IMPROVED GEOLOGICAL CHARACTERIZATION OF OLD HYDROCARBON FIELDS WITH SPARSE CONTROL POINTS: A CASE STUDY FROM THE SULIMAR QUEEN FIELD, SOUTHEAST NEW MEXICO

by

Maqsood Ali

Submitted in Partial Fulfillment
of the Requirements for the

Doctorate of Philosophy in Geology

New Mexico Institute of Mining and Technology
Department of Earth and Environmental Sciences

Socorro, New Mexico

October, 1997

TABLE OF CONTENTS

PART III

CHARACTERIZATION OF THE SULIMAR QUEEN FIELD

CHAPTER 4: GEOLOGIC MODEL FOR THE SULIMAR QUEEN FIELD

PART IV

SUMMARY AND CONCLUSIONS

LIST OF FIGURES

LIST OF TABLES

ACKNOWLEDGMENTS

This research was funded by the Department of Energy (contract No. DE-AC22-93BC14893), State of New Mexico, Landmark Graphics Corporation (Halliburton), Texaco, and Yates Petroleum.

I sincerely acknowledge the general discussions, assistance, and the criticisms of all my committee members. I would like to thank my committee for the opportunity to work with them on this multidisciplinary project. Drs. Adwait Chawathé, Ahmed Ouenes, and John Heller provided direction and insight throughout this research. I thank my academic advisor, Dr. Peter Mozley, for his guidance, assistance, and numerous stages of editing, and Drs. Dave Johnson, Allan Gutjahr, and Fred Phillips for their valuable input. I would like to specially thank my research advisor Dr. Adwait Chawathé for helping me to understand and use the concepts of fuzzy logic for petrographic data analysis and neural networks for predicting permeability using the petrographic data.

I would like to thank William Weiss for his help during this research and Liz Bustamante for editing this manuscript. I would also like to thank Martha Cather for her help in during the outcrop and petrographic studies and discussions on the depositional model.

New Mexico Bureau of Mines and Mineral Resources provided the core material used during this research.

Finally, this work simply would not have been possible without the love and guidance of my parents Mr. Syed Nazim Ali Kazmi and Mrs. Mumtaz Jehan.

ABSTRACT

The characterization of old hydrocarbon fields which are deficient in calibrated logs, cores, and reliable production data is a challenging task and no established methodology is available in the industry. The objective of this study was to characterize an old field—the Sulimar Queen—by developing new techniques and modifying existing ones to increase the quality and quantity of data. The Sulimar Queen field is producing from the Shattuck Member of the Queen Formation and is located in southeast New Mexico. The control points available from the Sulimar Queen field consisted of a core and modern logs from only one well, two core reports, and modern log suites from four wells. Only old gamma ray and neutron logs were available from the rest of the field. During the characterization of the Sulimar Queen field data from the Sulimar Queen field, analog reservoirs (adjacent fields), and Shattuck Member outcrops were used.

In the first step, the scale of permeability heterogeneity was established using cores from the Sulimar Queen and adjacent fields. The scale of permeability heterogeneity was found to be the same in the Sulimar Queen and adjacent fields.

A new technique for collecting and analyzing petrographic data was developed by combining minipermeameter and thin section analysis. This technique was developed in order to: (1) increase the quality and quantity of petrographic data related to permeability and (2) conserve the limited core material available from the Sulimar Queen field.

Fuzzy logic and neural network were used for the first time for petrographic data analysis and permeability prediction, respectively. Fuzzy logic algorithm was used to determine the control (ranking) of petrographic elements on permeability. The fuzzy logic algorithm is fast and unbiased and useful in dealing with large number of variables. Based on the results of the fuzzy logic ranking, a neural network was used successfully to predict permeability using the petrographic data.

Old gamma ray logs were first rescaled using the modern logs to increase their reliability. The rescaling of the gamma ray logs improved the identification of different porosity zones within the Shattuck Member. Rescaled gamma ray logs were used for the first time to predict porosity, sand thicknesses, and total water content.

The outcrop study of the Shattuck Member revealed that the sandstones were deposited in a mixed eolian and marine environment. The thicknesses of the sandstone units are variable and show lateral change from sandstone to evaporites. In the subsurface, similar lateral change from sandstone to evaporites is responsible for the formation of traps and the development of reservoirs in the Shattuck Member.

Information from thin sections, cores, logs, and outcrops was combined to develop the depositional model for the Shattuck Member in the Sulimar Queen and adjacent fields. The Shattuck Member was deposited in mixed lagoonal-sabkha-eolian environments. Based on the depositional model, a two layer simulation system was established. A history match of the primary performance was first achieved, and then the secondary performance was forecasted. A reasonable agreement between forecast and actual secondary performance attested to the credibility of the developed model.

Part I

CHAPTER 1: INTRODUCTION

The data required for detailed reservoir characterization ranges from mega-scale (>1 kilometer) to micro-scale (<1 centimeter). Mega-scale data define the spatial setting and the general architecture of the reservoir. Medium-scale information addresses variation of reservoir properties within the facies or individual reservoir units and sedimentary structures. Small-scale data comprises information on small-scale sedimentary structures, texture, mineralogy, and pore morphologies.

There are four basic sources of data for reservoir characterization: (1) the reservoir under consideration, (2) analog reservoirs, (3) outcrops similar to the specific reservoir, and (4) examples from modern environments. A complete set of reservoir data consists of static data such as lithological and stratigraphic details, seismic data, petrophysical properties, fluid properties, information on rock-fluid interaction, and dynamic data such as well test, production, and pressure data. Optimal data density is also critical in addition to the type and quality of data, and is governed by the type and scale of heterogeneity. The various scales of heterogeneity affect the reservoir performance in different ways, and are directly related to the size and part of the reservoir under consideration. The scale of heterogeneity dictates the selection of the methodology or tools to measure (identify) heterogeneity (Figure 1.1).

Mega-scale heterogeneities (thousands of meters horizontally and tens of meters vertically), e.g., faults and genetic units (Figure 1.2) are often clearly visible on seismic records or in well-to-well correlations. They can be analyzed on the basis of detailed well log correlations and sedimentological models derived from core descriptions. Within genetic units, characteristic patterns of permeability zonations are often present. These types of zonations classify as medium-scale heterogeneity and range in size from tens to thousands of meters horizontally and less than 10 meters vertically (Figure 1.2). These medium scale heterogeneities are much more difficult to evaluate than the large and

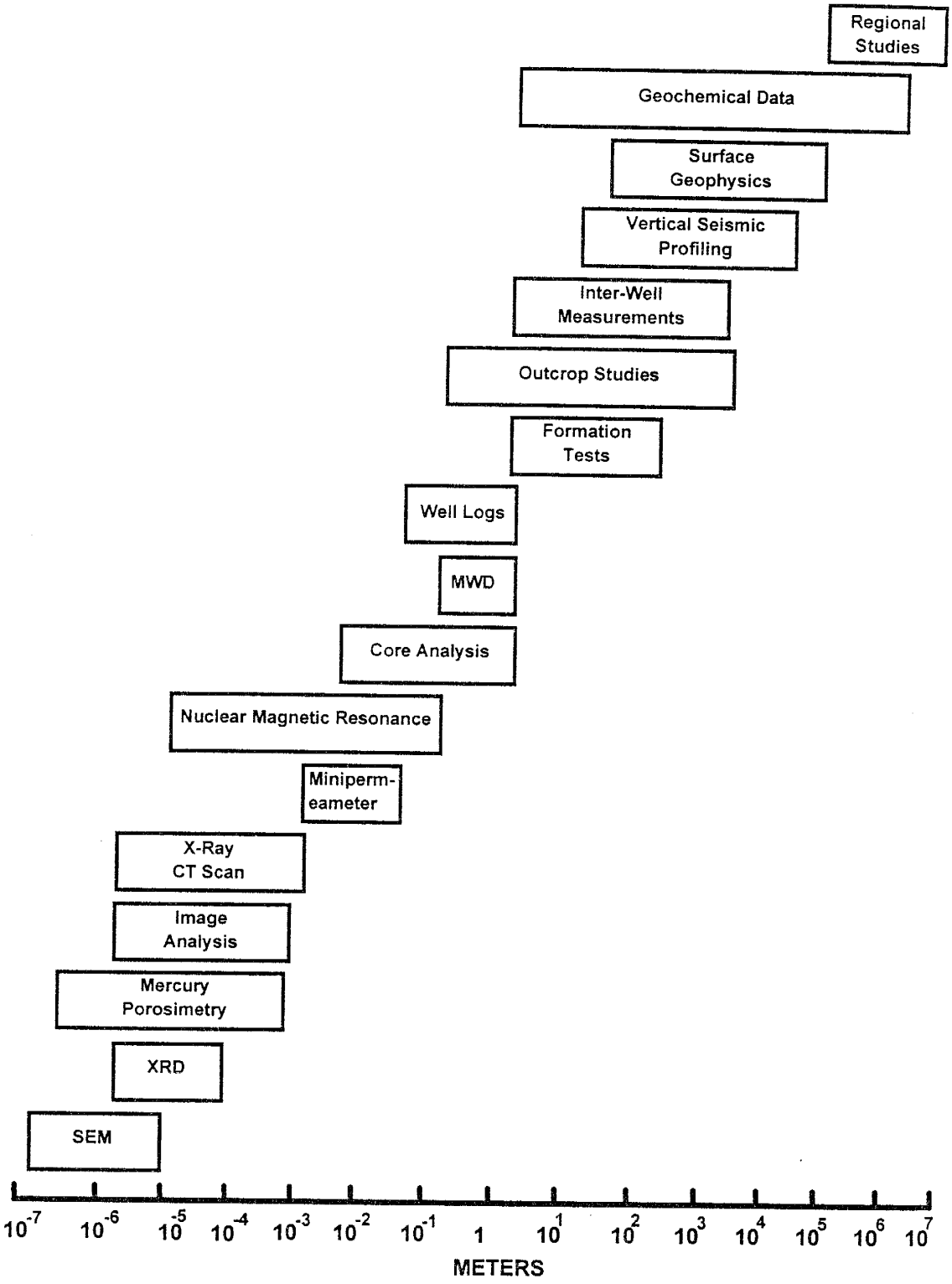

Figure 1.1: Scale of measurement of different methods and tools used in reservoir characterization (Jackson *et al.*, 1993).

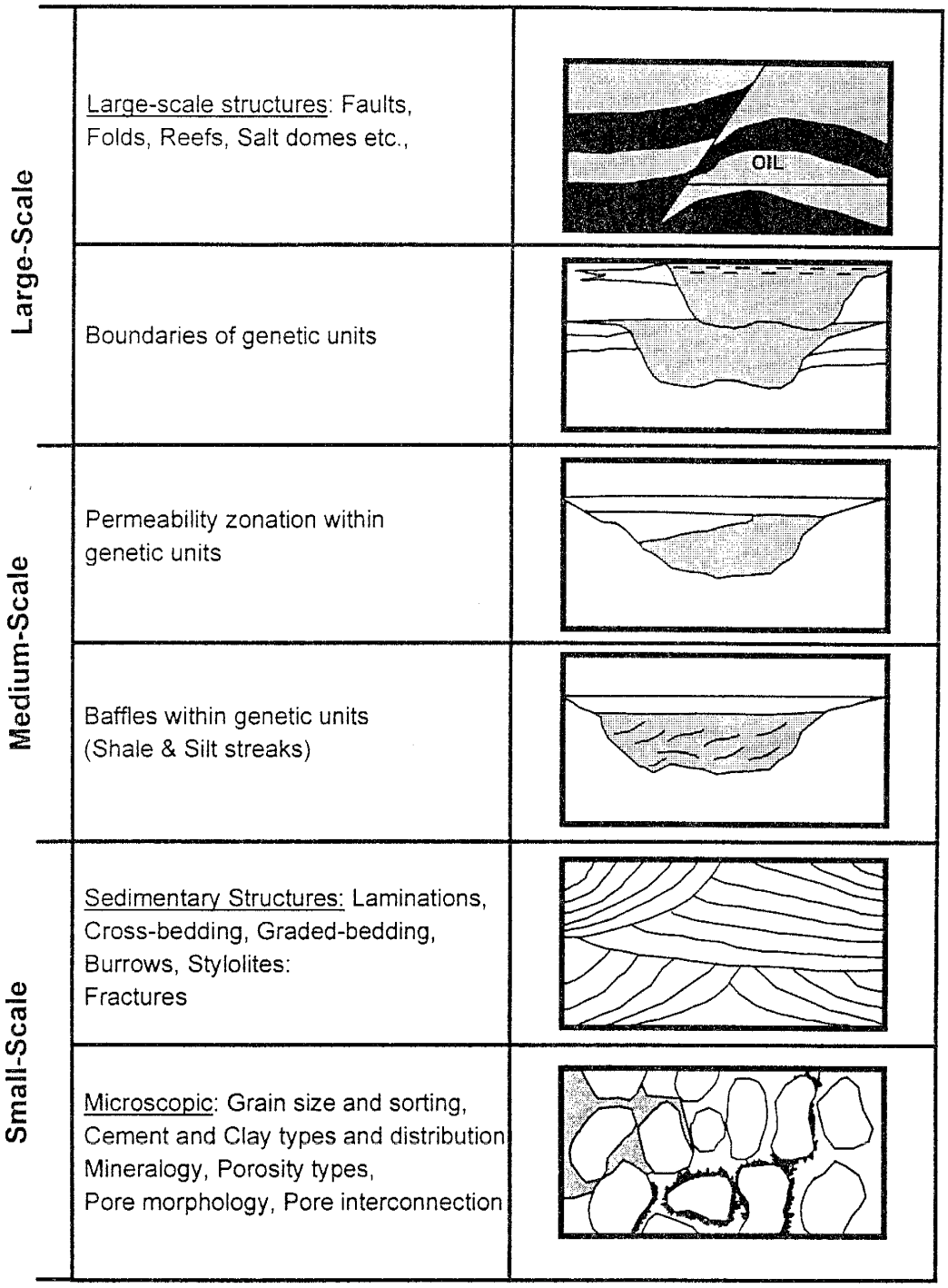

Figure 1.2: Types of reservoir heterogeneity (modified from Weber, 1986)

small-scale heterogeneities, and often require correlations between wells spaced at 100 meters or less (Weber, 1986). Crosswell tomography can also be used to evaluate medium-scale heterogeneities. Medium-scale heterogeneities affect interwell communication and injection/production behavior. Small-scale heterogeneities in the meter-to-micrometer range are only discernable in cores. Recovery problems in enhanced oil recovery operations are mostly due to small-scale heterogeneities in sedimentary structures, texture, and variations in pore geometry and distribution (Weber, 1986). This is due to nonuniform residual oil saturation distribution in the swept zones (Weber, 1986).

Although we know that the reservoirs are deterministic, i.e., there is only one actual representation of a particular reservoir, it is not economical or technically possible to sample the whole reservoir. Therefore, the data density should be at least statistically acceptable, and the models developed must be compatible with the geological understanding of the reservoir. However, in actual reservoir characterization problems, neither all types of data nor the appropriate data density may be available. A good example of this would be the oil fields developed before the 1970s which lack modern logs as well as core material. The drill cuttings available from these fields are not very reliable because a majority of the wells were drilled using cable tools. The economic constraints and risks involved prohibit both small and large operators from spending large sums of money on drilling new wells, coring, logging, and running special well-test operations in these old fields. Also, the production data available from these fields are sometimes unreliable. Under these circumstances the simulation/history-matching process may result in petrophysical properties (porosity, permeability, etc.,) far removed from reality. Hence, the characterization of such fields using available information is a challenging task, and no proven methodology is available in the industry.

This study describes a methodology developed for the characterization of an old field—the Sulimar Queen. The Sulimar Queen is typical of many old fields, in that it lacks quality reservoir data. In most cases, such a situation prevents an operator from investigating the true potential of such fields, and hence the methodology developed in

this study may be extended to old fields in general.

THE SULIMAR QUEEN FIELD

The Sulimar Queen field was developed in late 60s. Primary production was initiated in July 1968 and lasted until December 1971. A total of 20 wells produced 533,316 barrels of oil. A waterflood, initiated in 1972 and completed at the end of 1983, produced 1,112,033 barrels of incremental oil, tripling the primary production.

The field is deficient in core material, modern logs, and a complete production data set. The Sulimar Queen field is located in the Chaves County, southeast New Mexico (Figure 1.3A). The field is producing from the Upper Queen Formation also called the Shattuck Member. The Shattuck Member, colloquially called the Artesia Red Sand or Queen Sand is an excellent marker bed that can be correlated using well logs throughout the Northwest Shelf. The Shattuck sand, being radioactive, causes an increase in the gamma ray values (API) through the productive zone. To avoid the confusion due to different names, we used "Shattuck Member" in this study.

In the Sulimar Queen and adjacent fields, the Shattuck Member consists of 15 to 20 feet of generally greenish brown, gray, or red, very fine-grained arkosic sandstone (Table 1.1). The Sulimar Queen reservoir is a lenticular-shaped sand body elongated in a northeast direction. It occurs at an average depth of 2,000 feet. The reservoir is a stratigraphic trap caused by updip reduction of porosity and permeability in the oil-bearing sandstone intervals. The Shattuck Member was deposited in a mixed lagoonal-sabkha-eolian environments. The sand is internally complex and can only be successfully exploited if the distribution of the individual porosity and permeability zones within the reservoir is clearly understood.

For the characterization of the Sulimar Queen field, the only control points available consist of *one core, core reports from two wells, and modern log suites from four wells* (Figure 1.3B). From the rest of field only *old gamma ray and neutron logs* were available (Figure 1.3B). These old logs are also called perforating logs because they were mainly used to identify the reservoir zones, so that these zones can be perforated.

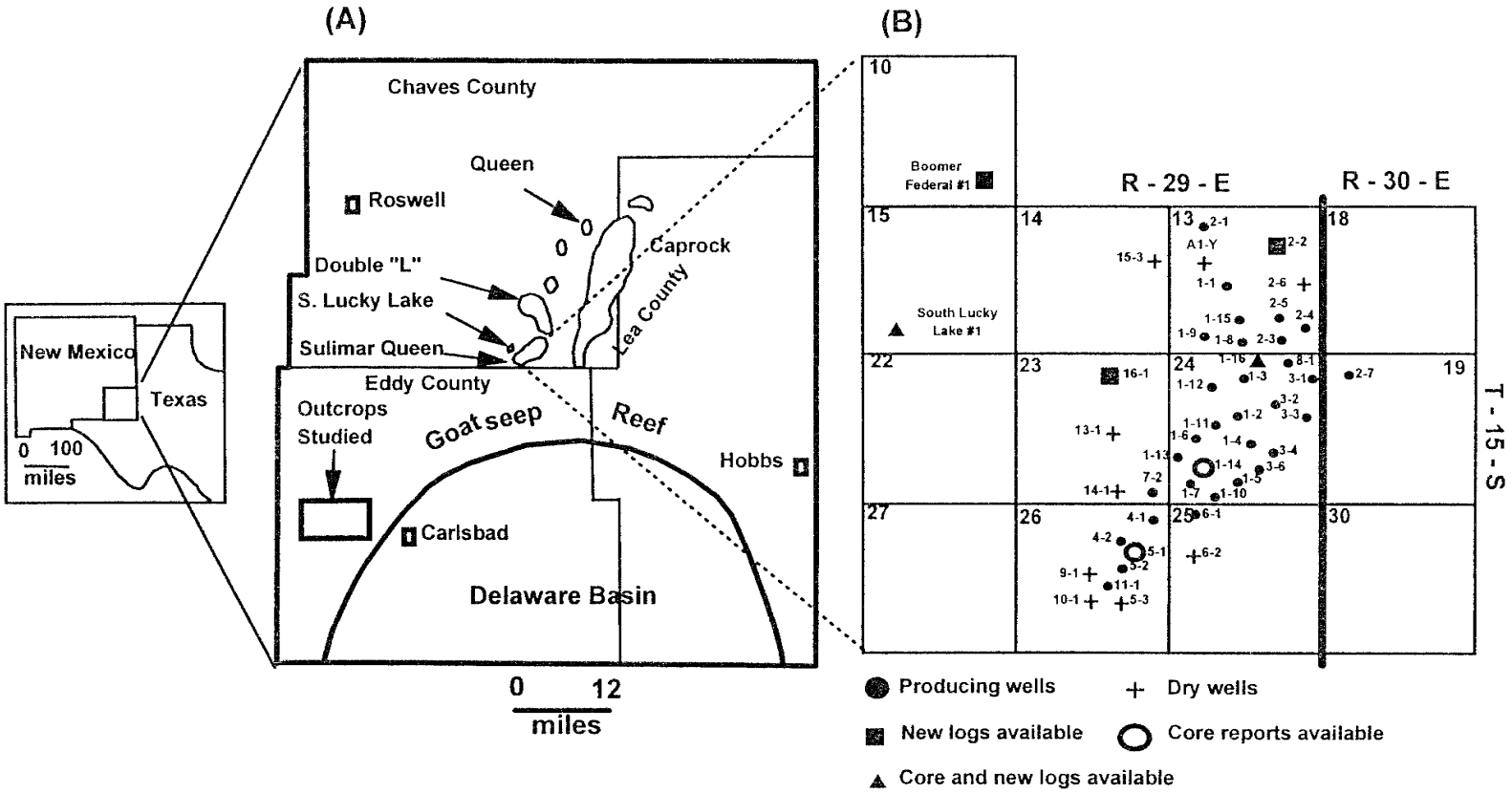

Figure 1.3: (A) Regional setting of the Sulimar Queen and adjacent fields. Stippled areas shows the indivudual field's size and shape. (B) Base map of the Sulimar Queen field showing the locations of the wells.

Some of the key properties of the Sulimar Queen reservoir are summarized in Table 1.1.

OBJECTIVES

The primary objective of this research was to develop new techniques, and modify existing ones, to increase the quality and quantity of data for the characterization of old fields with sparse and unreliable data. This was achieved by the successful characterization of an old field—the Sulimar Queen. The outcome of this study was to propose a practical methodology that independent operators can implement in order to make improved reservoir management decisions.

METHODOLOGY

In this section, the overall methodology developed to characterize the Sulimar Queen field is discussed. Figure 1.4 shows the assimilation of all the data types used in this study.

Identification of Similarities in the Reservoir Properties in the Sulimar Queen and Adjacent Fields

The first step in the characterization of the Sulimar Queen field was to determine the presence of similarities in the reservoir properties of the Sulimar Queen and adjacent fields. Since only one core was available from the field, additional cores and modern logs were obtained from the Queen and South Lucky Lake fields (Figure 1.3A). Several old gamma ray and neutron logs, and core reports from the neighboring Double "L" field were also obtained (Figure 1.3A). This information was collected to establish the similarities in the geological and petrophysical elements in the Shattuck Member in the Sulimar Queen and adjacent fields. It was critical to establish this behavior so that the relationships developed in Well 1-16, from which both modern logs and core were available, could be applied with confidence throughout the field.

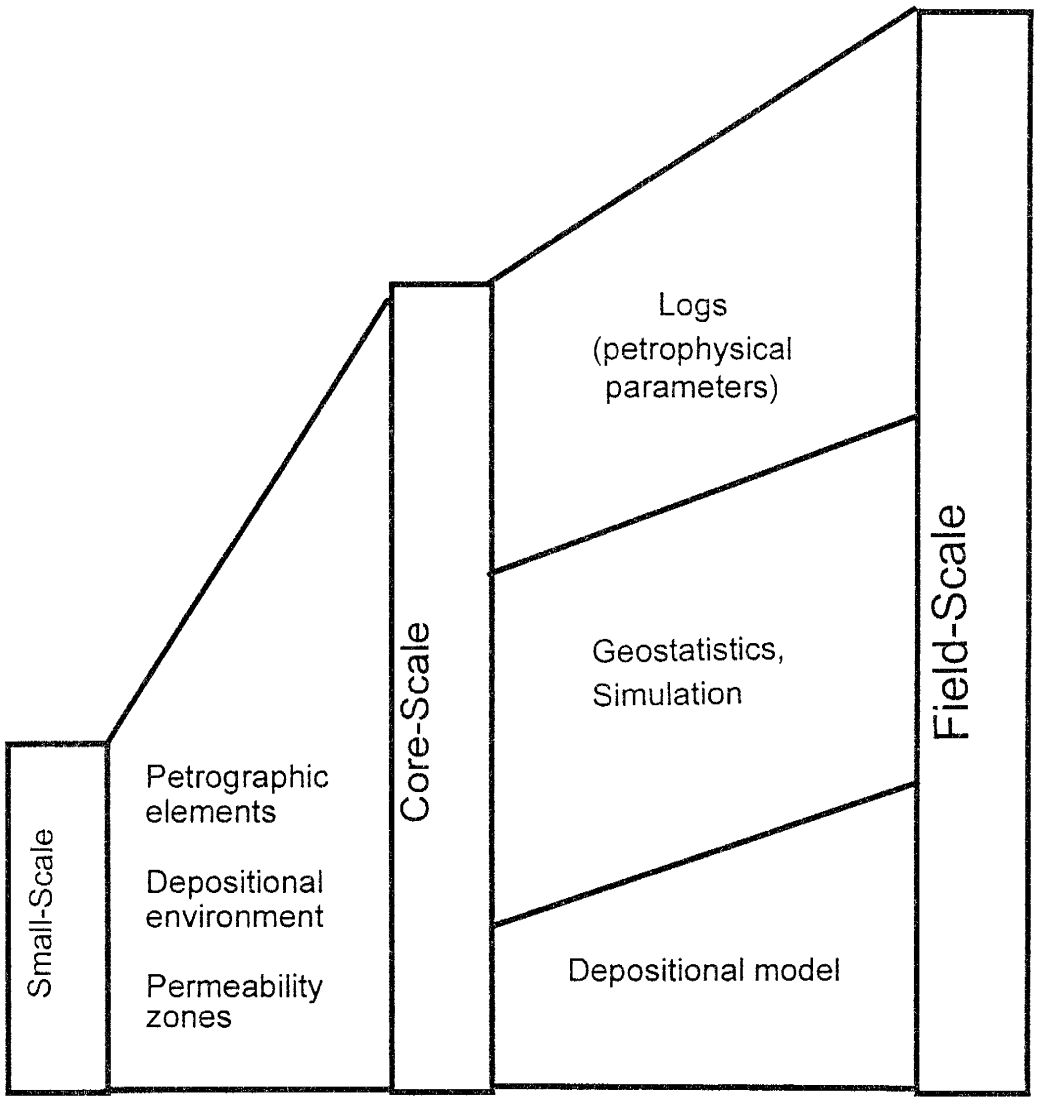

Figure 1.4: Assimilation of different data types for the characterization of the Sulimar Queen field.

Core Analysis

A small-scale heterogeneity study was conducted on the cores obtained from Sulimar Queen and adjacent fields in order to identifying micro-scale heterogeneities. Combining permeability studies made with the minipermeameter and thin section analysis allowed us to understand the petrographic influence on permeability. The core analysis was used to develop the depositional model. The overview of the core analysis is schematically depicted in Figure 1.5.

Small-scale heterogeneity study

For reliable characterization it is critical to establish the scale of permeability heterogeneity in the vertical direction using the cores. This was achieved by using a computer-controlled scanning minipermeameter (SMP). Several experiments were conducted to improve the capabilities of the SMP. Calibration of the SMP was done using standard core plugs and a probe minipermeameter on loan from UNOCAL Corporation.

Increasing the quality and quantity of petrographic data

After obtaining the permeability distribution from the minipermeameter, the next step was to collect enough samples for petrographic analysis from the only core available from the Sulimar Queen field. A new methodology was developed by utilizing the fine-scale grid on which permeability measurements were made using a minipermeameter. Because of this fine grid, each thin section contains more than one permeability measurement location. The area of investigation of the minipermeameter probe is very small and can be analyzed in the thin section. With this new technique the quality and quantity of petrographic data was increased. This methodology also helped to conserve the valuable core material.

The advantage of collecting a large set of data points is that detailed statistical analyses can be done and the control of each petrographic element on permeability can be evaluated. In addition to simple regression analysis, a fuzzy logic algorithm was applied

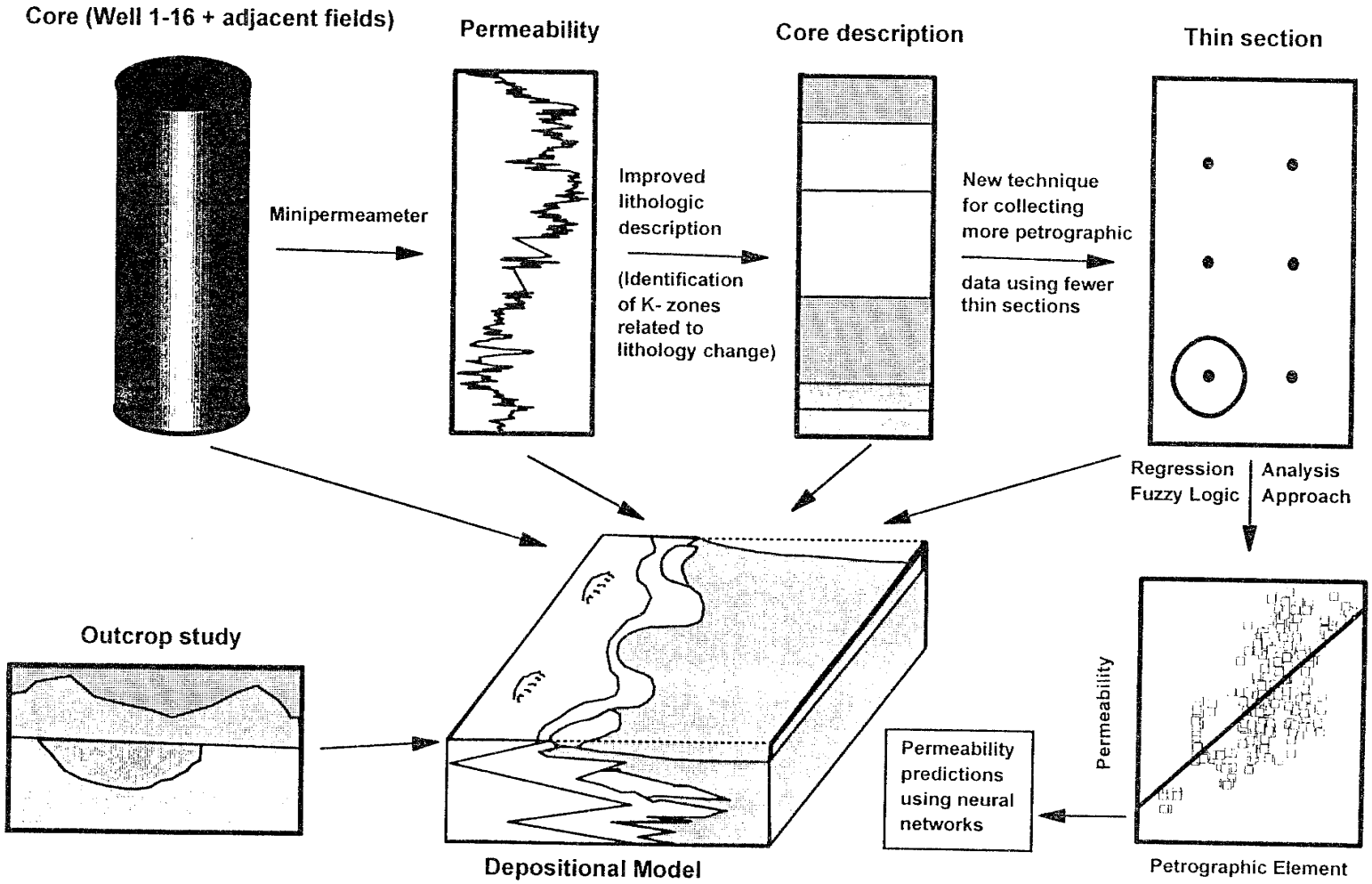

Figure 1.5: Generalized core evaluation and implementation to develop the depositional model.

to determine the importance (ranking) of each petrographic element in controlling permeability.

Outcrop Study

An outcrop study was conducted to supplement the subsurface information about the aerial distribution of the individual low and high permeability zones, heterogeneity on the interwell scale, and the lateral and vertical heterogeneity, (Figure 1.3A). The outcrops studied are present along and adjacent to Rocky Arroyo area (T-21-S, R-23-E & R-24-E; Eddy County, New Mexico). These outcrops are about 40 miles southwest of the Sulimar Queen field. Several sections were measured and described, and numerous core plugs and rock samples were collected. A field minipermeameter was used for making permeability measurements. Due to the malfunction of the field minipermeameter, rock samples and core plugs were collected to make porosity and permeability measurements in the lab. The Queen Formation weathers easily; therefore, well exposed and continuous outcrops are absent. As shown in Figure 1.5, the information obtained from the outcrops supplemented the core analysis and contributed to the development of the depositional model.

Log Analysis

With the exception of four modern log suites, only old gamma ray and neutron perforating logs were available from the field. The overview of the log analysis and its contribution is shown in Figure 1.6.

There were several problems with the old logs. These perforating logs were used only to identify the highly radioactive Shattuck Member. During the field development, various wireline companies were used to log the wells, resulting in a multitude of measurement scales. The logs were also not calibrated properly so the information from different wells could not be compared.

Gamma ray logs were rescaled based on the four modern logs, using a technique proposed by Barrett in 1994. Porosity and total water content distributions were obtained

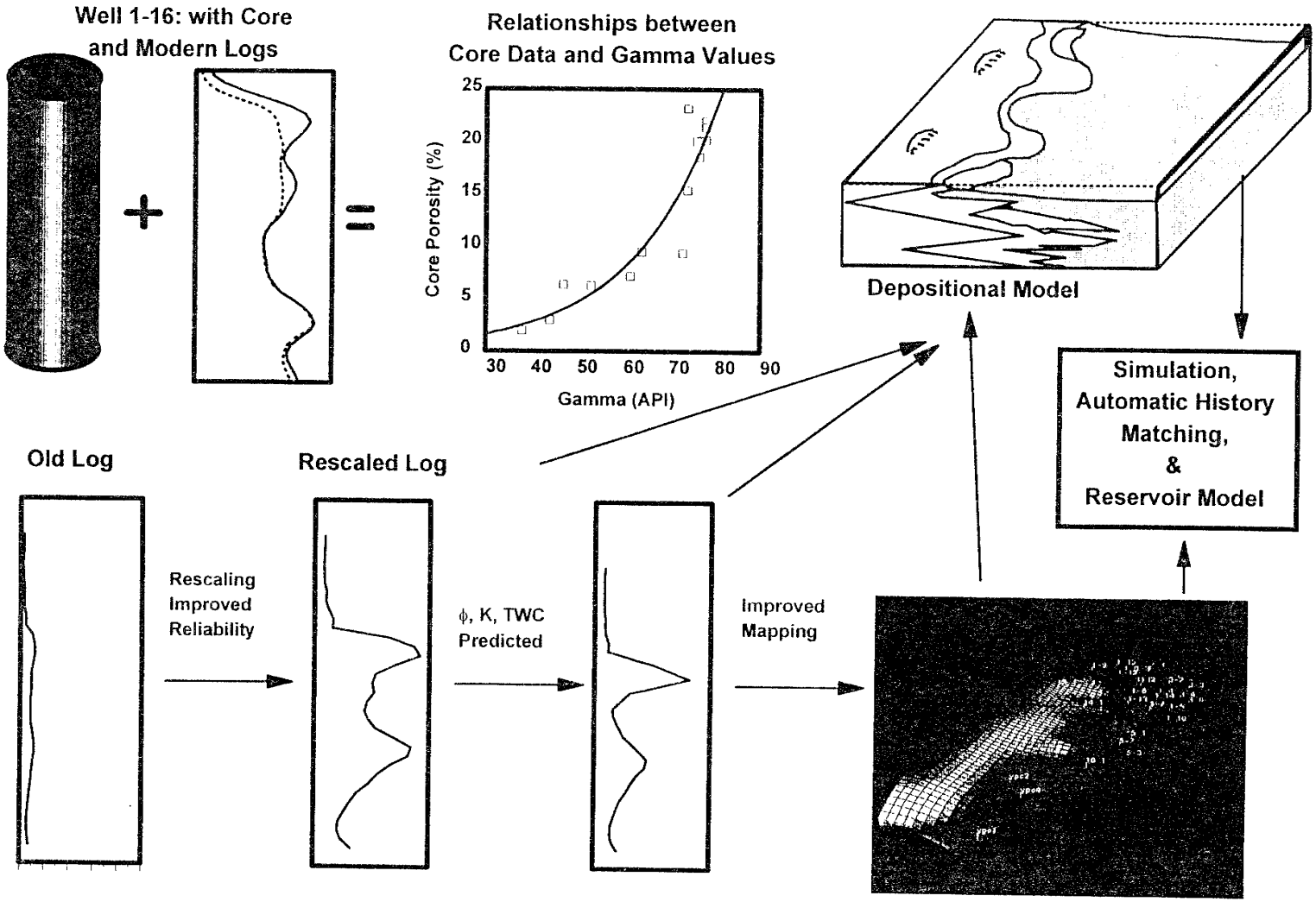

Figure 1.6: Generalized log evaluation techniques and their implementation towards developing the depositiona and simulation model.

throughout the field using the rescaled gamma ray logs. Mineralogic data from thin sections and XRD were also used to improve log analysis.

Statistical and Geostatistical Analysis

Core and outcrops permeability data were analyzed for the basic population statistics, using mean (arithmetic and harmonic) and variance. Data from cores and outcrops were also checked for the type of distribution, *i.e.*, normal, log-normal or power normal, etc. Arithmetic and harmonic averages of the permeability values were used to determine the horizontal and vertical permeabilities, respectively.

Variograms were generated using the core and outcrop permeability data. Kriging and inverse-distance weighting methods were used to generate porosity, permeability, and isopach maps.

Simulation and History Matching

The goal of the field-wide simulation was to match the primary producing histories of each well and then use the resulting reservoir description to forecast the waterflood response. A black oil simulator was used towards this objective. A two-layer, 6,000 grid block model was created to automatically match the primary production performance of each well. Once the simulator was calibrated with the primary performance, a waterflood forecast was made. The history matching was done using the simulated annealing method. The oil rates were used as the inner boundary condition to constrain the model, as they were the only reliable measurements in the field.

ORGANIZATION OF THE DISSERTATION

The efforts and results of this research are arranged in the form of individual papers. Some of the papers have already been accepted for publication in conference proceedings and others are being submitted for review. This dissertation is divided into four parts. An overview of the dissertation organization and the papers extracted from each chapter is shown in Figure 1.7.

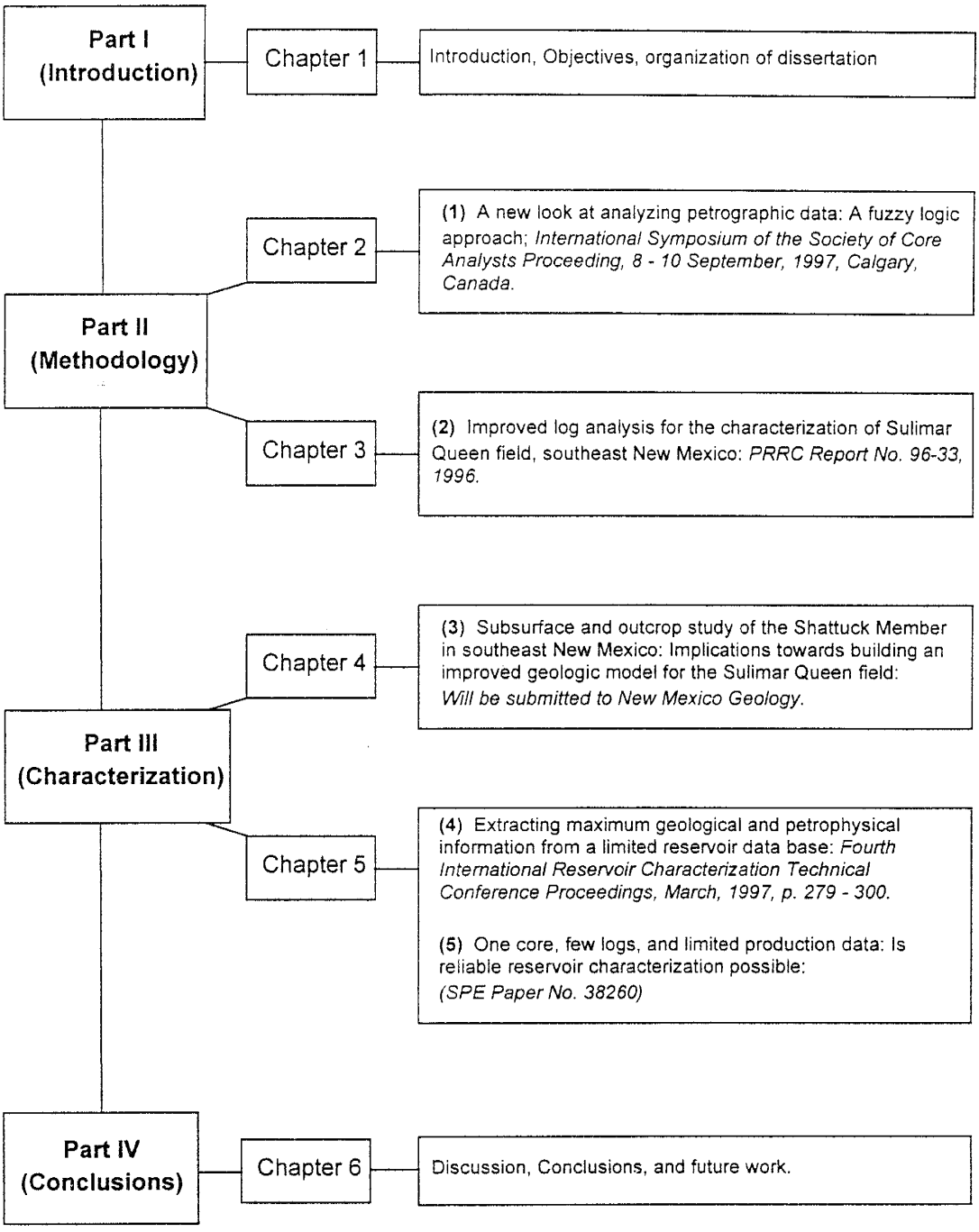

Figure 1.7: The overview of the dissertation organization and list of publications from each chapter.

Part II:

Following the introductory Chapter 1 (Part I), Part II discusses the methodology developed to improve the quality and quantity of data from a limited reservoir data base for the characterization of old fields. There are two chapters in this part.

Chapter 2 describes the details of the new methodology developed for collecting and analyzing petrographic data related to permeability. This work was presented as a poster and the paper will be published in the conference proceedings—Chawathe, A., *Ali, M.*, and Ouenes, A., *A new look at analyzing petrographic data: The fuzzy logic approach:* International Symposium of the Society of Core Analysts Proceedings, Calgary, Canada, 8 - 10 September, 1997. The implementation of fuzzy logic of the petrographic data was accomplished by Drs. Adwait Chawathé and Ahmed Ouenes. The author of this dissertation was responsible for the development of the new technique of collecting and analyzing petrographic data, which is the data used for the fuzzy logic analysis.

Chapter 3 describes the methodology used for the improved old log analysis. This work has been presented in the form of a PRRC Report (No. 96-33): *Ali, M.,* Chawathé, A., Ouenes, A., and Weiss, W., *Improved log analysis for the characterization of the Sulimar Queen field, southeast New Mexico:* This work was also presented at the final Review of the DOE Project (Contract no. DE-AC22-93BC14893) in Roswell, New Mexico. The author is responsible for most of the work described, while discussions were made with the coauthors.

Part III:

Part III of the dissertation consists of two chapters and is related to the characterization of the Sulimar Queen field.

Chapter 4 describes the assimilation of the information obtained from logs, cores, outcrops, and petrographic analysis to develop the depositional model for the Shattuck Member in the Sulimar Queen and surrounding area. This paper will be submitted for publication to New Mexico Geology: *Ali, M.*, and Cather, M., *Subsurface and outcrop*

study of the Shattuck Member in southeast New Mexico: Implications for building an improved geologic model of the Sulimar Queen field: The author is responsible for the core and petrographic analysis, outcrop study, log analysis, and building the depositional model. Martha Cather helped in the petrographic and outcrop studies.

Chapter 5 summarizes the methodology and results for the Sulimar Queen field. From this chapter two papers were published; (1) *Ali, M.*, Chawathé, A., Ouenes, A., Cather, M., and Weiss, W: *Extracting maximum petrophysical and geological information from a limited reservoir data base*: 4th International reservoir Characterization Technical Conference Proceedings, Houston, Texas, (2 - 4 March, 1997), p. 279 - 300. This paper will also be a part of a peer-reviewed AAPG book to be published next year. The author is responsible for the majority of the work described. The author is responsible for core analysis, logs rescaling, log analysis, prediction of porosity and total water content using rescaled gamma ray logs, petrographic analysis, statistical analysis, and developing the depositional model. Drs. Adwait Chawathé and Ahmed Ouenes were responsible for numerical simulation, Martha Cather helped in petrographic analysis, and William Weiss providing the logs and other field data. (2) Chawathé, A., Ouenes, A., *Ali, M.*, and Weiss, W., *One core, few logs and limited production data: Is reliable reservoir characterization possible?*: (SPE Paper no. 38260) Society of Petroleum Engineers, 67th Annual Western Regional Meeting, 25 - 27 June, 1997, Long Beach, California. William Weiss performed the transient pressure test and Drs Adwait Chawathé and Ahmed Ouenes were responsible for the global integration of all data in a black oil reservoir model. The author is responsible for the geological study.

Part IV:

Part IV consists of a discussion and conclusion section. In this section general conclusions, the methodology developed, and suggestions for future work are described.

Part II

Chapter 2: A New Approach for Collecting and Analyzing Petrographic Data*

INTRODUCTION

Small-scale permeability heterogeneities affect reservoir performance, especially during secondary and tertiary recovery. These heterogeneities are controlled by variations in petrographic elements such as porosity types, pore morphologies, mineralogy, texture, and type, amount, and distribution of clay and cement. In order to assess the influence of each variable on permeability, a comprehensive petrographic study is essential. Conventionally, correlations between permeability and petrographic elements are determined by using core plugs and thin sections, but there is a large difference in the volume of investigation of thin sections and core plugs. Permeability varies from point to point within most core plugs so that a thin section prepared from that core plug may not contain those petrographic elements that are representative of the core plug's permeability. As a consequence, such correlations may be misleading. In order to sample small-scale permeability heterogeneity a large number of core plugs are required. Because drilling core plugs is destructive to valuable cores, permeability heterogeneities on a small-scale cannot be analyzed in detail. The usual size of the core plug (2.5 centimeters diameter) also restricts the detailed investigation of permeability heterogeneities on a small-scale, especially in sedimentary structures with dimensions less than 2.5 centimeters. The size constraints imposed by core plugs to determine small-scale permeability heterogeneities can be overcome by making closely spaced permeability measurements with a minipermeameter.

Permeability measurements made with a minipermeameter have several

* Chawathe, A., Ali, M., Ouenes, A., and Weiss, W., *A new look at analyzing petrographic data: the fuzzy logic approach:* 1997 International Symposium of the Society of Core Analysts, Calgary, Canada, 8 - 10 September, 1997.

advantages: 1) a large amount of closely-spaced permeability data can be collected to reveal small-scale permeability heterogeneities, 2) the area of investigation of the minipermeameter probe tip is very small and can be examined in thin sections, and 3) as the permeability measurements are made on closely-spaced intervals, each thin section contains many permeability measurement points. Therefore, a large set of petrographic data directly related to permeability can be collected.

In this chapter, we first describe a new simple and efficient technique to make precise correlations between permeability and petrographic elements by combining minipermeameter and petrographic analysis. Second, we explore a new technique for analyzing the petrographic data using fuzzy logic. The former technique was applied to both sandstones and carbonates in order to determine their applicability. In Chapter 5, we describe the benefits of this technique in old fields.

METHODOLOGY

In the following sections methodology used to develop the new approach for collecting and analyzing petrographic data is described.

Minipermeameter

In order to obtain a large number of small-scale permeability measurements, a computer controlled scanning minipermeameter (SMP) was used in this study. Like other minipermeameters, the SMP is built around a constant-pressure air supply, a means to measure the air flow from the supply, and a soft silicon rubber probe tip which is pressed against the rock sample to achieve the seal. The SMP will be described briefly in this paper. For details see Suboor and Heller (1995).

In the SMP, both the air supply and the means for flow measurements are achieved by the use of a simple glass syringe (Figure 2.1). The gravitational force on a weight resting on the plunger produces a constant air pressure inside the syringe. An air pump is used to fill the syringe prior to each measurement. *The total time interval (T) required to inject a fixed volume of air from the syringe into the sample depends on the*

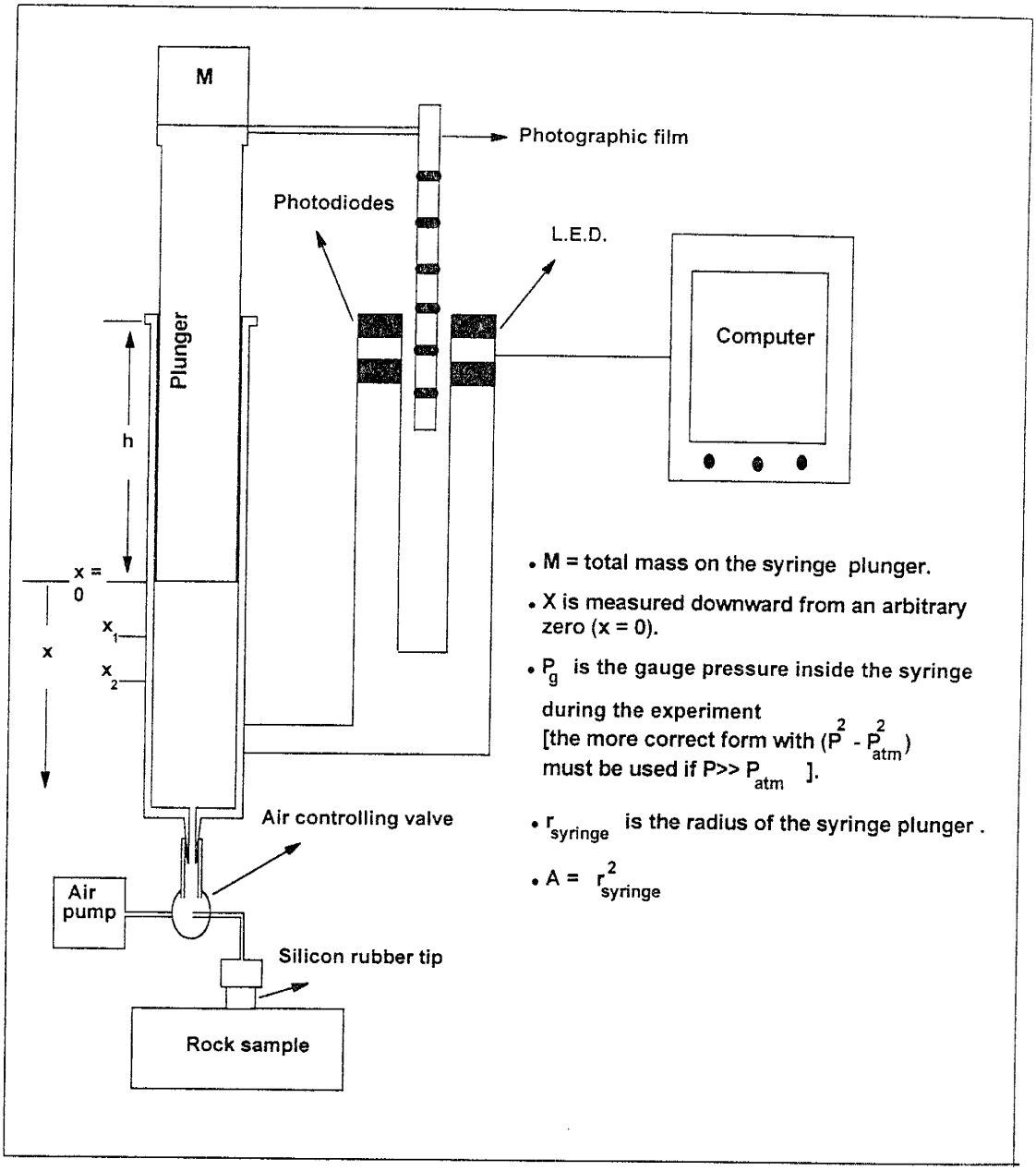

Figure 2.1: Schematic diagram of the scanning minipermeameter (SMP) device showing the motion of the plunger based on the forces that act on it (modified from Heller, 1992).

permeability of the rock sample precisely underneath the probe tip. Information on the position of the syringe plunger is obtained optically by means of commercial "edge detectors" that consist of a small light source (L.E.D) and photo detectors, mounted opposite to each other, through which a strip of photographic film attached to the syringe plunger moves. The permeability is calculated by a modified version of Darcy's law:

$$K = \frac{\mu A \Delta X}{aG\Gamma P_g}\left[\frac{1}{T} - \frac{1}{t_{lkt}}\right]$$

K = air permeability (darcy)

μ = viscosity of air (centipoise)

A = syringe area (centimeter squared)

Δx = distance traveled by the plunger from x_1 to x_2 (centimeters)

a = inner radius of tip (centimeters)

G = geometrical factor

Γ = pressure correction factor

P_g = gauge pressure inside syringe ($P - P_a$) (Fractions of a standard atmosphere).

P = absolute value of the applied pressure, and P_a = atmospheric pressure

T = time interval for syringe plunger to sink from x_1 to x_2 (seconds)

t_{lkt} = time interval in which the syringe plunger will move downwards by the distance Δx in the absence of flow into the rock (seconds)

The actual permeability of the sample is calculated by taking into account the leakage of air along the sides of the plunger in the form of the leak time (t_{lkt}). Leak time is determined by putting the probe tip on the leak pads, which have a smooth plastic surface, and measuring the time required by the plunger to travel the distance Δx.

Several experiments were conducted to calibrate and improve the accuracy of the SMP. One of the parameters that affects the permeability measurements is the quality of the seal between the probe tip and sample surface, because a slight leakage can give

erroneously high permeability values. This problem is more pronounced in sandstones than in carbonates. The sawing process to slab the cores produces smooth surfaces in carbonates, but due to the granular texture of sandstones, especially in medium and coarse grained samples, the surface remains rough enough to require larger weight/pressure on the probe tip to form a good seal. Several experiments were performed to determine the optimum weight for different probe sizes and rock permeabilities by gradually increasing the weight on the probe tip and finding the weight range at which the permeability values are stabilized (Figure 2.2). The results are summarized in Tables 2.1 and 2.2. For the same probe tip size, the optimum weight depends on the permeability of the sandstone samples. The permeability is, in turn, controlled by the grain size (i.e. the higher the permeability the larger the optimum weight on the probe tip; Table 2.1). For different probe-tip sizes, the optimum weight depends on the tip area that is in contact with the rock, and the bigger the tip area the larger the optimum weight (Table 2.2). In some cases when the weight is too large, the probe becomes distorted, causing leakage (Figure 2.2C). The SMPs permeabilities were compared with the standard homogeneous core plugs and a good correlation was obtained (Figure 2.3).

The surface of the slabbed cores were cleaned by vacuuming, before measuring permeabilities with the minipermeameter. The cleaning was done to remove the smaller grains and clay from the pores which may have moved into the pores during the cutting (slabbing) of the cores.

Improving the Quality and Quantity of Petrographic Data Related to Permeability

In order to sample the whole permeability range and improve the quality and quantity of the petrographic data related to permeability, a new methodology was developed by combining the minipermeameter and this section analysis. This new methodology consist of two main steps. In the first step permeability measurements are made on the slabbed cores on a fine scale grid. In the second step thin sections are made from the surface of the slabbed cores in such a way that the position of each permeability measurement can be located and analyzed on the thin section (Figure 2.4A).

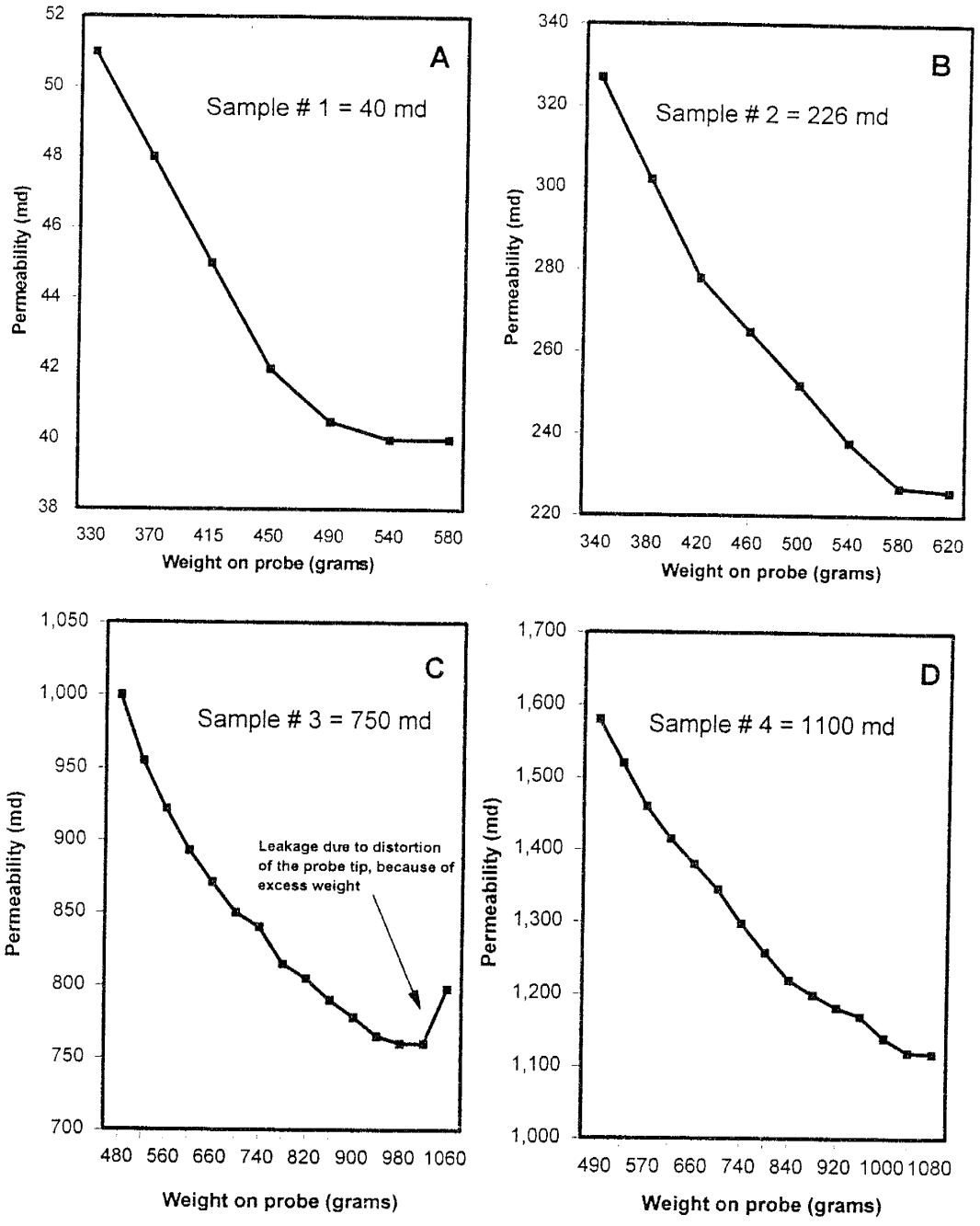

Figure 2.2: Calibration curves for the scanning minipermeameter, showing the relationships between weight on probe and permeability as observed in different standard core samples. If the weight on probe exceeds the strength of the probe tip, then leakage will occur (C) and the measured permeability will be very high.

Probe Tip Size (inches)	Probe Tip Area $(inches)^2$	Permeability (Range) (md)	Optimum Weight on Probe Tip (Range) (grams)
Inner Diameter = 0.125 Outer Diameter = 0.3125	0.0644	<1 - 300	500 - 600
		300 - 700	900 - 950
		700 - 2,000	1,000 - 1,500

Table 2.1: Optimum weight on probe tip of the minipermeameter for different permeability ranges. Note as the permeability increases so does the optimum weight.

Probe Tip Size (Inches)	Probe Tip Area $(inches)^2$	Optimum Weight on Probe Tip (grams)
Inner Diameter = 0.0625 Outer Diameter = 0.1875	0.0245	530 - 550
Inner Diameter = 0.125 Outer Diameter = 0.250	0.0368	750 - 800
Inner Diameter = 0.125 Outer Diameter = 0.375	0.098	1,200 - 1,250

Table 2.2. Optimum weight for different probe tip sizes. The optimum weight increases with increasing tip area.

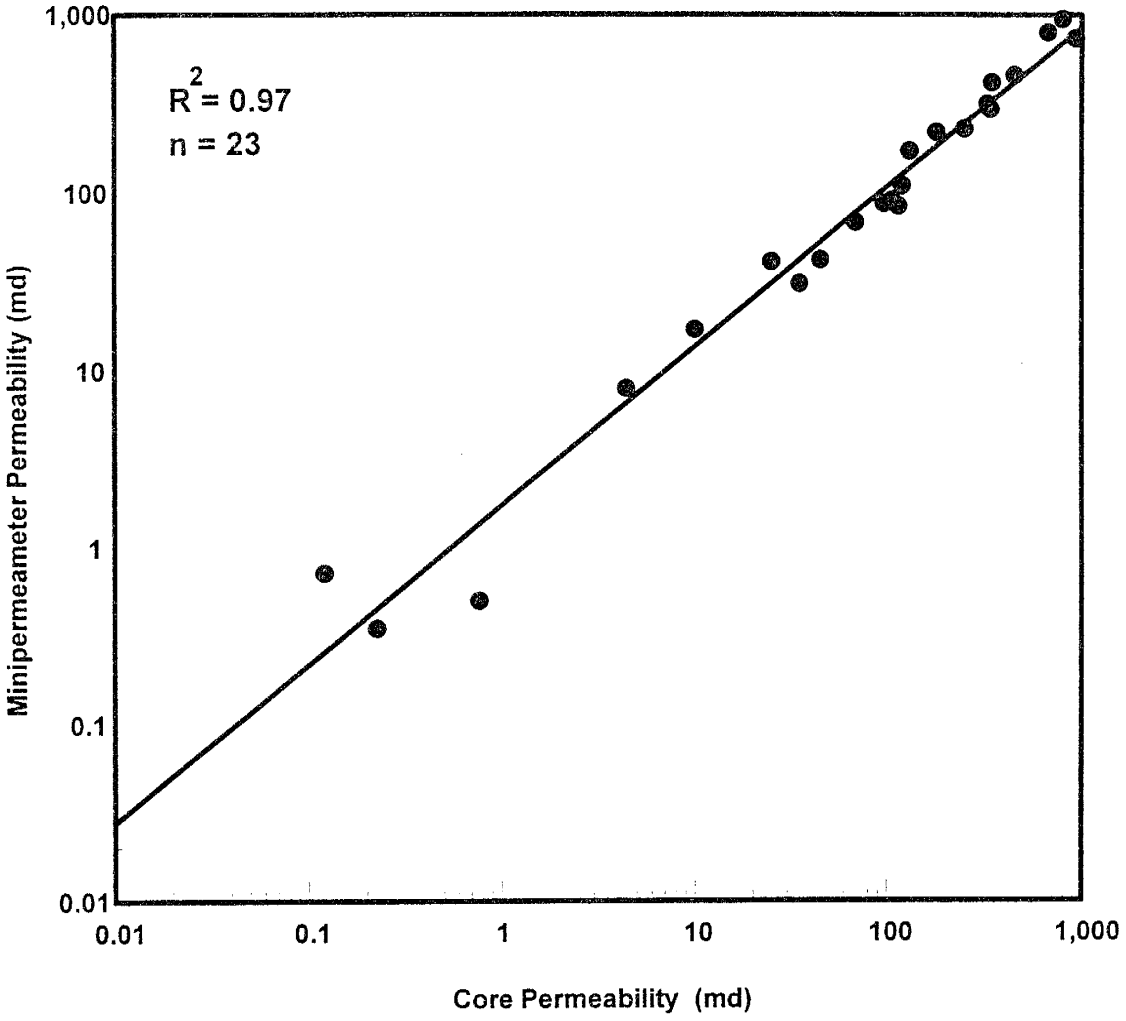

Figure 2.3: Comparison of core permeabilities obtained from Hassler-Sleeve and minipermeameter measurements.

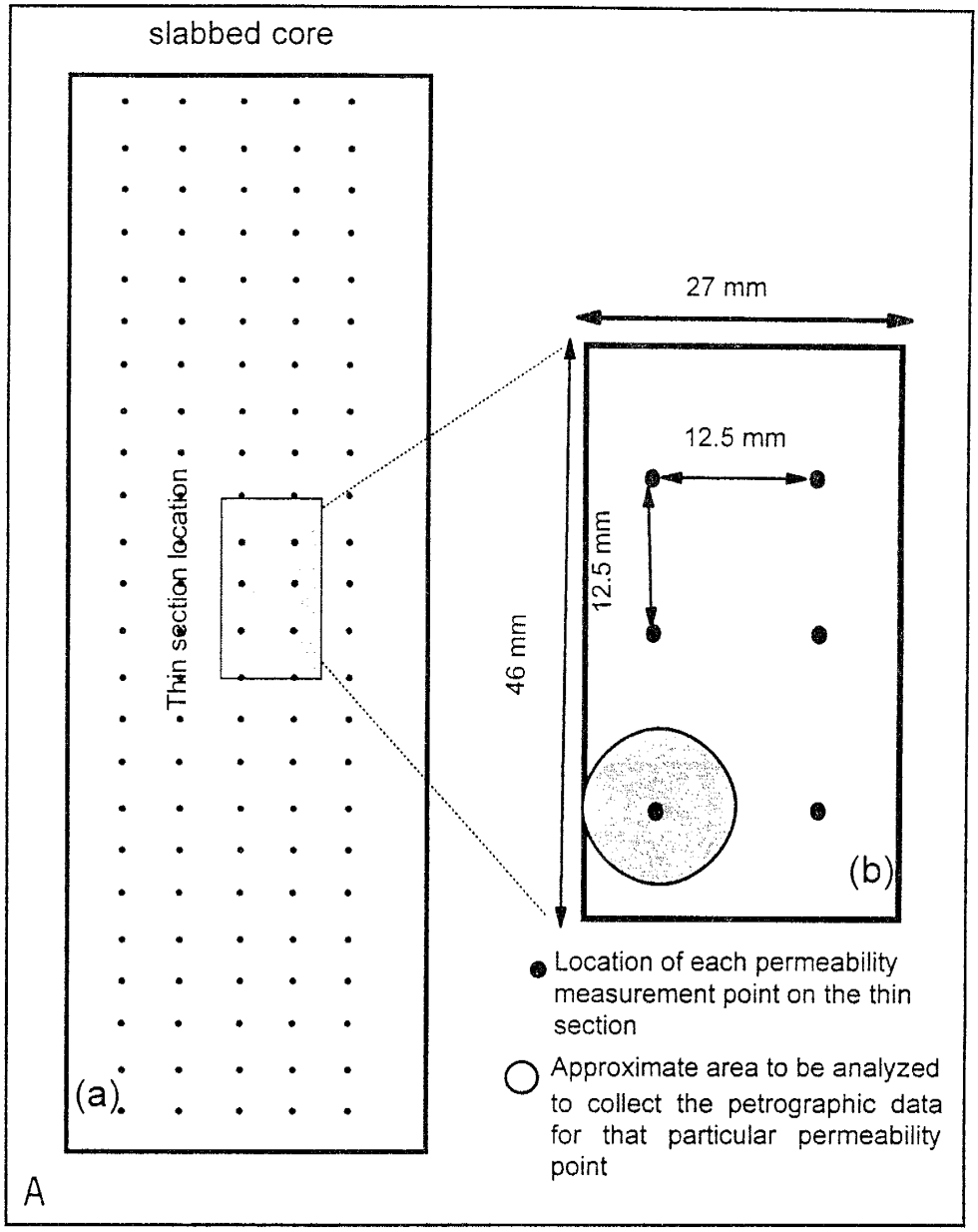

Figure 2.4A: (a) Grid on which permeability measurements were made. Five vertical profiles were generated by this grid. Thin section location is also shown. (b) Distribution of permeability measurement points on the thin section.

We concluded that this method allows for improved analysis based on the premises that: (1) the area of investigation of minipermeameter is very small and can be examined in thin section, thus increasing the quality of data, and (2) each thin section contains many permeability points, thus increasing the quantity of data (Figure 2.4A). The advantage of collecting a large set of data is that a detailed statistical analysis can be done, and the effects of each petrographic element on permeability can be determined accurately. This also helps assess the effects of diagenesis, and porosity evolution on permeability.

According to Goggin et al. (1988), the effective radius and depth of investigation of a minipermeameter probe tip is four times the internal radius of the probe tip. However, it was found during the calibration and permeability measurements with the minipermeameter, that the area of the core slab immediately under and around the probe tip exerts the main control over the permeability. After careful examination, the area of investigation of probe tips used to measure the permeability on the slabbed cores were established. For the probe tip with an inner radius of 0.125 inches (3.125 millimeters), the corresponding area on the thin section was 0.4 inches (10 millimeters) in diameter and for the probe tip with inner radius of 0.0625 inches (1.56 millimeters), the corresponding area on the thin section was 0.2 inches (5 millimeters) in diameter. In the absence of fractures, the area of investigation determined above can be used on both carbonates and sandstones. During the thin section analysis, depending on the number of permeability points (measured on the core, before thin section samples were cut) located on each thin section, the thin section was divided into that many circular regions of equal sizes and petrographic data was collected (Figure 2.4B). With this new method, data that would have required examination of 6-14 thin sections if conventional core plugs were used, were collected from a single thin section.

Once the petrographic data is collected, the second step is analysis. In order to assess the importance (ranking) of each petrographic element in controlling permeability, conventional regression analysis is performed. Linear, power, logarithmic, and exponential models are applied to the data, and the model that yields the best correlation

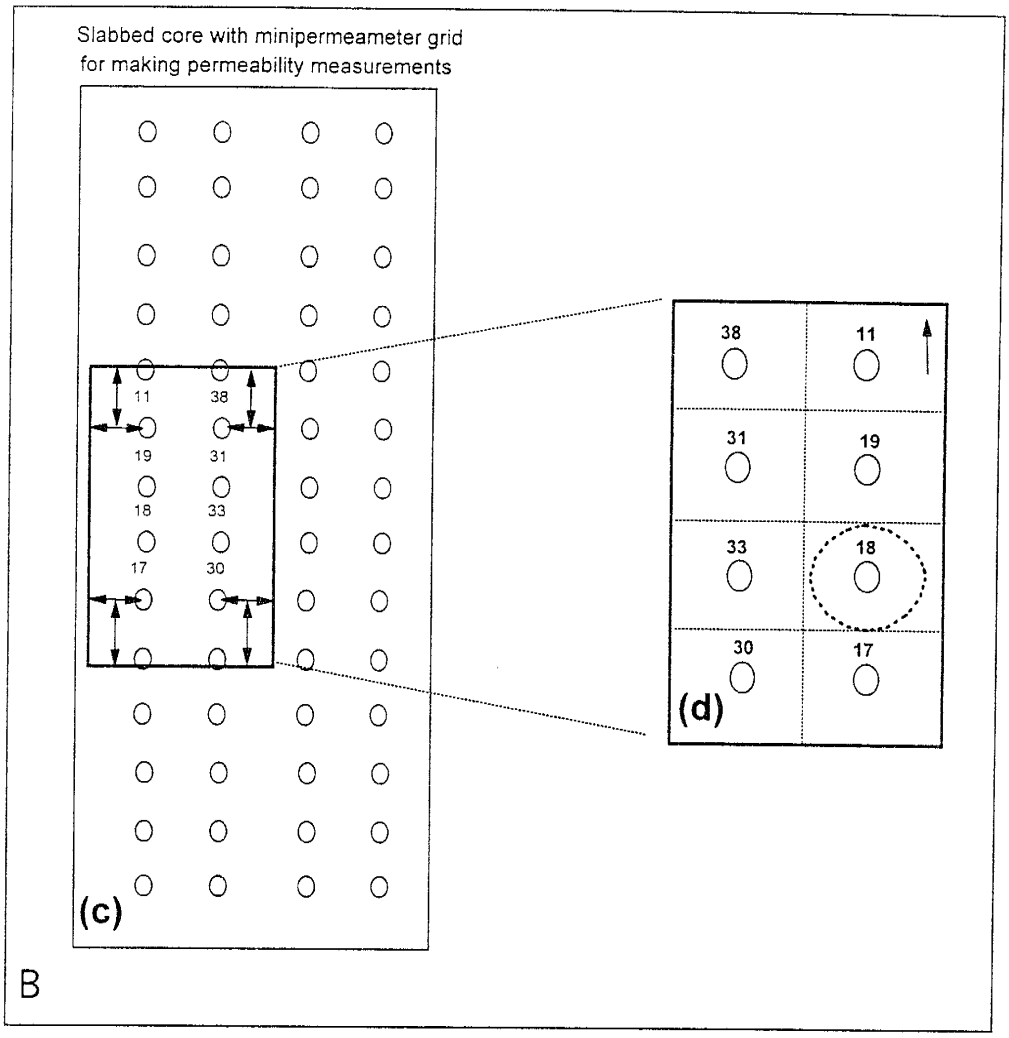

Figure 2.4B: The routine to prepare and collect data from the thin section containing many minipermeameter permeability measurements.

1. Record the distance from the edge of the thin section sample to the permeability points as shown in (c) (arrows). This is done, so that, after the thin section is made, the permeability measurement position can be located on the thin section accurately.

2. The locations of the individual permeability measurement points are flipped from left to right, because thin sections are made from the surface of the core slab (note the flipping of permeability locations from (c) to (d)).

3. Overlay a grid on the thin section so that the exact position of the permeability measurement point can be located (d) and petrographic data can be collected. Collect petrographic data either using the square or the circular area as shown in (d).

coefficient is usually chosen. It is important to realize that this conventional ranking technique compares the best regression models for different petrographic parameters, while ignoring the type of curve fit. Hence, the comparison is not entirely equitable. Once the best fit curves are obtained, the petrographic elements are ranked in descending order of their correlation coefficients, which also reflects the magnitude of their effect on permeability. At this stage, the petrographer, basing the decision on experience and intuition, supports (or modifies) this ranking of petrographic elements. In order to remove the qualitative interpretation, we used a quantitative approach—the fuzzy logic algorithm—to determine the importance (ranking) of each petrographic element in controlling permeability. The fuzzy logic algorithm compares all the parameters on the same basis and hence is superior to conventional regression analysis in that aspect. Depending on the ranking, the permeability may be estimated by using only the most important petrographic elements. In old fields, where the samples are scarce or not suited for making permeability measurements, thin section analysis may be used to estimate the permeability.

The Fuzzy Logic Algorithm

Computers cannot reason like the human brain. Computers "reason" when they manipulate precise facts that have been reduced to strings of zeros and ones and statements that are true or false (Kosko and Isaka, 1993). Fuzzy logic is a branch of machine intelligence that helps computers paint gray, common sense pictures of an uncertain world. Fuzzy logic manipulates such vague concepts as "warm" or "still dry" and thus helps engineers to build air conditioners, washing machines and other devices that judge how fast they should operate or shift from one setting to another even when the criteria for making those changes are hard to define (Kosko and Isaka, 1993).

In set theory, an element either does or does not belong to a set, e.g., a number 7 belongs completely to the set of odd numbers and not at all to the set of even numbers. In fuzzy sets elements only belong partially to the fuzzy sets, and they may also belong to more than one set (Kosko and Isaka, 1993). The only constraint on fuzzy logic is that an

element's degree of membership in complementary groups must sum to unity. Details of the fuzzy logic algorithm are beyond the scope of this dissertation and the interested reader is referred to Kosko and Isaka (1993) and Lin (1994).

More sophisticated techniques include the Partial Least Squares method and the Principal Component Analysis (the Karhunen-Loève transform; Martin and Neas, 1989). These techniques seek to identify the most significant inputs that contribute to a given output, and then model the system as a linear combination of the significant inputs. Non-linear systems, on the other hand, require more contemporary modeling techniques like neural networks, fuzzy systems, genetic algorithms, etc., which try to preserve the system's nonlinear nature. Although powerful, nonlinear techniques are plagued with erroneous solutions generated by the local minima in the solution space. These local minima worsen if the input space is large. Therefore, to efficiently model a nonlinear system, it is imperative to reduce the input space by identifying the significant inputs that contribute to a specific output.

In this study, most of the petrographic attributes examined in the thin sections contribute to permeability heterogeneity and each attribute alters permeability in a unique manner. It is difficult to accurately quantify this interaction between each of the petrographic parameters and permeability, thus emphasizing its non-linear nature.

Facing the dilemma of not knowing the explicit relationship between each petrographic attribute and permeability, the question of the most significant attributes that contribute to permeability was resolved using a fuzzy logic algorithm. This data-directed algorithm, developed by Lin (1994), compares the effect of each individual input parameter, x_i ($I = 1, 2, ..., N$, the petrographic elements), on the single output, y (the minipermeameter permeability). Assume that there are M training data points available and that x_{ik} ($k = 1, 2, ..., M$) are the i^{th} coordinates of each of the M training points. For each input variable x_i, the M data points are plotted in x_i-y space. For every point (x_{ik}, y_k) in x_i-y space, a fuzzy membership function is drawn for the input variable using

the following equation:

$$\Phi_{ik}(x_i) = exp[-(\frac{x_{ik} - x_i}{b})^2], \qquad k = 1,2,3,\ldots,m \qquad (1)$$

Each pair of Φ_{ik} and the corresponding y_k provides a fuzzy rule with respect to x_i. The rule is represented as "if x_i is $\Phi_{ik}(x_i)$, then y is y_k" (Lin, 1994). The normalizing factor "b" is generally taken as 10% of the length of the input parameter (x_i) interval. For M training data points, there are M training rules for each input variable. The fuzzy membership functions are then defuzzified using the centroid defuzzification rule to plot the fuzzy curves c_i for each input variable x_i using the following equation:

$$c_i(x_i) = \frac{\sum_{k=1}^{M} \Phi_{ik}(x_i) y_k}{\sum_{k=1}^{M} \Phi_{ik}(x_i)} \qquad (2)$$

The range of each fuzzy curve on the ordinate reflects the effect of each input parameter on the output.

There are few cases where fuzzy curves fail to identify significant inputs (Lin, 1994):

1. The first condition where fuzzy logic fails is when the data are not normally distributed. For a nonuniform data distribution, the range of the fuzzy curves of the input variables may not show the significance of the variables. Before performing the fuzzy logic analysis the data was normalized using the following equation:

$$Z = \frac{X - \mu}{\sigma} \qquad (3)$$

Where, Z is the normalized value, X is the raw value, μ is the mean, and σ is the standard deviation of the raw data. This creates a standardize normal distribution

with mean of *0* and standard deviation of *1*.

2. The other case where fuzzy curves fail to perform reliably is when data are highly correlated with each other. In this case, an unimportant element highly correlated with the most important element will be classified as an important element by the fuzzy logic analysis. On the other hand those elements which are not correlated with the most important elements, but do exert considerable control on permeability, will be classified as unimportant by the fuzzy logic.

Permeability and Thin Section Analysis

Sandstone and carbonate core samples from two formations were used in this study. One core from the Santa Rosa Formation (sandstone) and two cores from the San Andres Formation (carbonate) were analyzed. More than 5,000 permeability measurements were made on a fine grid using the minipermeameter in order to determine the scale of heterogeneity.

Santa Rosa Sandstone

A core sample from the Santa Rosa Formation (Newkirk Field, Guadalupe County, New Mexico) was used to study small-scale permeability heterogeneities and the relative importance (ranking) of each petrographic element controlling it. The Santa Rosa Sandstone (Triassic age) was named by Darton (1922) for medium to coarse-grained, white to buff sandstone that crops out in the vicinity of the city of Santa Rosa, Guadalupe County, New Mexico.

Permeability measurements were made on the slabbed core with the SMP on a rectangular grid with a horizontal interval of 0.5 inches and a vertical interval of 0.2 inches. This generated five vertical profiles along the length of the core (Figure 2.5). Approximately 1,200 permeability measurements were made. From the permeability distribution, seven permeability zones were recognized (Figure 2.5). The "horizontal permeability" was calculated using the arithmetic average and "vertical permeability" using the harmonic average of the minipermeameter data.

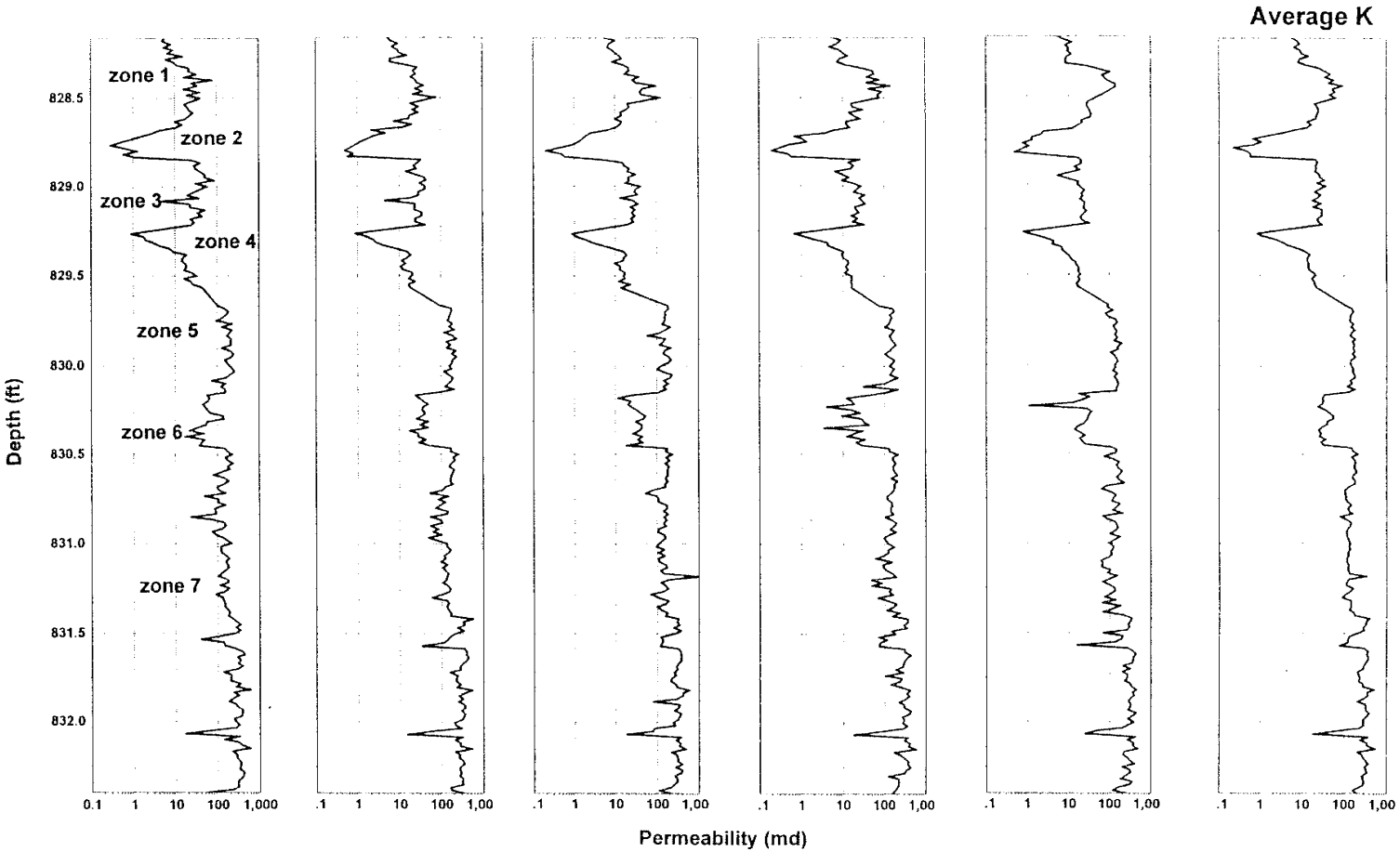

Figure 2.5: Permeability distribution in the Santa Rosa Sandstone core. Vertical spacing is 0.5 inches and horizontal spacing is 0.2 inches. Thin individual permeability zones can be correlated horizontally along the core. Note that averaging smoothens the original heterogeneity.

Twelve thin sections were made and 150 data points were collected. For each permeability data point 16 petrographic elements were collected. Permeability and petrographic data is given in Appendix A. The location of the thin sections and the distribution of the permeability measurement points on the thin sections are shown in Figure 2.6.

The inner radius of the probe tip used in this study was 0.0625 inches (1.56 millimeters). During thin section analysis, the area analyzed for each permeability measurement point had a diameter of 0.2 inches (5 millimeters).

San Andres Formation

The new methodology of collecting data was also applied to carbonates in order to judge the applicability of the methodology in carbonates. Carbonate cores from the San Andres Formation are much more heterogeneous than the Santa Rosa Sandstone. The San Andres Formation is one of the most prolific oil-bearing units in the Permian Basin. At its type locality in the San Andres mountains, New Mexico, the San Andres Formation consists of a 132 foot thick, basal, yellowish sandstone and 578 feet of overlying dark-gray to black limestone (Cowan and Harris, 1986).

The San Andres Formation samples used in this small-scale heterogeneity study were from two wells: State ACCT 2 #60, Lea County, New Mexico, and Mayers A-1 #17, Lea County, New Mexico. Both the cores were acquired from the New Mexico Bureau of Mines and Mineral Resources.

The core sample from Well State ACCT 2 #60 consists of light-gray dolomitized micritic-peloidal limestone (peloidal wackestone/packstone, according to Dunham's classification, 1962). Permeability measurements were made on a 18 foot long core on a 0.5 inch square grid. This generated six permeability profiles along the length of the core (Figure 2.7). About 2,000 permeability measurements were made (Appendix A). The core exhibits low to moderate permeability ranging from less than 1 md to 100 md. From the permeability distribution six individual low and high permeability zones were identified (Figure 2.7).

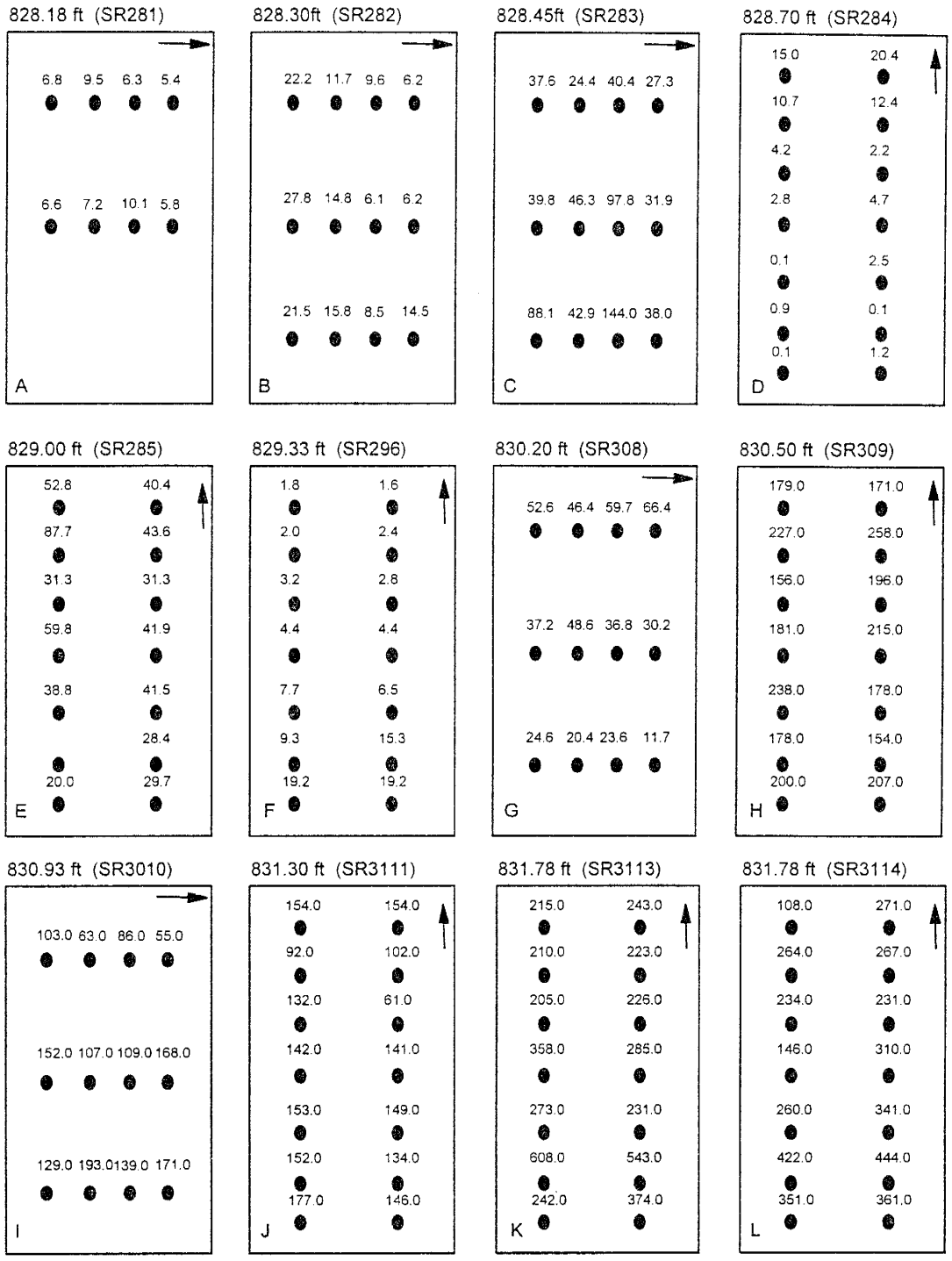

Figure 2.6: Distribution of permeability (md) measurements on the thin sections from the Santa Rosa Sandstone. Arrows shows the stratigraphic top. Permeability points are separated by a horizontal interval is 0.5 inches and vertical interval 0.2 inches. The inner radius of the probe tip was 0.0625 inches (1.56 mm). For each permeability point, the area to be analyzed has a diameter of 0.2 inches (5 mm).

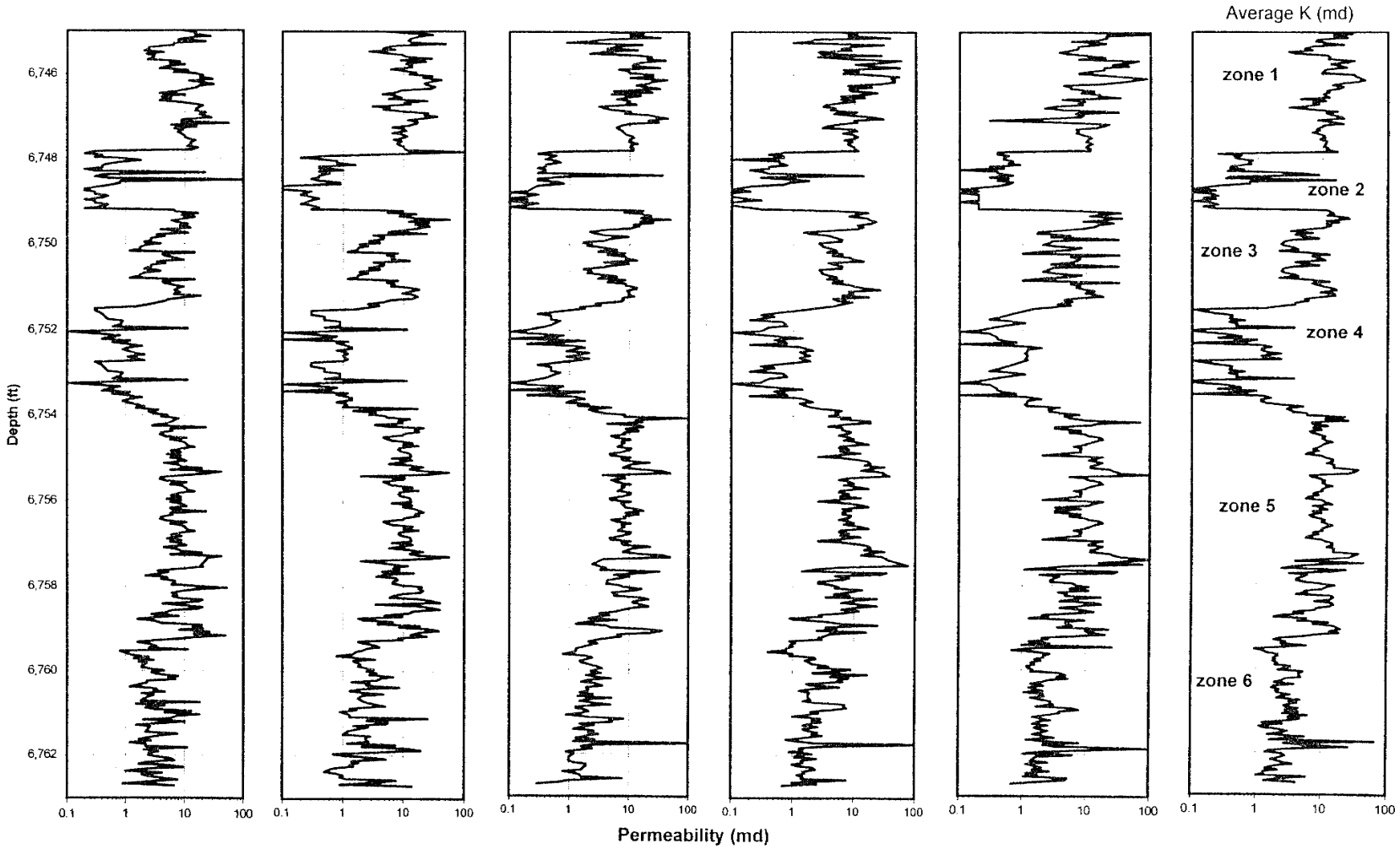

Figure 2.7: Permeability distribution in San Andres core sample composed of peloidal wackestone/packstone (Well: State ACCT 2 #60). Sample spacing is 0.5 inches in both horizontal and vertical directions.

Three different core intervals from Well Mayers A-1 #17 were selected based on the lithologic composition: (1) oolitic packstone, (2) peloidal wackestone, and (3) oolitic-peloidal wackestone/packstone. All these core samples contain vugs. Permeability measurements were made on two grids: (1) on the oolitic packstone, permeability measurements were made on a 0.2 inch square grid which generated six vertical profiles (Figure 2.8A), and (2) on both peloidal wackestone and oolitic-peloidal wackestone/packstone samples, permeability measurements were made on a rectangular grid with a horizontal interval of 0.3 inches and a vertical interval of 0.2 inches, which also generated six vertical profiles along the length of the core (Figure 2.8B & 2.8C). This increase in the sampling distance in the horizontal direction was adopted to avoid the larger vugs. More than 2,300 permeability measurements were made (Appendix A).

These are extremely heterogeneous cores and show heterogeneity in both vertical and horizontal directions (Figures 2.7 & 2.8). During petrographic analysis it was determined that permeability values above 1,000 md were due to air leakage around the probe tip because of a poor seal around larger vugs. These high permeability values were discarded.

Thirty-six thin sections were made from the cores and 324 data points were collected using the cores from two wells. For each data point, nine petrographic elements were analyzed (Appendix A). The location of the thin sections and the permeability measurement distribution on the thin sections are shown in Figures 2.12 & 2.10. Thin sections were made to analyze the mineralogy, pore morphologies, and the diagenesis.

The inner radius of the probe tip used in this study was 0.0625 inches (1.56 millimeters). During thin section analysis, the area analyzed for each permeability measurement point had a diameter of 0.2 inches (5 millimeters).

Thin section analysis

Samples for petrographic analysis were obtained in a pattern so that the whole range of permeability spectrum can be covered. All thin sections were impregnated with blue epoxy to accentuate pore structure under the microscope and to differentiate plucked

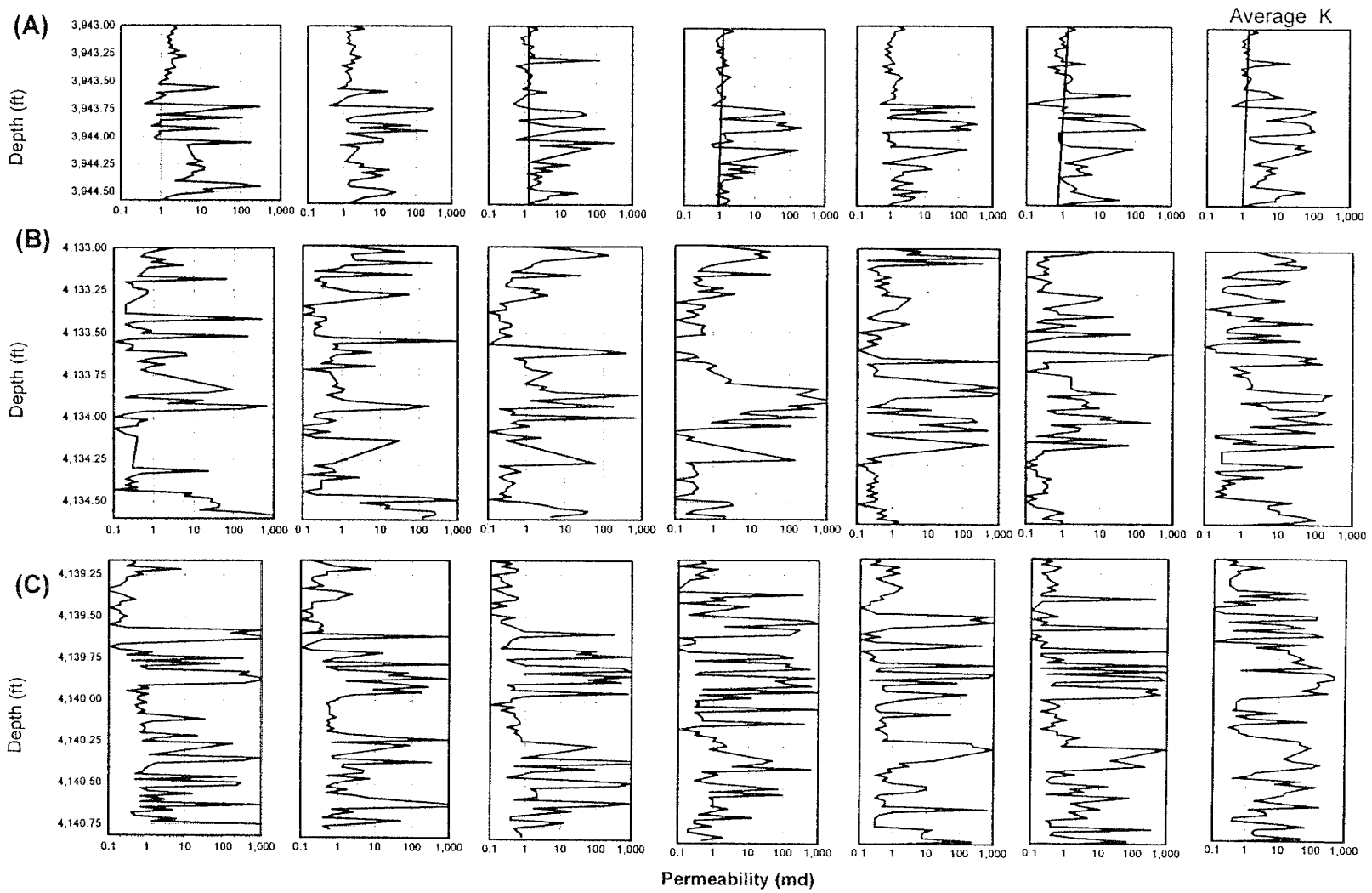

Figure 2.8: Permeability distribution in the San Andres core sample from Well Mayers A-1 #17. (A) Oolitic packstone, (B) Peloidal wackestone, and (C) Oolitic-peloidal wackestone/packstone. Note a large variation in permeability.

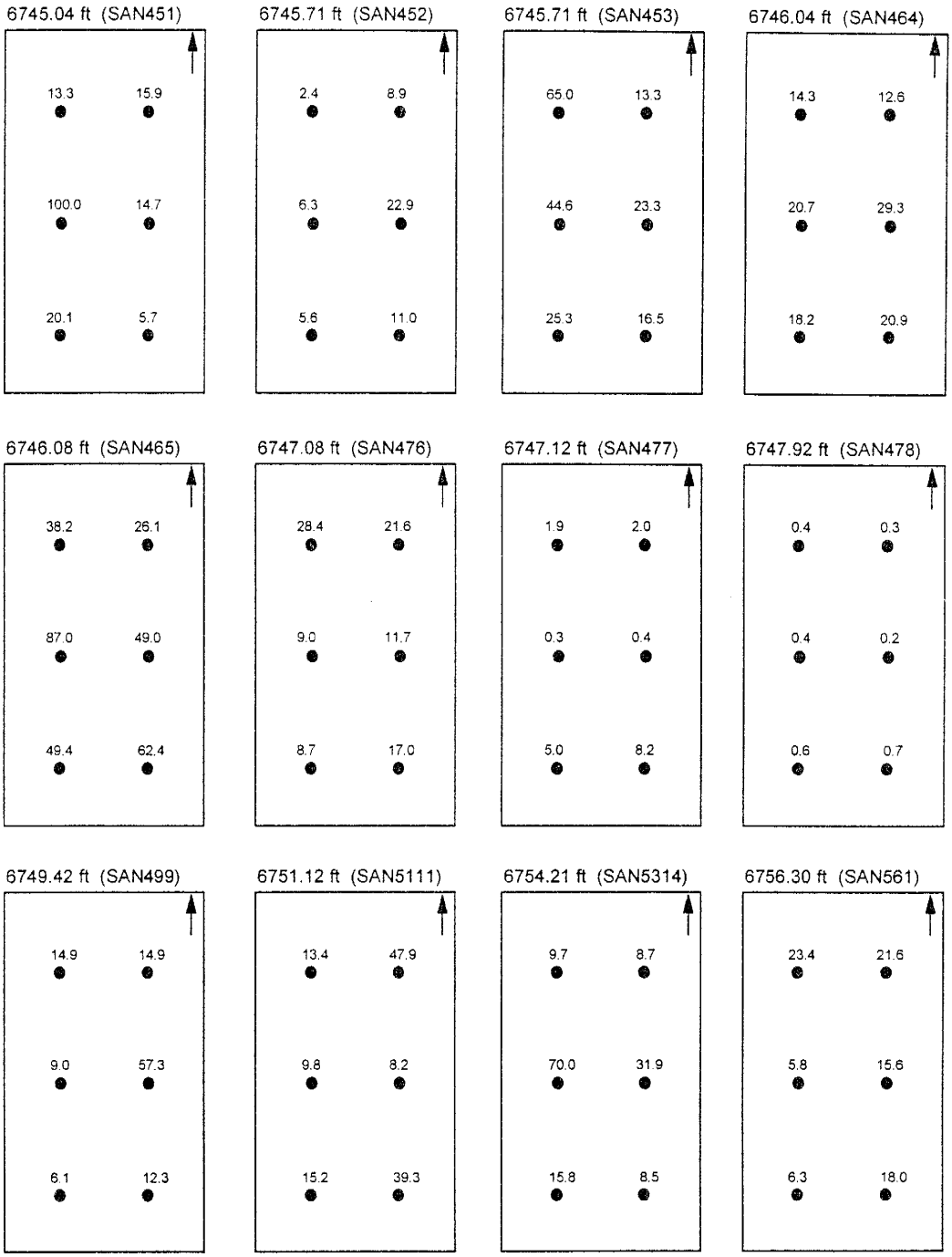

Figure 2.9: Distribution of permeability (md) measurements on the thin sections from the San Andres Formation (Well: State ACCT 2 #60, Peloidal Wackestone/Packstone). Arrows show the stratigraphic top. The horizontal and vertical interval between points is 0.5 inches. Probe tip has the inner radius of 0.0625 inches (1.56 mm). For each permeability point, the area to be analyzed has a diameter of 0.2 inches (5 mm)

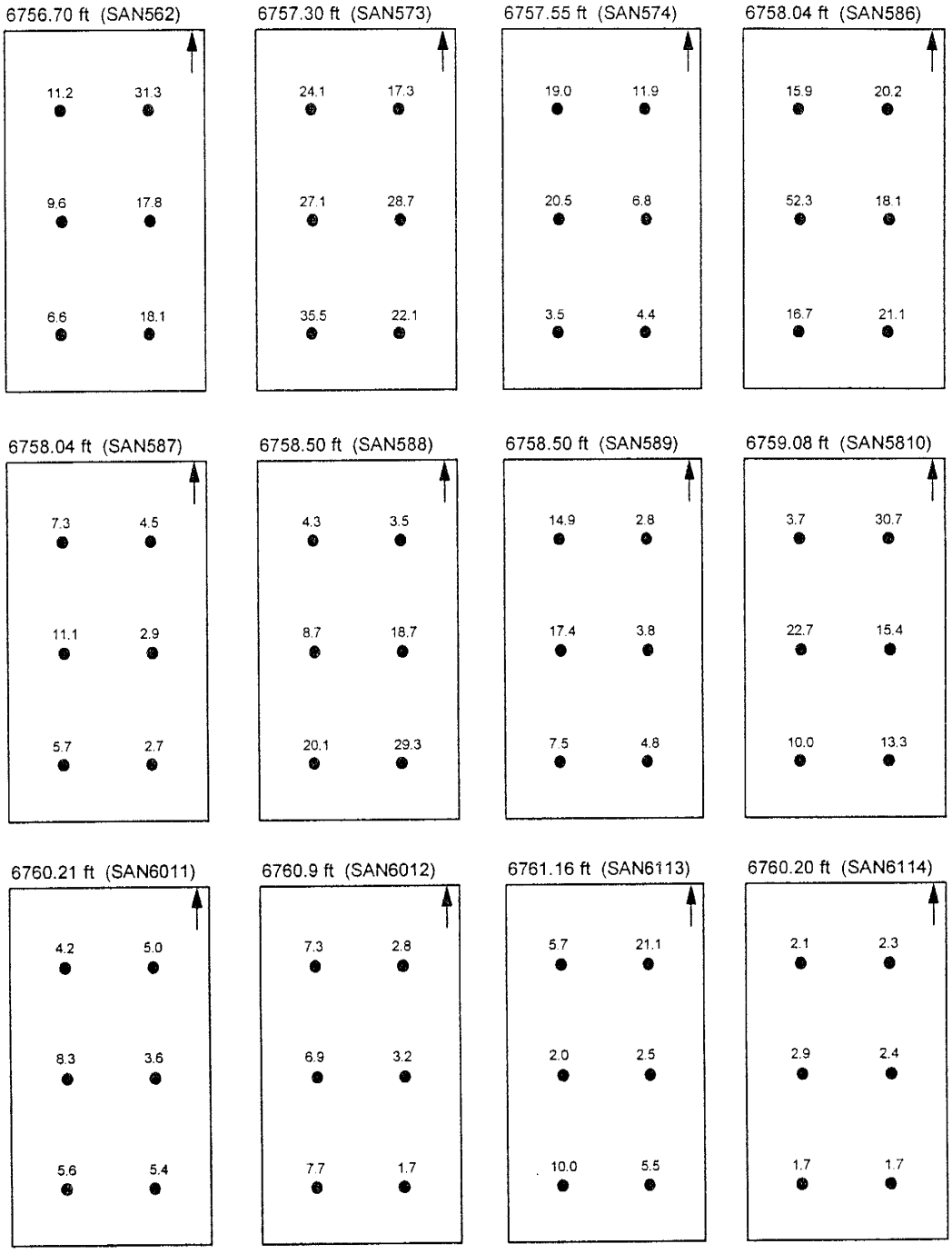

Figure 2.9: Continued.

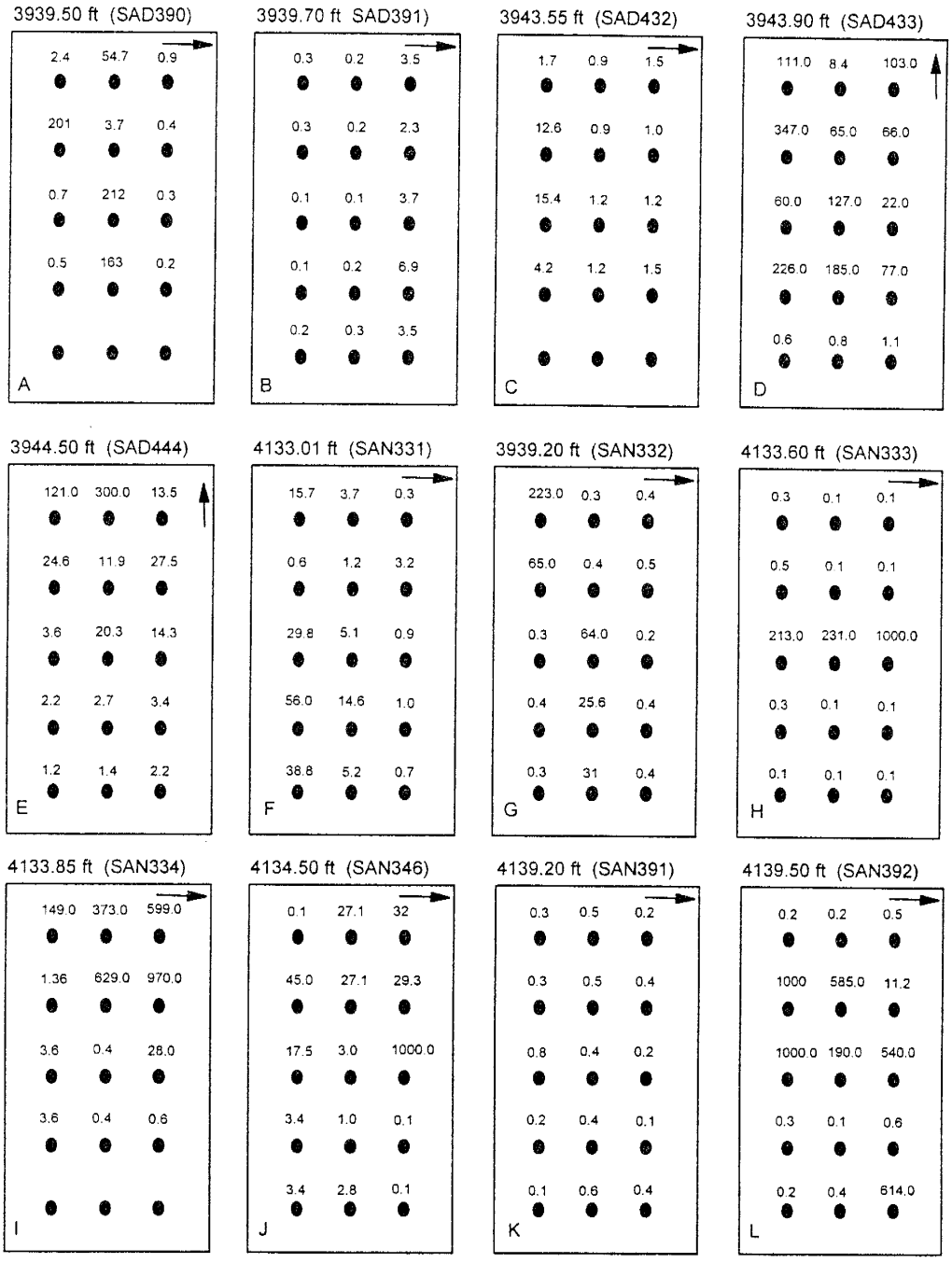

Figure 2.10: Distribution of permeability (md) measurements on the thin sections from the San Andres Formation (Well: Mayers A-1 #17). Arrows show the stratigraphic top. The horizontal and vertical interval between points is 0.3 inches. Probe tip has the inner radius of 0.0625 inches (1.56 mm). For each permeability point, the area to be analyzed has a diameter of 0.2 inches (5 mm). A - E: Oolitic Packstone; F - J: Peloidal Packstone; K - L: Oolitic-peloidal Wackestone/Packstone.

areas from true pores. The diagnostic stains Alizarin Red-S and potassium ferro cyanide were used to identify calcite, and ferroan-dolomite or ferroan-calcite, respectively. In addition to standard petrographic techniques, fluorescent petrography was used for the clear delineation of pore geometries and the distribution of micro-pores (method of Ruzyla and Jazeck, 1987).

Porosity definitions and petrographic criteria used in this study to identify different kinds of porosities in both sandstones and carbonates are given below.

Sandstones

Six types of porosity are present in the Santa Rosa Sandstone analyzed in this study. Although, criteria have been established for the recognition of secondary porosity in sandstones (Schmidt and McDonald, 1979), quantitative assessment of the contribution of the secondary porosity to the overall pore system remain difficult in practice. This is particularly true for the recognition of carbonate-cement dissolution pores, because petrographic criteria used to assess and quantify this type of porosity are highly subjective.

1. Primary intergranular pores: Intergranular pore spaces present between the grains which are not altered, fractured, or dissolved are assumed to be primary, but they might not be primary (e.g., if undetected cement dissolution occurred).
2. Secondary intergranular pores: Pore spaces of secondary origin between the constituent grains. Secondary intergranular pores are identified by the presence of corroded and partially dissolved grains surrounding the pores and by the presence of remnant cement in the pores.
3. Moldic pores: Pore spaces that are probably formed by the complete dissolution of grains. The main evidence is grain-sized and grain-shaped pore spaces.
4. Intraconstituent pores: Pore spaces present within the body of an individual grain or individual dolomite crystal. Intragranular and intracement pores are combined under this category because both are present in very minor amounts.
5. Oversized pores: Pore spaces larger than the diameter of the adjacent grains. These

pores are formed by the dissolution of gains and dolomite cement.

6. Microporosity: Pore spaces smaller than 5μm. Microporosity present in authigenic kaolinite is here also referred to as *redistributional porosity* in this study.

Carbonates

Six types of porosity are present in the San Andres Formation samples used in this study.

1. Intercrystalline pores: Pore spaces present between dolomite crystals.
2. Gradational intercrystalline pores: Pore spaces that are larger than the typical intercrystalline pores, but that cannot be classified as molds or vugs. These pores seem to have started as molds, but due to dolomitization the size of the pores was reduced and the shape of the mold was obliterated.
3. Moldic pores: Pore spaces formed by the complete dissolution of skeletal material. The outline of the skeletal grain is still recognizable.
4. Vugs: Pore spaces which are somewhat equant (i.e., length to width ratio <1.5:1), greater than 0.0625 mm in diameter, and are not fabric selective.
5. Primary intraparticle pores: Pore spaces present within skeletal grains (internal chambers) before the deposition of the sediments.
6. Secondary intraparticle pores: Pore spaces formed by the partial dissolution of the skeletal grains or ooids.

RESULTS AND DISCUSSION

Santa Rosa Sandstone

Petrographic analysis

The core sample from the Santa Rosa sandstone is composed of very fine to medium-grained, poorly to well sorted, subangular to subrounded, sublithic to quartz arenite. In the Santa Rosa Sandstone, quartz is the most abundant detrital grain and

dolomite the most abundant cement. Kaolinite occurs as authigenic vermicular pore filling cement. Rock fragments are comprised of shale fragments and chert. Feldspar (plagioclase and potassium feldspar) and muscovite are present consistently but never exceed 4%. The summary of the permeability, porosity, mineralogical, and textural data for each zone is given in Table 2.3.

The Santa Rosa sandstone has a paragenetic sequence that includes early quartz overgrowths, and late-stage dissolution of cement and detrital grains (feldspar), precipitation of kaolinite, and emplacement of oil. A generalized paragenetic sequence is shown in Figure 2.11. Authegenic quartz occurs as euhedral, syntaxial overgrowths on detrital quartz grains (Figure 2.12A). High intergranular volume of quartz-cemented regions indicate that the overgrowths formed prior to significant compaction (Figure 2.12A). Dolomite occurs in two morphologies: (1) coarse rhombic crystals with long axis up to 200 μm (0.2 mm) filling larger pores (Figure 2.12B), and (2) irregular poikilotopic patches ranging from 100 μm (0.1 mm) to 5000 μm (5 mm) in diameter (Figure 2.12B). In places, it appears that detrital grains are partially replaced by dolomite as shown in Figure 2.12B. In cases where only the margins of grains are replaced, much care is required to differentiate between the actual replacement and the grain-cement overlap in the plane of section (Figure 2.12B). This problem is usually more pronounced in thin section which are thicker than 30 μm. More definite evidence of replacement is provided by carbonate rhombs which penetrate into grains (Nockolds *et al.*, 1978) (Figure 2.12C).

The presence of rhombic embayments in quartz grains and overgrowths (Figure 2.12C) suggest the dissolution of carbonate (probably dolomite) cement which had replaced quartz grains and overgrowths. The size of the embayment in Figure 2.12C suggest that both the detrital grain and quartz overgrowths were partially replaced by the cement. Therefore, it may be appropriate to assume that quartz overgrowths predate dolomite cement. The absence of dolomite inclusions in the quartz overgrowths also suggests that quartz overgrowths predate dolomite cement. The presence of corroded grains and dolomite crystals indicate dissolution (Figure 2.12C) occurred after the

Zones	Thickness (inches)	Horizontal K (md)	Vertical K (md)	"σ" of Horizontal K (md)	Total Φ (%)	Primary Φ (%)	Secondary Φ (%)	Micro Φ (%)	Quartz (%)	Rock Fragments (%)	Clay (%)	Dolomite (%)	Pore size (mm)	Grain size (mm)
1	6.0	28.0	16.0	23.7	8.19	4.9	2.14	1.61	65.0	9.5	14.5	8.2	0.04 - 0.08	0.1 - 0.15
2	2.0	1.5	0.65	1.8	2.8	0.86	0.8	1.2	53.0	2.0	15.0	31.5	0.04	0.07 - 0.1
3	4.8	25.5	24.55	5.0	12.2	4.4	6.8	0.9	72.0	3.0	11.0	13.2	0.03 - 0.05	0.08 - 0.14
4	5.0	11.3	3.67	2.3	5.84	2.18	0.8	2.0	56.0	11.5	11.2	6.6	0.03 - 0.06	0.09 - 0.1
5	5.4	156.0	153.0	68.0	17.8	9.5	6.65	1.8	76.0	7.0	9.7	7.1	0.06 - 0.08	0.08 - 0.13
6	3.4	34.5	32.7	9.0	11.0	5.25	4.1	1.64	66.0	6.2	15.9	11.6	0.01 - 0.07	0.07 - 0.1
7	24.0	212.0	159.0	101.0	19.4	5.24	13.45	0.64	87.0	2.83	3.67	6.29	0.08 - 0.2	0.11 - 0.2

Table 2.3: Summary of average permeability, porosity, mineralogical, and textural data for each permeability zone in the Santa Rosa Sandstone. The horizontal permeability was calculated using the arithmetic average and vertical permeability using the harmonic average of the minipermeameter data.

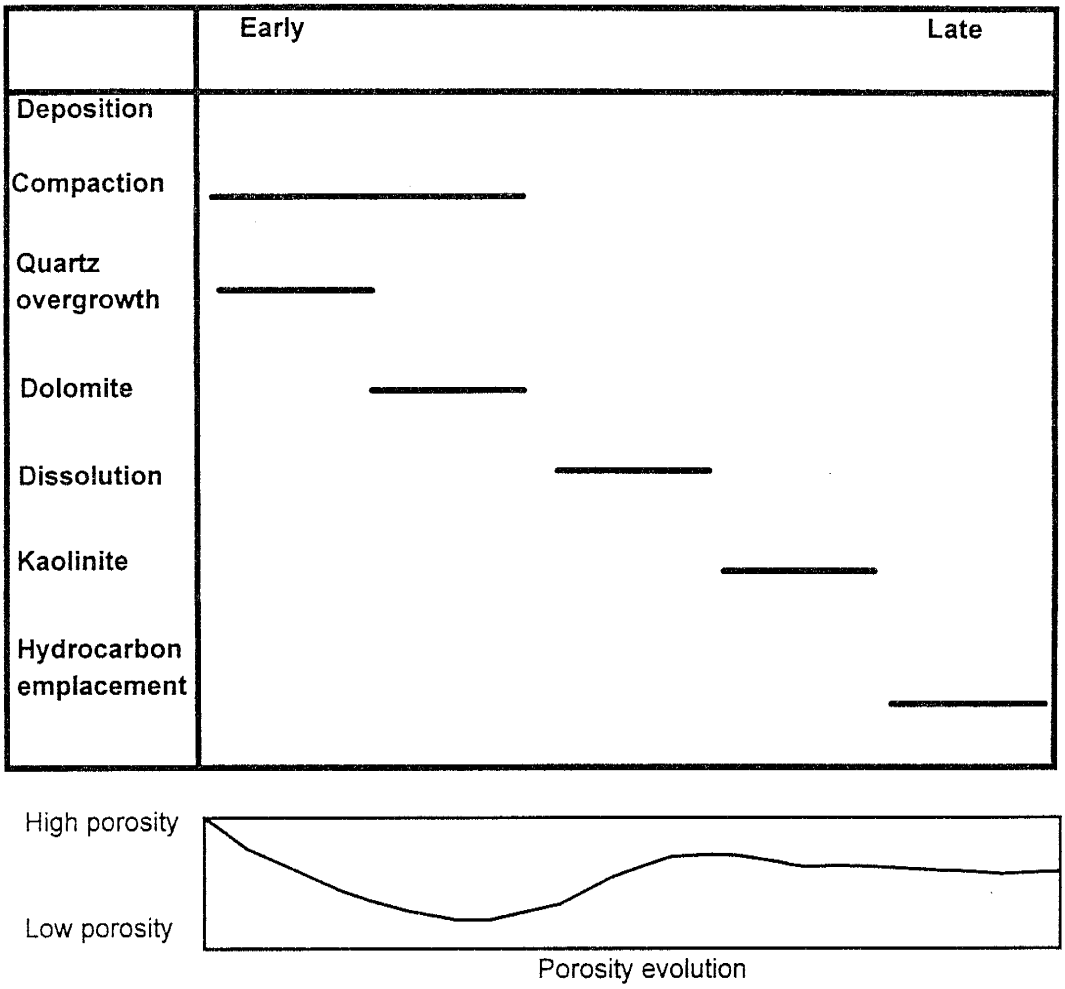

Figure 2.11: Generalized paragenetic sequence and porosity evolution for the Santa Rosa Sandstone.

Figure 2.12: Thin section photomicrographs showing the mineralogic components and diagenetic products in the Santa Rosa Sandstone. (Porosity in blue.)

A: Authigenic quartz occurs as euhedral, syntaxial overgrowths on detrital quartz grains (Q). (Thin section SR283, plane light)

B: Dolomite cement morphologies. Note a large rhombic crystal (D) about 0.23 mm long. Also, note dolomite replacing detrital grains (R). Possible grain-cement overlaps in the plane of thin section. (Thin section SR284, crossed polarizers)

C: Rhombic embayment in quartz overgrowth (O) formed by dissolution of a dolomite crystal that had partially replaced it. Note the residual oil (Arrow) in the partly dissolved rhombic dolomite crystal (D). (Thin section SR3114, plane light)

D: Authigenic kaolinite occupying grain-sized areas. Note the absence of kaolinite in primary pores (P) (Thin section SR296, plane light)

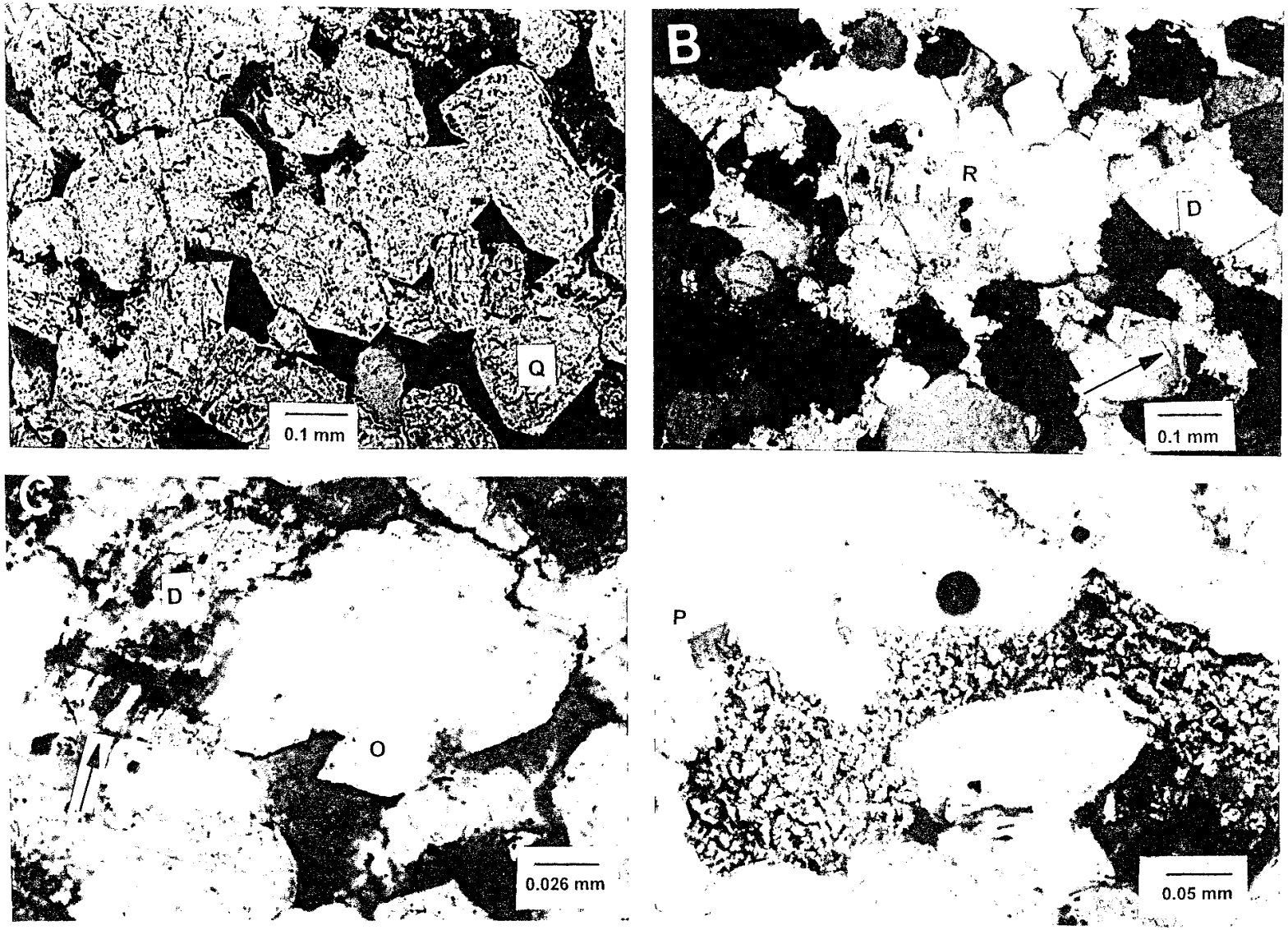
Q
0.1 mm
B
R
D
0.1 mm
C
D
O
0.026 mm
P
0.05 mm

precipitation dolomite cement, and therefore, dissolution also postdates quartz overgrowths.

Kaolinite is ubiquitous in the Santa Rosa Sandstone. It commonly occurs as vermiform pore filling cement and fills areas similar in size and shape to detrital grains (Figure 2.12D). Kaolinite can be considered to be authigenic in origin because of its well preserved vermicular stacks of platelets, presence in grain-sized and grain-shaped areas, and absence in the primary pores. The kaolinite probably precipitated in areas once occupied by detrital feldspar. The formation of most kaolinite may postdate precipitation of quartz overgrowths and dolomitic cement because it does not occur as inclusions in dolomite and quartz overgrowths.

Problem of quartz overgrowths

Authigenic quartz forms syntaxial overgrowths on the detrital quartz grains. The boundary between the detrital grain and the overgrowths may or may not be visible with standard petrographic techniques (Blatt, 1982). Quartz overgrowths are usually visible when they are marked by the presence of certain material between the detrital quartz grain and the overgrowths. This marking material could be red hematite cement, dark colored organic material, clay, etc. In the absence of these marking materials it is very difficult to differentiate between the detrital grain and overgrowths. Because quartz was formed very early in the diagenetic history of the Santa Rosa Sandstone, it does not have any marking material present between the detrital grain and quartz overgrowths. Overgrowths in the Santa Rosa Sandstone were identified due to the straight edges of the quartz grains (Figure 2.12A).

Cathodoluminescence petrography can be used to reveal overgrowths. During the cathodoluminescence analysis, the detrital grains luminesce and the overgrowths does not. This makes the identification of overgrowths very easy. The differences in luminescence between the detrital quartz grains and the overgrowths is a function of subtle differences in their trace element composition (Scholle, 1979).

In this study cathodoluminescence was not used during point count and detrital

quartz and the overgrowths were lumped together as detrital quartz. Therefore, we were unable to determine the influence of quartz overgrowths on permeability.

Porosity evolution

The pore system in the Santa Rosa Sandstone consists of the following types: primary porosity, secondary intergranular porosity, moldic porosity, intraconstituent porosity, oversized porosity, and microporosity.

The interplay of quartz overgrowths, cementation, and dissolution controlled the evolution of porosity (Figure 2.11). The high percentage of secondary porosity indicates that after quartz and dolomite precipitation, a moderate amount of primary porosity remained open to provide passage for the diagenetic fluids to gain access to dolomite cement and constituent grains. Feldspar and shale clasts have been partially to completely dissolved. However, secondary porosity created by the dissolution of feldspars enhances the effective pore system only if dissolution products are removed from the system. If the reaction products precipitate near or at the site of dissolution, then the dissolution may not result in a net increase in the effective porosity (Giles and Bore, 1990). Some part of the secondary porosity in the Santa Rosa may be considered as redistributional porosity resulting from dissolution of feldspar and precipitation of kaolinite in the volume originally occupied by detrital grains.

Among the secondary pores, secondary intergranular porosity is the most dominant type. Some secondary pores still follow the typical straight-edged outline of the primary pores, and are identified by the presence of remnant dolomite and corroded grain margins (Figure 2.13A). Irregular (non-polygonal) and elongated morphologies are the dominant type of secondary intergranular pores (Figure 2.13B & 2.13C). Due to the dissolution of grain margins and quartz overgrowths the pore throat size increased. In high permeability zones the pore-to-throat ratio is very small, and majority of pores and pore throats are of similar size (Figures 2.13B & 2.13C). The majority of the primary porosity (reduced primary porosity) consists of pores with polygonal outlines due to quartz overgrowths (Figure 2.13D). Quartz overgrowths, although providing support

Figure 2.13: Thin section photomicrographs showing the porosity types in the Santa Rosa Sandstone. (Porosity in blue.)

A: Primary polygonal shaped pores with minor amounts of secondary porosity and microporosity. Note the minor corrosion of grain margins producing slightly elongated pores. [(K = 40 md), Thin section SR283, plane light]

B: Mixture of primary and secondary intergranular pores. [(K = 97 md), Thin section SR283, plane light]

C: Dominantly secondary intergranular pores of elongated shape. Note the corroded grain margins and good interconnection between the pores. [(K = 197 md), Thin section SR3010, plane light]

D: Bigger size well interconnected secondary intergranular pores. [(K = 404 md), Thin section SR004, plane light]

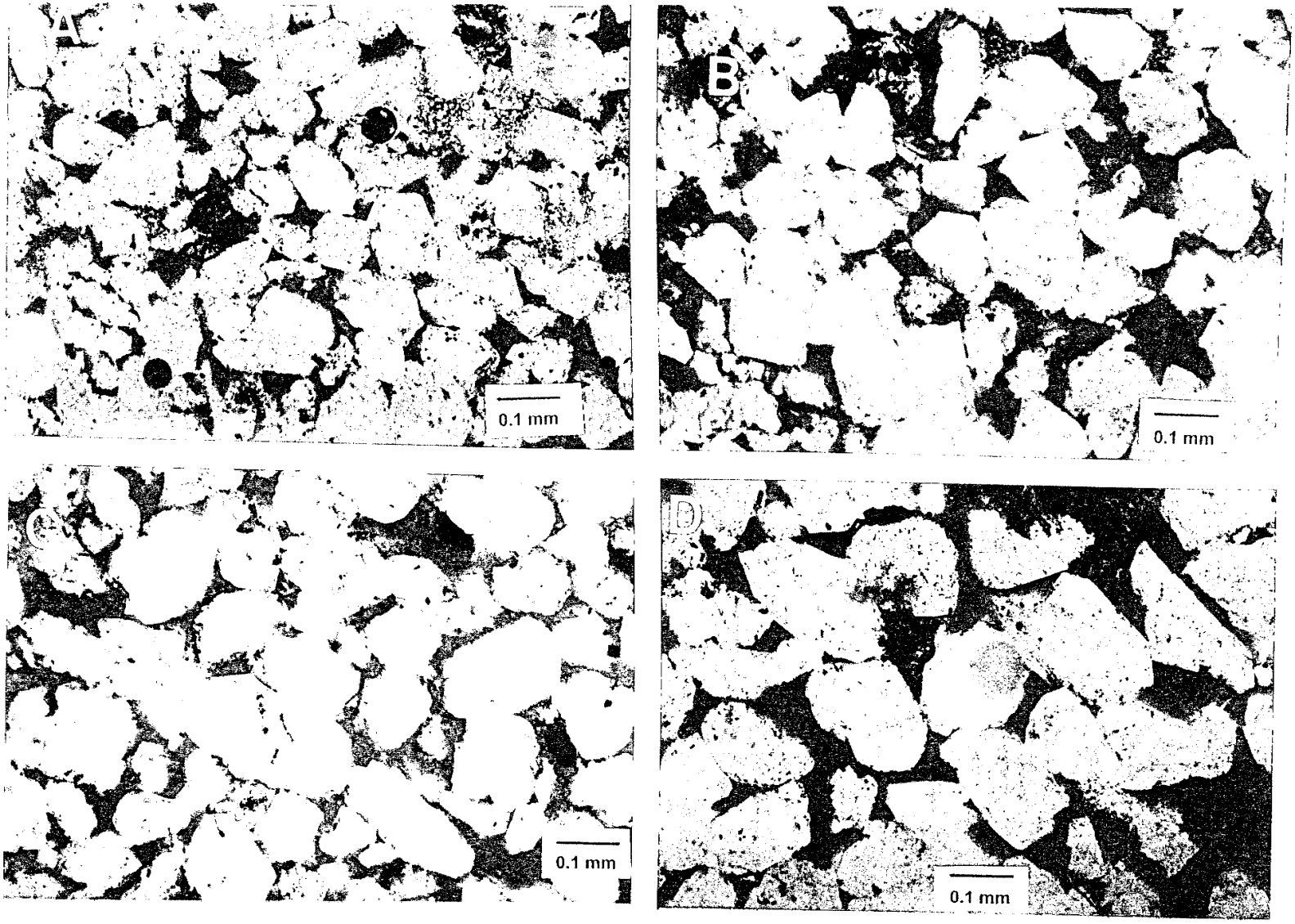
A
0.1 mm
B
0.1 mm
C
0.1 mm
D
0.1 mm

Figure 2.13: Continued

E: Pore system consists of a combination of primary, secondary, and micropores. [(K = 19.2 md), Thin section SR296, plane light]

F: Showing grain dissolution and intraconstituent porosity (Arrow). [Thin section SR296, plane light]

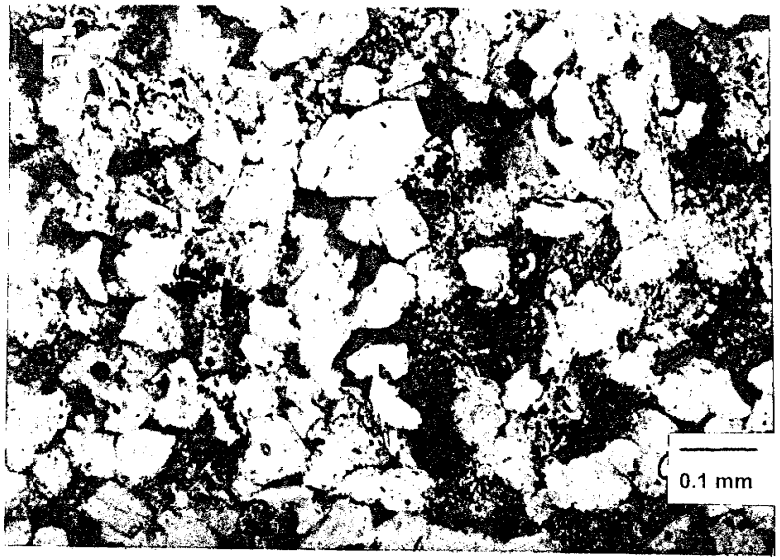
0.1 mm

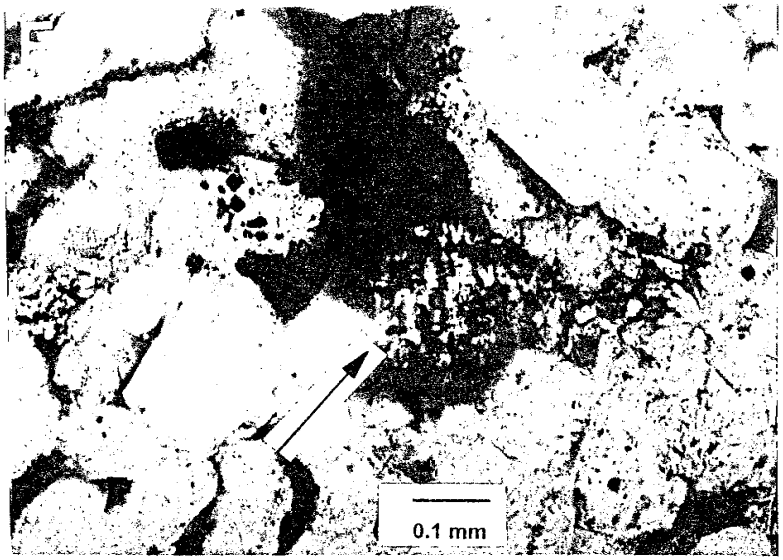
0.1 mm

against compaction, considerably reduced the volume of the primary pores as well as the connection between the pores. Microporosity is present among the kaolinite patches (Figure 2.13E). Oversized pores are only present in the highest porosity areas. Minor amounts of secondary intraconstituent pores are also present (Figure 2.13F).

Ranking of the petrographic elements in controlling permeability

Detailed data analysis was performed to determine the influence of petrographic elements on permeability. Before performing the analysis the data distribution was checked (Figures 2.14, 2.15, & 2.16) and data was normalized using Equation 3 (on page 31). The relationships investigated were between: (1) permeability and petrographic analysis using simple regression analysis (Figure 2.17), (2) total porosity and petrographic elements using simple regression analysis (Figure 2.18), and (3) permeability and petrographic elements using fuzzy logic analysis (Figure 2.19). The summary of the ranking for the top eight petrographic elements (out of sixteen collected) affecting permeability is given in Table 2.4.

The most important petrographic elements are the porosity types, as determined by the regression and fuzzy logic analysis. All the porosity types except for microporosity show a general increasing trend with permeability (Figure 2.17). Total porosity and permeability shows a good positive relationship (Figure 2.17A). However, for any given porosity there is a wide range of permeability. This is due to varying proportions of primary and secondary intergranular porosity in samples of similar total porosity.

Primary and total secondary porosity show very different trends with increasing permeability (Figures 2.17B & 2.17C). Primary intergranular porosity shows a general increasing trend for permeability less than 100 md, whereas, above 100 md the data becomes scattered. A good positive correlation exists between permeability and secondary porosity (Figure 2.17D). In general primary, total secondary, and secondary intergranular porosity increase as the total porosity increases (Figures 2.18A, 2.18B, & 2.18C). Microporosity and permeability show a poor negative correlation (Figure 2.17E).

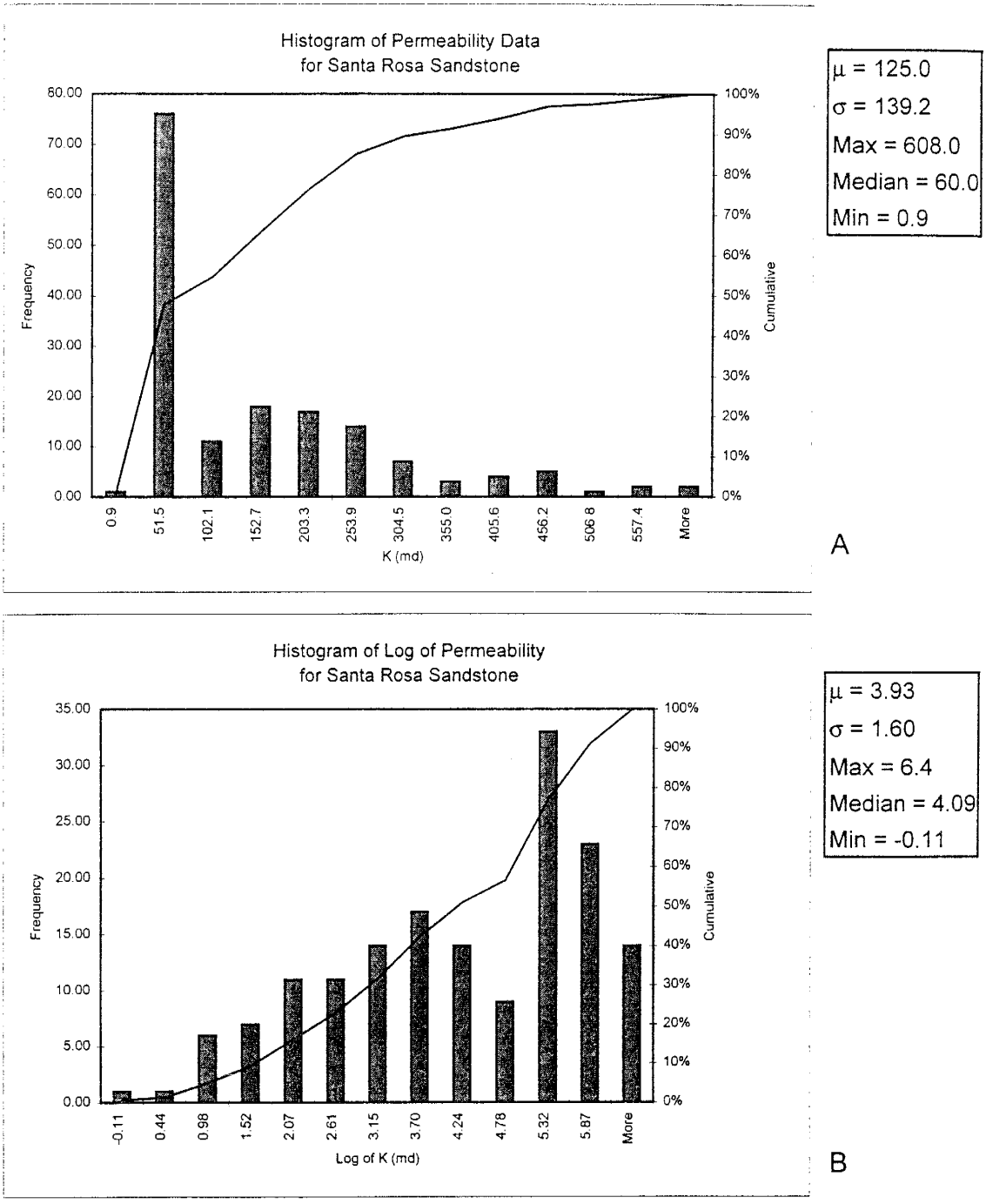

Figure 2.14: Histograms of permeability distribution in the Santa Rosa Sandstone. (A) Raw data; (B) Log transform. The data appears to be bimodal. Such a distribution is attributed to thick high permeability zone 7.

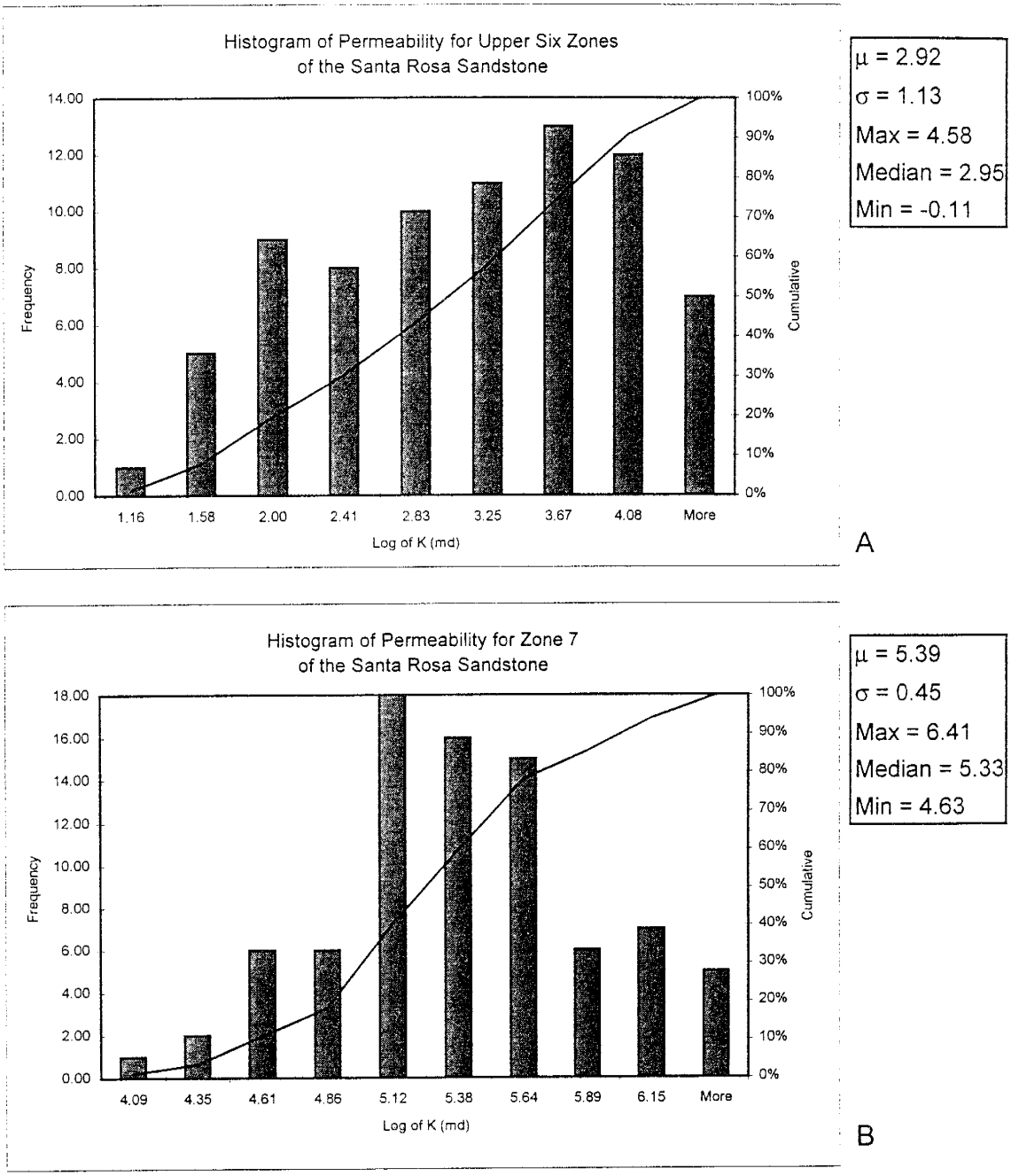

Figure 2.15: Histograms of log of permeability data for the Santa Rosa Sandstone. (A) Permeability data from the upper six zones; (B) Permeability data from zone 7.

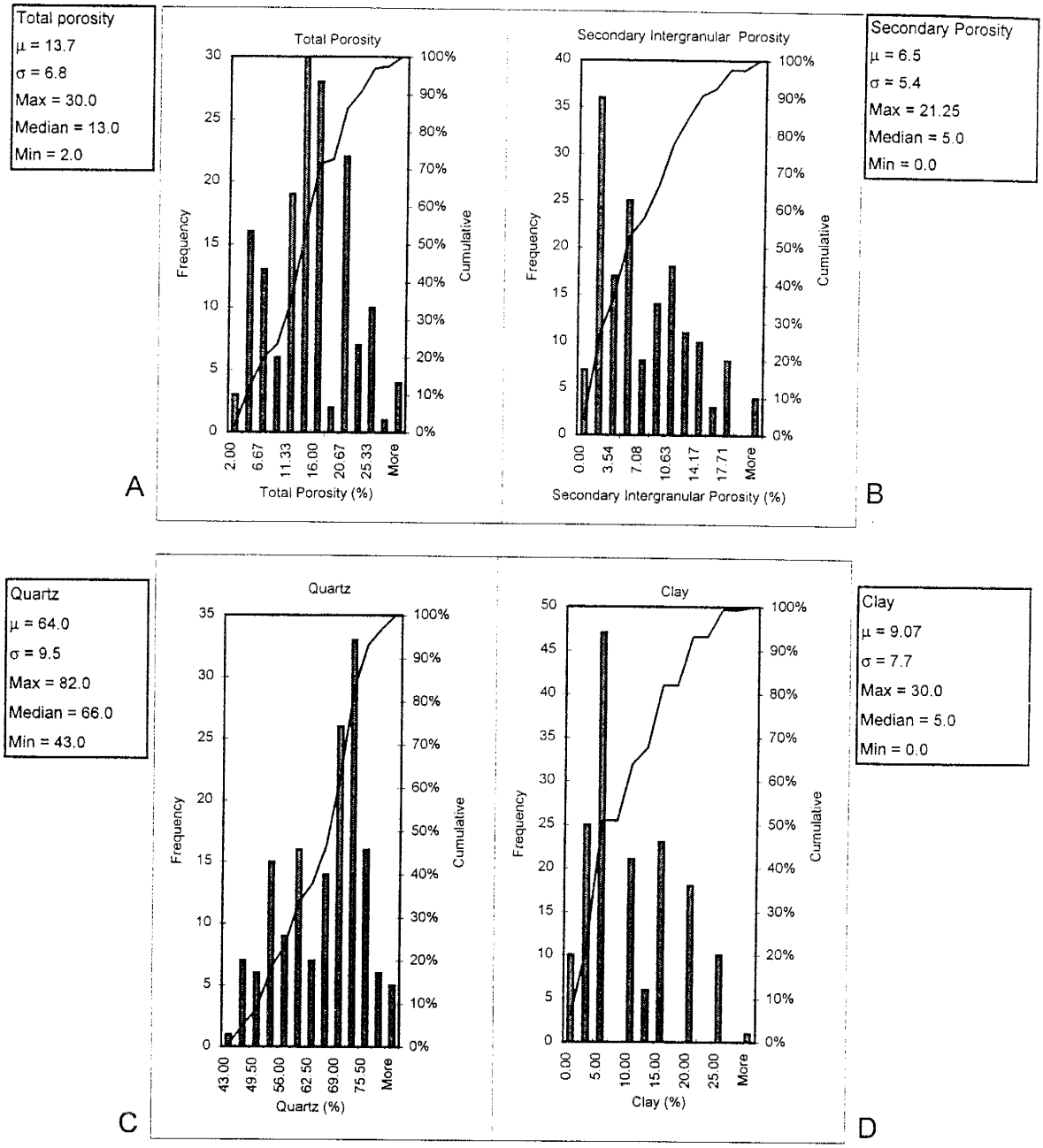

Figure 2.16: Histograms of the petrographic data for the Santa Rosa Sandstone.

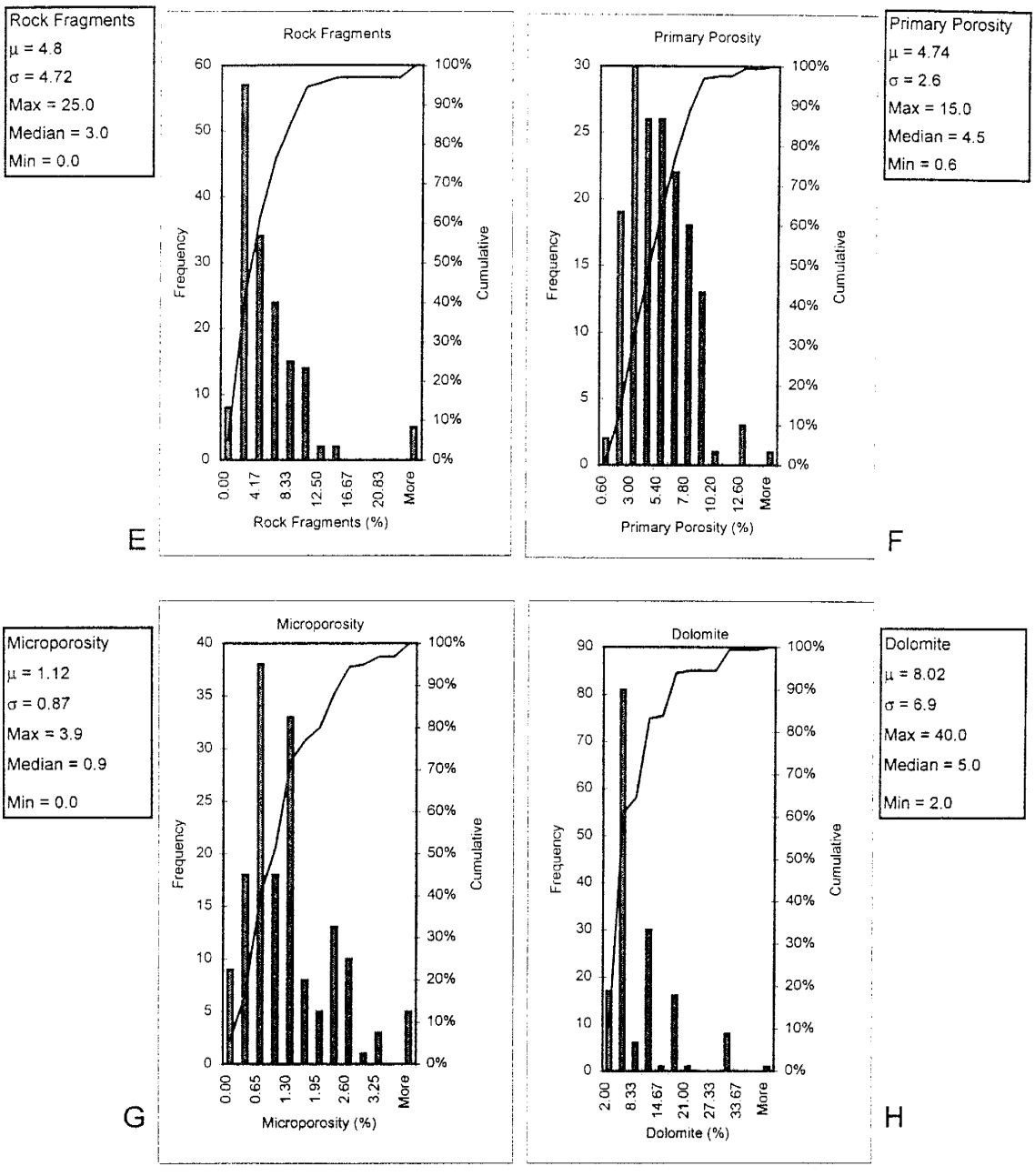

Figure 2.16: Continued.

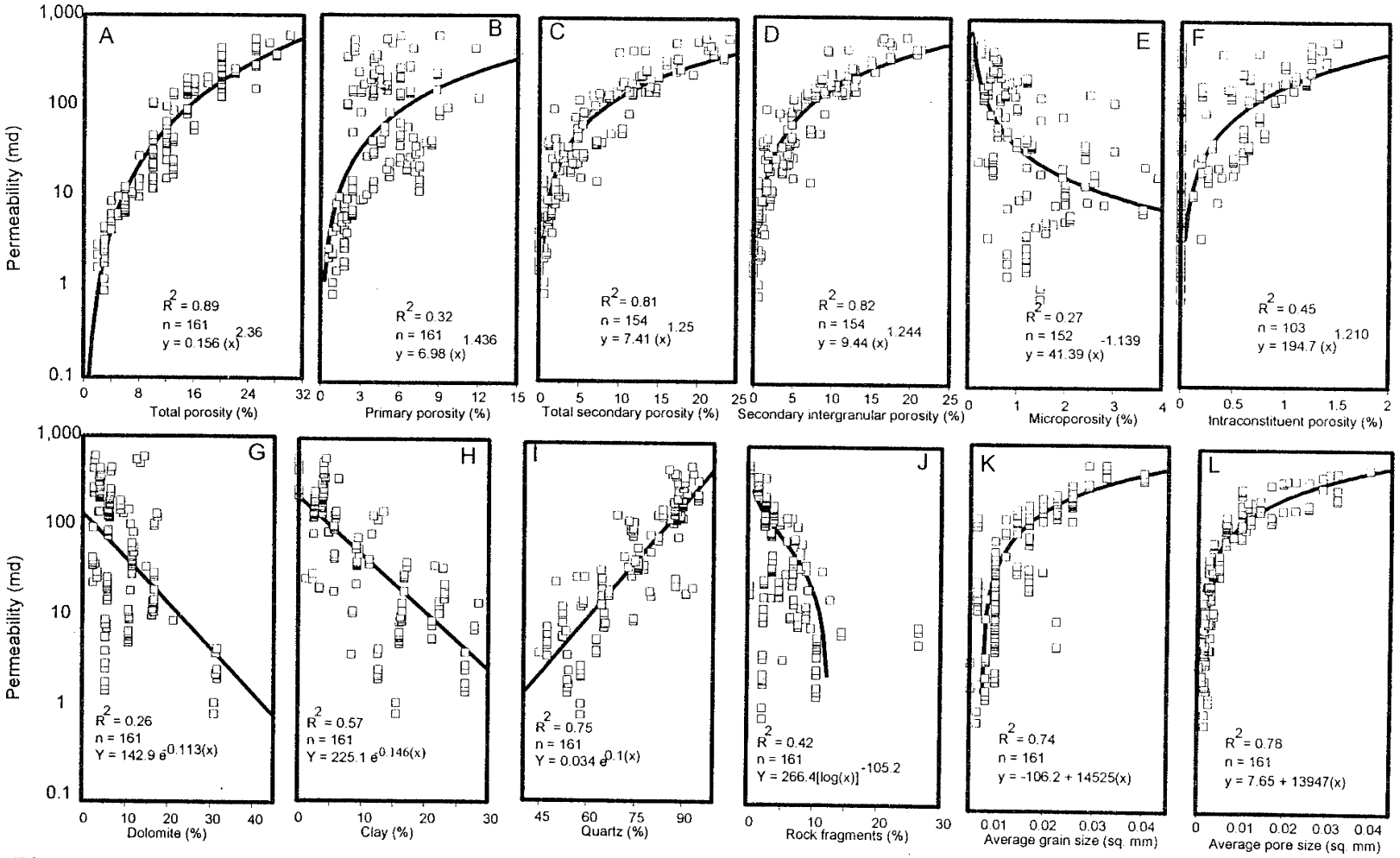

Figure 2.17: Relationships between permeability and different petrographic elements in the Santa Rosa Sandstone. The models which gave the best correlation coefficient were applied.

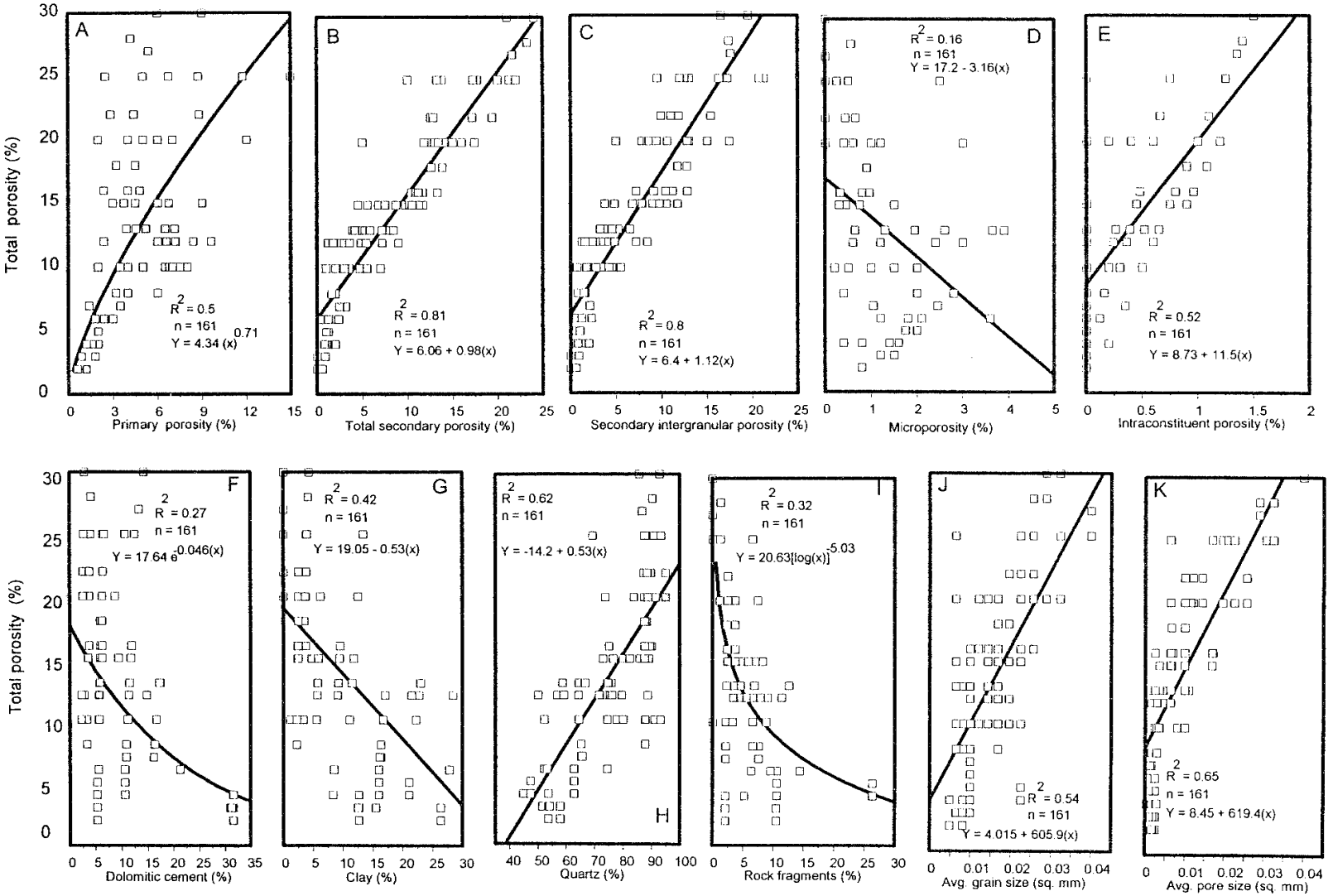

Figure 2.18: Relationships between total porosity and different petrographic elements in the Santa Rosa Sandstone.

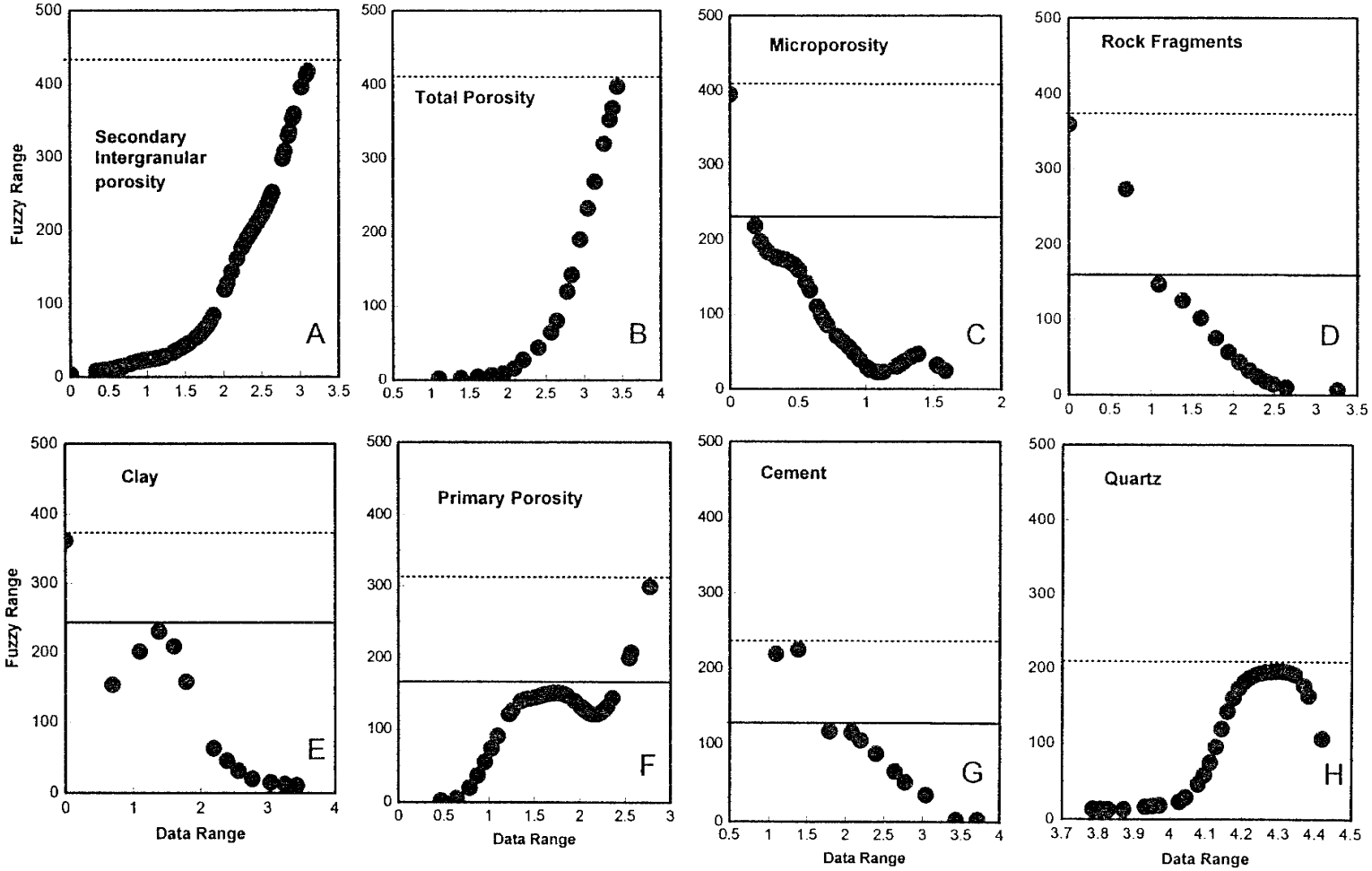

Figure 2.19: The fuzzy curves for the Santa Rosa Sandstone. The dotted lines represent the fuzzy range, whereas, the solid line represents the fuzzy range when isolated points are not considered.

Petrographic Elements	Amount (Ranges)	Correlation (R^2) with permeability (Regression Models)	Correlation (R^2) with total porosity (Regression Models)	Ranking based on R^2	Ranking based on fuzzy logic (Fuzzy Range)	Ranking based on fuzzy logic (isolated points removed)
Total ϕ	2 -30%	0.89 / Power		1	2 (396)	2 (396)
Secondary intergranular ϕ	0 - 22%	0.81/ Power	0.80/ Linear	2	1 (413)	1 (413)
Average pore size	20 - 200 μm	0.78/ Linear	0.65/ Linear	-	-	-
Detrital Quartz + Overgrowth	40 - 98%	0.75/ Exp.	0.62/ Linear	3	8 (210)	5 (210)
Average grain size	50 - 200 μm	0.74/ Linear	0.54/ Linear	-	-	-
Clay	0 - 25%	0.57/ Exp.	0.42/ Linear	4	5 (350)	3 (245)
Rock fragments	0 - 8%	0.42/ Log.	0.32/ Log.	5	4 (353)	7 (160)
Primary ϕ	0.5 - 15%	0.32/ Power	0.5/ Power	6	6 (297)	6 (165)
Micro-ϕ	0.5 - 4%	0.27/ Power	0.16/ Linear	7	3 (372)	4 (230)
Dolomite	2 - 40%	0.26/ Exp.	0.27/ Exp.	8	7 (222)	8 (130)

Table 2.4: List of the petrographic elements showing their importance in controlling permeability in the Santa Rosa Sandstone.

Microporosity also decreases with increasing porosity (Figure 2.18D).

Both dolomite and kaolinite show general decreasing trends as the permeability and total porosity increase (Figures 2.17G & 2.17H, 2.18F & 2.18G). For any given percentage of dolomite there is a wide range of permeability. This scattering of data is due to the presence of two dolomite morphologies. The isolated crystals cannot reduce effective porosity considerably and therefore, does not decreases permeability. However, poikilotopic cement decreases the effective porosity to a great extent, and therefore reduces the permeability significantly. As kaolinite is mostly present in areas similar in size and shape to detrital grains, it does not affect the pore throats and the interconnection between the pores. Kaolinite is only important in low and moderate permeability zones where it is present in considerable amounts. Permeability and total porosity show an increasing trend with the increase in quartz content (Figures 2.17I & 2.18H) and decreasing trend with increasing rock fragments (Figure 2.17J & 2.18I). Permeability and total porosity also increase as both grain and pore size increase (Figures 2.17K & 2.17L, 2.18J & 2.18K). The increase in pore size is in agreement with the increase in grain size.

For the most part, the fuzzy logic and conventional regression analyses are in good agreement, except for microporosity and quartz (Table 2.4). As mentioned earlier, to generate fuzzy curves the data distribution should be normal, and skewed data may give erroneous results. This seems to be the case with microporosity, although the histogram and cumulative probability distribution do not appear highly skewed (Figure 2.16G). Even though the data was normalized, using Equation 3, before creating fuzzy curves, sometimes the data distribution remains skewed. In the case of microporosity, the majority of the data dictated a fuzzy range of less than 207, but a single point caused the fuzzy range to jump to 372 (Figure 2.19D). This caused microporosity to be ranked in the third place according to fuzzy logic, whereas, the regression analysis ranked it at 7 (Figure 2.17E, Table 2.4). If we ignore the highest point, the fuzzy range becomes approximately 207, which will rank it at eighth place (Figure 2.19E). Based on the petrographic analysis, it is safe to assume that microporosity should not affect permeability considerably. The majority of the microporosity is present in the kaolinite.

Kaolinite is authigenic in origin and occupies only sand sized pores formed after the dissolution of feldspars.

The reason quartz was ranked low is related to the collection of petrographic data. During the petrographic analysis quartz overgrowths were not treated separately and were combined with the detrital quartz. This problem is explained in the mineralogy section. Because quartz overgrowths form around the grain in concentric circles, it reduces the pore throat size considerably. A sandstone may have a high intergranular porosity, but if it is affected by quartz overgrowths, will have a low permeability (effective porosity) because quartz overgrowths can reduce the pore interconnection considerably if present in even small amounts. It would have been too time-consuming to determine the control of quartz overgrowths on permeability. Also, our main intent was to develop the methodology, rather than the specific analysis of the Santa Rosa Sandstone.

Another reason due to which quartz may have been ranked low is its strong correlation with some low-ranked petrographic element. According to Lin (1994) another case where fuzzy curves fail is that when input variables are cross-correlated, and in this case a set of inputs may be obtained which will look good when they are analyzed separately. An alternative has been proposed by Lin (1994) that involves the use of fuzzy surfaces to quantify the effects of correlated variables. In this study, another possibility explored was to remove the isolated points from the fuzzy curves of all the elements and look at their fuzzy ranges (Figure 2.19 & Table 2.4 last column). This increased the ranking of quartz from 8 to 5.

An attempt was made to reduce cross-correlation by using the porosity and mineralogic data separately to perform the fuzzy logic analysis. When mineralogical elements were treated separately (no porosity types included) during the fuzzy logic analysis, the ranking obtained was: (1) rock fragments, (2) quartz, (3) clay, and (4) dolomite. This is considerably different from the ranking obtained using eight elements (Table 2.4). The removal of the outliers and classification of data into separate groups improved the results of the fuzzy logic analysis.

One important question to be considered during fuzzy logic analysis is whether

the elements that are present in high amounts (e.g., >20%) should be analyzed along with the elements that are present only in minor amounts (e.g., < 5%). It seems obvious intuitively that elements with higher percentages will be more influential than the ones with minor amounts. On the other hand, the control of cements and clays (especially clay types) cannot be judged on the basis of percentage alone, because the type and distribution of these elements are also very important. One element that can affect permeability considerably even if present in small amounts, is pore lining and bridging clay, especially illite and chlorite (Neashan, 1977).

Even though the fuzzy logic algorithm may have some limitations, it is still fast and more quantitative than the regression analysis because it compares all the input variable on the same basis. The comparison of fuzzy logic and regression analysis also indicated that the fuzzy logic results are reliable. Additionally, some of the limitations made evident by the fuzzy logic algorithm are also applicable to the conventional analysis. The fuzzy logic algorithm is also useful in ranking data sets consisting of large numbers of input variables. The normal distribution and absence of strong cross-correlation between the data is important for the correct application of fuzzy logic algorithm. A highly skewed data may cause the fuzzy logic to wrongly rank an unimportant variable as an important variable as observed in the case of microporosity, rock fragments, and clay (Figures 5.16C, 5.16D, & 5.16E).

San Andres Formation

Petrographic analysis

All the cores have been affected by micritization, pervasive dolomitization, and dissolution. Because of this the identification of the skeletal grains is very difficult. Only ooids partially retained their internal structure. The summary of the permeability and porosity data for each zone is given in Table 2.5.

Both oolitic packstone and oolitic-peloidal wackestone/packstone contain well

Zones	Thickness (ft)	Horizo-ntal K (md)	Vertical K (md)	"σ" of Horizontal K (md)	Total ϕ (%)	Intercrys-talline ϕ (%)	Intergran-ular ϕ (%)	Vuggy ϕ (%)	Intracons-tituent ϕ (%)	Vug size (mm)	Pore size (mm)
Well: State ACCT 2 #60 (Peloidal wackestone/packstone)											
1	3.00	14.3	10.4	8.4	7.41	4.64	0	0	0	-	0.1
2	1.00	1.2	0.3	3.1	0.5	0.5	0	0	0	-	0.03
3	1.50	8.2	5.0	5.6	7.22	5.12	0	0	0	-	0.11
4	2.50	1.2	0.1	1.4	0.5	0.5	0	0	0	-	0.03
5	5.25	11.6	1.1	7.0	7.45	5.4	0	0	0	-	0.1
6	2.50	3.9	2.4	7.5	3.2	2.18	0	0	0	-	0.05
Well: Mayers A-1 #117											
Oolitic packstone											
A	1.75	16.1	2.3	27.2	9.1	0.3	1.48	0.9	6.3	-	0.4
Peloidal packstone											
B	1.75	25.0	0.7	54.1	8.44	1.03	0	5.83	0	0.4	0.4
Oolitic-peloidal wackestone/packstone											
C	2.0	52.6	0.5	92.3	7.0	0.11	0	5.9	0	2.3	0.67

Table 2.5: Summary of permeability, porosity, and textural data for the San Andres Formation. The horizontal permeability was calculated using the arithmetic average and vertical permeability using the harmonic average of the minipermeameter data.

sorted detrital silt-sized material (Figure 2.20A & 2.20B). The well sorted nature of the silt-sized particles suggest an eolian origin (Mazzullo *et al.*, 1985). By analogy with modern settings, these ooid-dominated rocks were deposited in shallow water under moderate to high energy conditions. Todd (1976) suggested that the San Andres oolites were formed in water depths less than 15 feet and developed into linear banks or barrier bars in front of the lagoon.

Peloidal wackestone/packstone and peloidal wackestone do not contain any detrital silt-sized material (Figure 2.20C & 2.20D). Because of the microcrystalline nature of the dolomite, the original carbonate texture probably ranges from lime mud to skeletal/peloidal lime mud.

The San Andres Formation has a paragenetic sequence that includes early micritization and dissolution to late stage stylolitization, fracturing and hydrocarbon emplacement. A general paragentic sequence is shown in Figure 2.21. Both the skeletal grains and ooids show the effects of micritization (Figure 2.20). Ooids and less stable skeletal grains may have either undergone early dissolution or were not dolomitized and were later dissolved (Figure 2.20). The dissolution of the skeletal grains and formation of molds in dolomitized rocks is possible only if the matrix was dolomitized and skeletal grains were dissolved later. But when the majority of the skeletal grains along with the matrix are dolomitized, the presence of molds suggests dissolution of less stable skeletal grains (aragonite or high-magnesium calcite) before replacement (Figures 2.20C & 2.20D). Similar to molds, vugs were formed before dolomitization, probably by the solution enlargement of the molds (Figure 2.20B). The solution enlargement of the molds may have created the vugs. Although the bulk of dolomite is replacive in nature, in places dolomite crystals growing adjacent to open spaces show well developed rhombic shapes. Dolomite is present in two morphologies: (1) very finely to finely crystalline (<50μm) interlocking turbid crystals which replaced oolites and matrix (Figure 2.20A, 2.20B, & 2.20C), and (2) aphynocrystalline dolomite which replaced the skeletal grains (Figure 2.20D).

Anhydrite is only present in the peloidal wackestone/packstone. It is present in

Figure 2.20: Thin section photomicrographs showing ooids, peloids, matrix relationships, and dolomite morphologies in the San Andres Formation. (Porosity in yellow and blue.)

A: Oolitic packstone:
Pervasively dolomitized oolitic packstone. Ooids partially retain their internal structure and show the effects of dissolution. Note the presence of silt size quartz grains in the interparticle spaces. (Thin section SAD433, plane light)

B: Oolitic-peloidal wackestone/packstone:
Dolomitized peloids and ooids. The majority of ooids are recognized only on the basis of their shapes. Large sized vugs are typical of this interval. (Thin section SAN393, plane light)

C: Peloidal wackestone:
Dolomitized peloidal wackestone showing molds (m) and vugs (v). Dolomite is very finely crystalline. (Thin section SAN331, plane light)

D: Peloidal wackestone/packstone:
Dolomitized shell showing partially open intraparticle porosity (probably a foram). Dolomitized skeletal grains are present floating in anhydrite. (Thin section SAN464, plane light)

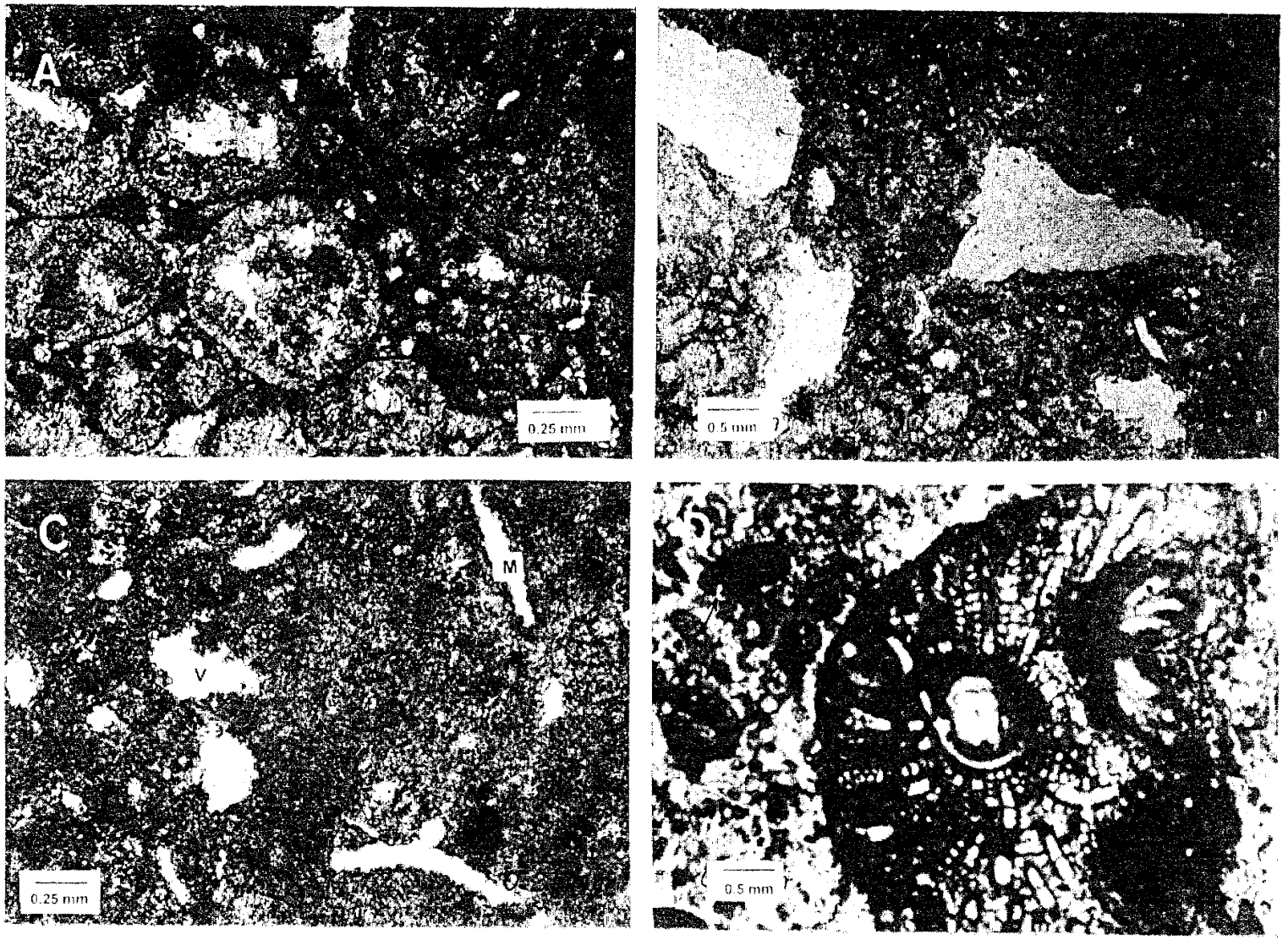
A
0.25 mm
0.5 mm
C
M
V
0.25 mm
0.5 mm

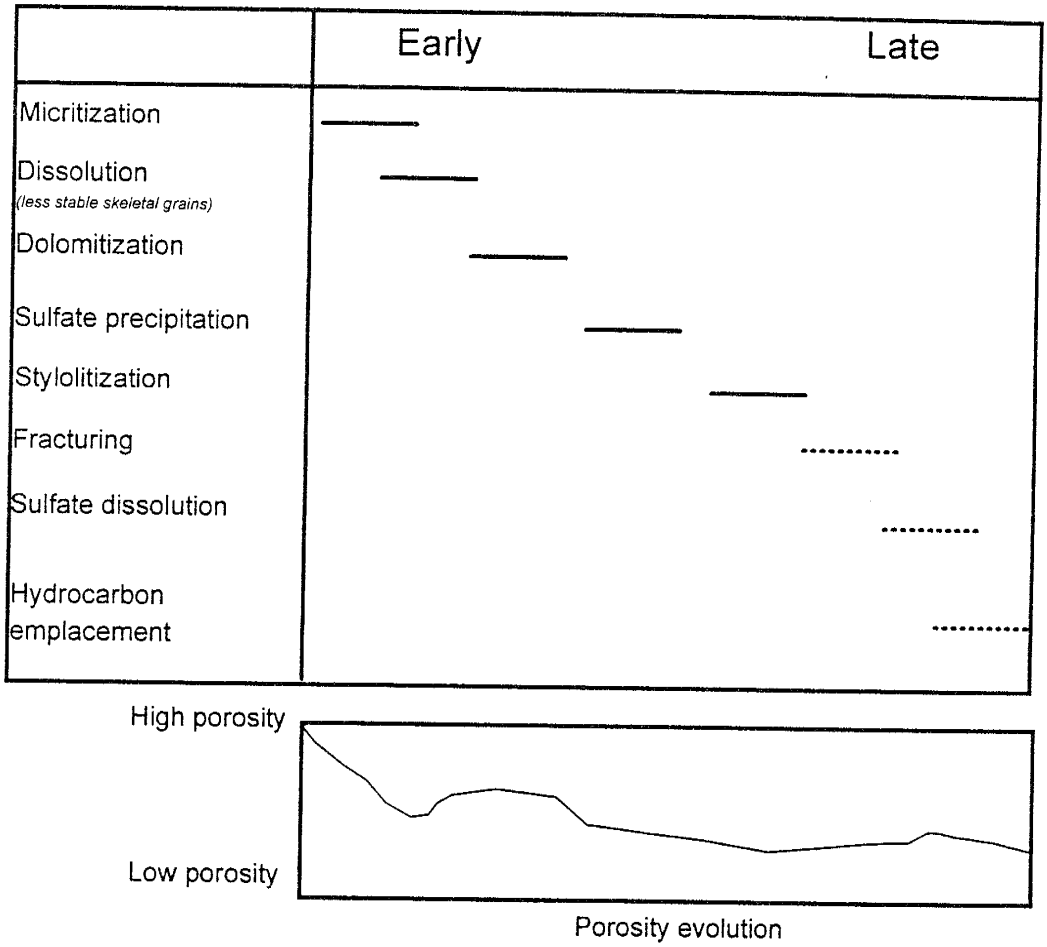

Figure 2.21: Generalized paragenetic sequence for the San Andres formation. Dashed lines show the range over which a given alteration may have occurred.

two morphologies: (1) isolated nodules containing randomly oriented (felted) crystals an coarse tabular crystals (Figures 2.22A & 2.22B), and (2) large patches of poikilotopic anhydrite that contains "floating" patches of dolomite and dolomitized skeletal grains (Figures 2.22C & 2.22D). The presence of dolomite inclusions and dolomitized skeletal grains with in anhydrite suggest that anhydrite postdates dolomite.

Stylolites occur as dark brown clay seams up to 0.25 mm thick (Figure 2.23A). According to the Wanless classification (1979), stylolites present in the San Andres Formation are the non-sutured seam solution type (Figure 2.23A). Anhydrite is present between stylolite seams. The decrease in the stylolite thickness around anhydrite indicates that anhydrite did not contribute the insoluble clayey material into the formatio of stylolite and hence, was precipitated before the formation of stylolites (Figure 2.23A). Minor fracturing of peloidal wackestone also occurred late in the diagenetic history.

Minor dissolution, especially of anhydrite, may have occurred after the formation of stylolites, suggesting considerable depth of burial, and therefore, can be considered as a late diagenetic event. The dissolution of anhydrite is manifested by the presence of pores in finely crystalline dolomite surrounded by pores of the same size and shape occupied by anhydrite (Figure 2.23B).

Porosity evolution

Based on petrographic analysis porosity is entirely secondary and consists of following types: intercrystalline pores, gradational intercrystalline pores, intraparticle pores, moldic pores, vugs, and fractures.

The dissolution of skeletal grains and pervasive dolomitization of the peloidal wackestone/packstone makes it difficult to identify different porosity types, because depositional textures have been completely obliterated (Figures 2.23A, 2.23B, & 2.23C). The shapes and sizes of the molds have been modified making it difficult to differentiate between molds, reduced molds, and intercrystalline pores (Figures 2.23B & 2.23D). In many instances, when pores are larger than typical intercrystalline pores but cannot be classified as molds or vugs, they have been classified as gradational intercrystalline pores

Figure 2.22: Thin section photomicrographs showing anhydrite morphologies in peloidal wackestone/packstone in the San Andres Formation.

A: Randomly oriented laths of anhydrite in a large vug (Thin section SAN476, crossed polarizers)

B: A small portion of anhydrite nodule consisting of coarse tabular anhydrite crystals (Thin section SAN6114, crossed polarizers)

C: A part of a large anhydrite patch containing floating patches of dolomite. Anhydrite appears to have replaced dolomite. Ghosts of some individual dolomite crystals are still recognizable (arrow). (Thin section SAN464, crossed polarizers)

D: Dolomitized skeletal grains floating in anhydrite (white). (Thin section SAN451, plane light)

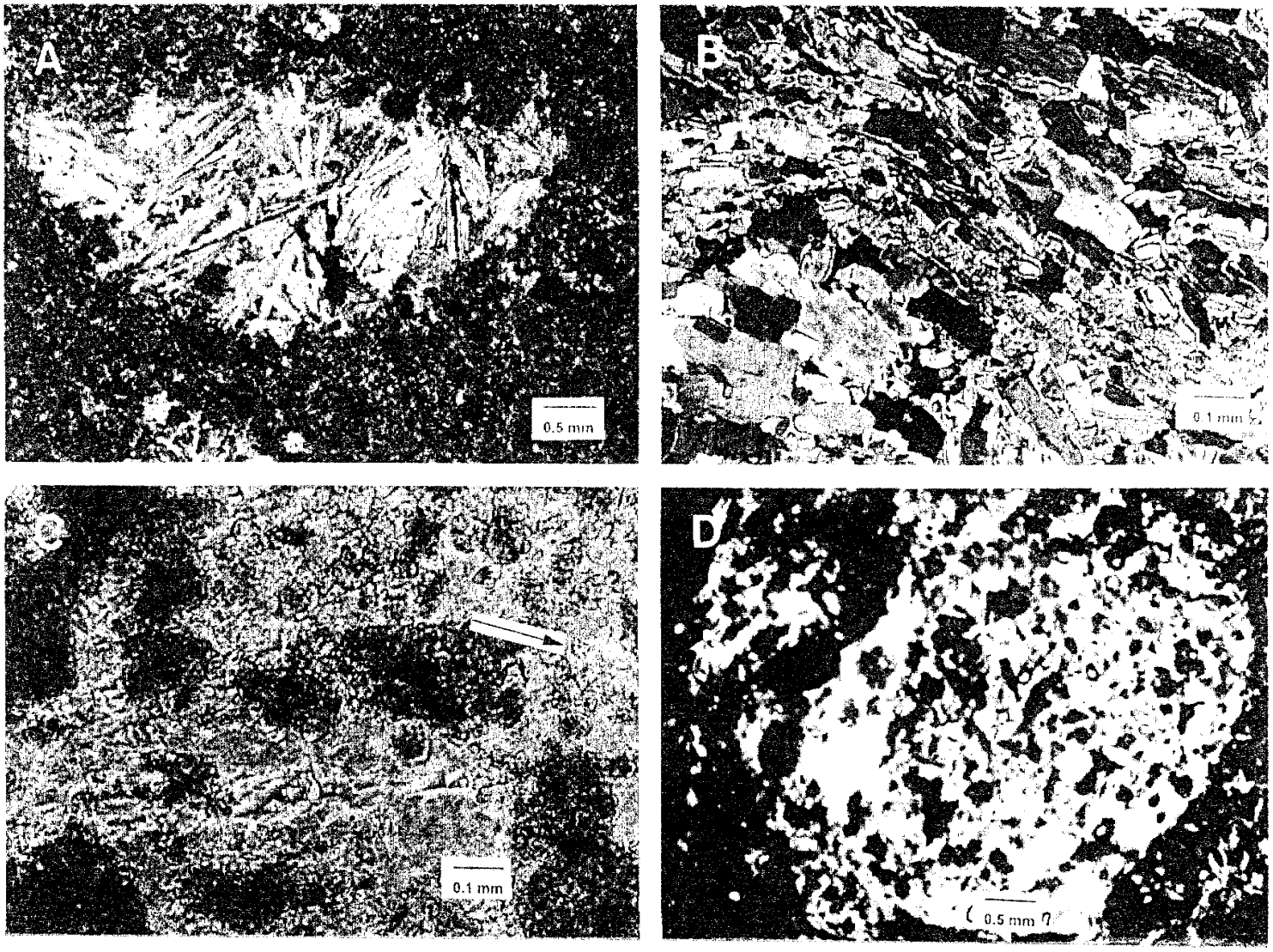
A
0.5 mm
B
0.1 mm
C
0.1 mm
D
0.5 mm

igure 2.23: Thin section photomicrographs showing late stage diagenetic effects and porosity types in peloidal wackestone/packstone
n the San Andres Formation. (Porosity in blue and yellow.)

: Stylolite in finely crystalline dolomite. Anhydrite is present within stylolite seams (arrow). (Thin section SAN465, crossed
olarizers)

: Intercrystalline (I) and vugular (V) porosity in dolomite. Vugs and intercrystalline pores occupied by anhydrite (white). (Thin
ection SAN5111, plane light)

: Intercrystalline porosity among dolomite crystals. (Thin section SAN5810, plane light)

: Vuggy porosity (V). (Thin section SAN453, plane light)

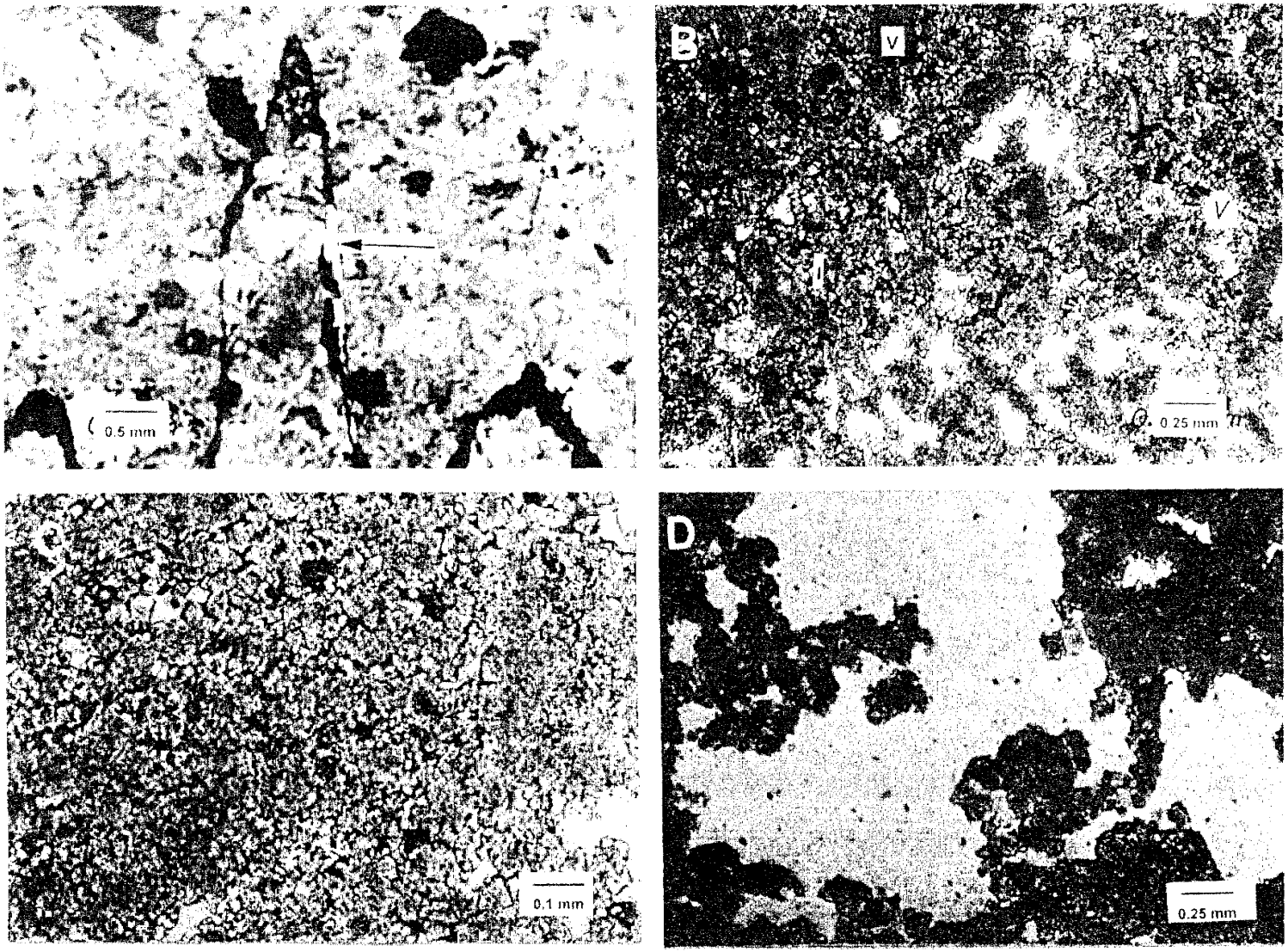
0.5 mm
B
V
V
0.25 mm
0.1 mm
D
0.25 mm

in this study (Figure 2.23B). The exact precursor for these kinds of pores is unknown. Proper intercrystalline pores are present between dolomite crystals (Figure 2.23C).

Intraparticle pores are only present in the oolitic packstone. Intraparticle pores were formed by the partial dissolution of ooids (Figure 2.24A) and range in size from 0.05 mm to 1 mm in length. The majority of these intraparticle (intraoolitic) pores appea to have poor interconnections (Figure 2.24A). Moldic pores are common in peloidal wackestone and range in size from 0.1 mm to 0.5 mm. The majority of these molds shov very poor interconnection with other pores (Figure 2.24B). In the peloidal wackestone/packstone, molds were formed early in the diagenetic history and were later filled by anhydrite. Based on the criteria given by Choquette and Pray (1970) for the recognition of pores, a small percentage of the open pores can be classified as molds (Figure 2.23B).

Vugs are present in all the core samples but are dominant in peloidal wackestone and oolitic-peloidal wackestone/packstone. The vugs range in size from <0.5 mm to 7.5 mm, and most are isolated (Figure 2.24C). In peloidal wackestone/packstone vugs are less than 0.5 mm in diameter and are in the category of "mesovugs" (0.0624 - 0.5 millimeters) according to Choquette and Pray's classification (1970) (Figure 2.25D). Fractures are present only in peloidal wackestone.

Relationship between permeability and petrographic elements

In the San Andres Formation only regression analysis was used to determine the control of petrographic elements on permeability. The fuzzy logic analysis was not applied for two reasons: (1) the applicability and reliability of the fuzzy logic as a tool for determining the ranking of petrographic elements in controlling the permeability was established using the Santa Rosa Sandstone and (2) the number of input variables (petrographic elements) were very few in the San Andres Formation.

In the core sample (peloidal wackestone/packstone) from well State ACCT 2 #60, the permeability heterogeneity is produced by the combined effects of dissolution, dolomitization, and anhydrite precipitation. The permeability is controlled by gradational

Figure 2.24: Thin section photomicrographs showing porosity types in oolitic packstone, oolitic-peloidal wackestone/packstone, and peloidal wackestone in the San Andres Formation. (Porosity in yellow and blue.)

A: Oolitic packstone:

Intraparticle (intraoolitic) is typical of this interval. Minor amounts of intercrystalline porosity are also present. Interconnection between pores is very poor. (Thin section SAD433, plane light)

B: Peloidal wackestone:

Molds and small vugs in dolomitized area. Majority of molds and vugs are isolated. (Thin section SAN334, plane light)

C: Oolitic-peloidal wackestone/packstone:

Large vugs are typical of this interval. Interconnection between vugs is very poor. (Thin section SAN393, plane light)

D: Peloidal wackestone:

Wide open fracture running through finely crystalline dolomite. A few vugs are also present. (Thin section SAN333, plane light)

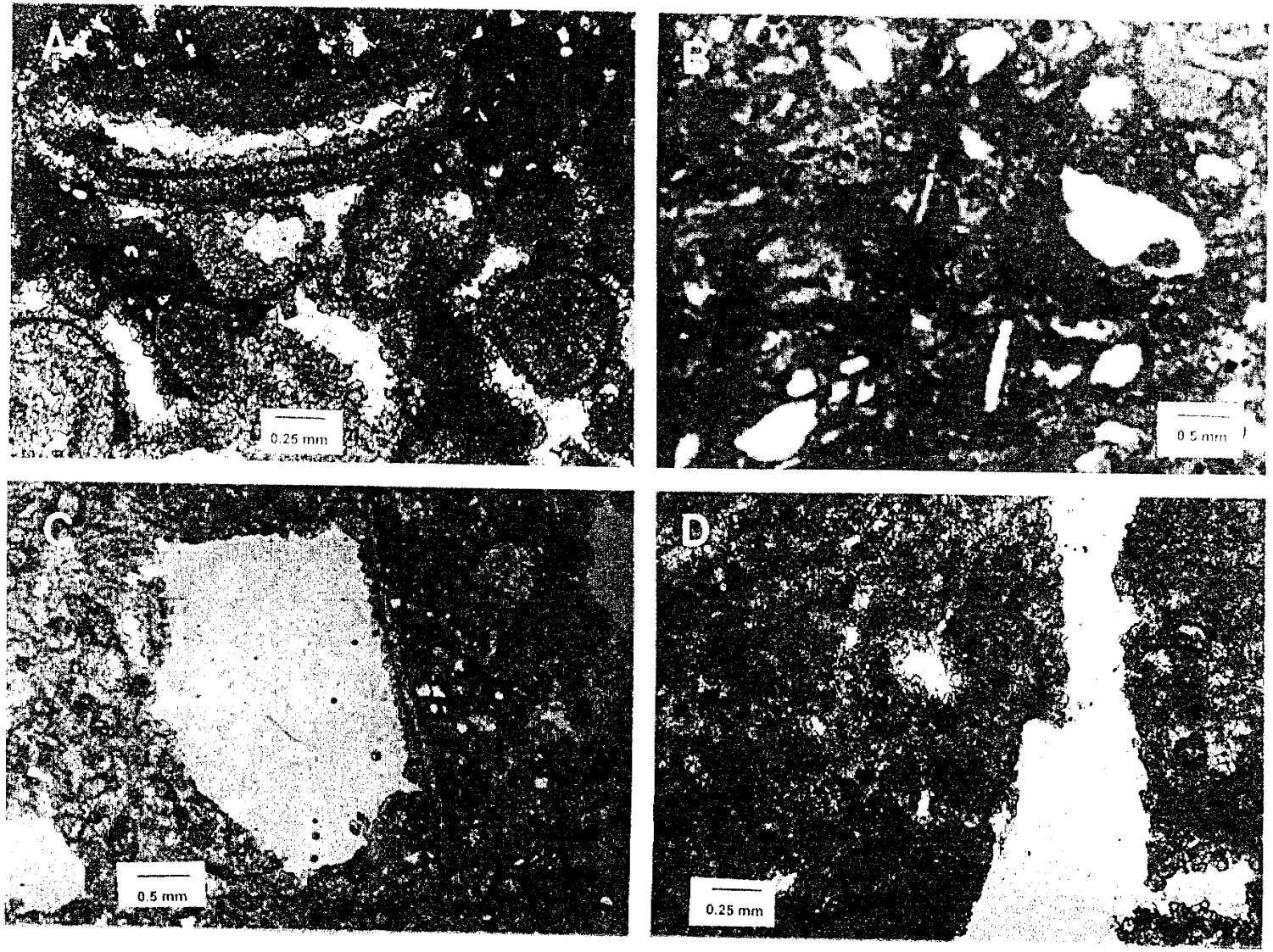
A
0.25 mm
B
0.5 mm
C
0.5 mm
D
0.25 mm

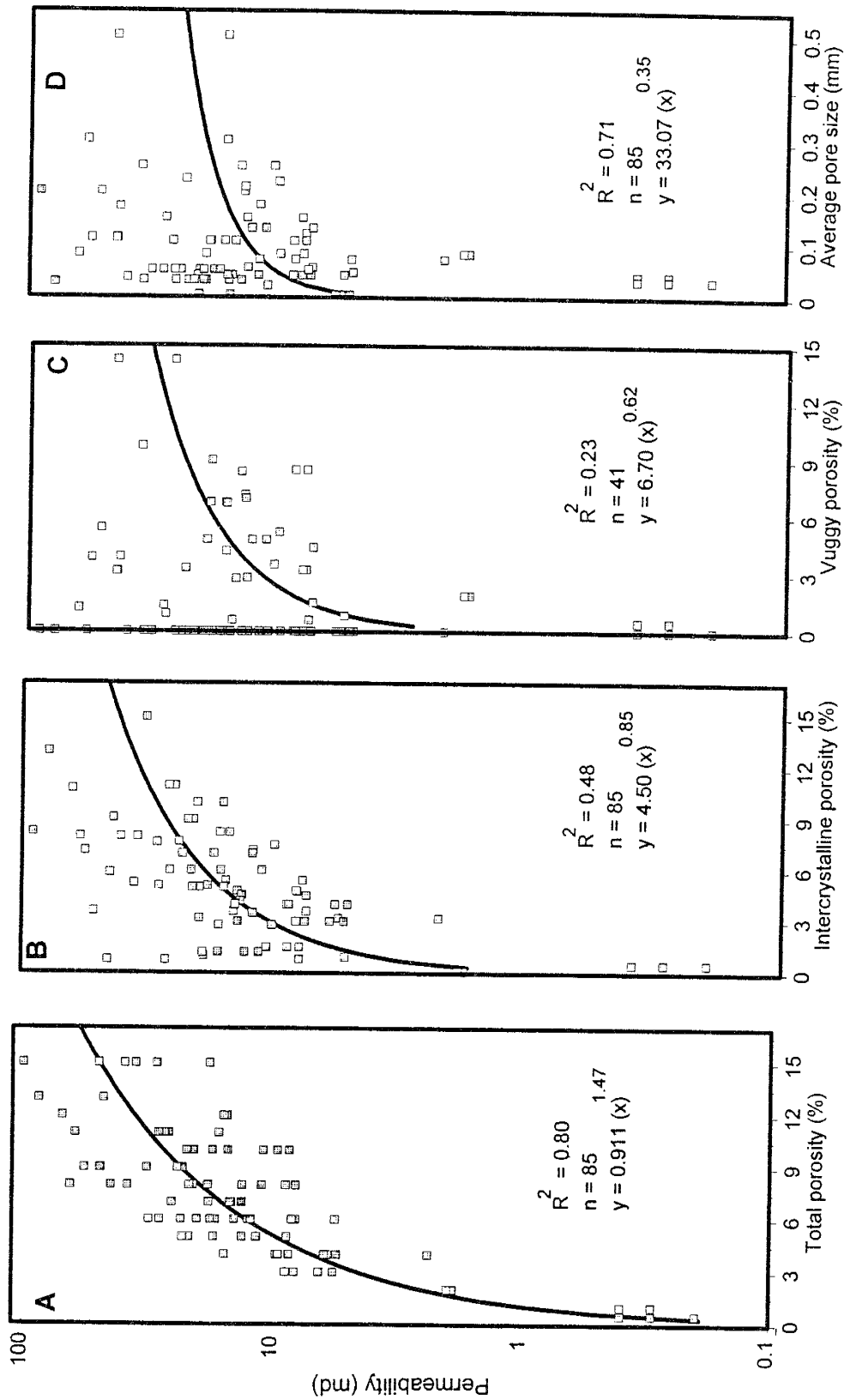

Figure 2.25: Relationships between permeability and petrographic elements in the San Andres Formation from Well STATE ACCT 2 #60.

intercrystalline and vuggy pores. Total porosity ranges from <1% to 15%, and shows a positive correlation with the permeability (Figure 2.25A). Intercrystalline and gradational intercrystalline porosity are the dominant porosity types and also exhibit a positive correlation with the permeability (Figure 2.25B). Vugs do not exert much control over permeability because they are isolated and are not very well connected (Figure 2.25C). Pore size shows a moderate control over permeability (Figure 2.25D). The wide range of pore sizes for the high permeability samples is due to the interplay of vuggy and gradational intercrystalline porosities. Small pore sizes showing high permeabilities are due to the dominance of well connected intercrystalline and gradational intercrystalline porosities, whereas larger pores associated with low permeabilities indicate isolated vugs.

The low permeability areas are characterized by interlocking euhedral crystals of dolomite (Figure 2.26A). Vugs, when present, associated with intercrystalline or gradational intercrystalline porosities, do not affect permeability considerably (Figure 2.26B). Gradational intercrystalline pores of elongated shape provide good interconnection between the pores (Figure 2.26C). When vugs and molds are associated with gradational intercrystalline porosity, they exhibit some of the highest permeabilities (Figure 2.26D).

In well Mayers A-1 #17 (oolitic packstone, oolitic-peloidal wackestone/packstone, and peloidal wackestone), the permeability heterogeneity is due to different porosity types and pore morphologies. The total porosity ranges from 1% to 45%. This wide range of porosity values is due to the presence of large vugs. There is a moderate positive correlation between total porosity and permeability (Figure 2.27A). The scattering of the data is due to isolated vugs and large intraconstituent pores exhibiting low permeability. Vuggy and intraconstituent porosities do not influence permeability, due to their isolated nature (Figures 2.27C & 2.27D). Average pore size ranges from 0.005 millimeters to 4 millimeters, with the majority of the pores less than 0.5 mm. There is a poor correlation between pore size and permeability (Figure 2.27E).

Vugs with poor interconnection exhibit low permeability (Figure 2.28A), whereas a slightly better interconnection between small vugs increases permeability (Figure

Figure 2.26: Thin section photomicrographs showing the relationship between permeability and porosity in peloidal wackestone/packstone in the San Andres Formation. (Porosity in blue and yellow.)

A: Dolomitized low porosity and permeability area. Note the interlocking habit of the crystals. [(K = 0.4 md),Thin section SAN477, plane light, 25x]

B: Vugs (V) with small percentage of intercrystalline porosity. Anhydrite is completely absent. [(K = 18 md), Thin section SAN5110, plane light]

C: A combination of intercrystalline and vuggy porosity. Permeability is moderately high despite the presence of anhydrite (White; A). [(K = 47.9 md), Thin section SAN5111, plane light]

D: A combination of vugs (V), molds (M), and intercrystalline pore exhibiting high permeability. [(K = 65 md), Thin section SAN453, plane light]

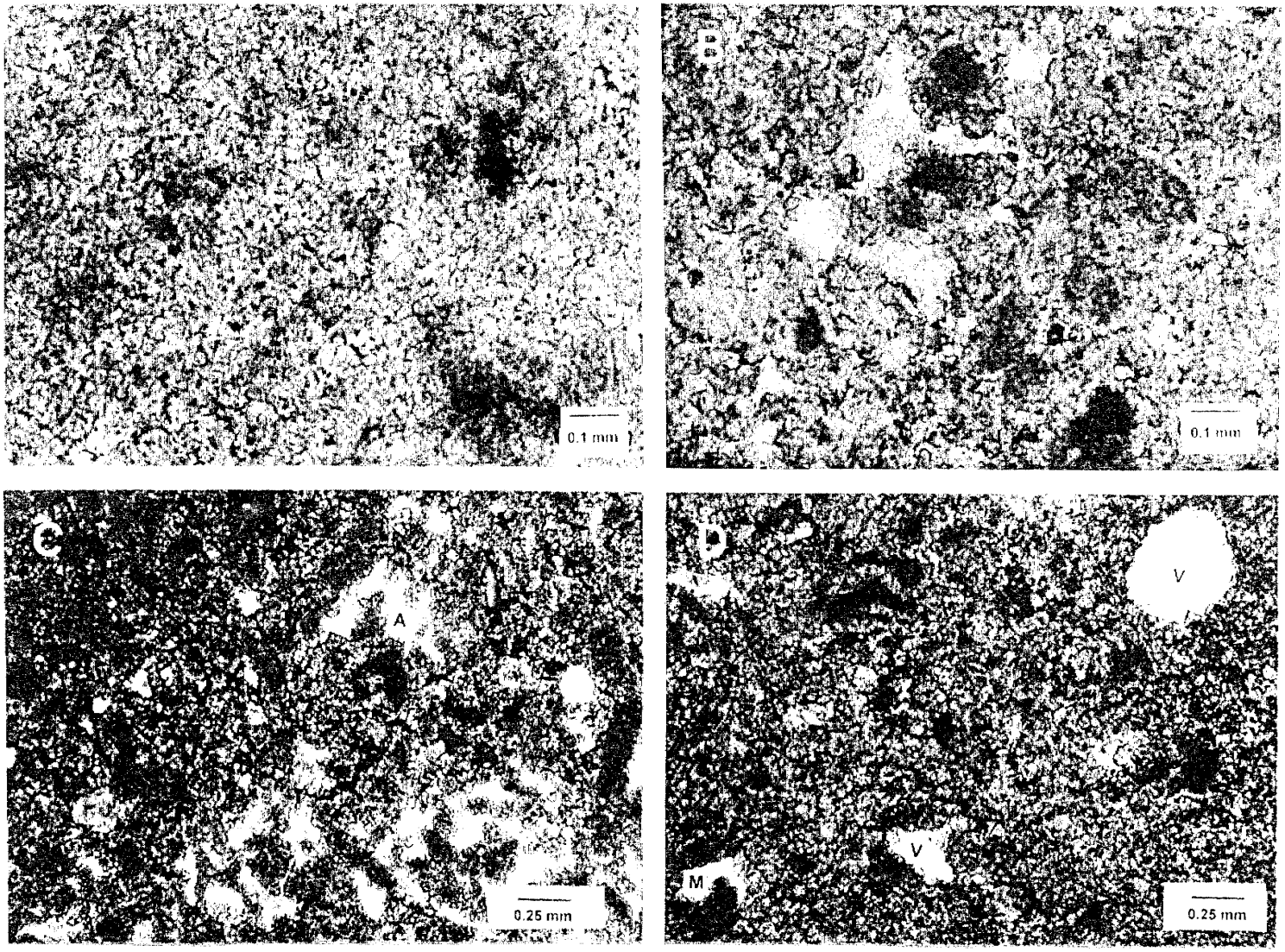
0.1 mm
B
0.1 mm
C
A
0.25 mm
D
V
V
M
0.25 mm

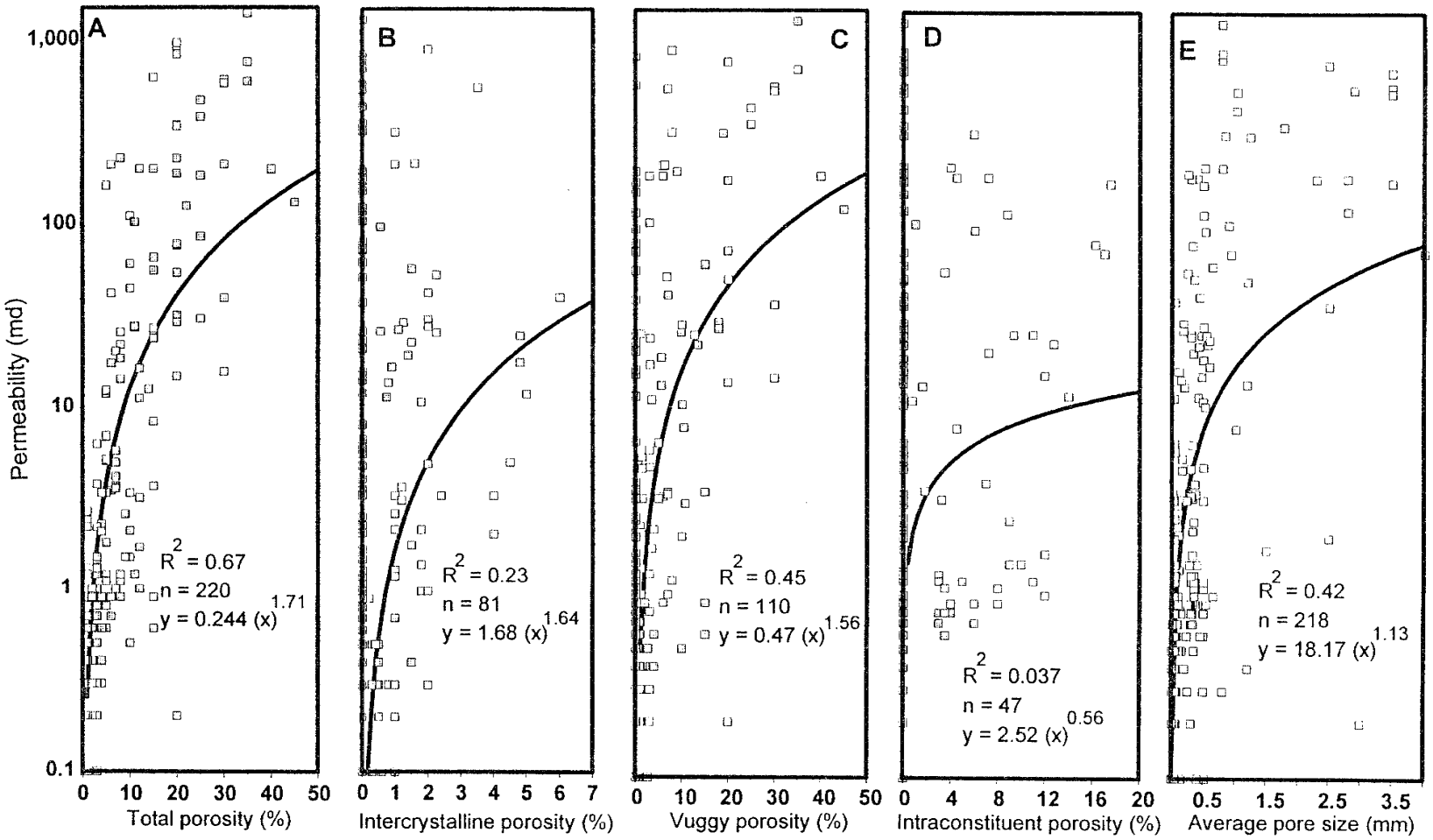

Figure 2.27: Relationships between permeability and petrographic elements in the San Andres Formation from Well Mayers A-1 # 17.

Figure 2.28: Thin section photomicrographs showing pore types present in peloidal wackestone and oolitic-peloidal wackestone/packstone in the San Andres Formation. (Porosity in yellow and blue.)

A: Isolated vugs of big size in microcrystalline dolomite. Even though vugs are big, the lack of interconnection give a low permeability value. [(K = 2.6 md), Thin section SAN345, plane light]

B: Combination of vugs, molds, and intercrystalline porosity. Due to slightly good interconnection permeability is high. [(K = 45 md), Thin section SAN346, plane light]

C: Isolated intraoolitic pores in dolomitized ooids exhibiting very low permeability. [(K = 0.8 md), Thin section SAD433, plane light]

D: A combination of intraoolitic and vugular porosity. This is the highest permeability point in oolitic packstone. [(K = 347 md), Thin section SAD433, plane light]

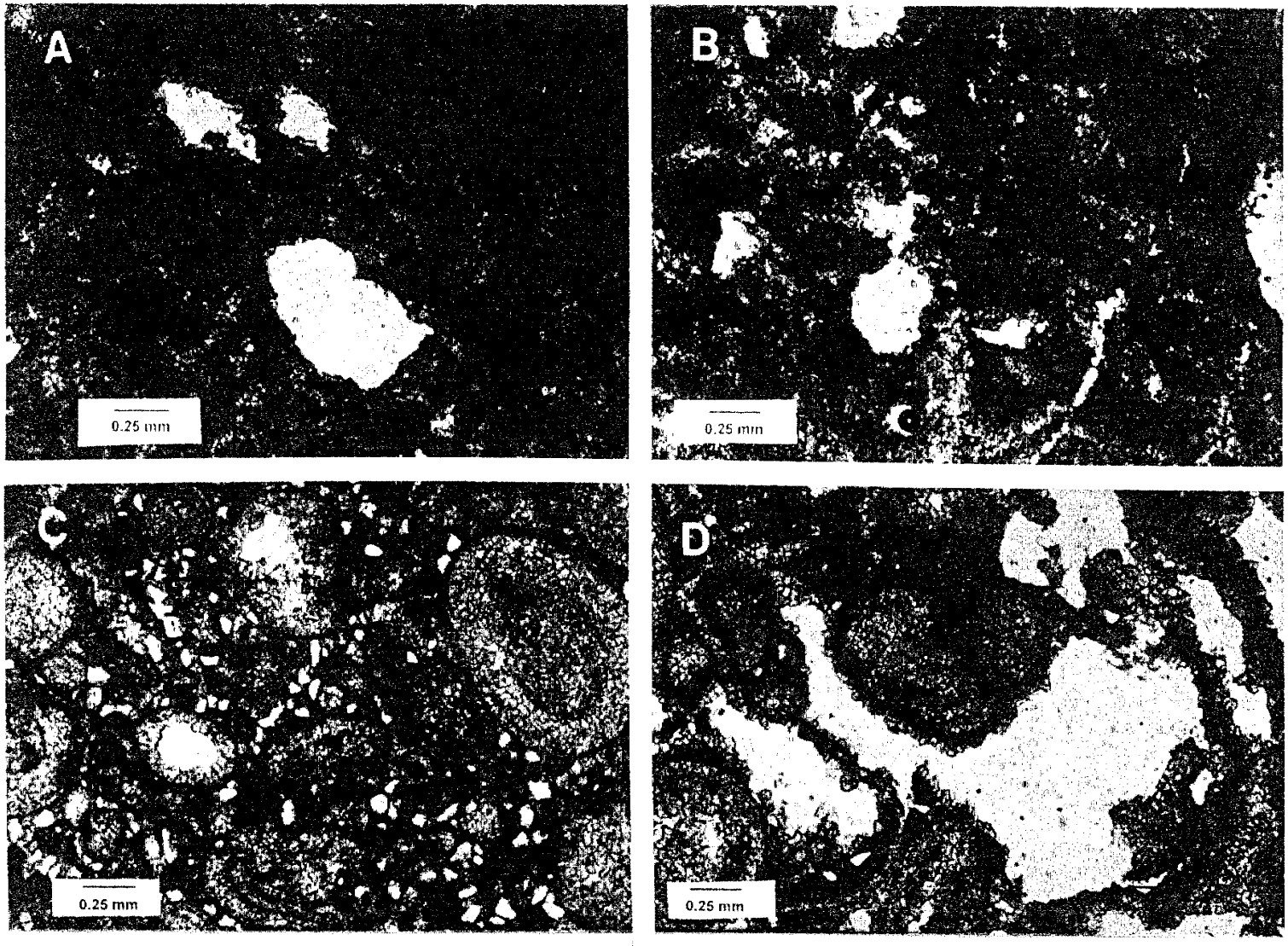
A
0.25 mm
B
0.25 mm
C
0.25 mm
D
0.25 mm

2.28B). Intraparticle (intraoolitic) pores are only present in the oolitic packstone. The majority of the intraparticle pores are isolated (Figure 2.28C). The highest porosities are exhibited by a combination of vuggy and intraconstituent porosities (Figure 2.28D). Fractures are present only in peloidal wackestone. They are open and affect permeability considerably (Figure 2.24D).

CONCLUSIONS

The computer-controlled scanning minipermeameter is very efficient and reliable for obtaining a large number of permeability measurements on a small scale. Proper calibration and optimum pressure on the probe tip is of prime importance for making reliable permeability measurements with the minipermeameter.

The new technique of combining the minipermeameter and petrographic analysis, is more accurate than the conventional techniques, to determine the influence of pore morphologies and textural elements on permeability. The summary of small-scale data and their uses is shown in Figure 2.29. The areas of investigation of the probe tip and thin sections are similar and therefore the correlations developed between permeability and petrographic elements are more accurate than those established using the conventional core plugs.

Since each thin section contains more than one permeability measurement, the new methodology allows sampling of the whole permeability range for petrographic analysis without destroying valuable core material. Because permeability measurements are made on a very fine grid, each thin section contains more than one permeability point (in most case between 6 - 10 permeability points). Therefore, a large set of petrographic data directly related to permeability can be collected using fewer thin sections. Detailed statistical analysis can also be done using this large set of reliable data.

The new technique of collecting petrographic data also allows the comparison of petrographic elements that have considerably different permeability values present adjacent to each other. This helps to understand subtle changes in the depositional conditions as well as porosity and permeability evolution through deposition and

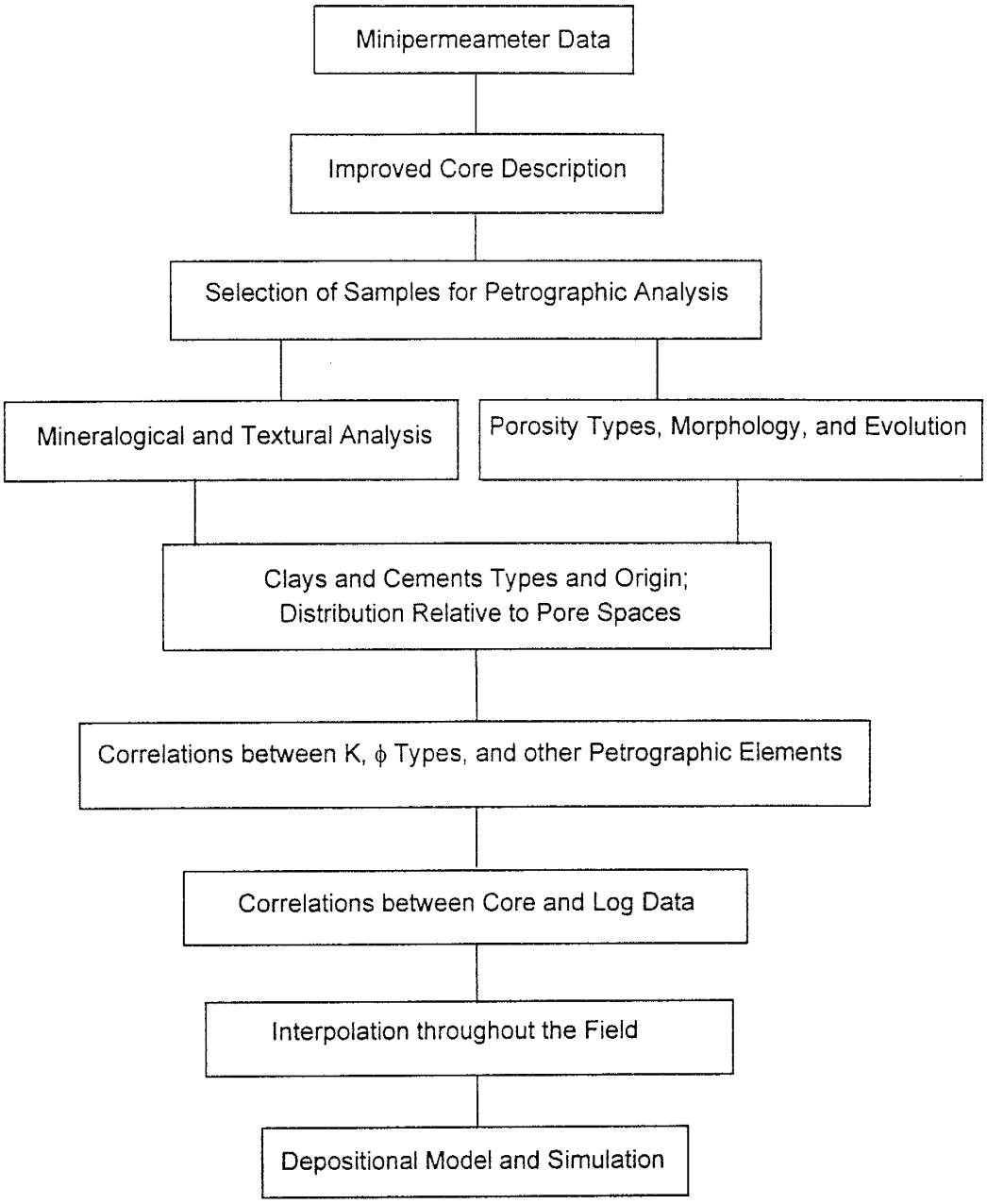

Figure 2.29: Summary of the uses of the small-scale data collected using the minipermeameter and thin sections.

diagenesis. Another important advantage of the presence of many permeability points on one thin section is that the interconnection between neighboring permeability points can be assessed qualitatively. For example, in most of the vuggy samples it was observed that the area adjacent to vugs exhibit permeability values less than 1 md, whereas vuggy areas had permeabilities as high as 1,000 md. This indicates that the matrix permeability is too low to allow interconnection between the vugs.

The minipermeameter is not reliable for making permeability measurements in vuggy samples. The problem is related to the relative sizes of the probe tip and the vugs. During this study it was noticed that when the vugs are smaller than 2 mm in diameter, a probe tip with an outer diameter of 8 mm (used in this study) can measure permeability quite accurately. However, when the vug size is larger than 2 mm or when vugs are present very close to each other, the chance of poor seal and leakage around the probe tip is very high. The minipermeameter should be used with caution in vuggy samples.

The fuzzy logic algorithm is fast, unbiased, and more quantitative than the conventional regression analysis, for establishing the ranking of petrographic elements in controlling permeability. The fuzzy logic approach should be used with caution in poorly distributed and cross-correlated data. The fuzzy logic algorithm was not tested for the carbonate samples because of fewer input variables.

The above studies on both sandstone and carbonates were conducted to assess the reliability and applicability of the methodology developed by combining minipermeameter and petrographic analysis. Carbonates rocks with different textures and compositions were used so that the efficiency of the methodology could be assessed. This methodology was developed to: (1) improve the reliability of the correlations developed between permeability and petrographic elements, and (2) to collect more petrographic data using few thin sections in situations where core material available is insufficient.

Once it was established that the methodology was less time consuming and improved the quality and quantity of permeability and petrographic data, it was used to characterize the Sulimar Queen field, which lacks sufficient core material.

CHAPTER 3: OLD LOG ANALYSIS*

INTRODUCTION

The physical properties of reservoir rocks that are of importance in formation evaluation and well log interpretation are:

- Electrical properties, when fully or partially saturated with water
- Radioactive properties, both natural or induced by neutron bombardment
- Elastic and acoustic wave propagation properties
- Density and thermal conductivity.

These properties form the basis of suites of well logs used extensively in oil and gas field operations that span exploration, drilling, well completion, and reserves evaluation. The classification of the geophysical well measurements are given in Table 3.1.

Wireline logging is necessary because geological sampling during drilling (drill cuttings) leaves an imprecise record of the formations encountered. Entire formations can be cored, but this is both slow and expensive. Logging is precise, but uncertain, in that it needs interpretation to bring the log to the level of quantifiable geological or petrophysical data. However, logs fill the gap between drill cuttings and cores. Table 3.2 summarizes the principal uses of open hole wireline logs. Logs are most useful when whole suites (e.g., resistivity, gamma, neutron, and density etc.) are available for reservoir characterization. For new fields modern calibrated logs are typically available (Table 3.2); therefore formation evaluation is not a significant problem.

A large number of oil fields developed prior to the 1970s lack modern reliable logs as well as sufficient core material. These fields contain very few log types (mainly

* Ali, M., Chawathé, A., Ouenes, A., and Weiss, W., 1996, *Improved Log Analysis for the Characterization of Sulimar Queen field, Southeast New Mexico:* PRRC Report No. 99-33, 35 pp.

Measurements	Log Type	Formation Parameters Measured
Mechanical Measurements	• Caliper	• Hole Diameter
Spontaneous Measurements	• Temperature • SP (self-potential) • Gamma Ray	• Borehole temperature • Spontaneous Electrical Current • Natural Radioactivity
Induced Measurements	• Resistivity • Induction • Sonic • Density • Neutron	• Resistance to Electrical Current • Conductivity of Electrical Current • Velocity of Sound Propagation • Reaction to Gamma-Ray Bombardment • Reaction to Neutron Bombardment

Table 3.1: Classification of wireline well log measurements (in 'open hole') (Rider, 1986).

Uses	General geology					Reservoir geology		Geochemistry		Petrophysics						Seismic	
	Lithology - general	Unusual Lithology: Volcanics, Evaporites	Mineral identification	Correlation: stratigraphy	Depositional environments	Fracture identification	Over-pressure identification	Source rock identification	Maturity	Porosity	Permeability	Shale volume	Formation water salinity	Hydrocarbon saturation	Gas identification	Interval velocity	Acoustic impedance
Caliper						-	-				-						
Temperature									+						-		
SP				-	-						-	+	*				
Resistivity	-	-		-	-		+	+		+			-	*	-		
Gamma Ray	-	-	+	-	-			+				+					
Spectral GR	-		+	+		-		+				+					
Sonic	+		-		-	+	+	+		*					-	*	*
Density	+	-	-	-		+	-	+		*					-		*
Neutron	+	-	-	-						*		-			-		

- (Essentially) qualitative use + Semi-quantitative uses * Strictly quantitative

Table 3.2: Principal uses of open-hole wireline logs (Rider, 1986).

old resistivity, gamma, and neutron logs), which sometimes makes reservoir characterization difficult. The economic constraints and risks involved prohibit both large and small operators from spending large sums of money on drilling new wells, coring, logging, and running special well test operations in these old fields. The characterization of such fields using available and poor-quality information is a challenging task.

This chapter describes a new methodology that uses old gamma ray and neutron logs for the characterization of old fields. The applicability of this methodology will be demonstrated by characterizing an old field—the Sulimar Queen (Figure 1.3). The Sulimar Queen field produces from the Shattuck Member. The Shattuck Member is an excellent marker bed that can be correlated using well logs across the Northwest Shelf. The Shattuck Member contains high concentrations of radioactive elements, thus an increase in the gamma ray API units leads to the identification of the productive zones. The productive zone is capped by an anhydrite bed approximately 10 foot thick.

Only old gamma ray and neutron logs were available from the Sulimar Queen field, with the exception of four modern log suites. Additionally two core reports (Wells: 1-15 & 5-1) along with old gamma ray and neuron logs were also available (Figure 1.3B). The old-style gamma ray-neutron perforating logs were thought to be useful only to identify the flow units of the productive interval (Weiss, 1997). During the field development, a number of different wireline companies were used to log the wells, resulting in a multitude of measurement scales. In the absence of other logs (e.g. resistivity, sonic, density etc.) correlations between core porosity, permeability, water saturation, and petrographic elements have to be made either with the neutron or gamma ray logs in order to predict reservoir characteristics throughout the field.

All the logs were digitized on 0.5 foot intervals using a commercially available log digitizing software called Neuralog & a Muratec Fax/Scanner..

OLD LOG ANALYSIS

For the characterization of the Sulimar Queen field only old neutron and gamma ray and neutron logs were available.

Neutron Logs

Neutron logging was introduced in 1941 by Well Survey, Inc (Pirson, 1963). Neutron logs are used principally for delineation of porous formations or porosity determination. They respond primarily to the amount of hydrogen in the formation. Thus, in clean formations where pores are filled with water or oil, the neutron log reflects the amount of liquid-filled porosity. The following general discussion about neutron logs is extracted from Rider (1986).

Neutrons are electrically neutral particles, each having a mass almost identical to the mass of a hydrogen atom. During neutron logging, high-energy (fast) neutrons are continuously emitted from a radioactive source in the sonde. These neutrons collide with nuclei of the formation materials. With each collision, the neutron loses some of its energy. The amount of energy lost per collision depends on the relative mass of the nucleus with which the neutron collides. Greater energy loss occurs when the neutron strikes a nucleus of practically equal mass—i.e., a hydrogen nucleus. Collisions with heavy nuclei do not slow neutrons considerably. Thus, the slowing and eventual capturing of the neutron depends largely on the amount of hydrogen in the formation. The capturing nucleus becomes intensely excited and emits a high-energy gamma ray of capture. Depending on the type of neutron tool, either these capture gamma rays or the neutrons themselves are counted by a detector in the sonde. Records of gamma radiation produced in response to the neutron bombardment is called "induced gamma ray logs".

When the hydrogen concentration of the material surrounding the neutron source is large, most of the neutrons are slowed and captured within a short distance of the source. On the other hand, if the hydrogen concentration is small, the neutrons travel farther from the source before being captured. Accordingly, the count rate at the detector increases for decreased hydrogen concentration, and vice versa.

Like other log types, neutron logs are also affected by the borehole conditions, mud invasion, rock types and the instruments used. Some of the most important factors affecting the response of neutron log tool are given below (Pirson, 1963):

- Due to caving the borehole becomes enlarged, and this gives rise to false high porosity.
- A thick mud cake results in high porosity between the tool and the formation, which causes the tool to measure an anomalously high porosity.
- The presence of casing decreases the counting rate and the porosity resolution of the tool. The cement column has a high percentage of combined water which affects the neutron curve.
- Because of the high percentage of bound water in shales, the neutron porosities are high. In order to determine the porosity in the shaly rocks, correction for shale contamination must be made using the gamma ray curves.

Subject to various assumptions and corrections, values of apparent porosity can be derived from any neutron log. However, certain effects, such as lithology, clay content, and amount and type of hydrocarbon, can be recognized and corrected only if additional porosity information—from sonic and/or density logs—is available (Schlumberger, 1987).

Porosity calculation from neutron logs

Old neutron logs with API counts were available from the Sulimar Queen field. All the neutron logs were run in cased holes; therefore, they were affected by the casing and cement. Some neutron logs had no scale so an arbitrary scale from 0 - 1,000 API units was used during digitizing. In the past, specific calibration curves were used by companies to evaluate their logs. In the Sulimar Queen field, the neutron logging was conducted by seven different companies with different scale-ranges and calibrations, therefore, calibration curves could not be used. In the absence of calibration curves, the logarithmic scale technique, which is particularly useful in clean rocks such as limestones

and dolomites (Pirson, 1963), was used.

It is recognized that porosity is related logarithmically to neutron counts. In the logarithmic scale technique, shales in a given section are assigned approximately 45% neutron porosity. Also, a low porosity value of 1% - 1.5% is assigned to known dense markers in the area. By doing this one may readily establish a porosity scale on the neutron log by lining up a logarithmic scale so that the assigned porosity values to the shale (45 %) and the dense zone (1%; anhydrite in the Sulimar Queen field) fall at the appropriate values (Figure 3.1). After that, porosity can be read directly from the logarithmic scale (Figure 3.1).

In the Sulimar Queen field, porosities were determined using the logarithmic scale and a few examples are shown in Figure 3.2. It is evident from Figure 3.2 that the neutron API values have no relationship with the porosity determined using the logarithmic technique. Because the neutron logs were run through the casing, a poor cementing job may have caused erroneous high porosity values in some wells especially in the anhydritic sections (Figures 3.2B & 3.2C). Porosities obtained using the logarithmic scale were erratic and unreliable. Therefore, the neutron logs were not used quantitatively. Nevertheless, the qualitative information provided by the neutron logs formed the basis for further formation evaluation and reservoir characterization.

In the Sulimar Queen field, a negative correlation was observed between the old gamma ray (API) and neutron (API) values, which suggests that porosity increases with the increase in gamma (lower neutron API counts indicates higher porosity) (Figure 3.3A & 3.3B). This relationship was also true for the Double "L" (Figures 3.3C & 3.3D) and other adjacent fields. Although, old neutron and gamma ray logs were not reliable, this behavior still helped to understand the overall relationship between gamma ray and porosity.

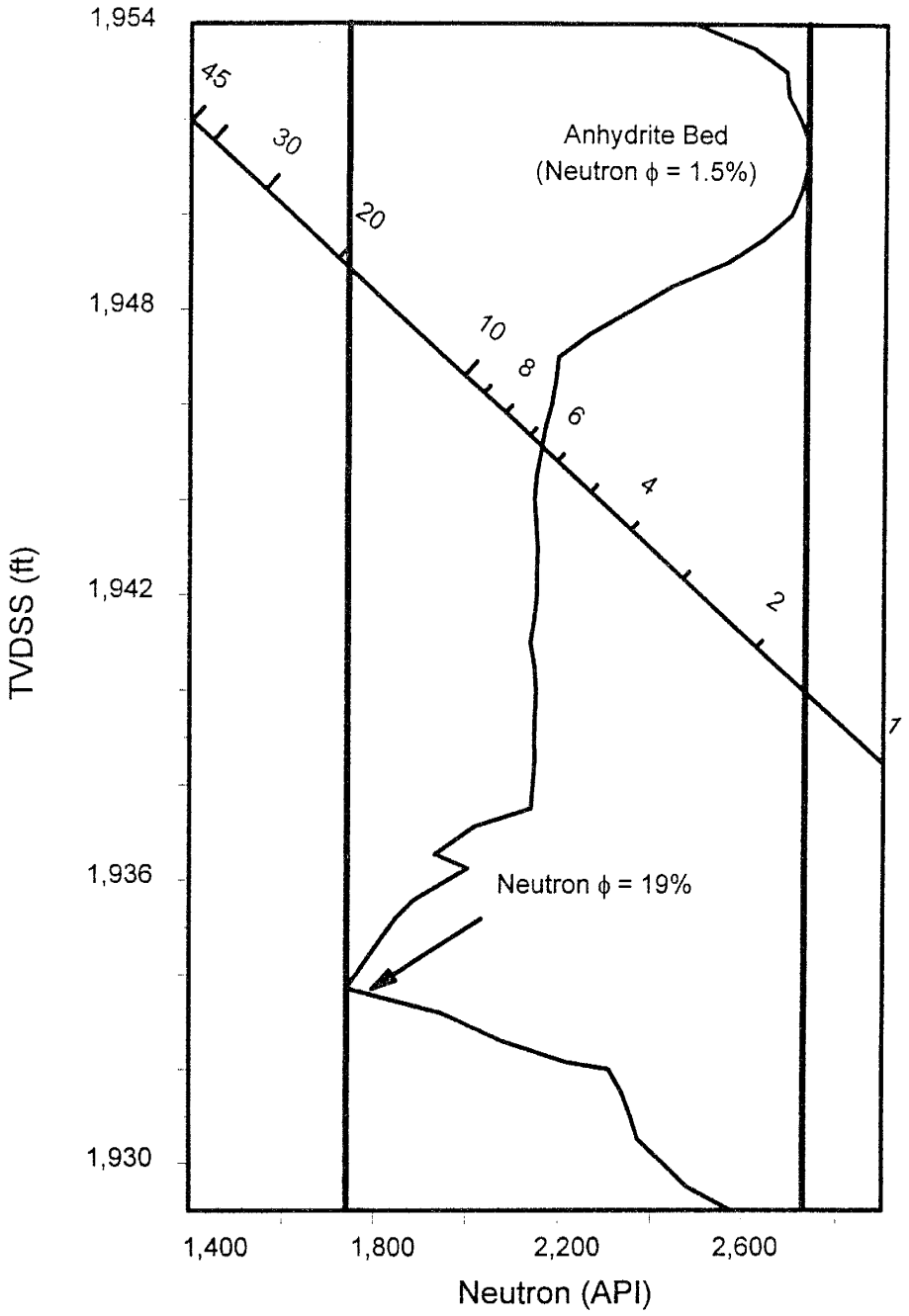

Figure 3.1: Showing the two point logarithmic plot technique to determine porosity from the old neutron logs.

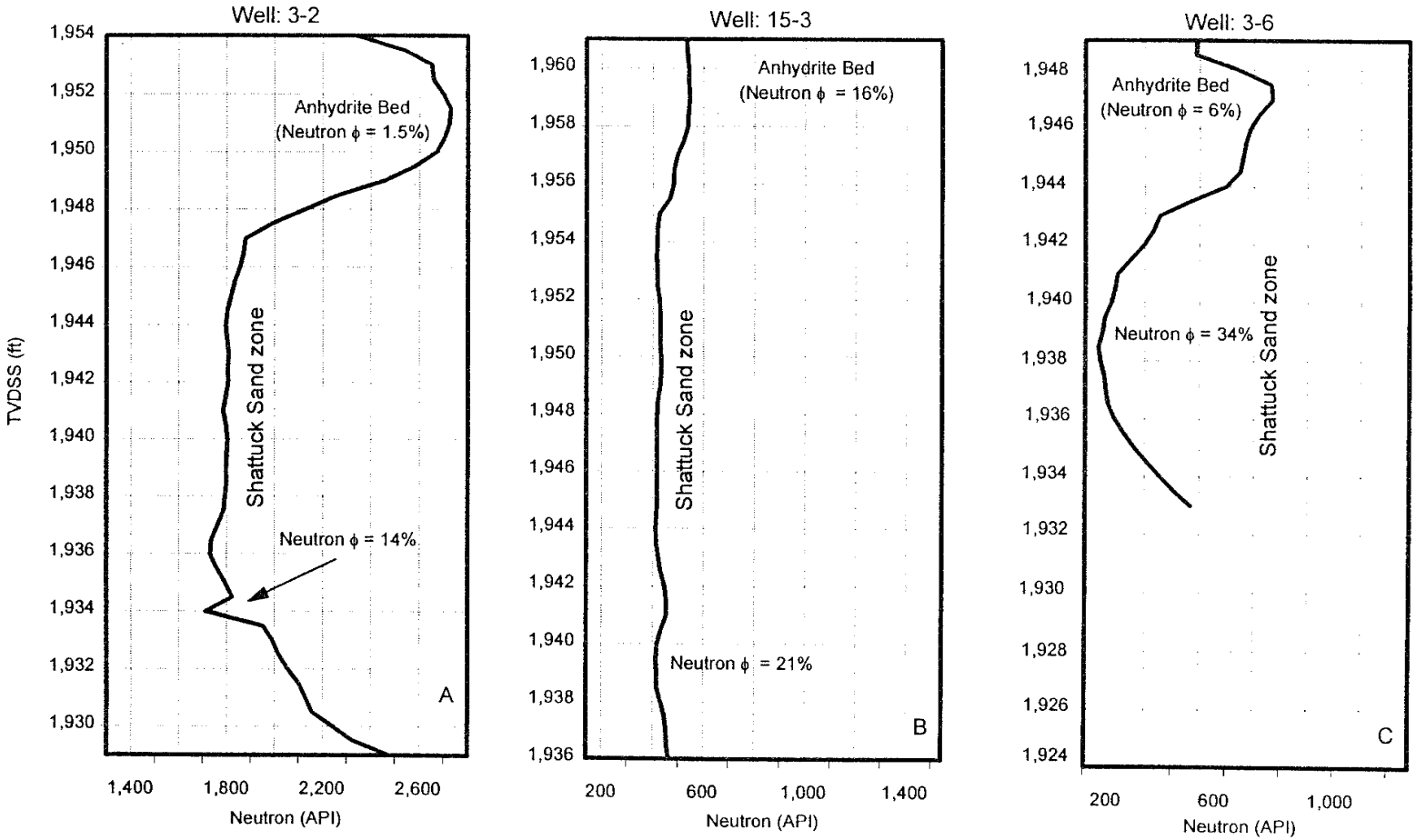

Figure 3.2: Varying scale ranges in the old neutron logs. Note the high porosity value in the anhydritic portion (B). Also note anomalously high porosity in the Shattuck sand zone (C). Porosities were determined from the neutron logs using the conventional logarithmic scale.

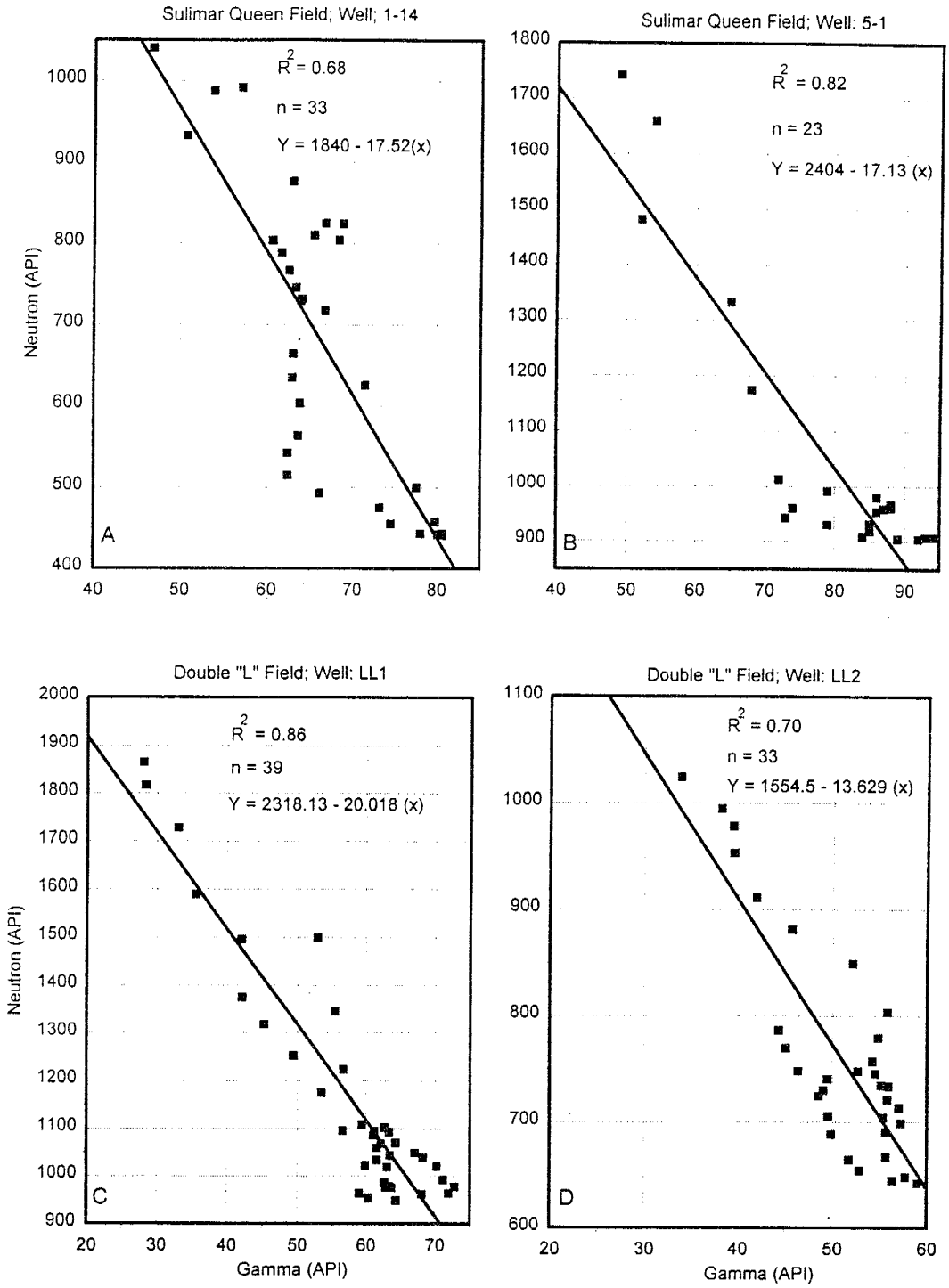

Figure 3.3: Plot of gamma ray and neutron log values. A negative correlation between gamma ray and neutron (API) values is evident. A high neutron API value means low porosity, therefore, porosity increases with increase in gamma ray count. Also, note a good correlation in neighboring Double "L" field (C & D).

Gamma Ray Logs

Gamma ray logs, that measure the natural radioactivity of rocks, were introduced in 1939 by Well Surveys, Inc. as a technique that could determine the lithology of cased wells that had never been logged before (Pirson, 1963). These are termed "natural gamma ray" logs and are different from the induced gamma ray logs discussed above. Such a gamma ray log is a record of a formation's radioactivity.

The following general discussion about gamma ray logs is mainly extracted from Rider (1986). Gamma rays are bursts of high energy electromagnetic waves which are highly penetrating even in dense matter. The radiation emanates from naturally occurring potassium and uranium and thorium, and nuclides in the decay chains of uranium and thorium in the formation. The geological significance of the radioactivity lies in the distribution of these three elements among the sedimentary rocks. Shales have the strongest radiation signature. It is for this reason that the simple gamma ray log has been called the "Shale Log," although it is quite insufficient to equate gamma ray emission with shale occurrence. Not all shales are radioactive, and all that is radioactive is not necessarily shale.

Gamma ray logs are affected to a certain degree by borehole diameter, mud additive (KCl), adjacent beds, bed thickness, casing and cement thickness, and the instrument used. Several correction techniques for these effects are available in the industry (Schlumberger, 1987). Logging speed is also very important in controlling the log behavior. Because gamma-ray radiations are discrete events, and are measured in the gamma ray tools by counting, there are restrictions on logging speed. A gamma ray tool that is pulled up too fast along the hole shows two defects: the shape of the beds is distorted and the full gamma ray count value is not achieved.

Modern gamma ray logs have some quantitative uses. Modern gamma ray logs are used to calculate the volume of shale in the formation, so that the neutron porosity can be corrected for the volume of shale present. The spectral gamma ray log can also be used to calculate the volume of radioactive minerals. Qualitatively, gamma ray logs can be used to identify lithology, mineralogy, unconformities, and facies; and are used to

correlate the facies between wells.

Since its inception in 1939, the gamma ray has been used primarily as a qualitative shale log. The earlier logs used Geiger counters or ionization chambers to detect the natural radioactivity of the formation (Pirson, 1963). Prior, to the 1960s the logs were run too fast (reducing the vertical bed resolution) and most of the counters were not efficient, resulting in relatively large statistical errors (Hilchie, 1982).

The gamma ray logs available from the Sulimar Queen field have several problems:

1. the logs were run by seven companies with different calibrations, sensor settings, and scales,
2. some of the logs had no scale; therefore, an arbitrary scale of 0 -100 API was used,
3. the statistical variations were enormous, making it difficult to decide which run to select,
4. although for most of the logs the logging speed was within the established limits, some logs were run fast. High speed decreases the vertical resolution of the beds and causes the gamma ray count to be low.

Due to these problems, the information from each well was not comparable (Figure 3.4). Anhydrite exhibits one of the lowest gamma ray values that should range between 0 - 10 API units (Dewan, 1983). But in some old gamma ray logs, the gamma API values in the anhydritic zones were higher (Figure 3.4C & 3.4D) than the sand zones in other wells (Figure 3.4B). Under these circumstances the old gamma ray could not be used to predict the reservoir properties, especially porosity, because the porosities predicted in the anhydritic zone in one well would have been higher than the porosities predicted in the sand zone of the other well.

The information about the tops of the formations was available from the drilling reports and scout cards, which helped to locate the Shattuck zone in the logs in cases where the anhydritic portion showed high gamma ray values. Neutron logs were also of qualitative assistance in identifying the reservoir zones throughout the field.

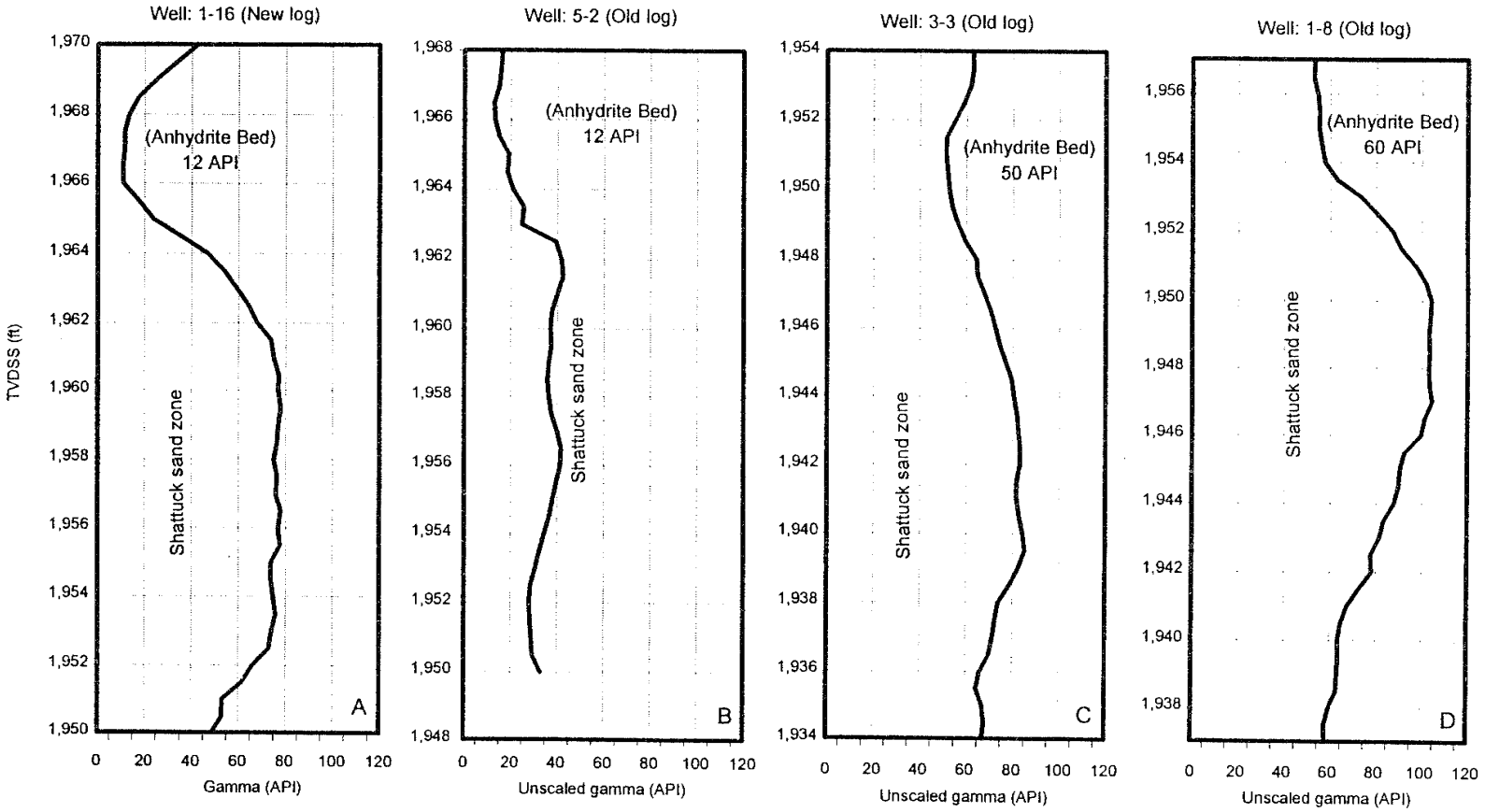

Figure 3.4: Comparison of new (A) and old gamma ray logs (B, C, D). Note the anomalously high gamma ray value in the anhydritic zone (C & D) and very low gamma ray values in the Shattuck sand zone (B).

In the absence of all other logs, it was critical to use the gamma ray logs as efficiently as possible, if reliable geologic characterization of the reservoir was to be accomplished. We needed to rely heavily on the logs, as they provided the only spatial measurement in the field. The gamma ray logs had problems, but these problems were not as severe as in the case of the neutron logs. Gamma ray logs had a small scale range (2 - 114 API units), whereas neutron logs have a large scale range (0 - 3,000 API units). The relative shape (not the API values) of the gamma ray logs were also consistent in each well, with low gamma values in the anhydritic portion and high values in the Shattuck sand zones (Figure 3.4). Because logging was carried out in cased holes, the gamma ray log is more reliable than the neutron log. The main problem with the gamma ray logs was their variable scale. Therefore, it was decided to increase the reliability of the old gamma ray logs by rescaling them to a common, known datum using the technique described by Barrett (1994).

Rescaling of old gamma ray logs

In order to make old gamma logs useful and reliable they should be normalized/rescaled using the modern calibrated logs, so that the information given by each well become comparable (Barrett, 1994). In Barrett's (1994) technique, several modern logs are needed to determine the representative value ranges of the logs in that area. The procedure used for the rescaling old gamma ray logs is described in the following section.

1. Modern logs were used to find the average high and low gamma ray value in the zone of interest. Four modern gamma ray logs (run after 1985) were available (Figure 3.5).

Histograms for the four modern gamma ray logs were compared to find the logging tool calibration and the representative histogram and its associated value ranges (Figure 3.6). To determine the value range, the histogram must include the productive interval along with the cap or nonreservoir units. The information related to the year the well was logged, value range, mean, and standard deviation for the Shattuck Member obtained from the modern logs are given in Table 3.3. Note the similarities in the gamma

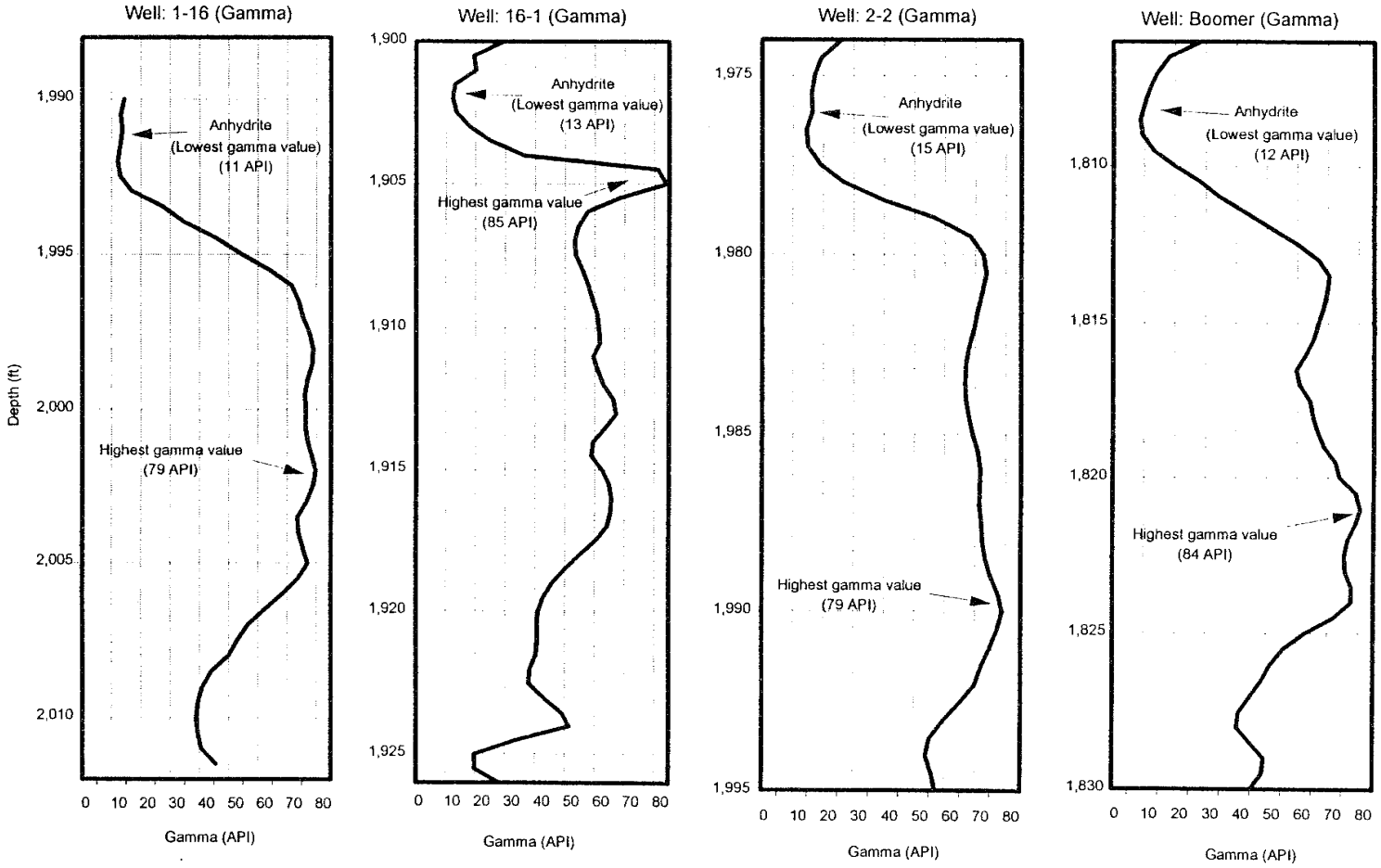

Figure 3.5: New gamma ray logs used to calculate the new high and low gamma ray values in the Shattuck Member in the Sulimar Queen field.

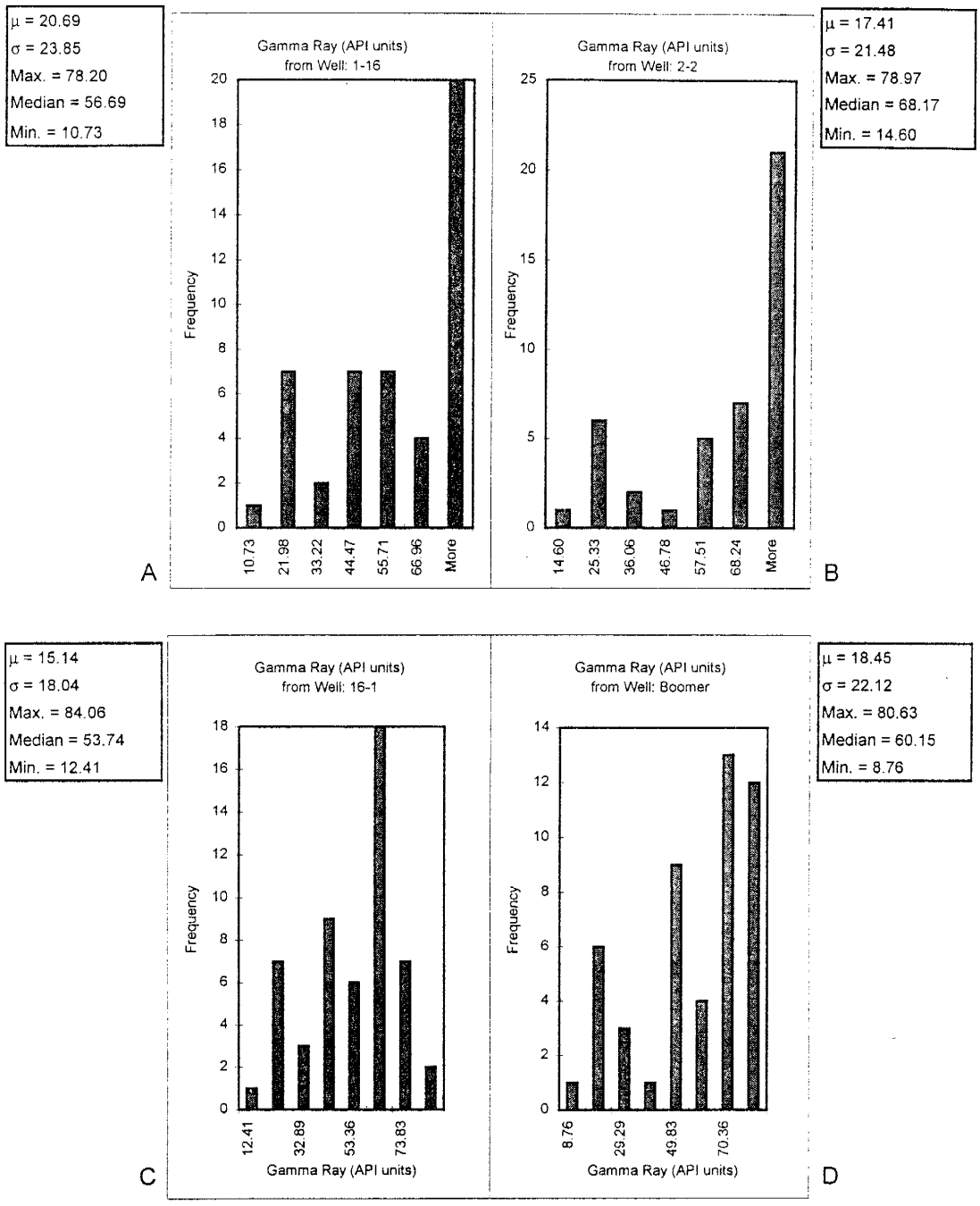

Figure 3.6: Histograms of modern gamma ray logs. Note the similar minimum and maximum value ranges. Average of the minimum and maximum of the four wells were used for the rescaling of old gamma ray logs.

Well	Year Drilled	Range (API)	Mean	Standard Deviation
1-16	1991	11 - 79	51	25
2-2	1990	15 - 79	47	20
Boomer	1990	12 - 84	50	24
16-1	1985	13 - 85	55	24

Table 3.3: Summary of the ranges, mean, and standard deviation for the Shattuck Member in modern gamma ray logs.

ray API value ranges, means, and standard deviations for the reservoir zone including the anhydritic cap (Table 3.3). The differences in range, mean, and standard deviation from different wells are within 15%, suggesting good calibration of the tools. For the old gamma ray logs from 36 wells, the gamma ray API value range was between 2 - 114 API units (Table 3.4). The mean values from different wells ranged between 20 - 70 API units and the standard deviation ranged between 10 - 34 API units, suggesting poor calibration of the tool. The data summary is given in Table 3.4.

In the Sulimar Queen field the presence of a 8 - 10 foot thick anhydrite bed above the reservoir provided the average low value of 12 API and an average high value of 80.5 API was found within the Shattuck Member (Figure 3.6).

$$New\ Average\ Low = 12\ API\ units$$

$$New\ Average\ High = 80.5\ API\ units$$

2. Once the new high and new low gamma ray values for the entire field are obtained, m for each well containing old gamma ray log can be calculated using the following relationship:

$$m = \frac{(new\ average\ high - new\ average\ low)}{(old\ average\ high - old\ average\ low)} \qquad (1)$$

old high and lows are different for different wells.

3. In this step b for each well containing old gamma ray logs is calculated using the following relationship:

$$b = new\ high - [m\ .\ (old\ high)] \qquad (2)$$

4. Once m and b for each well is obtained the old logs can be rescaled using the

Log Types	Scale Range (API units)	Range of Average Values (API units)	Range of Standard Deviation (API units)
Old Gamma Ray Logs (36 wells)	2 - 114	20 - 70	10 - 34
Rescaled Gamma Ray Logs (36 wells)	9 - 82	38 - 60	18 - 27
New Gamma Ray Logs (4 wells)	9 - 84	47 - 55	20 - 25

Table 3.4: Summary of the old, rescaled, and modern gamma ray log data. Note the similarity in the rescaled and new gamma ray log data. The rescaling of the old logs made them comparable with the new logs, as well as with each other.

following equation:

$$(Rescaled\ value)\ Y = mx + b \qquad (3)$$

where x is the old gamma ray value in API units at a particular depth.

Rescaling Example for Well 1-14:

New High = 80.5 API Units	New Low = 12.00 API units
Old High = 80.74 API units	Old Low = 34.46 API units

$$m = \frac{(80.5 - 12.0)}{(80.74 - 34.46)} = 1.48$$

$$b = 80.5 - [1.48\ (80.74)] = -39$$

Using m and b, the complete gamma ray log in Well 1-14 was rescaled (Figure 3.7A). Figure 3.7 shows the rescaling in wells 1-14 and 5-1. All the old gamma ray logs were rescaled by linearly shifting their histograms to match the modern gamma ray logs (Figure 3.8) (Appendix B).

Effects of rescaling

1. The increase in the reliability of the old gamma ray logs after rescaling is evident by the similarities of the scale ranges, mean, and standard deviation of the rescaled gamma ray logs with the new logs (Table 3.4).
2. Old logs from different wells became comparable to each other as well as with the

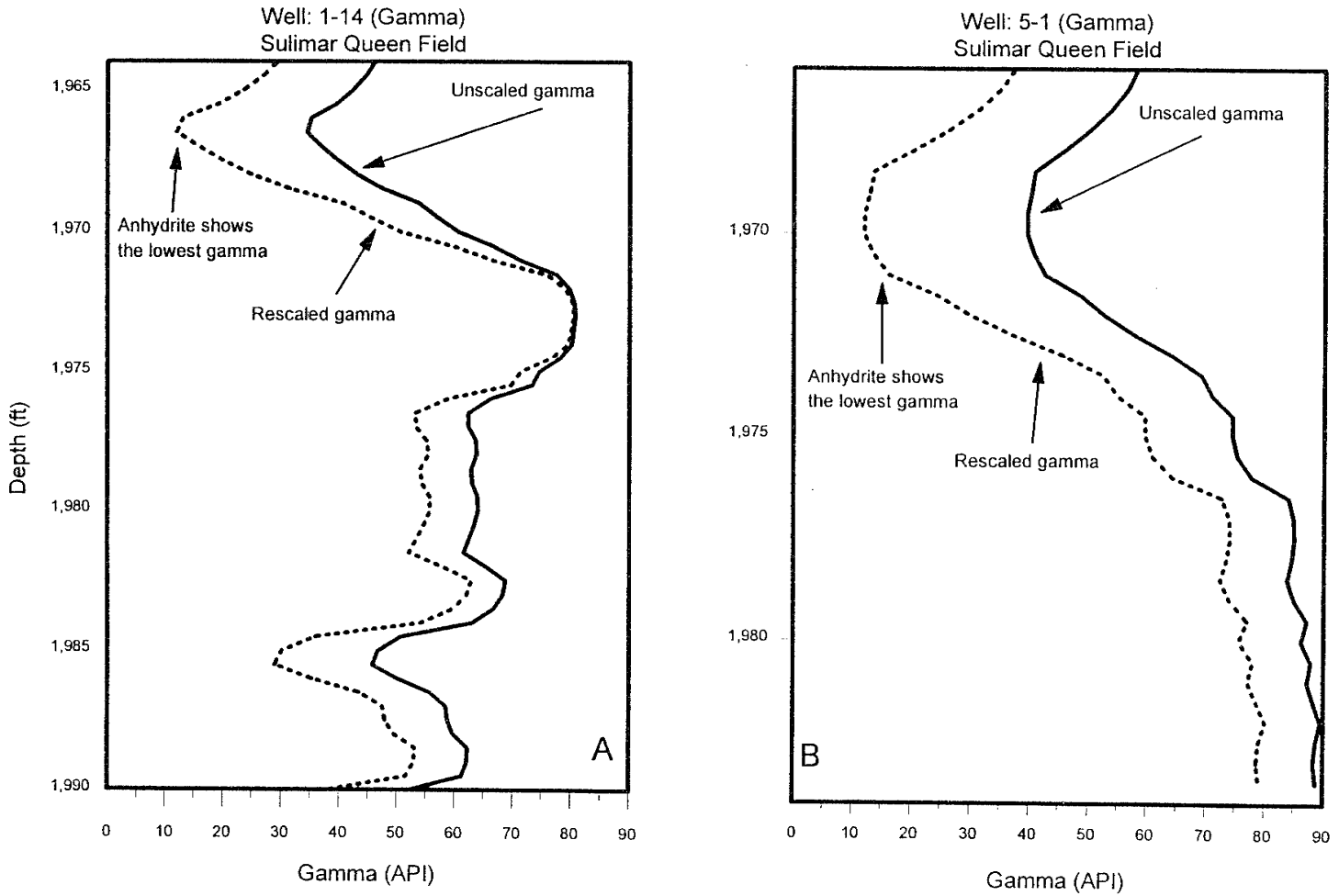

Figure 3.7: Comparison of unscaled and rescaled gamma ray logs. The rescaled logs have the minimum of 12 API and maximum of 80 API values. Note the identification of anhydritic portion in the rescaled gamma ray logs that were not easily identifiable in unscaled logs.

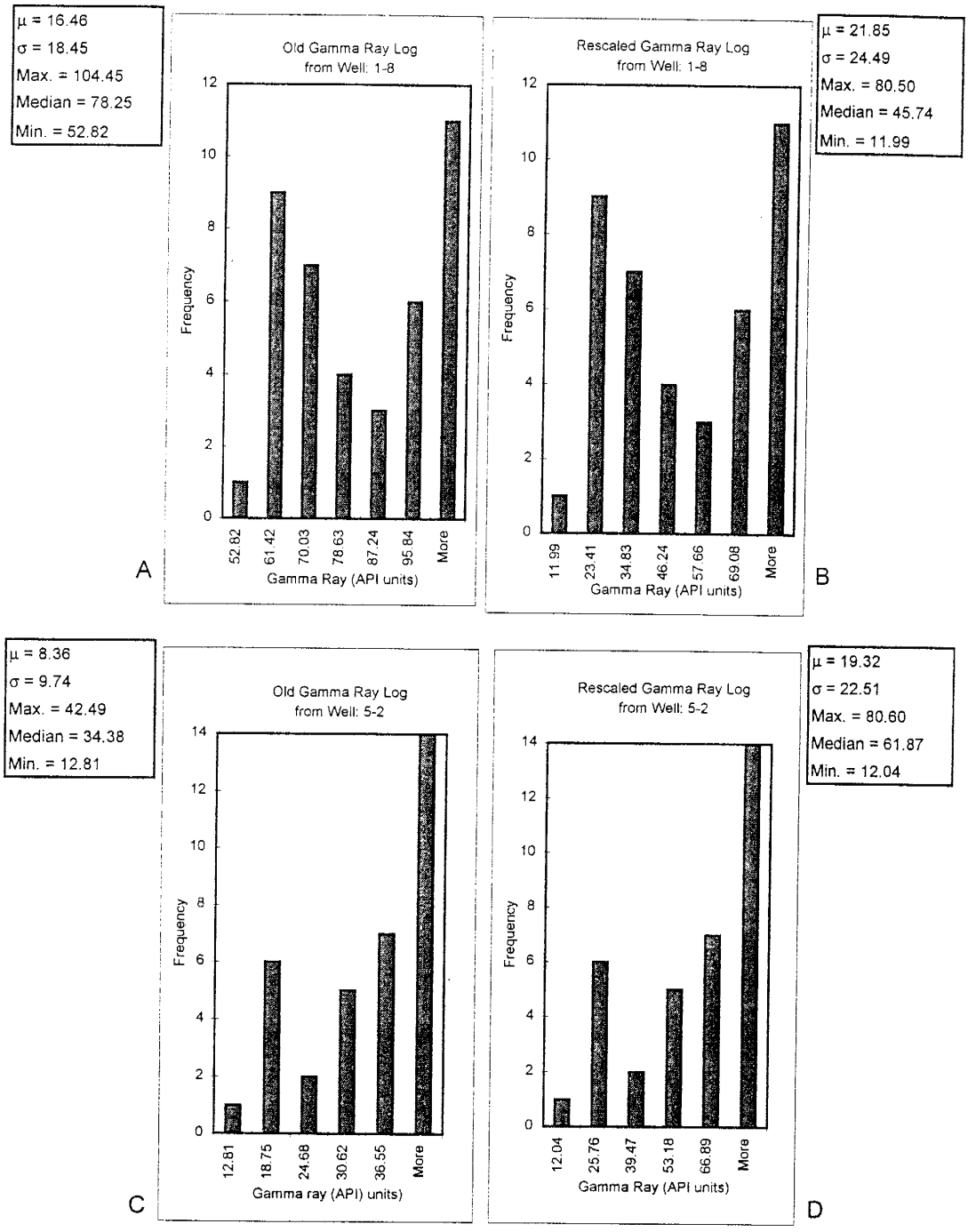

Figure 3.8: Comparison of the unscaled and rescaled gamma ray log histograms. Note the shift of data ranges from (A) to (B) and (C) to (D). Rescaling made the the old logs similar to the modern logs by bringing the low value to 12 API and high value to 80 API.

modern logs.

3. Figure 3.9 shows the improvement in the correlation coefficient between core porosity and gamma ray values, after rescaling. A comparison between the porosities derived from unscaled and rescaled gamma ray logs with the core porosities in wells 1-14 and 5-1 is given in Table 3.5. It is clear from the table that the porosity values predicted using the unscaled gamma ray logs are consistently higher than the core porosity, as evident from the residuals (Table 3.5). Also, the standard deviations for porosities derived from unscaled gamma ray logs is much higher than those derived from rescaled logs (Table 3.5).
4. Rescaling also made the gamma ray logs more useful for correlation as the individual zones became more obvious (Figure 3.10).

Relationship between gamma ray API values, porosity, and total water content

Based on the information obtained from the relationships between old gamma ray API values and neutron API values (Figure 3.3), the relationship between core porosity and gamma API values was also investigated (Figure 3.11). This was done in order to use the rescaled gamma ray logs for the prediction of petrophysical properties.

A positive correlation was observed between the core porosity and gamma ray values in the Sulimar Queen (Figure 3.12A), Queen (Figure 3.12B), Double "L" (Figure 3.12C), and South Lucky Lake (Figure 3.12D) fields. The similar positive relationships between gamma ray values and porosity in different fields suggested that this positive relationship is regional. As mentioned earlier, the core and modern logs were available only from one well (1-16); therefore, presence of this similar relationship between gamma ray values and total porosity in adjacent fields suggested that information from Well 1-16 may be applied throughout the field with relative confidence.

This positive relationship between porosity and gamma ray values is only good for the sand portion of the Shattuck Member as determined from the core description. In the Shattuck sand zone, the gamma-ray values are not controlled exclusively by the amount of clay as revealed by X-ray diffraction analysis. In fact, the gamma ray response is

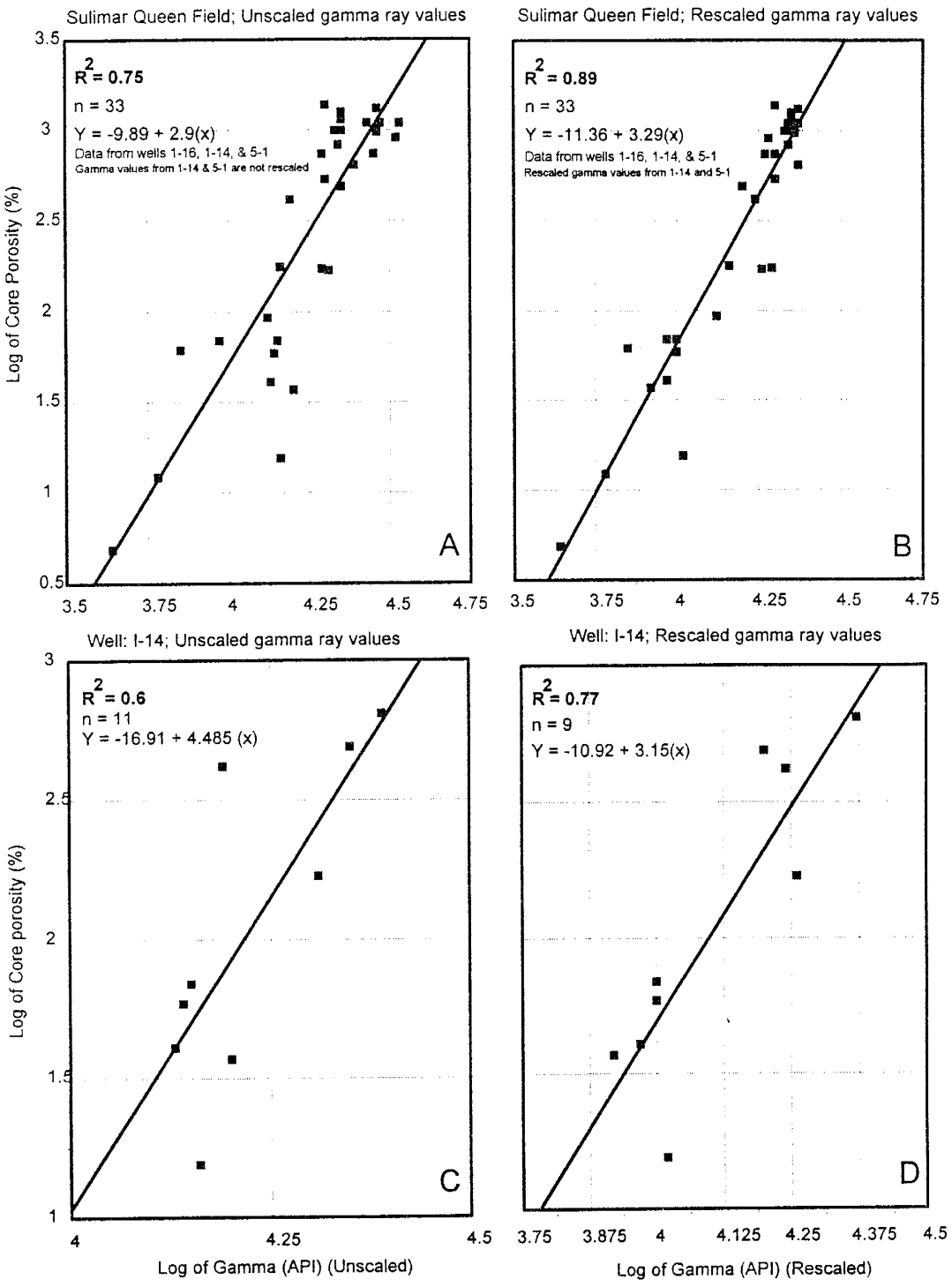

Figure 3.9: Plots showing the effects of rescaling on the correlations between core porosity and gamma ray values. Note the improvement of correlation from (A) to (B) and (C) to (D).

S. No	Well 1-14 (Sulimar Queen Field)					Well: 5-1 (Sulimar Queen Field)				
	Core Porosity (%)	Rescaled gamma derived porosity (%)	Residuals (Rescaled gamma derived porosity)	Unscaled gamma derived porosity (%)	Residuals (Unscaled gamma derived porosity)	Core porosity (%)	Rescaled gamma derived porosity (%)	Residuals (Rescaled gamma derived porosity)	Unscaled gamma derived porosity (%)	Residuals (Unscaled gamma derived porosity)
1	4.8	4.86	-0.06	8.18	-3.38	17.6	15.63	1.97	28.27	-10.67
2	14.7	11.4	3.3	14.54	0.16	17.7	16.8	0.9	29.8	-12.1
3	16.6	21.8	-5.2	22.57	-5.97	19.3	15.3	4	27.9	-8.6
4	9.3	14.51	-5.2	17.12	-7.82	21	19.6	1.4	33.31	-12.31
5	13.8	13.2	0.6	16.06	-2.26	21	20.6	0.4	34.6	-13.6
6	5	5.6	-0.6	8.99	-3.99	20.5	21.3	-0.8	35.4	-14.9
7	6.3	6.2	0.1	9.62	-3.32	21.1	21.8	-0.7	36.1	-15
8	5.9	5.8	0.1	9.25	-3.35	22.7	21.9	0.8	36.2	-13.5
9	3.3	6.3	-3	9.77	-6.47					
Mean	8.85	9.96		12.9		20.11	19.11		32.7	
Standard deviation	4.9	5.85		6.54		1.8	2.97		13.9	

● Standard deviations are calculated using the mean of core porosities.

● Residuals = core porosity - log derived porosity

Table 3.5: Summary of the porosities calculated using the unscaled and rescaled gamma ray logs. Porosities determined using the rescaled logs are very similar to the core porosities. Note high residuals and standard deviations in case of unscaled gamma derived porosities.

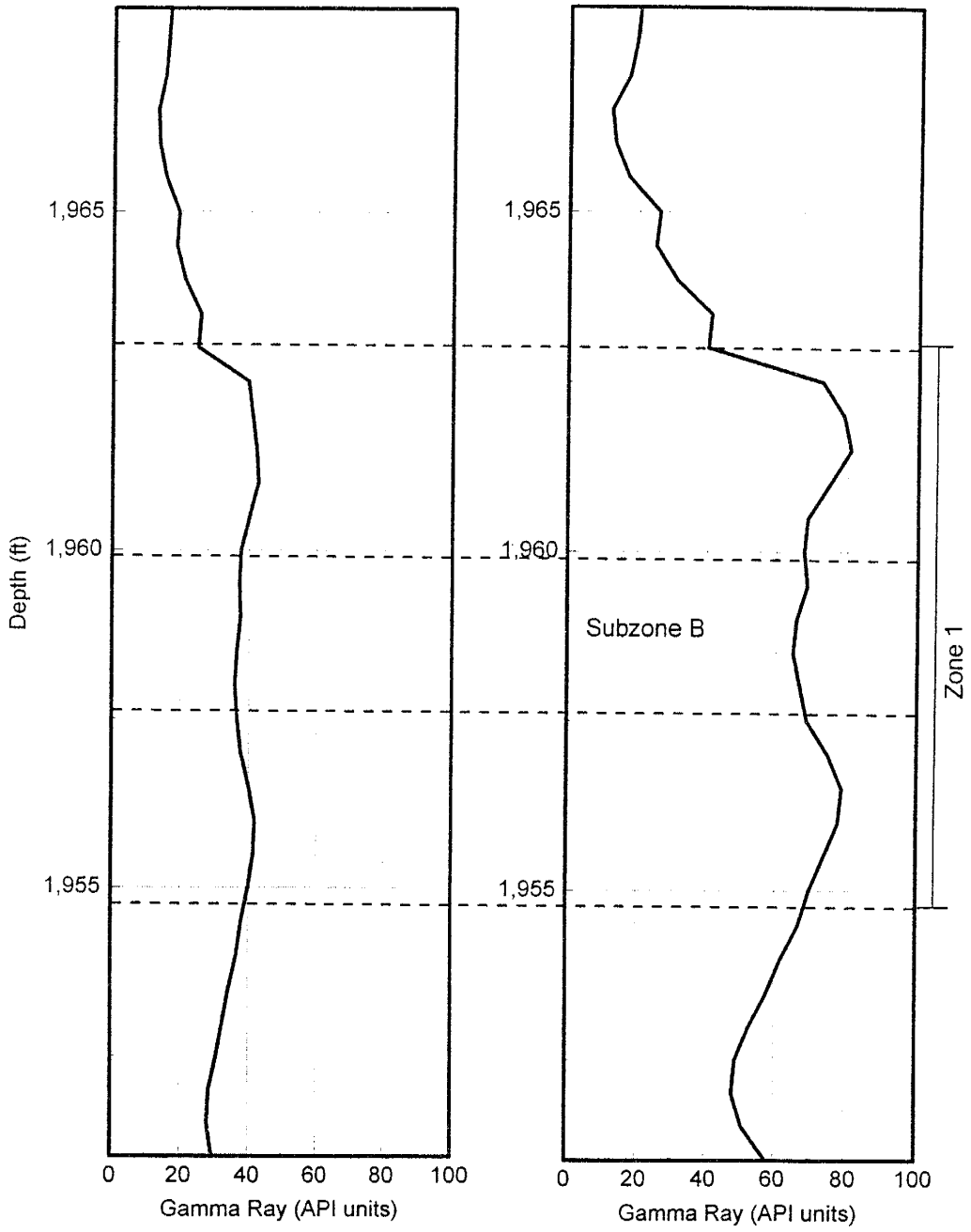

Figure 3.10: Showing the effects of rescaling on the identification of individual zones in Well 5-2.

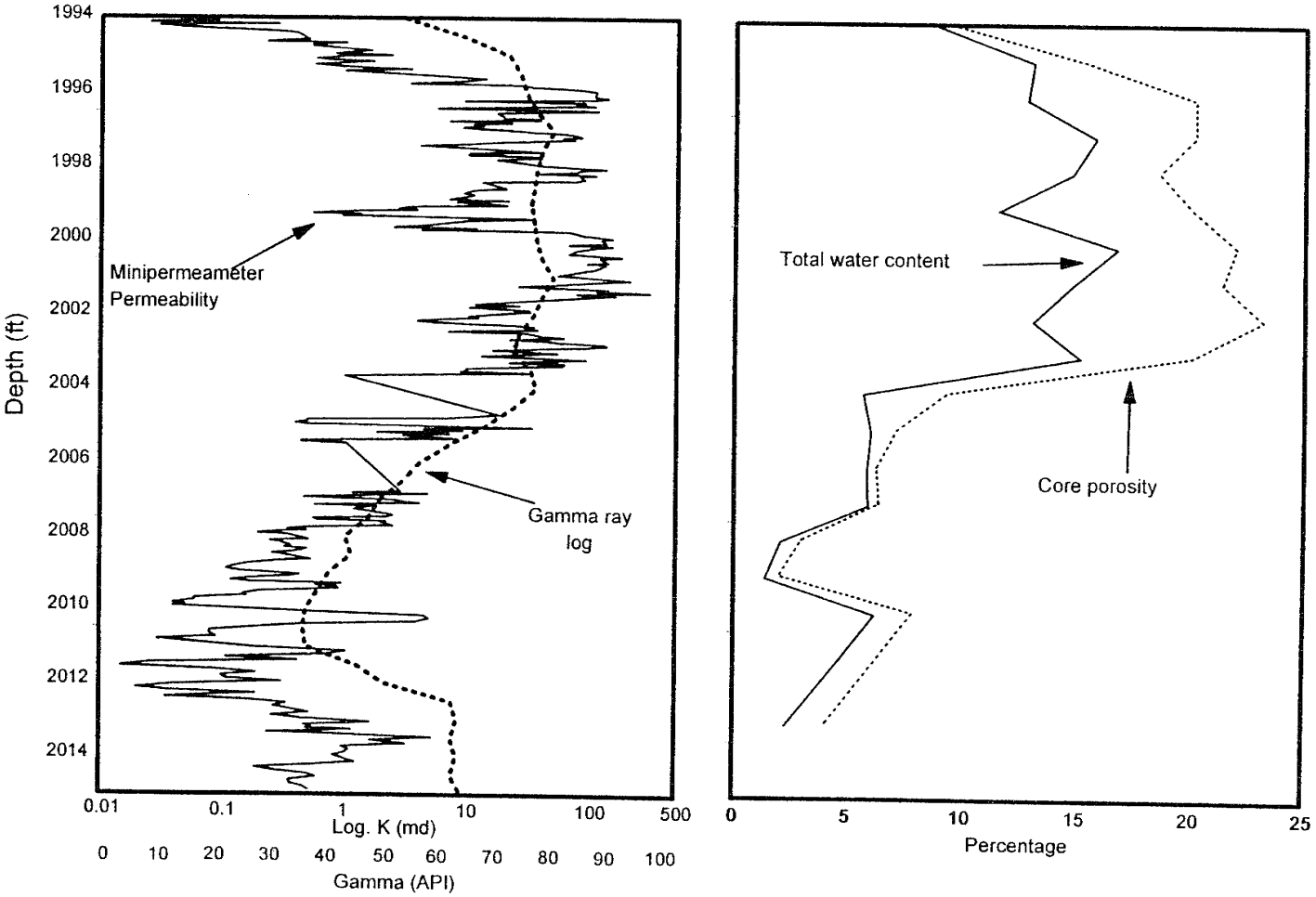

Figure 3.11: Plots showing the distribution of permeability, gamma ray, porosity, and total water content in Well 1-16 in the Sulimar Queen field. All parameters have the similar behavior.

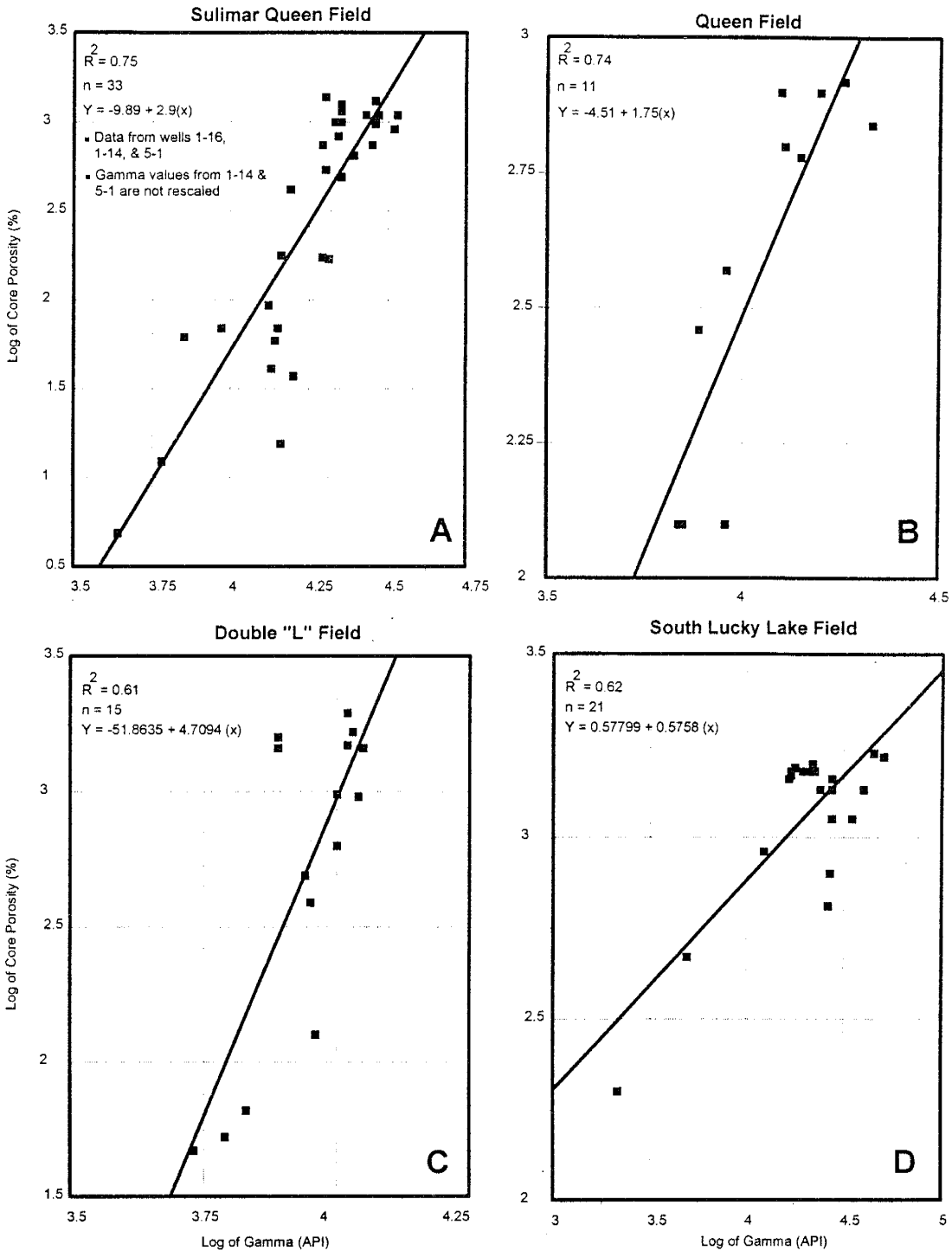

Figure 3.12: Plots showing positive correlations between gamma ray values and core porosities from Sulimar Queen (A) and three adjacent fields (B, C, & D). The data for the Sulimar Queen field consists of three wells (A).

controlled by the amount of uranium present, which was confirmed by the spectral gamma ray from one well in the Queen field (Figure 3.13). Unfortunately, in the Sulimar Queen field, spectral gamma ray log was not available in the Well 1-16 where core porosity, water saturation, permeability were available. A spectral gamma ray log from Well 16-1 in the Sulimar Queen field shows the presence of uranium in the Shattuck Member, but no porosity or water saturation was available (Figure 3.14) for cross-referencing. The uranium is assumed to be present in the formation water since gamma ray values are proportional to total water content (W_{TC}) (Figure 3.15).

The total water content represents the percentage of the total rock volume occupied by water:

$$W_{TC} = \frac{S_W}{100} \Phi \ (percentage)$$

The conventional way of representing the water saturation (S_W) as the percentage of porosity occupied by water was not used because of its inadequacy in conveying the amount of water present. For example, a 5% porosity with water saturation of 90% contains less volume of water than 20% porosity with only 35% water saturation. If we use the conventional representation of the water saturation, the relationship between gamma-ray response and volume of water could not be identified correctly (Figure 3.16). We suggest the use of total water content instead of conventional water saturation in order to understand the effect of radioactive species dissolved in water on the gamma ray behavior (Figure 3.16).

Relationship between air permeability and gamma ray values

Permeability measurements were made on the available core on a spacing of 0.5 inch using a minipermeameter. For the minipermeameter details see Chapter 2. Because the gamma-ray log data was available at a 0.5 foot interval, the permeability measurements were averaged on a 0.5 foot interval and plotted against the gamma-ray

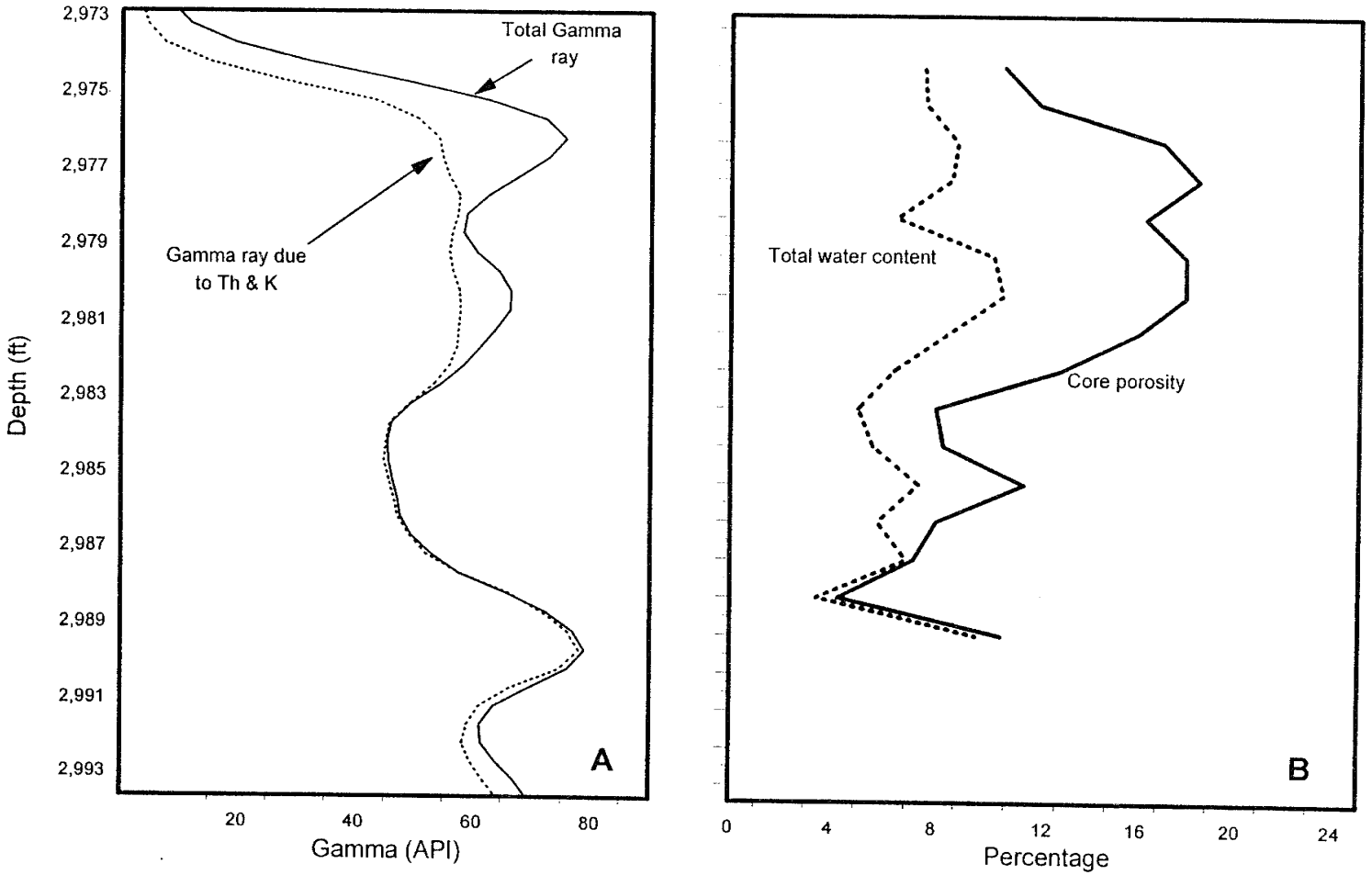

Figure 3.13: Plots showing the distribution of spectral gamma ray (A) and porosity and total water content (B) in the Queen field. Note as the porosity and total water content increase so does the total gamma ray response.

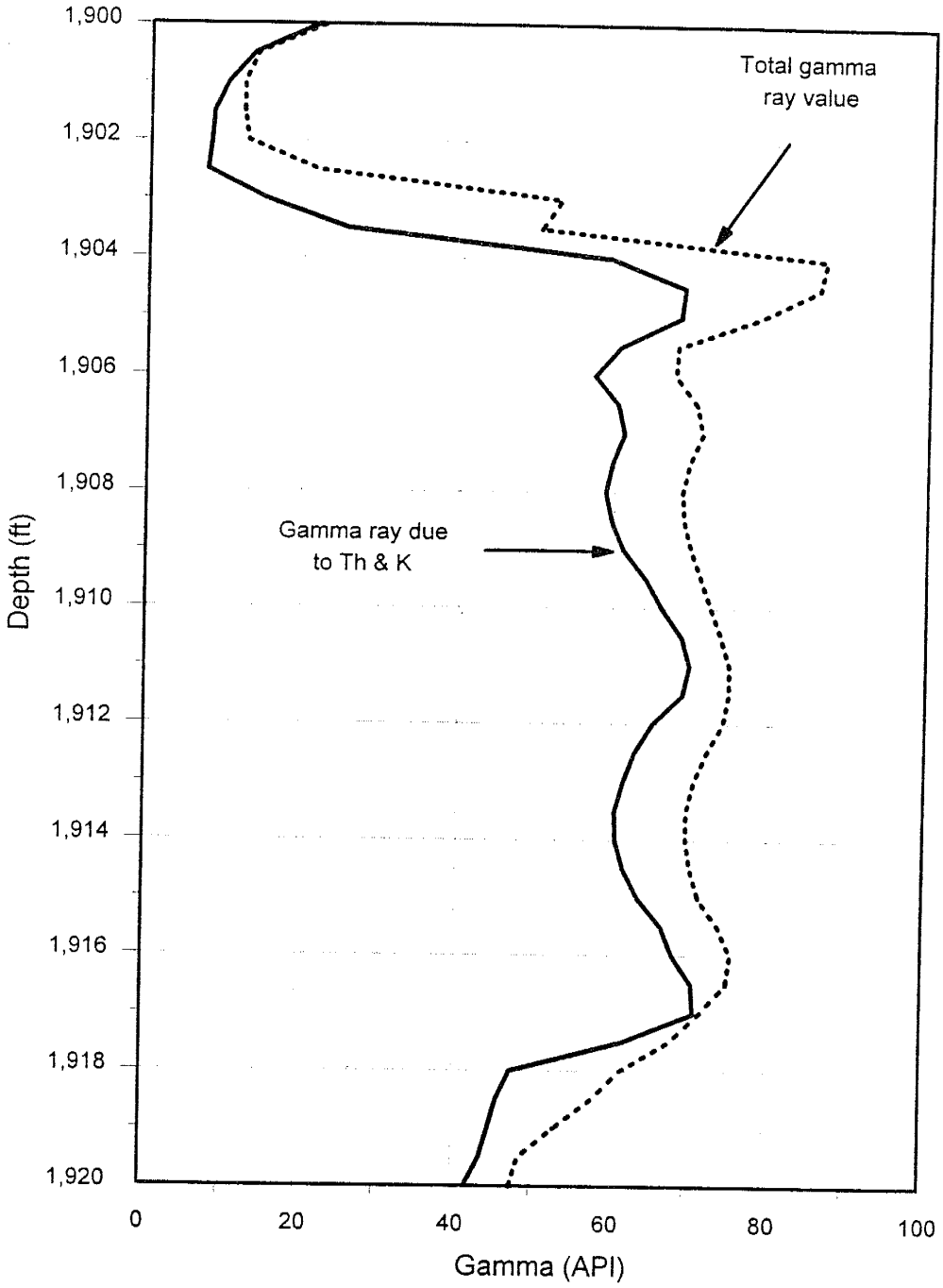

Figure 3.14: Spectral gamma ray log (Well: 16-1) of the Shattuck Member in the Sulimar Queen field. Note the separation in the total gamma (Uranium + Thorium + Potassium) and gamma ray due to Thorium + Potassium.

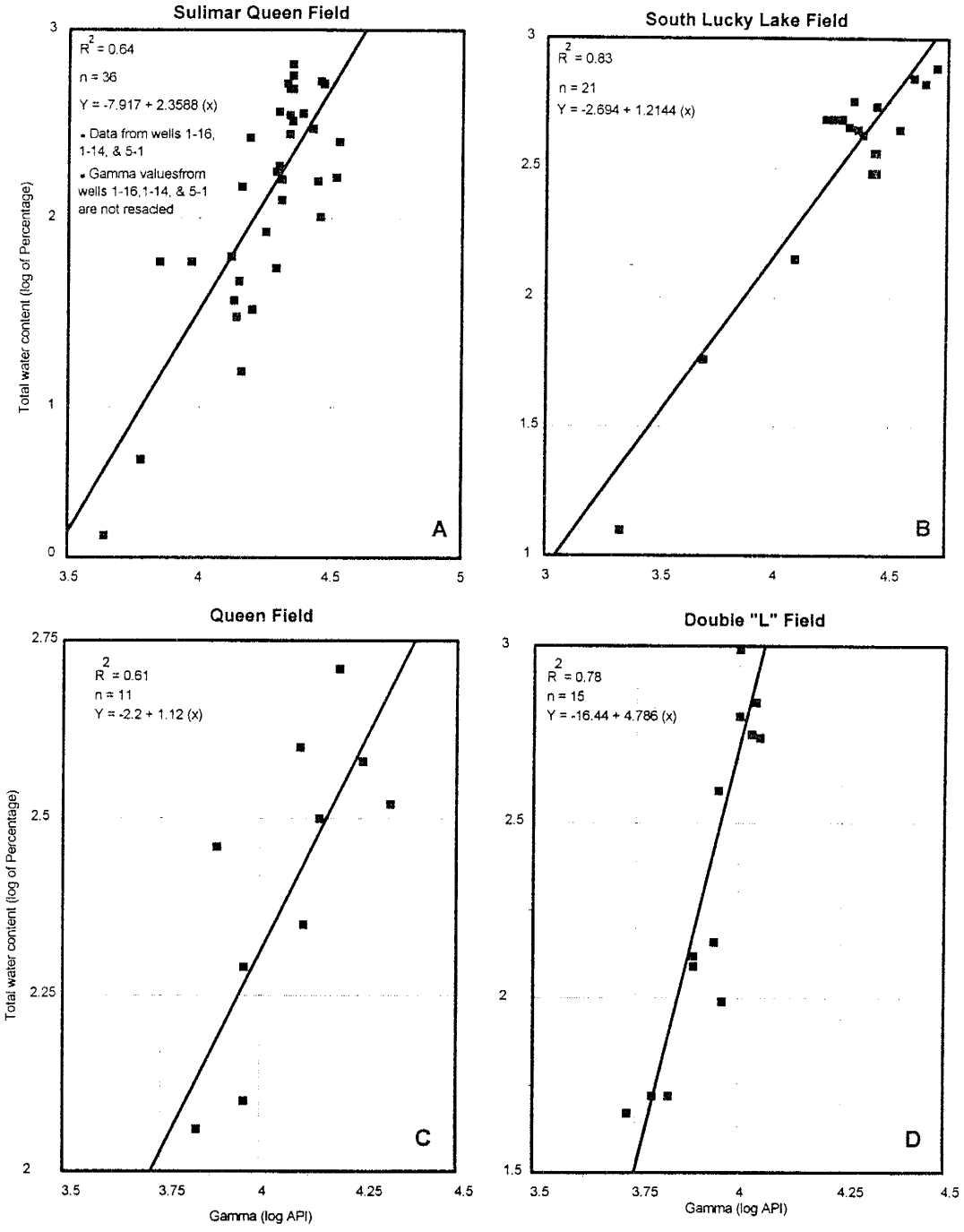

Figure 3.15: Plots showing positive correlations between gamma ray response and total water content from Sulimar Queen (A) and three adjacent fields (B, C, & D).

Gamma Value (API units)	Porosity (%)	Water Saturation (%)	Total Water Content (%)
64.0	9.5	93.0	8.8
74.0	15.4	85.0	13.1
77.0	20.2	78.0	15.7
78.0	20.2	64.0	12.92
76.5	18.6	79.0	14.6
76.5	20.1	58.0	11.66
78.0	22.0	76.0	16.7
78.0	21.4	69.0	14.8
74.0	23.2	57.0	13.2
76.0	20.1	76.0	15.3
73.0	9.4	61.0	5.7
61.5	7.2	84.0	6.1
53.0	6.3	93.0	5.86
47.0	6.4	93.0	5.9
44.0	3.0	68.0	2.06
38.0	2.0	69.0	1.38

A

* 6.4% porosity with 93% water saturation contains less water than a 20.2% porosity with only 64% water satutration

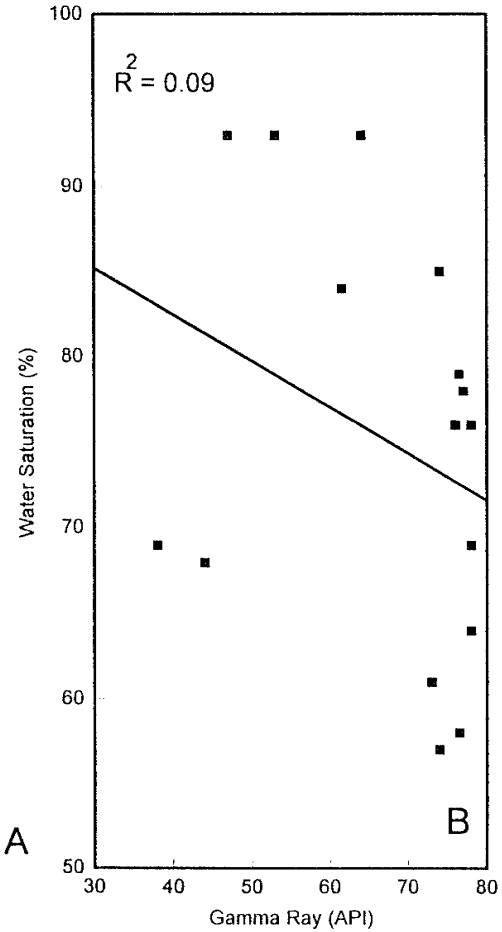

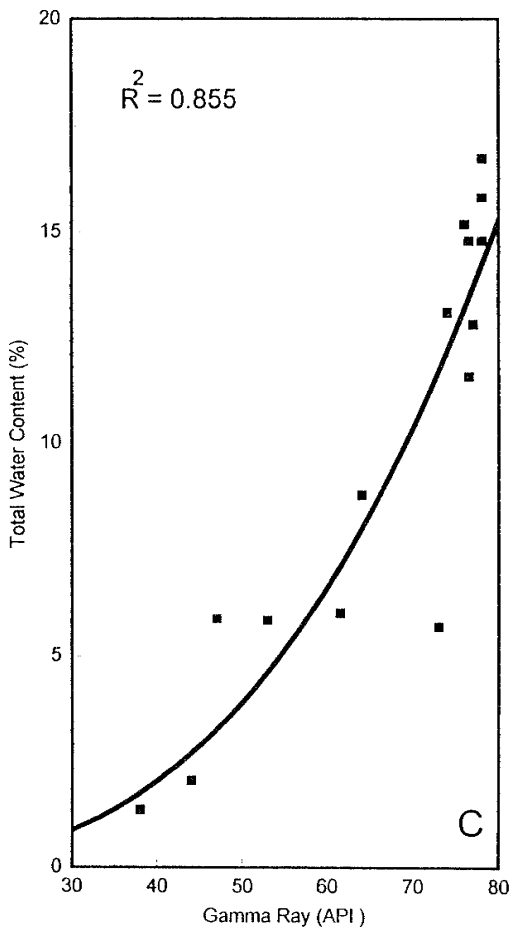

Figure 3.16: Relationship of gamma ray response with water saturation and total water content in Well 1-16. Summary of the data is given in (A). Conventional representation of water saturation does not convey the original amount of water. Gamma ray response and water saturation show a negative relationship (B), whereas, total water content and gamma ray shows a good positive correlation (C).

values. A good correlation was obtained in the Sulimar Queen (Figure 3.17A) and adjacent fields (Figures 3.17B & 3.17C).

A relationship between gamma-ray derived porosity and air permeability appears to be more reliable because it covers the whole permeability spectrum. When, permeability was predicted using gamma-ray values and the relationship in Figure 3.17A, the highest predictable permeability value was only 46 md. Whereas, when gamma-ray derived porosity and the relationship in Figure 3.18 was used, the highest permeability value predicted was 116 md, which is close to the minipermeameter measured permeabilities. Unfortunately, due to a lack of core material in Sulimar Queen field, the reliability of the permeability prediction could not be confirmed.

CONCLUSIONS

Old gamma-ray and neutron logs were the only log types available for the characterization of the Sulimar Queen field. Neutron logs were discarded due to a lack of reliability. Consistent and reliable gamma-ray logs were obtained by rescaling/normalizing old gamma ray logs using modern calibrated logs. Acknowledging that the logs were the only spatial control points, we established the presence of similar relationships between gamma ray values, porosity, total water content, and permeability in the Sulimar Queen and adjacent fields. This increased our confidence in applying the correlations developed in Well 1-16 throughout the field.

In the absence of other information, logs may be used unconventionally, if a particular reservoir exhibits certain features and properties that can be identified and associated with a certain log type. It is important to investigate the cause and effect relationship of a particular log response. Total water content (W_{TC}) should be used instead of conventional water saturation (S_W) in order to understand the effect of water content on a well log.

Rescaled gamma-ray logs were used to understand the distribution of porosity and total water. For the first time, gamma ray logs were used to predict porosity and total water content.

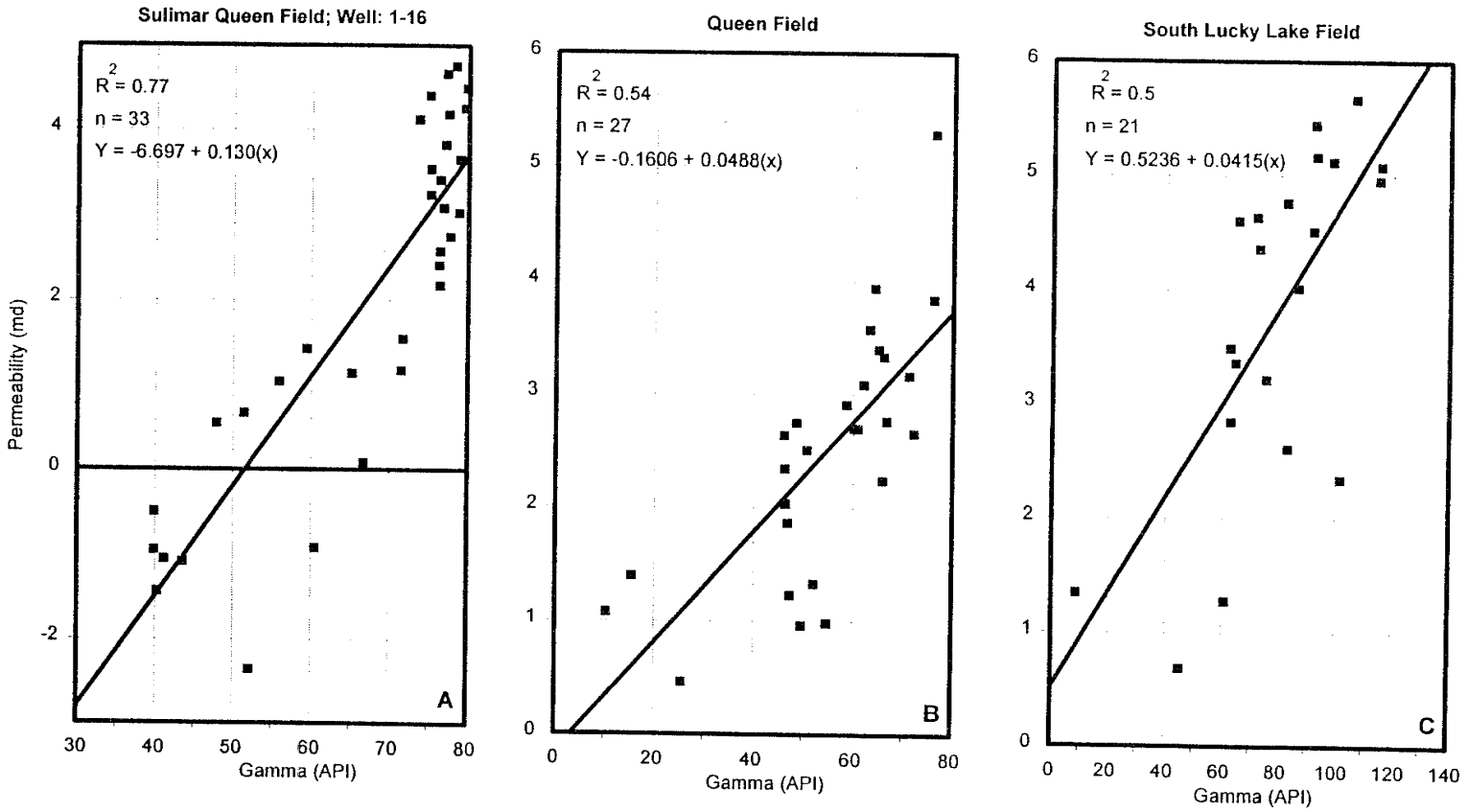

Figure 3.17: Plots showing the positive correlations between Gamma (API) values and air permeabilities. Adjacent fields also exhibit a good positive correlation (B & C).

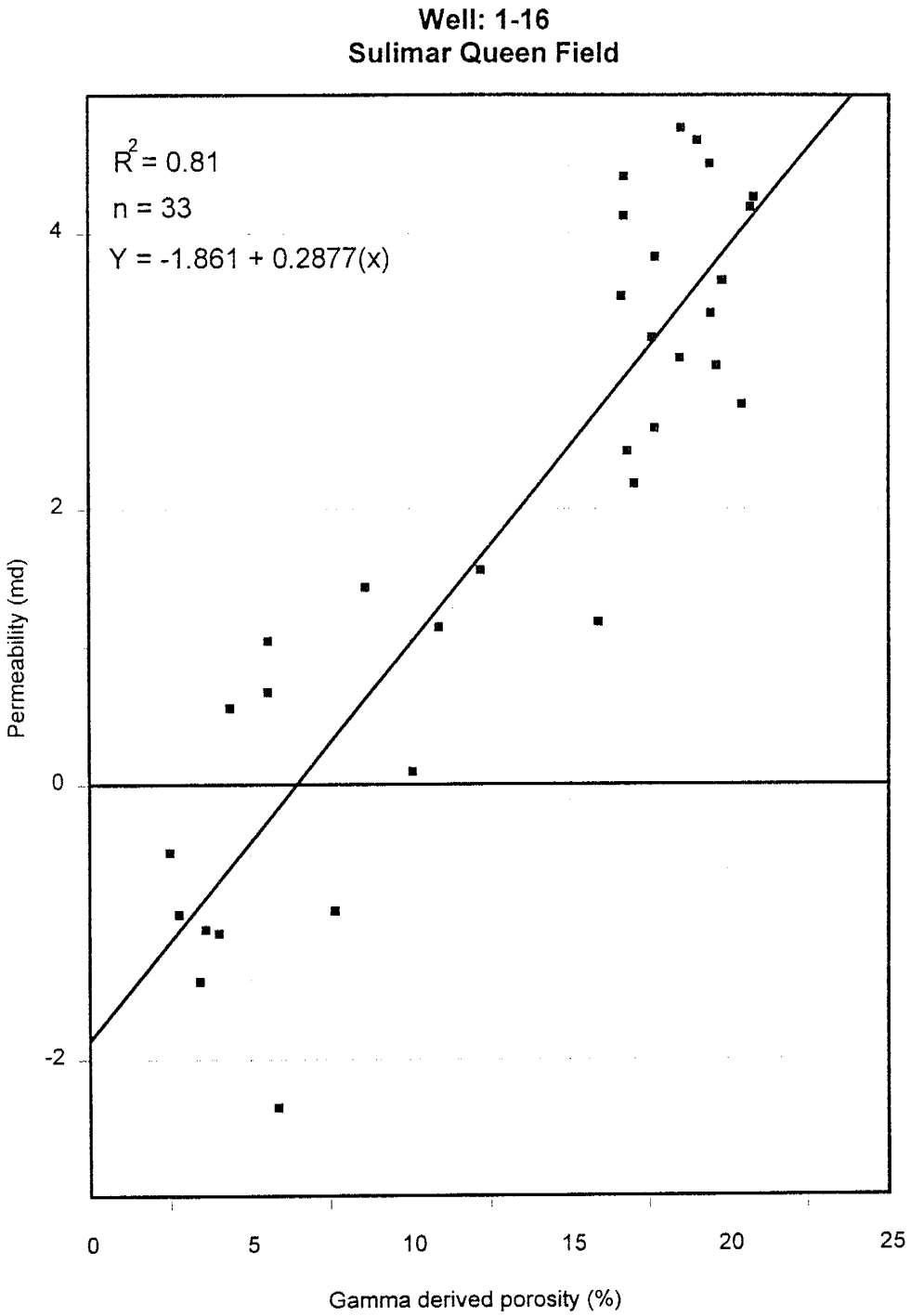

Figure 3.18: Plot showing the relationship between gamma ray derived porosity and air permeabilities. This relationship can be used to predict permeability in the field.

Another important observation of this study is that adjacent fields producing from the Shattuck Member also exhibit similar relationships between gamma ray, porosity, water saturation, and permeability. Therefore, in other Shattuck Member reservoirs, these relationships may be developed and used for improved geological characterization of fields, especially in the absence of reliable information.

Realizing the value of rescaling and building unconventional relationships between logs and reservoir properties, the PRRC (New Mexico Tech) has adopted this methodology for similar old fields in New Mexico.

PART III

CHAPTER 4: GEOLOGIC MODEL FOR THE SULIMAR QUEEN FIELD*

INTRODUCTION

The Queen Formation (Permian, Guadalupian) is a sequence of interbedded arkosic sandstones, silty sandstones, dolomitic mudstone, and evaporites that extends across a large part of the subsurface of the Permian Basin of southeast New Mexico and west Texas (Moran, 1954) (Figure 1.3A). The formation is part of the Artesia Group (Tiat et al., 1962), which is the back-reef facies of the Capitan-Goat Seep Reef complex that surrounded the Delaware Basin during the Guadalupian time (Figure 4.1). The Queen Formation was first named by Crandall (1929) for exposures near the Queen post office in Eddy County, New Mexico. Moran (1954) designated a new type section in Dark Canyon that has exposures of 421 feet of alternating sandstone and sandy dolomites. The uppermost 100 feet of sandstone is named the Shattuck Member (Newell *et al.*, 1953) with a type section on the Shattuck Valley escarpment. In the subsurface, the Queen Formation is from 300 to nearly 500 feet thick over much of the Northwest Shelf. The Shattuck Member, informally called Artesia Red Sand, thins from 100 feet near the reef at the shelf edge to about 15 to 25 feet in the Sulimar Queen and adjacent area.

In this chapter, the lithologic makeup, diagenesis, and distribution of the Shattuck Member are discussed. A model for the depositional environment and the development of reservoir through depositional and diagenetic history is proposed. Formation of the reservoir in the Shattuck Member is also discussed.

As mentioned in Chapter 1, the information available from the Sulimar Queen field is sketchy. Therefore, an outcrop study was conducted and additional cores were

---

* Ali, M., and Cather, M., *Subsurface and Outcrop Study of the Shattuck Member in the Southeast New Mexico: Implications towards Building an Improved Geologic Model for the Sulimar Queen Field*: paper in preparation for submission to New Mexico Geology.

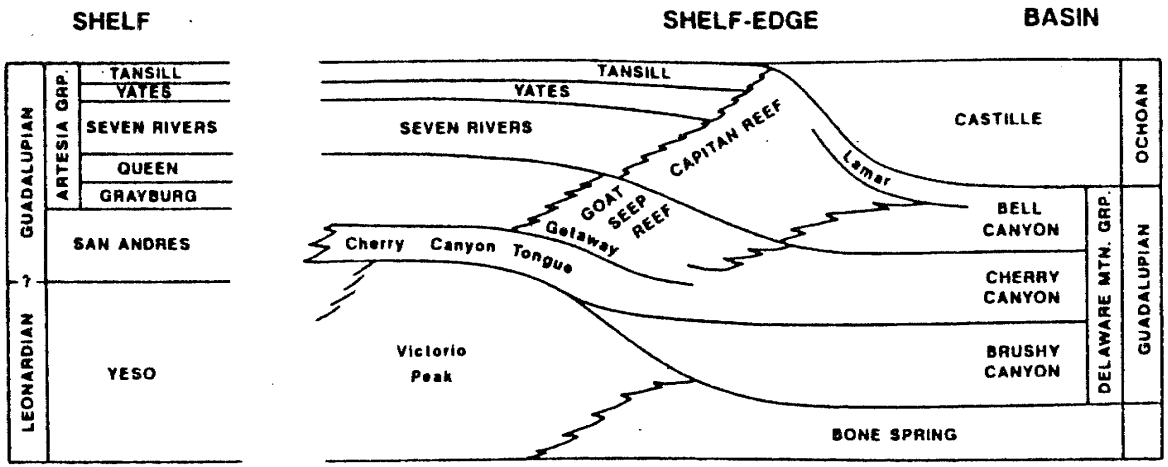

Figure 4.1: Stratigraphy of Late Permian sedimentary rocks on the Northwest Shelf and the adjacent shelf margin and basin. The Shattuck Member marks the top of the Queen Formation (Ward *et al.*, 1986).

collected from South Lucky Lake and Queen fields (Figure 1.3A). Geostatistical analyses were performed on permeability data from cores and outcrops. Geostatistical techniques were also used to generate the distribution of porosity, net thickness and structural top for the Sulimar Queen field. Before describing the details of the subsurface and outcrop studies, a brief overview of the geostatistical analysis is discussed in the following section.

GEOSTATISTICAL CONCEPTS

The application of geostatistics for reservoir description is now common. Geostatistics is a branch of statistics that considers the spatial relationship of geological variables. In many natural phenomena, measurements of a variable reveal that values measured close to each other are similar to each other. As the distance between the measurement points increases, the similarity between the points decreases. Geostatistical analyses are applied to capture such spatial relationships. Some geostatistical concepts will be described here briefly. Interested readers are referred to Journel and Huijbergts (1978) and Deutsch and Journel (1992) for further details. In applying geostatistical techniques, three basic steps need to be followed (Journel, 1989).

1. Determine Stationary Fields

Assumption of stationarity involves defining a region where the model based on sampled data is applicable. This assumption may be the most important step in geostatistical analysis. The ultimate answers that one obtains are consistent with this assumption.

Unfortunately, the assumption of stationarity is hard to prove or disprove. In reservoir data analysis, the definition of a region of stationarity is, by necessity, the entire region of interest. This may be because only few samples are available, and it is very difficult to separate them into different regions on a consistent basis. This problem may occur when examining areal or vertical data. The region of stationarity can be established by geological and statistical analysis of the data. There are different levels of stationarity.

The first order of stationarity relates to arithmetic mean being constant with the region of stationarity. For example, local means calculated in different regions within the region of stationarity should be constant. The second order of stationarity requires that the covariance is only a function of distance between two locations.

2. Spatial Analysis of Data

Once the region of stationarity is defined, spatial analysis of the data is conducted. A popular geostatistical tool for spatial analysis is the variogram. Covariance can also be used to quantify a spatial relationship. A variogram at a given distance is defined as:

$$\gamma(h) = \frac{1}{2n} \sum_{i=1}^{n} [\, V(X_i) - V(X_i + h) \,]^2$$

Where $\gamma\ (h)$ is the variogram, at the lag distance h, n is the total number of sample pairs at distance h, $V(x_i)$ and $V(x_i + h)$ form a sample pair h distance apart. Using this equation, variograms at various distances can be estimated (Figure 4.2A).

For statistically meaningful results, several numbers of pairs are needed at each lag distance. In many practical situations, however, sufficient pairs may not be available at a given distance. To eliminate this problem, a certain tolerance with respect to distance $[\gamma\ (h \pm \Delta h)]$ can be defined in the above equation (Figure 4.2B). Another restriction that can be imposed to ensure sufficient number of pairs for every lag distance h is to define the variogram only up to half the maximum distance between the sample pairs. The estimation of the variogram can also be extended to cases where the variogram not only depends on distance, but also on direction. If the variogram changes both as a function of distance and direction, that variogram is called anisotropic $[\gamma\ (h \pm \Delta h,\ \Theta \pm \Delta\Theta)]$ (Figure 4.2B).

Once the estimated variogram is calculated, the next step is modeling the variogram. Only certain models can be used to model the estimated variogram. This is

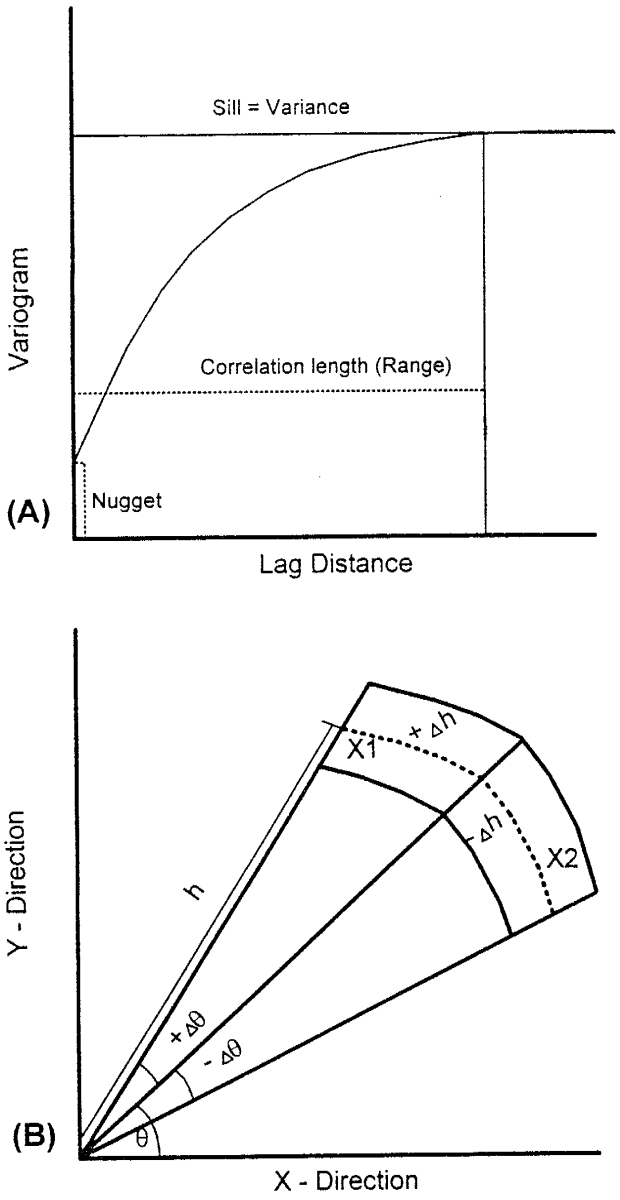

Figure 4.2: (A) An illustration of a variogram showing the range, sill, and nugget. Range is the distance over which data is correlated. Sill represents the variance. Nugget represents a random component in a regionalized variable. (B) An illustration showing the search window parameters for the variogram.

because the models have to satisfy the "condition of positive definiteness". This condition imposes a requirement that during estimation of a variable at an unsampled location, the associated error variance be always positive. The most common variogram models used are: spherical, exponential, and gaussian. In modeling estimated variograms, it is important to capture the basic features observed.

In many instances, the conventional definition of a variogram may not be appropriate, e.g., if sampling is biased. This is true in many reservoirs where more wells are drilled in an area that is the most promising. Only a few wells may be drilled in an area suspected to be of poor quality.

3. Estimate the Spatial Distribution

After modeling the variogram, the next step is to estimate the values of a variable at unsampled locations. A geostatistical technique used for estimation purposes is called kriging. Depending upon the type of estimation involved, different types of kriging techniques may be used.

- To estimate the point values **ordinary kriging** may be used. In this study we used ordinary kriging to estimate the reservoir properties.
- **Block kriging** is used to estimate the block values.
- **Co-kriging** may be used to estimate one variable by using its relationship with another extensively sampled variable.
- If the sample mean varies within the region of stationarity, **universal kriging** may be used.

Ordinary kriging is probably the simplest kriging method and provides an estimation of a point value at an unsampled location. In any of the four kriging methods, we assume that the estimated value is a linear combination of nearby sampled values. Mathematically, the estimated value at location X_0 is calculated as:

$$V(X_0) = \sum_{i=1}^{n} \lambda_i V(X_i)$$

where $V(X_i)$' are the sample values at locations X_i's, n is the total number of sample, and λ_i is a weight assigned to the sample value $V(X_i)$. In most instances, the weight assigned is between 0 and 1.

For details about kriging readers are referred to Journel and Huijbergts (1978) and Deutsch and Journel (1992).

In addition to kriging, a deterministic method called "inverse-distance weighting" was also used to estimate reservoir properties. This was done because of the problems encountered in the estimates obtained using ordinary kriging due to sparsely distributed data.

INVERSE-DISTANCE WEIGHTING METHOD

Inverse-distance techniques are often used to estimate the value of a parameter at locations where no specific data exists. This is done on a regular grid overlaying sparse, randomly located data. The technique estimates values at a point by weighting the influence of nearby data the most, and distant data the least.

$$g_i = \frac{\sum_{i=1}^{n} \frac{X_i}{d_i^P}}{\sum_{i=1}^{n} \frac{1}{d_i^P}}$$

where g_i is the estimated value at the grid location, and d_i is the distance between the grid location and the sample data. P is the power to which the distance is raised. The basis of this technique is that nearby data is most similar to the actual field conditions at the grid location. Depending on the site condition, distance may be weighted in different ways. If $P = 1$, this is a simple linear interpolation between points. Many people have found that $P = 2$ produces better results. In this case, close points are heavily weighted, and the more distant points are lightly weighted.

Conventional kriging can be considered more rigorous form of simple weighted

averaging procedure, but the problems related to local trends are similar for both kriging as well as simple weighted averaging procedures (Swan and Sandilands, 1995). Conventional kriging is based on the principal of minimizing error variance. In the process of minimizing error variance, the kriging process creates a smooth distribution of variables. In the absence of abundant data the kriged map will be overly smooth and the changes in the estimated values will be gradual.

SUBSURFACE STUDY

A detailed subsurface study for the Sulimar Queen field was carried out using the cores and rescaled gamma ray logs. In addition to one core available from the Sulimar Queen field, two cores were collected from the Queen and South Lucky fields. Additional lithologic information about the Shattuck Member was also available from the Double "L" field. For the locations of these fields see Figure 1.3A. This study was conducted to determine the distribution of reservoir properties and structure in the Sulimar Queen field. A detailed lithologic description of the core from well 1-16 (Sulimar Queen field) is shown in Figure 4.3. In the Sulimar Queen field, Zone 1 is the reservoir zone (details of reservoir properties are given in Chapter 5). The generalized lithologic makeup of the additional cores are similar to the one in Sulimar Queen field (Figure 4.3).

A small-scale permeability heterogeneity study was conducted on the available cores to determine the relationship between sandstone facies and the correlation length of permeability in the vertical direction. It was noted that sandstones deposited in different environments exhibit different means and standard deviations, and are the dominant control on the correlation length (Table 4.1). The histograms of the permeability distribution especially in the Sulimar Queen (Figure 4.4A) and South Lucky Lake (Figure 4.5A). fields show trimodal distribution. This distribution is may be due to individual permeability zones identified using the minipermeameter. The variograms were estimated in the vertical direction and a spherical model was applied (Figures 4.4, 4.5, & 4.6). Similar correlation lengths were observed for all the cores which is consistent with

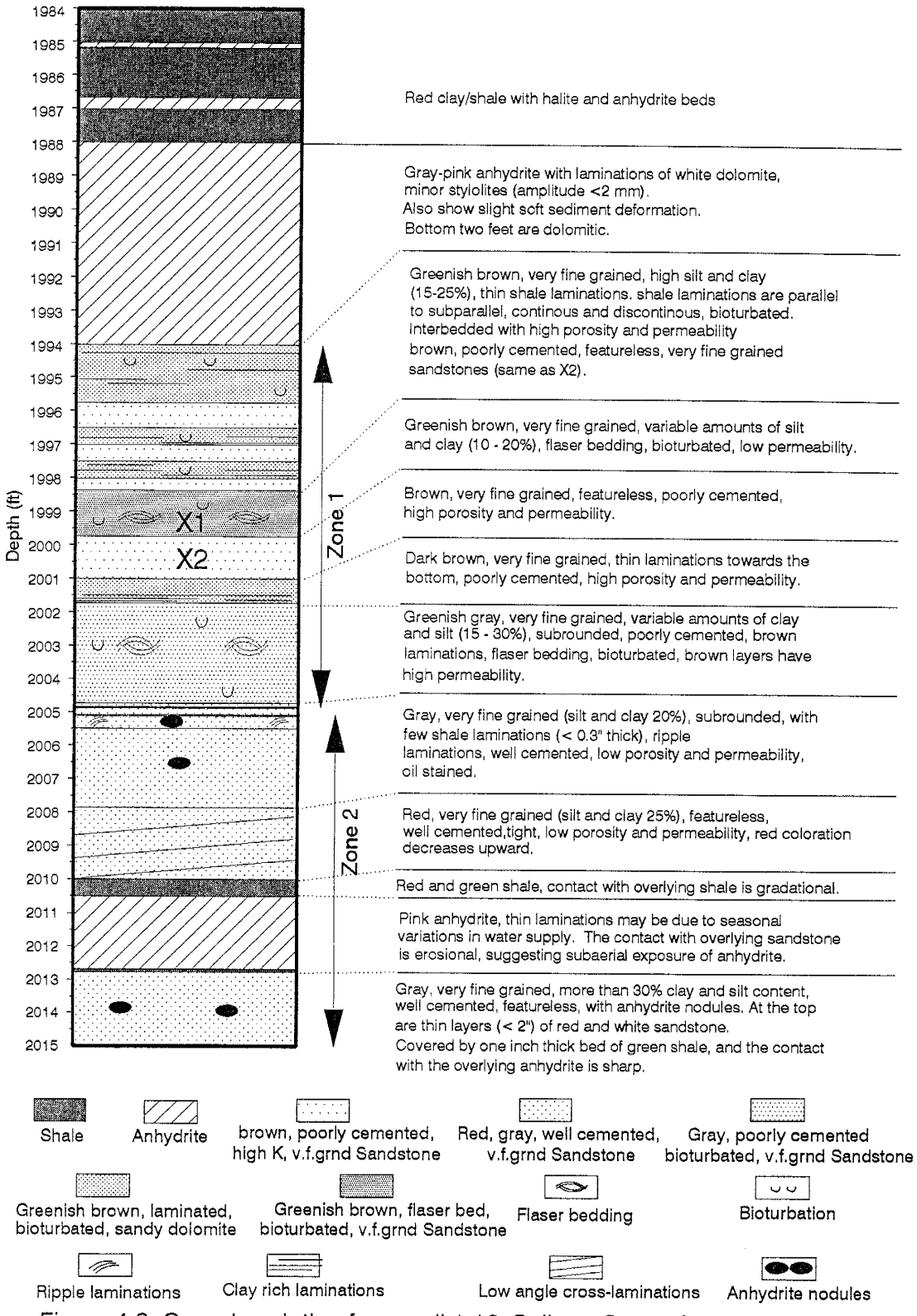

Figure 4.3: Core description from well 1-16, Sulimar Queen field.

Zones	Sulimar Queen field			South Lucky Lake field			Queen field		
	N	Mean	STD (σ)	N	Mean	STD (σ)	N	Mean	STD (σ)
Subzone A	38	0.68	0.60	41	3.63	1.39	44	2.80	2.07
Subzone B	24	9.90	7.30	22	11.52	5.62	45	2.48	1.67
Zone 1	259	37.30	43.00	240	87.39	86.17	319	24.00	44.00
Zone 2	247	1.06	1.30	151	0.83	1.04	181	1.67	1.30

Table 4.1: Summary of core permeability data from Sulimar Queen, South Lucky Lake and Queen fields.

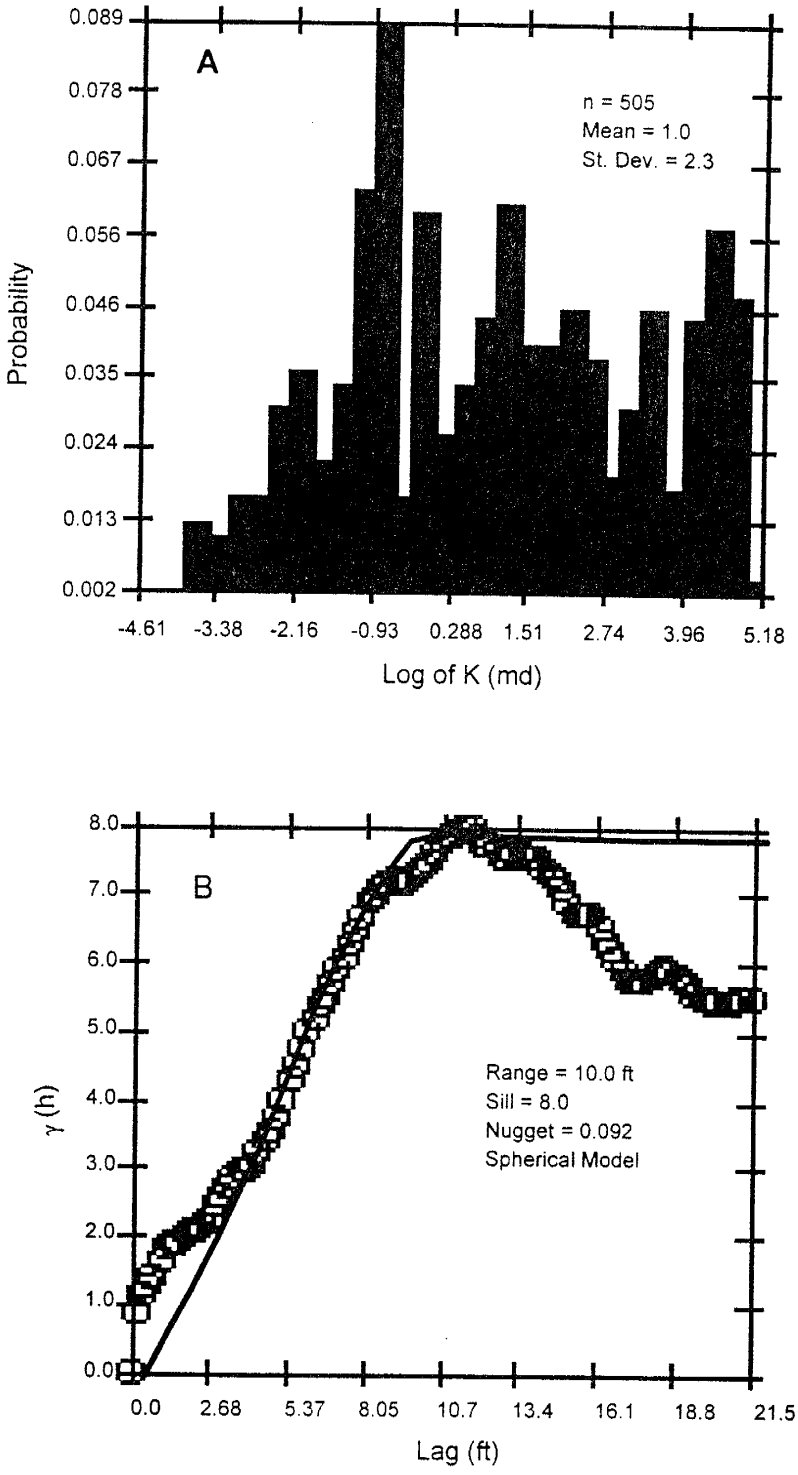

Figure 4.4: Histogram showing a probable trimodal distribution (A), and a vertical variogram estimate (B) of permeability data for Well 1-16 in the Sulimar Queen field.

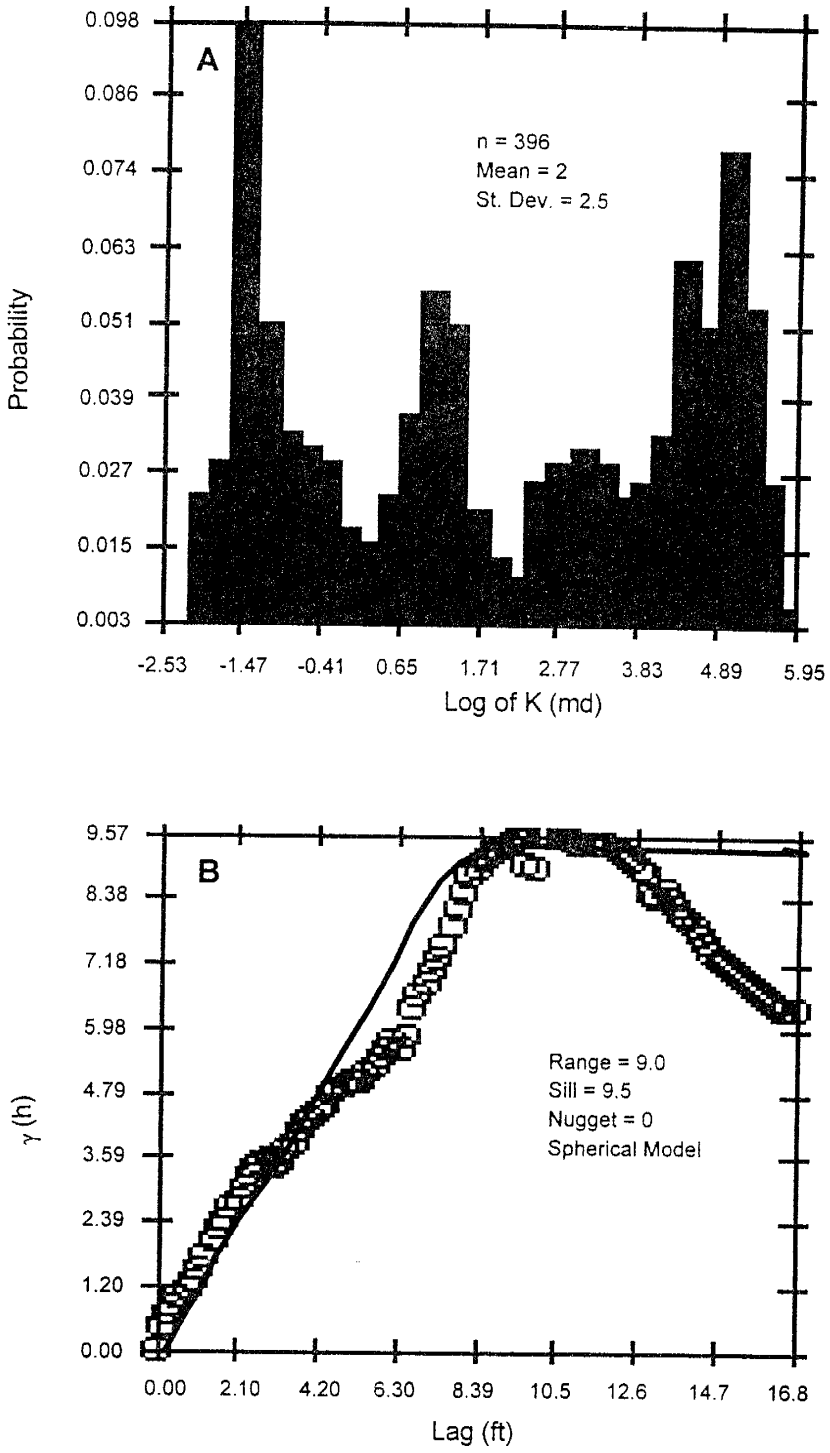

Figure 4.5: Histogram clearly showing a trimodal distribution (A), and a vertical variogram estimate (B) of the permeability data for the South Lucky Lake field.

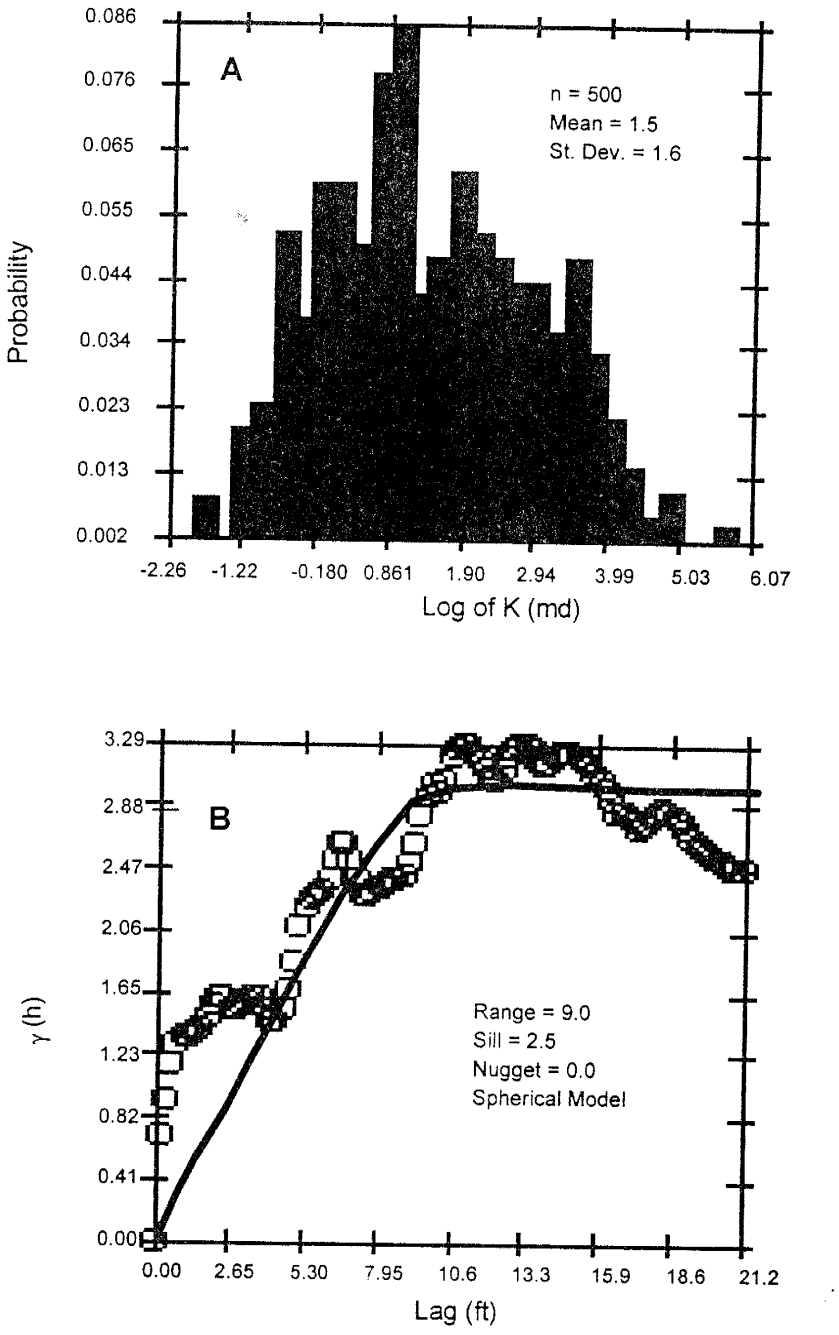

Figure 4.6: Histogram (A), and a vertical variogram estimate (B) of permeability data for the Queen field.

the observed facies distribution in the vertical direction (Figures 4.4, 4.5, & 4.6). The correlation lengths represent the approximate thickness of Zone 1 (reservoir zone) in all the cores from different fields (Figure 4.3). The Shattuck Member cores obtained from the nearby fields for analogy exhibit lithologic and permeability behavior similar to that in the Sulimar Queen field.

Lithologic Description

Anhydrite cap (1984 - 1994 feet; 2010 - 2012 feet)

A 10 foot thick, gray and pink colored, massive anhydrite bed is present at the top of the Shattuck Member in all the cores (Figures 4.3 & 4.7). Three beds of red clayey siltstone and beds of halite are present towards the top of this anhydritic unit. The anhydrite is dominantly laminated with minor amounts of nodular anhydrite. It also shows soft-sediment deformation (Figure 4.7). The bottom 2 feet of the anhydrite bed is composed of dolomitic anhydrite (Figure 4.7). There are thin laminations in the dolomitic anhydrite which indicate algal binding (Figure 4.7).

The uppermost sandstone underlying the anhydritic cap shows a gradual vertical change from anhydritic-cemented sandstones to dolomitic-cemented sandstones to sandy dolomite (Figure 4.7). Sandy dolomite also exhibits bioturbation (Figure 4.7). A thin zone in the dolomitic portion also contains oolites and micritized fossils.

Towards the lower part of the core, there is a 2 feet thick massive, thinly laminated and nodular bed of pink colored anhydrite.

Brown-gray sandstones (1995 - 2005.5 feet)

The greenish-gray and brown sandstone forms the reservoir zone in the Sulimar Queen field (Figure 4.8). These sandstones are composed of moderately to poorly sorted, very fine to fine-grained arkosic sandstones. Grains are angular to subangular, with minor amounts of medium sand-sized well-rounded quartz (Appendix C). These sandstones contain parallel to subparallel discontinuous shale laminations, flaser bedding,

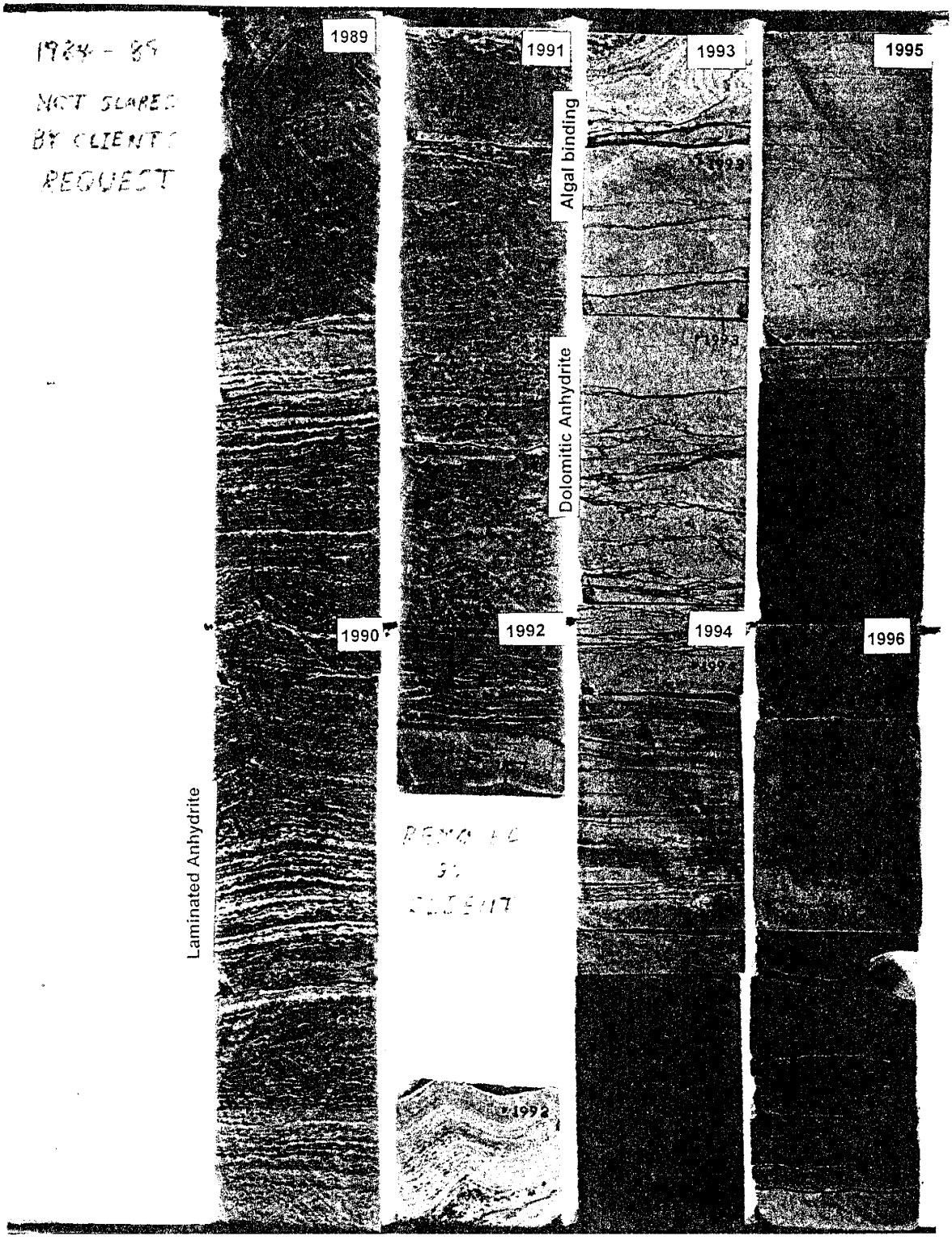

Figure 4.7: Laminated anhydrite cap (1989 - 1993 ft) and associated dolomite and sandy dolomite (1993 - 1995 ft). Underlying is the greenish-gray and brown sandstone of zone 1 (1995 - 1997 ft)

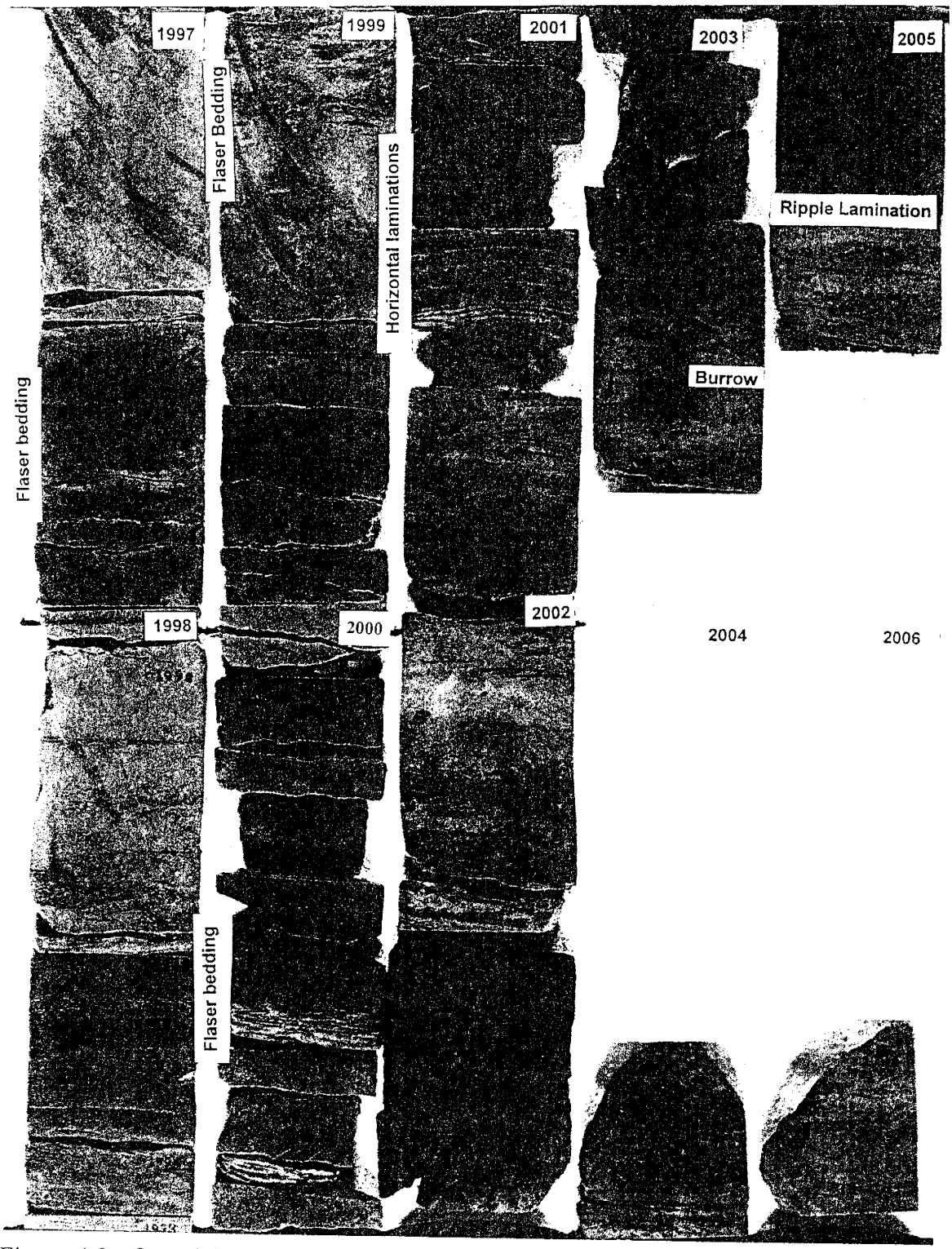

Figure 4.8: Greenish-gray and brown sandstone of Zone 1, exhibiting massive, parallel laminated, and bioturbated nature. Probably deposited in shallow lagoon.

minor cross laminations, and bioturbation (Figures 4.3 & 4.8). Sandstones are cemented mainly by anhydritic cement with minor amounts of dolomitic cement. Nodular anhydrite is completely absent in these sandstones. The loose packing of grains suggest that cement must have precipitated at shallow to moderate depths.

The upper part of this sandstone shows a gradual vertically change from anhydritic-cemented to dolomitic-cemented sandstones to sandy dolomite (Figure 4.7).

Gray and red sandstones (2005.5 - 2008 feet and 2013 - 2015 feet)

Massive, gray, moderately to well sorted, very fine-grained arkosic sandstone is present towards the lower part of the Shattuck Member (2013 - 2015 feet; Figure 4.9). These sandstones indicate intense haloturbation. Nodular anhydrite is the main cementing material along with some poikilotopic anhydrite.

A 2 foot thick anhydrite bed is present between the gray and red sandstones (Figure 4.9). At 2012.75 feet, there is an erosive contact between the gray sandstone and overlying anhydrite. At this contact, a 1-inch thick dolomitic sandstone bed is also present. This dolomitic bed grades upward into thinly laminated and nodular anhydrite (Figure 4.9). The upper contact of the anhydrite is also erosive with the overlying red, massive with minor cross-stratified, well sorted, well cemented, very fine-grained arkosic sandstone. This red sandstone grades upward into gray, moderately sorted, well cemented, haloturbated, very fine-grained arkosic sandstone.

Petrographic Analysis

A detailed petrographic analysis was conducted to determine the mineralogy and paragenesis.

Framework grains

Quartz is the most abundant detrital grain in all the sandstone types discussed in the lithologic description. It comprises 60% (arkosic) to 87% (subarkosic) of the framework grains. Most grains are common quartz, inclusion free with straight to slightly

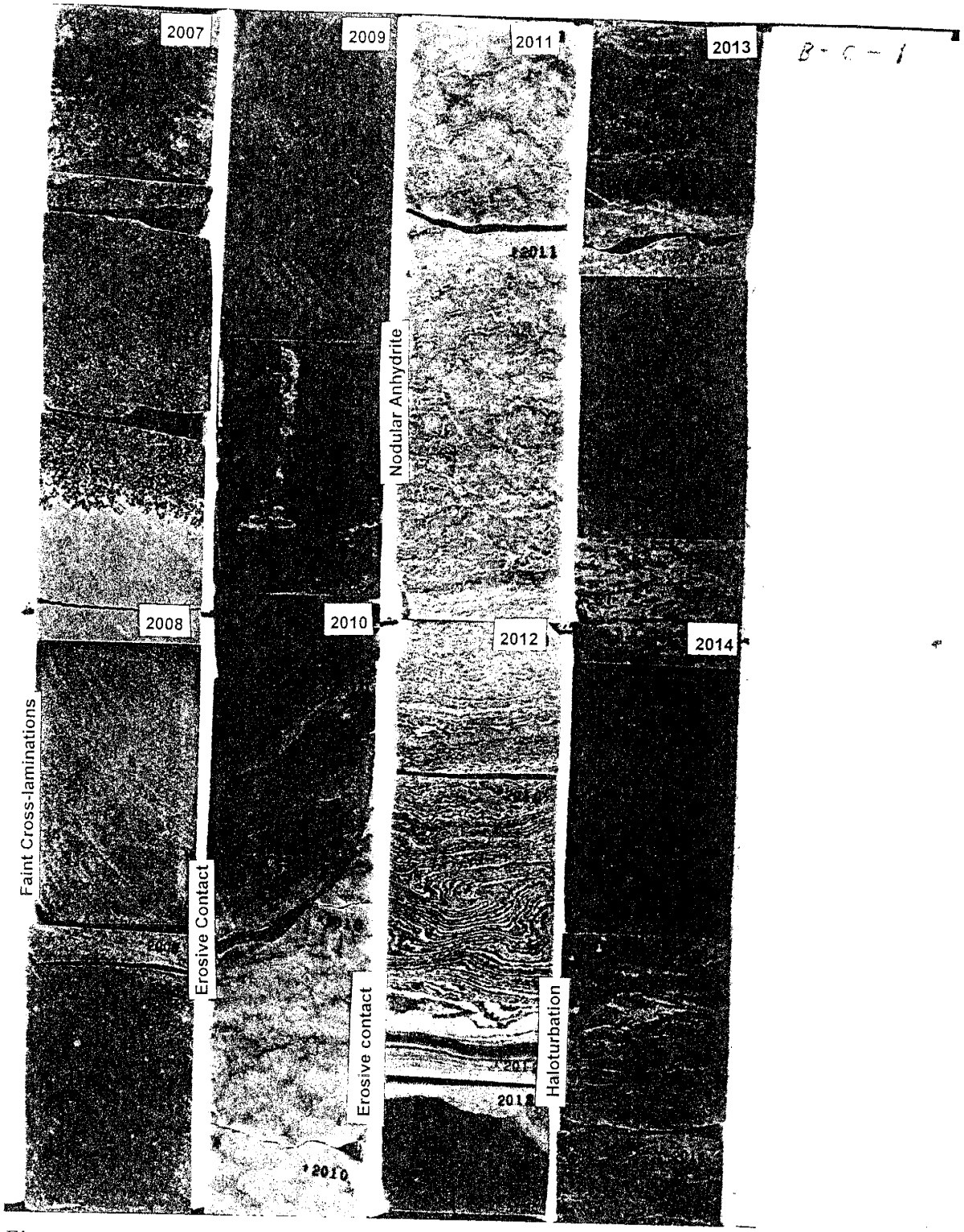

Figure 4.9: Gray and red sandstones of zone 2. These sandstones contain considerable amounts of nodular anhydrite (2007 - 2007.5 ft; 2013 - 2015 ft). Red sandstone show faint cross-stratifications (2007.5 - 20010 ft). Note the erosional contact between nodular anhydrite and red and green silty shale

undulose extinction. A few grains have fluid inclusions and contain probable mineral inclusions of rutile and tourmaline. Minor amounts of polycrystalline quartz (metamorphic) are also present.

Feldspar makes from 10 to 34 % of the framework grains. The majority of the feldspars are orthoclase. Minor amounts of plagioclase and microcline are also present. Most of the feldspars show alteration, mainly sericitization and vacuolization. Some skeletal feldspar grains are also present. It is possible that the feldspar grains either underwent direct dissolution, or were first replaced by anhydrite and this replacement material was later dissolved, leaving behind a skeletal appearance.

Rock fragments comprise about 3% of the detrital grains, and consist of metamorphic rock fragments, chert, carbonate rock fragments, and anhydrite cemented siltstones.

Authigenic minerals

(1) Anhydrite

Anhydrite is the most abundant cement and ranges from 0 to 35%. Anhydrite is present in two morphologies: (1) poikilotopic crystals surrounding many grains and locally replacing them (Figure 4.10A), and (2) fine-grained masses and nodules (Figure 4.10B). Poikilotopic anhydrite is the most dominant type.

The fine-grained anhydrite occurs as an interstitial pore fill and as small nodules. The individual crystals are rectangular and elongated. The detrital grains appears to be floating in the anhydrite nodule (Figure 4.10B). The close packing of grains around the nodules and the presence of detrital grains floating within the nodules indicates that the nodules were formed during very shallow burial (Figure 4.10B).

(2) Dolomite cement

Dolomite is the second most abundant authigenic mineral and occurs in two morphologies: (1) micritic (Figure 4.10C) and (2) large poikilotopic (Figures 4.10C &

Figure 4.10: Thin section photomicrographs showing the anhydrite and dolomite morphologies in the Shattuck Member.

A: Poikilotopic anhydrite surrounding many grains and replacing few grains (crossed polarizers)

B: Nodular anhydrite pushing the detrital grains around it. Probably formed during early diagenesis at the surface or shallow depth of burial (crossed polarizers)

C: Micritic and poikilotopic dolomite (crossed polarizers)

D: Poikilotopic dolomite replacing grains and probably anhydrite cement (crossed polarizers)

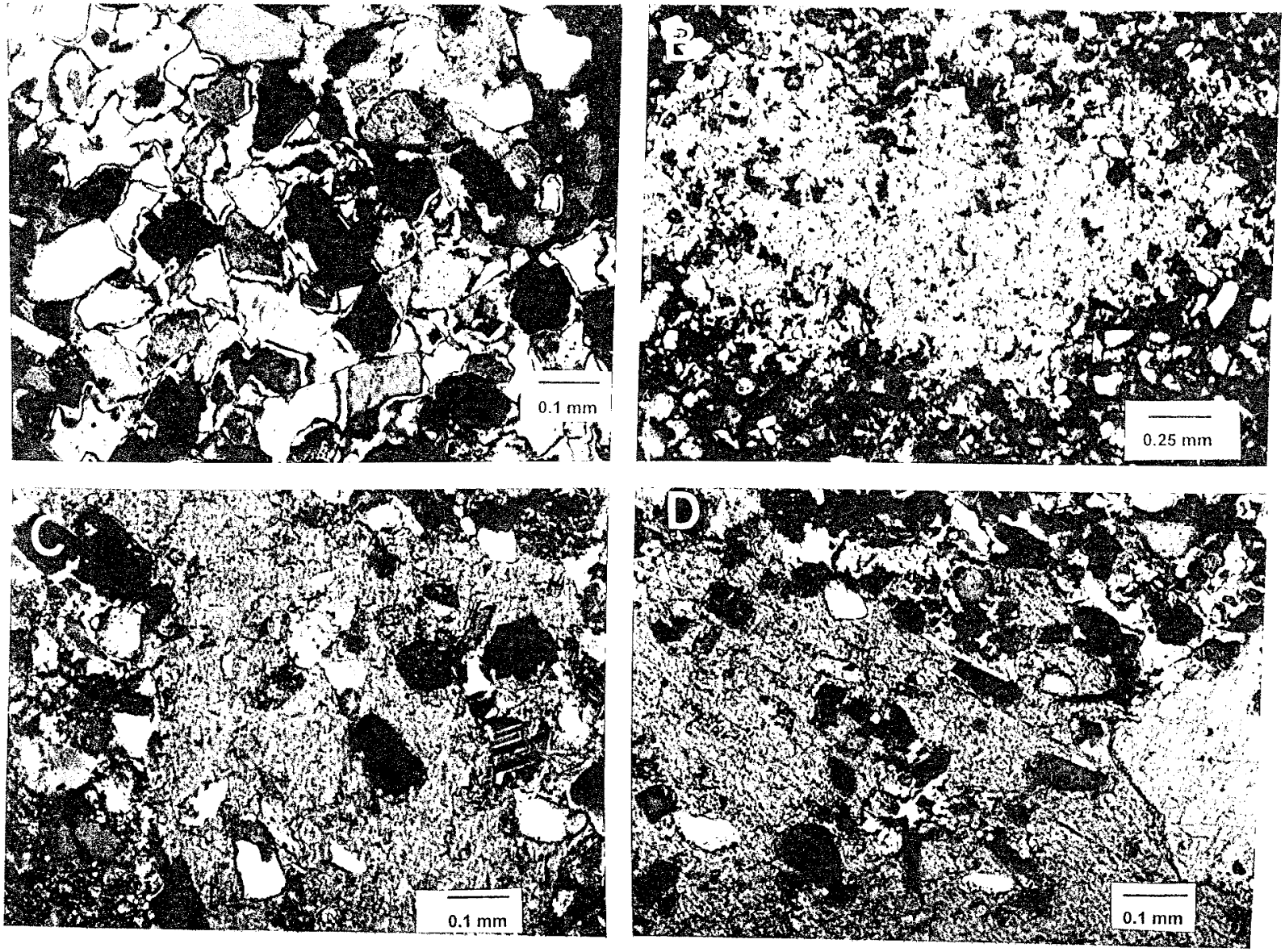
0.1 mm
0.25 mm
C
0.1 mm
D
0.1 mm

4.10D). Poikilotopic dolomite forms large patches surrounding several framework grains and contains inclusions of fine grained anhydrite cement (Figure 4.10D). The margins of grains are replaced by dolomite as visible in Figure 4.10C. The detrital grains appear floating within the poikilotopic patches, whereas around the patches the detrital grains show tangential/point contacts (Figures 4.10 C & 4.10D). This suggest that majority of the grains were replaced by dolomite during the growth of poikilotopic patches.

Micritic dolomite (2 μm) probably was calcitic or aragonitic lagoonal mud originally, which was dolomitized later. Its detrital origin is also supported by its presence only in the poorly sorted thin zones.

(3) Quartz and feldspar overgrowths

Quartz overgrowths are present in trace amounts which, in a few cases, completely surround the grains (Figure 4.11A). The presence of dust rims or hematite allows the identification of most of the overgrowths.

Minor amounts of feldspar overgrowths are also observed in the reservoir sandstone zone (Figure 4.11B).

(4) Hematite cement

Hematite is present in the uppermost (1984 - 1988 feet) and the lower part (2007 - 2010 feet) of the Shattuck Member. It occurs as thin rims surrounding the grains (Figure 4.11C) and staining early anhydrite cement. Since hematite coats grain and stains anhydritic cement, it is assumed that majority of the hematite was formed very early in the diagenetic history (Figure 4.11C). The presence of hematite between the grain-cement contact also suggest that hematite was formed before the precipitation of anhydritic cement (Figure 4.11C).

(5) Other cements

Chlorite rims are present in minor amounts (Figure 4.11D). The clay is light green and structureless in plane light. No chlorite fibers or plates growing perpendicular

Figure 4.11: Thin section photomicrographs showing some authigenic minerals in the Shattuck Member (Porosity in blue)

A: Quartz grain with overgrowth (O). Anhydrite replacing a probable feldspar grain with overgrowth (F) (crossed polarizers)

B: Partially dissolved feldspar grain (F) showing overgrowth (plane light)

C: Hematite coating around the detrital grains. Hematite also stains anhydrite cement (plane light)

D: SEM photomicrograph showing chlorite coating around grains. A probable authigenic feldspar (F), and other authigenic minerals are not coated by chlorite (C). Chlorite formed before overgrowths and precipitation of cement (500x)

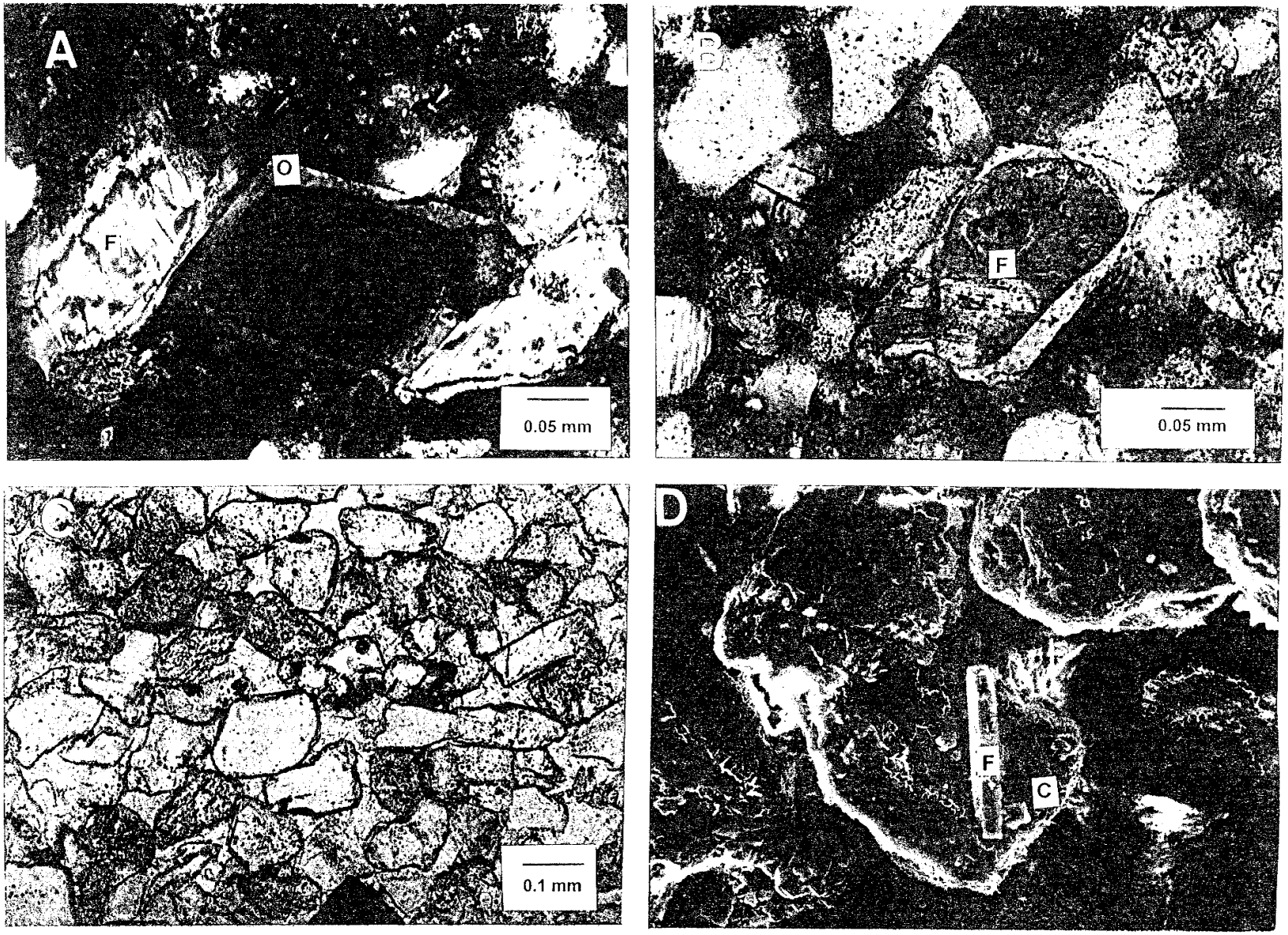
A
O
F
0.05 mm
B
F
0.05 mm
C
0.1 mm
D
F
C

Figure 4.11: Continued

E: A sericitized feldspar grain (F) (plane light)

F: Same view as (E) (Crossed polarizers)

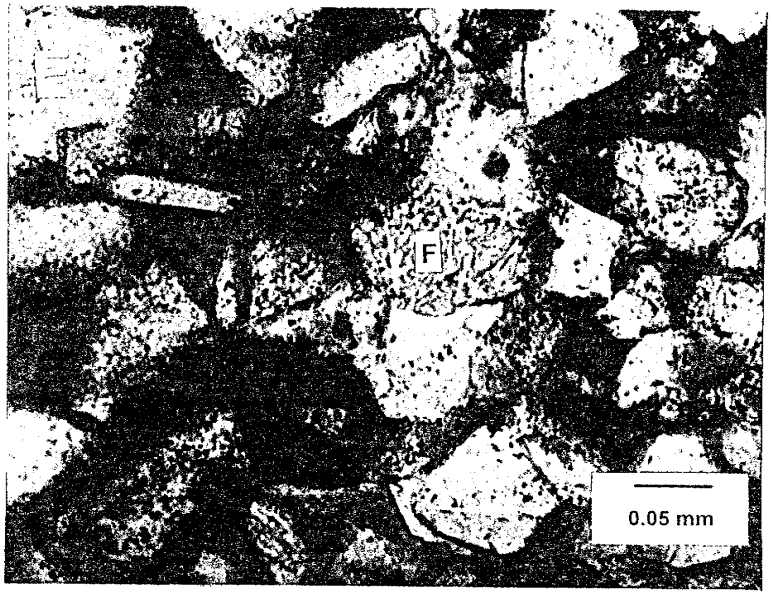
F
0.05 mm

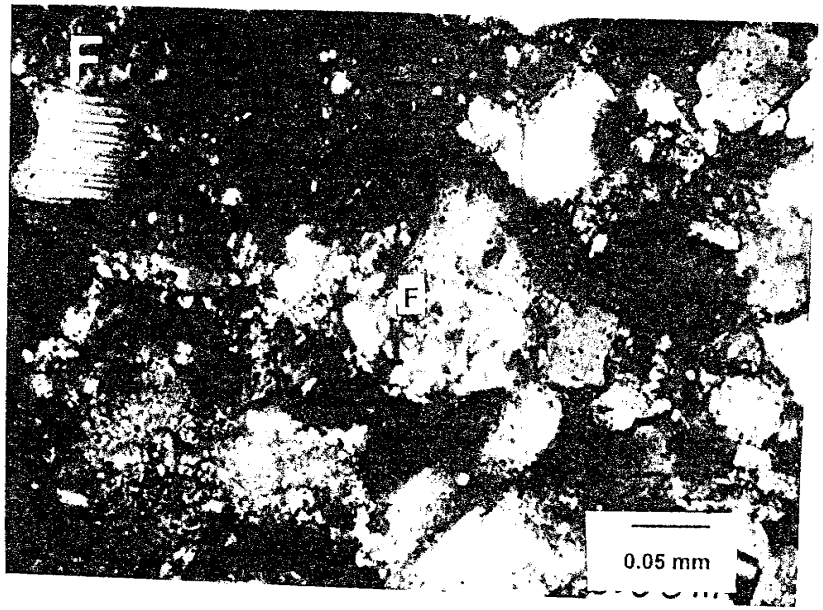
F
F
0.05 mm

to the detrital grains were identifiable in the thin sections but were visible under SEM (Figure 4.11D).

Pyrite occurs as isolated cubes and framboids in trace amounts. The presence of pyrite framboids indicate pyrite formation early in the diagenetic history in the sulphate-reducing zone (Gautier, 1985). The isolated cubes may be formed later as overgrowths on the pyrite framboids (Gautier, 1985).

Paragenetic sequence

The paragenetic sequence was determined using textural relationships. A generalized paragenetic sequence is shown in Figure 4.12. No one of the thin section contains all the diagenetic events because of the multiple depositional facies of the sandstone.

Early evaporite minerals (especially displacive nodular anhydrite) formed either at the sediment-water interface, or after shallow burial as indicated by the presence of displacive anhydrite (Figure 4.13A). Detrital grains were pushed apart, due to the displacive nature of the anhydrite, and appear floating in the anhydrite nodules (Figure 4.13A). Chlorite rims were formed around the detrital grains early in the diagenetic history, at least before quartz and feldspar overgrowths and poikilotopic anhydrite. This is suggested by the absence of chlorite rims around anhydrite crystals as well as feldspar overgrowth (Figure 4.13B). Hematite forms rims around detrital grains and stains clay matrix, early fine-grained anhydrite, and to some extent poikilotopic anhydrite. This indicates that hematite precipitation continued until cements were precipitated or it was redistributed during their growth (Figure 4.11C). Therefore, hematite developed at the surface or shallow burial depths and reddening continued until porosity was reduced by later cements, because it also stains the anhydrite cement (Figure 4.11C). Hematite also predates quartz overgrowth because of its presence between the quartz grain and the overgrowth (Figure 4.13C).

Feldspar grains are affected by sericitization and dissolution. Although alteration of feldspars has been considered to reflect climatic conditions at the time and/or site of

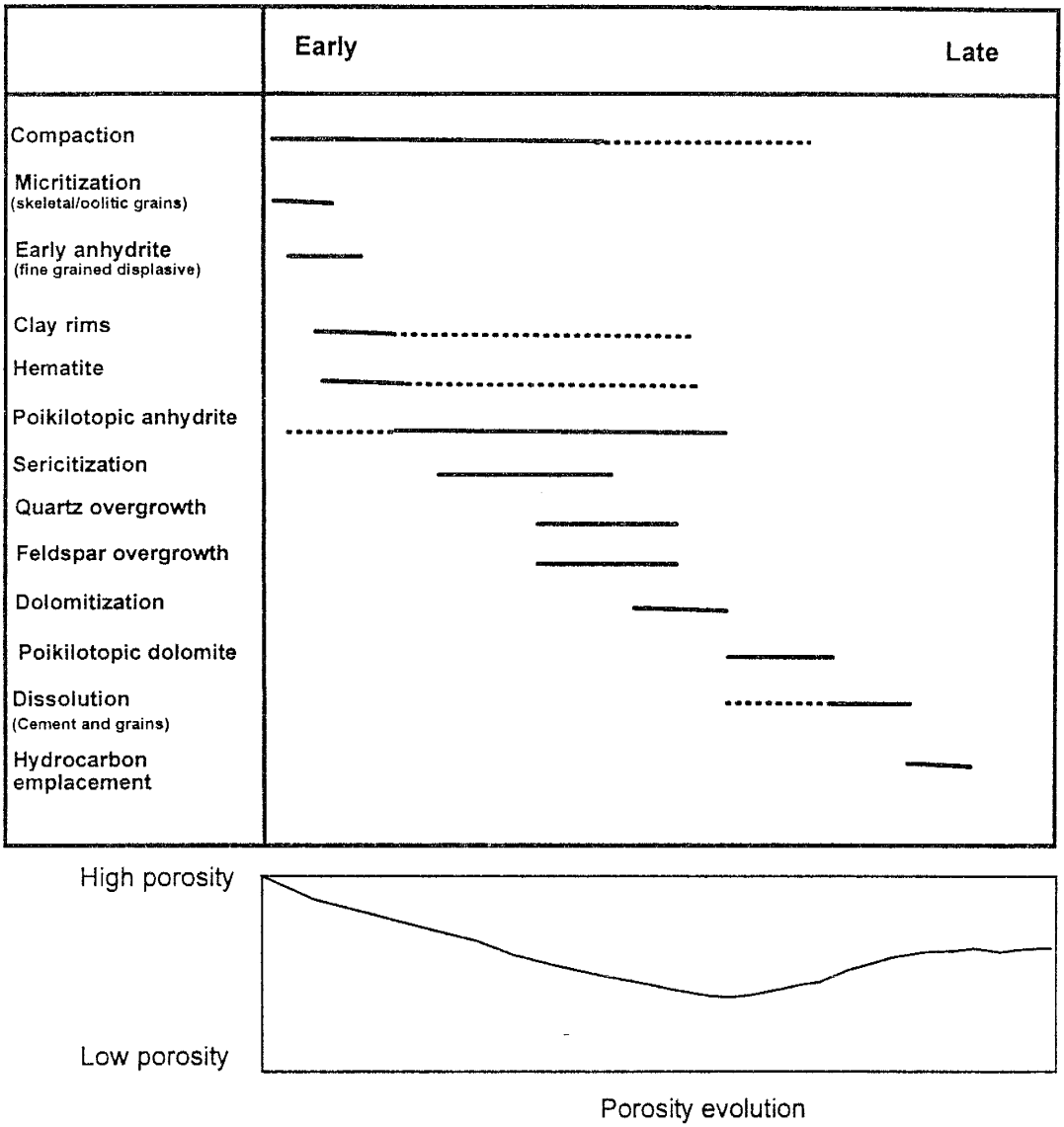

Figure 4.12: Generalized paragenetic sequence for the Shattuck Member in the Sulimar Queen and adjacent fields.

Figure 4.13: Thin section photomicrographs showing some of the paragenetic sequences in the Shattuck Member (Porosity in blue)

A: Early displasive anhydrite nodules (crossed polarizers)

B: SEM photomicrograph showing the relationships between chlorite (C), anhydrite (A), and feldspar overgrowth (F). Chlorite precipitated before overgrowth and anhydrite precipitation (2000x)

C: Hematitic stains between the quartz grain and the overgrowth (Arrow) (plane light)

D: SEM photomicrograph showing the relationship between overgrowths and chlorite (1000x)

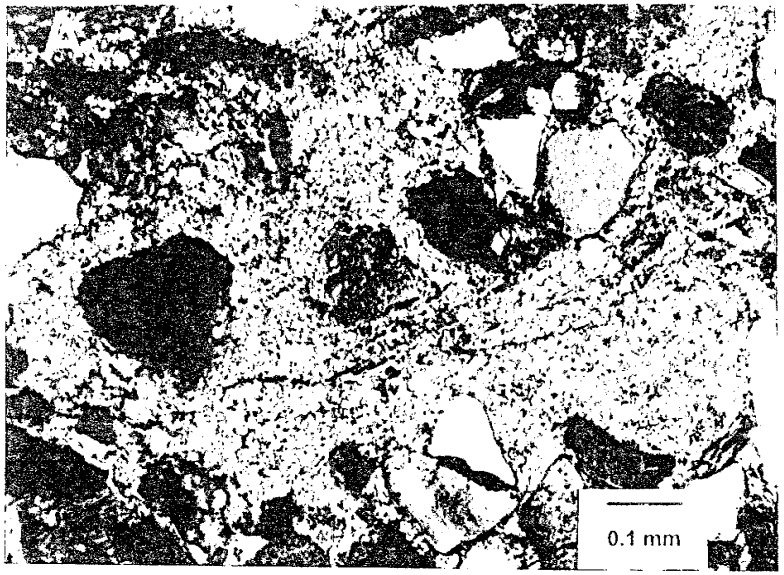
0.1 mm

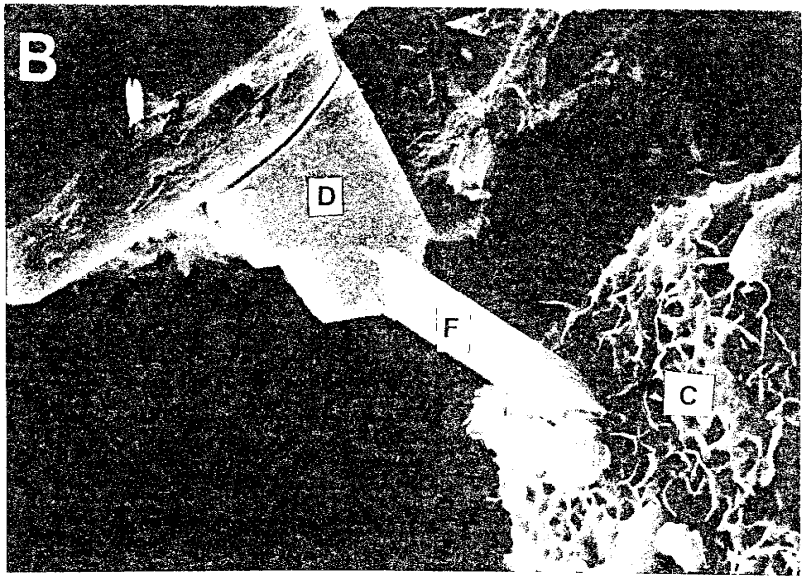
B
D
F
C

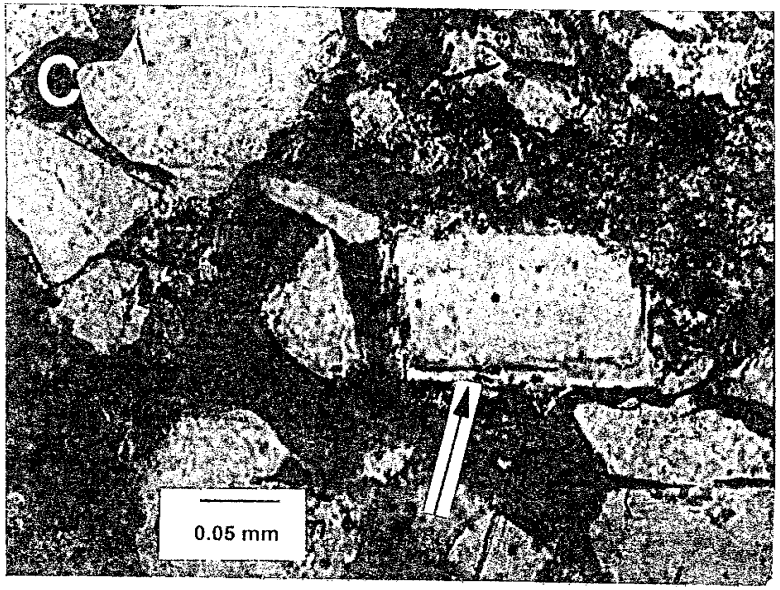
C
0.05 mm

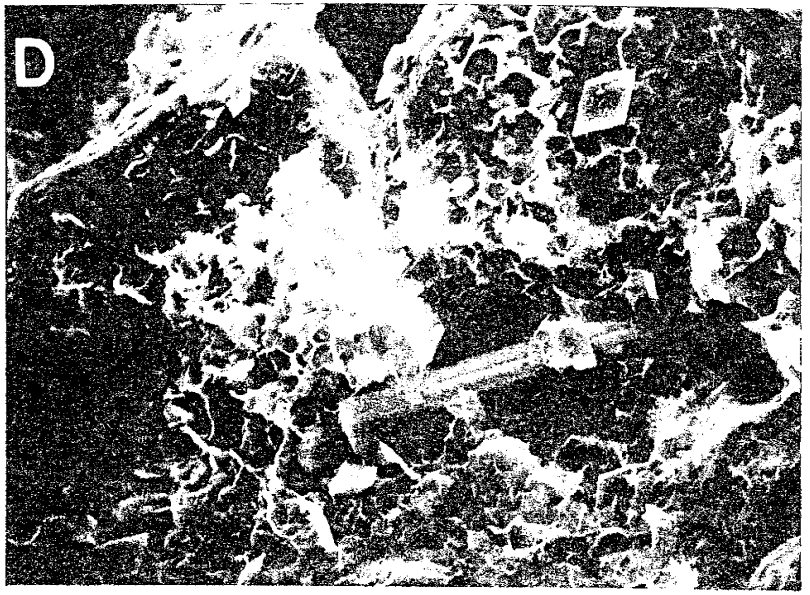
D

Figure 4.14: Thin section photomicrographs showing some of the diagenetic sequences in the Shattuck Member (Porosity in blue)

A: Poikilotopic dolomite containing floating grains and anhydrite cement. Dolomite formed after anhydrite (crossed polarizers)

B: Poikilotopic dolomite (crossed polarizers)

C: Dissolution of grains and cement (plane light)

D: Patchy distribution of cement formed by dissolution (plane light)

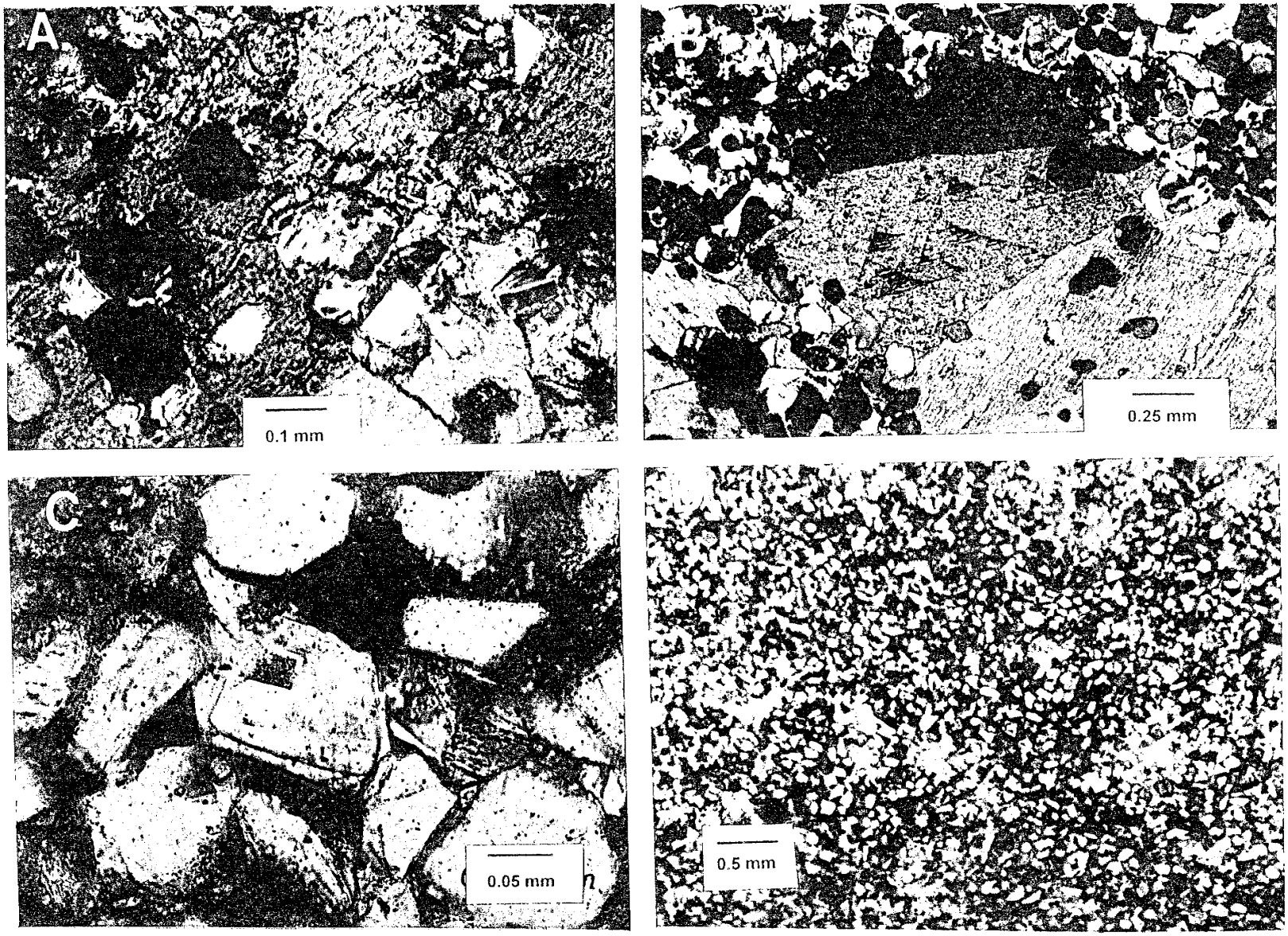
A
0.1 mm
B
0.25 mm
C
0.05 mm
0.5 mm

deposition of the feldspar grains, chemical alteration of feldspar grains can take place as easily and rapidly during diagenesis as during surface weathering (Blatt, 1982). In the Shattuck Member the sandstones that are well cemented by early poikilotopic anhydrite do not show considerable alteration of feldspar grains (Figure 4.11C), whereas the zones which escaped early cementation or were not extensively cemented have sericitized feldspars (Figures 4.11E & 4.11F). The sericitization was identified due to the high birefringence and speckled, micaceous texture (Figures 4.11E & 4.11F). Since no illite was found distributed within the pores, it is possible that the sericitization might have occurred during weathering.

Quartz and feldspar overgrowths were formed during or after the formation of clay rims, hematite, poikilotopic anhydrite, and sericitization. Dust rims of hematite are present between the grains and overgrowths, and thus hematite precedes the formation of overgrowths (Figure 4.13C). Chlorite rims were formed before the overgrowths and may have continued during the precipitation because they are not present on the overgrowths (Figures 4.13B & 4.13D). Some partially dissolved feldspar grains with undissolved overgrowths suggest that selective dissolution of detrital feldspars followed the precipitation of overgrowths (Figure 4.11B).

The precipitation of poikilotopic anhydrite may have taken place before and after the quartz and feldspar overgrowth precipitation. The absence of overgrowths in areas which are very well cemented by anhydrite indicates that poikilotopic anhydrite precipitated before the overgrowths (Figure 4.11C). Some feldspar grains have been selectively replaced anhydrite (Figure 4.11A). This selective replacement may have occurred after the precipitation of overgrowths. Dolomitization took place after the initiation of the anhydrite precipitation because it contains floating anhydrite crystals (Figures 4.10D & 4.14A).

It is difficult to pinpoint the occurrence of dissolution in the diagenetic history. The dissolution of feldspar grains with overgrowths suggest that dissolution took place at least after the precipitation of overgrowths (Figure 4.11B). Dissolution also created the patchy distribution of anhydritic and dolomitic cement (Figure 4.14D). The assumption

that dissolution created the patchy distribution is based on the fact that the grain packing is similar in the cemented and uncemented (areas where cement was dissolved) regions (Figure 4.14D). If the cement was precipitated originally in patches, then the uncemented regions would have close packing of the grains. Therefore, dissolution can be regarded as the late diagenetic event at least after the precipitation of quartz and feldspar overgrowths and anhydrite and dolomite cement. The oil stains both primary and secondary pores (Figure 4.11E) and the emplacement of hydrocarbons may be regarded as the last diagenetic event because there is no indication of any other diagenetic event occurring after the oil emplacement.

OUTCROP STUDY

Outcrop exposures of reservoir rocks provide laterally continuous sampling of rock characteristics, and provide lateral information on scales not available from reservoir data. Outcrop studies are cheap and valuable sources of good quality geological data. The constraints in utilizing outcrop data for the reservoir characterization are:

1. The availability and accessibility of outcrops analogous to the reservoir.
2. Differences in facies architecture, diagenetic imprints, tectonic structure etc., between outcrops and reservoir.

The limitations of applying information from analogous depositional systems to reservoir simulation models, result from the underlying assumptions that:
(1) the statistics of facies dimensions, (2) frequencies of facies occurrence, and
(3) interconnectedness of particular facies within a particular depositional system are transferable from one deposit to another. In a particular case some properties can be transferred, but it is important to assess the degree of similarity and the applicability of data from outcrops.

Keeping the above limitations in mind, an outcrop study of the Shattuck Member was conducted. The overall objective of the outcrop study was to understand how the depositional processes controlled the distribution of the lithologic and permeability facies within the Shattuck Member.

Methodology

There are several Queen Formation outcrops present in Eddy County, southeast New Mexico (Figure 4.15). The Queen Formation exposures are not suited for detailed and continuous outcrop studies because it weathers into slopes that are covered with rubble (Figure 4.16). After reconnaissance of the outcrops present in Eddy County, certain outcrops were selected for study (Figure 4.15). Five sections were studied—four in the Rocky Arroyo area and one in the Bone Tank Draw area (Figure 4.15).

Initially, a TEMCO field minipermeameter was used to collect the permeability data. However, this minipermeameter had operational problems due to high ambient temperatures (> 100°F) and its use was discontinued. Instead, core samples were drilled from the outcrops and permeability measurements were made in the laboratory using an automatic scanning minipermeameter available at the Petroleum Recovery Research Center (New Mexico Tech). Approximately 600 core plugs and hand samples were collected. Core plugs were drilled more than 1.5 inches in length so that permeability data could be collected from rocks less affected by surficial weathering. For each section a detailed sketch was made showing lithofacies and their distribution.

The Rocky Arroyo area (T-21-S, R-24-E) is about 40 miles southwest of the Sulimar Queen field, and about 11 miles landward from the Goat Seep Reef. The Bone Tank Draw area is about 35 miles southwest of the Sulimar Queen field and about 16 miles landward from the Goat Seep Reef. The Sulimar Queen field is located 20 miles north of the Goat Seep Reef (Figure 1.3A). The Sulimar Queen field exhibits relatively different facies and depositional environments from the outcrops studied in the Rocky Arroyo area but is quite similar to the outcrops in the Bone Tank area. Because of the poor exposure, we were unable to collect data on a regular grid except for Section 1.

The objective of the outcrop study was to observe the interwell and field-scale heterogeneities and the small-scale data was available from the cores, Therefore, permeability data were collected on a coarse grid. Additionally, time limitations and insufficient personnel, as well as bad exposures, hampered the small-scale permeability study.

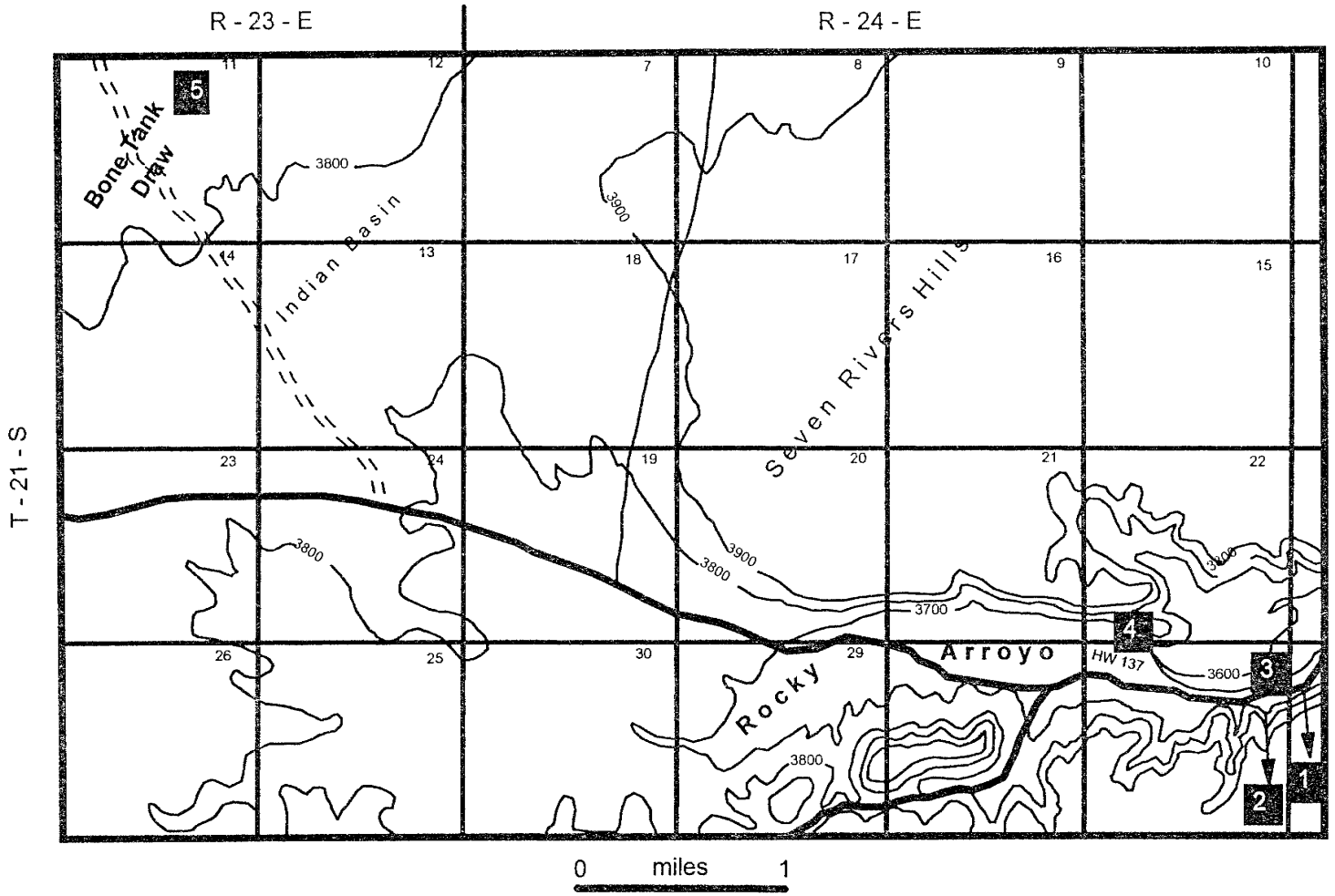

Figure 4.15: Locations of the Shattuck Member outcrops in Eddy County. Locations of the sections studied are shown (numbers in the boxes).

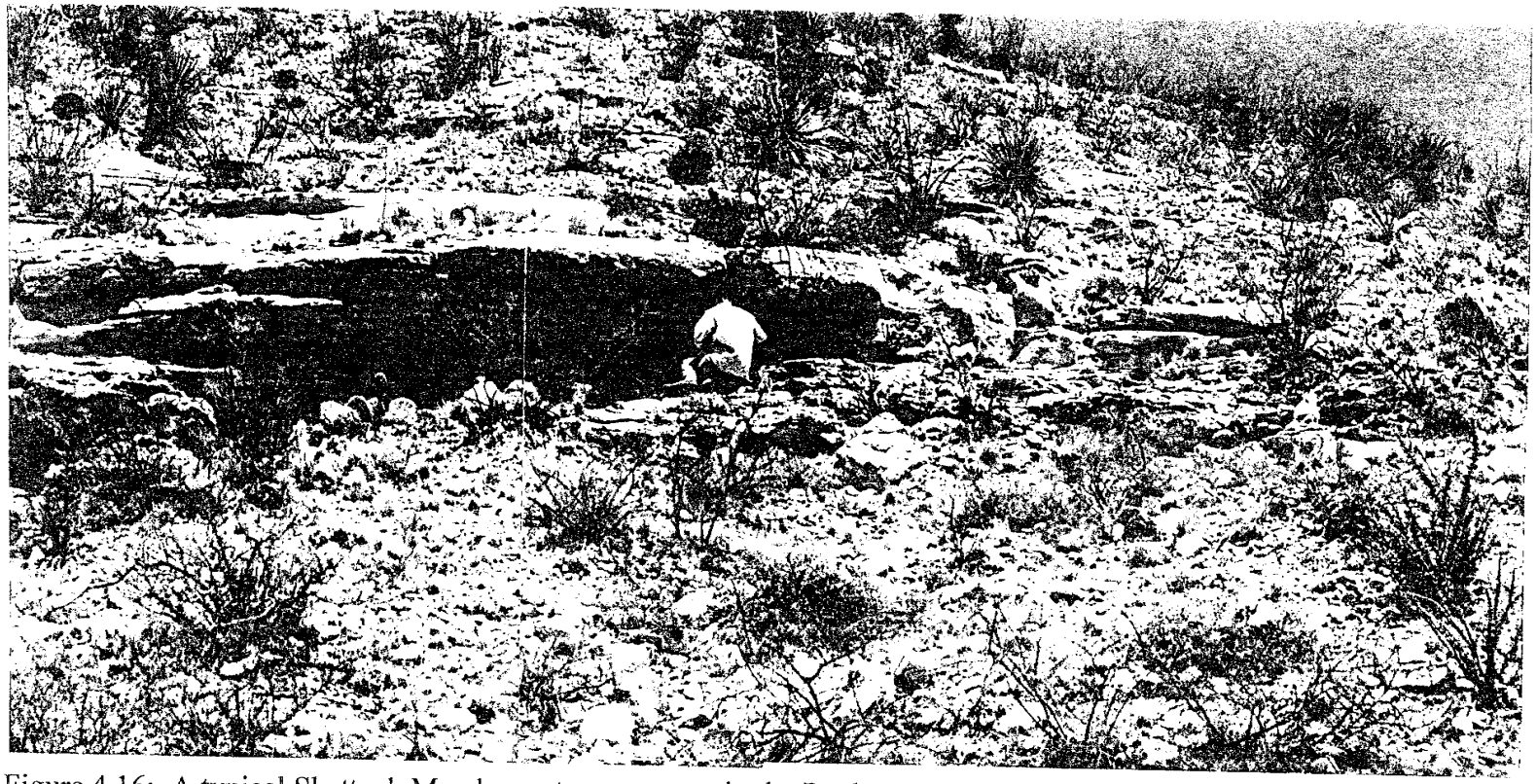

Figure 4.16: A typical Shattuck Member outcrop present in the Rocky Arroyo area. Most of the oucrops are covered with rubble.

Rocky Arroyo Area

Four sections (Sections 1, 2, 3, & 4) were studied in the Rocky Arroyo area (Figure 4.15). In the study area Rocky Arroyo runs east-west (Figure 4.15). Sections 1, 3, & 4 run east-west and are perpendicular to the Goat Seep reef complex. Section 2 runs north-south and is parallel to the Goat Seep reef complex.

Section 1

Section 1 runs east-west along the south wall of the Rocky Arroyo and has a lateral extent of 450 feet (Figure 4.17). This section is about 35 feet thick, much thicker than the Shattuck Member in the subsurface.

More than 220 core plugs were collected on a coarse regular grid (Figure 4.17). Samples were collected at a horizontal interval of 50 feet and vertical interval of 5 feet. Later, the area between 50 -100 feet, and 150 - 200 feet was sampled at a horizontal interval of 10 feet and vertical interval of 2 feet in order to capture heterogeneity on relatively smaller-scale (Figure 4.17).

Section 1 can be divided into 7 individual units (Figure 4.17). Statistics of individual units are given in Table 4.2. At the base of the section is a light yellow, gray, well cemented, moderately sorted, thickly bedded, fine to very fine-grained sandstone unit (Unit A; Figure 4.17). The individual beds are inclined and the fresh surfaces on these individual foresets show flaser bedding and thin discontinuous laminations of very fine silts and clays (Figure 4.18). Ripple bedding in which finer-grained (silt and mud) laminations drape over ripples or are confined to ripple troughs are called flaser bedding (Collins and Thompson, 1982). The presence of flaser bedding implies that both sand and mud were available during the deposition and that periods of current activity alternate with periods of quiescence (Reineck and Singh, 1975). During periods of current activity, the sand is transported and deposited as ripples, while the mud is held in suspension. As the current weakens, mud deposits in the troughs as well as on the crest of the ripple. At the start of the next cycle, ripple crests are eroded away and new sand is deposited in the form of ripples, burying and preserving ripple beds with mud flaser in the trough.

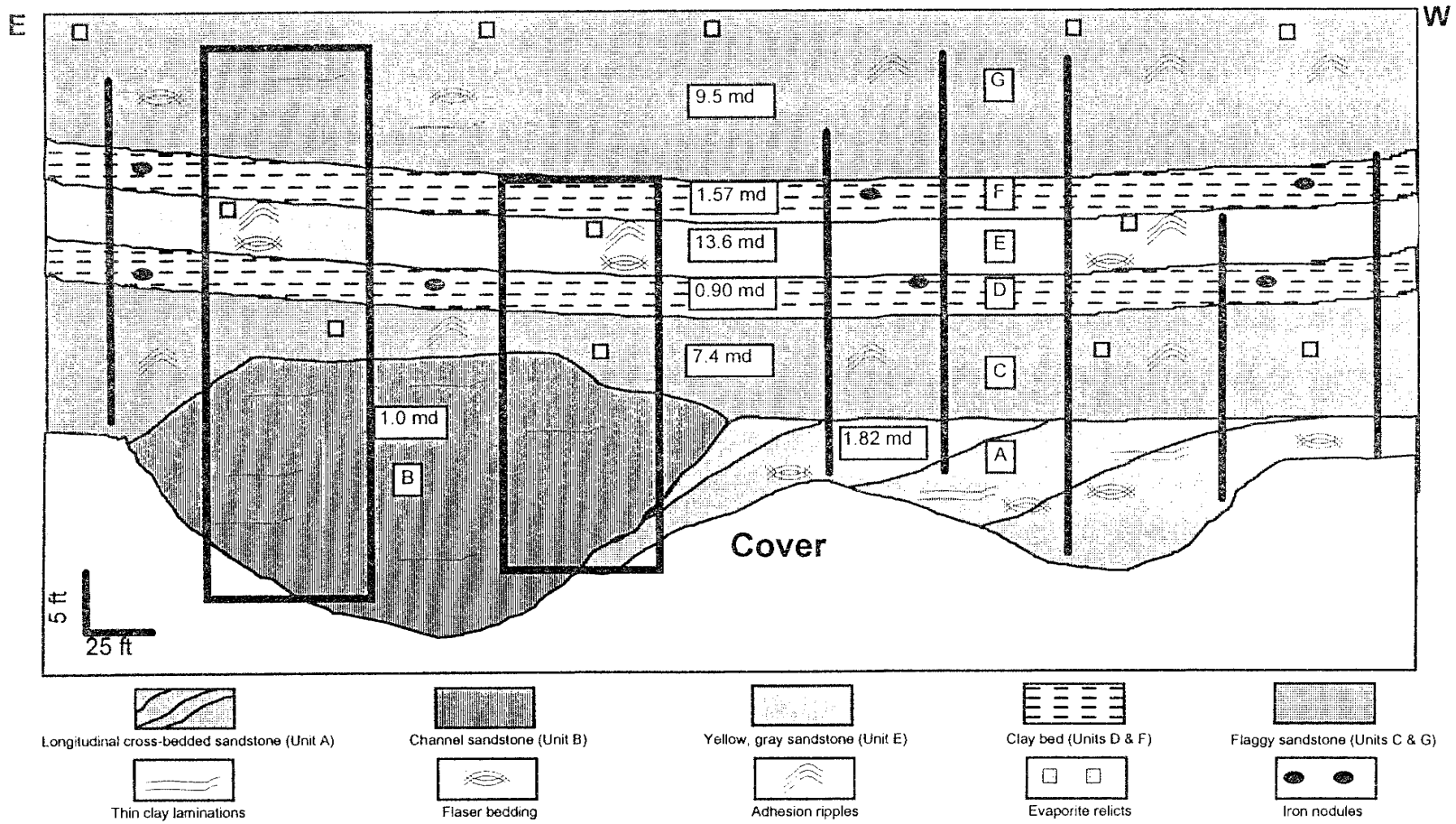

Figure 4.17: Section 1 of the Shattuck Member in the Rocky Arroyo area, showing the extent of individual units. Sampling transects are shown by vertical solid lines (horizontal interval is 50 ft, and vertical interval is 2 ft). Boxes show the areas at which samples were collected at a horizontal interval of 10 ft and vertical interval of 2 ft. The numbers are the average permeabilities of each unit in millidarcies.

Units	Section 1			Section 2			Section 3		
	N	Mean	STD (σ)	N	Mean	STD (σ)	N	Mean	STD (σ)
Unit A	37	1.82	1.20	10	3.75	1.20	-	-	-
Unit B	57	1.00	1.00	-	-	-	-	-	-
Unit C	36	7.40	8.40	10	11.80	4.80	10	14.40	3.70
Unit D	10	0.40	0.32	10	0.88	0.31	10	0.87	0.23
Unit E	33	13.60	19.60	13	11.70	24.90	10	10.40	3.70
Unit F	17	1.57	1.30	10	0.85	0.54	9	1.28	1.03
Unit G	37	9.50	9.70	16	16.00	7.47	4	78.20	23.20

Table 4.2: Summary of the permeability data from the Shattuck Member outcrops on the south wall of the Rocky Arroyo.

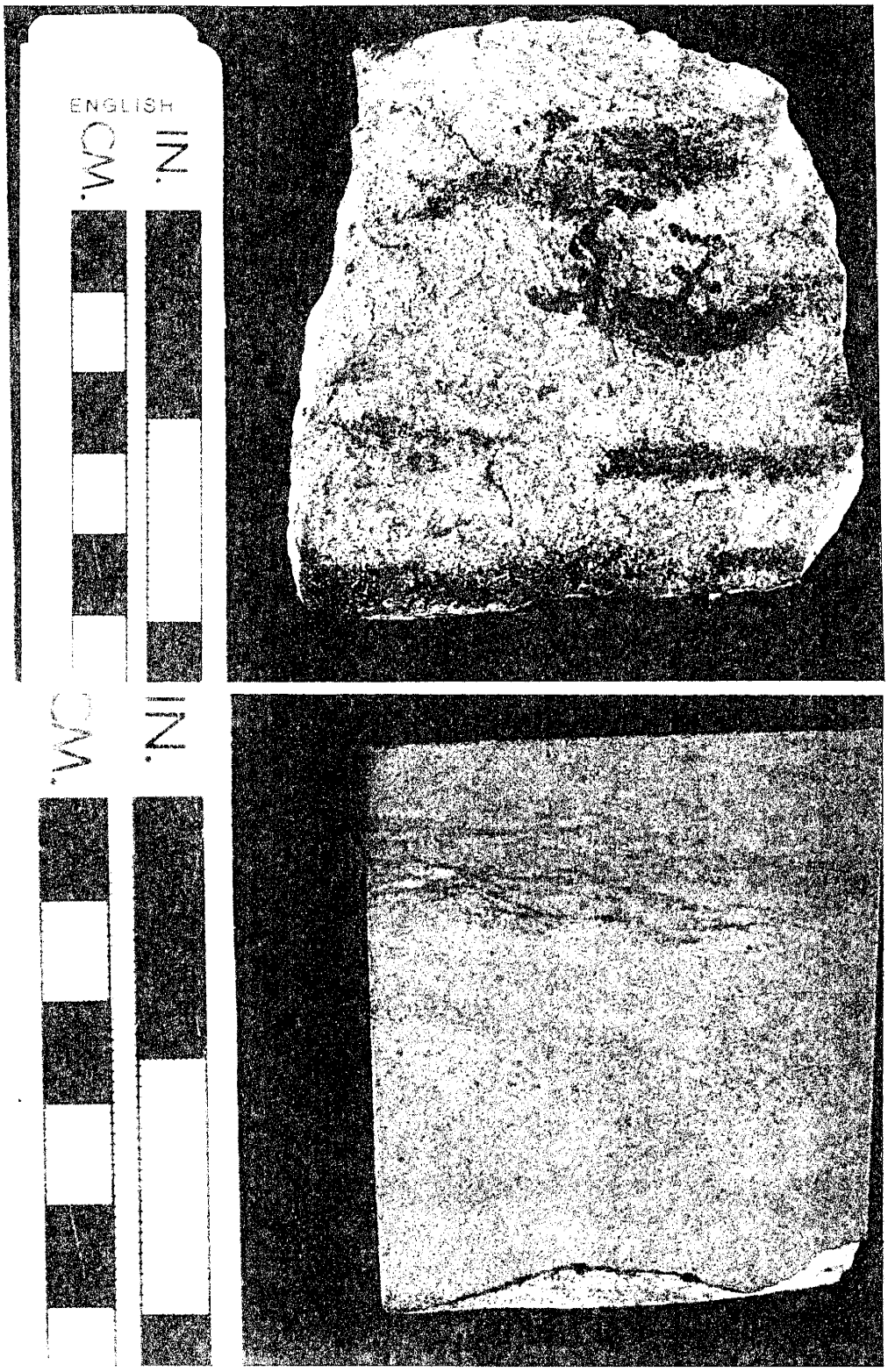

Figure 4.18: Hand samples from Unit A showing flaser bedding (A) and thin clay laminations (B).

Our interpretation of the depositional environment for this unit— inferred from its lateral contact to a channel-like sand body (Unit B), moderate sorting, and the presence of silt and clay laminations and flaser bedding— is in an intertidal environment, probably as longitudinal cross-beds associated with a tidal channel (Figure 4.17). Longitudinal cross-bedding is very common in intertidal flat environments (Reineck and Singh, 1975). The lateral shifting of tidal channels on tidal flats produce beds, which in contrast to other types of cross-beds, run parallel to the current direction, and is thus called longitudinal cross-bedding (Reineck and Singh, 1975). According to the Reineck and Singh (1975) each inclined layer in itself is a bed (Figure 4.17) and contains different types of bedding, e.g., thinly laminated sand/mud bedding, small ripple-bedding, lenticular and flaser bedding, and thick mud layers. Individual beds in Unit A contains thin silt and clay laminations and flaser bedding (Figure 4.18).

Unit A has very low permeability ranging between 1 - 4 md (average 2.1 md). The actual thickness of unit A could not be determined because its lower contact is not exposed.

Unit B is in lateral contact with Unit A and has a massive channel shape (Figures 4.17 & 4.19). It is grayish-yellow with gray and yellow laminations visible on fresh surfaces (Figure 4.20), moderately sorted, well cemented, fine to very fine-grained sandstone. Based on the shape of this unit, we assume its deposition in a channel (probably, a tidal channel). Although fining upward sequence of a channel-fill is absent, the grain size distribution and sequence primarily depends on the available material. Unit B is classified as a tidal channel based on its channel-like shape and its lateral association with the longitudinal cross-bedded Unit A. Unit B has low permeability ranging between 0.01 - 5.5 md (average 1.0 md).

Overlying Units A and B is a 4 foot thick, yellow, gray, moderately cemented, fine grained flaggy sandstone (Unit C) (Figure 4.17). This unit contains evaporite relicts and exhibits adhesion ripples (Figure 4.21). Adhesion ripples are formed when dry sand is blown across a wet sediment surface and sticks to the surface on impact. Capillary rise of moisture helps to further trap grains by constantly wetting the new surface and eventually

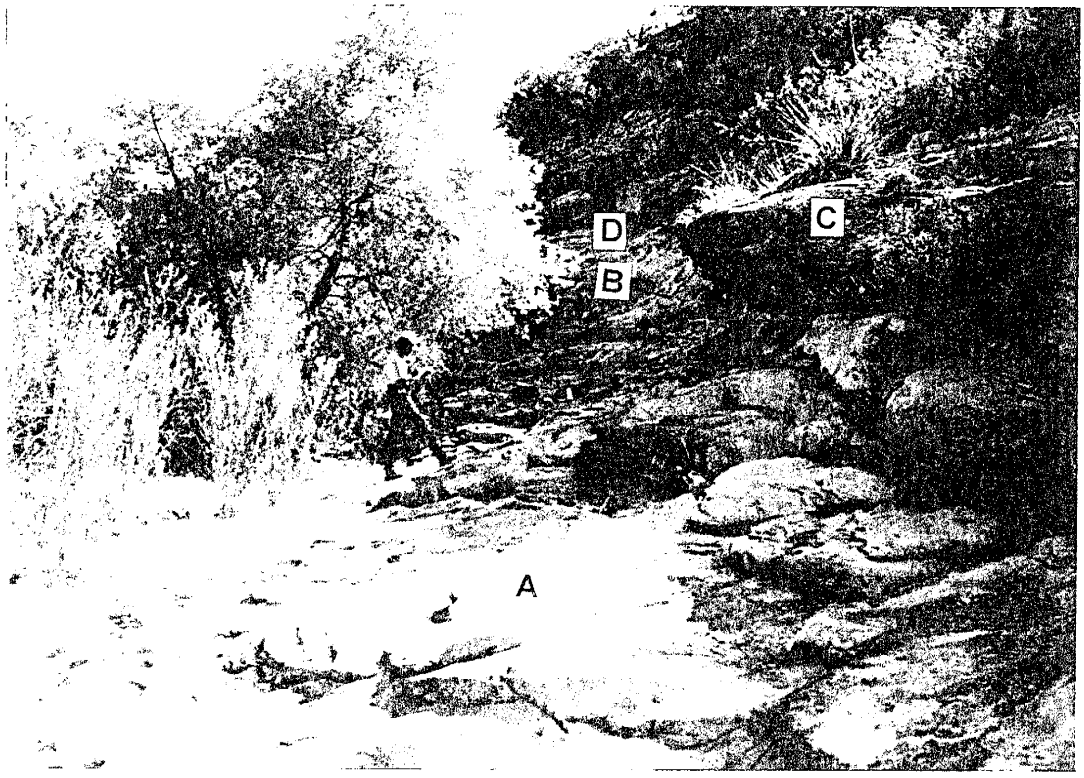

Figure 19: Photograph showing the relationship between Units A, B, C, and D in Section 1 in the Rocky Arroyo area.

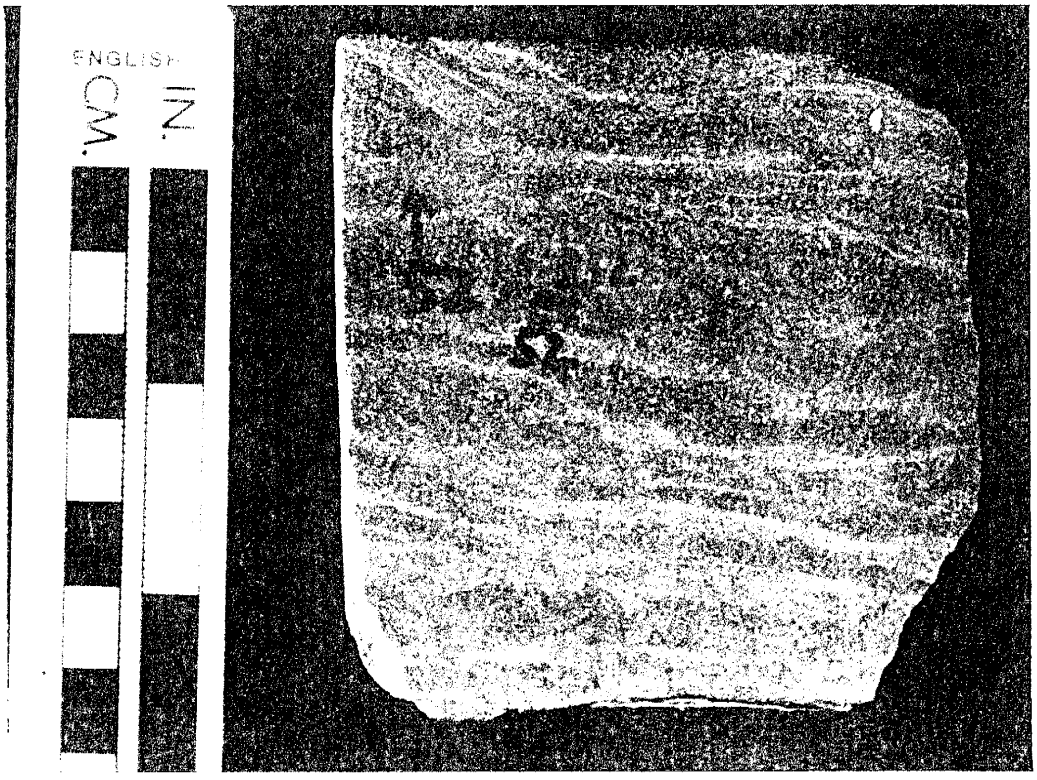

Figure 4.20: Hand sample from Unit B showing gray and yellow laminations.

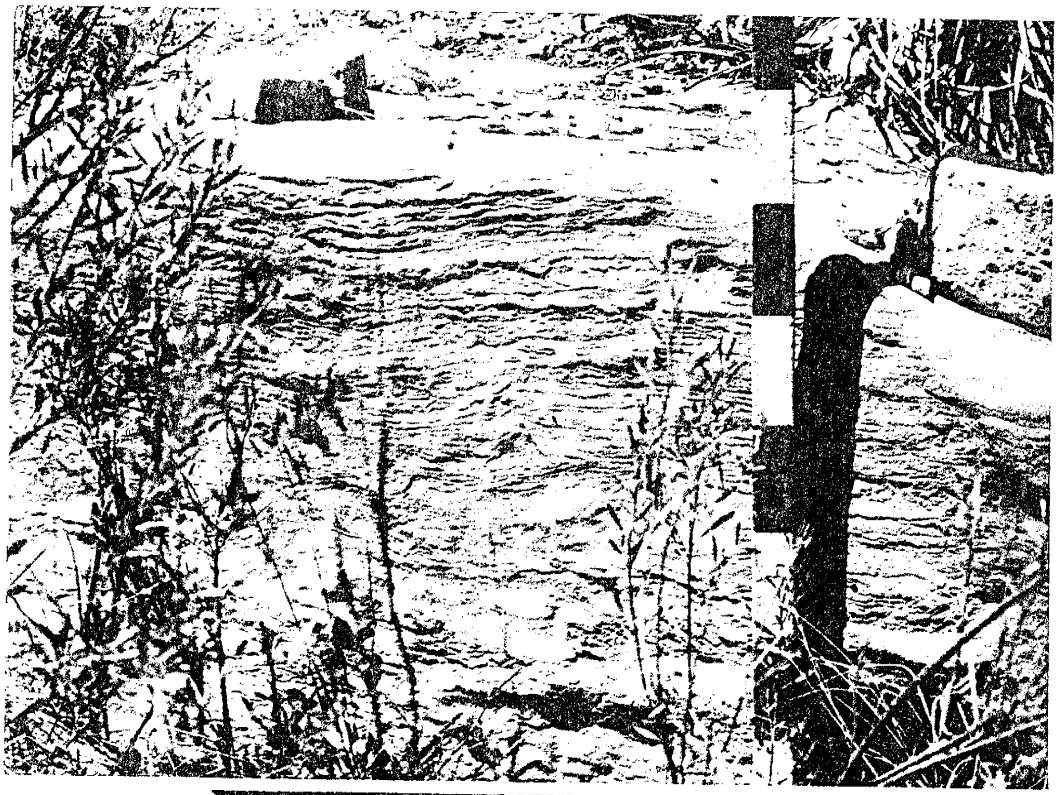

(A)

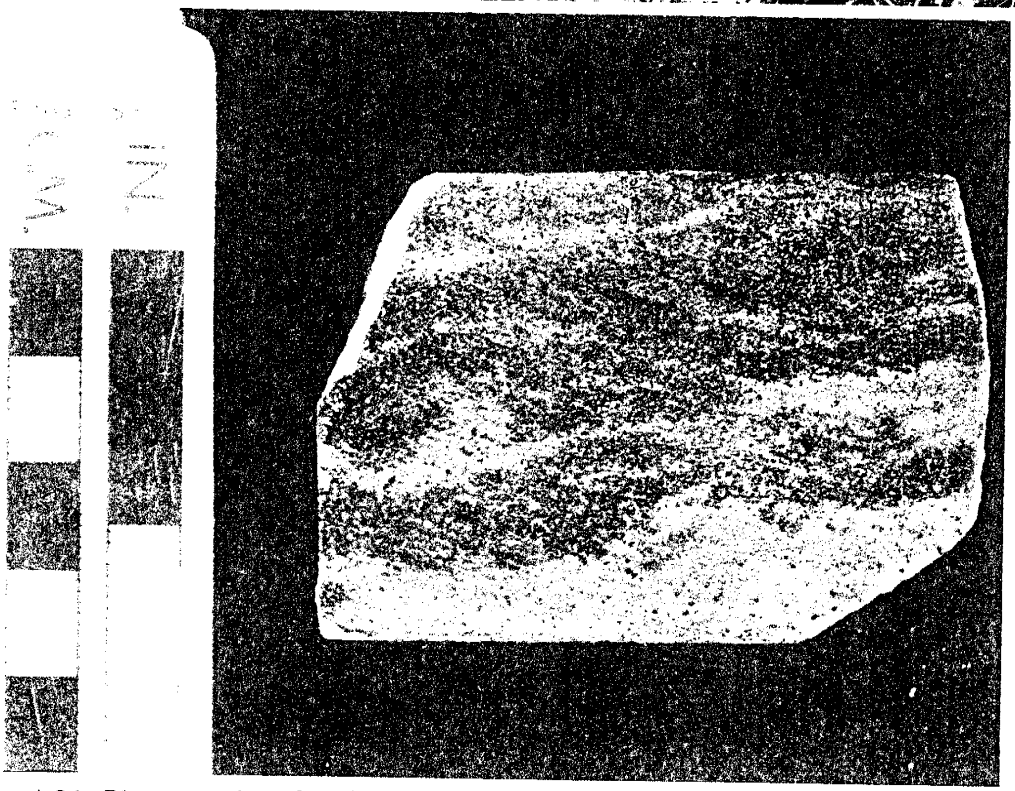

(B)

Figure 4.21: Photographs of Unit C outcrop showing adhesion ripples (A) and a hand sample showing irregular bedding surfaces formed due to adhesion ripples (B).

an irregular, blistered, but sometimes ripple-like surface develops (Collins and Thompson, 1982). According to Glennie (1970), adhesion ripples are extremely important in the deposition of inland sabkha. Because of the presence of adhesion ripples and evaporite relicts, Unit C may be assigned an eolian or sabkha environment of deposition. It shows moderate permeability ranging between 1 - 36 md (average 7.4 md) and is continuous over the entire length of the section.

A 2 foot thick bed of clay (Unit D) is present above Unit C (Figure 4.17). It is thinly to moderately bedded, moderately cemented, and contains numerous small pure iron concretions. It probably represents deposition in calm water conditions (probably a lagoon) as finely disseminated iron is commonly deposited in deltaic, lagoonal, and estuarine environments (Tucker, 1981). Based on the prevailing geologic setting during the deposition of Queen Formation (Guadalupian), we suggest the deposition of Unit D in a lagoonal/salina environment. Unit D exhibits the lowest permeability ranging between 0.2 - 1.16 md (average 0.7 md).

Unit E is 4 foot thick and consists of yellow, moderately to thinly bedded (flaggy), moderately to poorly cemented, fine-grained sandstone. The fresh surfaces show yellow and gray laminations. The lower part of this unit shows flaser bedding, while the upper part exhibits adhesion ripples and abundant evaporite relicts (Figure 4.22). Unit E probably represents a upward transition from lagoonal/salina to sabkha/eolian environments. The lower part which exhibits flaser bedding was probably deposited in aqueous environment. Flaser bedding may have formed due to waves generated by the storms in a lagoon/salina. The upper part which exhibits adhesion ripples and abundant evaporite relicts was deposited in a sabkha/eolian environment. The lower part of Unit E has low permeabilities (1- 5 md), whereas, the upper part has high permeabilities (4 - 176 md). Overlying Unit E is 2 foot thick Unit F, which is similar to Unit D (Figure 4.17).

The rest of Section 1 consists of a 10 foot thick, yellow and gray, moderately to poorly cemented, with abundant evaporite relicts, very fine to fine-grained sandstone bed (Unit F; Figure 4.17). The eastern part of this unit shows flaser bedding as well as thin

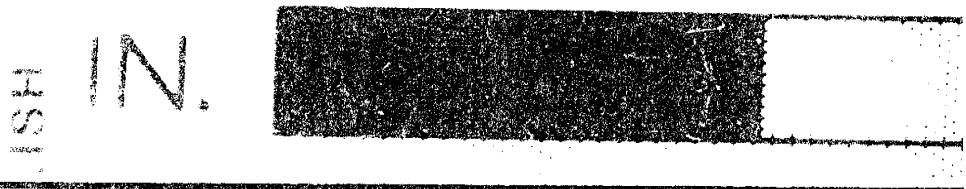

(A)

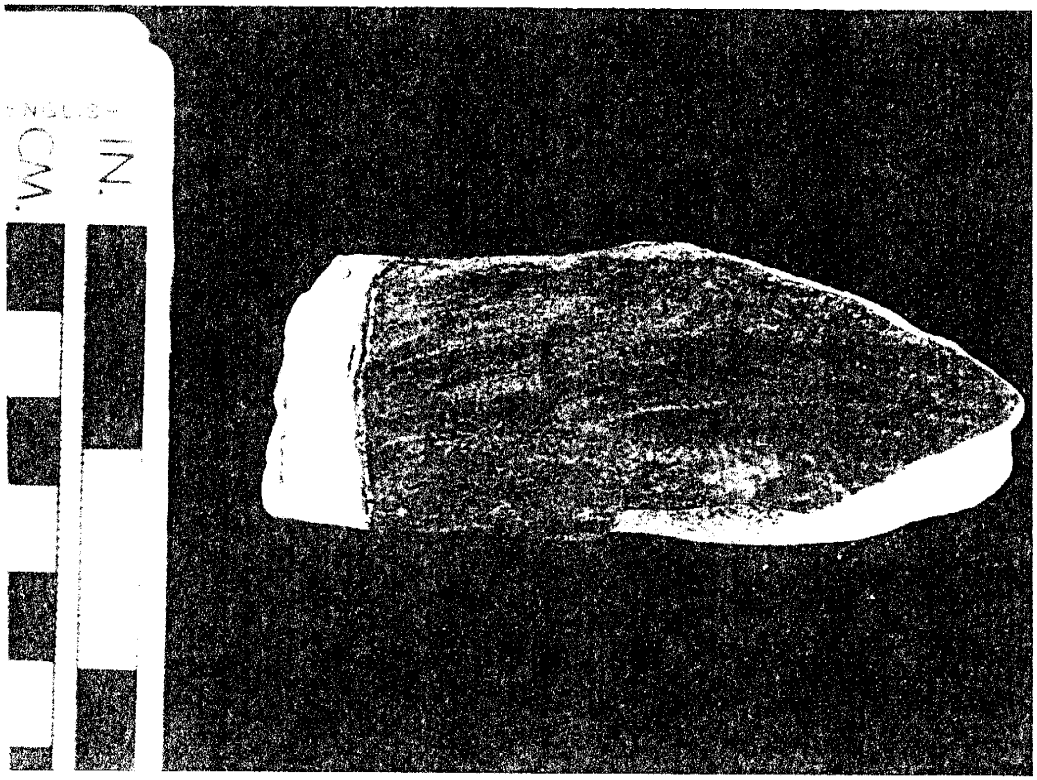

(B)

Figure 4.22: Hand samples from Unit E showing flaser bedding (A) and adhesion ripples (B).

clay laminations (lagoon/salina) and the western part exhibits adhesion ripples and evaporite relicts (sabkha/eolian). Therefore, this unit was probably deposited in a laterally merging aqueous (eastern part) and sabkha/eolian environment (western part). Permeability ranges between 1 - 95 md (average 9.5 md).

Section 2

In order to acquire a three-dimensional distribution of individual units Section 2 was measured in a north-south direction perpendicular to the eastern end of Section 1. Section 2 is located about 1,500 feet southwest of Section 1 (Figure 4.15). It has a lateral extent of 300 feet. Individual units exhibit sheet-like geometry as opposed to varying thicknesses observed in the east-west direction in Section 1. This suggests that in the Rocky Arroyo area most of the depositional changes occurred perpendicular to the Goat Seep reef complex. The contact between the overlying Seven Rivers Formation, including the transition zone is also clearly visible. Section 2 exhibits units similar to Section 1, with the exception of Unit B (Figure 4.23). Unit B is absent in Section 2. The lithology and the average permeability distributions are the same as Section 1 (Table 4.2; Figures 4.17 & 4.23). About 70 permeability measurements were made.

Section 3

Section 3 runs east-west along the south wall of Rocky Arroyo, and has a lateral extent of 800 feet. Section 3 is located 2,500 feet west of Section 1 (Figure 4.15). At this location, 30 - 35 feet of Shattuck Member is exposed (Figure 4.24). In Section 3, Units A and B are not exposed. Section 3 consists of Units C, D, E, F, and G. More than 30 permeability measurements were made on an irregular grid. This section is more permeable than Sections 1 and 2 (Table 4.2; Figure 4.24). The grain size distribution as well as sedimentary structures are similar to Section 1.

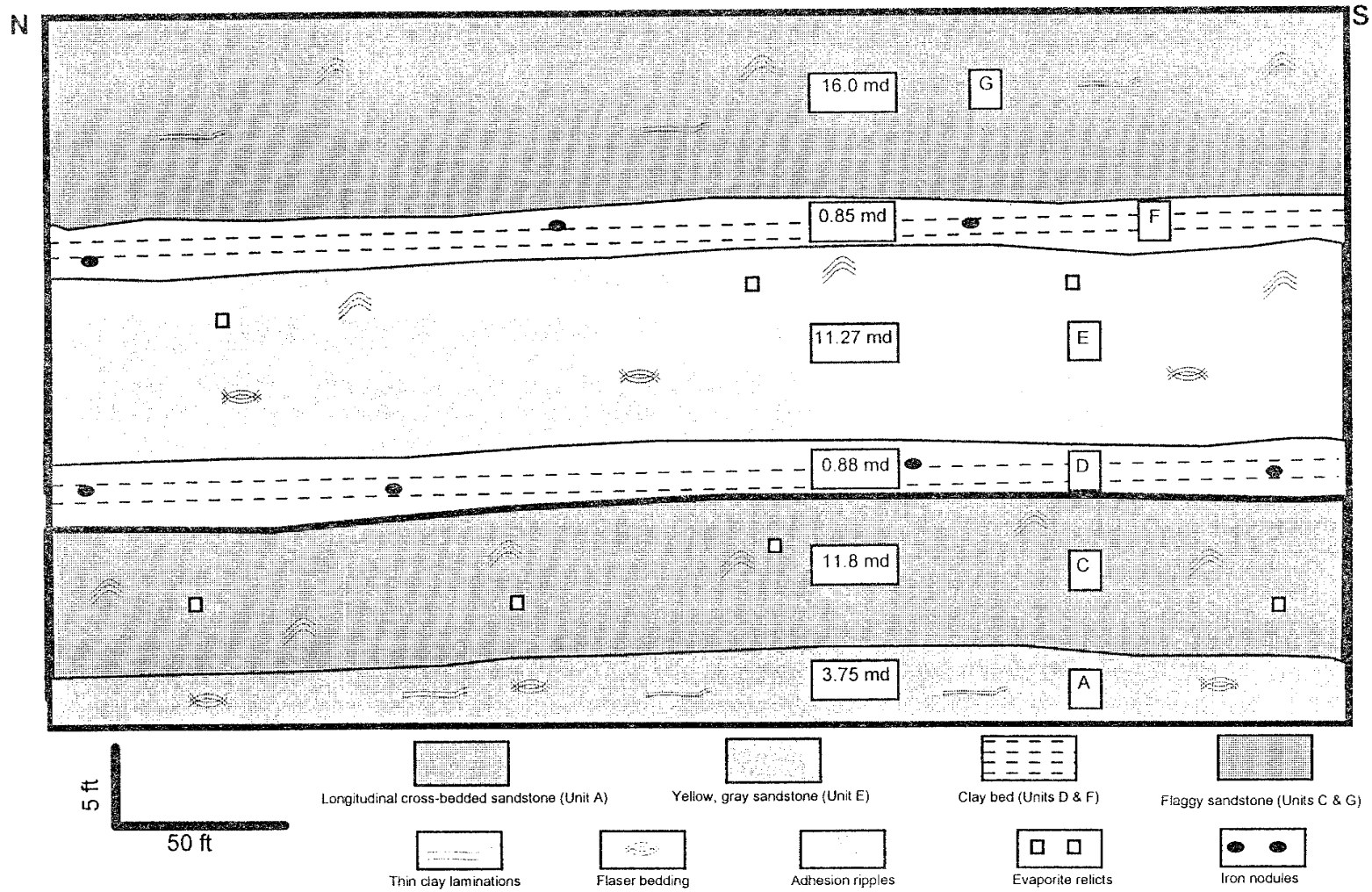

Figure 4.23: Section 2 runs north-south perpendicular to Sections 1. Unit B (channel sand) is missing in this section. Permeabilities are similar to Section 1.

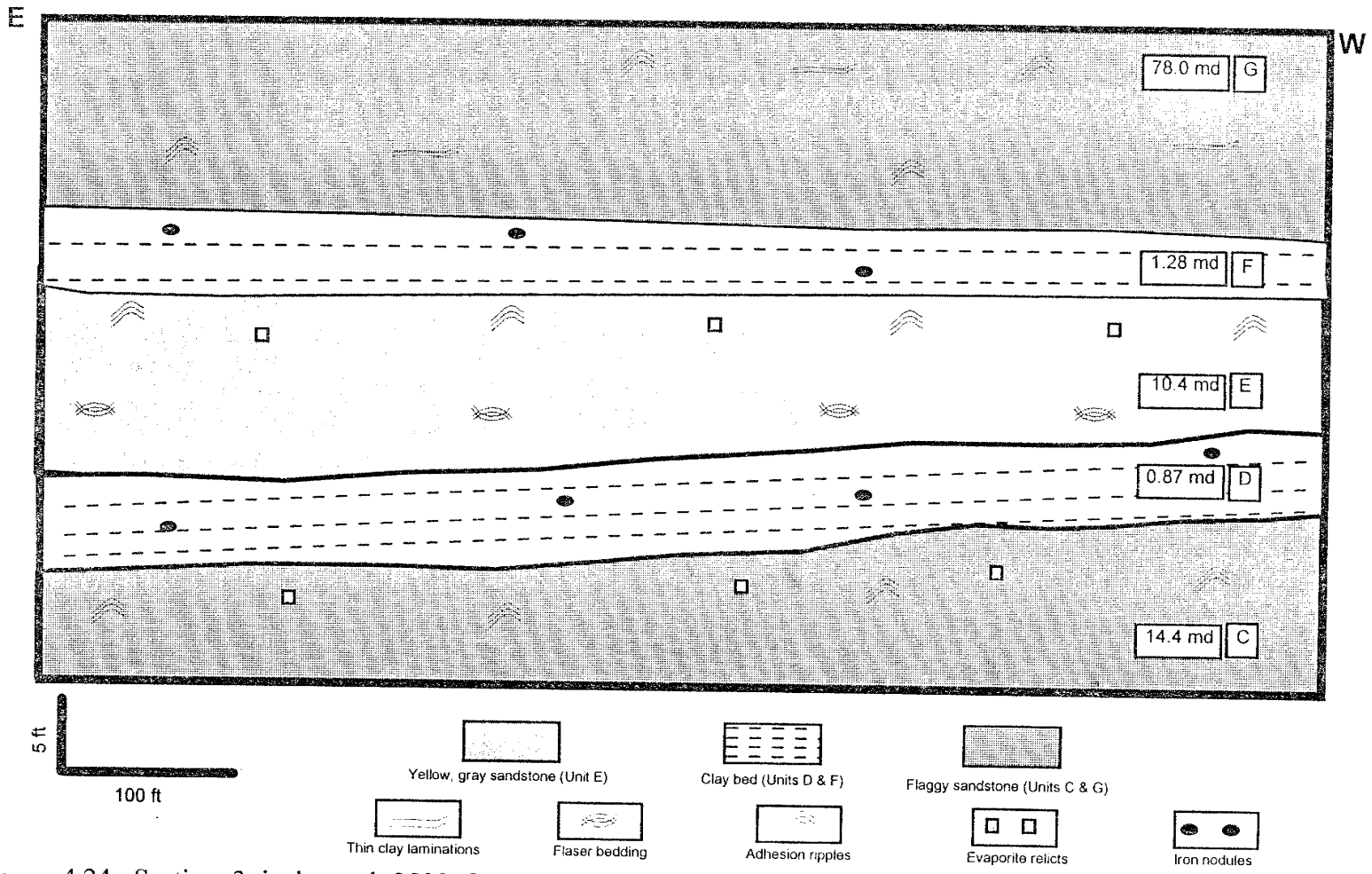

Figure 4.24: Section 3 is located 2500 feet west of Section 1. In this section Units A and B arenot exposed. Permeabilities are also higher than the Sections 1 & 2.

Section 4

Section 4 runs east-west, has a lateral extent of 1,500 feet, and was measured along the north wall of Rocky Arroyo. This section lies 3,000 feet northwest of Section 3 (Figure 4.15). Unlike Sections 1 and 3, individual units exhibit typical sheet-like geometry (Figure 4.25). Here the Shattuck Member is exposed in its entirety, underlain by the Queen dolomite and overlain by the Seven Rivers Formation. Section 4 is 55 feet thick and consists of very fine to fine and silty sandstone interbedded with thin beds of clayey siltstone. This section can be divided into two units—Unit 1 and Unit 2 (Figure 4.25)—and cannot be correlated with individual units of Sections 1 through 3.

The upper 17 feet (Unit 1) are yellow to yellowish orange, thinly bedded, moderately cemented, fine-grained, silty sandstone (Figure 4.25). Permeability ranges between 10 md and 86 md (average 39.0 md). Unit 2 is a 35 foot thick sequence consisting of 4 thick sandstone beds (average thickness 8 feet) interbedded with two 2-foot thick clayey siltstones (Figure 4.25). The sandstones are yellow and pink, moderately cemented, fine-grained to silty sandstones. These sandstones are moderately to thinly bedded and exhibits cross and wavy laminations. There are no differences in the permeabilities between the sandstones and silty sandstones. Due to the poor quality of clayey siltstones samples, no permeability measurements were made on them. Again, due to bad exposure of this section, permeability measurements were not made on regular grids. About 100 permeability measurements were made. Permeability ranges between 7 md and 95 md (average 34 md; Table 4.3). Towards the west the whole section changes from silty sandstone to dominantly evaporitic within a distance of one mile.

Depositional environment of the Shattuck outcrops in the Rocky Arroyo area

The depositional environments of Shattuck Member outcrops in the Rocky Arroyo and adjacent areas are a matter of debate. We suggest, based on this preliminary study, that the Shattuck Member was deposited in combined lagoonal/salina and sabkha/eolian environments. The reason for contradicting a dominantly eolian environment of deposition, as proposed by Mazzullo *et al.*, (1984, 1985), lies in the absence of typical

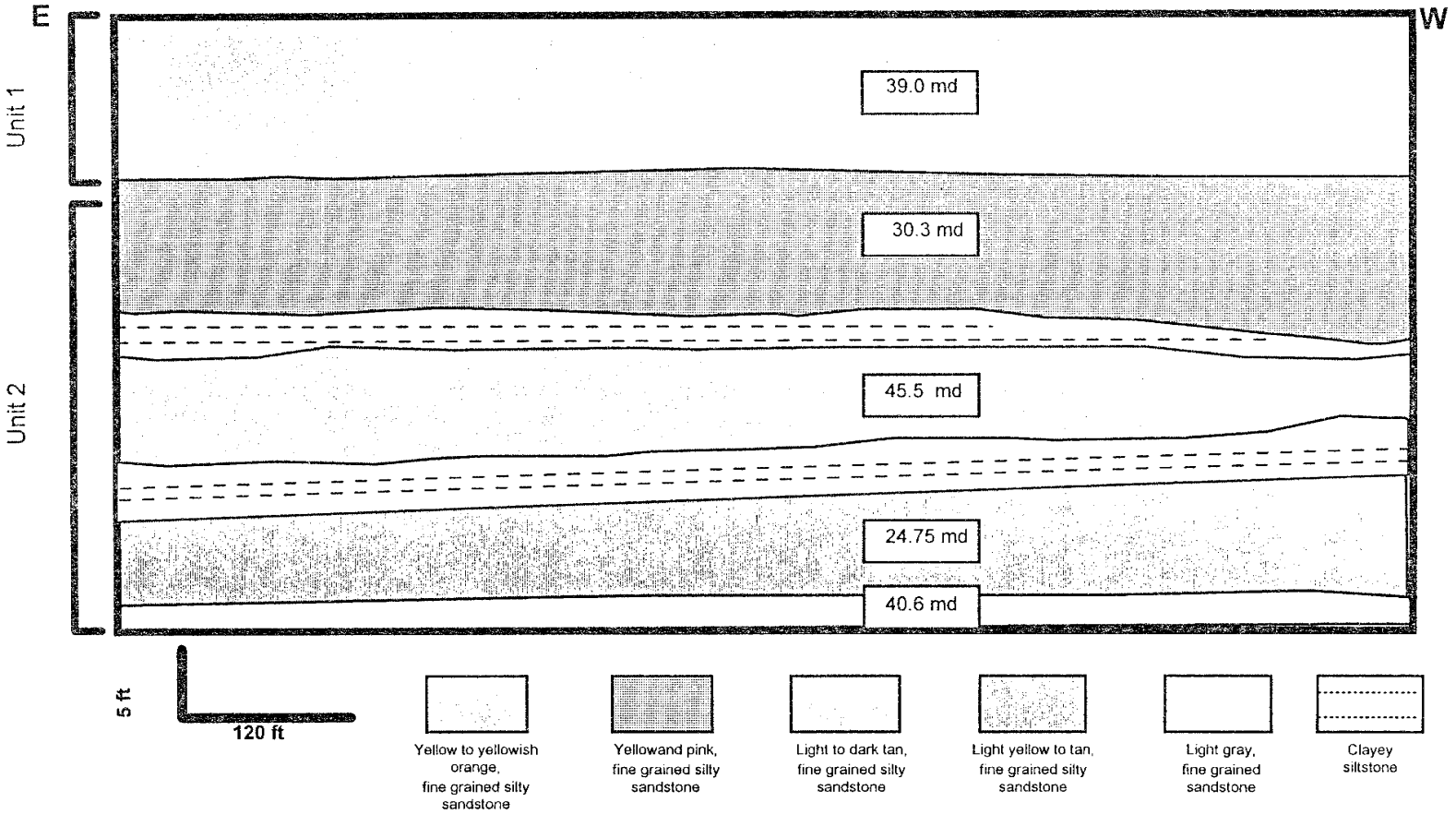

Figure 4.25: Section 4 is located about 3,000 feet northwest of Section 2. Unlike Sections 1 and 2, in this section individual individual units exhibits sheet-like geometry. Permeabilities are considerably higher than Sections 1, 2, & 3. Unit 1 is yellowish orange, thinly bedded, moderately cemented, fine grained sandstone. Unit 2 consists of 4 sandstone beds interbedded with 2 siltstone beds. Sandstones are yellow, tan, pink, moderately to thinly bedded, fine grained to silty sandstone.

Section 4			
Units	N	Mean	STD (σ)
Unit 1	25	39.00	19.60
Unit 2	16	30.30	10.90
	11	45.50	24.70
	20	24.70	12.90
	25	40.60	10.40

Table 4.3: Summary of permeability data from the Shattuck Member outcrop on the north wall of Rocky Arroyo.

eolian features, which Mazzullo also acknowledges (Mazzullo, 1985). The presence of flaser laminations, minor cross- and wavy-laminations, poor to moderate sorting, detrital clay matrix as well as clay layers, and bioturbation points towards deposition in an aqueous (lagoon/salina) environments. Mazzullo *et al.*, (1985) suggested the reworking of the eolian sands by marine currents and waves. In some units the presence of adhesion ripples and evaporite relicts does suggest sabkha/eolian deposition. Therefore, the Shattuck Member in the outcrops is probably not the product of a single depositional environment, but a combination of lagoonal/salina and sabkha/eolian processes.

Bone Tank Draw

Section 5

Section 5 is exposed in the Bone Tank Draw area (Figure 4.15). This section of the Shattuck Member is located about 16 miles landward of the reef, similar to the Sulimar Queen field, which is 20 miles landward of the Goat Seep Reef. The Shattuck Member at Section 5 exhibits similar lithologic characteristics to the Shattuck Member in the subsurface. This section consists of 11 - 15 foot thick sandstone sequence overlain and underlain by gypsum (Figure 4.26).

Section 5 consists of three small subsections separated by a horizontal interval of 200 feet (Figure 4.26). The individual subsections runs east-west and are subparallel to each other (Figure 4.26).

The base of Section 5 consists of a 10 foot thick sequence of thick-bedded red and grayish-green gypsum (Unit X) with minor siltstone intercalations. Overlying is a 6 foot thick bed of dark-gray to brown color, cross-bedded (with horizontal bounding surfaces), moderately cemented, very fine-grained gypsiferous sandstone (Unit Y). The formation of this bed may be attributed to a very shallow watertable or a wet surface over which dunes were migrating. According to Stokes (1968), the areas where groundwater is not too deep, e.g., in sand dunes migrating over an inland sabkha, water rises in the sand dunes and the cohesive action of water holds wet sand grains together, and the dry sand

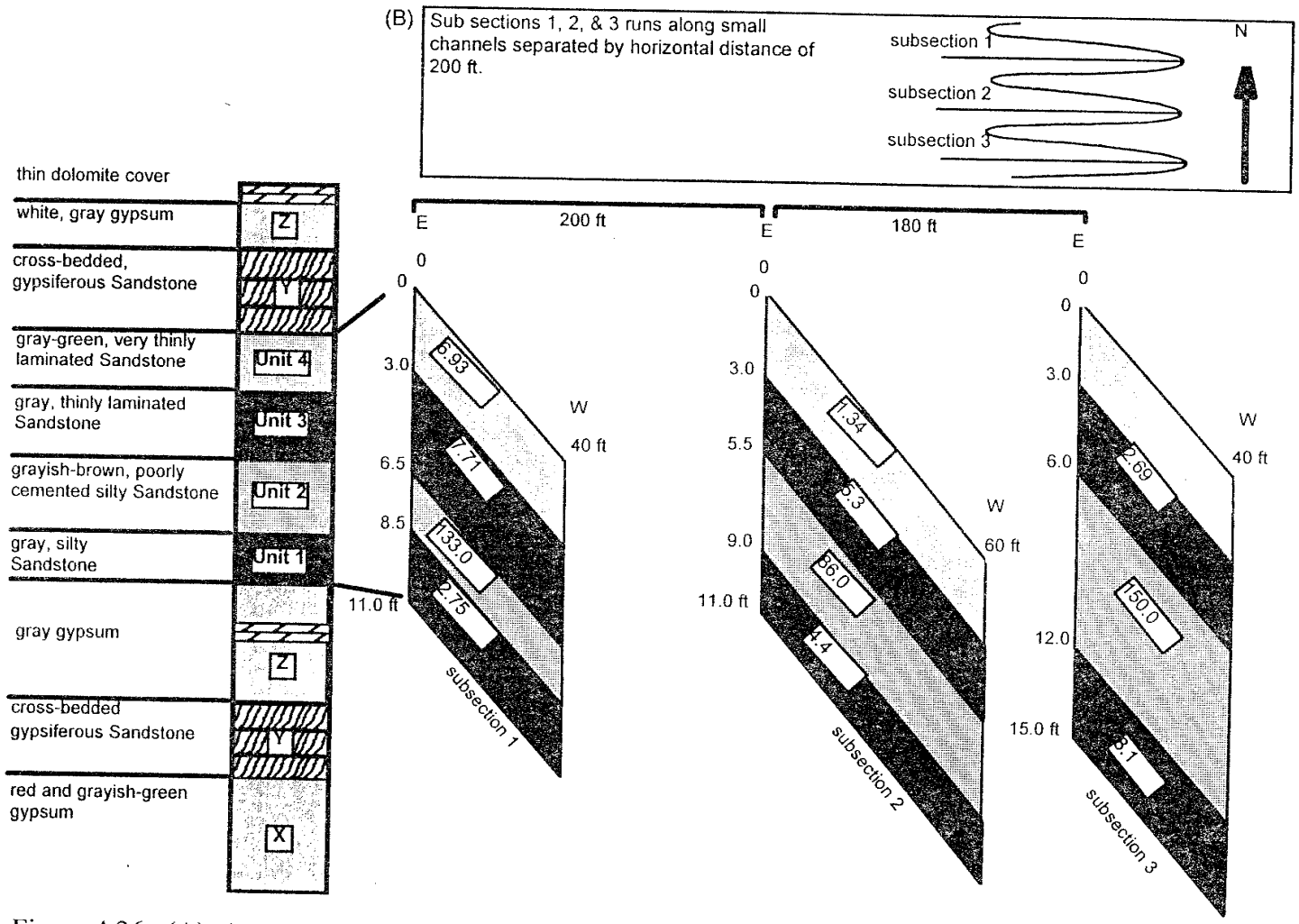

Figure 4.26: (A) A composite stratigraphic sequence of Section 5. The numbers inside the units are average permeabilities in millidarcies. (B) The individual subsections run east-west and are separated by distances of about 200 ft.

above this surface is removed, producing a rather smooth, horizontal surface. As new sand dunes migrate over this surface and the process is repeated several times, several smooth surface may be produced (Figure 4.26). McKee (1966) reported the presence of horizontal to sub-horizontal bounding surface in the white sand dunes in New Mexico, which were formed without any groundwater effect.

Overlying the cross-bedded gypsiferous sandstone is a 8 foot thick, white and gray gypsum bed (Unit Z) with a 6 inches thick dolomite bed (Figure 4.26).

Sandstone sequence

Overlying the gray gypsum is a sandstone sequence comprised of four individual units. Approximately 120 permeability measurements were made. A summary of permeability data is given in Table 4.4.

Unit 1 is the lowermost unit (Figure 4.26) and consists of gray, moderately cemented, moderately bedded, very fine-grained, argillaceous, silty sandstone. Unit 1 shows no sedimentary structures and exhibits low permeability ranging between 1 md and 19 md (average 7 md). The northern section (subsection 1) contains carbonate cement, whereas subsections 2 and 3 have gypsum cement. This unit has variable thickness and thickens towards the south (Subsection 3).

Unit 2 is a grayish-brown, poorly cemented, moderately to poorly sorted, very fine- grained silty sandstone. It contains variable amounts of clay and exhibits thin clay laminations. In the north (Subsection 1) its thickness is 2 feet but in the south Unit 2 becomes 6 feet thick (Subsection 3). This unit has the highest permeability among the sandstone units, ranging between 10 md and 447 md (average 140 md).

Unit 3 is a gray to light green, moderately cemented, moderately to poorly sorted, very fine-grained silty sandstone. Fresh surfaces show discontinuous, less than 1 mm thick, parallel to subparallel laminae of gray and light green color. Unit 3 shows intense bioturbation. In the northern part (Subsection 1) carbonate cement is present and in the southern part (Subsection 2 & 3) gypsiferous cement is present. This unit exhibits the lowest permeabilities, ranging between less than 1 md and 8 md (average 4.7 md).

Units	Subsection 1			Subsection 2			Subsection 3		
	N	Mean	STD (σ)	N	Mean	STD (σ)	N	Mean	STD (σ)
Unit 1	3	2.95	1.53	3	4.50	2.85	6	8.10	5.56
Unit 2	7	133.00	73.00	16	86.00	45.10	17	150.00	122.80
Unit 3	14	7.71	5.35	10	5.30	1.97	17	2.69	2.21
Unit 4	11	6.93	3.13	5	1.34	0.72	-	-	-

Table 4.4: Summary of permeability data from the Shattuck Member outcrop in the Bone Tank Draw area.

Unit 4 is a gray to light green, thinly laminated, moderately cemented, very fine grained silty sandstone. Unit 3 and 4 are similar to each other when fresh surfaces are observed. Unit 4 can be differentiated from Unit 3 in the field based on their different weathering behaviors. Unit 4 weathers into thin sandstone layers due to the presence of thin clay layers between the sandstone layers. Fresh surfaces show parallel to subparallel laminations, flaser bedding, and bioturbation. This unit has the lowest permeability among the sandstone units, which ranges between less than 1 md and 5 md (average 3 md).

Overlying the sandstone sequence is a cross-bedded gypsiferous sandstone similar to one towards the bottom of this section (Unit Y). Overlying the cross-bedded gypsiferous sandstone is a 4 foot thick white gypsum bed (Unit Z) which is in turn overlain by a 6 inches thick white dolomite layer similar to the one in the lower part of this section. This section probably presents a complete cycle of sedimentation.

Based on the presence of overlying and underlying bedded gypsum, cross-bedded gypsyferous sandstone, and sandstones with clay laminations, flaser bedding, and bioturbation, a mixed salina/lagoonal and eolian environment of deposition may be attributed to Section 5. Sandstones and bedded gypsum were deposited in salina/lagoonal environment, whereas the cross-bedded gypsyferous sandstone was deposited in the eolian environment.

Petrographic Analysis

A petrographic analysis of the outcrop samples was performed to identify the similarities and differences with the subsurface samples, especially the diagenetic sequence. A generalized paragenetic sequence for the Shattuck Member outcrops is given in Figure 4.27.

The Shattuck sandstones in the outcrops are composed of angular to subangular, poorly to moderately sorted, poorly to well cemented, fine to very fine-grained arkosic sandstone. The Shattuck Member outcrops have detrital compositions similar to the subsurface Shattuck Member as described previously.

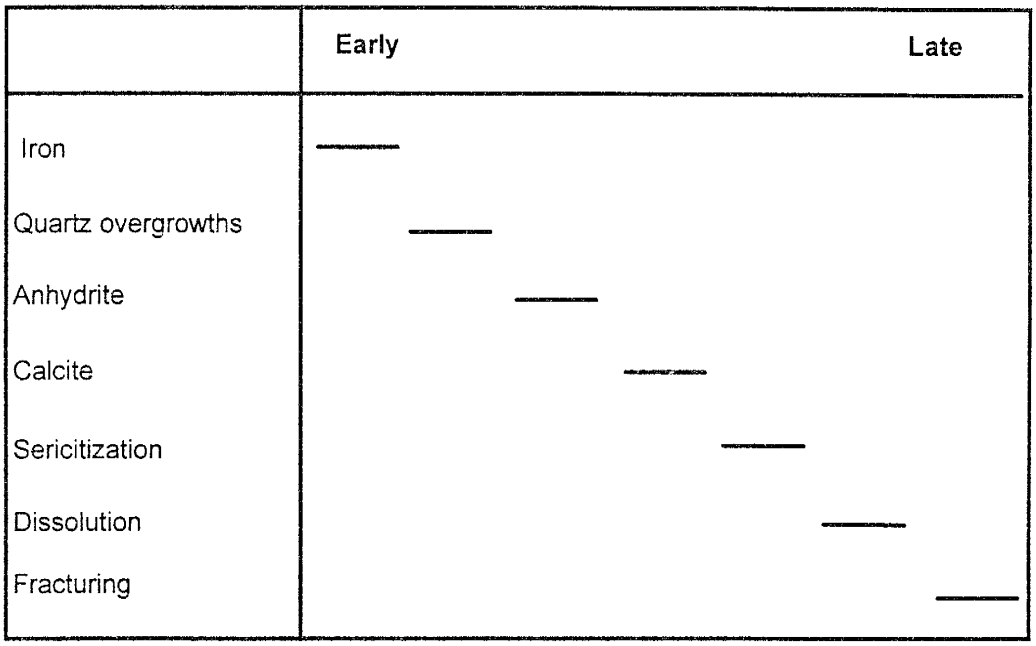

Figure 4.27: Generalized paragenetic sequence for the Shattuck Member in the outcrops.

In outcrops, quartz grains show syntaxial overgrowths containing inclusions of probable iron oxide. In the outcrops, silica also occurs as pore-filling cement, whereas in the subsurface it only occurs as overgrowths. Feldspars show considerable alteration ranging from sericitization to partial to complete dissolution similar to subsurface.

The main cementing material is finely crystalline calcite, whereas in the subsurface the cementing material is dominantly anhydrite and dolomite. In Section 5, gypsum is the dominant cementing material. Similar to the subsurface, iron (hematite) cement is present in almost all samples in trace amounts.

Both primary and secondary porosity are present. Porosity types consist of primary, secondary intergranular, intraconstituent, and moldic porosity. Secondary porosity is dominant in high permeability samples. Secondary porosity is formed by the dissolution of cement and constituent grains, mainly feldspar. In the subsurface, porosity was also created by the dissolution of cement and detrital grains, mainly feldspar.

As stated before, bad exposures of the Shattuck Member in both Rocky Arroyo and Bone Tank Draw prohibited the collection of permeability data on a regular grid with the exception of Section 1. The outcrop study was conducted to collect the "soft geological" information about the depositional environment, lithologies, and areal distribution of individual units. Outcrops around both Sections 1 and 5 (which were studied in detail) within a radius of one mile show drastic changes in lithologic makeup and depositional environments. Section 4, which is located one mile north of Section 1, exhibits completely different lithologic characteristics, is 55 feet thick and has high permeabilities. Section 4 changes from clastic to completely evaporitic composition within a lateral distance of one mile towards the west. Similarly, isolated outcrops approximately 3,000 feet north and northwest of section 5 are evaporitic and lack sandstone units.

Similar changes from sandstone to evaporites also occur in the subsurface and these changes are responsible for the formation of reservoirs (stratigraphic traps) in the Shattuck Member. It was also noted both in the subsurface and outcrops that the thickness of the sandstone units changes rapidly over short distances. The deposition of

the Shattuck Member in both outcrop and in the subsurface took place in a mixture of aqueous and eolian environments. Information obtained from the outcrops were useful in understanding the overall behavior of the Shattuck Member in the southeast New Mexico.

DEPOSITIONAL MODEL

Background

The Northwest Shelf was a broad, flat area that borders the Delaware Basin in the west Texas and southeast New Mexico during Permian time (Figure 1.3A). The Delaware Basin was a deep structural depression covering 10,000 square miles was surrounded by flat shelves that slope at a very low angle to the basin (Newell *et al.*, 1953). In the early Permian, the Delaware Basin subsided rapidly and accumulated a thick sequence of sediments. The basin continued to deepen and receive sediments until subsidence slowed in the mid-Permian and reefs began to develop around its border in Guadalupian time (Adams, 1965).

The Northwest Shelf was developed before the Permian, when numerous reefs were formed along its trend in late Pennsylvanian time. By Guadalupian time the shelf was 250 - 300 miles wide (Jacka and Franco, 1974). Early Permian rocks of the shelf area (Yeso and San Andres Formations) are mostly dolomites with thin interbeds of fine-grained sandstone. Middle and Upper Guadalupian rocks of the shelf area are called the Artesia Group (Figure 4.1). These are dolomites, sandy dolomites, fine sandstones, siltstones, red evaporitic silty shales, and evaporites. Landward, dolomites grade first to sandstones, then to evaporitic silty shales and evaporites (Newell *et al.*, 1953). Late Permian evaporites that filled the Delaware Basin also covered lagoonal areas of the Northwest Shelf and the red beds deposited above these are the last sediments of the Permian (Newell *et al.*, 1953).

As reported by Ball (1971) and Jacka and Franco (1984), the paleoclimate over much of the western interior was hot and arid in the Permian. During the Permian time, the Northwest Shelf of the Delaware Basin was situated in low latitude equatorial region

which created the hot and arid climate (Fischer, 1988).

Detailed facies models for the Queen and other shelf formations are presented by Williams (1967, 1968), Kendall (1969), Silver and Todd (1969), Ball *et al.*, (1971), Meissner (1972), Jacka and Franco (1974), and Ward *et al.*, (1986).

Models of Jacka and Franco (1974); and Silver and Todd (1969)

In the following section a summary of the depositional model proposed by Jacka and Franco (1974) is presented. Figure 4.28 illustrates the facies association described by Jacka and Franco (1974). They recorded seven depositional environments in the Permian shelf: (1) reef, (2) backreef apron, (3) lagoon, (4) intertidal zone, (5) coastal sabkha, (6) continental sabkha, and (7) deflation flats. They considered three general hypotheses to explain the Guadalupian depositional cycles, which are given below.

(1) Alternating tectonic subsidence and uplift caused intervals of submergence and emergence and caused the depositional cycles.

Tectonic processes are not known to rhythmically reverse themselves within relatively short time intervals. Evidence indicate that during Guadalupian time the Permian Basin was characterized by extreme tectonic quiescence (Adams, 1965). For these reasons, Jacka and Franco (1974) rejected any tectonic control hypothesis.

(2) Seaward progradation of coastal and continental sabkha deposits progressively infilled shelf lagoons. Continuous subsidence of the shelf area eventually caused an episode of submergence, followed again by progradation and progressive infill of lagoons. Regressive phases of depositional cycles reflect seaward progradation of coastal and continental sabkha facies and progressive lagoonal infilling.

According to Jacka and Franco (1974), this may have largely occurred during high still stands of sea level when climates were arid. It is difficult to explain repeated episodes of transgression, which followed regressive phases, wholly within the context of continuous subsidence.

(3) Glacially controlled eustatic sea level fluctuations, superimposed upon continuous subsidence of the shelf, caused alternating submergence and subaerial exposures. Based

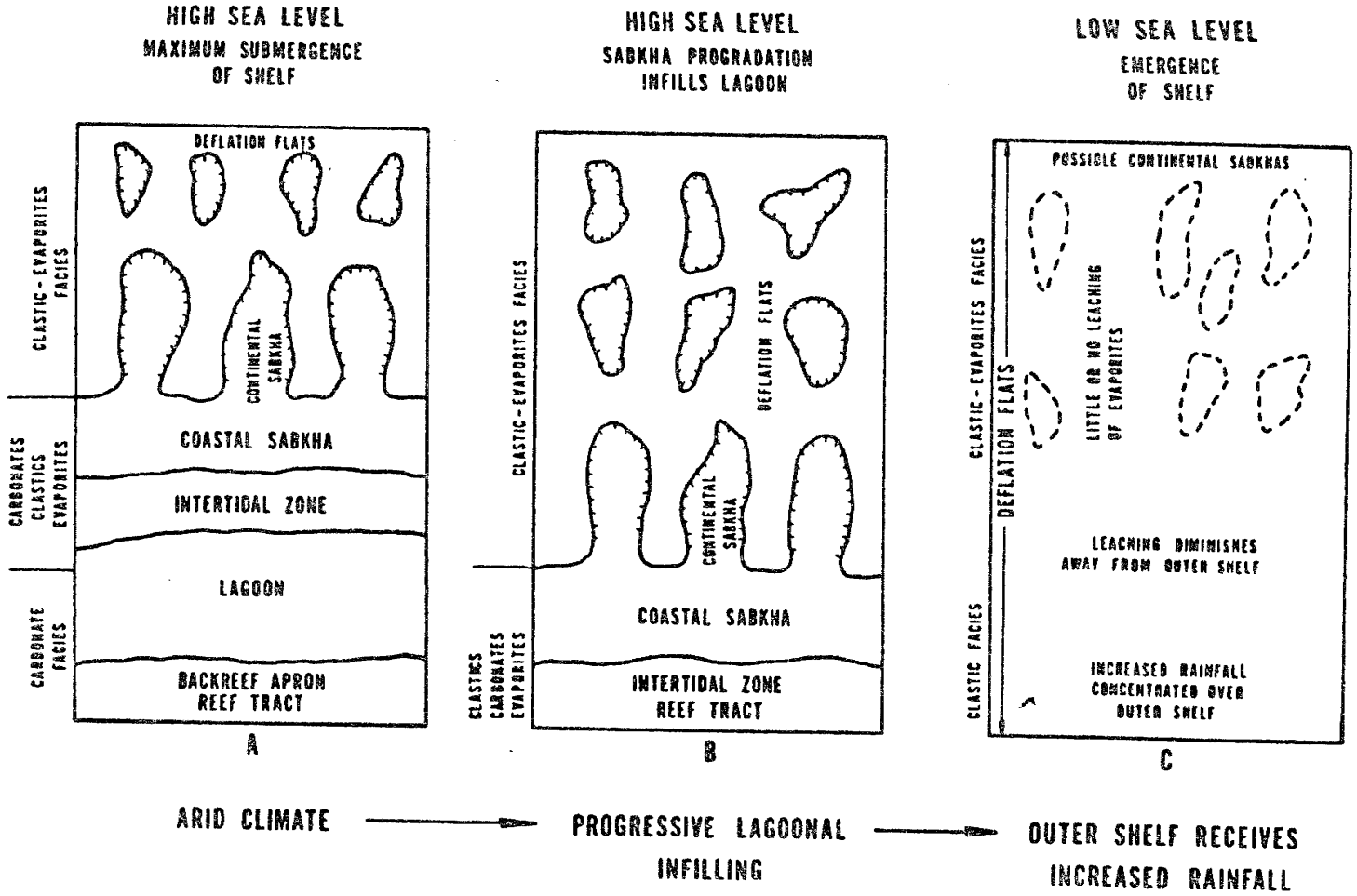

Figure 4.28: Model of sabkha progradation into lagoon. (A) Facies relationships that characterized Permian high stand of sea level when climates were arid (interglacial-interpluvial intervals). (B) Facies relationships that reflect progradation of coastal and continental sabkhas and deflation flat with progressive lagoonal infilling. (C) Facies relationships that characterized Permian low stands of sea level when the outer shelf received increased rainfall (glacial-pluvial interval) (Jacka and Franco, 1974).

on diagenetic evidence and Guadalupian climate, Jacka and Franco (1974) support the idea of climatic changes associated with major sea level fluctuations. No details of the diagenetic evidence as well as the sea level fluctuations and associated climatic changes are given in the paper by Jacka and Franco (1974). According to Jacka and Franco (1974), in Guadalupian time high stands of sea level were characterized by arid climates and precipitation of evaporites in coastal and continental sabkhas (interglacial-interpluvial interval) (Figure 4.28A). With continued aridity the sabkha and continental facies migrated seaward and filled the lagoon (Figure 4.28B). As the sea level dropped and rainfall increased over the outer shelf, carbonates were calichified (development of vadose diagenetic environment), some evaporites were leached, and accumulation of sediments ceased (Figure 4.28C).

Based on the magnitude and frequency of sea level fluctuations and because of associated climatic changes, the glacio-eustatic hypothesis is favored by Jacka and Franco (1974) as the major source of transgression and regression. Silver and Todd (1969) proposed a similar model for Guadalupian sediments. Clastics were all deposited as supratidal or continental facies and prograded across the lagoon only during extreme low stands of sea level.

In the model of Jacka and Franco (1974), most of the sands were deposited by eolian processes, and were deflation flat sediments; only the brine-pan deposits were water laid. Deflation flats occur inland from coastal sabkhas and they surround or engulf continental sabkhas (Figures 4.28A & 4.28B, Jacka and Franco, 1974). Deflation flat sediments are fine-grained, locally silty sands that were cemented by dolomite and anhydrite during early burial. They contain mud crack clasts and casts, adhesion ripples, and lenses of well-rounded medium to coarse quartz grains as lag deposits. Some dunes may have developed over parts of the deflation surfaces. Some evaporites were precipitated at the surface.

Model of Ball *et al.*, (1971)

The interpretation of Ball *et al.*, (1971) differs from the ones just described on several points (Figure 4.29).

(1) Barrier islands developed behind the reef and had associated sabkha and tidal-flat deposits on their flanks. William's (1969) model, although similar to the one of Jacka and Franco (1974), does include a barrier island facies behind the reef. Outcrop studies, particularly Williams (1967), have documented the presence of these carbonate shoals in the Queen Formation.

(2) Lagoonal sediments include quartz sands, evaporitic dolomites and bedded evaporites.

(3) The facies did not prograde as stripes parallel with the shelf edge.

(4) The shelf was never completely emergent. There are no marine sands in either Jacka and Franco's (1974) or Silver and Todd's (1969) models. Ball *et al.* (1971) found traction-current features in outcrops of the quartz and carbonate sands that indicate transport parallel with the shelf edge indicating marine deposition.

(5) The only areas that show evidence of subaerial exposure are the carbonate shoals that contain pisolitic caliche zones (vadose zone pisolites). These are interpreted to be the highest points on the shelf.

(6) Deposition of sand was continuous, and was not restricted to low stands of sea-level.

Depositional Model

We propose a depositional model which is similar to that of Ball *et al.*, (1971). One important concern is that the above mentioned depositional models dealt with the entire Queen and to a certain degree underlying and overlying formations, whereas we are presenting a depositional model only for the Shattuck Member. Therefore, we are dealing with a very short time interval, and the migration of different depositional environments within the Shattuck Member may have occurred due to minor sea level fluctuations.

We developed the model after assimilating all the information from cores,

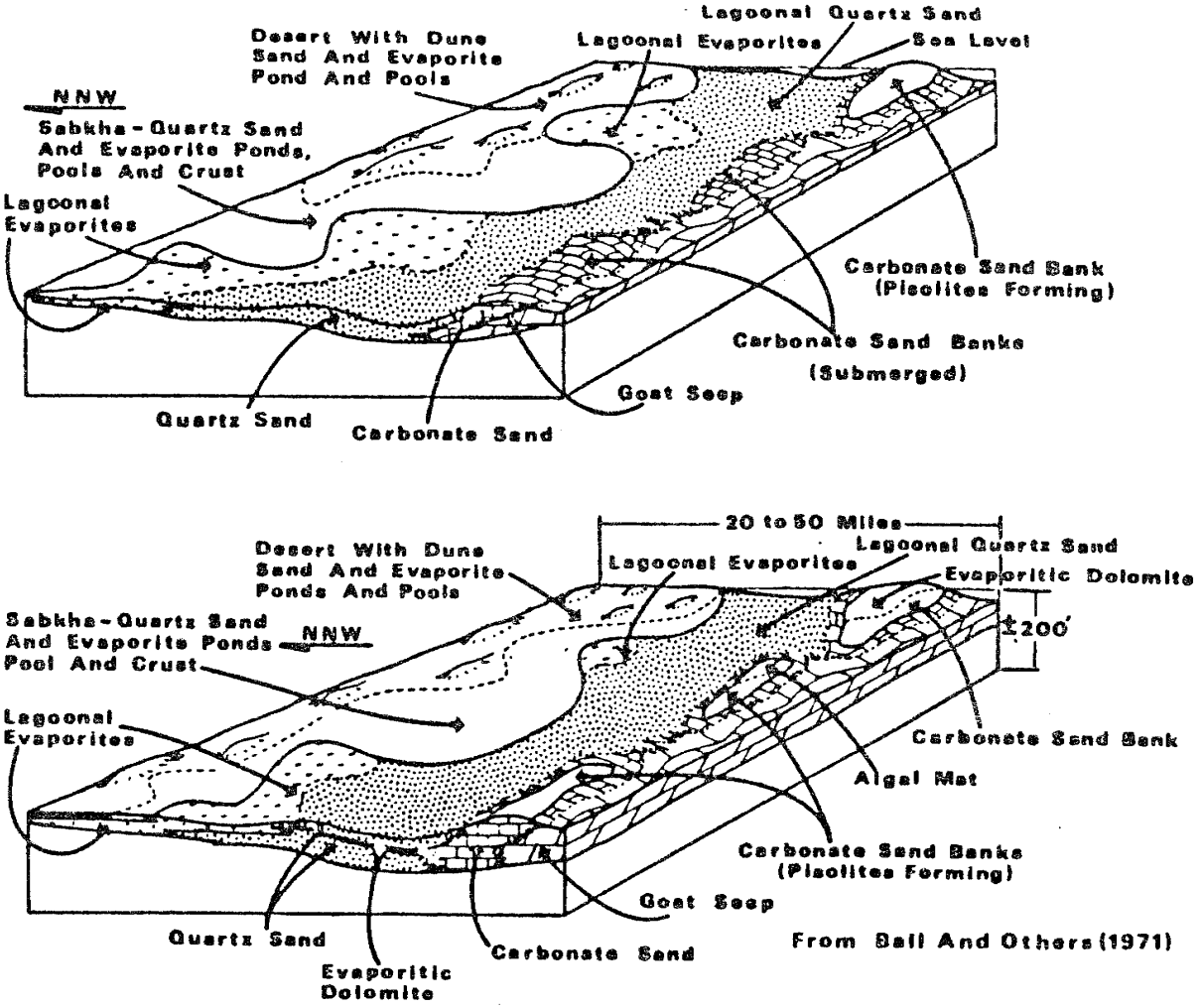

Figure 4.29: Model of interfingering lagoonal, sabkha, and eolian sandstone (Ball *et al.*, 1971).

petrographic analyses, logs, lithologic description of cores and chip analyses, and outcrop data.

North-south and east-west cross-sections for the net sand (sand portions with > 6% porosity) in the Sulimar Queen field are shown in Figures 4.30 & 4.31. Rescaled gamma ray logs were used to construct the cross-sections. There are minor structural elements in the north-south cross-section (Figure 4.30), but this small anticline-like feature is not exclusively responsible for the formation of the reservoir, and probably only controlled the distribution of gas cap. An east-west cross-section shows a variable dip towards the east (Figure 4.31). The thickness of the net sand also increases towards the east.

Based on the literature survey of the depositional environment of the Artesia Group (Guadalupian) in the Northwest Shelf, following assumptions were made:
(1) Goat Seep and Capitan reefs separated the Northwest Shelf from the Delaware Basin,
(2) barrier islands were present behind the Goat Seep and Capitan reefs. A lagoon developed between the barrier islands and land,
(3) the lagoonal part present towards the land was shallow and probably had restricted circulation,
(4) sandstones, silty sandstones, and evaporites were deposited towards the landward portion of the lagoon,
(5) sabkha and desert environments were present landward of the lagoon,
(6) due to minor sea-level changes or climatic changes (rainfall and wind direction and strength) or supply of detrital material, lagoonal, sabkha, and eolian environments migrated back and forth and created the present distribution of the Shattuck Member in the Sulimar Queen and adjacent fields,
(7) based on the distribution of the Goat Seep reef, the Sulimar Queen field is located towards the landward portion of the lagoon (Figure 1.3A).

In the Sulimar Queen, and the surrounding area, the Shattuck Member was deposited in a mix of coastal sabkha, shallow saline lagoon (with variable energy and depth), and eolian environments (dry eolian sand sheets of Malicse and Mazzullo, 1990)

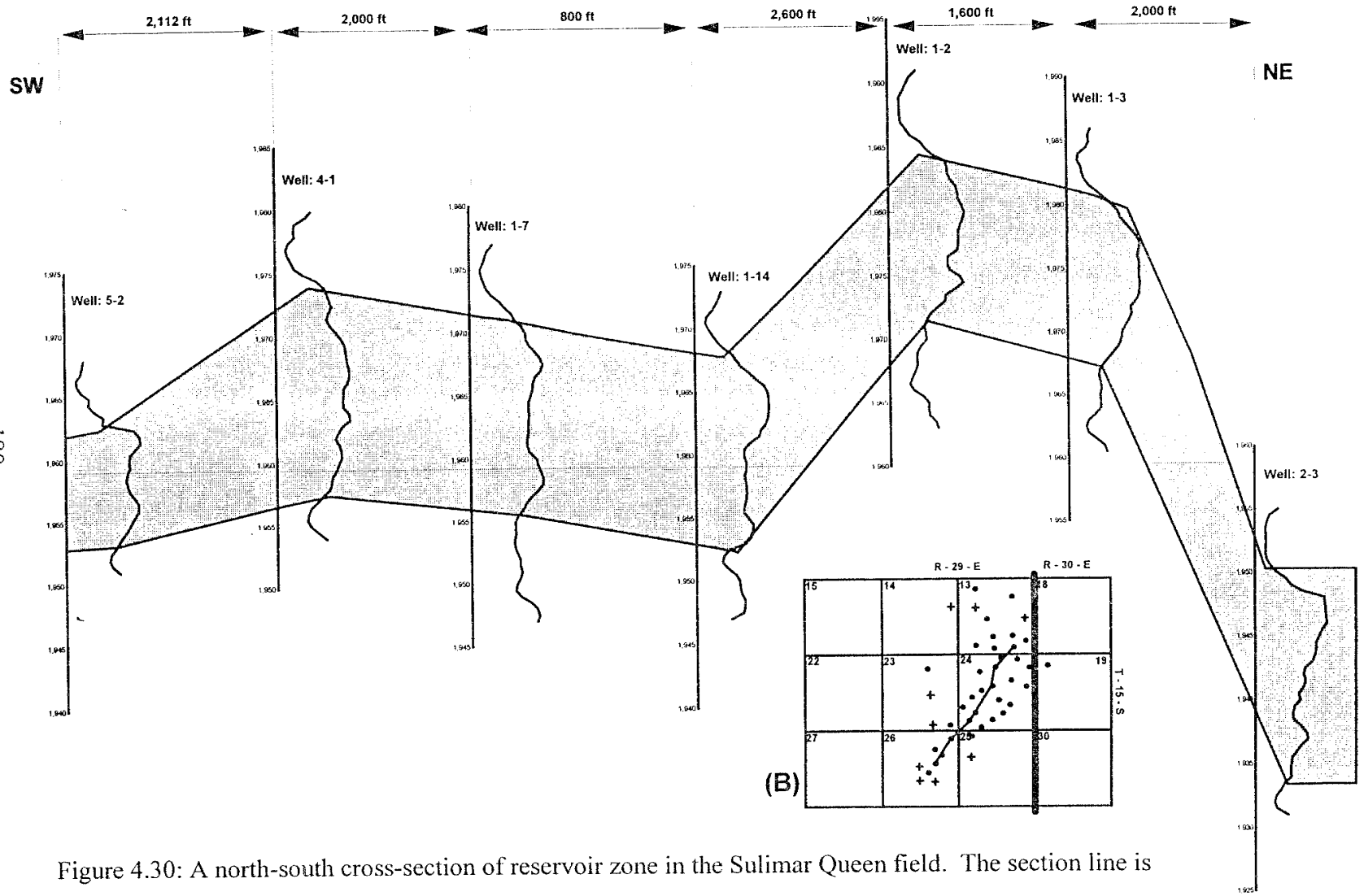

Figure 4.30: A north-south cross-section of reservoir zone in the Sulimar Queen field. The section line is shown in B.

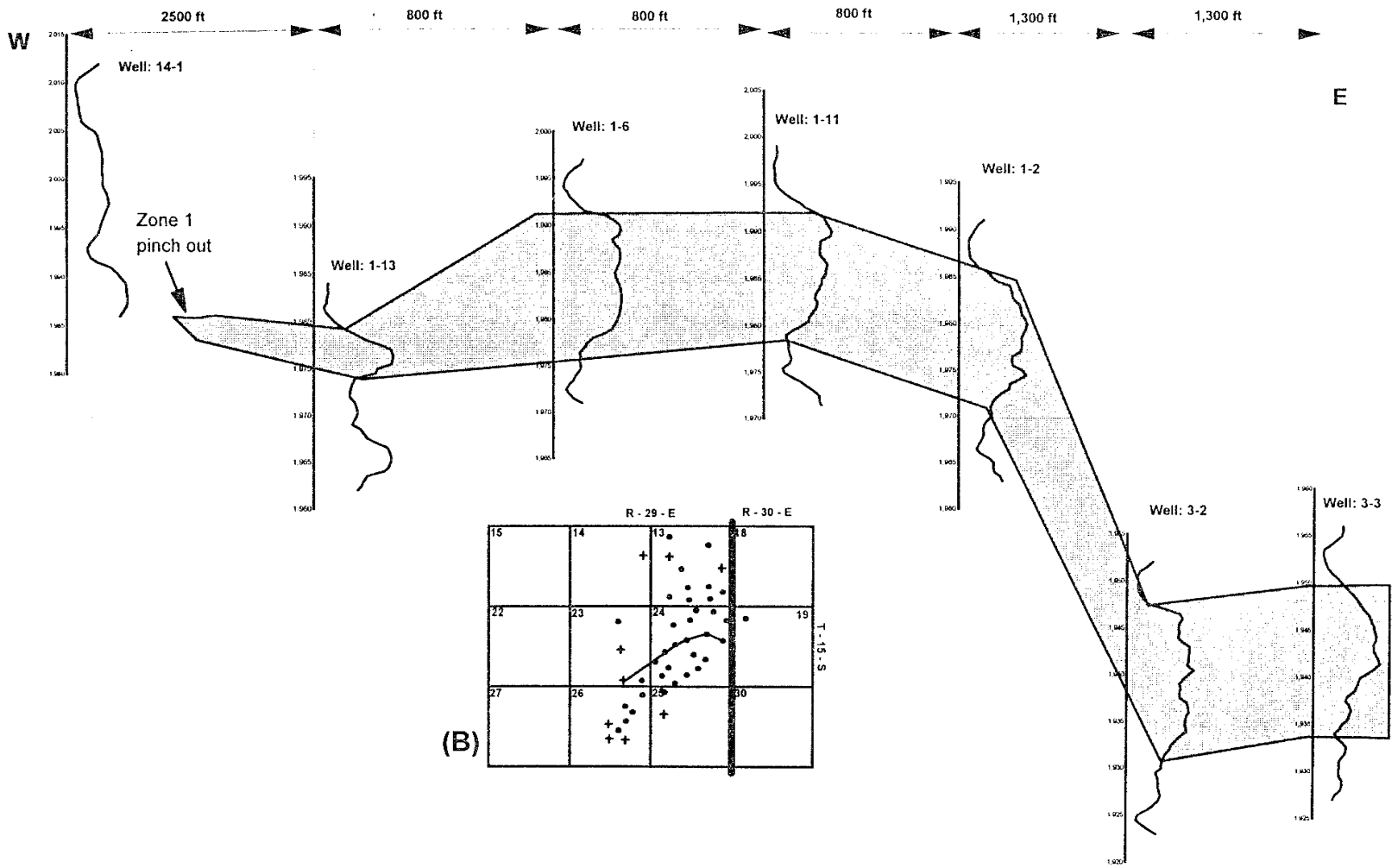

Figure 4.31: An east-west cross-section of reservoir zone in the Sulimar Queen field. The section line is shown in B.

(Figure 4.32). The depositional environments were established based on: (1) the information available in the literature about the geologic history of the Permian Basin and (2) the variations in grain size and sorting, poorly developed sedimentary features (flaser bedding, wavy laminations, ripple laminations, cross laminations, bioturbation, and haloturbation), and the distribution of overlying and underlying anhydrite (Figure 4.32) observed in the cores and outcrop (Section 5).

Zone 2

Zone 2 consists of the bottom 10 feet of the Shattuck Member and consists of gray and red sandstones and anhydrite (Figure 4.32). Massive, gray, moderately to well sorted, very fine-grained arkosic sandstone is present towards the lower part of the Shattuck Member (2013 - 2015 feet; Figure 4.9 & 4.32). Gray sandstone exhibits extensive haloturbation due to the growth of the displacive anhydrite nodules and contains very thin discontinuous clay laminations (Figures 4.9 & 4.32). The gray sandstone is overlain by a dominantly nodular anhydrite bed (Figures 4.9 & 4.32).

Nodular anhydrite forms when gypsum precipitates displacively within the sediments. With increasing concentration of pore fluids across the sabkhas, gypsum crystals are replaced by a fine mush of equant and lath-shaped anhydrite crystals (Tucker, 1981). Continued precipitation of anhydrite results in closely-packed nodules with host sediments restricted to thin stringers. The nodular texture produced is referred to as chicken-wire anhydrite (Tucker, 1981). Nodular anhydrite forms above the water table in the capillary zone (Warren, 1991). According to Kendal and Warren (1988) the nodular anhydrite usually indicates deposition in a sabkha.

Both the lower and upper contacts of the nodular anhydrite present in Zone 2 are erosive (Figure 4.9). According to Warren (1991), erosion surface in the sandstone with nodular anhydrite and the capping nodular anhydrite are the most important features of a sabkha sequence, as observed in Abu Dhabi. Because of the nodular morphology of anhydrite beds, the presence of nodular anhydrite in the underlying gray sandstone, and the presence of erosional surfaces, a sabkha depositional environment is assigned to the

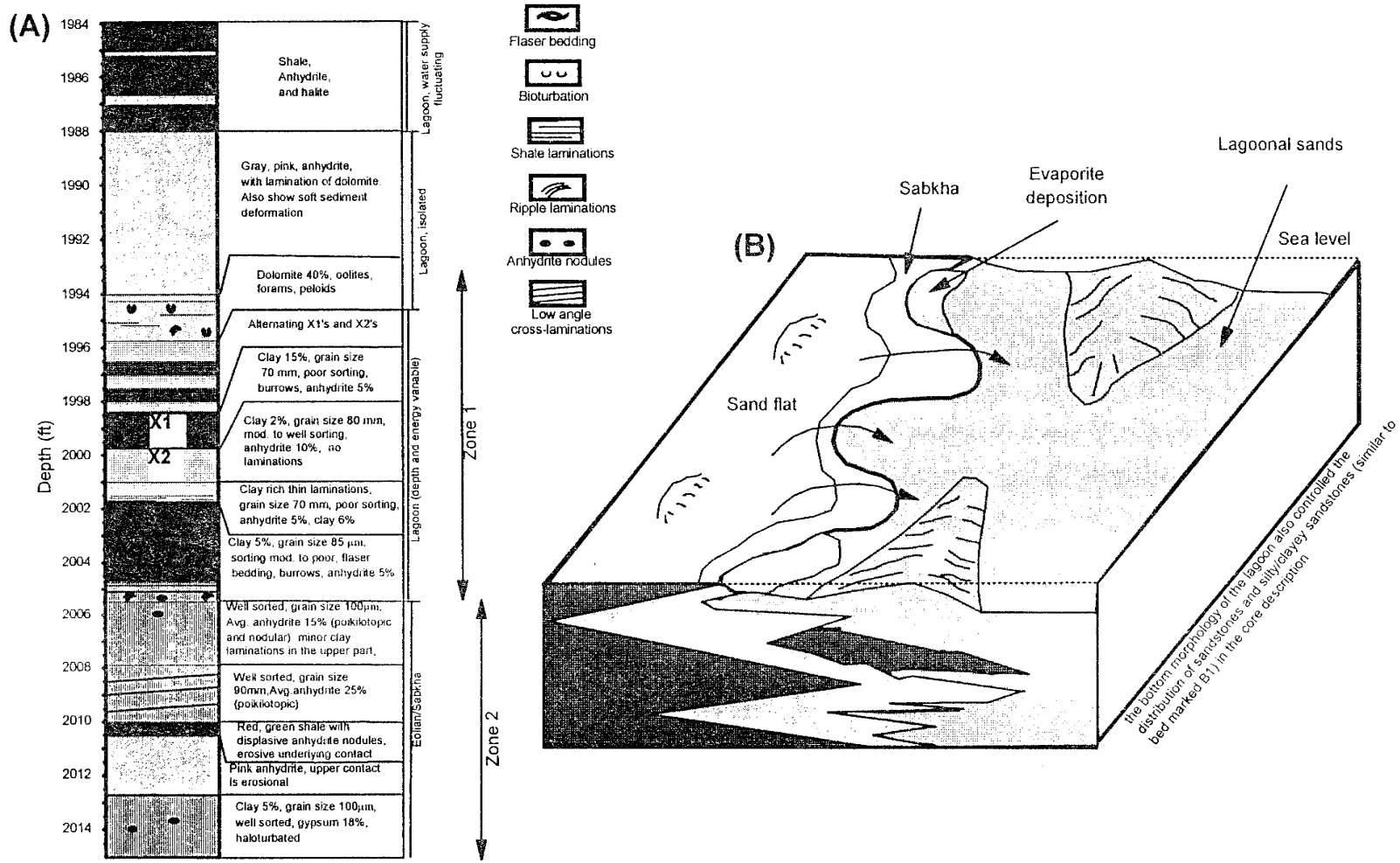

Figure 4.32: (A) Core description along with inferred depositional environments. (B) Generalized depositional model for the Shattuck Member in the Sulimar Queen and adjacent fields. The interfingering of different environments created the present distribution of the Shattuck Member.

gray sandstone and nodular anhydrite.

Overlying the anhydrite is a 5 foot thick sequence of red and gray, well sorted sandstone (Figure 4.9). The red sandstone grades upward into gray sandstone. The red color is mainly due to hematite (Fe_2O_3), whereas the gray color could be due to the presence of organic matter or pyrite (FeS_2) (Berner, 1971). We assume that the gray coloration is due to the presence of pyrite, because there is no mention in the literature about the presence of considerable amount of organic matter, which can cause gray coloration alone. If this is the case, the upward change from red to gray color probably represents a change from an oxidizing to a slightly reducing conditions.

These sandstones exhibit weak low angle cross-stratification in the red sandstone and haloturbation in the gray sandstone (Figure 4.9). We assume that the cross-laminated and well sorted red sandstone in Zone 2 was deposited in an eolian (sand flat) environment (Figure 4.32). In the Shattuck Member, low angle cross-bedded sandstones deposited in sand flats were also reported by Malicse and Mazzullo (1990). The presence of haloturbation (anhydrite nodules) in the gray sandstone (similar to bottom gray sandstone) indicate its deposition in a sabkha environment.

The distribution of Zone 2 was traced throughout the field using the rescaled gamma ray logs. Zone 2 thicken and become dominant in the western part of the field.

Zone 1

Zone 1 is the main reservoir zone. Zone 1 consists of the upper 12 feet of the Shattuck Member and consists of greenish-gray and brown sandstones (Figure 4.32). The sandstones are composed of moderately to poorly sorted, very fine to fine-grained arkosic sandstones. These sandstones contain parallel to subparallel, continuous and discontinuous silt laminations, flaser bedding, wavy bedding, minor cross laminations, and bioturbation (Figures 4.3 & 4.8). Nodular anhydrite is completely absent in Zone 1.

The upper part of Zone 1 shows a gradual vertical change from anhydrite-cemented to dolomite-cemented sandstones to sandy dolomite (Figure 4.7). Zone 1 grades upward through sandy dolomite into laminated anhydrites. This transition was

observed in the cores from Sulimar Queen and adjacent fields. The gradation of these sandstones vertically into bedded evaporites, especially laminated anhydrite, indicates deposition in a lagoon or a large salina (Kerr and Thomson, 1963). The laminated morphology and the regional extent of the overlying anhydrite points towards deposition in a lagoon/large salina instead of local ponds. The Shattuck Member outcrop (Section 5 in the Bone Tank Draw area also contains a laminated anhydrite bed above the sandstone sequence, which could be regarded as equivalent to the subsurface anhydrite bed.

The distribution of sediments and sedimentary structures within a lagoon is controlled mainly by hydrographic conditions and availability of sediments (Reineck and Singh, 1975). Sands can be brought into the lagoon by several means—storms, tidal channels, rivers, or by wind blowing from land (desert) towards the lagoon. The alternating clay rich beds (X1; Figure 4.32), which contain thin laminations of clayey-silty sandstone with the featureless poorly to moderately-sorted sandstone beds (X2; Figure 4.32), suggest either a minor fluctuation in the energy of the lagoon or in the supply of sand from the land. The sands were probably supplied to the lagoon by the winds blowing from the desert as well as by occasional rain storms.

Presence of flaser bedding, wavy laminations, horizontal laminations, bioturbation, minor ripple laminations (Figure 4.8), trace amounts of well rounded and frosted grains, and absence of nodular anhydrite indicate that much of the deposition of these sandstones took place in a lagoonal/salina environment.

The Shattuck Member present in the Sulimar Queen field was deposited in the part of the lagoon present towards the land as inferred from the location of the Goat-Seep reef relative to the Sulimar Queen field. We assume that diurnal tides were not responsible for the formation of flaser beds. Flaser beds were probably formed due to the wind-induced tides. In shallow waters, the sediment surface may be strongly influenced by waves actively driven by winds (forced waves; Collins and Thompson, 1982), which can cause the formation of ripples and flaser bedding. We suggest that strong wind-induced tides created the flaser bedding (Figure 4.18A) and weaker wind-induced tides formed the continuous and discontinuous horizontal and wavy laminations

(Figure 4.18B), which are frequently present in Zone 1. Elliot (1986) reported the formation of silt/sand laminae in Laguna Madre due to slight wave agitation.

The lack of evidence of subaerial exposure and sedimentary structures typical of sabkha, fluvial, or eolian environments also supports the deposition of sandstones in Zone 1 in a lagoonal environment. The absence of fossils in the sandstones may be attributed to hypersaline conditions.

We conclude that the Shattuck Member in the Sulimar Queen and adjacent fields was deposited in an imperceptible merging of lagoonal, sabkha, and eolian environments that produced the widespread sheet-like geometry. Eolian sands blew into the lagoon when winds blew seaward. Sea-level fluctuations were probably small, but they caused the interfingering of quartz sands (Zone 1 and Zone 2) of different environments.

RESERVOIR DEVELOPMENT

The reservoir in the Sulimar Queen field was formed due to a stratigraphic trap. This stratigraphic trap is also affected by a minor structural element (Figures 4.30 & 4.31). The trap was formed by the updip pinch out of porosity and permeability in the Shattuck Member. Generalized diagenetic pathways for the reservoir and non-reservoir zones are shown in Figure 4.33. The reservoir zone (Zone 1) was deposited in the lagoonal environment and escaped extensive cementation by anhydrite, whereas, the non-reservoir zone (Zone 2) was deposited in a mixture of eolian and sabkha environments and was affected by early pervasive cementation by anhydrite. Since the lagoonal facies escaped early cementation by anhydrite, it had enough porosity and permeability to allow the fluids responsible for dissolution to flow freely through them.

The distribution of reservoir properties such as net sand thickness, total thickness, and porosity were determined by using kriging and inverse-distance weighting methods. The histogram for the sand thickness show a bimodal distribution, probably suggesting that the Sulimar Queen field consists of two separate regions (Figure 4.34A). Because only few data points were available the field was not divided into two separate areas. The variogram estimated for the net sand thickness showed a correlation length of 400 feet

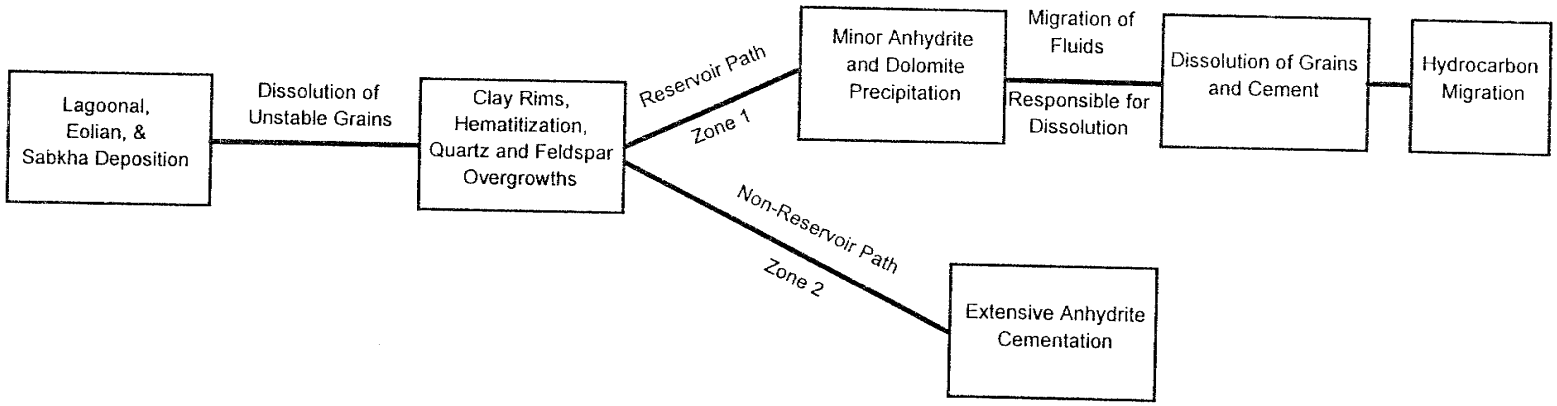

Figure 4.33: Diagenetic paths of reservoir and non-reservoir sandstones in the Shattuck Member.

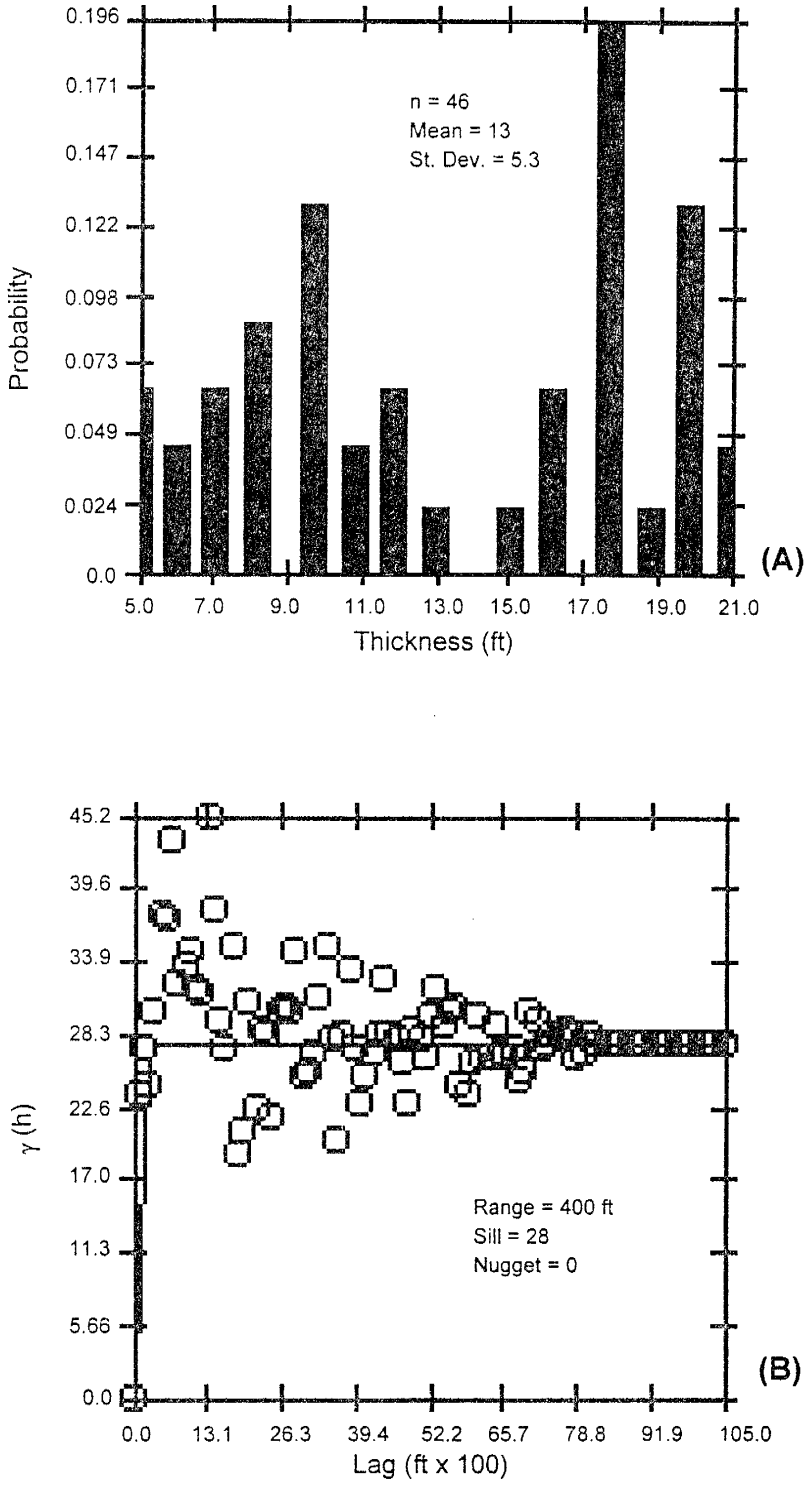

Figure 4.34: Histogram showing a bimodal distribution (A) and variogram estimate (B) for the thickness of the Shattuck sand in the Sulimar Queen field.

(Figure 4.34B). It was also difficult to model the variogram correctly because of the bivariate distribution of data.

Based on the variogram model, net sand thickness distribution was obtained using ordinary kriging. Kriging failed to capture the distribution of the net sand thickness because data points were few and irregularly distributed (Figure 4.35). On the other hand, the inverse-distance weighting method gave more meaningful distribution of the net sand thickness (Figure 4.36). The reason we consider this distribution meaningful is based on the information available from logs and depositional model. The overall thickness of the net sand increases towards the east (Figure 4.36).

The distribution of the Shattuck Sand (Zone 1 & 2) was also obtained in order to gain insight on the depositional environment (Figures 4.37 & 4.38). The total sand thickness is variable and shows no particular pattern, but on the whole it increases towards the southwestern part of the field. Because of the absence of any particular pattern, the total sand thickness distribution was not helpful in providing any additional information concerning depositional conditions.

Similar to thickness maps, porosity distribution maps in the reservoir zone as well as in the Shattuck Sand (Zone 1 & 2) were also generated. The porosity distribution (Figure 4.39A) was not suitable for generating reliable variograms (Figure 4.39B). For the porosity distribution a correlation length of 400 feet was obtained (Figure 4.39B). The porosity in the reservoir zone (Zone 1) is much higher in the northwestern part of the reservoir (Figures 4.40 & 4.41). In the Shattuck sand (Zone 1 & 2) porosity is much lower than the reservoir zone and does not show any particular pattern (Figures 4.42 & 4.43). The absence of a definite pattern may be due to the masking effect of Zone 2.

A structure map at the top of the Shattuck Member shows a dip in the east and southeast direction with structural nosing in the eastern part of the reservoir (Figure 4.44). The oil-water contact is located in the eastern and southeastern part of the reservoir and the oil-gas contact in the higher areas in the western part of the reservoir.

The reservoir zone is not restricted to only the thickest or thinnest parts of the Shattuck Member. Therefore, the reservoir was formed through a combination of:

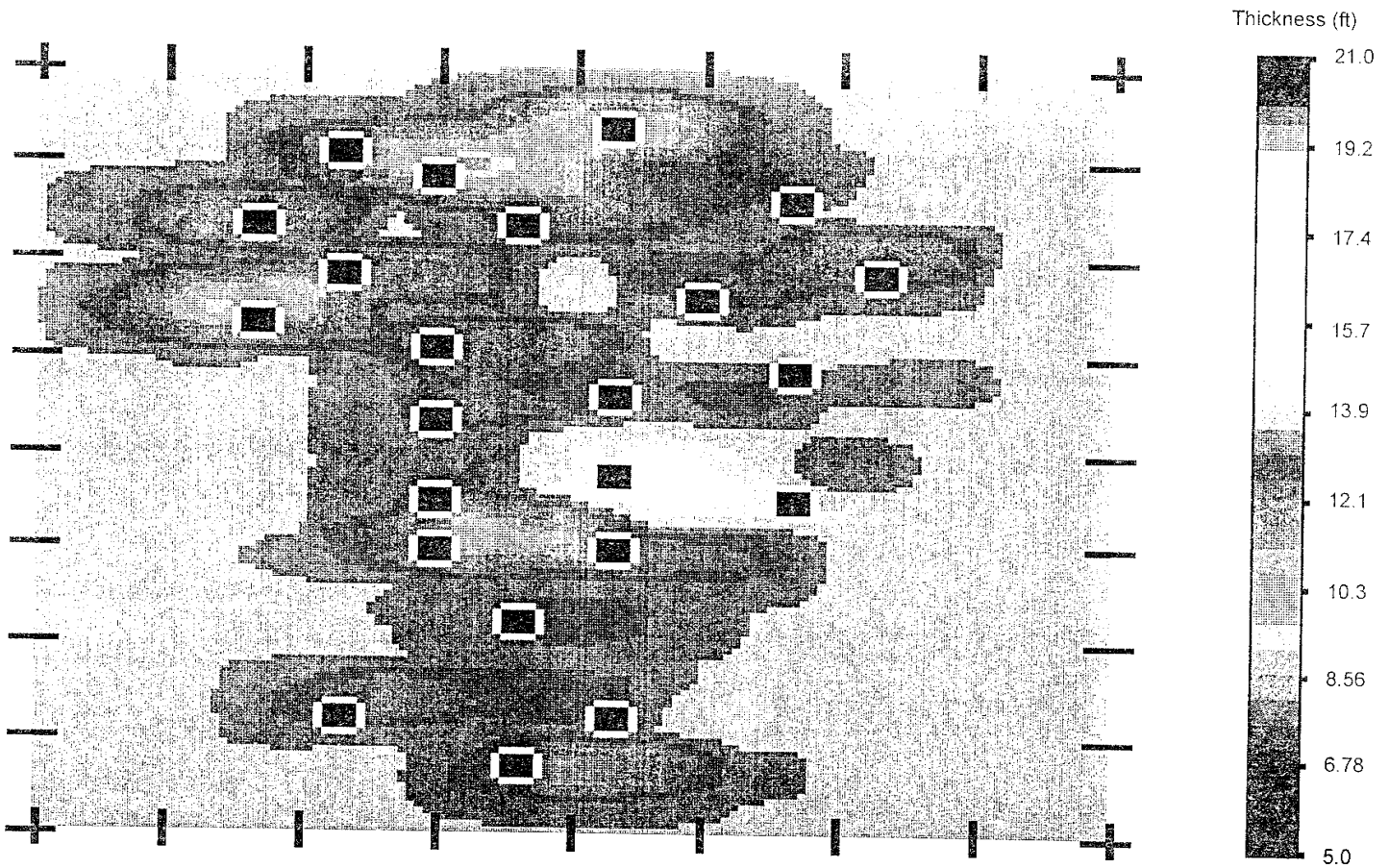

Figure 4.35: Net sand thickness map constructed using ordinary kriging. The map is featureless and does not show the changes in thickness.

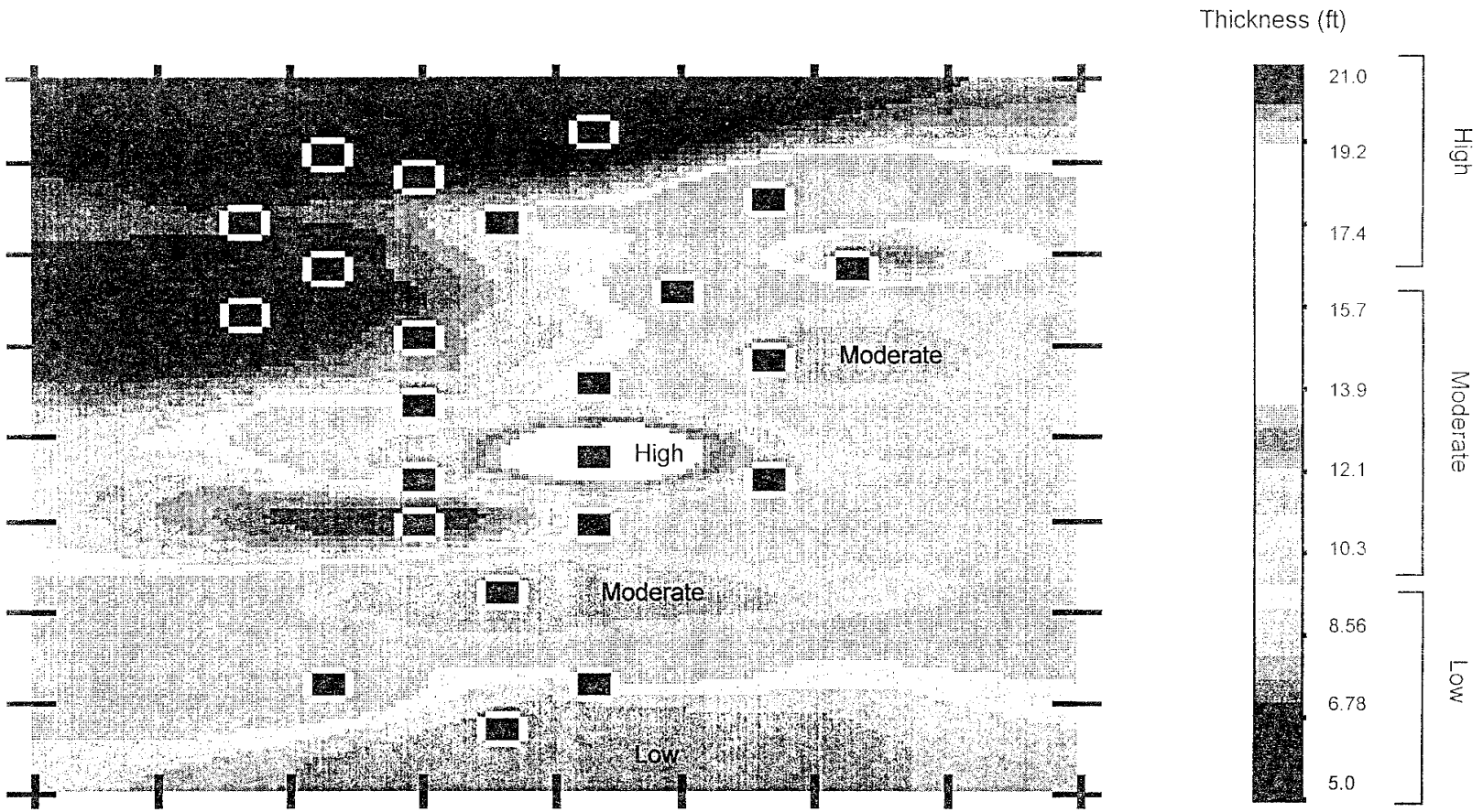

Figure 4.36: Thickness distribution of the net sand in the Sulimar Queen field. This distribution was obtained using the inverse-distance weighting method.

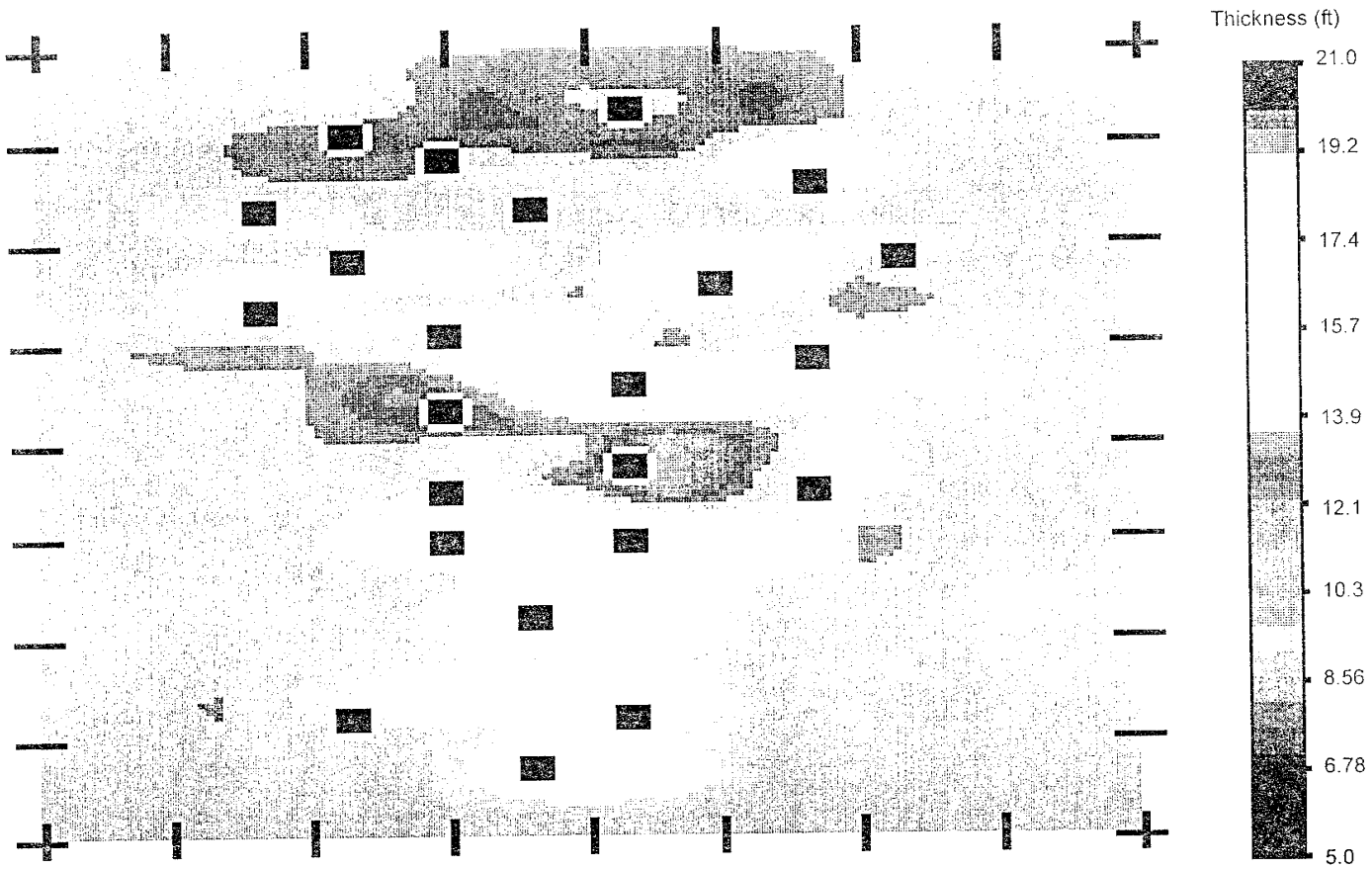

Figure 4.37: Total sand (Zone 1 & Zone 2) thickness map constructed using oridinary kriging. The map fails to depict the details.

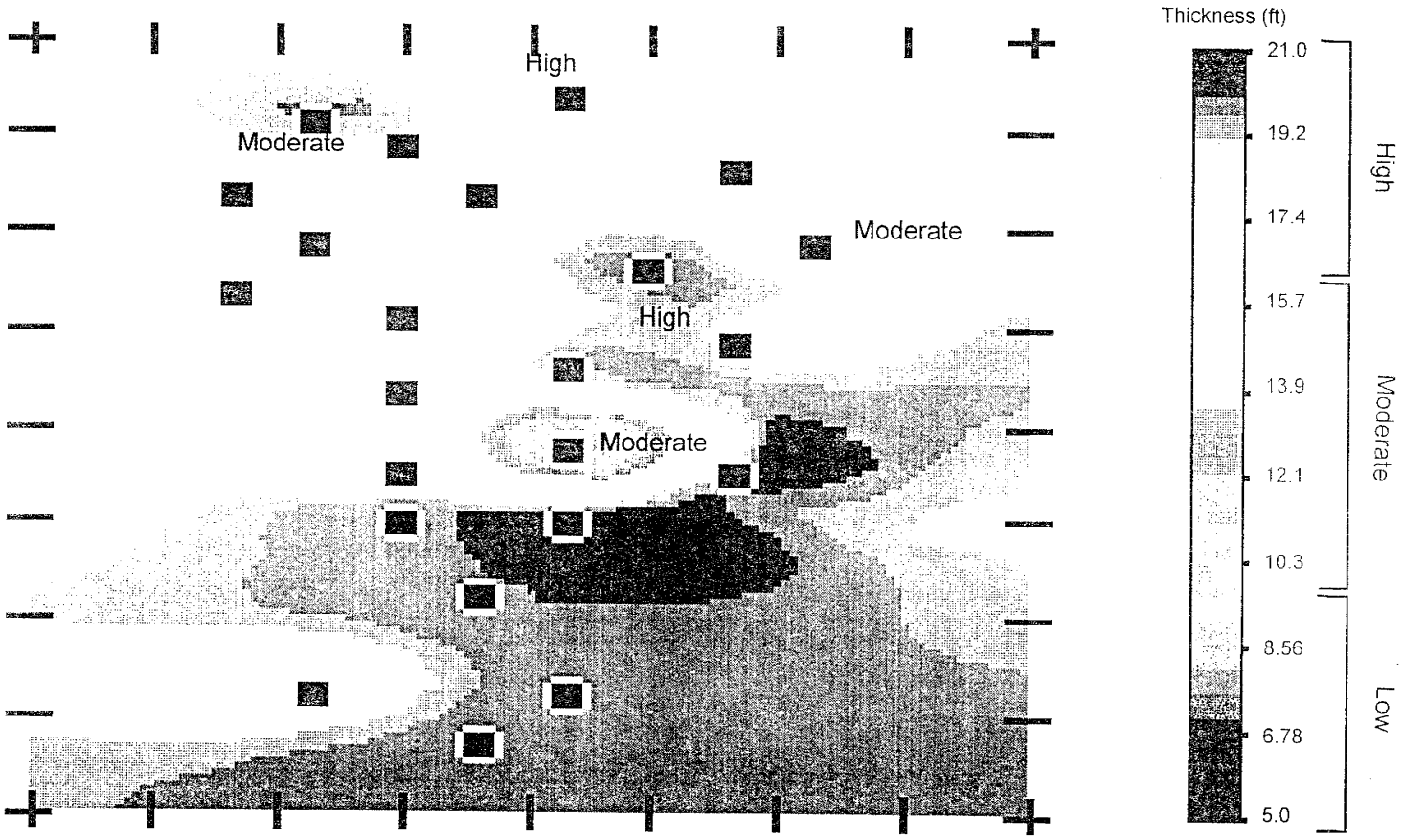

Figure 4.38: Total sand (Zone 1 & Zone 2) thickness map constructed using the inverse-distance weighting method.

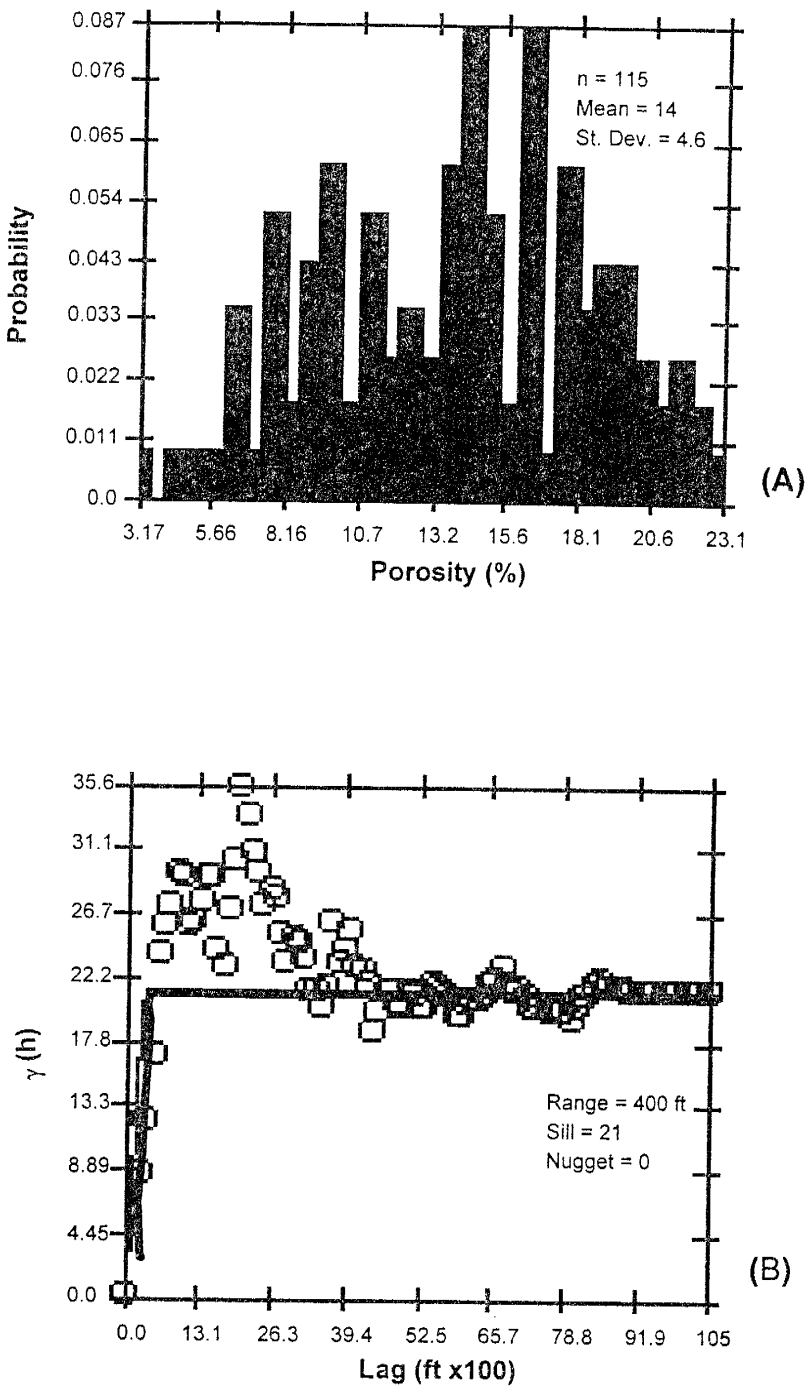

Figure 4.39: Histogram (A) and variogram estimate (B) for the porosity in the Shattuck sand in the Sulimar Queen field.

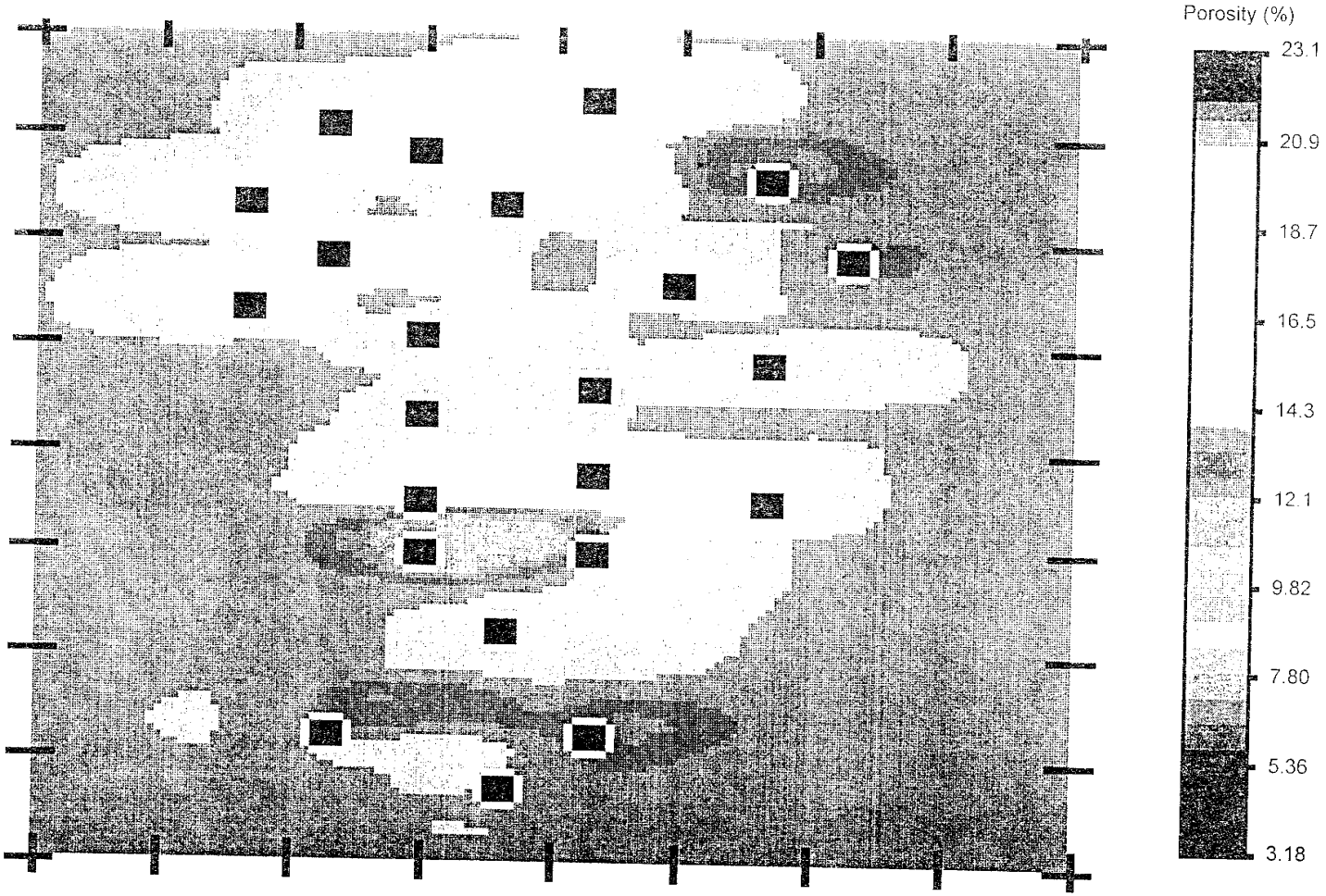

Figure 4.40: Porosity distribution in Zone 1 of the Sulimar Queen field. Map constructed using ordinary kriging.

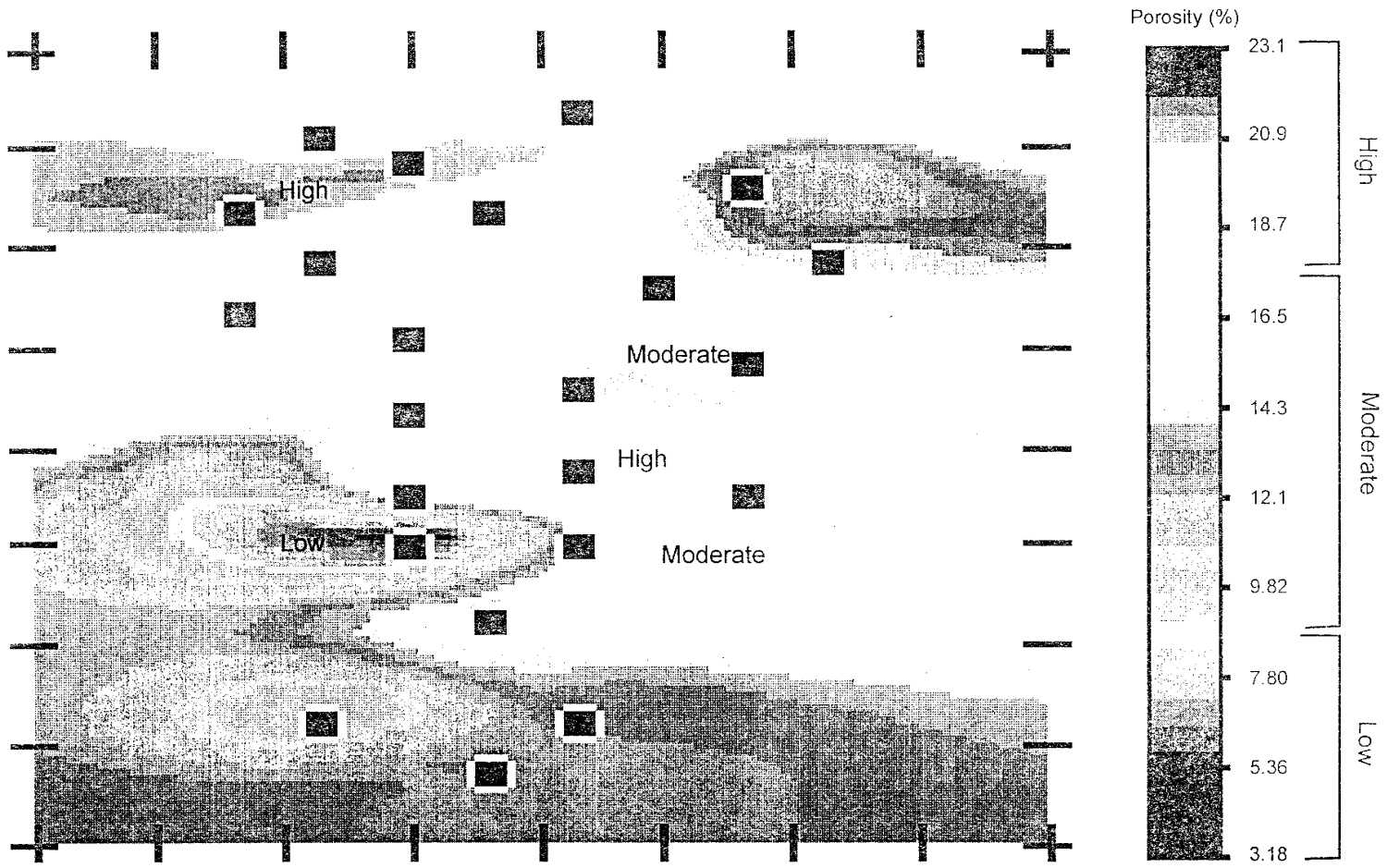

Figure 4.41: Porosity distribution in Zone 1 of the Sulimar Queen field. Map constructed using the inverse-distance weighting method.

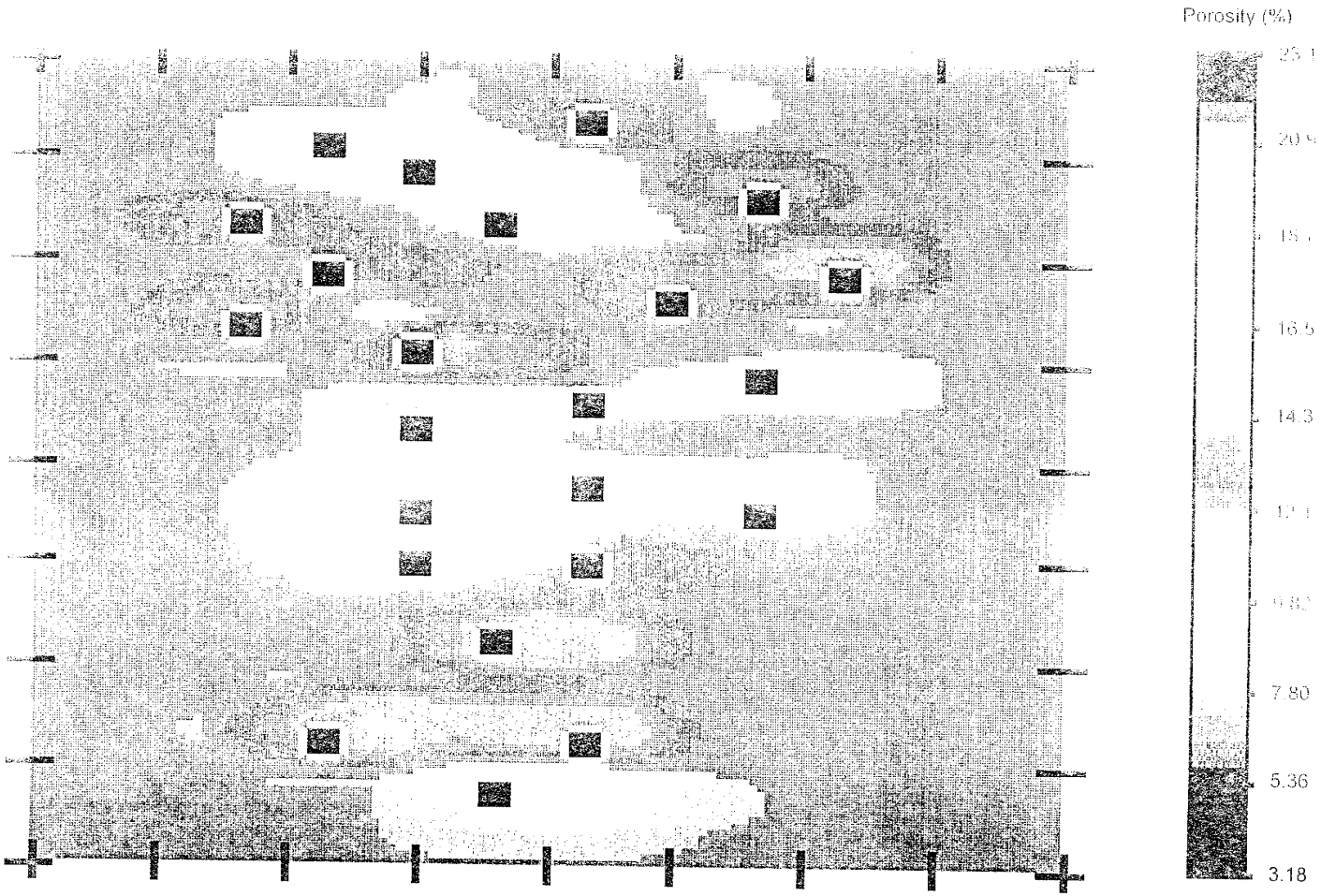

Figure 4.42: Porosity distribution in whole Shattuck Member (Zone 1 & Zone 2) in the Sulimar Queen field. Map constructed using ordinary kriging.

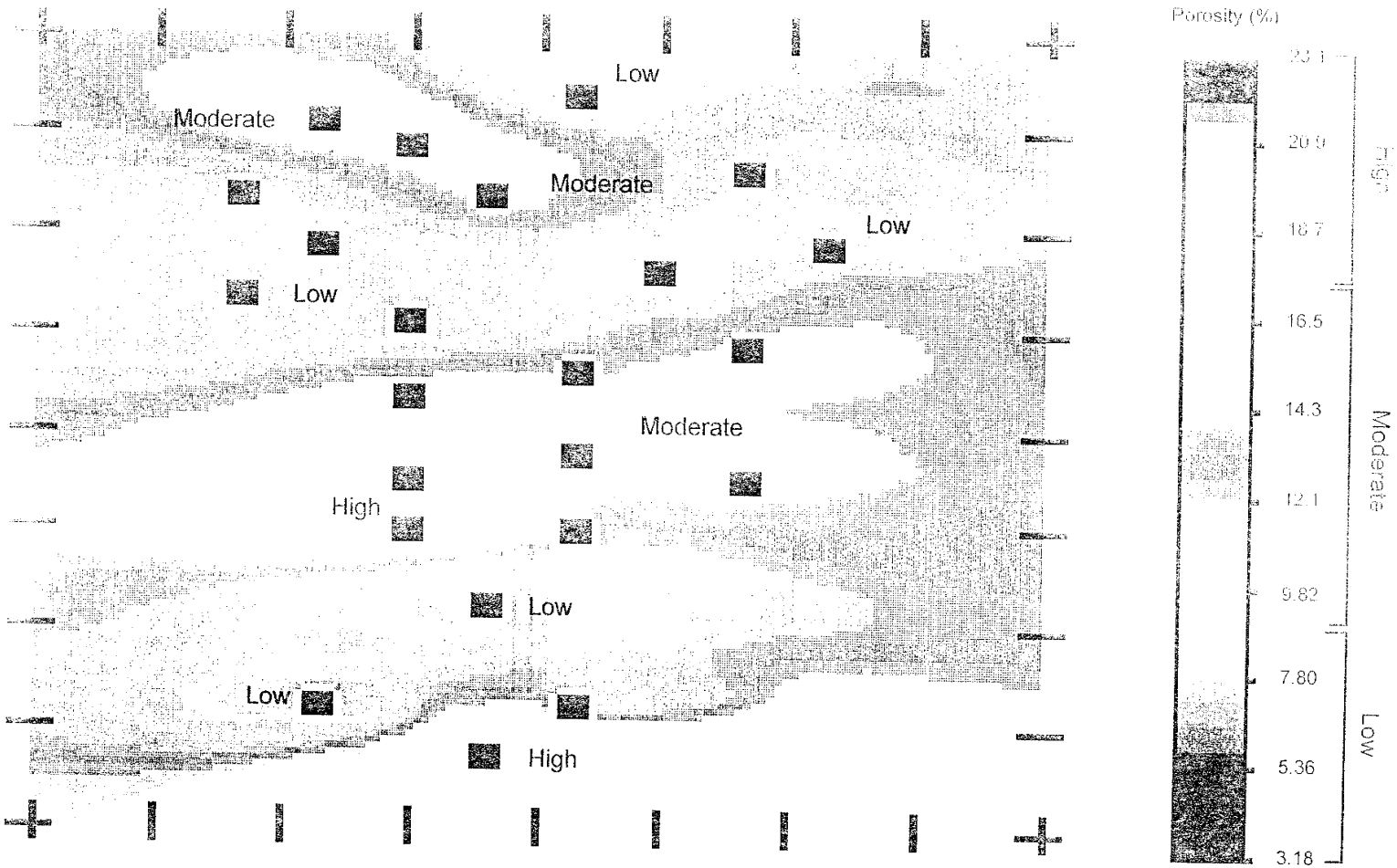

Figure 4.43: Porosity distribution in whole Shattuck Member (Zone 1 & Zone 2) in the Sulimar Queen field. Map constructed using the inverse-distance weighting method.

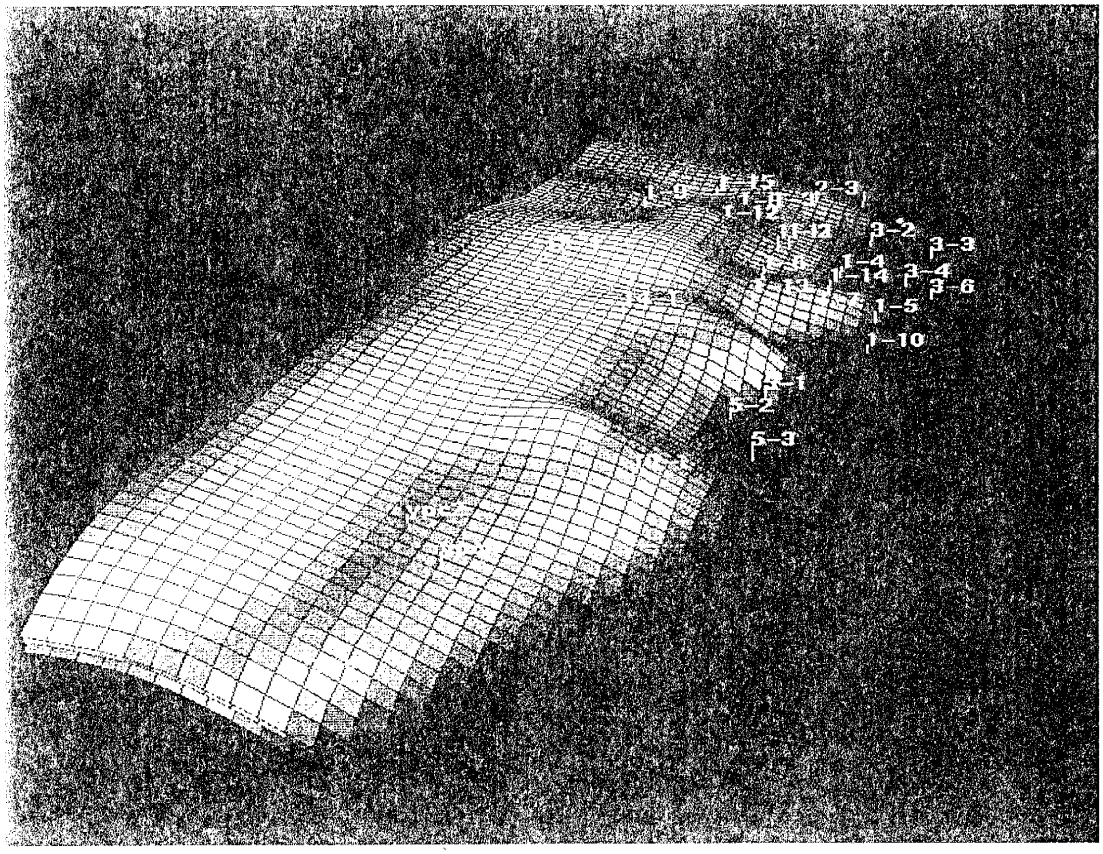

Figure 4.44: Top of the Sullimar Queen structure produced using inverse-distance weighting method.

(1) depositional environment (lagoonal sands), (2) diagenetic history (lagoonal sands escaped pervasive cementation by anhydrite), (3) dissolution, and (4) minor structural control.

CONCLUSIONS

The Shattuck Member in the Sulimar Queen and adjacent fields is a product of three depositional environments—Lagoonal-Sabkha-Eolian. The large areal extent and small vertical range of the Shattuck sandstones were produced by the interfingering of these environments in response to slight changes in sea-level and shifts in wind direction. As terrigenous input slowed, and then ceased, dolomite cemented sands and sandy dolomite were deposited in the lagoon. With more restriction, salinity increased to the point of gypsum saturation and bedded gypsum was precipitated (now anhydrite). The extensive nature of the overlying anhydrite also suggests deposition in a shallow saline lagoon. The absence of fauna within the sandstone portions of the Shattuck Member is perhaps due to hypersaline conditions.

The outcrop study also suggests deposition in a mixture of aqueous and dry environments. Considerable evidence of similar depositional environments for the outcrops and subsurface exists, especially in the Bone Tank Draw area. The permeability data from the outcrops were not suited for detailed geostatistical analysis. On the other hand, the outcrop study did provide an insight into facies relationships and their lateral and vertical distribution in the Shattuck Member. This information was included in the development of depositional and reservoir model.

The petrographic analyses show that sandstones are poorly to moderately sorted, angular to subangular, very fine to fine-grained arkoses. Diagenesis began with the generation of anhydrite nodules, gypsum blades, and hematite at the surface and very shallow burial depths. Later chlorite, quartz, and feldspar cements precipitated. Poikilotopic anhydrite and later dolomite precipitated later. A stage of dissolution followed and recreated porosity in the reservoir zone.

The development of secondary porosity created potential hydrocarbon reservoir. Oil and gas were trapped by the updip pinch-out of porosity. The reservoir was formed by a combination of depositional environment, diagenetic history, and minor structural elements.

Kriging to generate the distribution of thickness and porosity distribution was not adequate, due to limited and irregularly spaced data points.

CHAPTER 5: CHARACTERIZATION OF THE SULIMAR QUEEN FIELD*

INTRODUCTION

Limited and unreliable data has been the bane of reservoir characterization. This is especially true for fields that were developed before the 70's, when field development was more art than science. Producers struggling with re-engineering such fields have to evaluate every shred of available information to optimize modern production operations. This is a common problem faced by most operators today.

In most cases, this situation prevents an operator from investigating the future potential of such fields. For example, an infill drilling program would require at least the spatial mapping of key reservoir properties. For most old fields, porosity or permeability may not be available even at the well locations. The Sulimar Queen unit is typical of many old fields lacking high-quality reservoir data (Figure 1.3B).

Primary production from the Sulimar Queen was initiated in July 1968 and lasted until December 1971. A total of 20 wells produced 533,316 barrels of oil. A waterflood, initiated in January 1972 and completed at the end of 1983, produced 1,112,033 barrels of incremental oil, tripling primary production.

This field is deficient in core material, modern logs, and a complete production data set. The Sulimar Queen field is located in the Chaves County, southeast New Mexico, USA (Figure 1.3). A modern well—Well 1-16—was drilled in 1990 by

---

* Ali, M., Chawathé, A., Ouenes, A., Cather, M., and Weiss, W., 1997, *Extracting Maximum Petrophysical and Geological Information from a Limited Reservoir Data Base*: Fourth International Reservoir Characterization Technical Conference Proceedings, Houston, Texas, 2 - 4 March, 1997, p. 279 - 300.

* Chawathé, A., Ouenes, A., Ali, M., and Weiss, W., 1997, *One Core, Few Modern logs, and Limited Production Data: Is Reliable Reservoir Characterization Possible*: Society of Petroleum Engineers, Sixty-Seventh Annual Western Regional Meeting, Long Beach, California, 25 - 27 June, 1997, p. 109 - 122.

by McClellan Oil Corporation/Tech. Research Oil Field Corporation. This well was logged and cored using modern equipment.

For the characterization of the field, the only control points available consisted of one core, core reports from two wells, and modern log suites from four wells. From the rest of the field only old gamma ray and neutron logs were available. Neutron logs, because of their wide scale ranges and anomalous high and low porosity values, were discarded and not used in this study. Two additional cores were obtained from the adjacent fields, and additional outcrop studies were conducted to supplement the database (Figure 1.3). Cores and logs from the adjacent fields (South Lucky Lake and Queen fields) were collected to capture the regional behavior of the Shattuck Member, so that the correlations developed in the Sulimar Queen field could be verified.

An understanding of the reservoir structure and developing characteristic measures for heterogeneity classification are essential to maximize oil production from producing reservoirs. The physical phenomena associated with oil recovery have been relatively well understood for some time. Nevertheless, there have been disappointing gaps between model predictions based on laboratory and field tests, and the actual production of oil. The scarcity of detailed reservoir data has contributed to such failures. A unique opportunity for a detailed and integrated study existed at the Sulimar Queen, which was available as a research field.

One goal of the Sulimar Queen study was to use the integrated data to explain the improved oil recovery in response to waterflood and to share the insight gained in this study with operators re-engineering reservoirs similar to the Sulimar Queen. The reservoir characterization methodology, resulting from history-matching the primary production to predict secondary recovery performance, can be readily utilized by oil and gas producers.

The challenge of the Sulimar Queen project was to develop a reasonable reservoir model using limited and old data—a common problem with reservoirs in the Permian Basin. Typically, old well logs (gamma ray-neutron perforating logs) and production history are the only data available for this maturing area.

In this chapter, the integration of all the assimilated data, which spans from the micro-scale (thin sections) to mega-scale (outcrops), to characterize the Sulimar Queen will be discussed. Applications of new artificial intelligence tools, such as fuzzy logic, to correlate thin-section data with permeability were developed. Neural networks were applied to predict permeability using petrographic data. The use of geostatistics and simulated annealing to build simulation-scale property distributions are discussed. The final version of the conditioned Sulimar Queen model includes a previously undetected gas cap.

The following sections briefly describe the data gathering, analysis and integration pertaining to various scales and sources of data.

SMALL-SCALE HETEROGENEITY STUDY

The first objective was to analyze the scale of heterogeneity in the vertical direction from the available cores. Permeability measurements were made using a computer controlled minipermeameter (Chapter 2), and approximately 5,000 permeability measurements were made (Appendix C). The inner radius of the SMP probe tip used was 0.125 inches (3.125 mm). On the core from Sulimar Queen field (Well 1-16) permeability measurements were made on a square grid with an interval of 12.5 mm, which created five vertical permeability profiles along the length of the core (Figure 5.1). The histograms of the permeability distribution are shown in Figure 5.2. The average of the five profiles for the cores from Sulimar Queen, South Lucky Lake, and Queen fields are shown in Figure 5.3. The permeability varied from less than 0.1 md to 500 md, and the scale of permeability heterogeneity was the same for three cores (Figure 5.3). This similarity suggested that the vertical permeability heterogeneity in the Sulimar Queen and adjacent fields may be caused by the same depositional and diagenetic events. This similar behavior provided the first confirmation of the assumption that the data from the adjacent fields may be used.

The producing zone of the Shattuck Member consists of greenish-gray and brown, very fine-grained arkosic sandstone. It is bounded at the top and the bottom by anhydrite

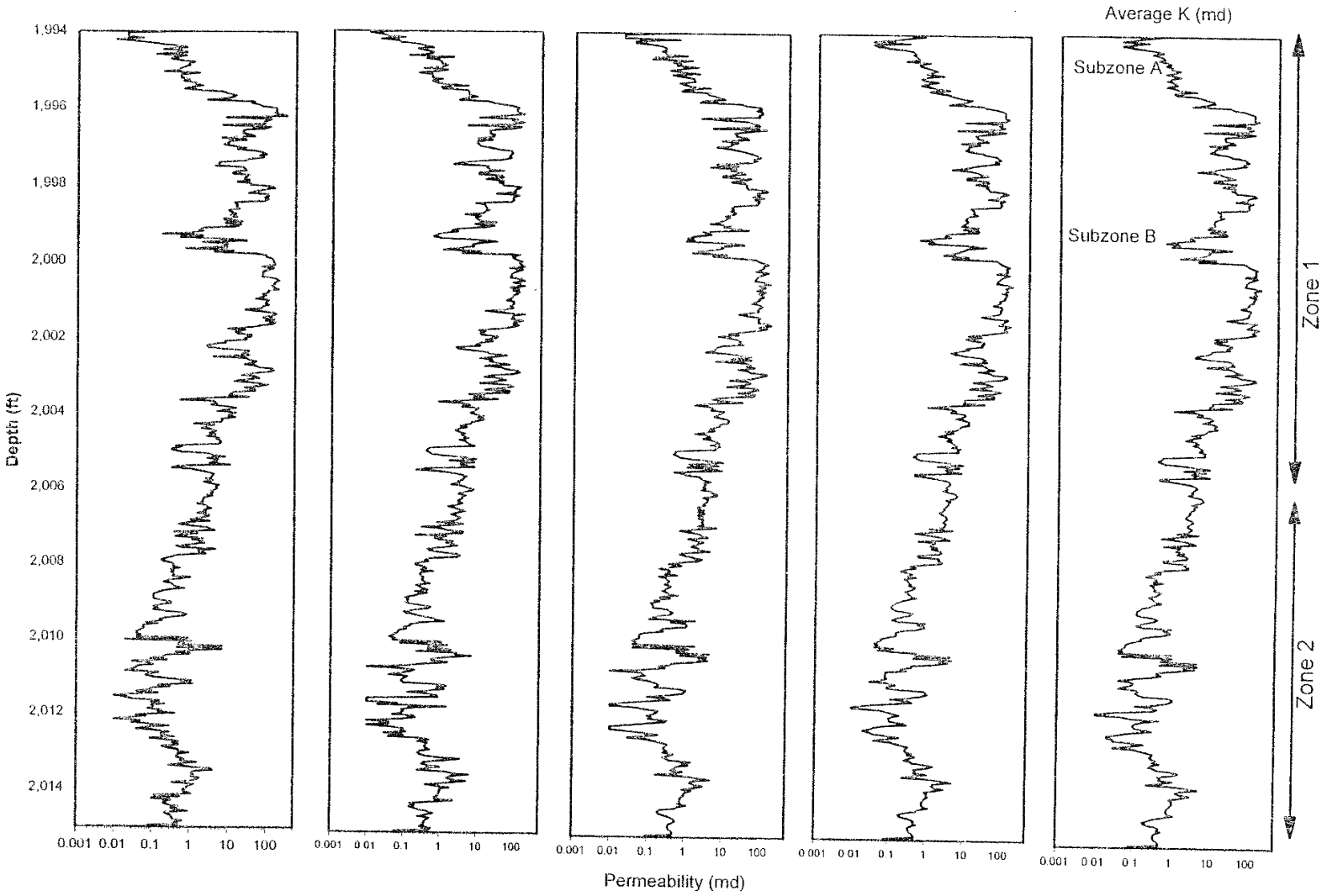

Figure 5.1: Permeability distribution in the Shattuck Member. Vertical and horizontal spacing is 0.5 inches.

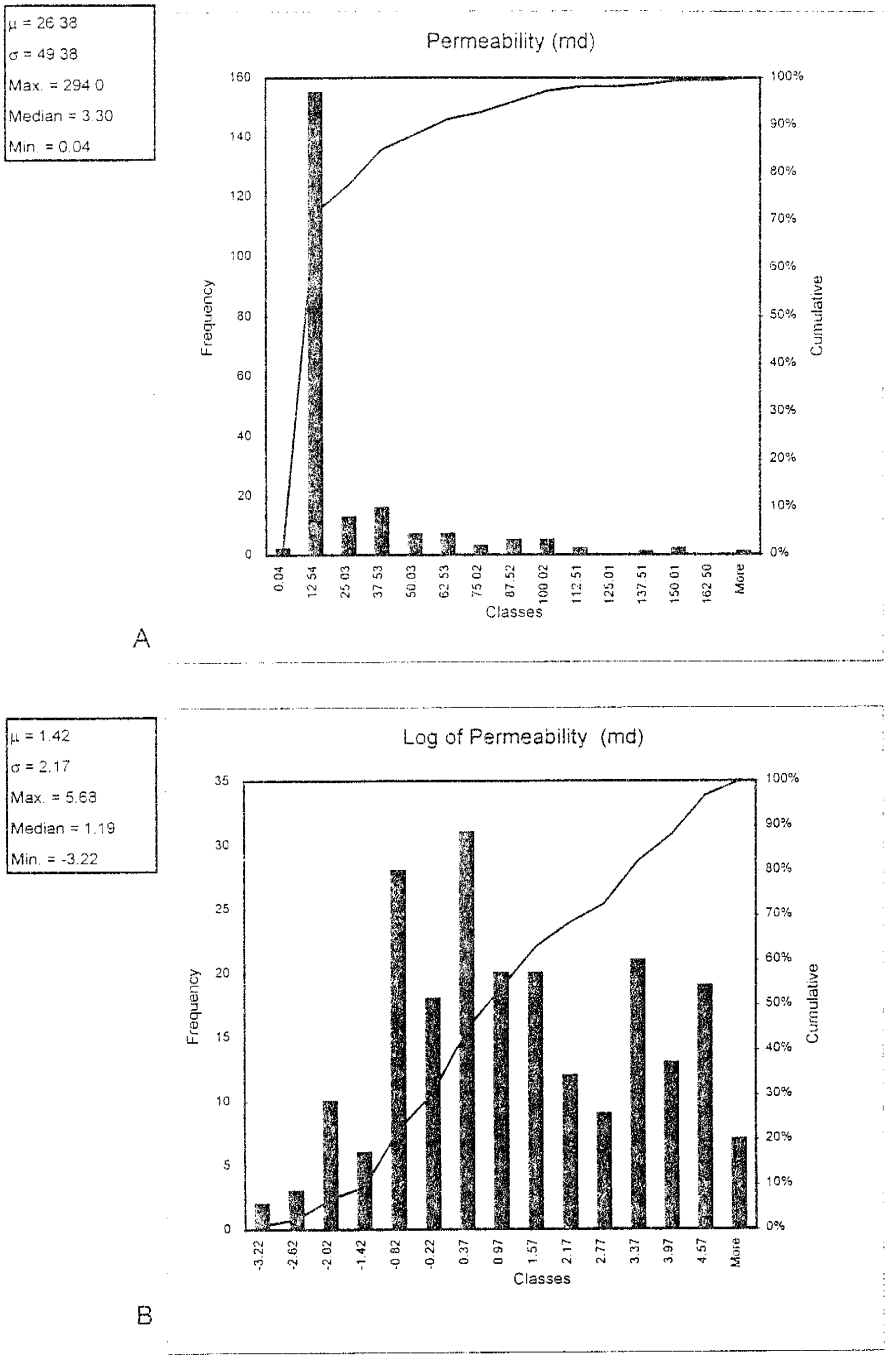

Figure 5.2: Histograms of combined permeability distribution in the Shattuck Member from the Sulimar Queen and South Lucky Lake fields. (A) raw data (B) log transform

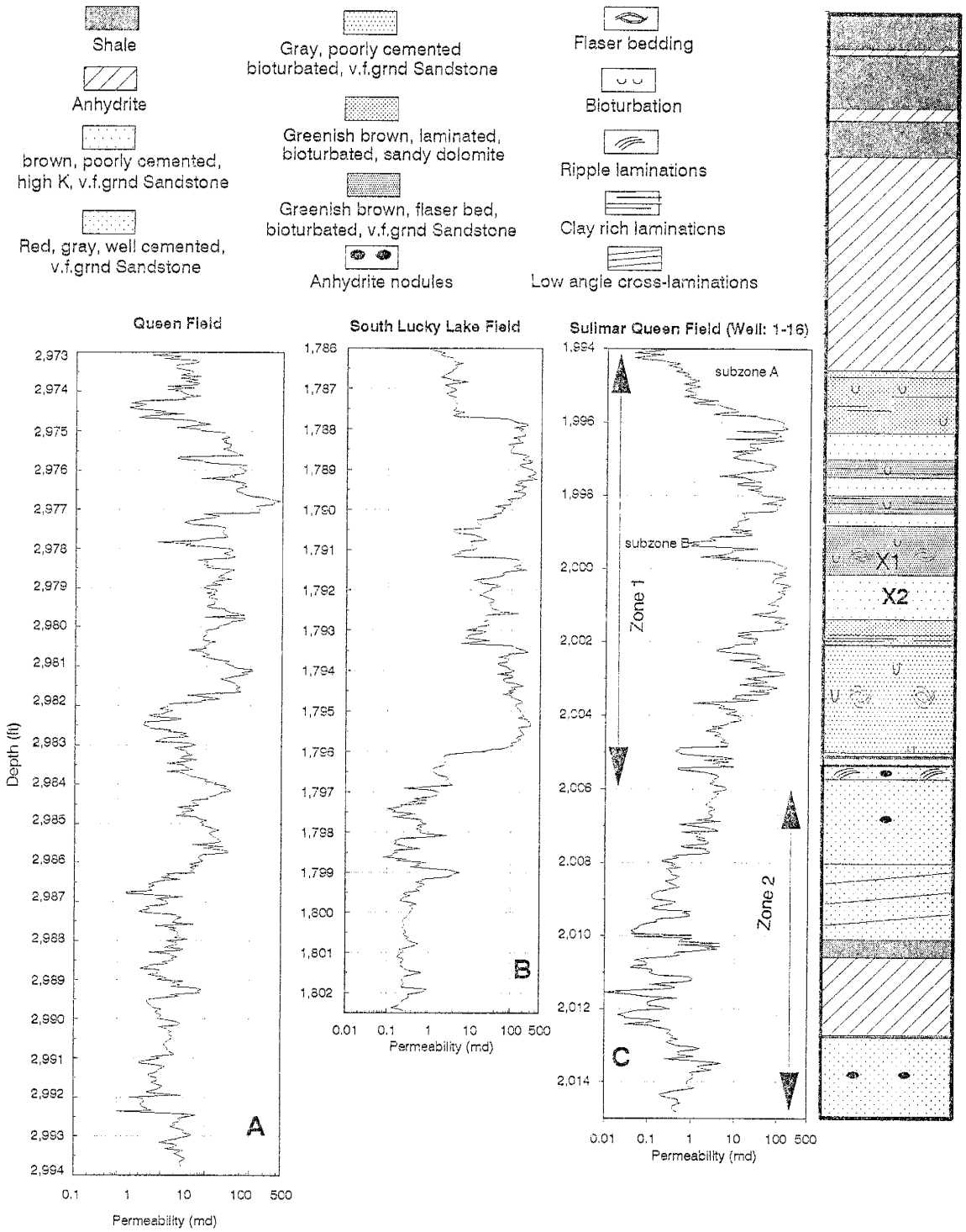

Figure 5.3: Permeability distribution in the cores from Queen (A), South Lucky Lake (B), and Sulimar Queen field (C). Core description from the Sulimar Queen field is also shown beside the permeability distribution. Note the similar permeability distribution, especially between South Lucky Lake (B) and Sulimar Queen field (C).

(Figure 5.3). The permeability heterogeneity is caused by minor changes in the depositional conditions, in which minor changes in the lithology correlate with changes in permeability (Figure 5.3). Since permeability measurements made on a small-scale identified small-scale lithologic heterogeneities, the reexamination of the core also improved the lithologic description. On the basis of permeability distribution, the reservoir was divided into two separate layers, an upper high permeability layer (Zone 1) with two thin low permeability subzones (subzone A & B) and a lower tighter layer (Zone 2) as illustrated in Figure 5.3.

Improving the Quantity and Quality of Petrographic Data

Once the permeability distribution was obtained, the second step was to collect enough samples for the petrographic analysis, so that the control of petrographic elements such as porosity types, pore morphologies, mineralogy, textures, and type, amount, and distribution of clay and cement in creating permeability heterogeneity could be determined. Because only one core was available from the field, it was critical not to destroy it. In the Shattuck Member, permeability heterogeneities exist on a small-scale (Figures 5.1 & 5.3) and the whole range of permeability distribution cannot be sampled using core plugs. The new technique of collecting petrographic data described in Chapter 2 was applied here to conserve the valuable core material. A large set of petrographic data was obtained so that detailed statistical analyses could be done in order to determine the effects of each petrographic element on permeability and to assess the control of diagenesis and porosity evolution on permeability.

Petrographic Data Collection and Analysis

Thirty-three thin sections were made from the cores and a total of 267 data points were obtained (i.e., approximately 8 data points from each thin section). The location of the thin sections and the permeability measurement distribution on each thin section are shown in Figure 5.4. A summary of permeability, porosity, mineralogical, and textural data is given in Table 5.1. Twenty petrographic elements collected for each permeability

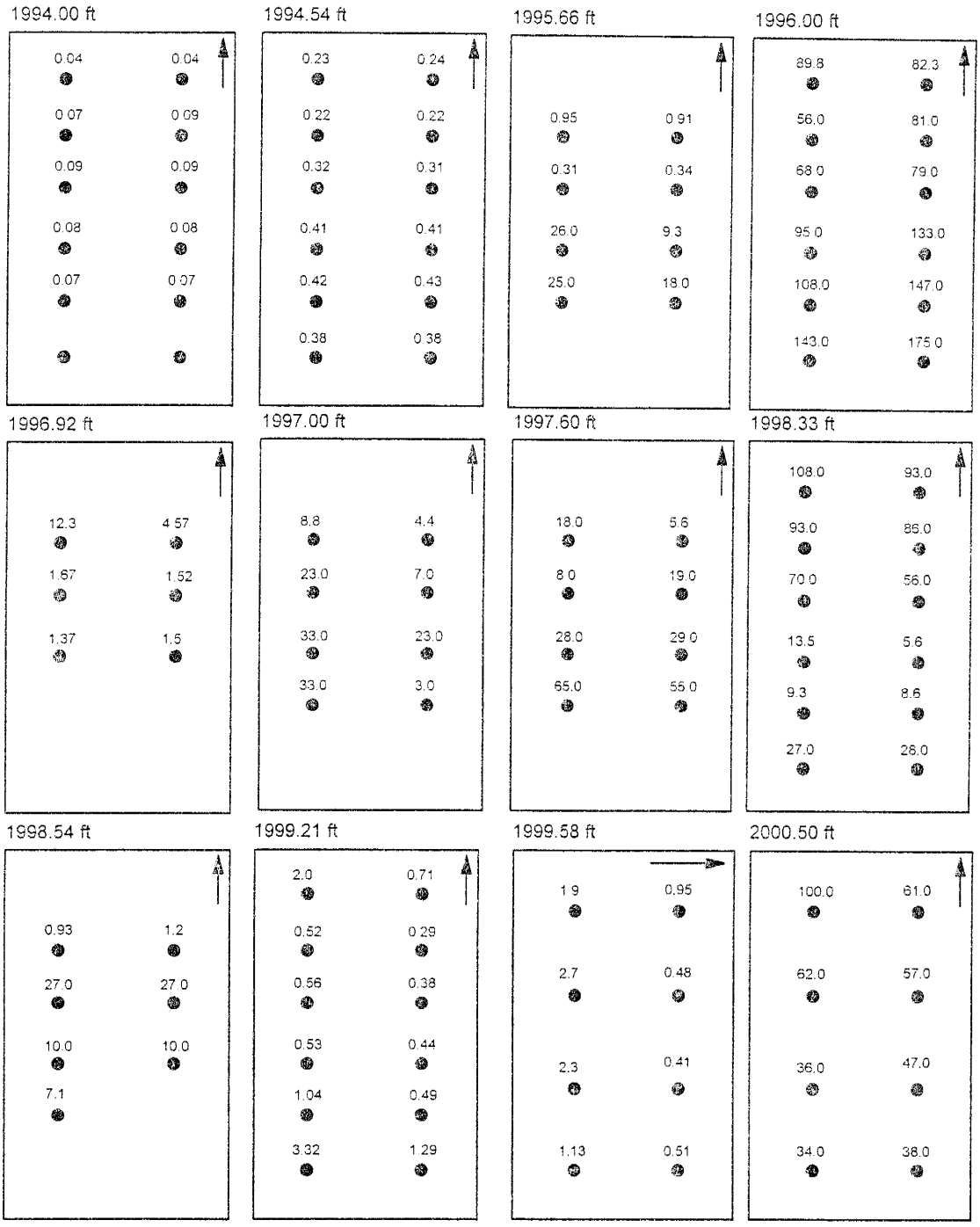

Figure 5.4: Distribution of permeability points on the thin sections from the Shattuck Member. Arrows show the stratigraphic top. The horizontal and vertical interval between permeability points is 0.25 inches. The probe tip has inner radius of 0.125 inches (3.15 mm). For each permeability point, the area analyzed has an approximate diameter of 0.4 inches (10 mm).

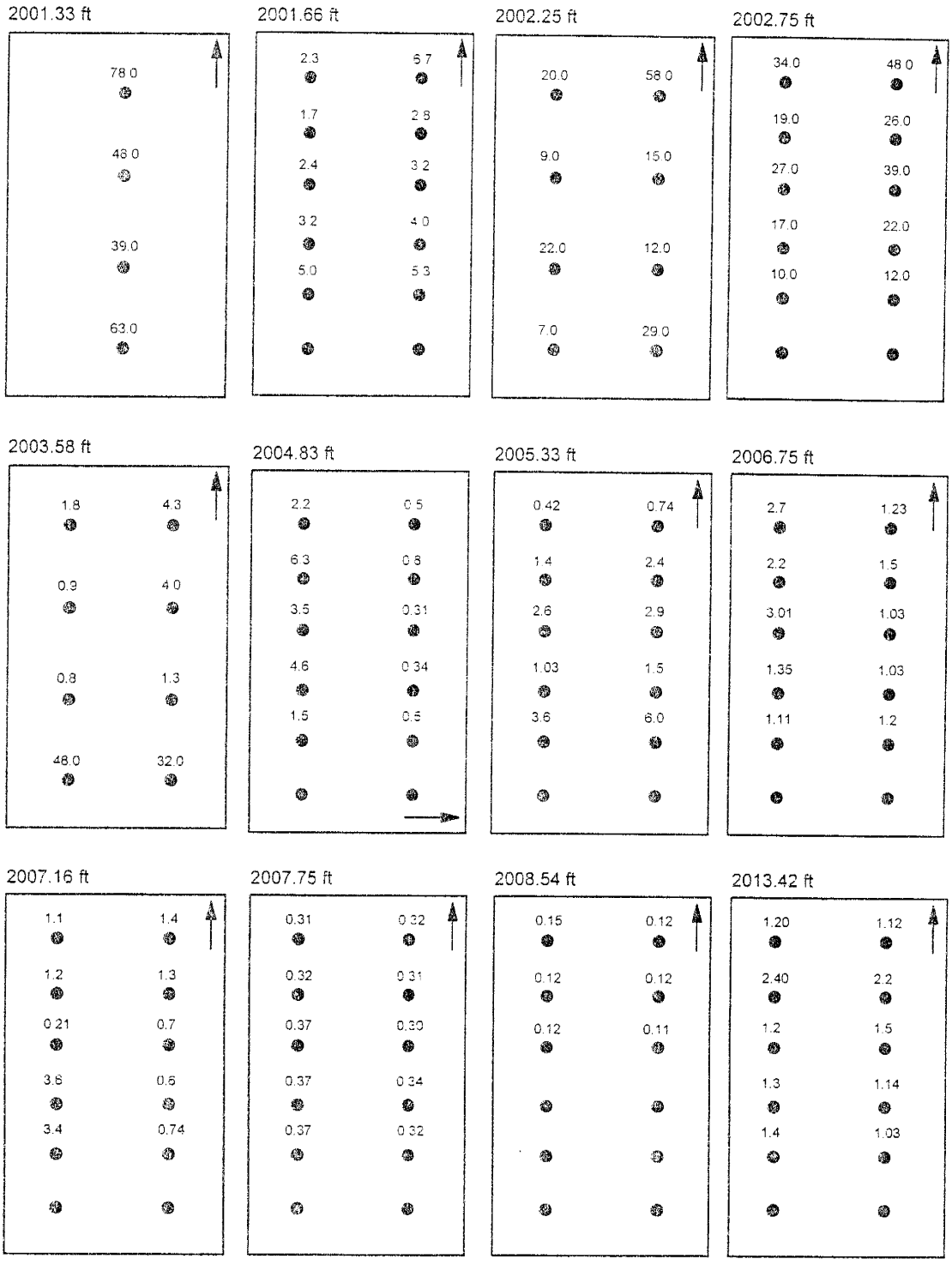

Figure 5.4: Continued.

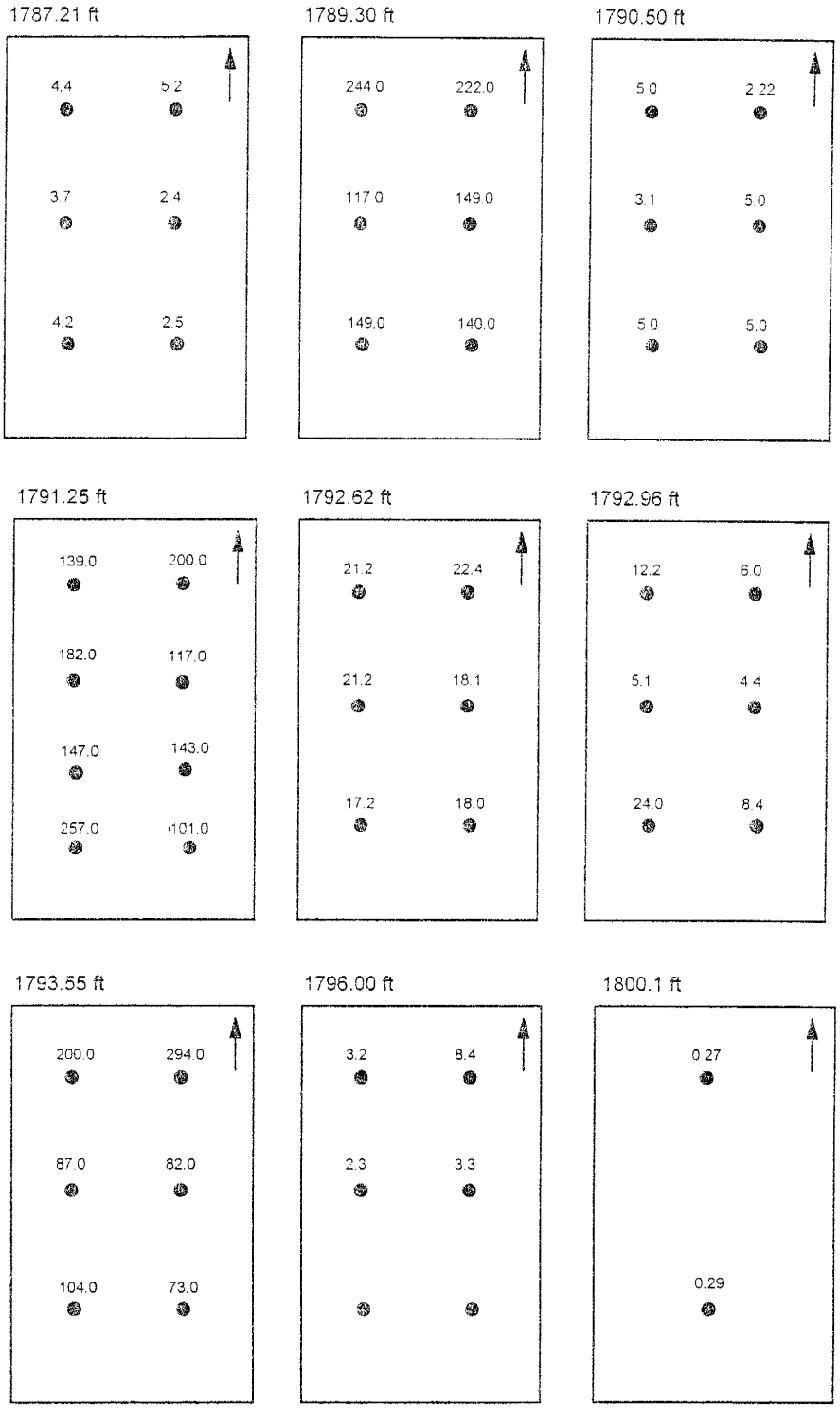

Figure 5.4: Continued. Samples from South Lucky Lake field.

point were: total porosity, total secondary porosity, secondary intergranular porosity, microporosity, intraconstituent porosity, moldic porosity, microfractures, quartz, feldspar, rock fragments, anhydrite, dolomite, clay, dead oil, pore size, grain size, grain sorting, pore sorting, and pore interconnection (Appendix C).

Petrographic data analysis using regression and fuzzy logic

Petrographic analysis was done to establish the ranking of each petrographic element in controlling the permeability using simple regression analysis and fuzzy logic algorithm. Prior to generating the fuzzy curves for these petrophysical attributes, histograms were plotted for each attribute. The histograms for the most important petrographic elements are shown in Figure 5.5. The histograms ensure that the data have approximately gaussian distribution. Heavily skewed data may result in erroneous results from the fuzzy logic algorithm. Histograms for moldic and intraconstituent porosity were skewed even after normalization and hence the fuzzy logic results pertaining to these parameters were considered inconclusive. Moldic and intraconstituent porosities are present in minor amounts (<3%) and exhibit poor relationships with the permeability (regression analysis). Therefore, it was assumed that they impart no control over permeability and these parameters were eliminated from analysis, which improved the fuzzy logic results. In cases where it is known that the heavily skewed parameters are important in controlling the permeability, the data can be normalized using the normal score transform (Deutsch and Journel, 1992).

The results of simple regression analysis and the fuzzy logic algorithm are shown in Figures 5.6, 5.7, & 5.8 and Tables 5.2 & 5.3. Both simple regression analysis and the fuzzy logic algorithm have been discussed in detail in Chapter 2. Table 5.3 compares the ranking of the top ten (out of sixteen) elements obtained from the fuzzy logic algorithm with the results of conventional regression analysis. It is evident from Table 5.3 that the most important petrographic elements (ranking 1 to 5) controlling permeability are accurately predicted by the new algorithm, which is the primary objective of this type of analysis.

Zones	Thickness (ft.)	Horizontal K (md)	Vertical K (md)	"σ" of Horizontal K (md)	Total ϕ (%)	Primary ϕ (%)	Secondary ϕ (%)	Micro ϕ (%)	Quartz (%)	Feldspar (%)	Rock Fragments (%)	Clay (%)	Dolomite (%)	Anhydrite (%)	Pore Size (μm)	Grain Size (μm)
Zone 1	9.0	37.33	1.57	43.0	8.2	0.93	7.2	1.7	51.5	14.6	2.6	6.0	11.15	4.5	24.5	76.6
Subzone A	1.8	0.68	0.26	0.6	3.0	0.77	2.0	2.1	44.6	4.3	0.73	2.0	42.3	2.0	10.0	45.4
Subzone B	1.8	9.9	3.63	7.3	3.2	0.11	3.1	1.5	45.0	17.0	5.3	15.2	7.2	6.4	11.85	70.0
Zone 2	10.0	1.06	0.18	1.3	4.8	0.10	4.8	1.3	52.2	16.5	0.63	2.4	1.3	19.8	14.8	88.0
Zone 1 without Zone A	7.2	43.2	6.7	44.0	9.3	0.96	8.3	1.6	53.0	16.8	3.01	6.7	4.5	5.0	27.6	83.2

Table 5.1: Summary of average permeability, porosity, mineralogical, and textural data for each permeability zone in the Shattuck Member. The horizontal permeability was calculated using the arithmetic average and vertical permeability was calculated using the harmonic average of the minipermeameter data.

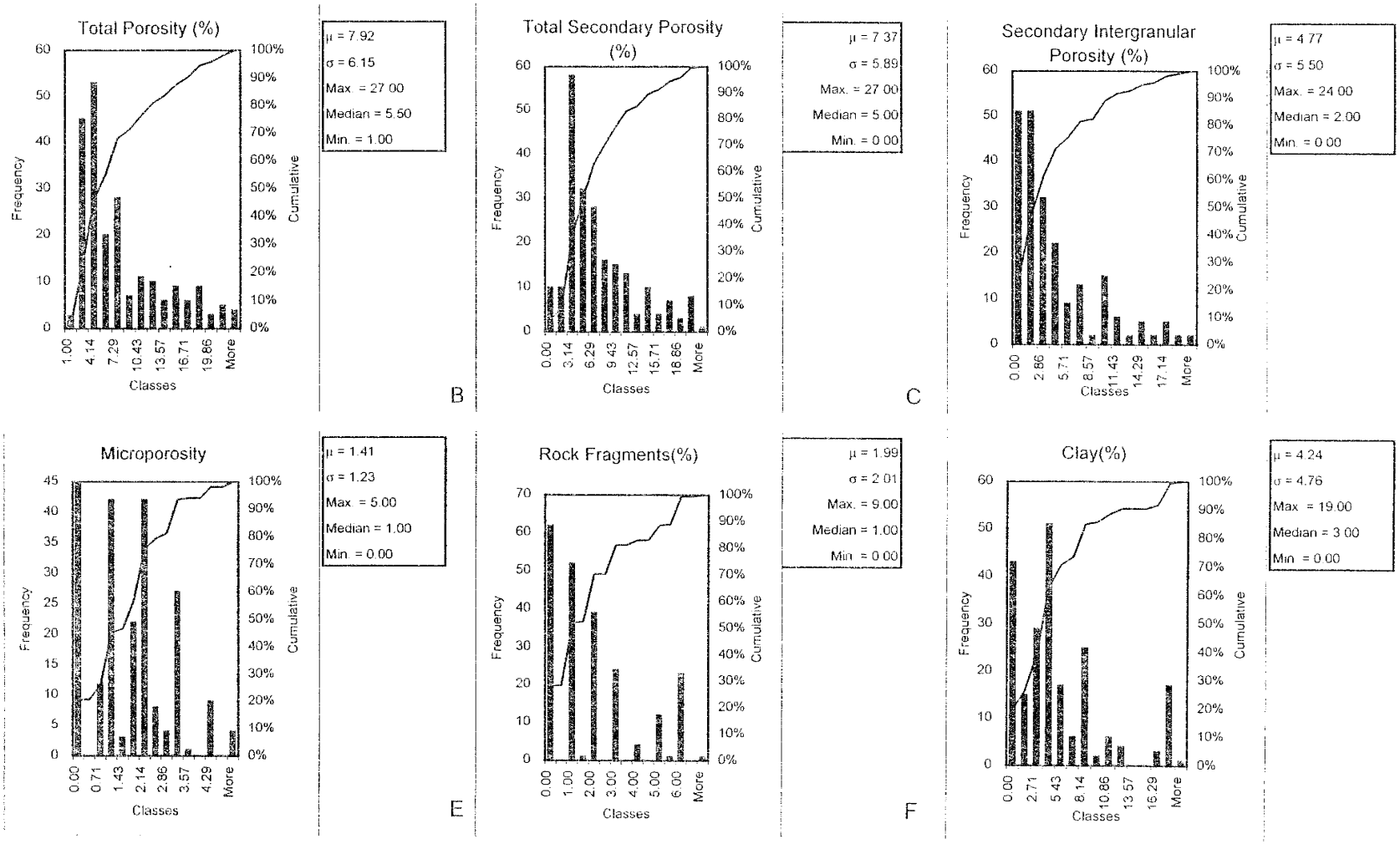

Figure 5.5: Histograms of petrographic data for the Shattuck Member in the Sulimar Queen and South Lucky Lake fields.

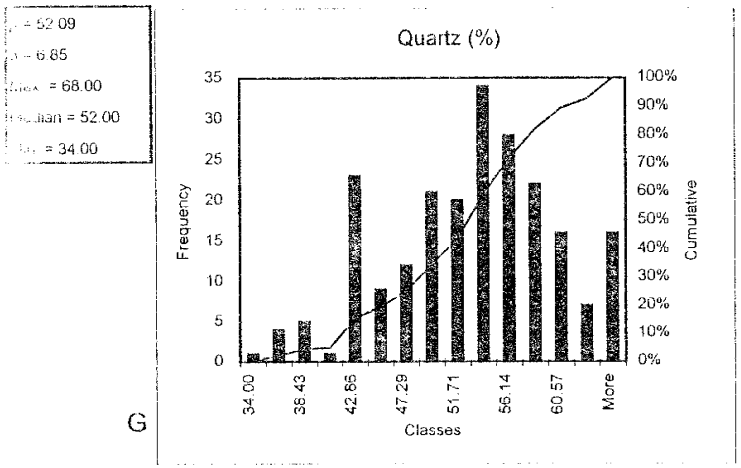

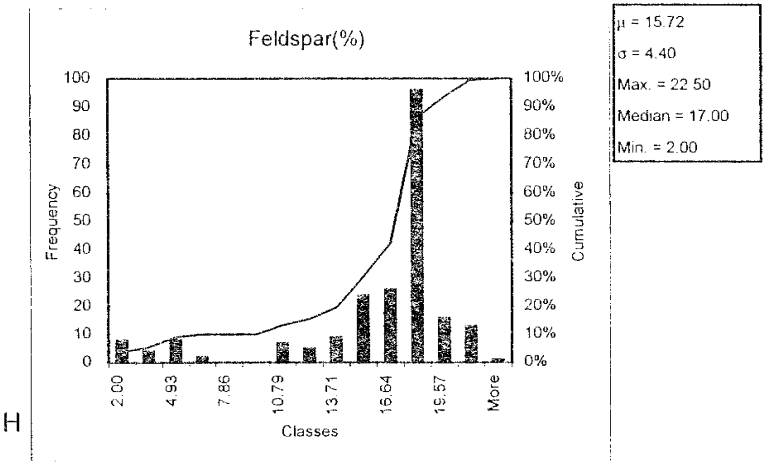

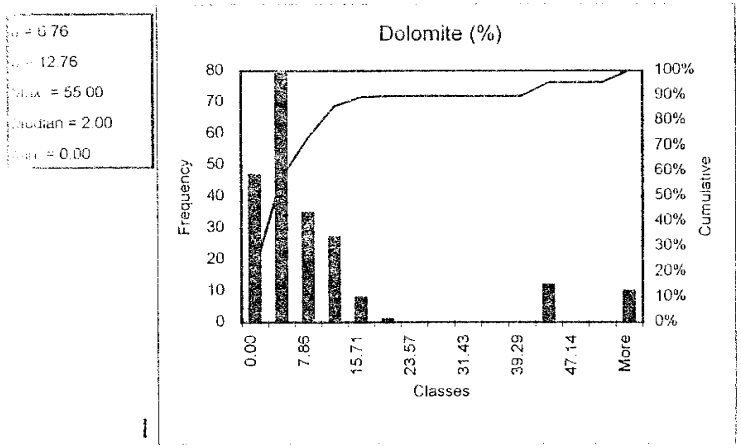

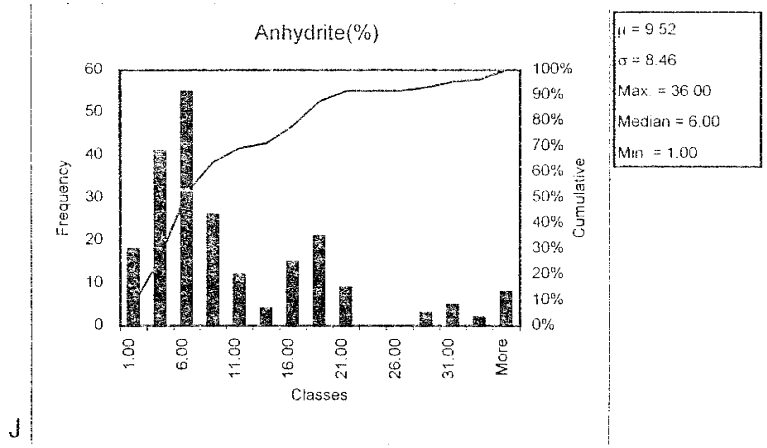

Figure 5.5: Continued.

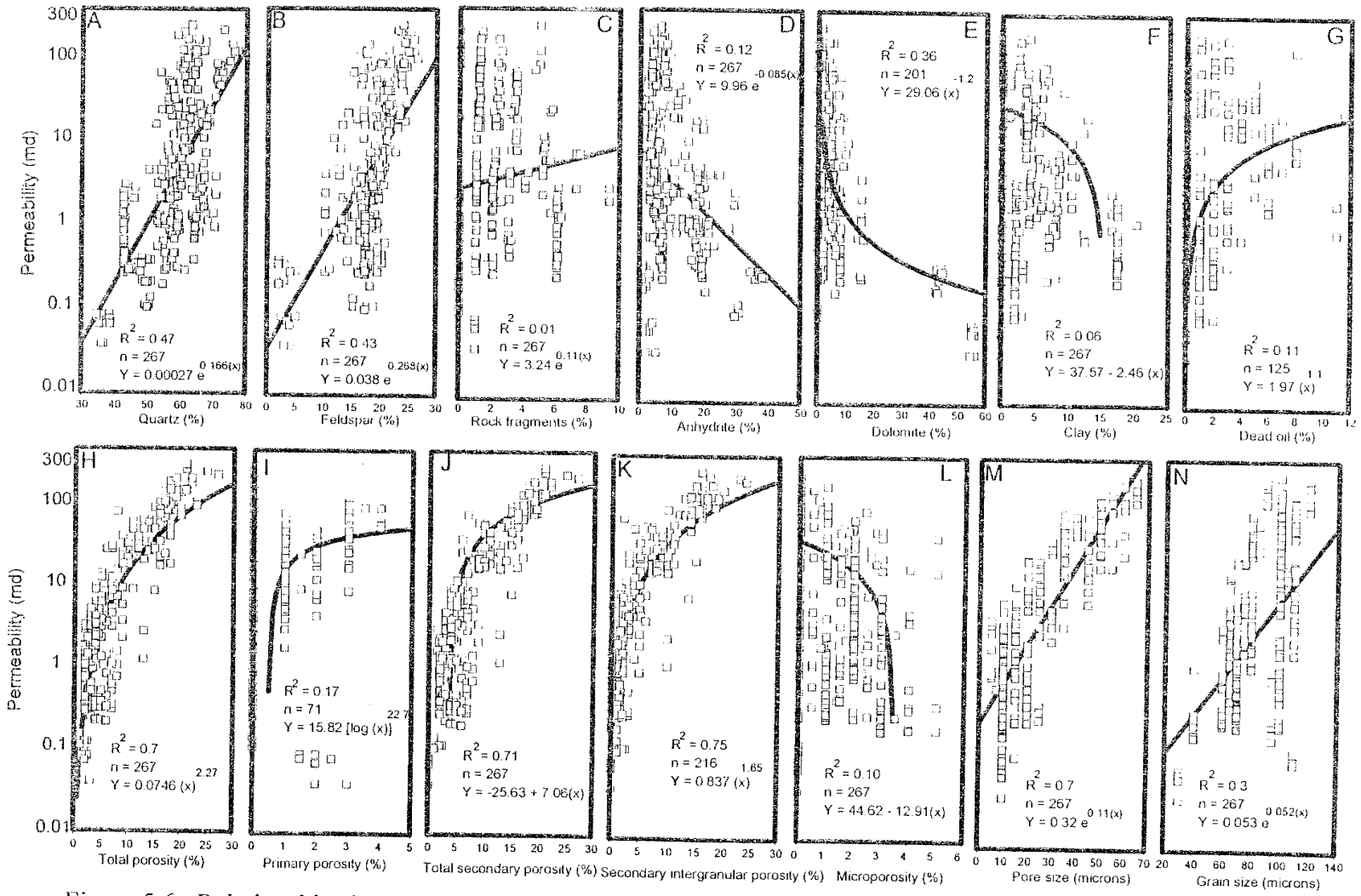

Figure 5.6: Relationships between permeability and different petrographic elements in the Shattuck Member, Sulimar Queen and South Lucky Lake fields.

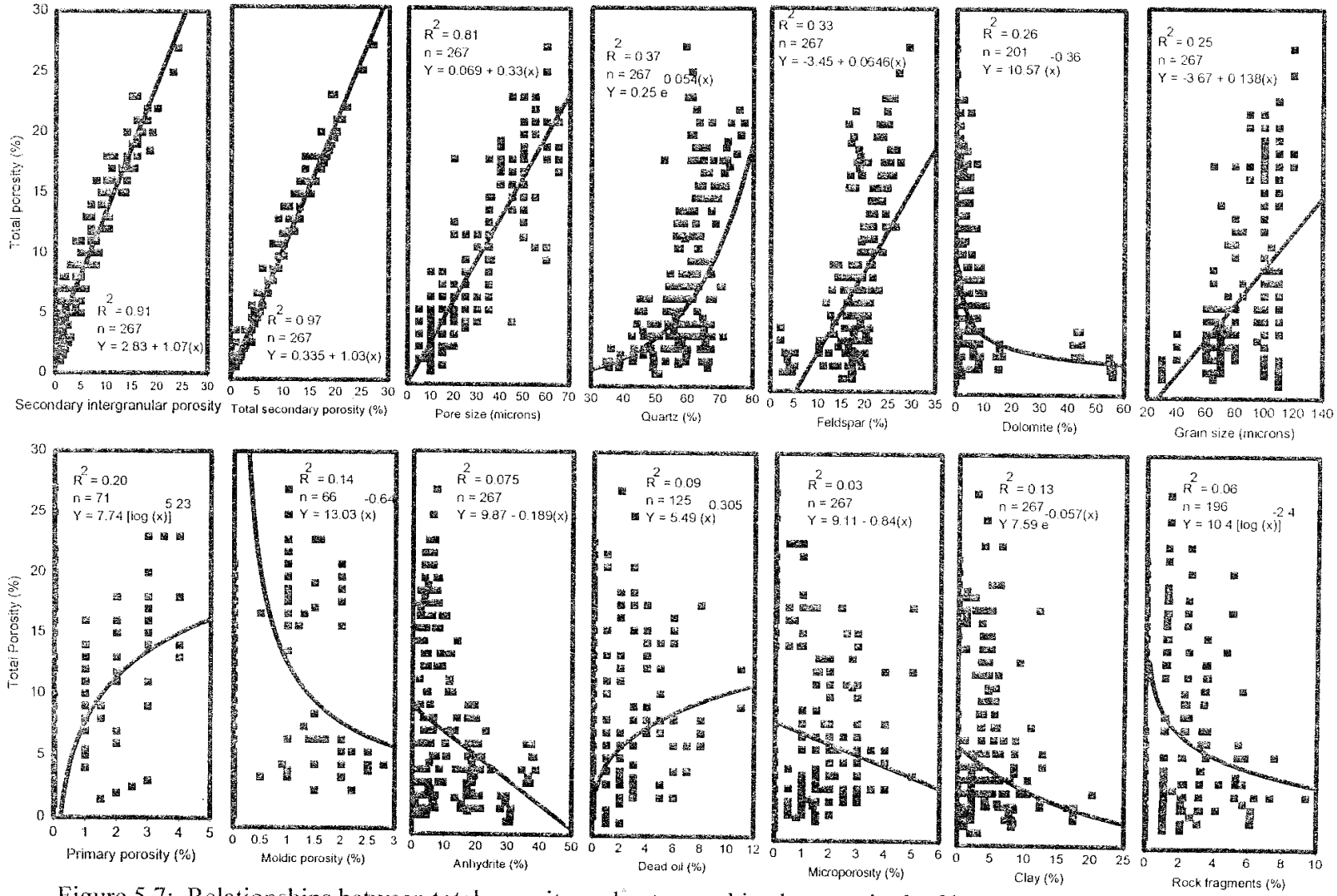

Figure 5.7: Relationships between total porosity and petrographic elements in the Shattuck Member, Sulimar Queen and South Lucky Lake fields.

Petrographic elements	Amount (Ranges)	Correlation (R^2) with permeability	Correlation (R^2) with total Porosity	Ranking based on R^2 with permeability
Secondary intergranular ϕ	0 - 27%	0.75	0.91	1
Total Secondary ϕ	0 - 27%	0.71	0.97	2
Total ϕ	0 - 27%	0.70	-	3
Pore size (microns)	0 - 70 μm	0.70	0.81	4
Quartz	0 - 75%	0.47	0.37	5
Feldspar	0 -26%	0.43	0.33	6
Dolomite	0 - 55%	-0.36	-0.26	7
Grain size (microns)	0 - 120 μm	0.30	0.25	8
Intraconstituent ϕ	0 - 3.5%	0.21	0.36	9
Primary ϕ	0 - 4%	0.17	0.20	10
Moldic ϕ	0 - 3%	0.13	0.14	11
Anhydrite	0 - 40%	-0.12	-0.07	12
Dead oil	0 - 11%	0.11	0.09	13
Micro- ϕ	0 - 5.5%	-0.10	-0.03	14
Clay	0 - 21%	-0.06	-0.13	15
Rock Fragments	0 - 9%	0.01	-0.06	16

Table 5.2: Summary of the petrographic elements and their relationship (R^2) with permeability and total porosity in the Shattuck Member. The ranking shows the importance of petrographic elements in controlling the permeability, as determined by the conventional regression analysis.

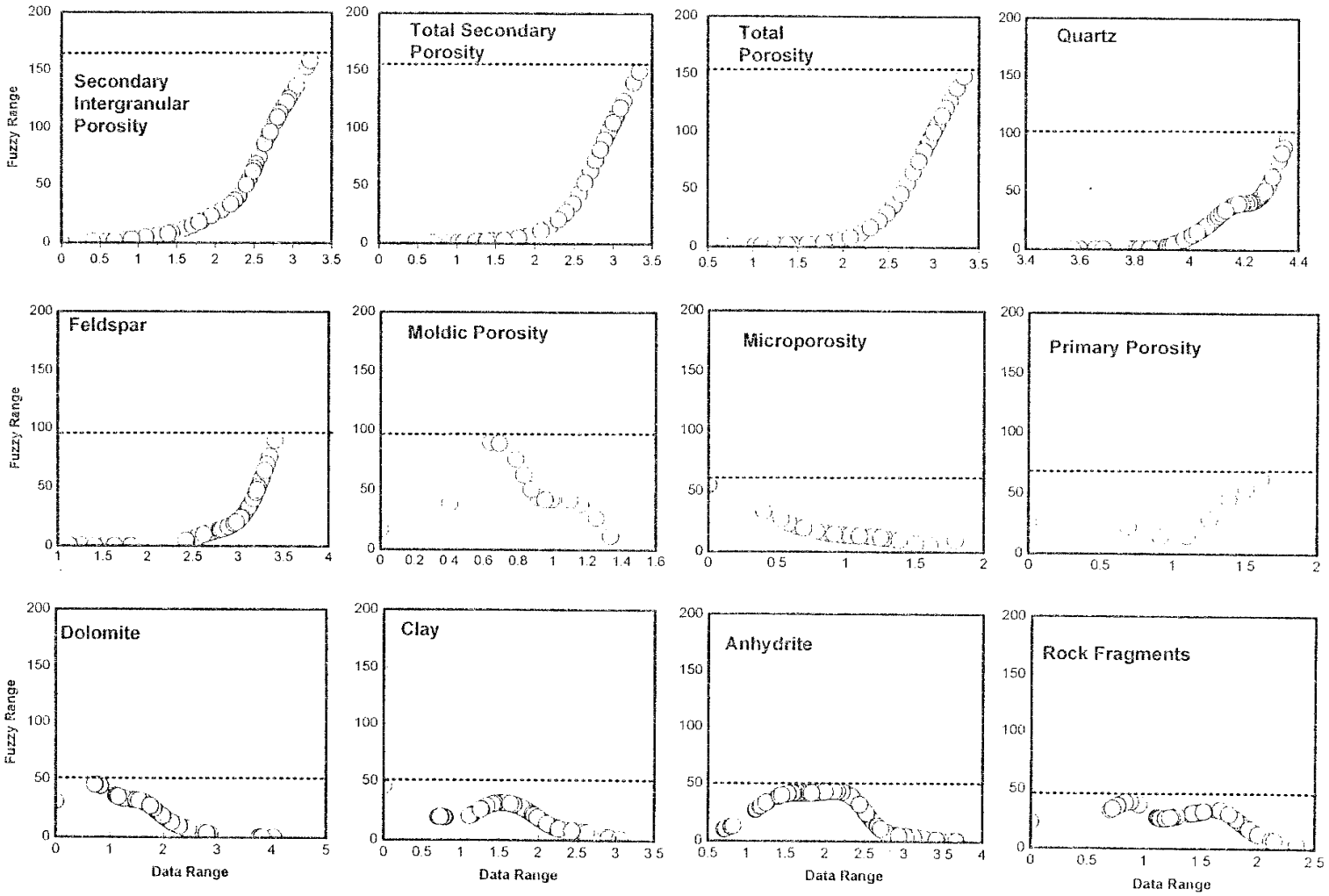

Figure 5.8: Fuzzy-curves for the Shattuck Member. Fuzzy range on the Y-axis determines the control of that element on permeability.

Petrographic elements	Ranking due to regression	Ranking due to fuzzy logic
Secondary intergranular ϕ	1	1
Total secondary ϕ	2	2
Total ϕ	3	3
Quartz	4	4
Feldspar	5	5
Dolomite	6	7
Anhydrite	7	9
Microporosity	8	6
Clay	9	8
Rock fragments	10	10

Table 5.3: Comparison of conventional and fuzzy logic based ranking of petrographic elements in controlling permeability in the Shattuck Member.

Depending on the ranking, permeability can be estimated by using the most significant petrographic elements. The results of the fuzzy logic algorithm were in excellent agreement with conventional regression analysis (Table 5.3). The advantage of using fuzzy logic analysis lies in the speed of analysis. In conventional regression analysis, each petrographic element is plotted against permeability individually, whereas in the fuzzy logic method all the petrographic elements are compared at the same time with permeability, therefore, it is much faster and more quantitative.

Mineralogy

A detailed petrographic analysis was also done to determine the paragenetic sequence, porosity evolution, and the depositional environment. A generalized paragenetic sequence is shown in Figure 5.9.

The petrographic analysis indicated that quartz and feldspars are the dominant detrital grains, whereas anhydrite and dolomite are the dominant cements. Both quartz and feldspar overgrowths are ubiquitous throughout the reservoir but never exceed 2% (Figure 5.10A). Most of the feldspar grains are altered (sericitized) and the majority of the intraconstituent porosity is present among the partially dissolved feldspar grains especially in Zone 1 (Figure 5.10A). Quartz and feldspar grains are also coated with clay and hematite (Figure 5.10B). These clay rims consist of authigenic chlorite. Hematite is more conspicuous in the low permeability part (Zone 2), where it coats grains and also stains the anhydrite (poikilotopic) cements. Both quartz and feldspar ranked in the middle with respect to controlling the permeability based on the fact that as their percentage increases, the percentage of anhydrite and dolomite cement decreases.

The rock fragments consist of metamorphic rock fragments, chert, carbonate rock fragments, and anhydrite cemented siltstone. Rock fragments do not exert much control over the permeability because of their low percentage and fine sand size. Only when clay fragments form the pseudomatrix as they get squeezed between the harder grains, both porosity and permeability are reduced.

Dolomicrite might have originally been lime mud which was diagenetically

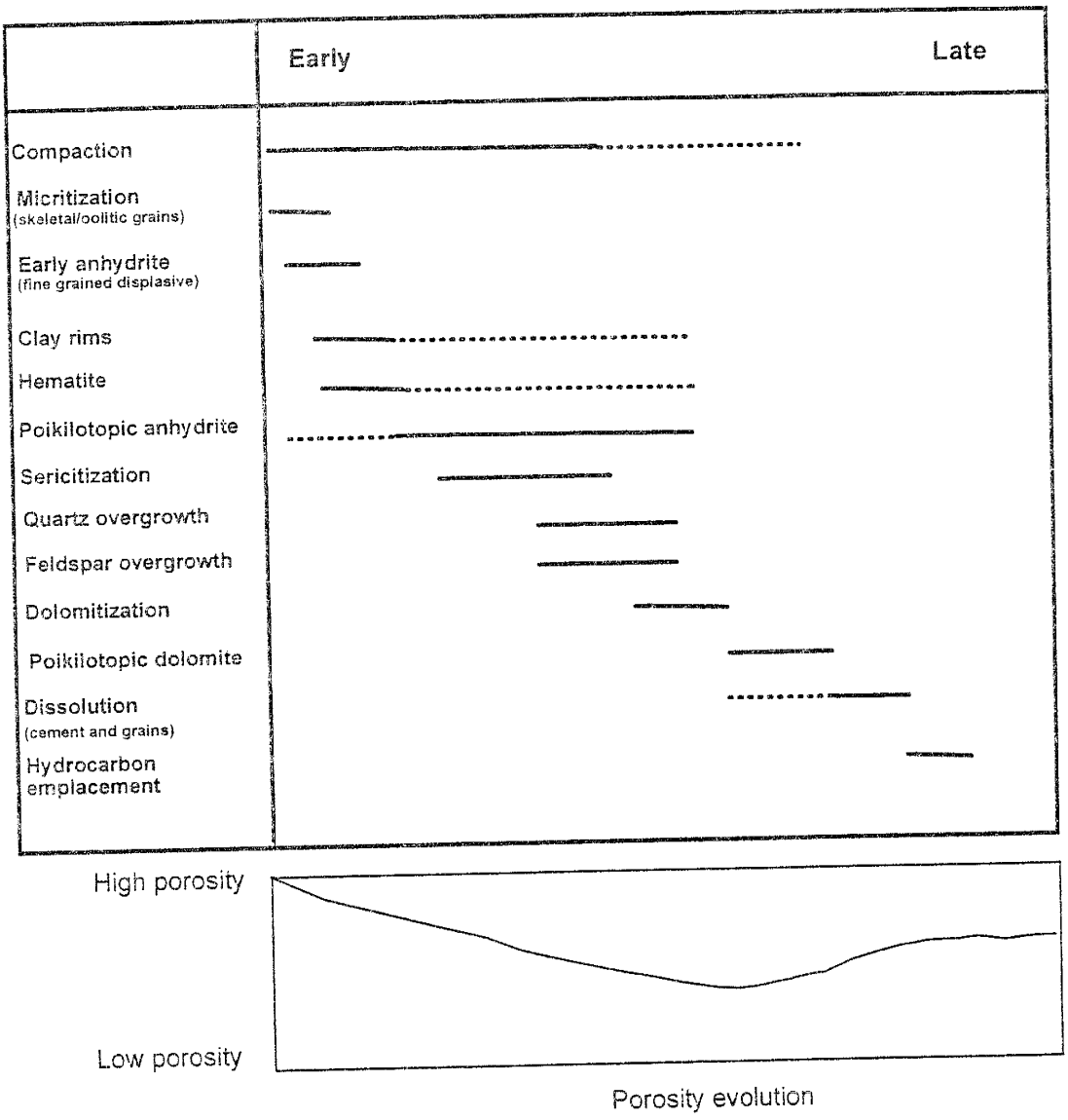

Figure 5.9: Generalized paragenetic sequence for the Shattuck Member in the Sulimar Queen and adjacent fields.

Figure 5.10: Thin section photomicrographs showing the mineralogic makeup and diagenetic products in the Shattuck Member. (Porosity in blue.)

A: Quartz (Q) and feldspar (F) grains. Quartz overgrowth (Q) and partially altered feldspar (F) grains visible. (Thin section 1994.80, plane light)

B: Hematite coating in moderately sorted well cemented (anhydrite) part of the Shattuck Member. (Thin section 2009.0, plane light)

C: Displacive anhydrite. (Thin section 1986.0, crossed polarizers)

D: Poikilotopic pore filling anhydrite. (Thin section 2008.65, crossed polarizers)

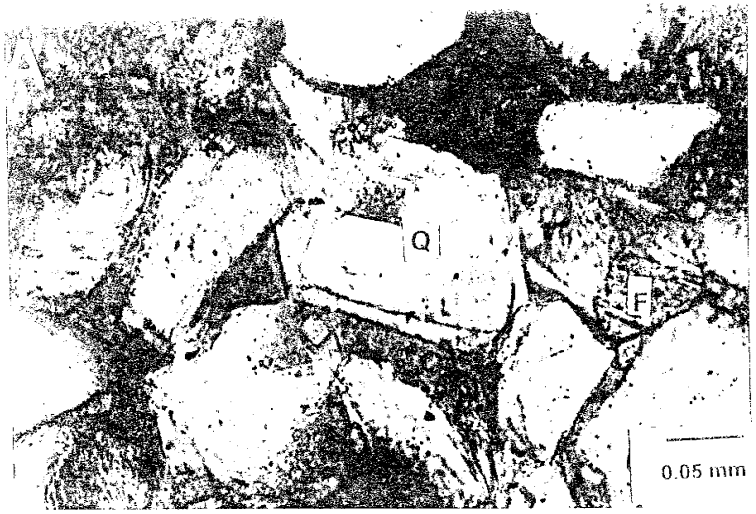
A
Q
F
0.05 mm

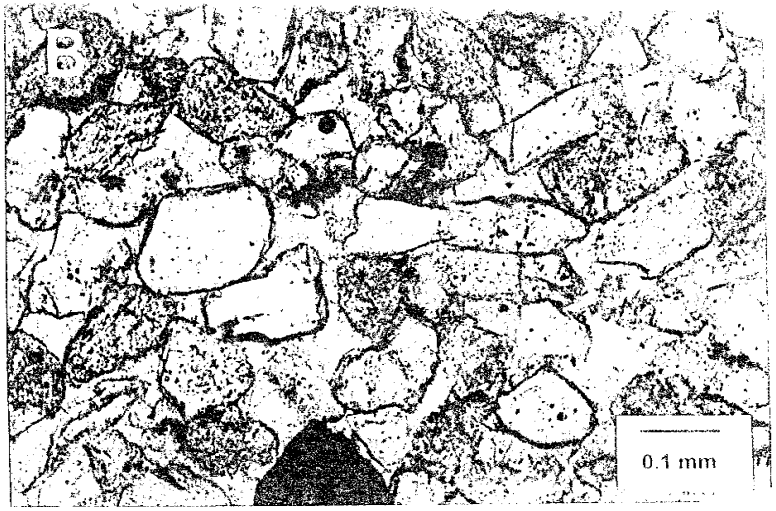
B
0.1 mm

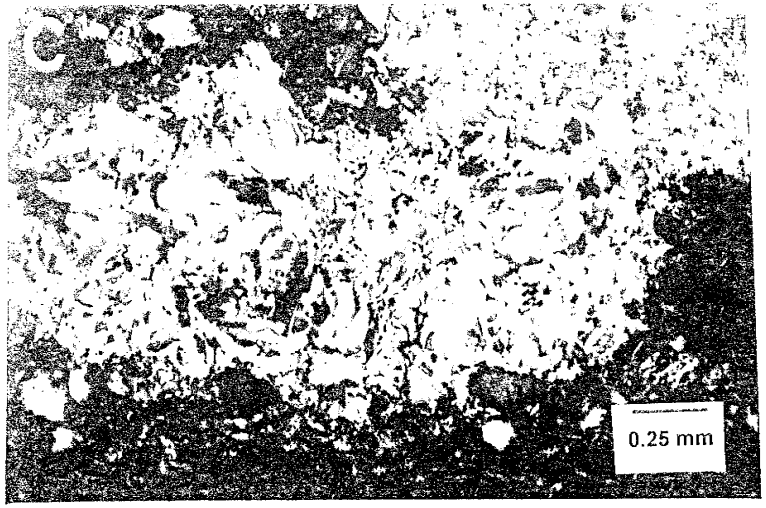
C
0.25 mm

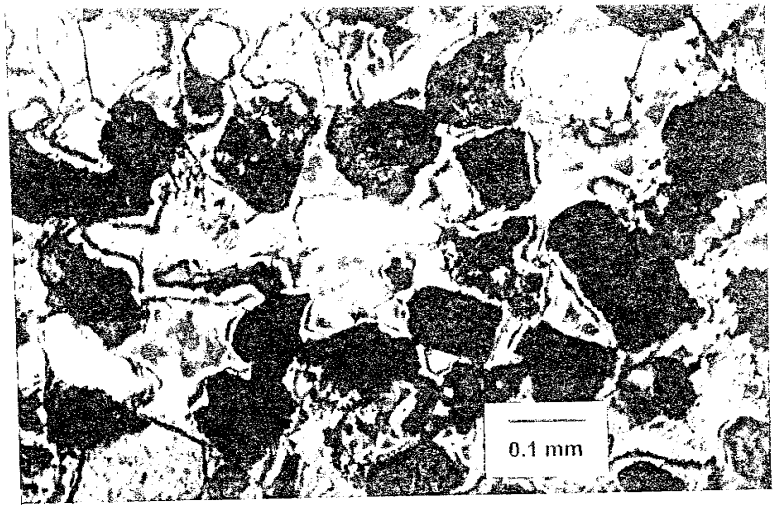
0.1 mm

Figure 5.10: Continued

E: Microdolomite. (Thin section 1995.80, crossed polarizers)

F: Poikilotopic dolomite with coarse anhydrite crystals floating in it. (Thin section 1995.80, crossed polarizers)

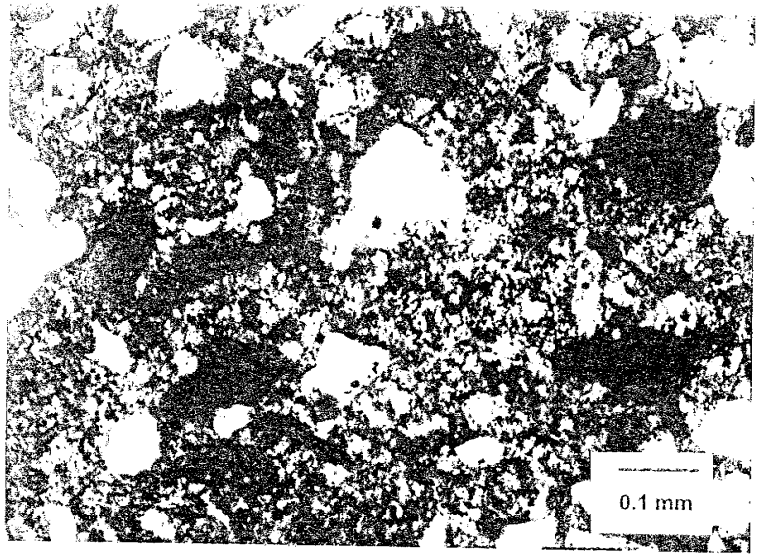
0.1 mm

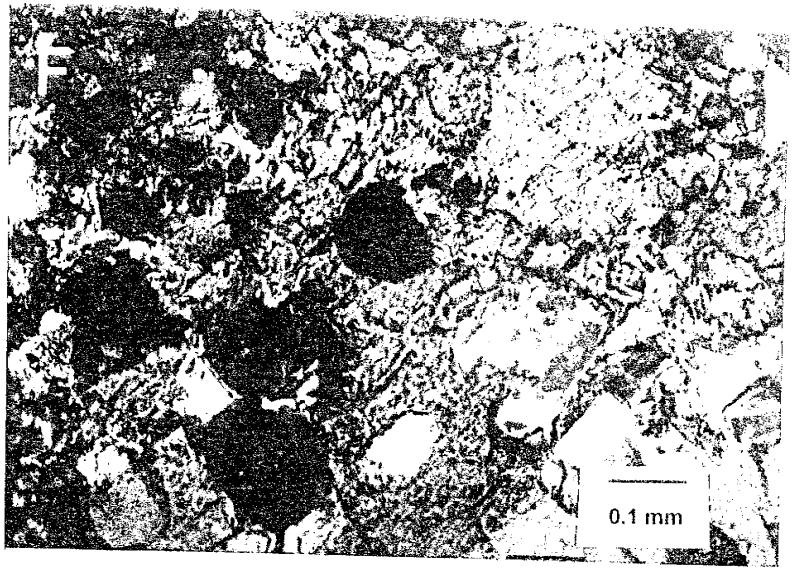
F
0.1 mm

altered to dolomicrite. Dolomicrite could be identified easily due to its exclusive presence in the primary pores. Dolomicrite is present in substantial amounts only in the thinly laminated, poorly sorted, silty sandstone zones not thicker than 2 inches (Zone 1). This is the reason why clay does not affect the permeability and is close to the bottom of the conventional ranking (Table 5.2).

Cement is present in the form of anhydrite and dolomite. Anhydrite is present in two morphologies: (1) fine crystalline nodules, mainly in the upper silty-shaly zone at the top and in Zone 2 of the Shattuck Member (Figure 5.10C), and (2) coarse, pore-filling, large patches of poikilotopic crystals surrounding several grains (Figure 5.10D). It is the poikilotopic morphology which has affected the permeability especially in Zone 2. Dolomite is present in two morphologies: (1) micritic dolomite, probably formed by the dolomitization of the carbonate mud (Figure 5.10E), and (2) large poikilotopic patches (Figure 5.10F). The presence of the inclusions of dolomicrite and anhydrite in the poikilotopic dolomite suggest that poikilotopic dolomite postdates both of them (Figure 5.10F). Both dolomite and anhydrite have also replaced the detrital grains. Based on the correlation coefficient and fuzzy logic analyses, dolomite seems more important than anhydrite in controlling permeability. The dead oil present reduced porosity and the interconnection between the pores; therefore, its effect on permeability was also acknowledged.

Porosity types

Different porosity types present in the Shattuck Member are shown in Figure 5.11. Among the porosities, secondary intergranular porosity is the most dominant type and exerts the most influence on the permeability (Table 5.2 and Figures 5.11D, & 5.6K). As the dissolution increases, the secondary intergranular porosity increases and the interconnection between the pores becomes good (Figure 5.11D).

As the amount of secondary porosity increases, so does the pore size because of increased dissolution. The interconnection between the pores also improved, due to dissolution and enlargement of pores. This explains why the pore size is very important

Figure 5.11: Thin section photomicrographs showing different porosity types in the Shattuck Member. (Porosity in blue.)

A: Primary pores of polygonal shape. The interconnection between the pores is poor.
[(K = 4.4 md), Thin section 1997.0, plane light]

B: Microporosity among the microdolomite. [(K = 1.67 md), Thin section 1996.11, plane light]

C: The effects of channel pores on permeability. Dominantly primary pores interconnected through channels (may be formed by dissolution of anhydritic cement), exhibiting slightly higher porosity. [(K = 12.3 md), Thin section 1996.11, plane light]

D: Well developed secondary intergranular porosity. [(K = 90 md), Thin section 1996.0, plane light]

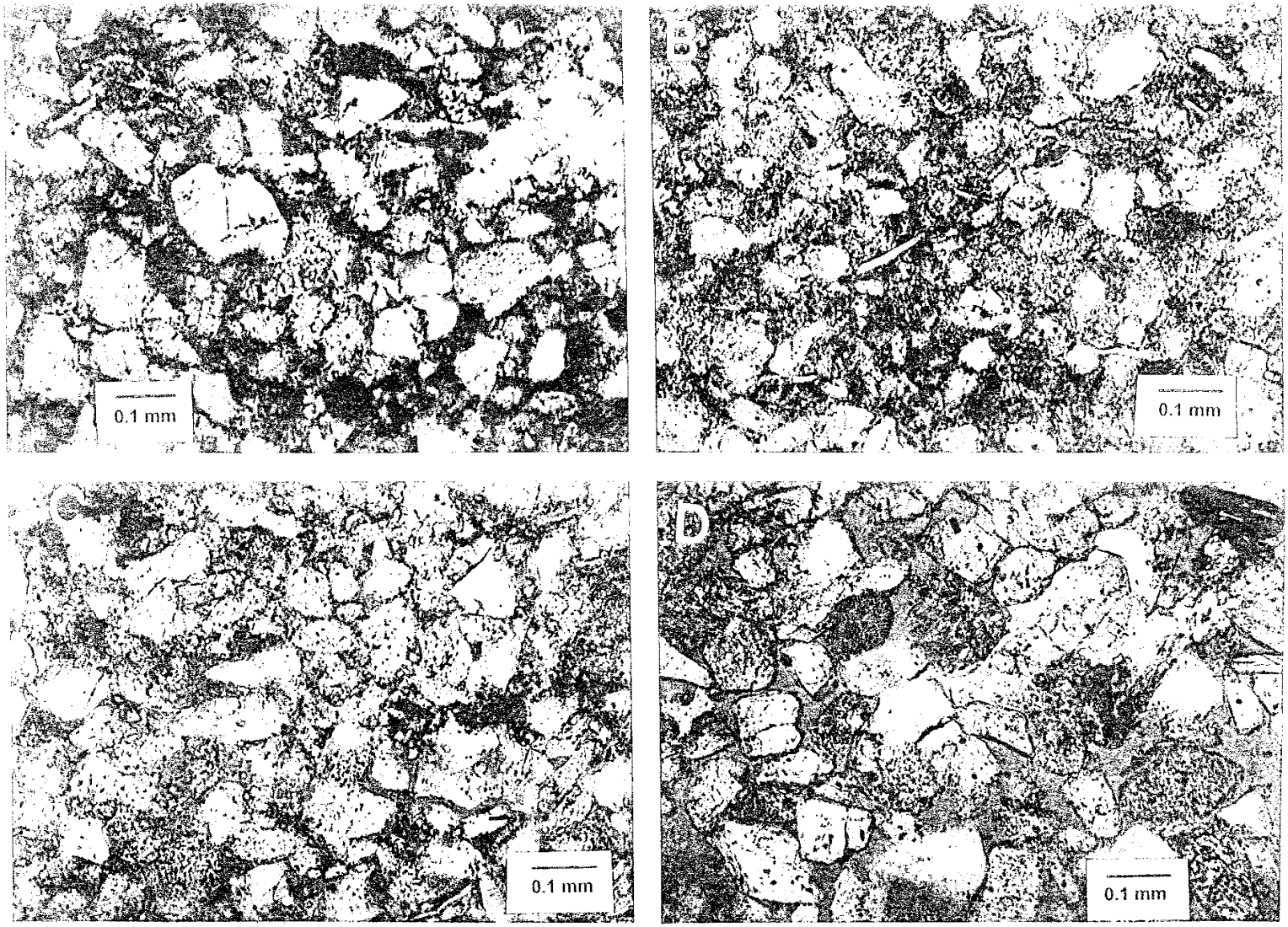
A
0.1 mm
B
0.1 mm
C
0.1 mm
D
0.1 mm

Figure 5.11: Continued

E: Patchy distribution of anhydritic cement. This distribution is caused by the partial dissolution of anhydrite. [(K = 108.0 md), Thin section 1998.4, plane light]

F: Typical discontinuous thin laminations in zone 1. [(K = 2.4 md), Thin section 2001.8, plane light]

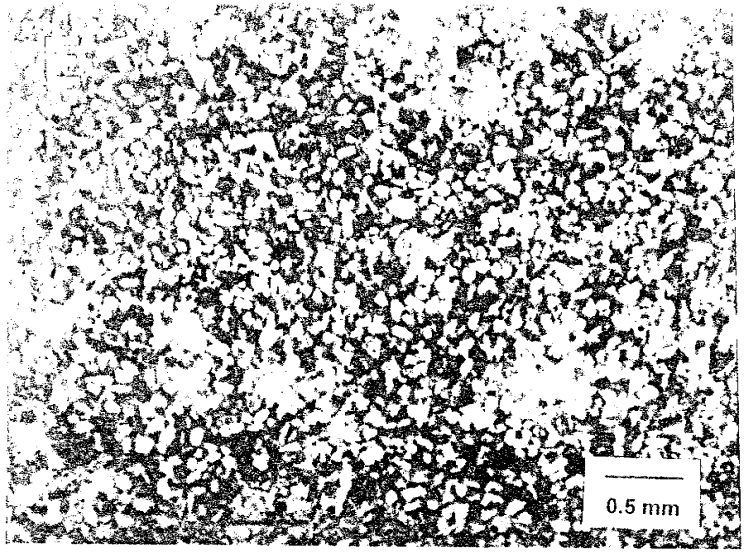
0.5 mm

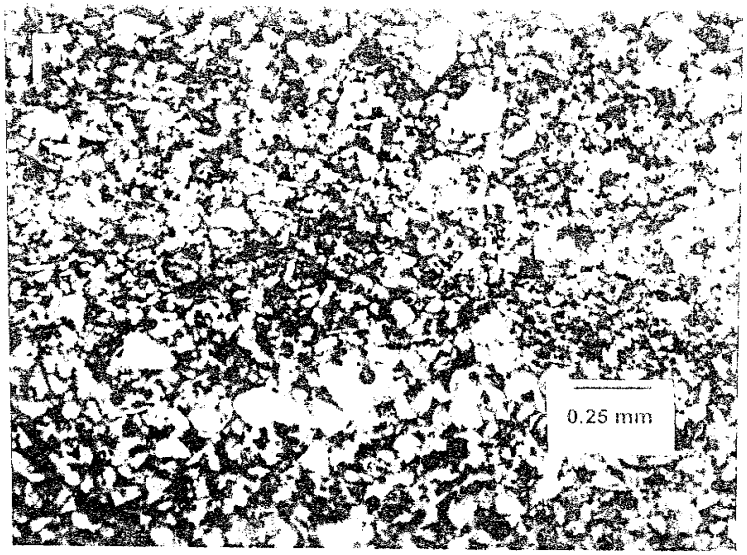
0.25 mm

in controlling the permeability (Figures 5.11D & 5.6M). The relationship between the grain size and permeability is not good (Table 5.2 and Figure 5.6N). The larger grains are present in the well-sorted part of the reservoir (Zone 2). Zone 2 was affected by early anhydrite cementation and almost all the original porosity was lost (Figure 5.10B). The moderately-sorted lagoonal sandstones (Zone 1) were not affected by early cementation and enough primary porosity was available for the fluids responsible for dissolution to move freely through the system and produce secondary porosity and the patchy distribution of anhydrite (Figure 5.11E). Poorly sorted thin laminae of clay cause local low porosity and permeability areas in the high permeability Zone 1 (Figure 5.11F).

The relation of total porosity to other petrographic elements was also investigated (Figure 5.7). Except for moldic porosity and microporosity, all other types of porosity increases as the total porosity increases (Figure 5.7). Total porosity increases with the increase in grain and pore size, but decreases with the increase in dolomite and anhydrite (Figure 5.7). Total porosity increases with the increase in quartz and feldspar and decreases with the increase in the amount of rock fragments and clay (Figure 5.7).

Figure 5.8 shows the fuzzy curves resulting from the fuzzy logic method. The first row represents the petrophysical parameters that have the largest influence on the permeability, and most of them are the porosity types. This is evident from the range of each fuzzy curve on the corresponding ordinate. For example, the fuzzy curve for total secondary porosity exhibits a range of approximately 160, whereas feldspar and anhydrite exhibit ranges of approximately 90 and 45 respectively. H ere, the total porosity has greater influence than feldspar which, in turn, affects permeability more than anhydrite.

From Table 5.3 we can also see that the fuzzy logic algorithm ranked microporosity in the 6th place. From conventional ranking, we see that microporosity was ranked 8th. In the case of Sulimar Queen field, we know that microporosity should affect permeability more than dolomite which, appears to be in agreement with the fuzzy logic prediction.

From the petrographic analysis, we decided that Zone 1 should be the main reservoir because it was not affected by anhydrite cementation. Zone 1 was affected

considerably by dissolution and thus has the highest porosity and permeability. The detailed petrographic analysis also helped to understand the subtle changes in the lithologies. The identification the grain size and sorting, millimeter-thick clay laminations, and anhydrite cement types during the petrographic analysis also improved the depositional model. The well sorted and moderate to well rounded red sandstones with low-angle cross-bedding was assigned an eolian (sand flat) environment. Moderate to well sorted gray sandstones with anhydrite nodules (haloturbation) were assigned sabkha environment. On the other hand, poorly to moderately sorted sandstones that were cemented with poikilotopic anhydrite and contained continuous and discontinuous thin (millimeter thick) clay laminations, wavy laminations, and flaser bedded were assigned a lagoonal/salina environment. The details of the depositional model are given in Chapter 4.

PERMEABILITY PREDICTION USING ARTIFICIAL INTELLIGENCE

The fields of statistics and neural networks are closely related. The principle difference between the two fields is that, historically, statistics has focused on linear problems, which are relatively tractable, while neural networks excel with nonlinearities (Smith, 1993). In the following paragraphs, the basics of neural networks and their use in predicting permeability using the petrographic elements is discussed briefly.

Overview of Neurocomputation

This overview of neurocomputation is extracted from Haykin (1994). Neural networks are designed to duplicate the way the brain processes data to recognize patterns. Therefore, neural networks can be trained to identify certain patterns and then predict the outcome for some complex situations. The human brain acts like a natural neural net and is composed of a chaotic connections of neurons. It is a highly complex, nonlinear, and parallel information processing system. A typical neuron receives input from many other neurons. It also send outputs to other neurons, which can be considered inputs for other neurons. During brain development, we learn because the strengths of the connections

between neuron change with time. The response of a particular neuron to the other connected neurons does not remain constant. It may increase or decrease over a given time period, depending on experience or learning.

Like an individual neuron, a neural network has inputs and like an individual neuron, a neural network produces output. A neural net emulates the behavior of the brain in a rudimentary manner. Like an individual neuron, the network calculates its outputs as a function of its inputs.

According to Aleksander and Morton (1990):

A neural network is a machine that is designed to model the way in which the brain performs a particular task. A neural network is a massively parallel distributed processor that has a natural propensity for sorting experimental knowledge and making it available for us. It resembles the brain in two respects:

1. *Knowledge is acquired by the network through the learning process.*
2. *Interneuron connection strengths known as synaptic weights are used to store the knowledge.*

Physically, the neural net consists of layers of interconnected processing elements called neurons (Figure 5.12). These layers are called input, hidden, and output layers.

Neural Network Training

The formal training of the neural net is done by either supervised or unsupervised algorithms. The feedforward backpropagation (FFBP) algorithm is an example of the supervised training algorithm (Rumelhart and McClelland, 1986). Feedforward in the FFBP algorithm refers to the fact that there are no recurrent loops in the network that provide an active feedback, i.e., the output from a given node does not cycle back immediately to the same node. The interaction between the layers is governed through connections of variable strengths referred to as weights. In the case of supervised learning, the net is repeatedly presented with numerous pairs of input and corresponding desired outputs. In the beginning, the weights are initialized randomly. The data at the

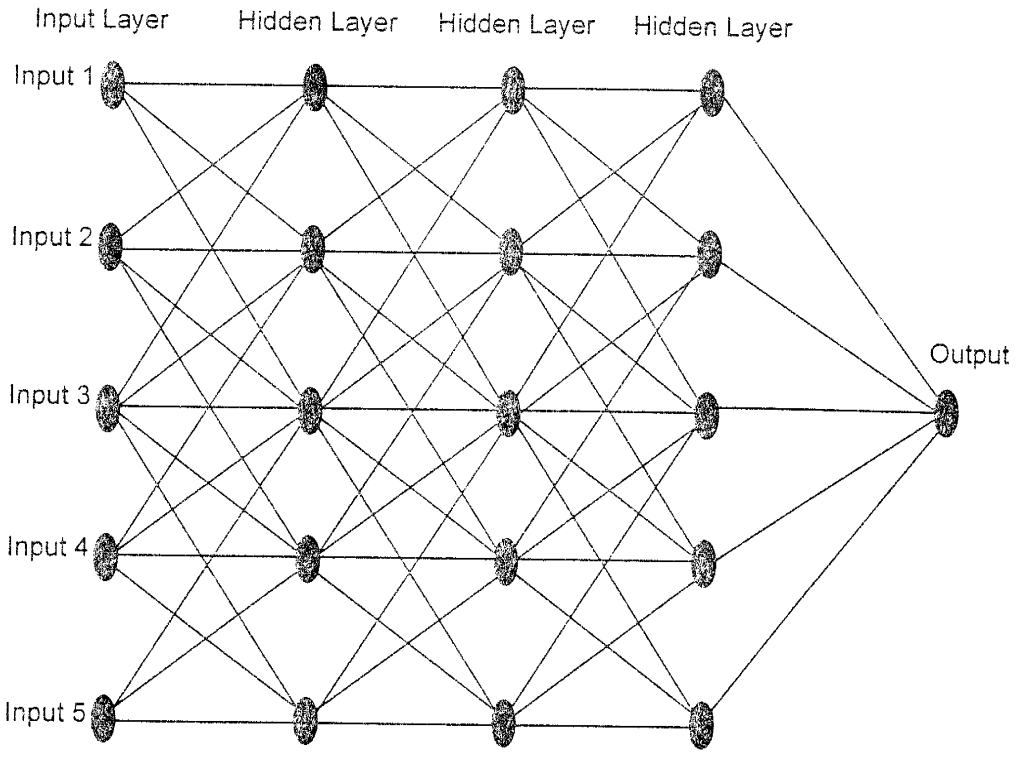

Figure 5.12: The generalized architecture of the neural network.

input layer is processed by neurons and the results are fed forward to the hidden layer. The hidden layer neurons perform similar data processing and pass the results to the output layer. The data at the output layer are then compared against the "desired output" and an error term is calculated. This term is then backpropagated through the net. This process is continued until the error term generated at the output layer falls within a specified tolerance. At this point, the neural net is considered to be trained.

A major characteristic of the neural net used for this study is its ability to converge very fast and provide robust solutions. The fast convergence is achieved through the implementation of the scaled conjugate gradient (SCG) algorithm (Møller, 1994). The scaled conjugate gradient algorithm, a variant of the conjugate gradients method, replaces the common backpropagation algorithm, which uses the steepest gradient method to modify the weight space. The SCG method uses the second-order (or the curvature) information to determine the global minimum. The algorithm attains this by maintaining the Hessian weight matrix positive-definite throughout the training phase. The result is bypassing of the local minima and thus faster training (Chawathé et al, 1997). The details of the neural networks, FFBP algorithm, and the SCG method are out of the scope of this dissertation. Interested readers are referred to Haykin, (1994) and Møller, (1993).

From the preceding discussion, it is clear that a neural network derives its computing power through its massively parallel distributed structure and its ability to learn. This makes the neural network capable of solving complex non-linear problems.

Methodology

Neural networks were used to predict permeability using the petrographic elements in the Shattuck Member. Initially, sixteen petrographic elements were available for each permeability measurement. As mentioned before, the fuzzy logic algorithm allowed the recognition of the top ten elements controlling the permeability (Table 5.3).

The modified feedforward error backpropagation network (Figure 5.12) constructed was tested for various combinations to optimize the neural network. This

was done by changing the following parameters:

1. input petrographic elements,
2. number of input petrographic elements,
3. number of data points used for training (sample size).
4. number of hidden layers of the neural network,
5. correlation coefficient used for training.

It is necessary to optimize the net for several reasons:

1. To reduce the effects of the noise: Sometimes minimizing error on the training data does not minimize the error on the whole population (Smith, 1993). This happens because of the noise. Noise may be caused by measurement error or exclusion of some parameters which appear insignificant.

2. To reduce the overfitting of the model: Overfitting occurs for several reasons. It may happen due to unusually large numbers of hidden nodes, which causes the network's output to fit the data too closely. The net learns the noise in addition to the underlying functional relationship. Backpropagation is the form of a mapping function that is very flexible and the gradient-descent learning process is so relentless that, unless we prevent it, overfitting may cause serious problems (Smith, 1993). In this study, this problem was minimized through the use SCG algorithm.

One important way to achieve fast and accurate training is to maintain a low dimensionality of the input layer. If the input layer comprises of few neurons, the corresponding weight matrix can be maintained small and manageable. Additionally, unnecessary inputs result in noise contribution to the actual signal. To achieve the minimum necessary dimensionality of the input layer, we used the results of the fuzzy logic algorithm, as will be discussed in the following paragraphs.

Neural Network Implementation

The data from Well 1-16 from the Sulimar Queen field was used to train and test the neural net.

Training

The net was optimized with 149 data points. The training data points used for the optimization were selected in order to cover the whole range of permeability and petrographic data. The optimization was based on the "closeness" of the prediction of the remaining 70 data points from Well 1-16. An optimum net was chosen that required one hidden layer with all the layers completely connected (Figure 5.13). The net was trained using 149 data points for a correlation coefficient of 0.94. The correlation coefficient is a linear least square measure between the desired output and the training output. Training was done for the following three combinations:

1. 149 data points with top ten petrographic elements as determined by the fuzzy logic algorithm (Table 5.3).
2. 149 data points with top five petrographic elements as determined by the fuzzy logic algorithm (Table 5.3).
3. 149 data points with top three petrographic elements as determined by the fuzzy logic algorithm (Table 5.3).

Testing

Once the training was completed using the 149 data points, permeability was predicted in the Sulimar Queen field. The permeability was predicted using ten (Figure 5.14A), five (Figure 5.14B), and three (Figure 5.14C) petrographic elements. It is obvious from Figure 5.14 that the prediction of permeability using ten petrographic elements gave the best result. The predictions made using five petrographic elements are also good (Figure 5.14B). The network was able to learn the relationship of petrographic elements in controlling the permeability. In addition to being able to predict the permeability, examining Figures 5.14B & 5.14C clearly shows the importance of the

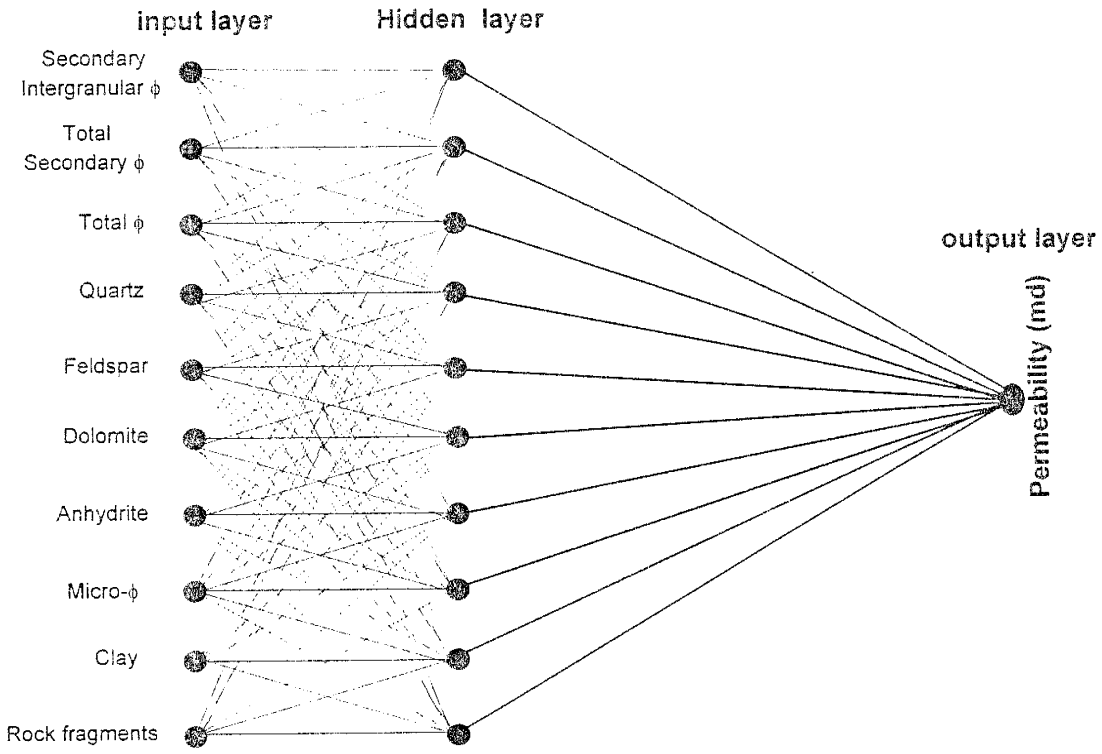

Figure 5.13: Neural network architecture used to predict permeability in the Sulimar Queen and South Lucky Lake fields. The size of the input layer was determined using the fuzzy logic approach. Top ten petrographic elements were used. The first layer was fully connected.

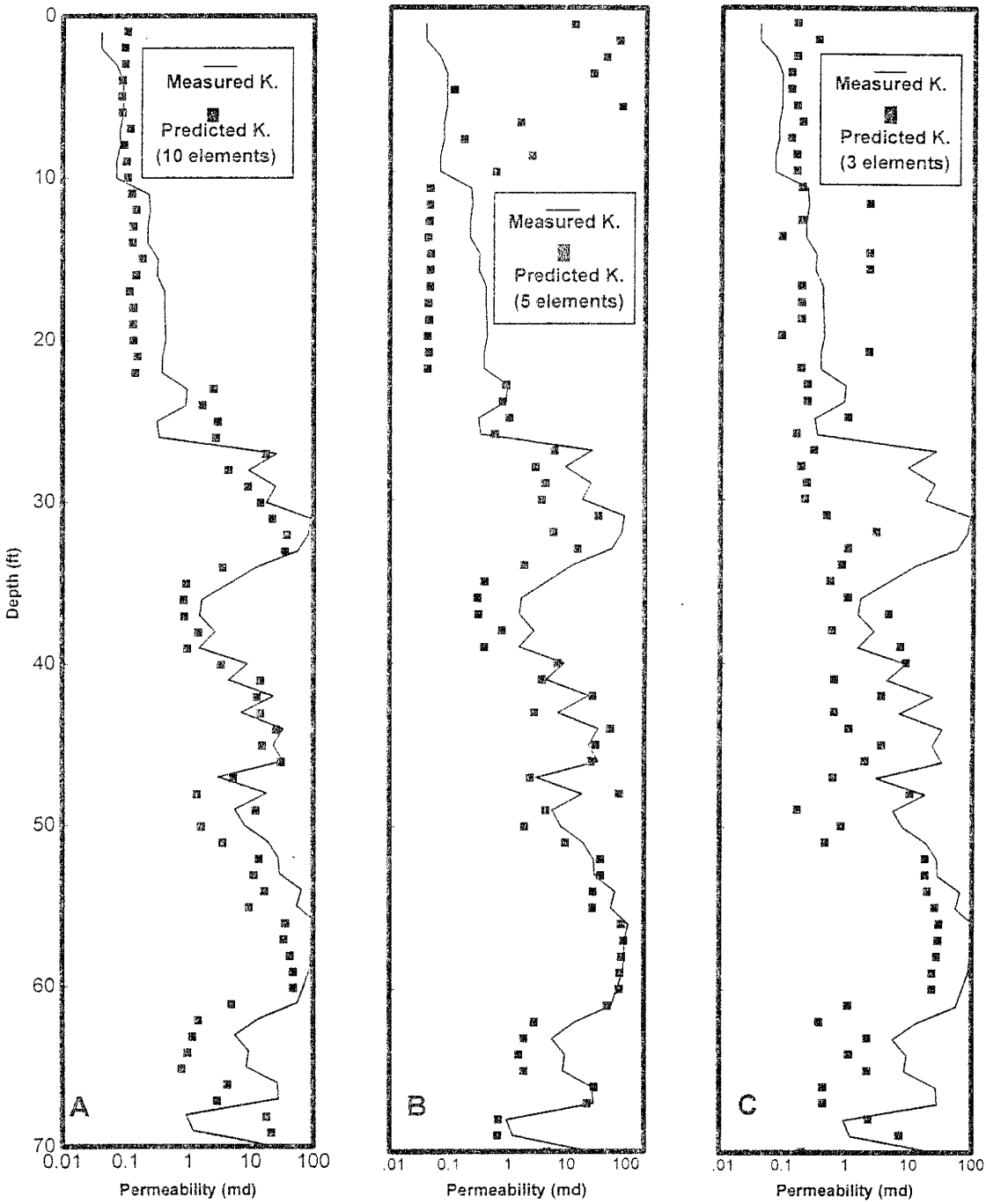

Figure 5.14: Comparison of the neural-network predicted permeabilities and the measured permeabilities; (A) using top ten petrographic elements, (B) using top five petrographic elements, and (C) using top three petrographic elements.

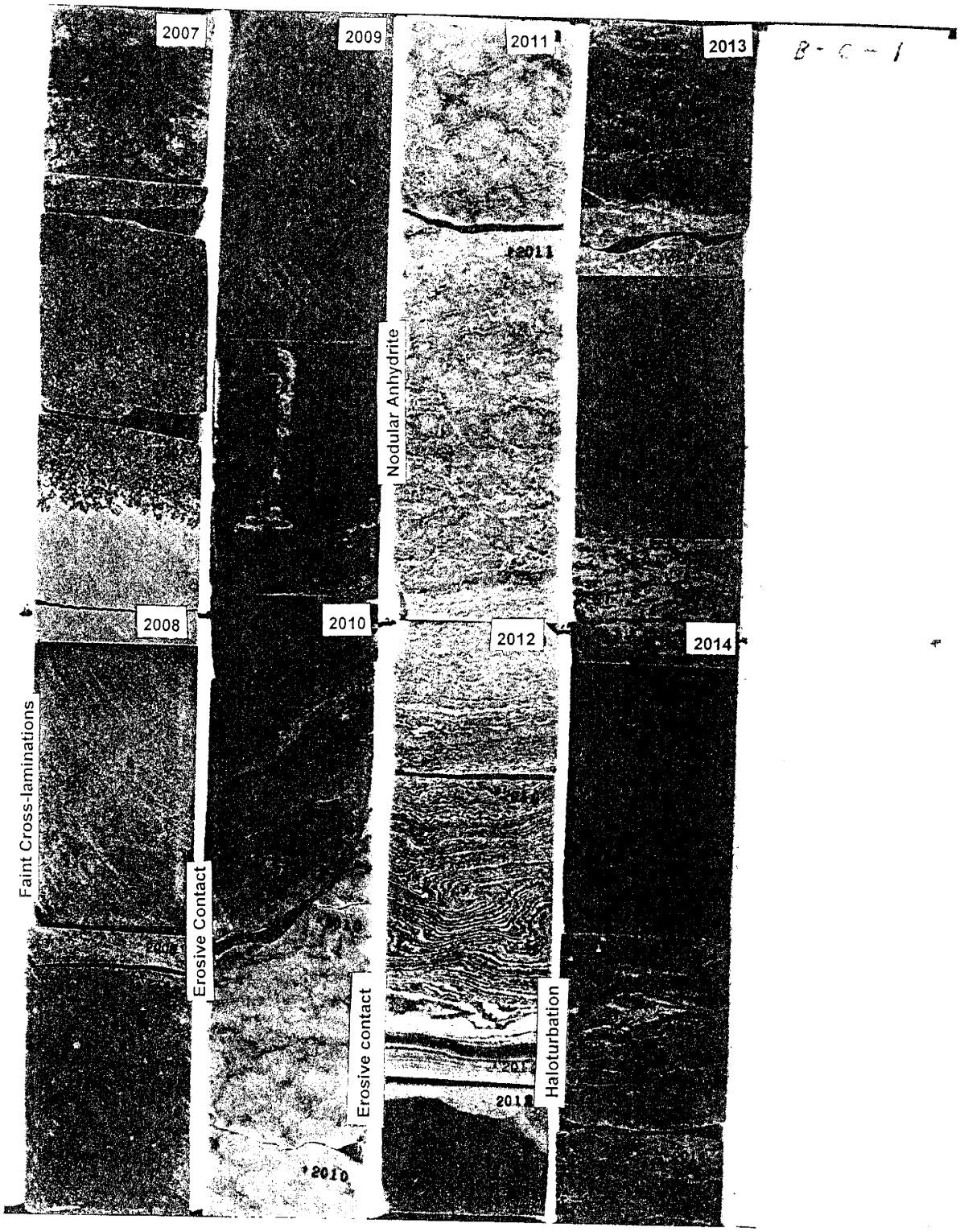

Figure 4.9: Gray and red sandstones of zone 2. These sandstones contain considerable amounts of nodular anhydrite (2007 - 2007.5 ft; 2013 - 2015 ft). Red sandstone show faint cross-stratifications (2007.5 - 20010 ft). Note the erosional contact between nodular anhydrite and red and green silty shale

undulose extinction. A few grains have fluid inclusions and contain probable mineral inclusions of rutile and tourmaline. Minor amounts of polycrystalline quartz (metamorphic) are also present.

Feldspar makes from 10 to 34 % of the framework grains. The majority of the feldspars are orthoclase. Minor amounts of plagioclase and microcline are also present. Most of the feldspars show alteration, mainly sericitization and vacuolization. Some skeletal feldspar grains are also present. It is possible that the feldspar grains either underwent direct dissolution, or were first replaced by anhydrite and this replacement material was later dissolved, leaving behind a skeletal appearance.

Rock fragments comprise about 3% of the detrital grains, and consist of metamorphic rock fragments, chert, carbonate rock fragments, and anhydrite cemented siltstones.

Authigenic minerals

(1) Anhydrite

Anhydrite is the most abundant cement and ranges from 0 to 35%. Anhydrite is present in two morphologies: (1) poikilotopic crystals surrounding many grains and locally replacing them (Figure 4.10A), and (2) fine-grained masses and nodules (Figure 4.10B). Poikilotopic anhydrite is the most dominant type.

The fine-grained anhydrite occurs as an interstitial pore fill and as small nodules. The individual crystals are rectangular and elongated. The detrital grains appears to be floating in the anhydrite nodule (Figure 4.10B). The close packing of grains around the nodules and the presence of detrital grains floating within the nodules indicates that the nodules were formed during very shallow burial (Figure 4.10B).

(2) Dolomite cement

Dolomite is the second most abundant authigenic mineral and occurs in two morphologies: (1) micritic (Figure 4.10C) and (2) large poikilotopic (Figures 4.10C &

Figure 4.10: Thin section photomicrographs showing the anhydrite and dolomite morphologies in the Shattuck Member.

A: Poikilotopic anhydrite surrounding many grains and replacing few grains (crossed polarizers)

B: Nodular anhydrite pushing the detrital grains around it. Probably formed during early diagenesis at the surface or shallow depth of burial (crossed polarizers)

C: Micritic and poikilotopic dolomite (crossed polarizers)

D: Poikilotopic dolomite replacing grains and probably anhydrite cement (crossed polarizers)

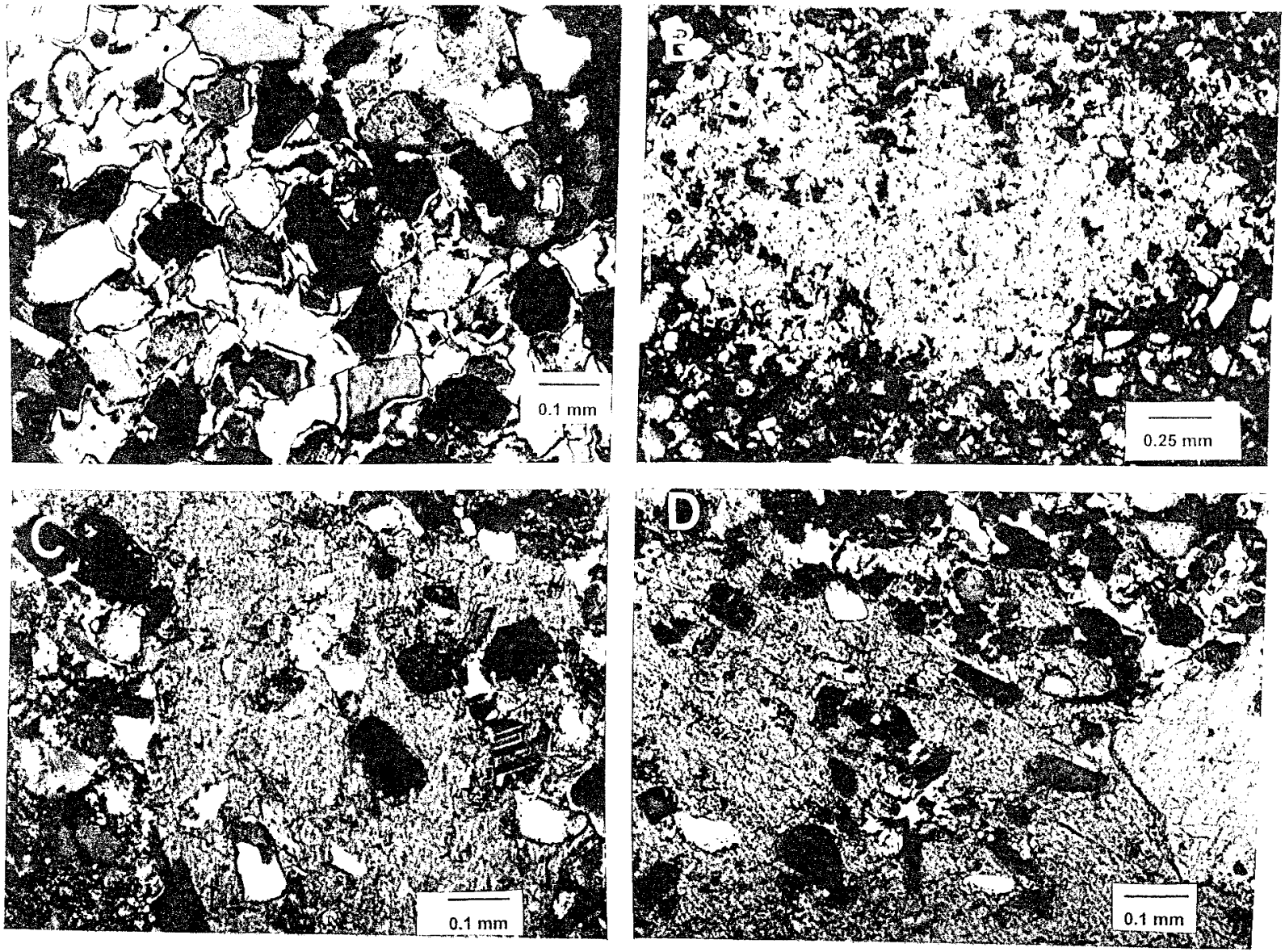
0.1 mm
0.25 mm
C
0.1 mm
D
0.1 mm

4.10D). Poikilotopic dolomite forms large patches surrounding several framework grains and contains inclusions of fine grained anhydrite cement (Figure 4.10D). The margins of grains are replaced by dolomite as visible in Figure 4.10C. The detrital grains appear floating within the poikilotopic patches, whereas around the patches the detrital grains show tangential/point contacts (Figures 4.10 C & 4.10D). This suggest that majority of the grains were replaced by dolomite during the growth of poikilotopic patches.

Micritic dolomite (2 μm) probably was calcitic or aragonitic lagoonal mud originally, which was dolomitized later. Its detrital origin is also supported by its presence only in the poorly sorted thin zones.

(3) Quartz and feldspar overgrowths

Quartz overgrowths are present in trace amounts which, in a few cases, completely surround the grains (Figure 4.11A). The presence of dust rims or hematite allows the identification of most of the overgrowths.

Minor amounts of feldspar overgrowths are also observed in the reservoir sandstone zone (Figure 4.11B).

(4) Hematite cement

Hematite is present in the uppermost (1984 - 1988 feet) and the lower part (2007 - 2010 feet) of the Shattuck Member. It occurs as thin rims surrounding the grains (Figure 4.11C) and staining early anhydrite cement. Since hematite coats grain and stains anhydritic cement, it is assumed that majority of the hematite was formed very early in the diagenetic history (Figure 4.11C). The presence of hematite between the grain-cement contact also suggest that hematite was formed before the precipitation of anhydritic cement (Figure 4.11C).

(5) Other cements

Chlorite rims are present in minor amounts (Figure 4.11D). The clay is light green and structureless in plane light. No chlorite fibers or plates growing perpendicular

Figure 4.11: Thin section photomicrographs showing some authigenic minerals in the Shattuck Member (Porosity in blue)

A: Quartz grain with overgrowth (O). Anhydrite replacing a probable feldspar grain with overgrowth (F) (crossed polarizers)

B: Partially dissolved feldspar grain (F) showing overgrowth (plane light)

C: Hematite coating around the detrital grains. Hematite also stains anhydrite cement (plane light)

D: SEM photomicrograph showing chlorite coating around grains. A probable authigenic feldspar (F), and other authigenic minerals are not coated by chlorite (C). Chlorite formed before overgrowths and precipitation of cement (500x)

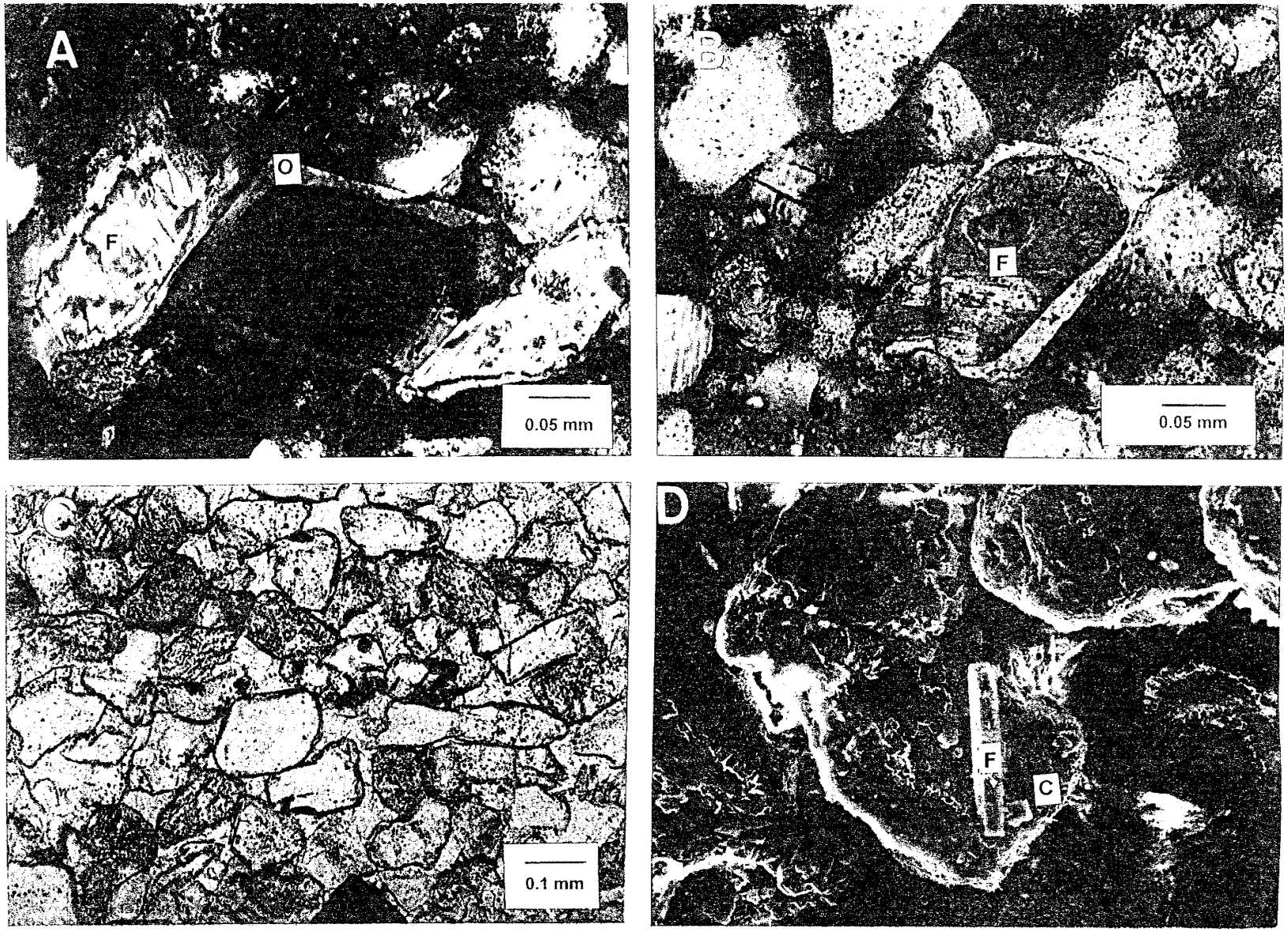
A
O
F
0.05 mm
B
F
0.05 mm
C
0.1 mm
D
F
C

Figure 4.11: Continued

E: A sericitized feldspar grain (F) (plane light)

F: Same view as (E) (Crossed polarizers)

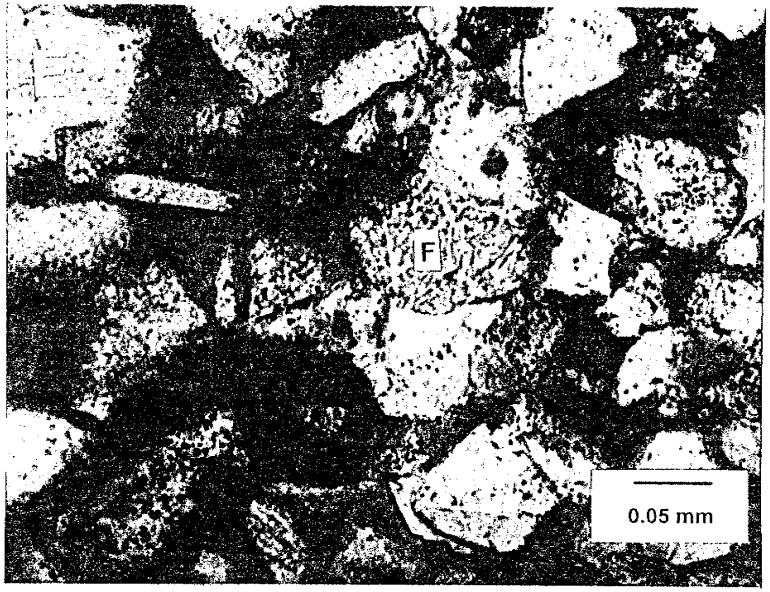
F
0.05 mm

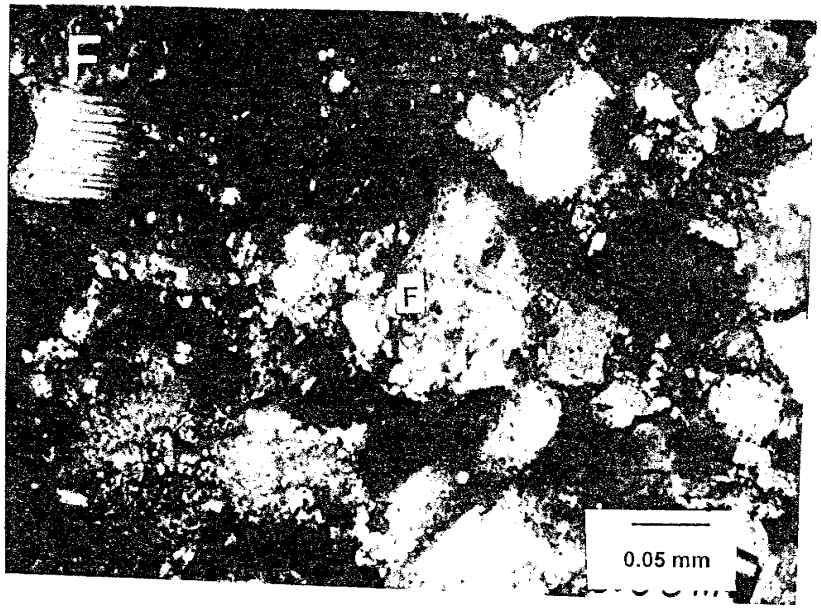
F
F
0.05 mm

to the detrital grains were identifiable in the thin sections but were visible under SEM (Figure 4.11D).

Pyrite occurs as isolated cubes and framboids in trace amounts. The presence of pyrite framboids indicate pyrite formation early in the diagenetic history in the sulphate-reducing zone (Gautier, 1985). The isolated cubes may be formed later as overgrowths on the pyrite framboids (Gautier, 1985).

Paragenetic sequence

The paragenetic sequence was determined using textural relationships. A generalized paragenetic sequence is shown in Figure 4.12. No one of the thin section contains all the diagenetic events because of the multiple depositional facies of the sandstone.

Early evaporite minerals (especially displacive nodular anhydrite) formed either at the sediment-water interface, or after shallow burial as indicated by the presence of displacive anhydrite (Figure 4.13A). Detrital grains were pushed apart, due to the displacive nature of the anhydrite, and appear floating in the anhydrite nodules (Figure 4.13A). Chlorite rims were formed around the detrital grains early in the diagenetic history, at least before quartz and feldspar overgrowths and poikilotopic anhydrite. This is suggested by the absence of chlorite rims around anhydrite crystals as well as feldspar overgrowth (Figure 4.13B). Hematite forms rims around detrital grains and stains clay matrix, early fine-grained anhydrite, and to some extent poikilotopic anhydrite. This indicates that hematite precipitation continued until cements were precipitated or it was redistributed during their growth (Figure 4.11C). Therefore, hematite developed at the surface or shallow burial depths and reddening continued until porosity was reduced by later cements, because it also stains the anhydrite cement (Figure 4.11C). Hematite also predates quartz overgrowth because of its presence between the quartz grain and the overgrowth (Figure 4.13C).

Feldspar grains are affected by sericitization and dissolution. Although alteration of feldspars has been considered to reflect climatic conditions at the time and/or site of

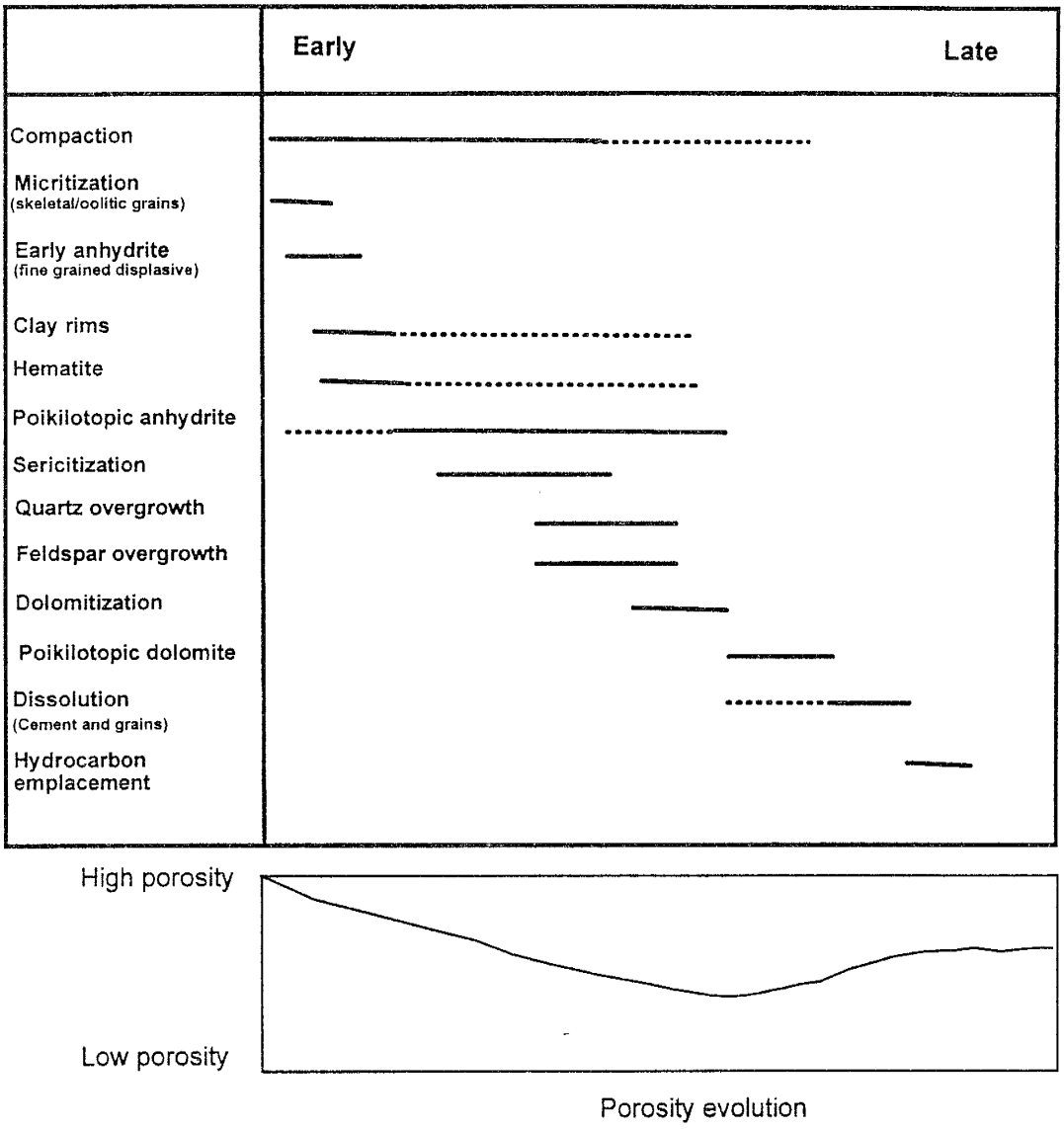

Figure 4.12: Generalized paragenetic sequence for the Shattuck Member in the Sulimar Queen and adjacent fields.

Figure 4.13: Thin section photomicrographs showing some of the paragenetic sequences in the Shattuck Member (Porosity in blue)

A: Early displasive anhydrite nodules (crossed polarizers)

B: SEM photomicrograph showing the relationships between chlorite (C), anhydrite (A), and feldspar overgrowth (F). Chlorite precipitated before overgrowth and anhydrite precipitation (2000x)

C: Hematitic stains between the quartz grain and the overgrowth (Arrow) (plane light)

D: SEM photomicrograph showing the relationship between overgrowths and chlorite (1000x)

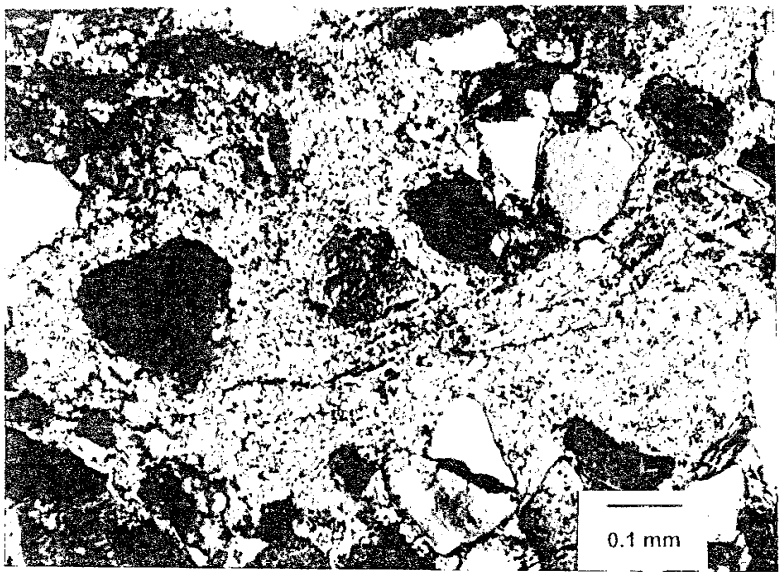
0.1 mm

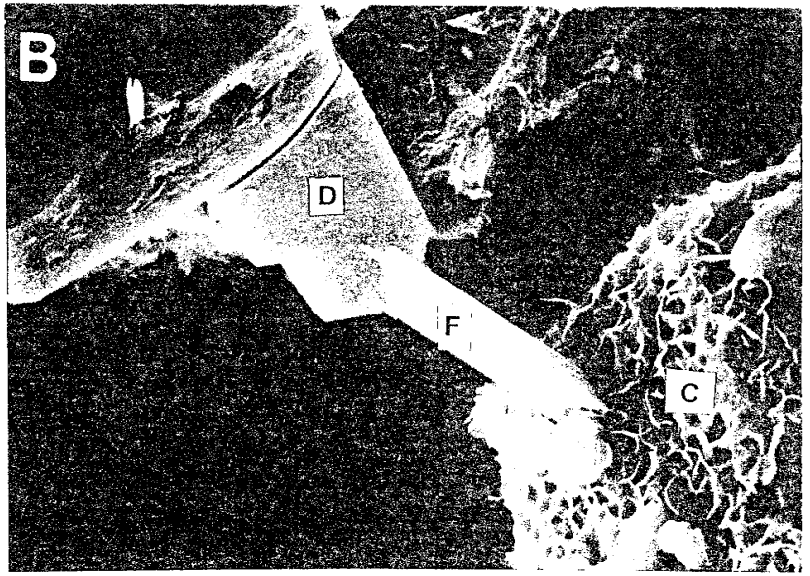
B
D
F
C

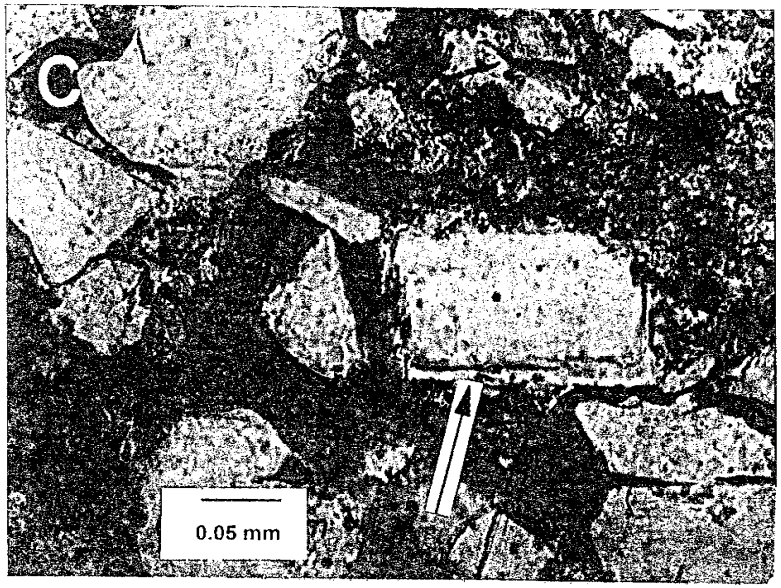
C
0.05 mm

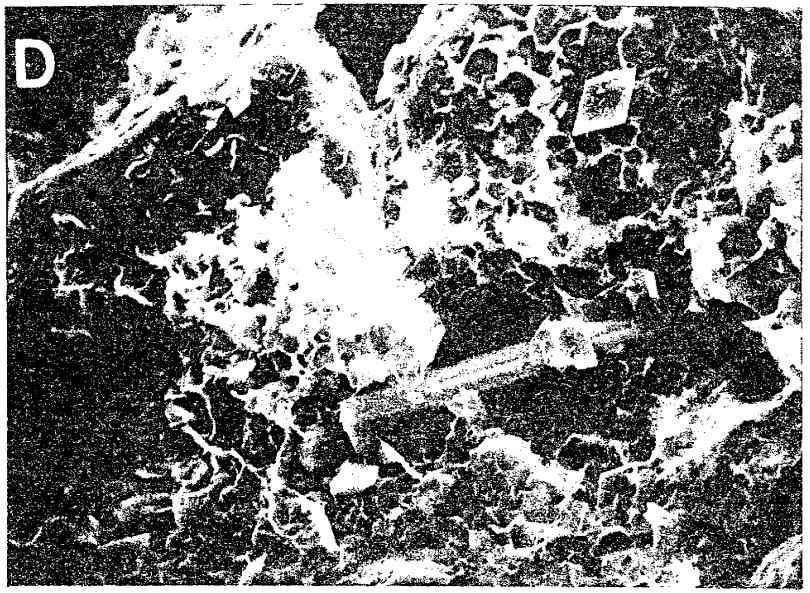
D

Figure 4.14: Thin section photomicrographs showing some of the diagenetic sequences in the Shattuck Member (Porosity in blue)

A: Poikilotopic dolomite containing floating grains and anhydrite cement. Dolomite formed after anhydrite (crossed polarizers)

B: Poikilotopic dolomite (crossed polarizers)

C: Dissolution of grains and cement (plane light)

D: Patchy distribution of cement formed by dissolution (plane light)

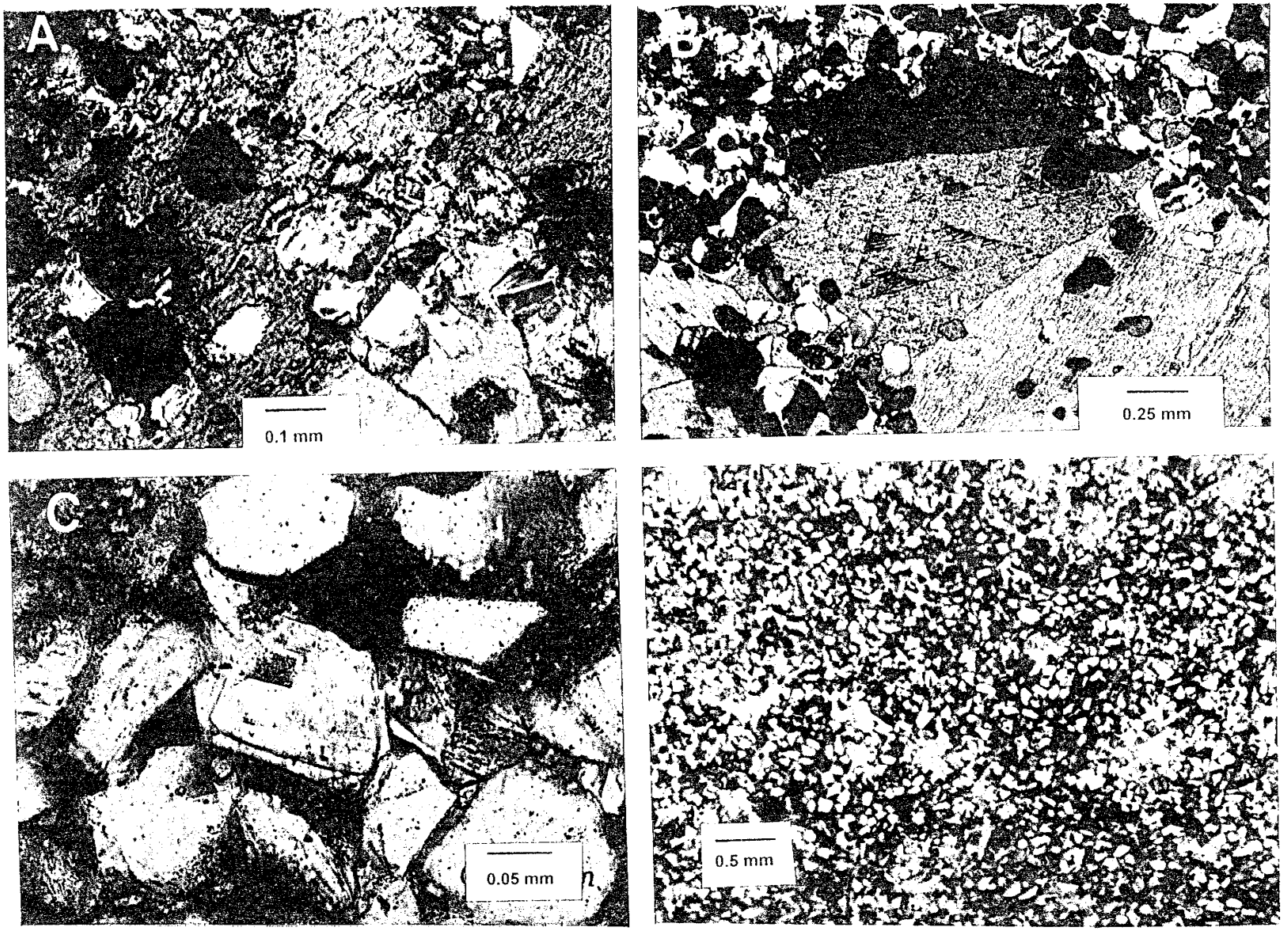
A
0.1 mm
B
0.25 mm
C
0.05 mm
0.5 mm

deposition of the feldspar grains, chemical alteration of feldspar grains can take place as easily and rapidly during diagenesis as during surface weathering (Blatt, 1982). In the Shattuck Member the sandstones that are well cemented by early poikilotopic anhydrite do not show considerable alteration of feldspar grains (Figure 4.11C), whereas the zones which escaped early cementation or were not extensively cemented have sericitized feldspars (Figures 4.11E & 4.11F). The sericitization was identified due to the high birefringence and speckled, micaceous texture (Figures 4.11E & 4.11F). Since no illite was found distributed within the pores, it is possible that the sericitization might have occurred during weathering.

Quartz and feldspar overgrowths were formed during or after the formation of clay rims, hematite, poikilotopic anhydrite, and sericitization. Dust rims of hematite are present between the grains and overgrowths, and thus hematite precedes the formation of overgrowths (Figure 4.13C). Chlorite rims were formed before the overgrowths and may have continued during the precipitation because they are not present on the overgrowths (Figures 4.13B & 4.13D). Some partially dissolved feldspar grains with undissolved overgrowths suggest that selective dissolution of detrital feldspars followed the precipitation of overgrowths (Figure 4.11B).

The precipitation of poikilotopic anhydrite may have taken place before and after the quartz and feldspar overgrowth precipitation. The absence of overgrowths in areas which are very well cemented by anhydrite indicates that poikilotopic anhydrite precipitated before the overgrowths (Figure 4.11C). Some feldspar grains have been selectively replaced anhydrite (Figure 4.11A). This selective replacement may have occurred after the precipitation of overgrowths. Dolomitization took place after the initiation of the anhydrite precipitation because it contains floating anhydrite crystals (Figures 4.10D & 4.14A).

It is difficult to pinpoint the occurrence of dissolution in the diagenetic history. The dissolution of feldspar grains with overgrowths suggest that dissolution took place at least after the precipitation of overgrowths (Figure 4.11B). Dissolution also created the patchy distribution of anhydritic and dolomitic cement (Figure 4.14D). The assumption

that dissolution created the patchy distribution is based on the fact that the grain packing is similar in the cemented and uncemented (areas where cement was dissolved) regions (Figure 4.14D). If the cement was precipitated originally in patches, then the uncemented regions would have close packing of the grains. Therefore, dissolution can be regarded as the late diagenetic event at least after the precipitation of quartz and feldspar overgrowths and anhydrite and dolomite cement. The oil stains both primary and secondary pores (Figure 4.11E) and the emplacement of hydrocarbons may be regarded as the last diagenetic event because there is no indication of any other diagenetic event occurring after the oil emplacement.

OUTCROP STUDY

Outcrop exposures of reservoir rocks provide laterally continuous sampling of rock characteristics, and provide lateral information on scales not available from reservoir data. Outcrop studies are cheap and valuable sources of good quality geological data. The constraints in utilizing outcrop data for the reservoir characterization are:

1. The availability and accessibility of outcrops analogous to the reservoir.
2. Differences in facies architecture, diagenetic imprints, tectonic structure etc., between outcrops and reservoir.

The limitations of applying information from analogous depositional systems to reservoir simulation models, result from the underlying assumptions that:
(1) the statistics of facies dimensions, (2) frequencies of facies occurrence, and (3) interconnectedness of particular facies within a particular depositional system are transferable from one deposit to another. In a particular case some properties can be transferred, but it is important to assess the degree of similarity and the applicability of data from outcrops.

Keeping the above limitations in mind, an outcrop study of the Shattuck Member was conducted. The overall objective of the outcrop study was to understand how the depositional processes controlled the distribution of the lithologic and permeability facies within the Shattuck Member.

Methodology

There are several Queen Formation outcrops present in Eddy County, southeast New Mexico (Figure 4.15). The Queen Formation exposures are not suited for detailed and continuous outcrop studies because it weathers into slopes that are covered with rubble (Figure 4.16). After reconnaissance of the outcrops present in Eddy County, certain outcrops were selected for study (Figure 4.15). Five sections were studied—four in the Rocky Arroyo area and one in the Bone Tank Draw area (Figure 4.15).

Initially, a TEMCO field minipermeameter was used to collect the permeability data. However, this minipermeameter had operational problems due to high ambient temperatures (> 100°F) and its use was discontinued. Instead, core samples were drilled from the outcrops and permeability measurements were made in the laboratory using an automatic scanning minipermeameter available at the Petroleum Recovery Research Center (New Mexico Tech). Approximately 600 core plugs and hand samples were collected. Core plugs were drilled more than 1.5 inches in length so that permeability data could be collected from rocks less affected by surficial weathering. For each section a detailed sketch was made showing lithofacies and their distribution.

The Rocky Arroyo area (T-21-S, R-24-E) is about 40 miles southwest of the Sulimar Queen field, and about 11 miles landward from the Goat Seep Reef. The Bone Tank Draw area is about 35 miles southwest of the Sulimar Queen field and about 16 miles landward from the Goat Seep Reef. The Sulimar Queen field is located 20 miles north of the Goat Seep Reef (Figure 1.3A). The Sulimar Queen field exhibits relatively different facies and depositional environments from the outcrops studied in the Rocky Arroyo area but is quite similar to the outcrops in the Bone Tank area. Because of the poor exposure, we were unable to collect data on a regular grid except for Section 1.

The objective of the outcrop study was to observe the interwell and field-scale heterogeneities and the small-scale data was available from the cores, Therefore, permeability data were collected on a coarse grid. Additionally, time limitations and insufficient personnel, as well as bad exposures, hampered the small-scale permeability study.

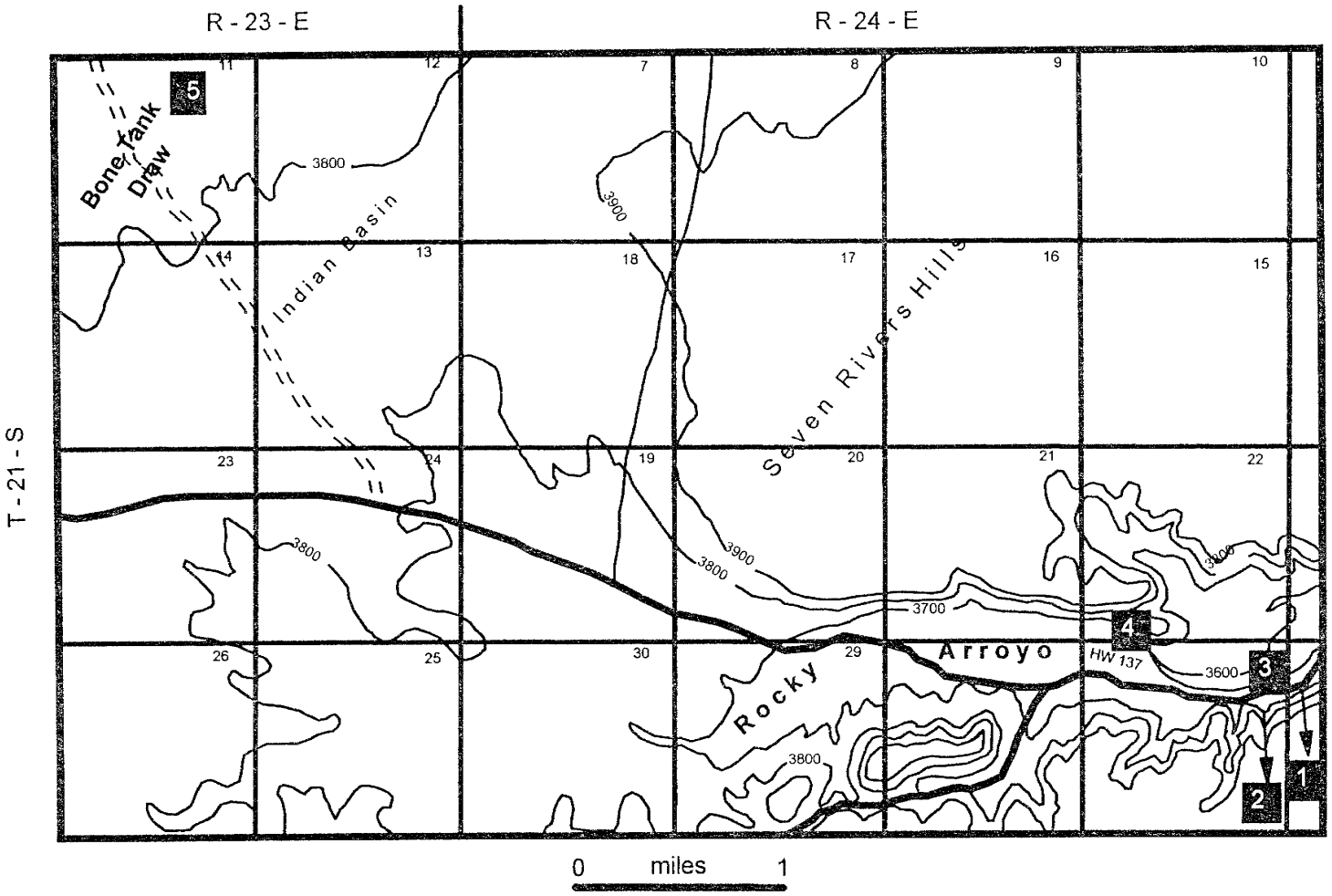

Figure 4.15: Locations of the Shattuck Member outcrops in Eddy County. Locations of the sections studied are shown (numbers in the boxes).

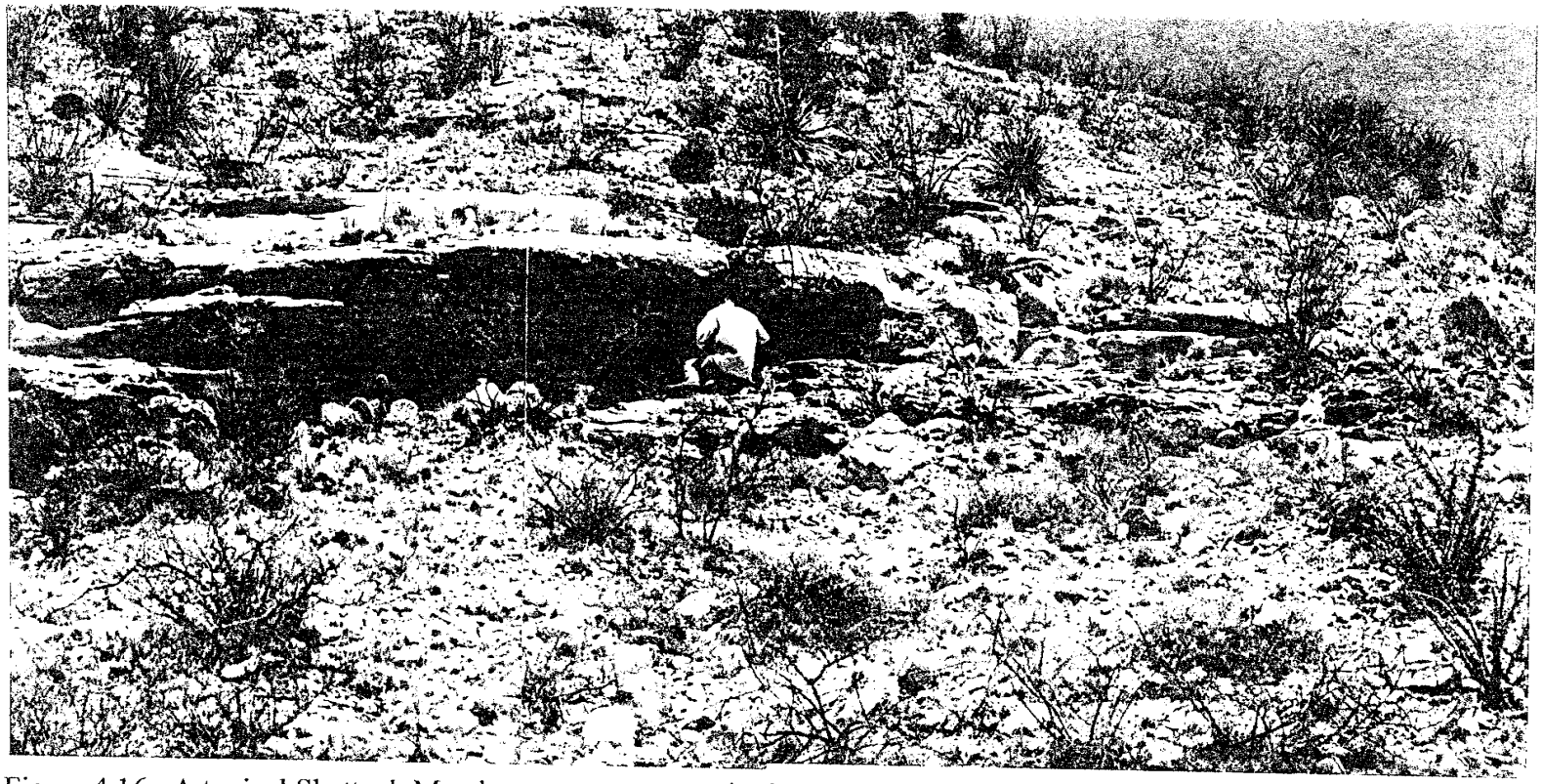

Figure 4.16: A typical Shattuck Member outcrop present in the Rocky Arroyo area. Most of the oucrops are covered with rubble.

Rocky Arroyo Area

Four sections (Sections 1, 2, 3, & 4) were studied in the Rocky Arroyo area (Figure 4.15). In the study area Rocky Arroyo runs east-west (Figure 4.15). Sections 1, 3, & 4 run east-west and are perpendicular to the Goat Seep reef complex. Section 2 runs north-south and is parallel to the Goat Seep reef complex.

Section 1

Section 1 runs east-west along the south wall of the Rocky Arroyo and has a lateral extent of 450 feet (Figure 4.17). This section is about 35 feet thick, much thicker than the Shattuck Member in the subsurface.

More than 220 core plugs were collected on a coarse regular grid (Figure 4.17). Samples were collected at a horizontal interval of 50 feet and vertical interval of 5 feet. Later, the area between 50 -100 feet, and 150 - 200 feet was sampled at a horizontal interval of 10 feet and vertical interval of 2 feet in order to capture heterogeneity on relatively smaller-scale (Figure 4.17).

Section 1 can be divided into 7 individual units (Figure 4.17). Statistics of individual units are given in Table 4.2. At the base of the section is a light yellow, gray, well cemented, moderately sorted, thickly bedded, fine to very fine-grained sandstone unit (Unit A; Figure 4.17). The individual beds are inclined and the fresh surfaces on these individual foresets show flaser bedding and thin discontinuous laminations of very fine silts and clays (Figure 4.18). Ripple bedding in which finer-grained (silt and mud) laminations drape over ripples or are confined to ripple troughs are called flaser bedding (Collins and Thompson, 1982). The presence of flaser bedding implies that both sand and mud were available during the deposition and that periods of current activity alternate with periods of quiescence (Reineck and Singh, 1975). During periods of current activity, the sand is transported and deposited as ripples, while the mud is held in suspension. As the current weakens, mud deposits in the troughs as well as on the crest of the ripple. At the start of the next cycle, ripple crests are eroded away and new sand is deposited in the form of ripples, burying and preserving ripple beds with mud flaser in the trough.

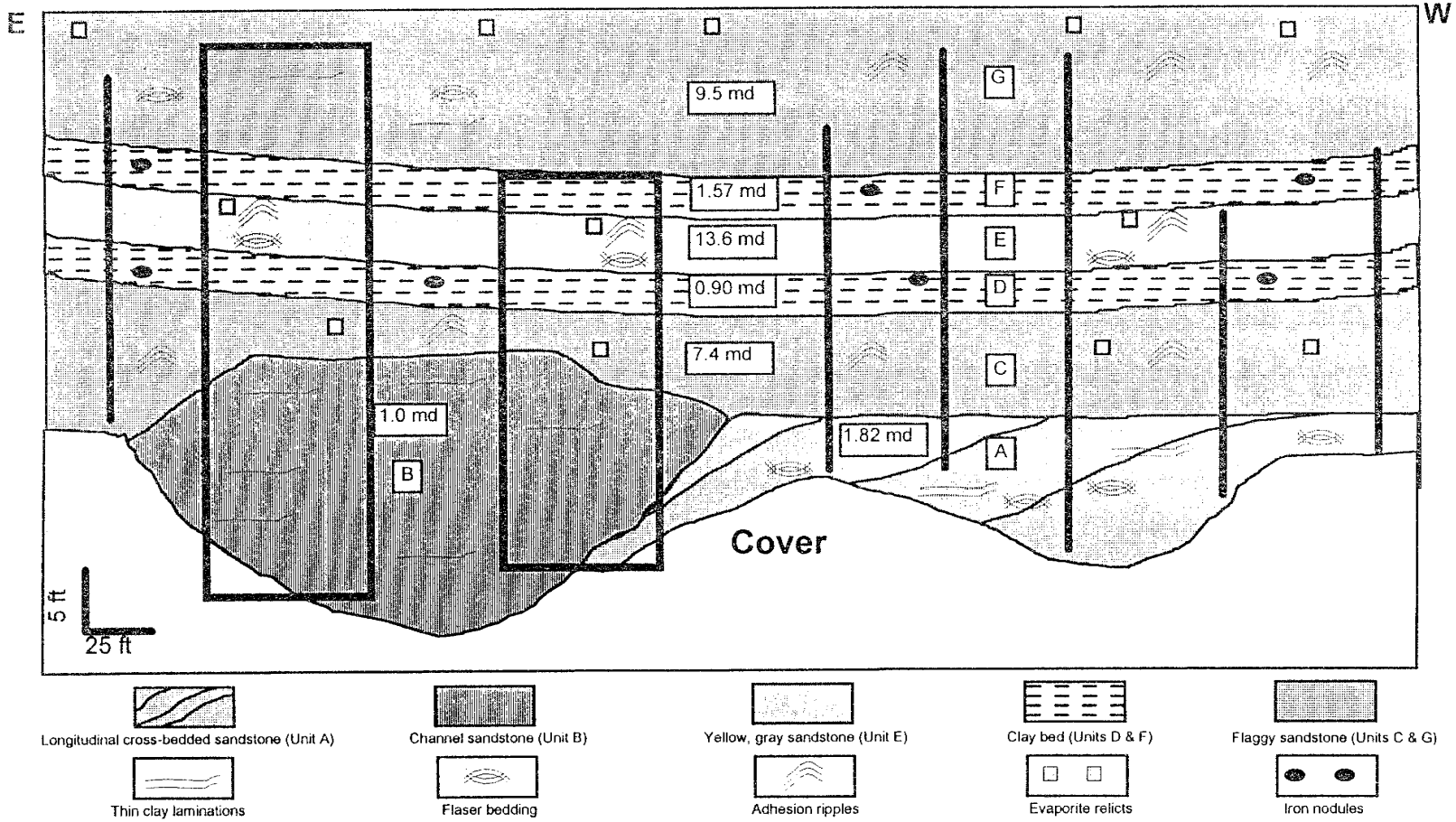

Figure 4.17: Section 1 of the Shattuck Member in the Rocky Arroyo area, showing the extent of individual units. Sampling transects are shown by vertical solid lines (horizontal interval is 50 ft, and vertical interval is 2 ft). Boxes show the areas at which samples were collected at a horizontal interval of 10 ft and vertical interval of 2 ft. The numbers are the average permeabilities of each unit in millidarcies.

Units	Section 1			Section 2			Section 3		
	N	Mean	STD (σ)	N	Mean	STD (σ)	N	Mean	STD (σ)
Unit A	37	1.82	1.20	10	3.75	1.20	-	-	-
Unit B	57	1.00	1.00	-	-	-	-	-	-
Unit C	36	7.40	8.40	10	11.80	4.80	10	14.40	3.70
Unit D	10	0.40	0.32	10	0.88	0.31	10	0.87	0.23
Unit E	33	13.60	19.60	13	11.70	24.90	10	10.40	3.70
Unit F	17	1.57	1.30	10	0.85	0.54	9	1.28	1.03
Unit G	37	9.50	9.70	16	16.00	7.47	4	78.20	23.20

Table 4.2: Summary of the permeability data from the Shattuck Member outcrops on the south wall of the Rocky Arroyo.

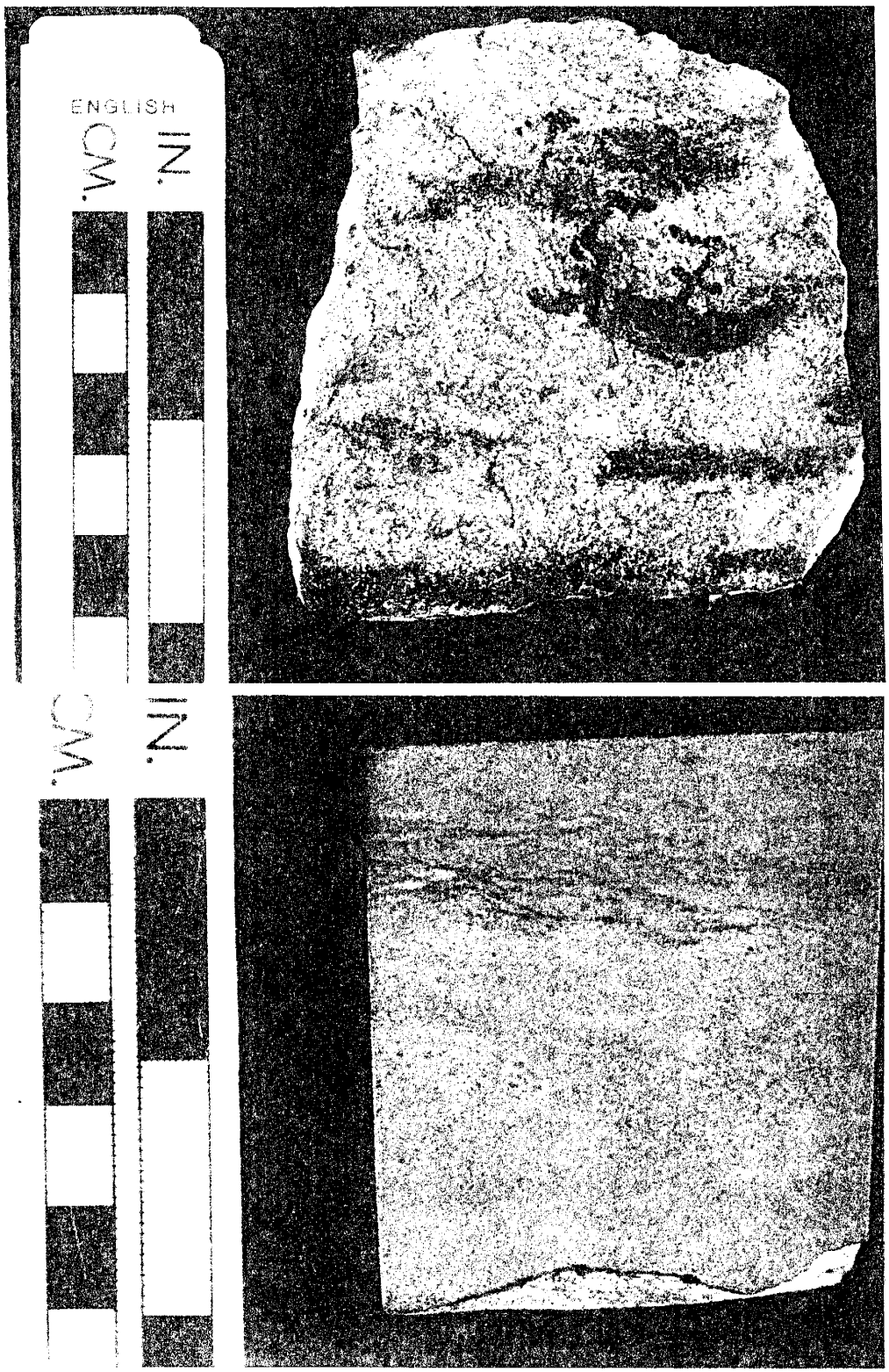

Figure 4.18: Hand samples from Unit A showing flaser bedding (A) and thin clay laminations (B).

Our interpretation of the depositional environment for this unit— inferred from its lateral contact to a channel-like sand body (Unit B), moderate sorting, and the presence of silt and clay laminations and flaser bedding— is in an intertidal environment, probably as longitudinal cross-beds associated with a tidal channel (Figure 4.17). Longitudinal cross-bedding is very common in intertidal flat environments (Reineck and Singh, 1975). The lateral shifting of tidal channels on tidal flats produce beds, which in contrast to other types of cross-beds, run parallel to the current direction, and is thus called longitudinal cross-bedding (Reineck and Singh, 1975). According to the Reineck and Singh (1975) each inclined layer in itself is a bed (Figure 4.17) and contains different types of bedding, e.g., thinly laminated sand/mud bedding, small ripple-bedding, lenticular and flaser bedding, and thick mud layers. Individual beds in Unit A contains thin silt and clay laminations and flaser bedding (Figure 4.18).

Unit A has very low permeability ranging between 1 - 4 md (average 2.1 md). The actual thickness of unit A could not be determined because its lower contact is not exposed.

Unit B is in lateral contact with Unit A and has a massive channel shape (Figures 4.17 & 4.19). It is grayish-yellow with gray and yellow laminations visible on fresh surfaces (Figure 4.20), moderately sorted, well cemented, fine to very fine-grained sandstone. Based on the shape of this unit, we assume its deposition in a channel (probably, a tidal channel). Although fining upward sequence of a channel-fill is absent, the grain size distribution and sequence primarily depends on the available material. Unit B is classified as a tidal channel based on its channel-like shape and its lateral association with the longitudinal cross-bedded Unit A. Unit B has low permeability ranging between 0.01 - 5.5 md (average 1.0 md).

Overlying Units A and B is a 4 foot thick, yellow, gray, moderately cemented, fine grained flaggy sandstone (Unit C) (Figure 4.17). This unit contains evaporite relicts and exhibits adhesion ripples (Figure 4.21). Adhesion ripples are formed when dry sand is blown across a wet sediment surface and sticks to the surface on impact. Capillary rise of moisture helps to further trap grains by constantly wetting the new surface and eventually

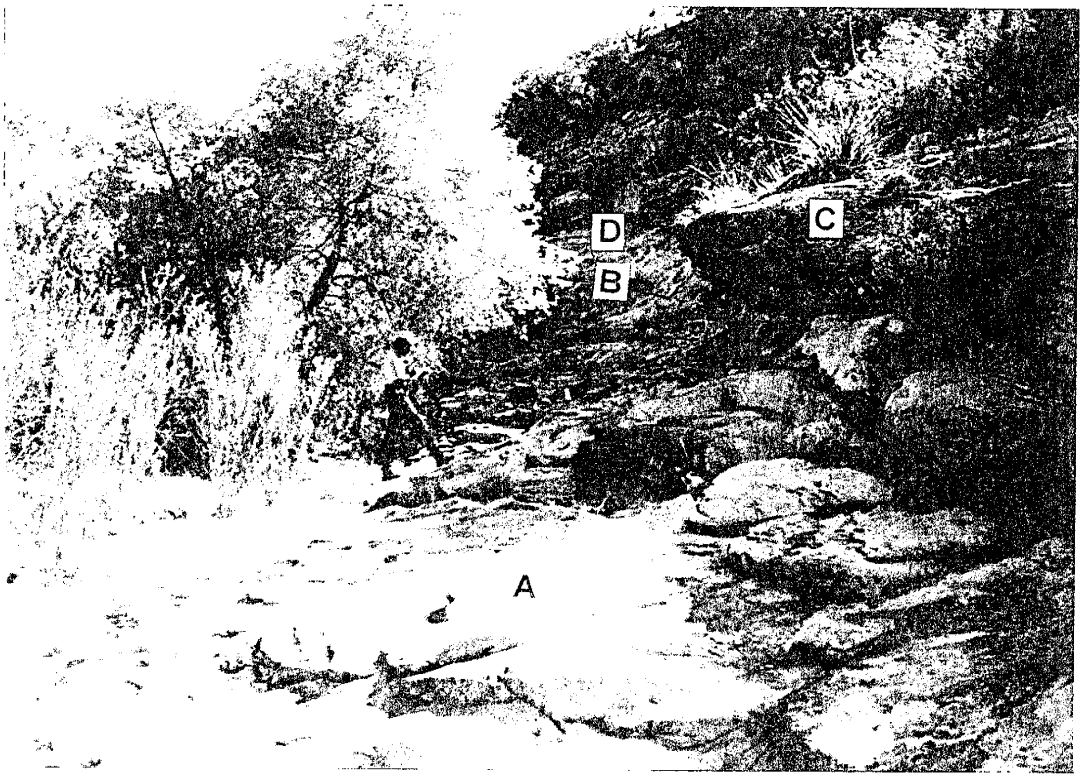

Figure 19: Photograph showing the relationship between Units A, B, C, and D in Section 1 in the Rocky Arroyo area.

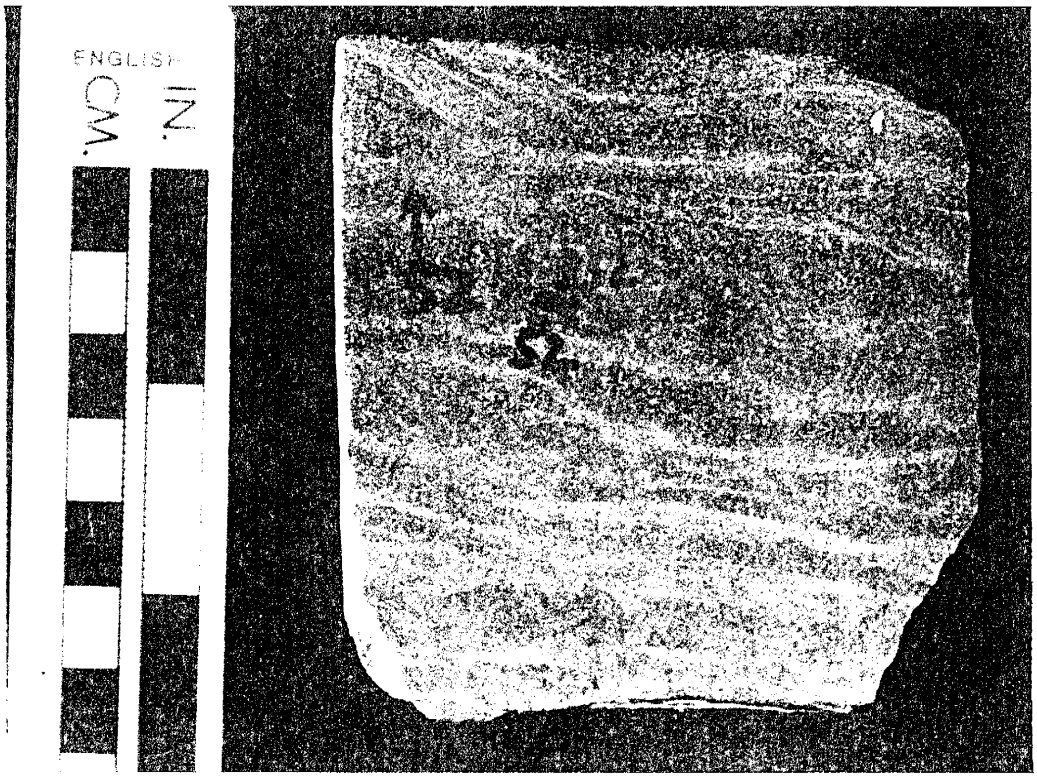

Figure 4.20: Hand sample from Unit B showing gray and yellow laminations.

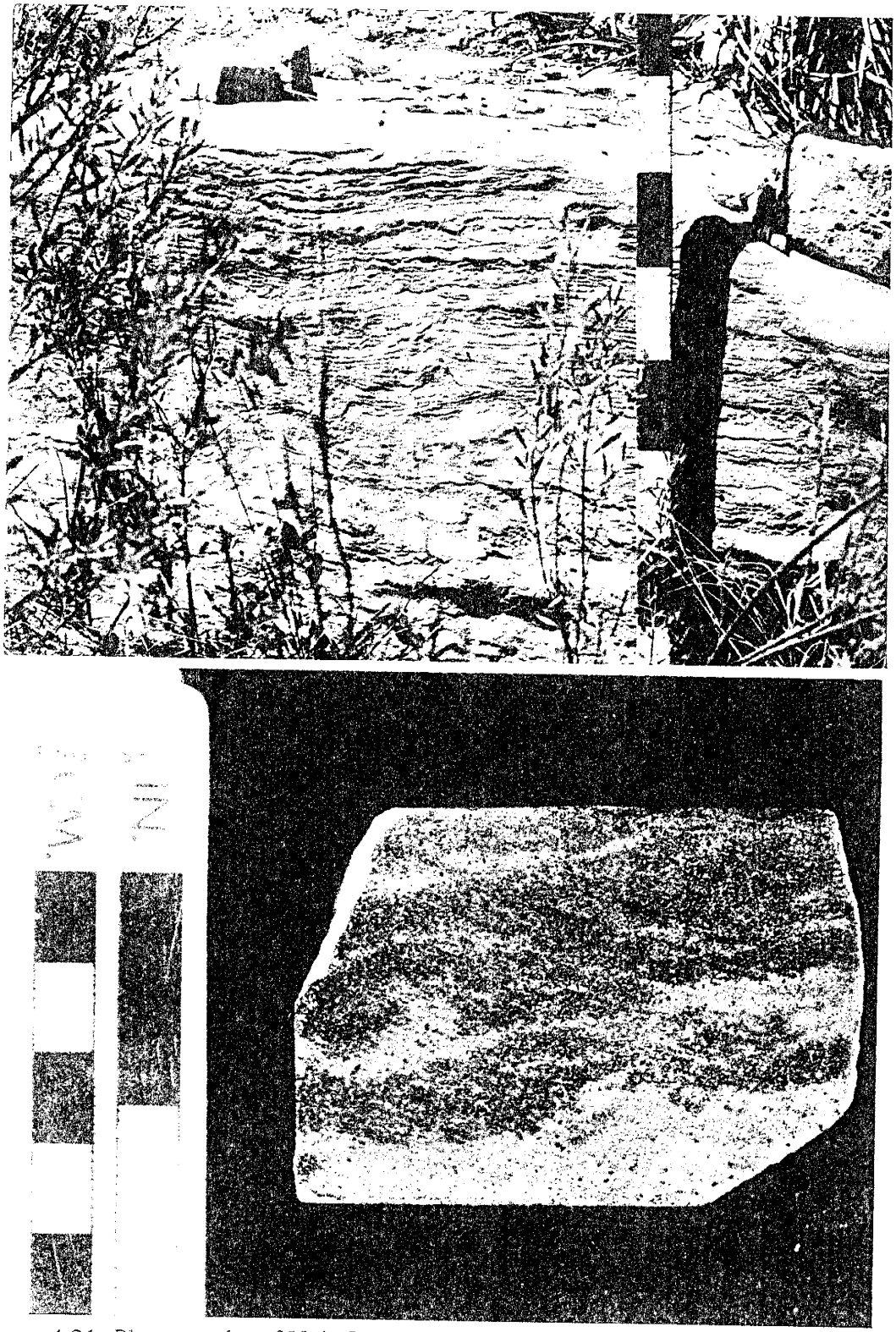

Figure 4.21: Photographs of Unit C outcrop showing adhesion ripples (A) and a hand sample showing irregular bedding surfaces formed due to adhesion ripples (B).

an irregular, blistered, but sometimes ripple-like surface develops (Collins and Thompson, 1982). According to Glennie (1970), adhesion ripples are extremely important in the deposition of inland sabkha. Because of the presence of adhesion ripples and evaporite relicts, Unit C may be assigned an eolian or sabkha environment of deposition. It shows moderate permeability ranging between 1 - 36 md (average 7.4 md) and is continuous over the entire length of the section.

A 2 foot thick bed of clay (Unit D) is present above Unit C (Figure 4.17). It is thinly to moderately bedded, moderately cemented, and contains numerous small pure iron concretions. It probably represents deposition in calm water conditions (probably a lagoon) as finely disseminated iron is commonly deposited in deltaic, lagoonal, and estuarine environments (Tucker, 1981). Based on the prevailing geologic setting during the deposition of Queen Formation (Guadalupian), we suggest the deposition of Unit D in a lagoonal/salina environment. Unit D exhibits the lowest permeability ranging between 0.2 - 1.16 md (average 0.7 md).

Unit E is 4 foot thick and consists of yellow, moderately to thinly bedded (flaggy), moderately to poorly cemented, fine-grained sandstone. The fresh surfaces show yellow and gray laminations. The lower part of this unit shows flaser bedding, while the upper part exhibits adhesion ripples and abundant evaporite relicts (Figure 4.22). Unit E probably represents a upward transition from lagoonal/salina to sabkha/eolian environments. The lower part which exhibits flaser bedding was probably deposited in aqueous environment. Flaser bedding may have formed due to waves generated by the storms in a lagoon/salina. The upper part which exhibits adhesion ripples and abundant evaporite relicts was deposited in a sabkha/eolian environment. The lower part of Unit E has low permeabilities (1- 5 md), whereas, the upper part has high permeabilities (4 - 176 md). Overlying Unit E is 2 foot thick Unit F, which is similar to Unit D (Figure 4.17).

The rest of Section 1 consists of a 10 foot thick, yellow and gray, moderately to poorly cemented, with abundant evaporite relicts, very fine to fine-grained sandstone bed (Unit F; Figure 4.17). The eastern part of this unit shows flaser bedding as well as thin

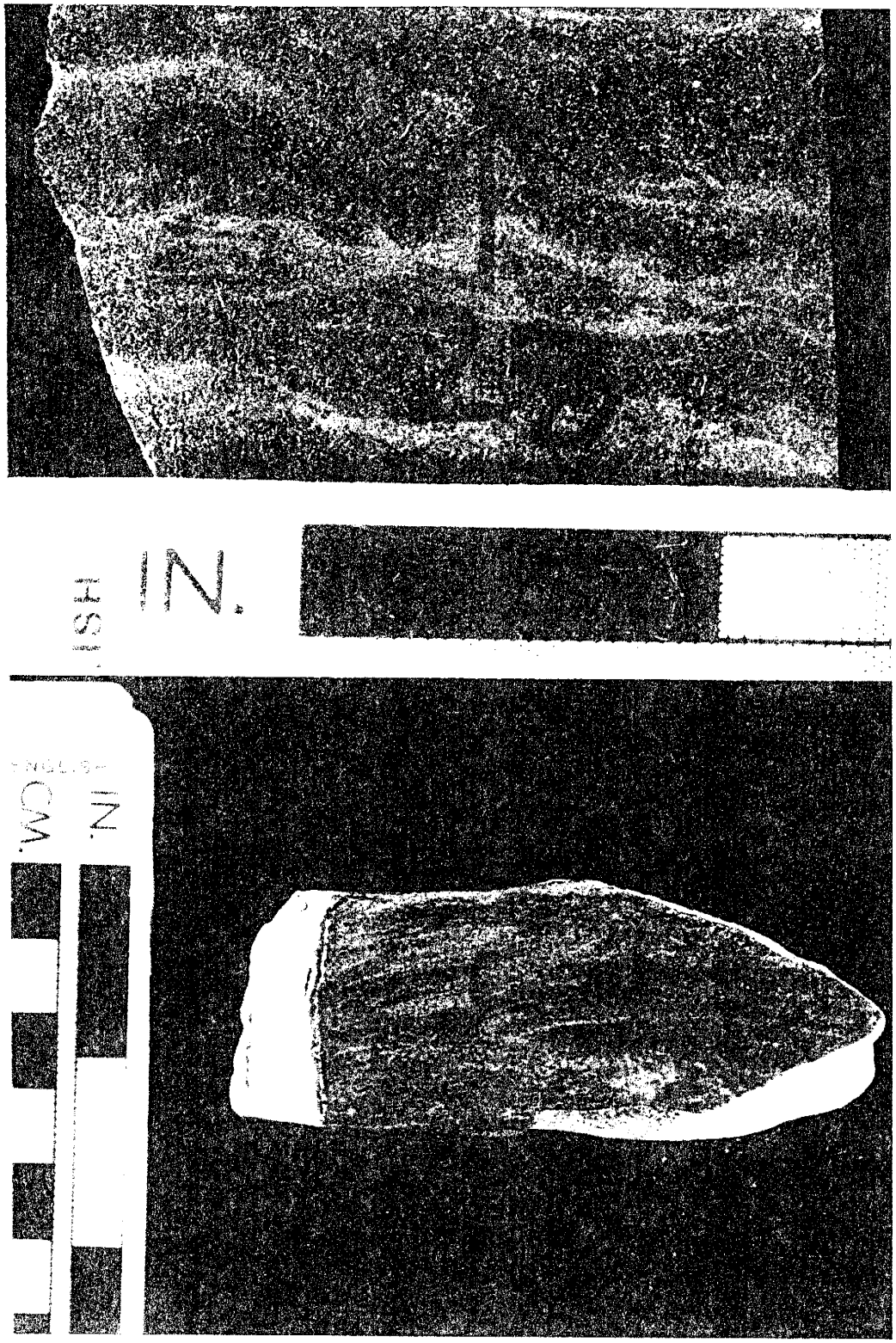

Figure 4.22: Hand samples from Unit E showing flaser bedding (A) and adhesion ripples (B).

clay laminations (lagoon/salina) and the western part exhibits adhesion ripples and evaporite relicts (sabkha/eolian). Therefore, this unit was probably deposited in a laterally merging aqueous (eastern part) and sabkha/eolian environment (western part). Permeability ranges between 1 - 95 md (average 9.5 md).

Section 2

In order to acquire a three-dimensional distribution of individual units Section 2 was measured in a north-south direction perpendicular to the eastern end of Section 1. Section 2 is located about 1,500 feet southwest of Section 1 (Figure 4.15). It has a lateral extent of 300 feet. Individual units exhibit sheet-like geometry as opposed to varying thicknesses observed in the east-west direction in Section 1. This suggests that in the Rocky Arroyo area most of the depositional changes occurred perpendicular to the Goat Seep reef complex. The contact between the overlying Seven Rivers Formation, including the transition zone is also clearly visible. Section 2 exhibits units similar to Section 1, with the exception of Unit B (Figure 4.23). Unit B is absent in Section 2. The lithology and the average permeability distributions are the same as Section 1 (Table 4.2; Figures 4.17 & 4.23). About 70 permeability measurements were made.

Section 3

Section 3 runs east-west along the south wall of Rocky Arroyo, and has a lateral extent of 800 feet. Section 3 is located 2,500 feet west of Section 1 (Figure 4.15). At this location, 30 - 35 feet of Shattuck Member is exposed (Figure 4.24). In Section 3, Units A and B are not exposed. Section 3 consists of Units C, D, E, F, and G. More than 30 permeability measurements were made on an irregular grid. This section is more permeable than Sections 1 and 2 (Table 4.2; Figure 4.24). The grain size distribution as well as sedimentary structures are similar to Section 1.

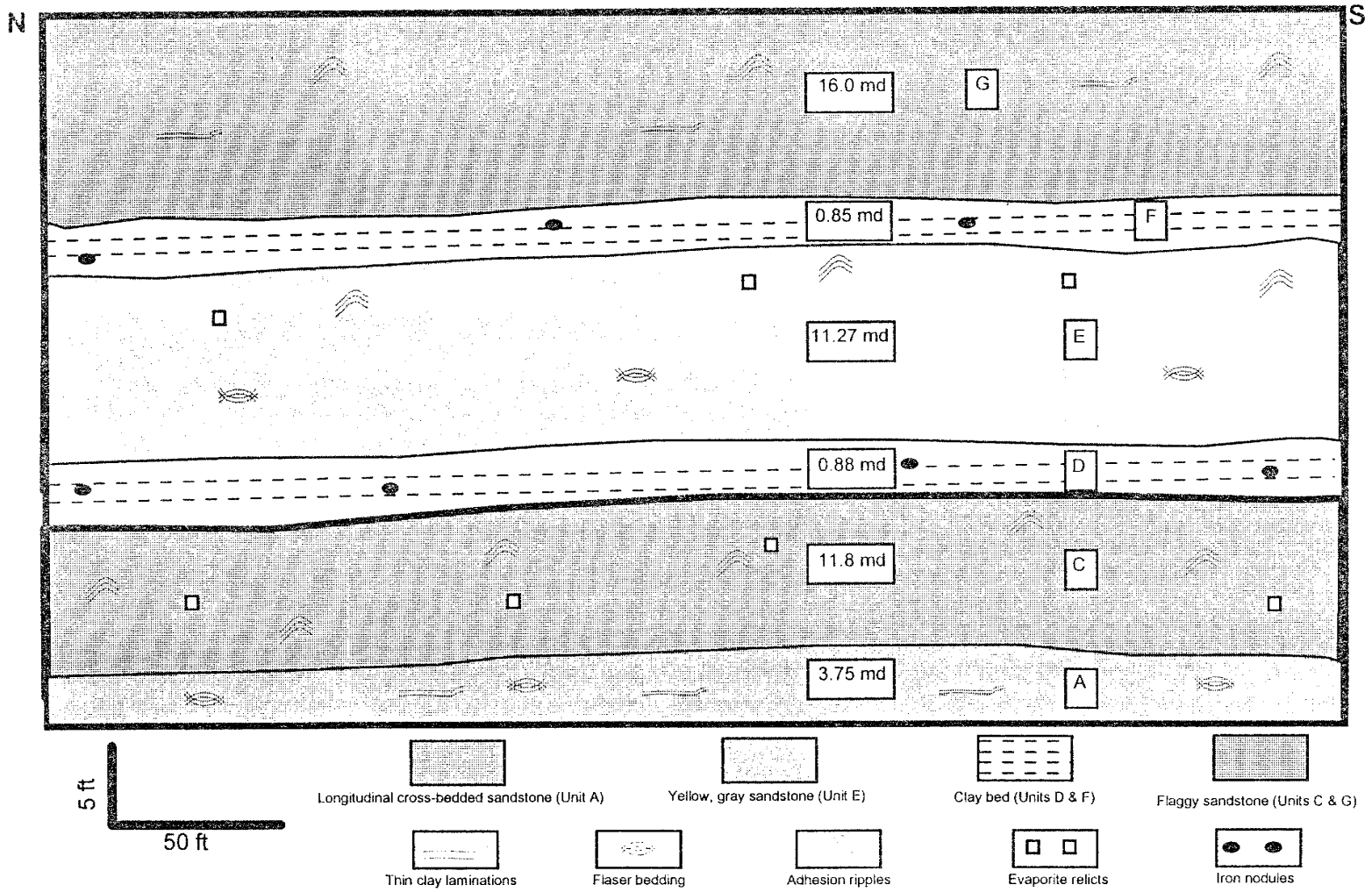

Figure 4.23: Section 2 runs north-south perpendicular to Sections 1. Unit B (channel sand) is missing in this section. Permeabilities are similar to Section 1.

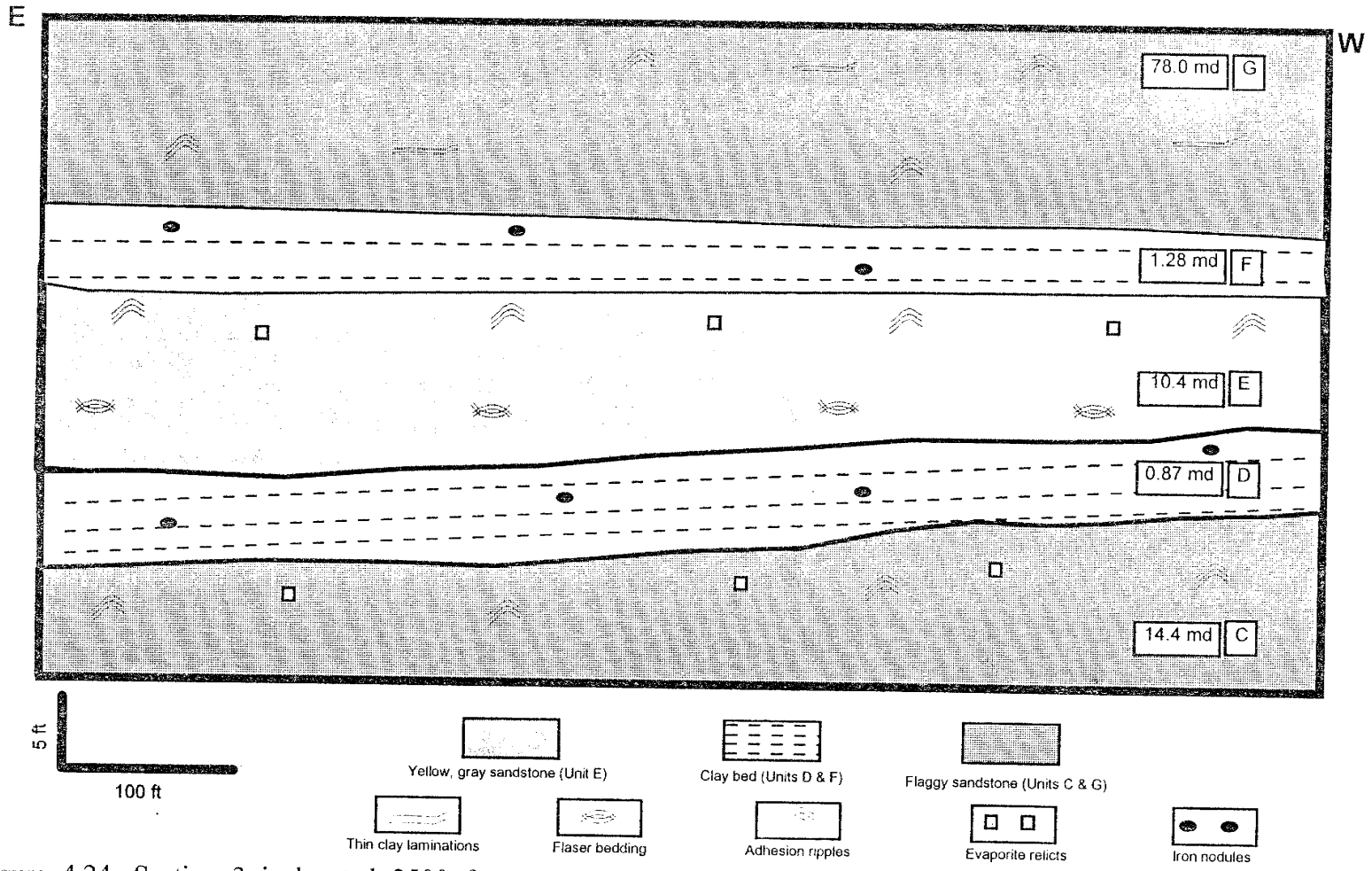

Figure 4.24: Section 3 is located 2500 feet west of Section 1. In this section Units A and B arenot exposed. Permeabilities are also higher than the Sections 1 & 2.

Section 4

Section 4 runs east-west, has a lateral extent of 1,500 feet, and was measured along the north wall of Rocky Arroyo. This section lies 3,000 feet northwest of Section 3 (Figure 4.15). Unlike Sections 1 and 3, individual units exhibit typical sheet-like geometry (Figure 4.25). Here the Shattuck Member is exposed in its entirety, underlain by the Queen dolomite and overlain by the Seven Rivers Formation. Section 4 is 55 feet thick and consists of very fine to fine and silty sandstone interbedded with thin beds of clayey siltstone. This section can be divided into two units—Unit 1 and Unit 2 (Figure 4.25)—and cannot be correlated with individual units of Sections 1 through 3.

The upper 17 feet (Unit 1) are yellow to yellowish orange, thinly bedded, moderately cemented, fine-grained, silty sandstone (Figure 4.25). Permeability ranges between 10 md and 86 md (average 39.0 md). Unit 2 is a 35 foot thick sequence consisting of 4 thick sandstone beds (average thickness 8 feet) interbedded with two 2-foot thick clayey siltstones (Figure 4.25). The sandstones are yellow and pink, moderately cemented, fine-grained to silty sandstones. These sandstones are moderately to thinly bedded and exhibits cross and wavy laminations. There are no differences in the permeabilities between the sandstones and silty sandstones. Due to the poor quality of clayey siltstones samples, no permeability measurements were made on them. Again, due to bad exposure of this section, permeability measurements were not made on regular grids. About 100 permeability measurements were made. Permeability ranges between 7 md and 95 md (average 34 md; Table 4.3). Towards the west the whole section changes from silty sandstone to dominantly evaporitic within a distance of one mile.

Depositional environment of the Shattuck outcrops in the Rocky Arroyo area

The depositional environments of Shattuck Member outcrops in the Rocky Arroyo and adjacent areas are a matter of debate. We suggest, based on this preliminary study, that the Shattuck Member was deposited in combined lagoonal/salina and sabkha/eolian environments. The reason for contradicting a dominantly eolian environment of deposition, as proposed by Mazzullo *et al.*, (1984, 1985), lies in the absence of typical

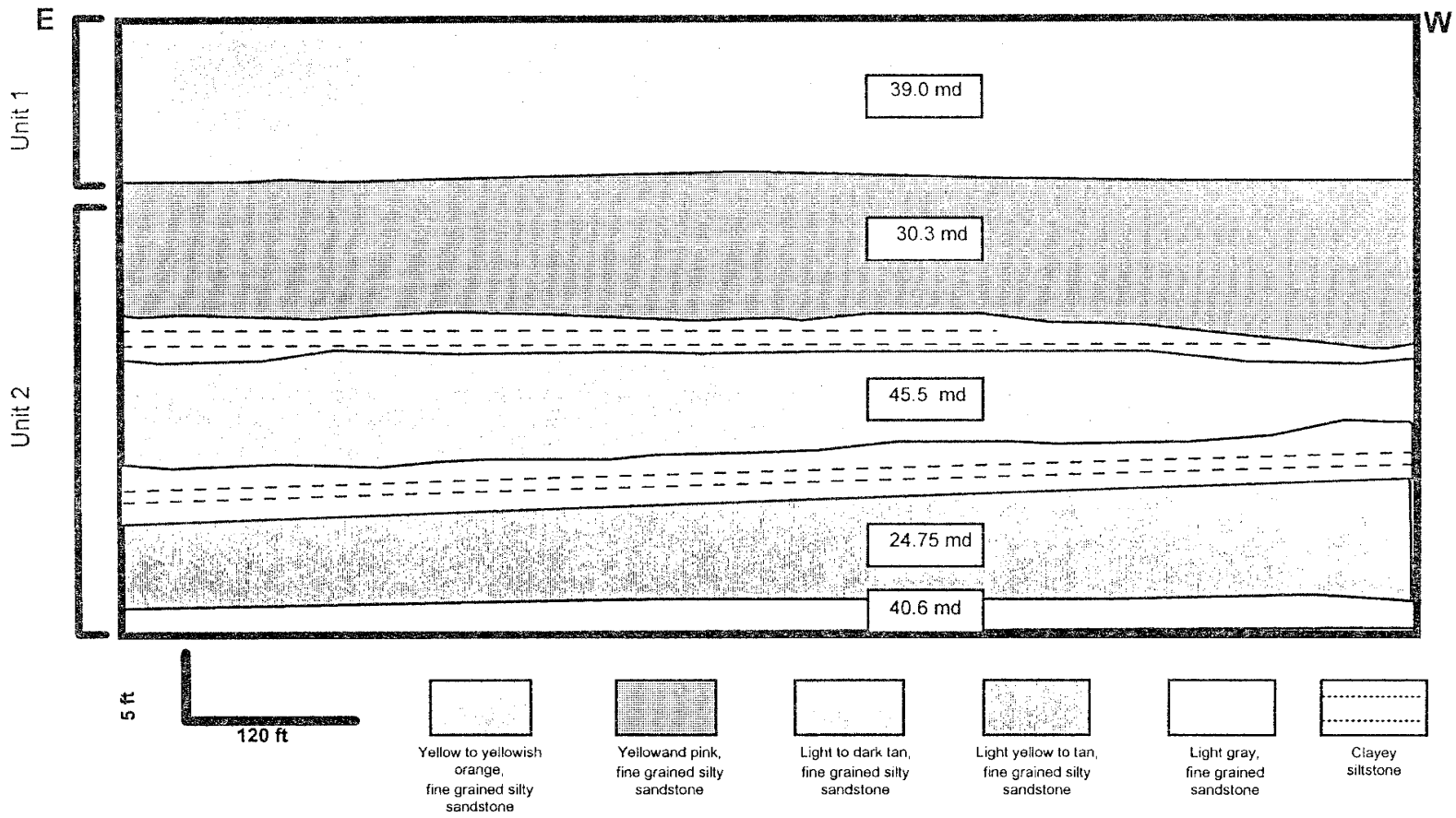

Figure 4.25: Section 4 is located about 3,000 feet northwest of Section 2. Unlike Sections 1 and 2, in this section individual individual units exhibits sheet-like geometry. Permeabilities are considerably higher than Sections 1, 2, & 3. Unit 1 is yellowish orange, thinly bedded, moderately cemented, fine grained sandstone. Unit 2 consists of 4 sandstone beds interbedded with 2 siltstone beds. Sandstones are yellow, tan, pink, moderately to thinly bedded, fine grained to silty sandstone.

Section 4			
Units	N	Mean	STD (σ)
Unit 1	25	39.00	19.60
Unit 2	16	30.30	10.90
	11	45.50	24.70
	20	24.70	12.90
	25	40.60	10.40

Table 4.3: Summary of permeability data from the Shattuck Member outcrop on the north wall of Rocky Arroyo.

eolian features, which Mazzullo also acknowledges (Mazzullo, 1985). The presence of flaser laminations, minor cross- and wavy-laminations, poor to moderate sorting, detrital clay matrix as well as clay layers, and bioturbation points towards deposition in an aqueous (lagoon/salina) environments. Mazzullo *et al.*, (1985) suggested the reworking of the eolian sands by marine currents and waves. In some units the presence of adhesion ripples and evaporite relicts does suggest sabkha/eolian deposition. Therefore, the Shattuck Member in the outcrops is probably not the product of a single depositional environment, but a combination of lagoonal/salina and sabkha/eolian processes.

Bone Tank Draw

Section 5

Section 5 is exposed in the Bone Tank Draw area (Figure 4.15). This section of the Shattuck Member is located about 16 miles landward of the reef, similar to the Sulimar Queen field, which is 20 miles landward of the Goat Seep Reef. The Shattuck Member at Section 5 exhibits similar lithologic characteristics to the Shattuck Member in the subsurface. This section consists of 11 - 15 foot thick sandstone sequence overlain and underlain by gypsum (Figure 4.26).

Section 5 consists of three small subsections separated by a horizontal interval of 200 feet (Figure 4.26). The individual subsections runs east-west and are subparallel to each other (Figure 4.26).

The base of Section 5 consists of a 10 foot thick sequence of thick-bedded red and grayish-green gypsum (Unit X) with minor siltstone intercalations. Overlying is a 6 foot thick bed of dark-gray to brown color, cross-bedded (with horizontal bounding surfaces), moderately cemented, very fine-grained gypsiferous sandstone (Unit Y). The formation of this bed may be attributed to a very shallow watertable or a wet surface over which dunes were migrating. According to Stokes (1968), the areas where groundwater is not too deep, e.g., in sand dunes migrating over an inland sabkha, water rises in the sand dunes and the cohesive action of water holds wet sand grains together, and the dry sand

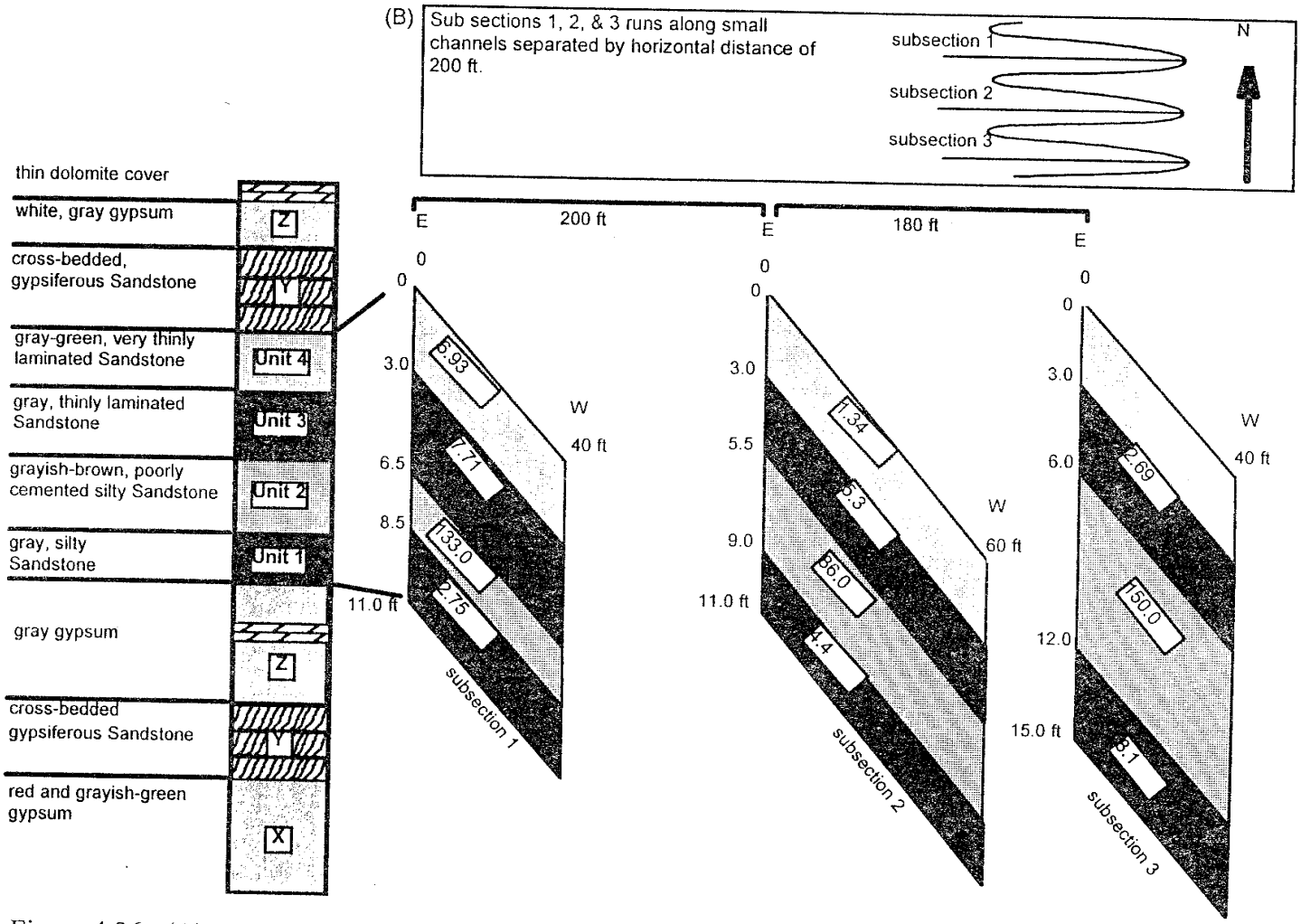

Figure 4.26: (A) A composite stratigraphic sequence of Section 5. The numbers inside the units are average permeabilities in millidarcies. (B) The individual subsections run east-west and are separated by distances of about 200 ft.

above this surface is removed, producing a rather smooth, horizontal surface. As new sand dunes migrate over this surface and the process is repeated several times, several smooth surface may be produced (Figure 4.26). McKee (1966) reported the presence of horizontal to sub-horizontal bounding surface in the white sand dunes in New Mexico, which were formed without any groundwater effect.

Overlying the cross-bedded gypsiferous sandstone is a 8 foot thick, white and gray gypsum bed (Unit Z) with a 6 inches thick dolomite bed (Figure 4.26).

Sandstone sequence

Overlying the gray gypsum is a sandstone sequence comprised of four individual units. Approximately 120 permeability measurements were made. A summary of permeability data is given in Table 4.4.

Unit 1 is the lowermost unit (Figure 4.26) and consists of gray, moderately cemented, moderately bedded, very fine-grained, argillaceous, silty sandstone. Unit 1 shows no sedimentary structures and exhibits low permeability ranging between 1 md and 19 md (average 7 md). The northern section (subsection 1) contains carbonate cement, whereas subsections 2 and 3 have gypsum cement. This unit has variable thickness and thickens towards the south (Subsection 3).

Unit 2 is a grayish-brown, poorly cemented, moderately to poorly sorted, very fine- grained silty sandstone. It contains variable amounts of clay and exhibits thin clay laminations. In the north (Subsection 1) its thickness is 2 feet but in the south Unit 2 becomes 6 feet thick (Subsection 3). This unit has the highest permeability among the sandstone units, ranging between 10 md and 447 md (average 140 md).

Unit 3 is a gray to light green, moderately cemented, moderately to poorly sorted, very fine-grained silty sandstone. Fresh surfaces show discontinuous, less than 1 mm thick, parallel to subparallel laminae of gray and light green color. Unit 3 shows intense bioturbation. In the northern part (Subsection 1) carbonate cement is present and in the southern part (Subsection 2 & 3) gypsiferous cement is present. This unit exhibits the lowest permeabilities, ranging between less than 1 md and 8 md (average 4.7 md).

Units	Subsection 1			Subsection 2			Subsection 3		
	N	Mean	STD (σ)	N	Mean	STD (σ)	N	Mean	STD (σ)
Unit 1	3	2.95	1.53	3	4.50	2.85	6	8.10	5.56
Unit 2	7	133.00	73.00	16	86.00	45.10	17	150.00	122.80
Unit 3	14	7.71	5.35	10	5.30	1.97	17	2.69	2.21
Unit 4	11	6.93	3.13	5	1.34	0.72	-	-	-

Table 4.4: Summary of permeability data from the Shattuck Member outcrop in the Bone Tank Draw area.

Unit 4 is a gray to light green, thinly laminated, moderately cemented, very fine grained silty sandstone. Unit 3 and 4 are similar to each other when fresh surfaces are observed. Unit 4 can be differentiated from Unit 3 in the field based on their different weathering behaviors. Unit 4 weathers into thin sandstone layers due to the presence of thin clay layers between the sandstone layers. Fresh surfaces show parallel to subparallel laminations, flaser bedding, and bioturbation. This unit has the lowest permeability among the sandstone units, which ranges between less than 1 md and 5 md (average 3 md).

Overlying the sandstone sequence is a cross-bedded gypsiferous sandstone similar to one towards the bottom of this section (Unit Y). Overlying the cross-bedded gypsiferous sandstone is a 4 foot thick white gypsum bed (Unit Z) which is in turn overlain by a 6 inches thick white dolomite layer similar to the one in the lower part of this section. This section probably presents a complete cycle of sedimentation.

Based on the presence of overlying and underlying bedded gypsum, cross-bedded gypsyferous sandstone, and sandstones with clay laminations, flaser bedding, and bioturbation, a mixed salina/lagoonal and eolian environment of deposition may be attributed to Section 5. Sandstones and bedded gypsum were deposited in salina/lagoonal environment, whereas the cross-bedded gypsyferous sandstone was deposited in the eolian environment.

Petrographic Analysis

A petrographic analysis of the outcrop samples was performed to identify the similarities and differences with the subsurface samples, especially the diagenetic sequence. A generalized paragenetic sequence for the Shattuck Member outcrops is given in Figure 4.27.

The Shattuck sandstones in the outcrops are composed of angular to subangular, poorly to moderately sorted, poorly to well cemented, fine to very fine-grained arkosic sandstone. The Shattuck Member outcrops have detrital compositions similar to the subsurface Shattuck Member as described previously.

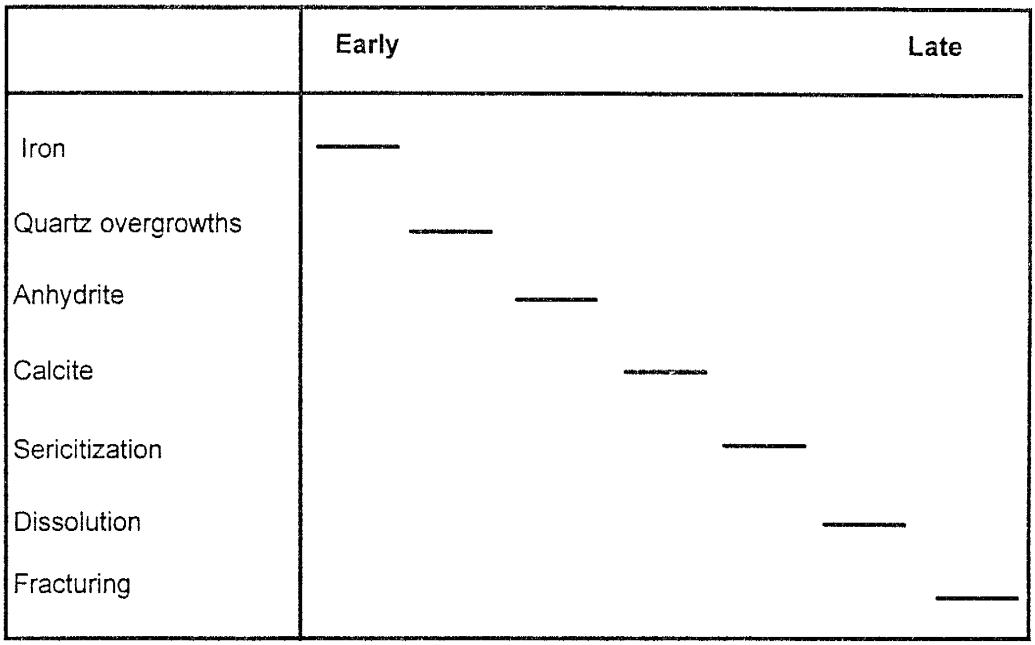

Figure 4.27: Generalized paragenetic sequence for the Shattuck Member in the outcrops.

In outcrops, quartz grains show syntaxial overgrowths containing inclusions of probable iron oxide. In the outcrops, silica also occurs as pore-filling cement, whereas in the subsurface it only occurs as overgrowths. Feldspars show considerable alteration ranging from sericitization to partial to complete dissolution similar to subsurface.

The main cementing material is finely crystalline calcite, whereas in the subsurface the cementing material is dominantly anhydrite and dolomite. In Section 5, gypsum is the dominant cementing material. Similar to the subsurface, iron (hematite) cement is present in almost all samples in trace amounts.

Both primary and secondary porosity are present. Porosity types consist of primary, secondary intergranular, intraconstituent, and moldic porosity. Secondary porosity is dominant in high permeability samples. Secondary porosity is formed by the dissolution of cement and constituent grains, mainly feldspar. In the subsurface, porosity was also created by the dissolution of cement and detrital grains, mainly feldspar.

As stated before, bad exposures of the Shattuck Member in both Rocky Arroyo and Bone Tank Draw prohibited the collection of permeability data on a regular grid with the exception of Section 1. The outcrop study was conducted to collect the "soft geological" information about the depositional environment, lithologies, and areal distribution of individual units. Outcrops around both Sections 1 and 5 (which were studied in detail) within a radius of one mile show drastic changes in lithologic makeup and depositional environments. Section 4, which is located one mile north of Section 1, exhibits completely different lithologic characteristics, is 55 feet thick and has high permeabilities. Section 4 changes from clastic to completely evaporitic composition within a lateral distance of one mile towards the west. Similarly, isolated outcrops approximately 3,000 feet north and northwest of section 5 are evaporitic and lack sandstone units.

Similar changes from sandstone to evaporites also occur in the subsurface and these changes are responsible for the formation of reservoirs (stratigraphic traps) in the Shattuck Member. It was also noted both in the subsurface and outcrops that the thickness of the sandstone units changes rapidly over short distances. The deposition of

the Shattuck Member in both outcrop and in the subsurface took place in a mixture of aqueous and eolian environments. Information obtained from the outcrops were useful in understanding the overall behavior of the Shattuck Member in the southeast New Mexico.

DEPOSITIONAL MODEL

Background

The Northwest Shelf was a broad, flat area that borders the Delaware Basin in the west Texas and southeast New Mexico during Permian time (Figure 1.3A). The Delaware Basin was a deep structural depression covering 10,000 square miles was surrounded by flat shelves that slope at a very low angle to the basin (Newell *et al.*, 1953). In the early Permian, the Delaware Basin subsided rapidly and accumulated a thick sequence of sediments. The basin continued to deepen and receive sediments until subsidence slowed in the mid-Permian and reefs began to develop around its border in Guadalupian time (Adams, 1965).

The Northwest Shelf was developed before the Permian, when numerous reefs were formed along its trend in late Pennsylvanian time. By Guadalupian time the shelf was 250 - 300 miles wide (Jacka and Franco, 1974). Early Permian rocks of the shelf area (Yeso and San Andres Formations) are mostly dolomites with thin interbeds of fine-grained sandstone. Middle and Upper Guadalupian rocks of the shelf area are called the Artesia Group (Figure 4.1). These are dolomites, sandy dolomites, fine sandstones, siltstones, red evaporitic silty shales, and evaporites. Landward, dolomites grade first to sandstones, then to evaporitic silty shales and evaporites (Newell *et al.*, 1953). Late Permian evaporites that filled the Delaware Basin also covered lagoonal areas of the Northwest Shelf and the red beds deposited above these are the last sediments of the Permian (Newell *et al.*, 1953).

As reported by Ball (1971) and Jacka and Franco (1984), the paleoclimate over much of the western interior was hot and arid in the Permian. During the Permian time, the Northwest Shelf of the Delaware Basin was situated in low latitude equatorial region

which created the hot and arid climate (Fischer, 1988).

Detailed facies models for the Queen and other shelf formations are presented by Williams (1967, 1968), Kendall (1969), Silver and Todd (1969), Ball *et al.*, (1971), Meissner (1972), Jacka and Franco (1974), and Ward *et al.*, (1986).

Models of Jacka and Franco (1974); and Silver and Todd (1969)

In the following section a summary of the depositional model proposed by Jacka and Franco (1974) is presented. Figure 4.28 illustrates the facies association described by Jacka and Franco (1974). They recorded seven depositional environments in the Permian shelf: (1) reef, (2) backreef apron, (3) lagoon, (4) intertidal zone, (5) coastal sabkha, (6) continental sabkha, and (7) deflation flats. They considered three general hypotheses to explain the Guadalupian depositional cycles, which are given below.

(1) Alternating tectonic subsidence and uplift caused intervals of submergence and emergence and caused the depositional cycles.

Tectonic processes are not known to rhythmically reverse themselves within relatively short time intervals. Evidence indicate that during Guadalupian time the Permian Basin was characterized by extreme tectonic quiescence (Adams, 1965). For these reasons, Jacka and Franco (1974) rejected any tectonic control hypothesis.

(2) Seaward progradation of coastal and continental sabkha deposits progressively infilled shelf lagoons. Continuous subsidence of the shelf area eventually caused an episode of submergence, followed again by progradation and progressive infill of lagoons. Regressive phases of depositional cycles reflect seaward progradation of coastal and continental sabkha facies and progressive lagoonal infilling.

According to Jacka and Franco (1974), this may have largely occurred during high still stands of sea level when climates were arid. It is difficult to explain repeated episodes of transgression, which followed regressive phases, wholly within the context of continuous subsidence.

(3) Glacially controlled eustatic sea level fluctuations, superimposed upon continuous subsidence of the shelf, caused alternating submergence and subaerial exposures. Based

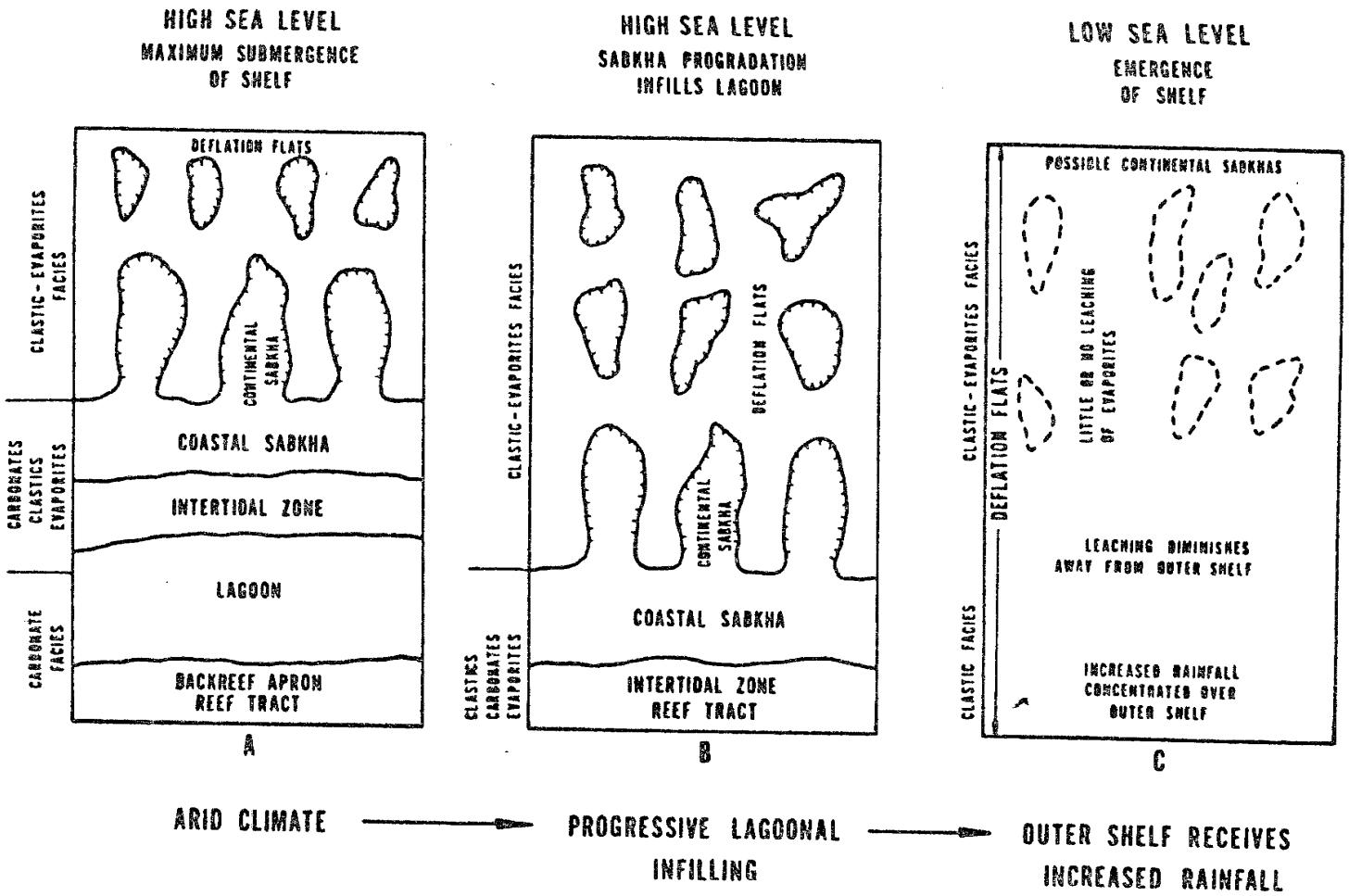

Figure 4.28: Model of sabkha progradation into lagoon. (A) Facies relationships that characterized Permian high stand of sea level when climates were arid (interglacial-interpluvial intervals). (B) Facies relationships that reflect progradation of coastal and continental sabkhas and deflation flat with progressive lagoonal infilling. (C) Facies relationships that characterized Permian low stands of sea level when the outer shelf received increased rainfall (glacial-pluvial interval) (Jacka and Franco, 1974).

on diagenetic evidence and Guadalupian climate, Jacka and Franco (1974) support the idea of climatic changes associated with major sea level fluctuations. No details of the diagenetic evidence as well as the sea level fluctuations and associated climatic changes are given in the paper by Jacka and Franco (1974). According to Jacka and Franco (1974), in Guadalupian time high stands of sea level were characterized by arid climates and precipitation of evaporites in coastal and continental sabkhas (interglacial-interpluvial interval) (Figure 4.28A). With continued aridity the sabkha and continental facies migrated seaward and filled the lagoon (Figure 4.28B). As the sea level dropped and rainfall increased over the outer shelf, carbonates were calichified (development of vadose diagenetic environment), some evaporites were leached, and accumulation of sediments ceased (Figure 4.28C).

Based on the magnitude and frequency of sea level fluctuations and because of associated climatic changes, the glacio-eustatic hypothesis is favored by Jacka and Franco (1974) as the major source of transgression and regression. Silver and Todd (1969) proposed a similar model for Guadalupian sediments. Clastics were all deposited as supratidal or continental facies and prograded across the lagoon only during extreme low stands of sea level.

In the model of Jacka and Franco (1974), most of the sands were deposited by eolian processes, and were deflation flat sediments; only the brine-pan deposits were water laid. Deflation flats occur inland from coastal sabkhas and they surround or engulf continental sabkhas (Figures 4.28A & 4.28B, Jacka and Franco, 1974). Deflation flat sediments are fine-grained, locally silty sands that were cemented by dolomite and anhydrite during early burial. They contain mud crack clasts and casts, adhesion ripples, and lenses of well-rounded medium to coarse quartz grains as lag deposits. Some dunes may have developed over parts of the deflation surfaces. Some evaporites were precipitated at the surface.

Model of Ball *et al.*, (1971)

The interpretation of Ball *et al.*, (1971) differs from the ones just described on several points (Figure 4.29).

(1) Barrier islands developed behind the reef and had associated sabkha and tidal-flat deposits on their flanks. William's (1969) model, although similar to the one of Jacka and Franco (1974), does include a barrier island facies behind the reef. Outcrop studies, particularly Williams (1967), have documented the presence of these carbonate shoals in the Queen Formation.

(2) Lagoonal sediments include quartz sands, evaporitic dolomites and bedded evaporites.

(3) The facies did not prograde as stripes parallel with the shelf edge.

(4) The shelf was never completely emergent. There are no marine sands in either Jacka and Franco's (1974) or Silver and Todd's (1969) models. Ball *et al.* (1971) found traction-current features in outcrops of the quartz and carbonate sands that indicate transport parallel with the shelf edge indicating marine deposition.

(5) The only areas that show evidence of subaerial exposure are the carbonate shoals that contain pisolitic caliche zones (vadose zone pisolites). These are interpreted to be the highest points on the shelf.

(6) Deposition of sand was continuous, and was not restricted to low stands of sea-level.

Depositional Model

We propose a depositional model which is similar to that of Ball *et al.*, (1971). One important concern is that the above mentioned depositional models dealt with the entire Queen and to a certain degree underlying and overlying formations, whereas we are presenting a depositional model only for the Shattuck Member. Therefore, we are dealing with a very short time interval, and the migration of different depositional environments within the Shattuck Member may have occurred due to minor sea level fluctuations.

We developed the model after assimilating all the information from cores,

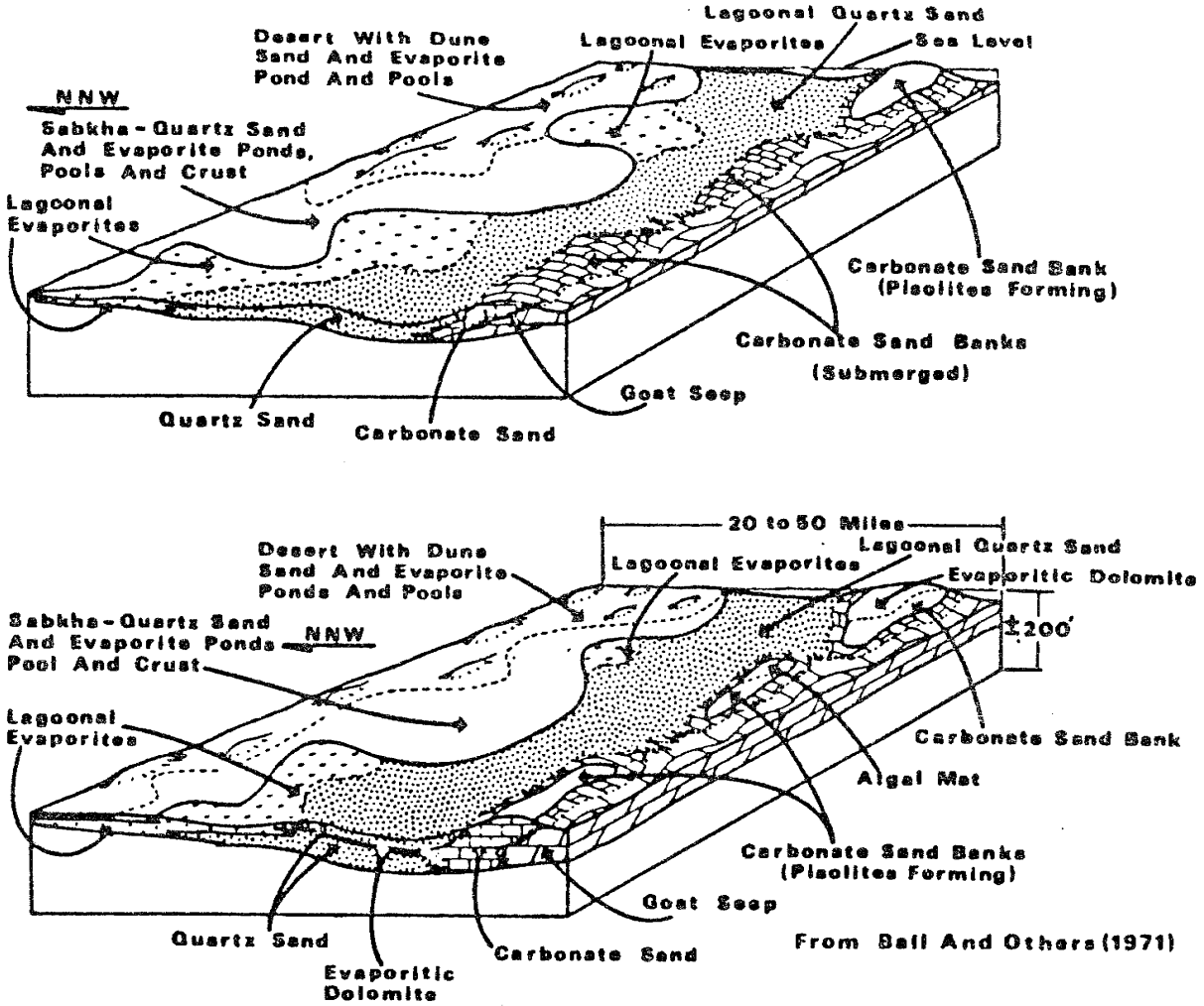

Figure 4.29: Model of interfingering lagoonal, sabkha, and eolian sandstone (Ball *et al.*, 1971).

petrographic analyses, logs, lithologic description of cores and chip analyses, and outcrop data.

North-south and east-west cross-sections for the net sand (sand portions with > 6% porosity) in the Sulimar Queen field are shown in Figures 4.30 & 4.31. Rescaled gamma ray logs were used to construct the cross-sections. There are minor structural elements in the north-south cross-section (Figure 4.30), but this small anticline-like feature is not exclusively responsible for the formation of the reservoir, and probably only controlled the distribution of gas cap. An east-west cross-section shows a variable dip towards the east (Figure 4.31). The thickness of the net sand also increases towards the east.

Based on the literature survey of the depositional environment of the Artesia Group (Guadalupian) in the Northwest Shelf, following assumptions were made:
(1) Goat Seep and Capitan reefs separated the Northwest Shelf from the Delaware Basin,
(2) barrier islands were present behind the Goat Seep and Capitan reefs. A lagoon developed between the barrier islands and land,
(3) the lagoonal part present towards the land was shallow and probably had restricted circulation,
(4) sandstones, silty sandstones, and evaporites were deposited towards the landward portion of the lagoon,
(5) sabkha and desert environments were present landward of the lagoon,
(6) due to minor sea-level changes or climatic changes (rainfall and wind direction and strength) or supply of detrital material, lagoonal, sabkha, and eolian environments migrated back and forth and created the present distribution of the Shattuck Member in the Sulimar Queen and adjacent fields,
(7) based on the distribution of the Goat Seep reef, the Sulimar Queen field is located towards the landward portion of the lagoon (Figure 1.3A).

In the Sulimar Queen, and the surrounding area, the Shattuck Member was deposited in a mix of coastal sabkha, shallow saline lagoon (with variable energy and depth), and eolian environments (dry eolian sand sheets of Malicse and Mazzullo, 1990)

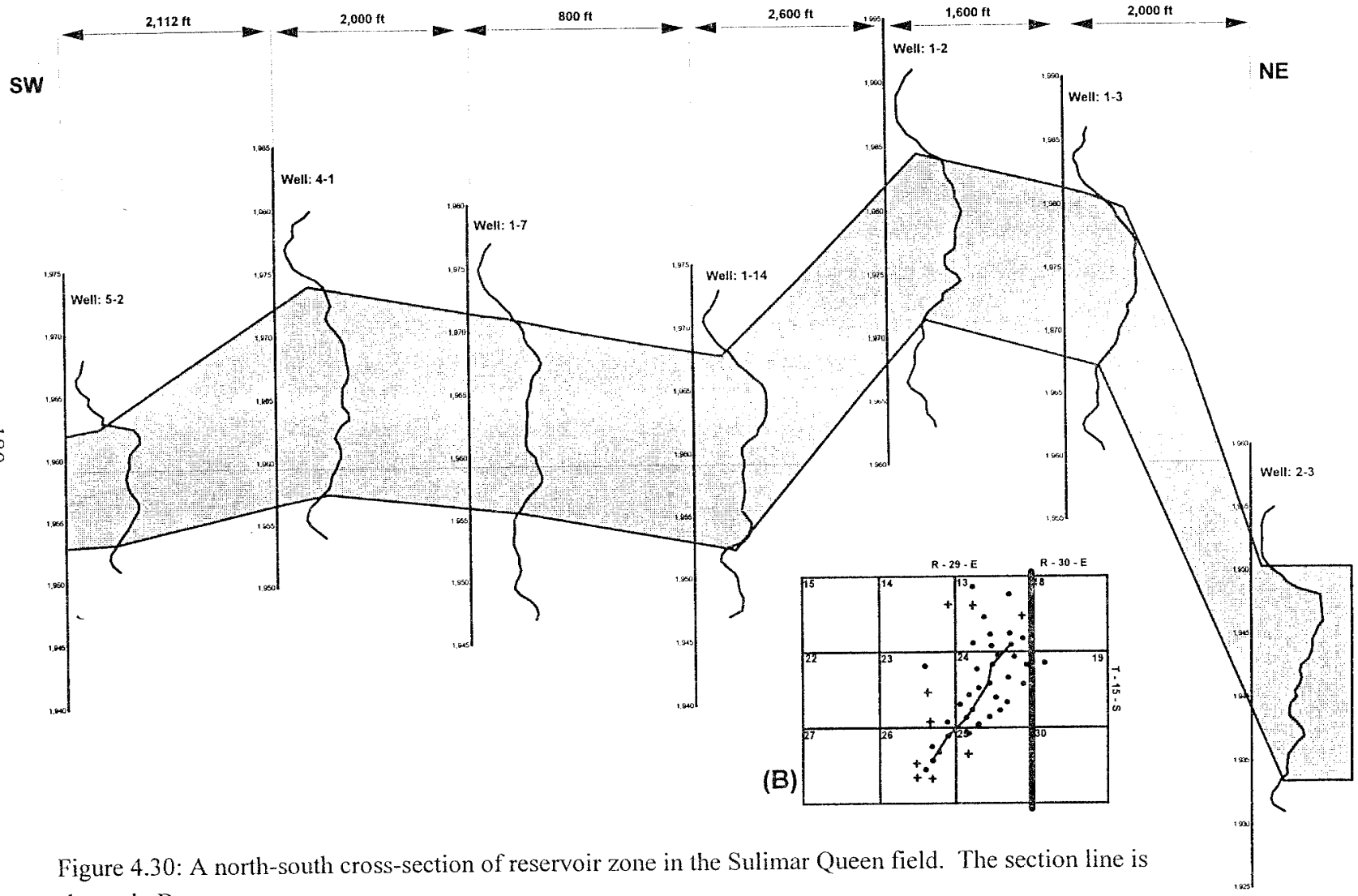

Figure 4.30: A north-south cross-section of reservoir zone in the Sulimar Queen field. The section line is shown in B.

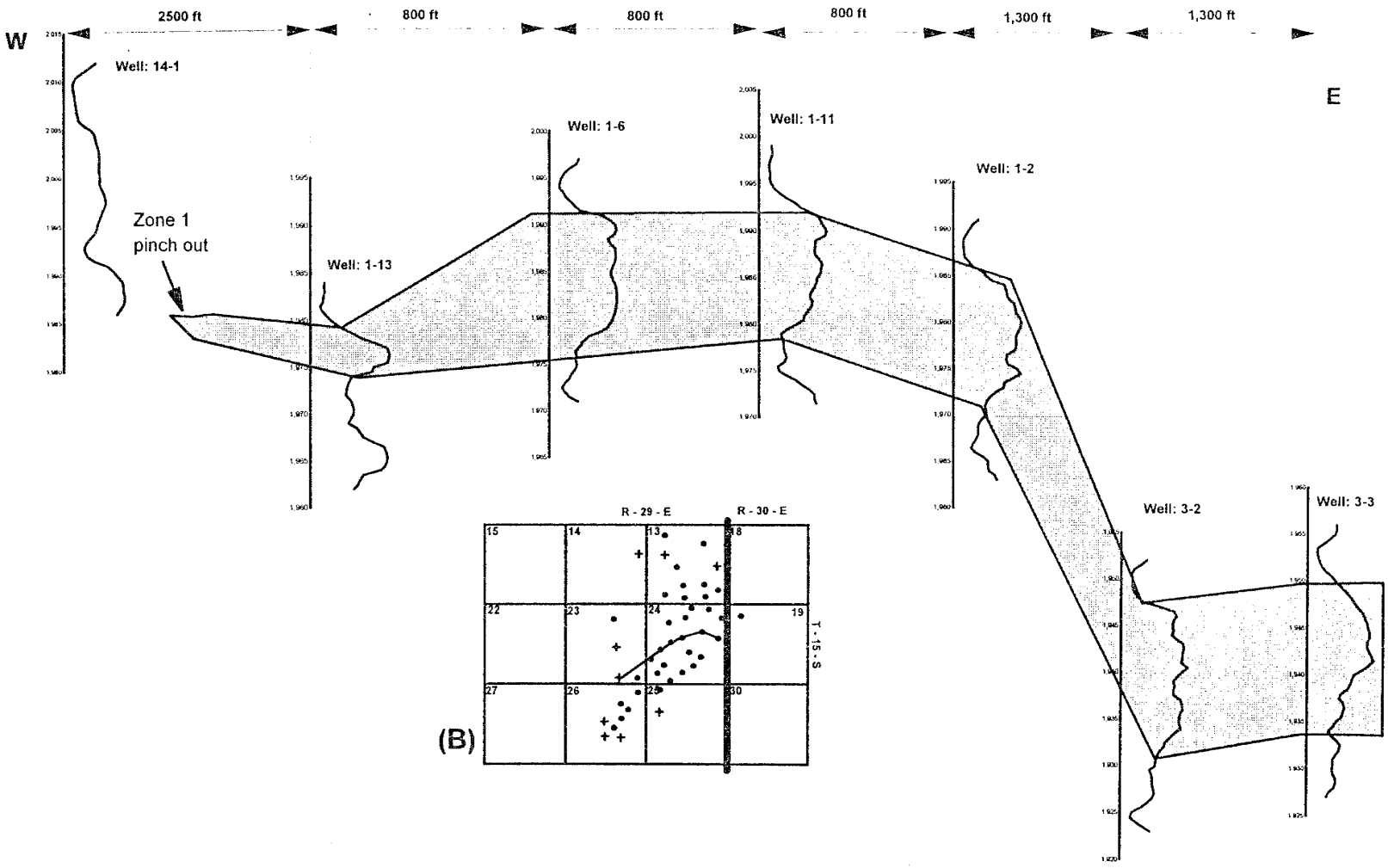

Figure 4.31: An east-west cross-section of reservoir zone in the Sulimar Queen field. The section line is shown in B.

lower ranked elements in producing local heterogeneities.

We studied three combinations in order to examine the capability of the neural network to predict the permeabilities from limited petrographic data. The petrographic elements used in case of three elements are commonly available from most petrographic analyses. If observed closely, the predictions made by limited elements were reasonable and successful in capturing the general permeability trend (Figure 5.14C).

The Power of the Neural Network

As mentioned before, additional core from a well in the South Lucky Lake field was also collected for analogy. South Lucky Lake field is located 1.5 mile west of the Sulimar Queen field (Figure 1.3 A). Permeability measurements were made and thin section analysis were done on the South Lucky Lake field core. Thin section analysis revealed that the depositional and diagenetic sequences as well as bulk mineralogies were similar for Sulimar Queen and South Lucky Lake fields. Based on this information, it was decided to use the neural network to predict permeability from the petrographic data, in the South Lucky Lake field. It is evident from Figure 5.15 that the net did a good job of predicting the permeabilities, although the data from the South Lucky Lake field were never seen by the net. The only problems encountered were with the prediction of the low permeabilities. As mentioned earlier, this may be due to measurement errors in the low permeabilities.

The correlation between the predicted and the measured/desired permeabilities using the top ten petrographic elements are shown in Figure 5.16. For the test data from the same well (1-16) an R^2 of 0.70 was achieved, whereas for the South Lucky Lake an R^2 of 0.63 was obtained.

A neural network is useful to predict permeabilities because it is capable of learning and solving nonlinear problems fast. Using the neural network, we exceeded the boundaries of conventional multiple regression. By predicting permeabilities in a field different from that of the training data set, we showed that neural networks are powerful tools for predicting permeability from petrographic data. In the old fields, with proper

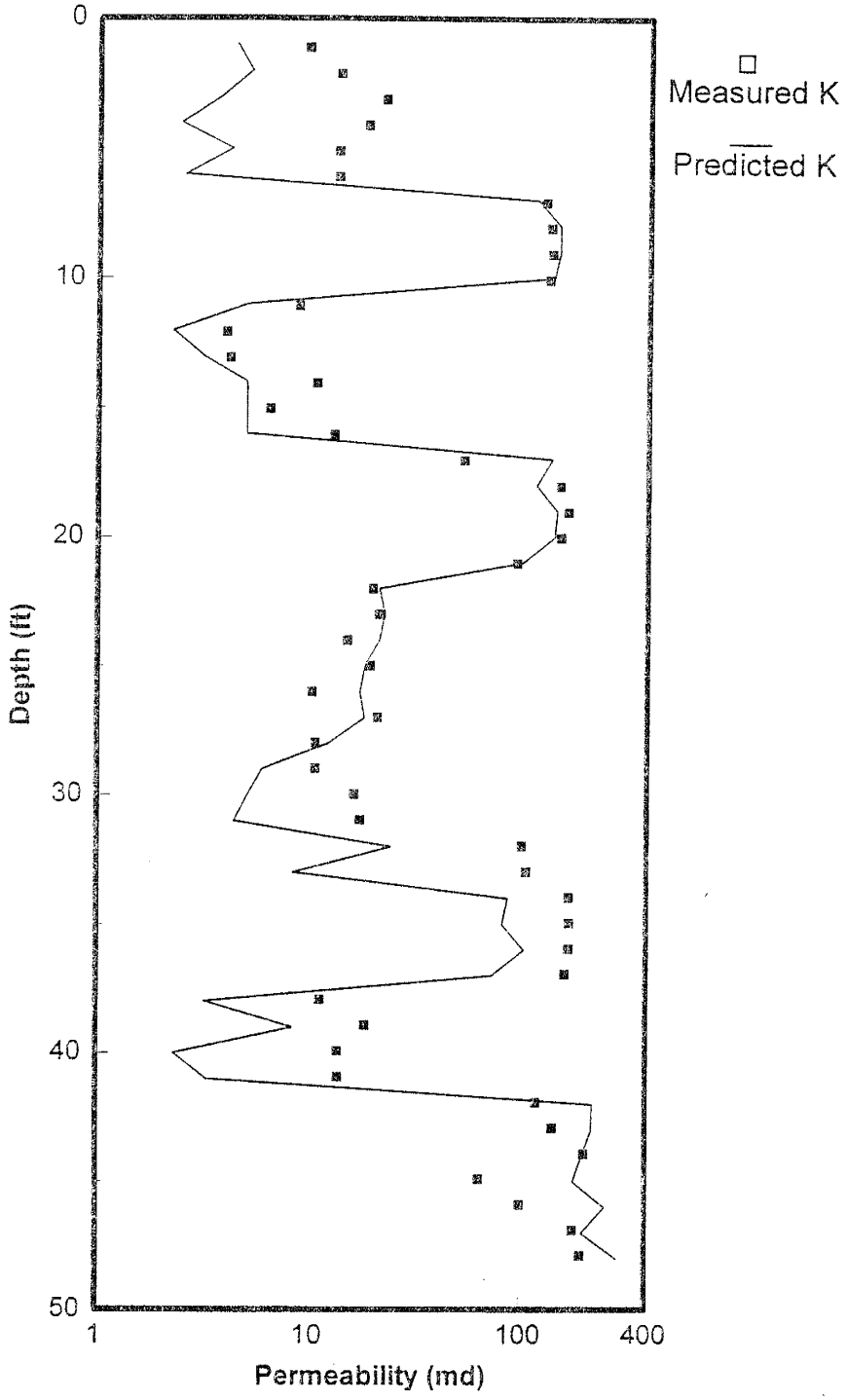

Figure 5.15: Comparison of the neural-network predicted permeabilities and measured permeabilities in the South Lucky field. Data from South Lucky Lake were never seen by the neural-network

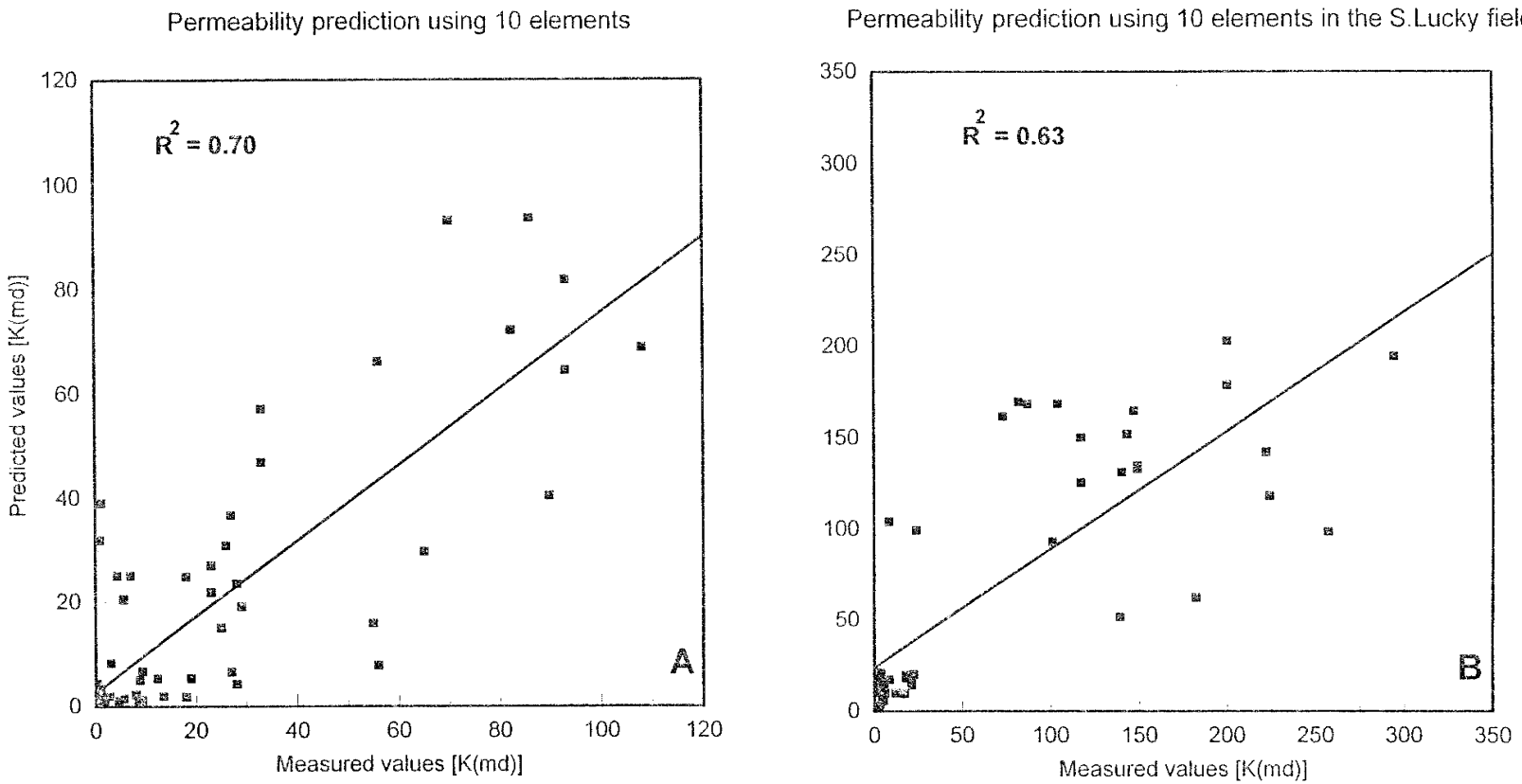

Figure 5.16: Results of the neural-network testing in the Sulimar Queen field (A) and prediction in the South Lucky Lake field (B).

training, thin section data can be used to predict permeability using the neural net. The petrographic data required for the prediction is usually available from conventional petrographic analysis. In the old fields, petrographic data collected from thin sections made from the drill cuttings can also be used to predict permeability.

LOG ANALYSIS

As mentioned previously, only four modern log suites were available, and the rest of the field contained only old gamma ray and neutron logs. Due to the absence of other logs (e.g., resistivity, sonic, density, etc.) and the unreliability of the old neutron logs, correlations between core porosity, total water content, and permeability had to be made with gamma ray logs in order to predict these properties in the uncored wells. Details of the log analysis are given in Chapter 3. In the following sections log analysis and its application for the characterization of the Sulimar Queen field will be discussed briefly.

Developing Relationships of Gamma Ray with Porosity, Total Water Content, and Permeability

A positive relationship between core porosity and the gamma ray response was developed in the Sulimar Queen field (Figure 5.17) as well as in the Queen field, which may be expressed as (Figure 5.17):

$$\phi = 0.334 e^{0.0526(\gamma)} \qquad (1)$$

where ϕ is the porosity in percent and γ represents the gamma ray value in the API units.

Similar relationships between gamma ray and porosity were also observed in the adjacent fields (Chapter 3). This increased our confidence in using the correlation between core porosity and gamma ray, developed in one well (Well 1-16) to be used for predicting porosity throughout the field (Figure 5.17). As revealed from the core analysis, this relationship is only good for the sand portion of the Shattuck Member.

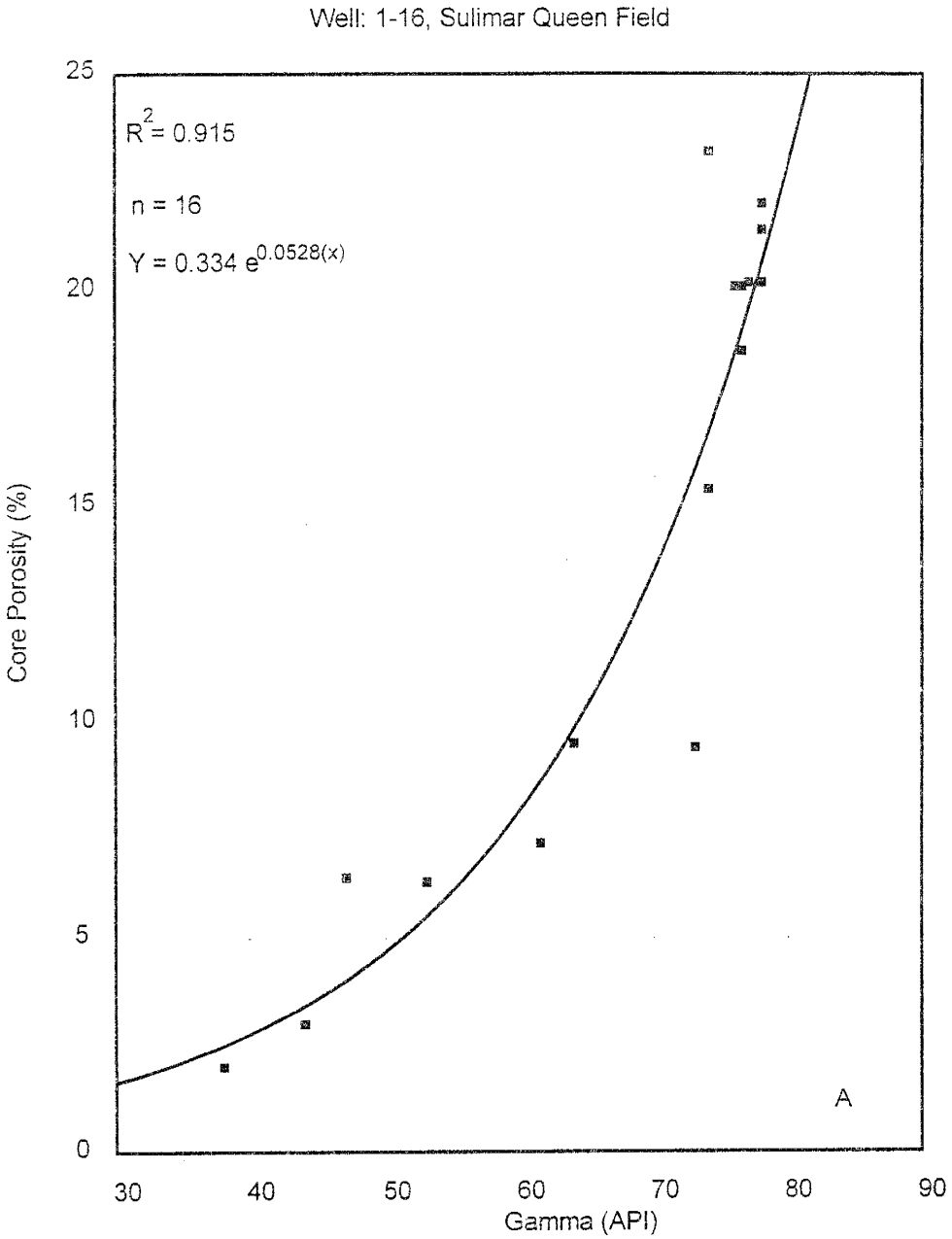

Figure 5. 17: Plot showing the relationship between gamma ray values and core porosity in the Sulimar Queen field.

Petrographic and XRD analysis suggested that in the Shattuck zone, the gamma ray values are not controlled by the amount of clay. The gamma ray response is partially controlled by the amount of potassium feldspar and partially by uranium (confirmed by the spectral gamma ray log from one well in the Queen field) (Figure 5.18A).

Uranium is generally associated with acid igneous rocks, which contain on average 4.65 ppm of uranium (Rider, 1986). However, the mineral does form soluble salts, especially the uranyl ion (UO_2^{2+}) and in this form is present in river and sea waters (Rider, 1986). The direct precipitation of uranium requires strongly reducing conditions and is rarely found in the natural environment. Uranium is often found associated with high organic content sediments ("black shales" e.g., North Sea Jurassic "hot shales," Bjørlykke *et al.*, 1975). A small amount of uranium can strongly affect the total gamma ray value of the gamma ray log. For example, Bjørlykke *et al.*, (1975) showed that in the Black Kimmeridigian shale (North Sea) only 5.27 ppm of uranium was responsible for 66% of the gamma ray log response, whereas 10.44 ppm of thorium accounted for 33% and 1.34% of potassium only 6% of the gamma ray log response. However, the available literature contains no evidence of the presence of high organic matter that can account for the uranium in the Shattuck Member.

Although no water analyses were available from the Sulimar Queen field, we assume that the uranium is present in the water as uranium salt based on the positive relationship between gamma ray values and total water content. It is noted that permeable zones sometimes have higher uranium salt content than less permeable zones (Schlumberger, 1987). This seems to be the more likely scenario to explain the positive relationships of gamma ray values with porosity, total water content, and permeability in the Shattuck Member.

Total water content showed a relationship similar to that of core porosity and gamma ray response. The following relationship developed in Well 1-16 was then used with caution to predict the total water content (W_{TC}) (Figure 5.19):

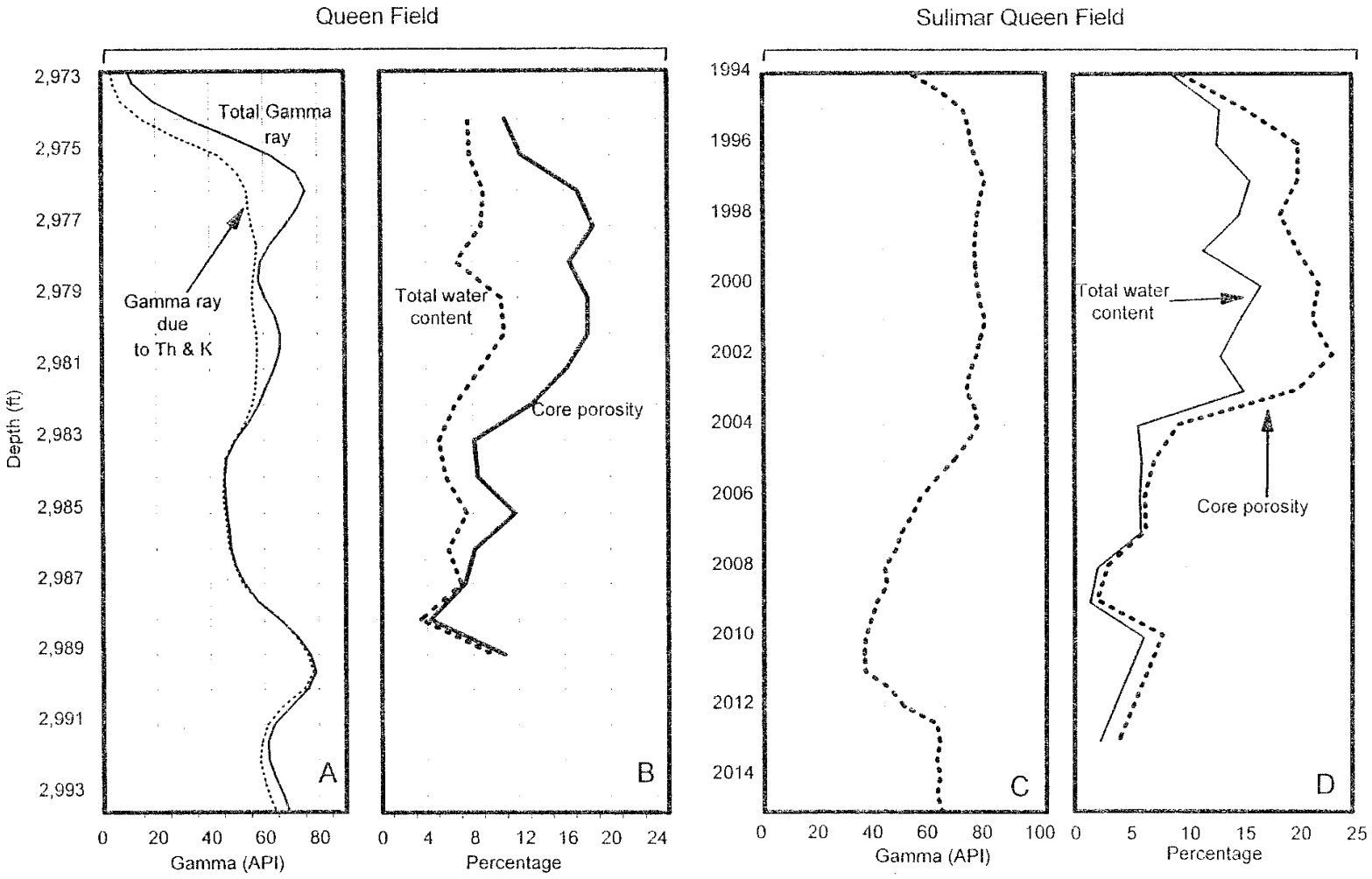

Figure 5.18: Plots showing the distribution of spectral gamma ray (A) and porosity and total water content (B) in the Queen field. Also shown is the gamma ray log (C) and porosity and total water content (D) in the Sulimar Queen field. As the porosity and total water content increase so does the gamma ray value

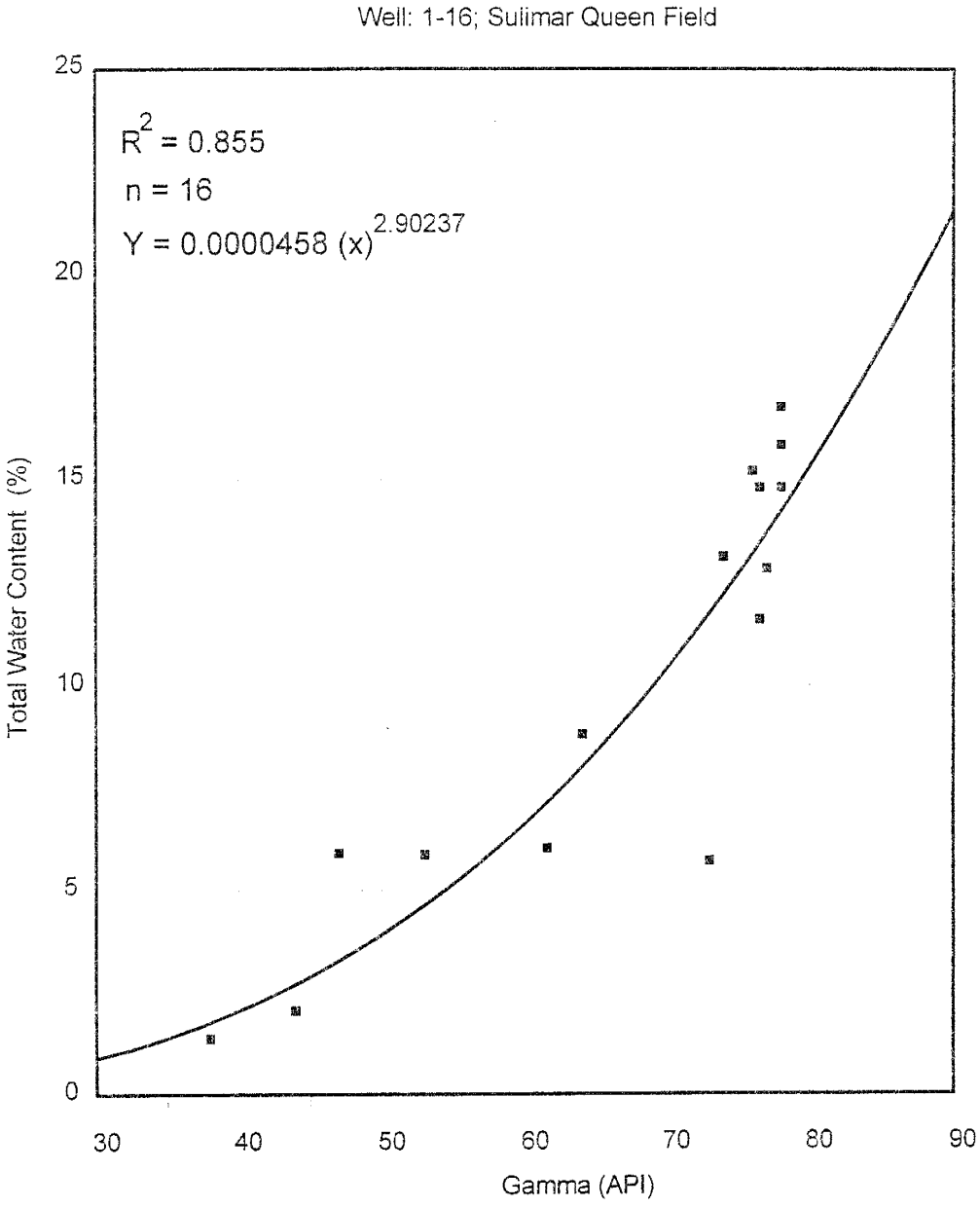

Figure 5. 19: Plot showing the relationship between total water content and gamma ray values in the Sulimar Queen field.

$$W_{TC} = 4.6 \times 10^{-5} \gamma^{2.9} \quad (2)$$

W_{TC} is the total water content in percentage, and γ the gamma ray value in API units.

The total water content can be converted to water saturation, using:

$$S_W = [\frac{W_{TC}}{\phi}] \times 100 \quad (3)$$

Total water content was used instead of water saturation in order to understand the effects of dissolved water contents on gamma ray response (Chapter 3).

Improving the Reliability of Old Gamma Ray Logs

The methodology to improve the reliability of old gamma ray logs is given in Chapter 3. The rescaling of the old gamma ray logs was done because the porosity (Equation 1) and total water content (Equation 2) obtained from the *unscaled* old gamma ray logs were erroneous. Also, due to different scale ranges of the old gamma ray logs, the extrapolation beyond the range of original data values (Well 1-16) yielded incorrect results. Examples of a few rescaled logs are shown in Figure 5.20.

The increase in the reliability of the old gamma ray logs after rescaling is also evident from the improved correlation coefficient between the core porosity and the gamma ray values (Figure 5.21). The gamma ray derived porosity (Equation 1) and total water content (Equations 2) were compared with the core porosities and total water content in Wells 1-14 and 5-1 for reliability (Figures 5.22 and 5.23).

Porosity calculated from the rescaled gamma ray logs also captured the presence of individual high and low porosity zones that were not distinguishable in the porosities obtained from unscaled gamma ray logs (Figure 5.24). Porosity and total water content were predicted throughout the field using the rescaled logs.

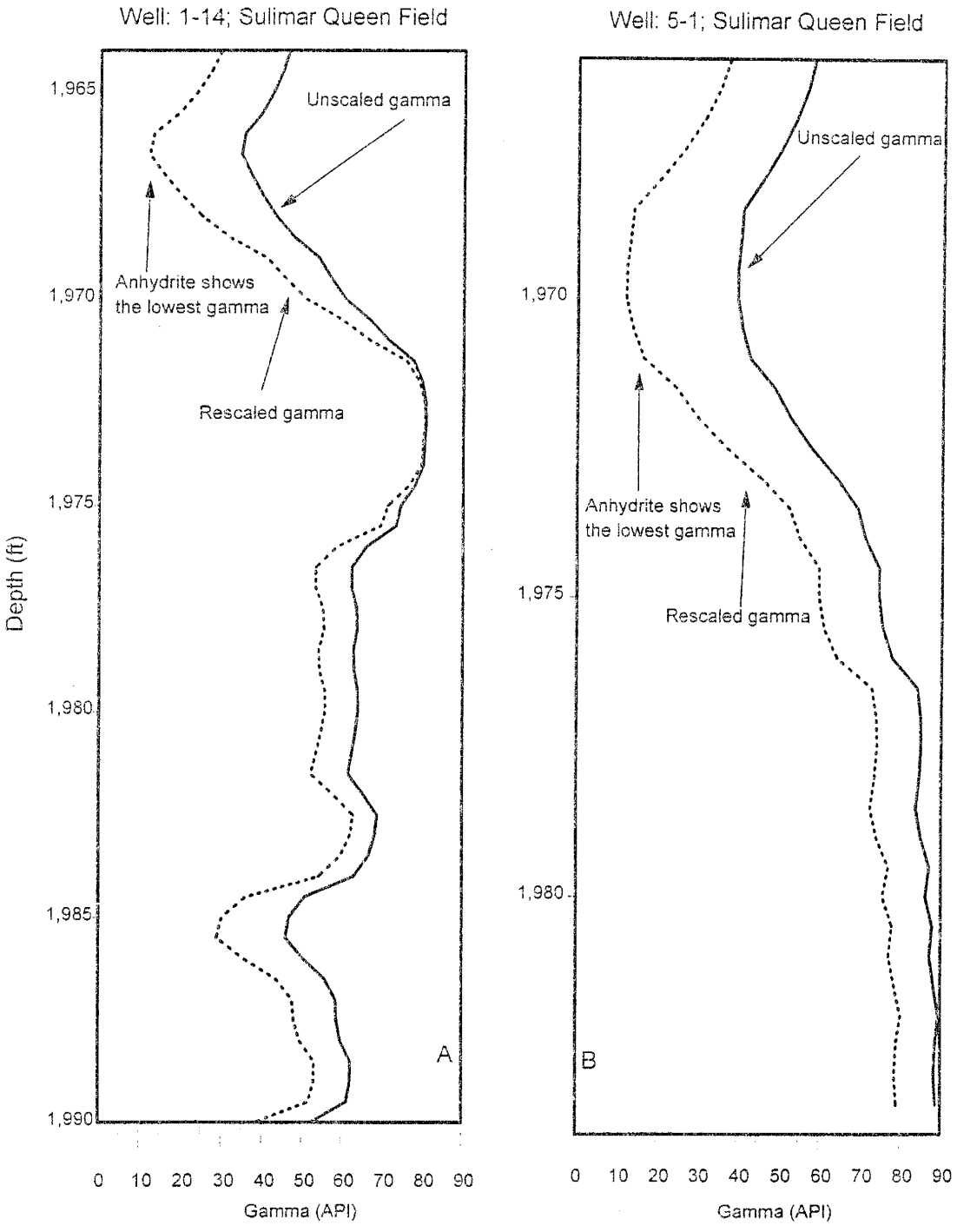

Figure 5.20: Comparison of unscaled and rescaled gamma ray logs. The rescaled logs have the minimum of 12 API and maximum of 80 API values. Note the presence of anhydritic portion in the rescaled gamma ray logs which were not identifiable in unscaled logs.

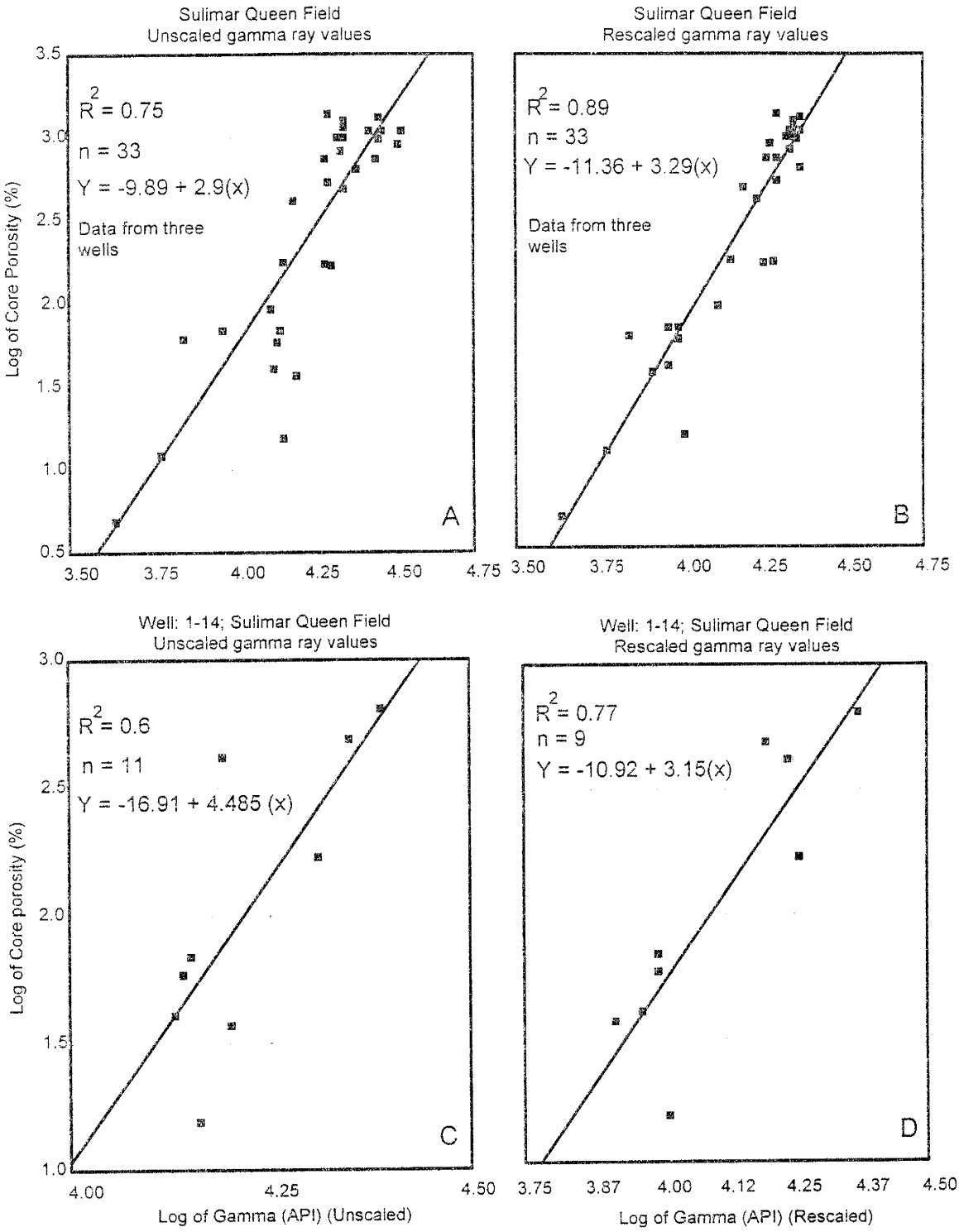

Figure 5.21: Plots showing the effects of rescaling on the correlations between core porosity and gamma ray values. Note the improvement of correlation from (A) to (B) and (C) to (D).

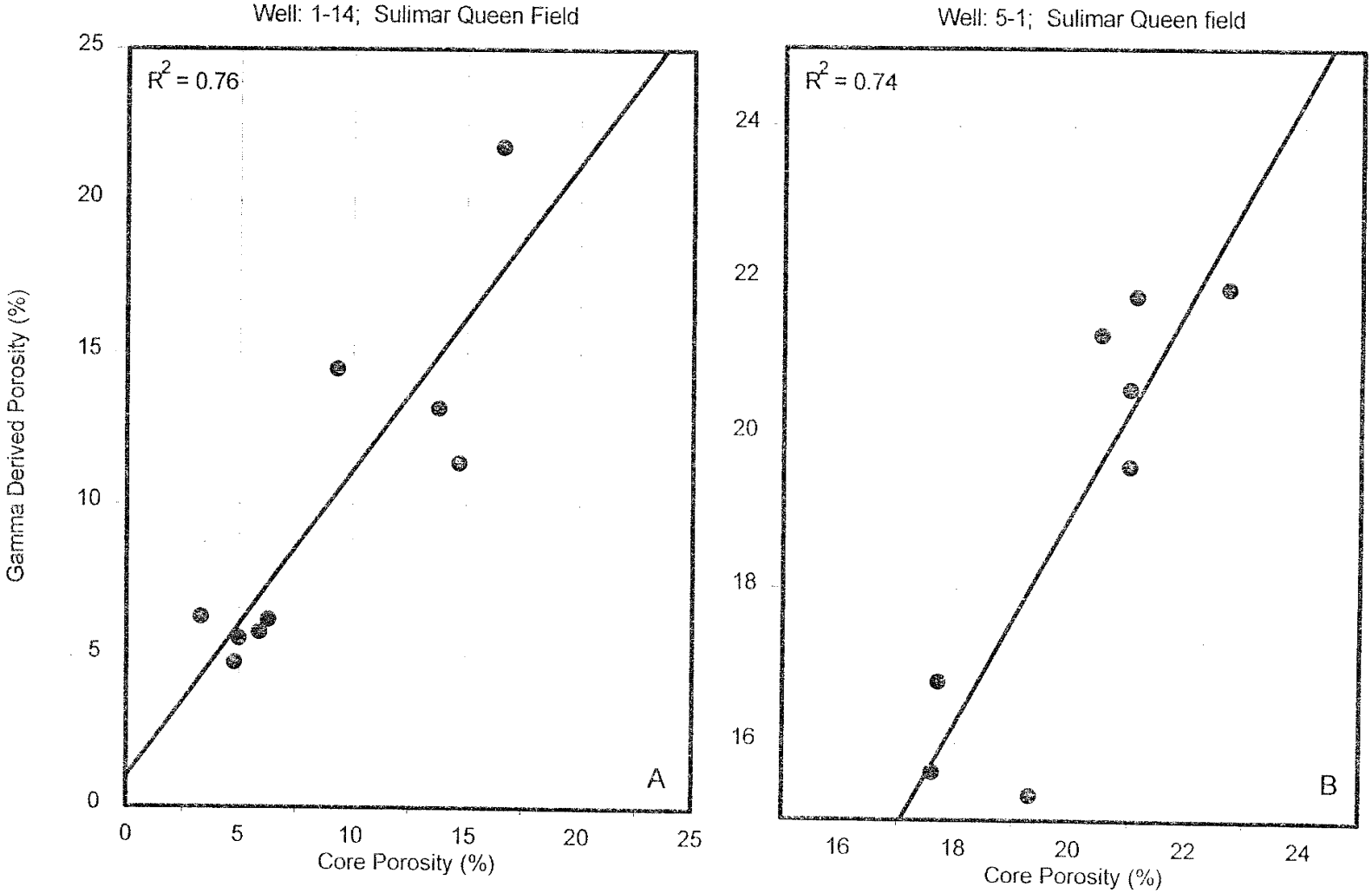

Figure 5.22: Comparison of core porosity and the porosity predicted using rescaled gamma ray logs in the Sulimar Queen field.

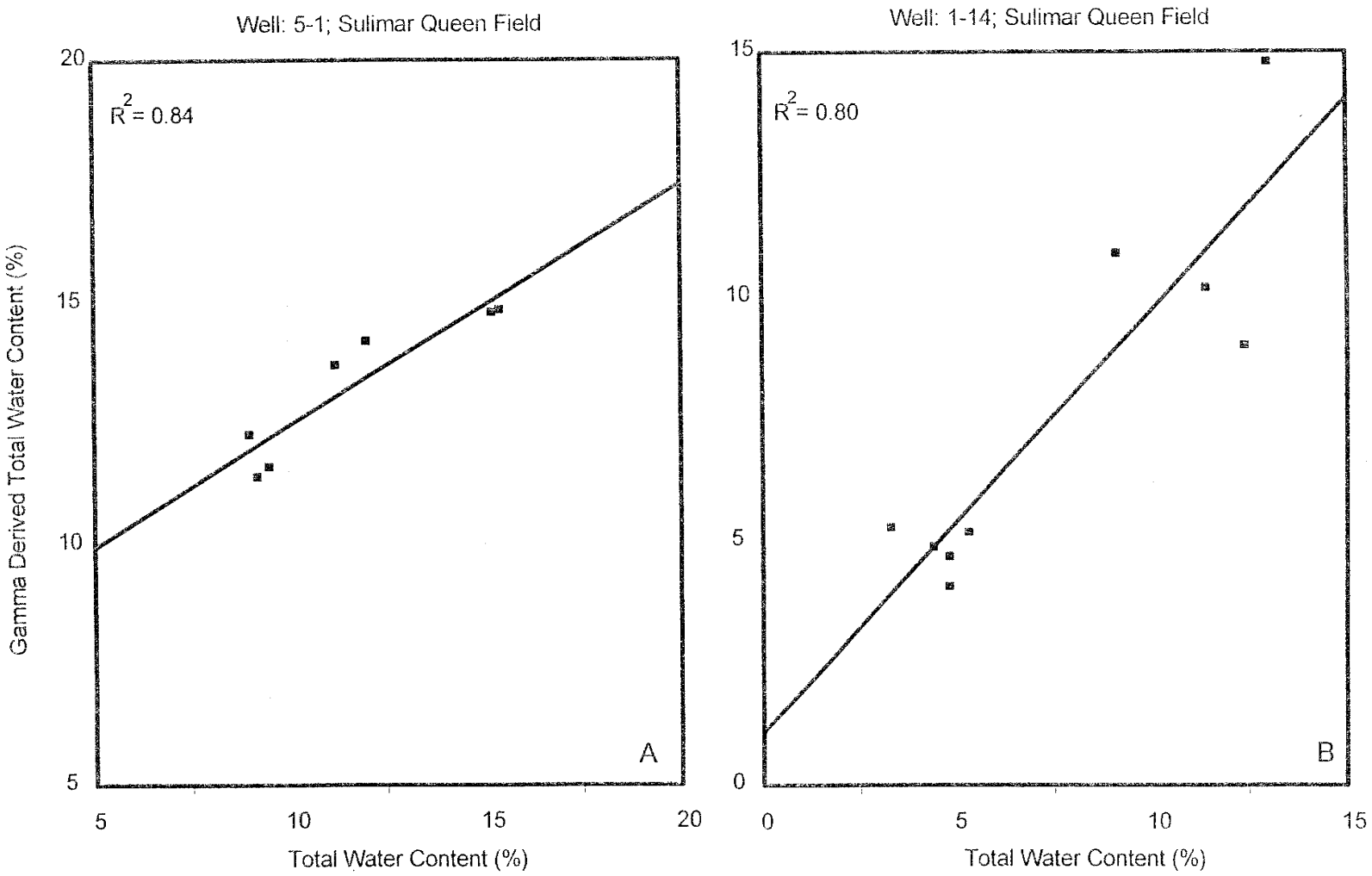

Figure 5.23: Comparison of core derived and rescaled gamma ray log derived total water content. Note a strong correlation in both wells.

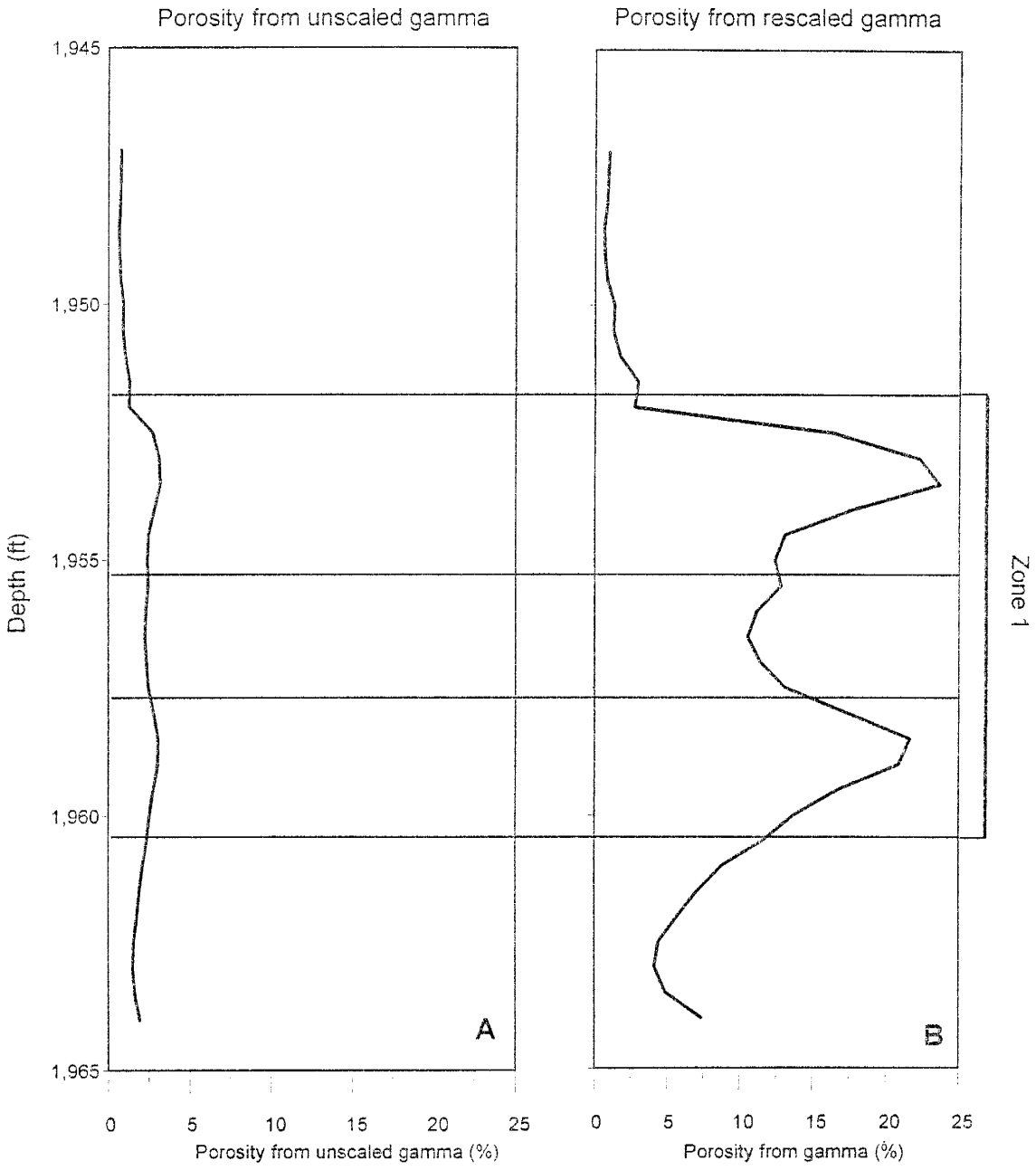

Figure 5.24: Comparison of porosity distribution as calculated from unscaled (A) and rescaled (B) gamma ray logs in Well 5-2. High and low porosity zones are clearly visible in the porosity derived from rescaled gamma ray log (B).

OUTCROP ANALYSIS

An outcrop analog study combined with geostatistics is essential in understanding the stratigraphic behavior of the rock units on a regional scale. Without a 3-D seismic survey of the Sulimar Queen, the outcrop provided the only measure of the large-scale geologic behavior of the system. The objectives of the outcrop study were to collect quantitative information on dimensions and geometries of sand bodies, to determine fluid flow barriers, and to evaluate the spatial distribution of the reservoir properties.

Five outcrop sections were measured and described. Permeability measurements were made with a field minipermeameter and numerous core and rock samples were collected. The locations of the outcrops are shown in Figures 1.3 & 4.15. Two sections were studied in detail: Section 1 in the Rocky Arroyo and Section 5 in the Bone Tank Draw area.

Rocky Arroyo (Section 1)

The longest section, and the one studied in most detail, is called Section 1 (Figure 5.25). This section runs east-west along the south wall of Rocky Arroyo and has a lateral extent of about 450 feet. Thirty to thirty-five feet of the Shattuck Member is exposed here, and the exposure can be divided into seven different units based on lithology and permeability (Figure 5.25). Sandstones are light gray to yellowish tan and fine to very fine-grained. Sedimentary structures are rare, but include parallel and wavy laminations, flaser bedding, and minor cross-bedding. The upper part of some bedding surfaces contains dessication cracks and gypsum rosettes. The gypsum rosettes are usually formed in sabkha (Kendall and Warren, 1988), eolian sandstones (Hanford, 1988), and brine-saturated interdune sediments (Hanford, 1988). The association of gypsum rosettes and dessication cracks probably suggest a shallow body of hypersaline brine, although dessication cracks can form subaqueously (Collins and Thompson, 1982).

The best-exposed portions of Section 1 were sampled on an interval of 10 feet horizontally and 2 feet vertically; it is believed that this interval should reveal the most heterogeneities within the sampled section. Permeabilities range from less than 1 md to

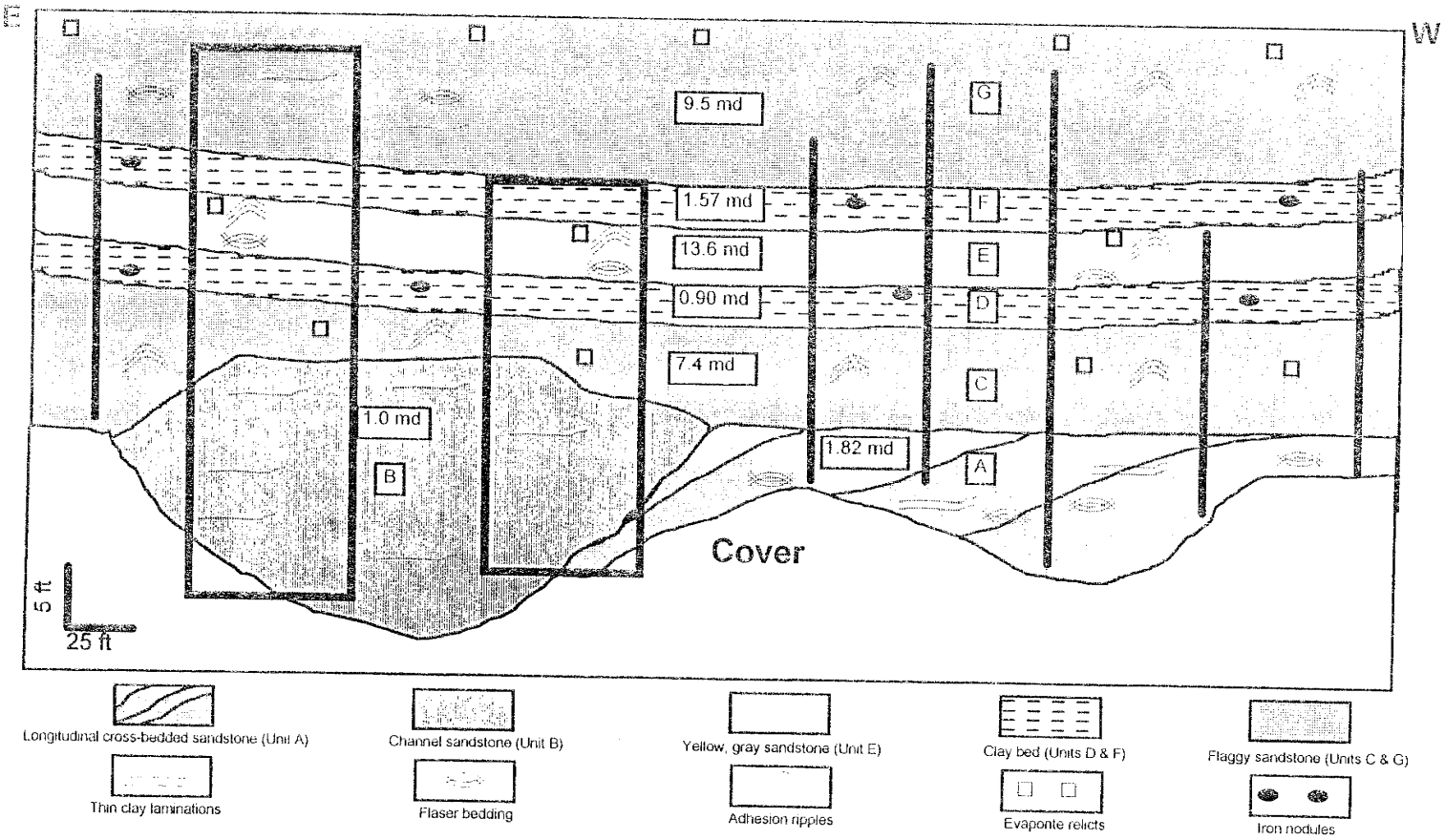

Figure 5.25: Section 1 in the Rocky Arroyo (south wall). Sampling transects are shown by vertical solid lines (horizontal interval 50 ft., and vertical interval 2 ft.). The numbers are the average permeability value of each unit in millidarcies. Boxes show the area in which samples were collected at a horizontal interval of 10 feet. and vertical interval of 2 feet.

176 md for Section 1; some units show much greater permeability variation than others. The low permeability sandstones are moderately-sorted and fine-grained and have been tightly cemented with carbonate and quartz cements. This outcrop also contain two clay-rich layers with extremely low permeabilities. Grain size analysis of Section 1 showed that there was an overall positive correlation between grain size and permeability in this outcrop.

Bone Tank Draw (Section 5)

Section 5 (Bone Tank Draw) is located about 7 miles to the northwest of Rocky Arroyo Section 1. It is located about 16 miles landward of the position of the Goat Seep reef (Figure 1.3), further away from the reef than any of the other outcrops studied. The Sulimar Queen field is about 20 miles north of the Goat Seep Reef, and exhibits relatively different facies and depositional environment from the outcrops studied in Rocky Arroyo; however, it is quite similar to the outcrop in the Bone Tank Draw section.

Figure 5.26 shows a schematic of a measured cross-section of the Bone Tank Draw. The Shattuck outcrop in Bone Tank Draw is 11 - 15 ft thick sandstone, overlain and underlain by massive and bedded gypsum, interbedded with red siltstone. The sands can be divided into four thin units that persist throughout the outcrop area. Sedimentary structures include parallel or subparallel laminations, flaser bedding, and occasional wavy bedding similar to that seen in the Sulimar Queen reservoir rocks. Permeabilities are generally low in much of the sandstone, averaging about 5 md; however, there is one poorly cemented sandstone layer with an average permeability of 140 md. This layer is laterally continuous throughout the Bone Tank Draw outcrop, but varies in thickness, thickening to the south.

One feature that is apparent from the permeability studies of the Rocky Arroyo and Bone Tank Draw outcrops is that the Shattuck sandstone is not a single unit, but can be divided into smaller subunits based on variations in lithology, sedimentary structures, depositional environment, and, ultimately, permeability. The observation of groundwater seepage at the outcrop face demonstrates that there is definitely preferential fluid flow

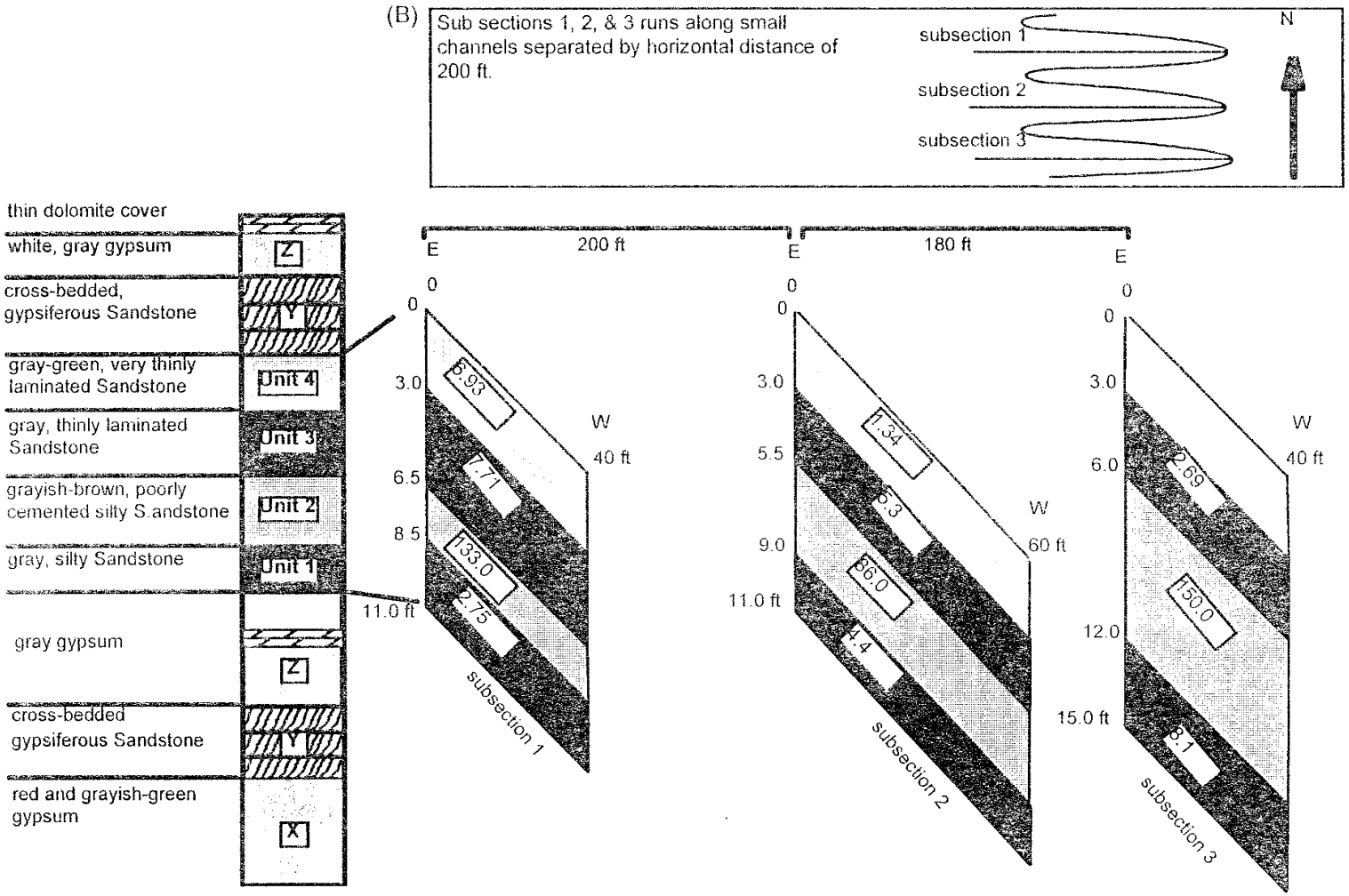

Figure 5.26: A composite stratigraphic sequence of section 5. The numbers inside the units are average permeabilities in millidarcies. (B) The individual subsections run east-west and are separated by distances of about 200 ft.

within some layers.

Although exposures of outcrops were too limited to perform a rigorous geostatistical analysis based on a regular grid, the close similarities of the outcrop, particularly the Bone Tank Draw section, to the Shattuck sandstone seen in the Sulimar Queen Well 1-16 core provided a compelling reason to study the outcrops. The geological information gathered about depositional environment, lithologies, aerial distribution of individual units, and sedimentary structures were important in understanding and modeling the distribution and facies architecture of the Shattuck Member in the subsurface. Individual units are laterally continuous over the space of a single outcrop (a few hundred feet at most), but it is difficult to correlate units over distances of several hundreds of feet.

Integration in the Sulimar Queen Model

This information was incorporated into the geological model of the Shattuck and was one of the reasons the reservoir was subdivided into only two layers, rather than the three lithologies that can be seen in the core. The clayey siltstones appear to be too discontinuous and unpredictable in nature to be included in the reservoir model. Sandstones seem to be more laterally continuous in outcrop; thus, we felt justified in extending them across areas of the Sulimar Queen field where well data was not available.

The characterization effort focused on building reservoir models that honor the existing and derived data. The two major steps involved in this approach were: (1) to identify the major lithofacies classes and, more importantly, their spatial distribution, and (2) to estimate the petro-geological properties within each class of lithofacies. In the first step, geology and log data were used to locate the two major geologic zones affecting rock properties. These two major zones were deposited in different environments. One was deposited in the eolian and sabkha environment and the other in a lagoonal environment. The next step involved estimating the porosity, permeability, and initial water saturation in each zone.

DEPOSITIONAL ENVIRONMENT

Two opposing interpretations for the deposition of the Queen Formation are available in the literature. Boyd (1958), Pray (1977), and Sarg (1977) proposed an aqueous "all wet" depositional model. They attribute the deposition to a subsiding lagoon based on the lack of evidence for extensive subaerial exposure in the Queen or the adjacent formations in the Guadalupe Mountains in Texas and New Mexico. On the other hand, Silver and Todd (1969), Mazzullo *et al.*, (1984) (1985), and Malisce and Mazzullo (1990) suggest an eolian/continental environment.

During Guadalupian time, the Northwest Shelf was a flat, slowly subsiding platform to the north of the Delaware Basin (Figure 1.3). During Queen deposition, a broad lagoon was present between carbonate sand shoals and the land-sea margin (Ball, 1971).

In this section the depositional model is described very briefly. The details of the depositional model developed for the Shattuck Member are given in Chapter 4. In the Sulimar Queen and the South Lucky Lake fields, the Shattuck Member was deposited in a mixed coastal sabkha, shallow lagoon (with variable energy and depth), and eolian (dry eolian sand sheets of Malisce and Mazzullo, 1990) environments (Figure 5.27). These environments were established based on the variations in grain size and sorting, poorly developed sedimentary features (flaser bedding, ripple laminations, cross laminations, bioturbation, and haloturbation), and the distribution of overlying and underlying anhydrite (Figure 5.27).

Zone 2 consists of gray and red sandstone beds and nodular anhydrite (Figure 5.27A). Zone 2 is considered to be deposited in a mixed eolian and sabkha environment due to the presence of nodular anhydrite, cross-laminations, and moderate to well sorting. The combined distribution of the bottom sabkha and eolian sandstones (Zone 2; Figure 5.27) can be traced throughout the field because of their low gamma ray values (API). These sandstones thicken and completely replace the overlying lagoonal reservoir facies, forming a trap in the western part of the field.

Zone 1 was deposited in a shallow lagoon with variable depth and energy level

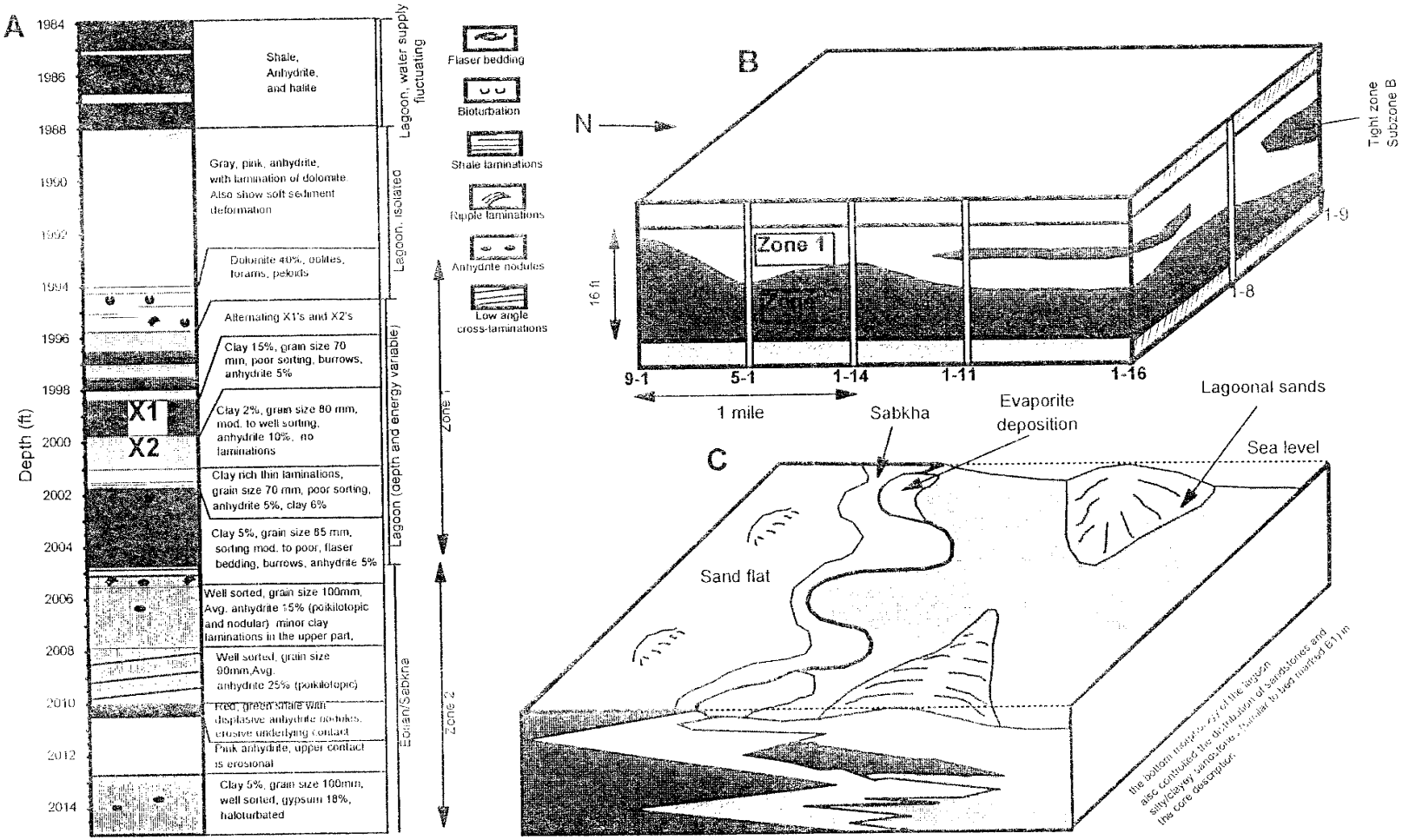

Figure 5.27: (A) Core description along with inferred depositional environments. (B) Block diagram of the Sulimar Queen field showing the distribution of the Zone 1, Zone 2, and low permeability subzone B within Zone 1. (C) Generalized depositional model for the Shattuck Member in the Sulimar and adjacent fields. The interfingering of different environments created the present distribution of the Shattuck Member.

and exhibits flaser bedding, bioturbation, thin shale laminations, and moderate to poor-sorting. For details about the depositional environment, see Chapter 4. Zone 1 (Figure 5.27) lacks evidence of subaerial exposure and sedimentary structures typical of sabkha, fluvial, or eolian environments. The absence of curled clay flakes, clay pebbles, mud cracks with sandy infills, cross-stratification, and channel or flood plain deposits, supports its deposition in a lagoon. Zone 1 grades upward through sandy dolomite into laminated anhydrite assumed to be deposited in a lagoon. This transition was observed in the cores from the Sulimar Queen as well as the adjacent fields. This regional extent of anhydrite points towards deposition in a lagoon instead of local ponds or salinas.

The Shattuck Member in the Sulimar Queen and adjacent fields was deposited in a mixed lagoonal-sabkha-eolian environment. The Sulimar Queen and adjacent fields were formed due to combining effects of lagoon bottom morphology, migration of different depositional environments in response to minor sea level fluctuations, the distribution of lagoonal anhydrite and anhydrite cemented sabkha and eolian sandstone, minor structural features, and, most importantly, the development of secondary porosity.

TRANSIENT PRESSURE TESTS

To determine the spatial variation in permeability, a transient pressure testing was used. Pressure build-up, interference, and an inverse-DST were considered to estimate the permeability of several different wells. Build-up testing was not acceptable because it required very long shut-in periods. A fast and inexpensive inverse-DST procedure was applied that produced results which were confirmed by an interference test.

The lack of reliable spatial permeability data needed to characterize the Sulimar Queen for numerical simulation was a problem. Estimating permeability from pressure build-up tests, utilizing an automatic acoustic fluid level device to record bottomhole pressure, had proved inadequate. As with many fields at the end of their productive life, much of the Sulimar Queen pumping equipment had been sold, which limited the use of pressure build-up testing. Additionally, the reservoir pressure was quite low (~900 psi), resulting in low producing rates which require long shut-in periods to reach the radial

flow period.

Build-up and inverse-DST tests gave permeability estimates at the well and a value of skin. The build-up testing procedure is well known, but the inverse-DST operation is not common in petroleum literature. Hydrologists call this method "slug testing." Ferris and Knowles (1954) with the US Geological Survey, originated the idea of slug testing. Earlougher and Kersch (1974) introduced the concept to the oilfield with their logarithmic-type curve for short-time transient testing. Ramey and Agarwal (1975) refined the idea by applying it to drill stem testing. They developed a semi-log type curve that seemed applicable to the Sulimar Queen problem.

Figure 5.28 shows a typical drill stem test. Point *A* is the hydrostatic pressure on the gauge prior to opening the tool to flow the well. This results in a decrease in pressure to Point *B*. In the inverse-DST, pressure at A is prior to loading the hole, or P_0 in Equation (4):

$$P_D = \frac{P_{wf} - P_0}{P_i - P_0} \tag{4}$$

where P_D is the dimensionless pressure and P_{wf} is the flowing borehole pressure. In a slug test, the pressure increase is due to loading the hole with water to an imposed pressure, P_i in Equation 4. From Point *B* to Point *C* in the DST, the pressure increases due to closing of the tester valve. The pressure, P_{wf}, in Equation 4, decreases with time when loading the hole with water is stopped. Thus, the name inverse-DST, rather than slug test, is appropriate for oilfield work. The Ramey and Earlougher type curve analysis only applies when the well does not flow to the surface during a DST. In a similar manner, surface pressure is not appropriate when loading a well with water during an inverse-DST.

The first Sulimar Queen inverse-DSTs were conducted at the injection Well 1-2 and the producing Well 1-16 on April 29, 1994. A hot oil truck was used to load

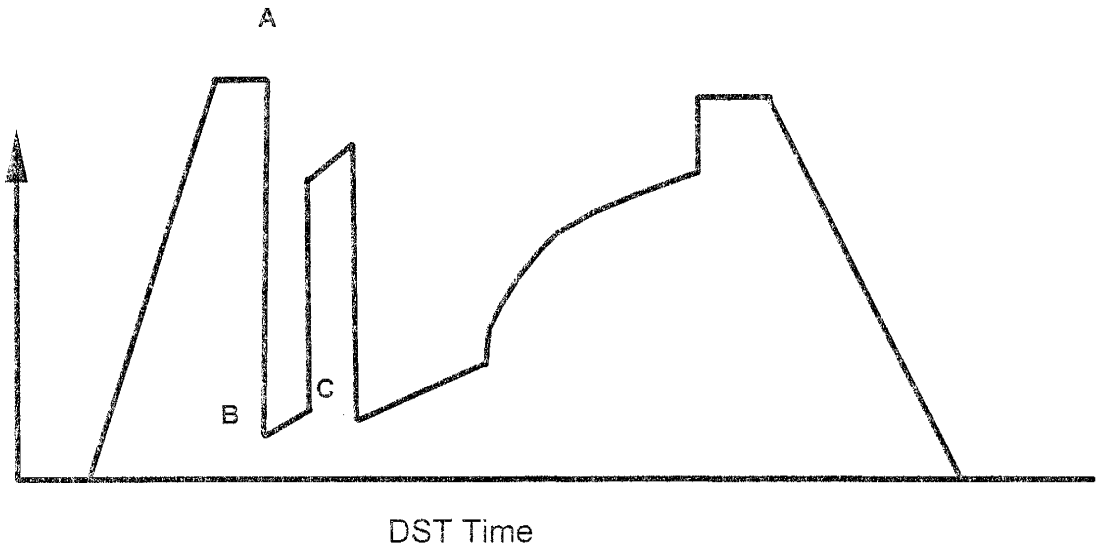

Figure 5.28: A typical drill-stem test.

Well 1-16 with fresh water and an automatic acoustic fluid level device was used to record the bottomhole pressure. The dimensionless pressure versus the pressure decline time for Well 1-16 is presented as a semi-log plot (Figure 5.29). This plot was matched to the type curve presented by Ramey *et al.*, (1975). From the match points, the permeability was found to be 13.3 md.

The permeability value obtained from the transient testing provided the initial guess for the average permeability used in simulation grid blocks for history-matching purposes. This value also supported the values obtained from core analyses.

GLOBAL INTEGRATION IN A BLACK OIL RESERVOIR MODEL

Integrating the descriptive reservoir data from the outcrop study, petrographic analyses, and the field tests with the dynamic production history was achieved by automatically history-matching the field primary performance on a well-by-well basis. An innovative approach to automatic history-matching involved developing correlations for scale-up of the small-scale log and core properties to grid block size. A depth-to-free-gas saturation correlation was developed that indicated the presence of a gas cap. The variables in the correlating equations were estimated using a global optimization technique to match the primary gas and water producing rates. The flow equations were constrained with the oil rate, which is the most precisely measured among the dynamic data. After deriving the reservoir model that honors primary production, the secondary performance was forecast and compared to the actual history. A reasonable agreement between forecast and actual secondary performance attested to the reliability of the developed model.

After rescaling the old-style gamma ray logs and using a porosity-gamma ray correlation derived from the Well 1-16 core, it was possible to quantify the characterization of the Sulimar Queen. Geological examination of the cores and outcrops and reservoir engineering observations led to the distinction between two major flow units: the upper producing sand and the bottom anhydrite-cemented sands. Hence, as an initial geological model, a two-layer system representing the two flow units was

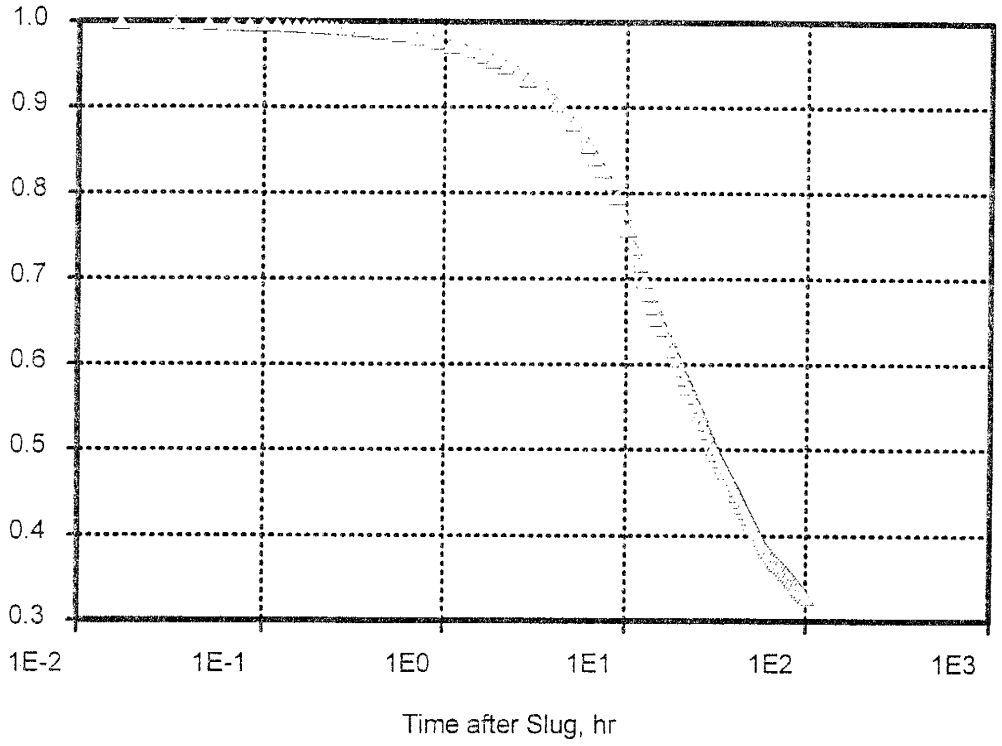

Figure 5.29: Dimensionless pressure versus time.

established. A grid of 3,000 horizontal blocks was constructed. The block size was 200 feet x 200 feet.

The process of rescaling also improved the log signatures for detecting the anhydrite sequences bounding the pay sand, which helped in delineating the sand thickness and the top of the structure for the 36 wells present in the field. Once the top of the structure was accurately identified in all the wells, inverse-distance weighting method was applied to obtain the top of the structure (Figure 5.30).

From the gamma ray logs, porosity logs were derived at each well using the porosity-gamma ray correlation. The structural top of the Queen was chosen by using a 6% cut-off value for the porosity below the overlying anhydrite layer. The separation between the first layer (productive sand) and the second layer (tight sand) was picked at each well location, using a marker from the porosity log. Based on this criterion, the Sulimar Queen presented three different possibilities. In the east the reservoir thins but includes mainly productive sand. In the west, the reservoir is thick, but the entire thickness is occupied by tight sands. In the middle of the reservoir, both productive and tight sand coexist in different proportions (Figure 5.31). These variable thicknesses were mapped through the reservoir and used as input in the reservoir model.

After defining the volume of the reservoir, rock properties needed to be assigned to each gridblock. The average porosity for each layer (Zone 1 & Zone 2) was obtained by using a simple arithmetic average of the porosity logs obtained using the relationship developed between core and gamma ray log data in Well 1-16. At this stage, two porosity values, one for Zone 1 and one for Zone 2, were available at each well location. The inverse-distance weighting method was used to estimate the spatial distribution of porosity in the lateral direction for each layer. Other mapping techniques were tried, including geostatistical mapping, but the resulting realizations proved inaccurate. Additionally, the simulation of the Sulimar Queen required the spatial distribution of permeability, and gas and water saturation. The permeability was assumed to be correlated to porosity by a power function, based on analysis of the core and well test

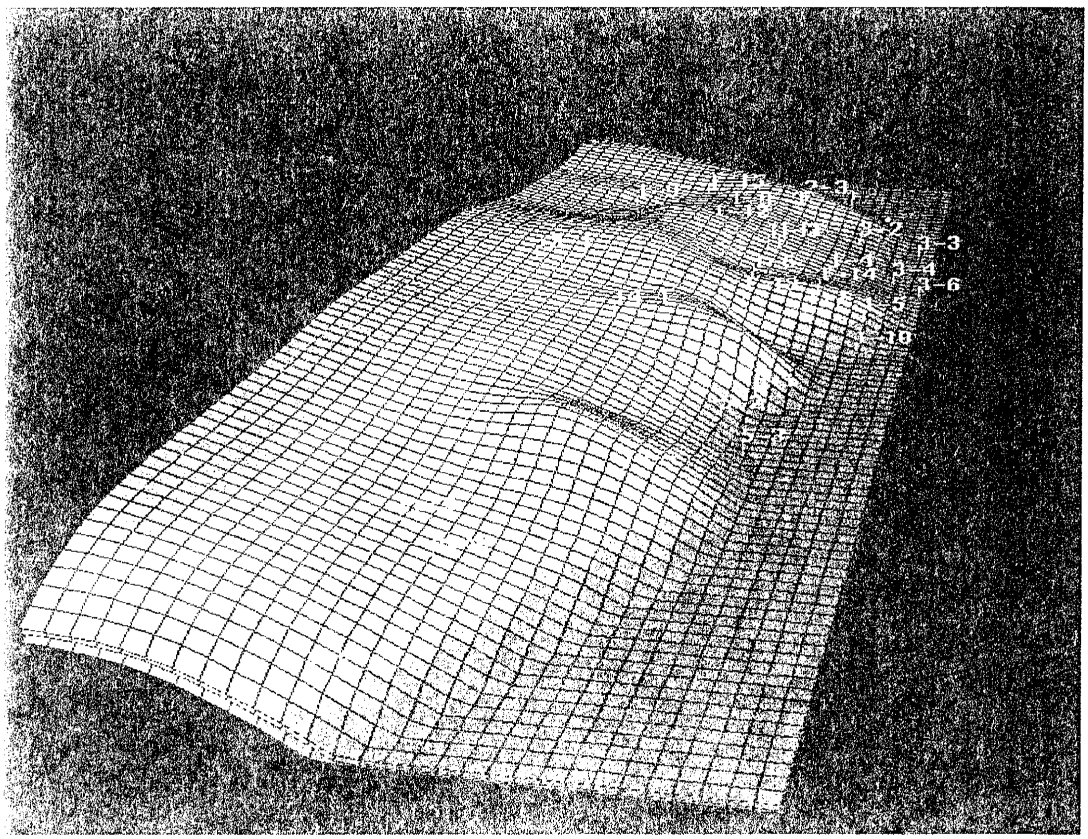

[illegible] se-distance
[illegible]

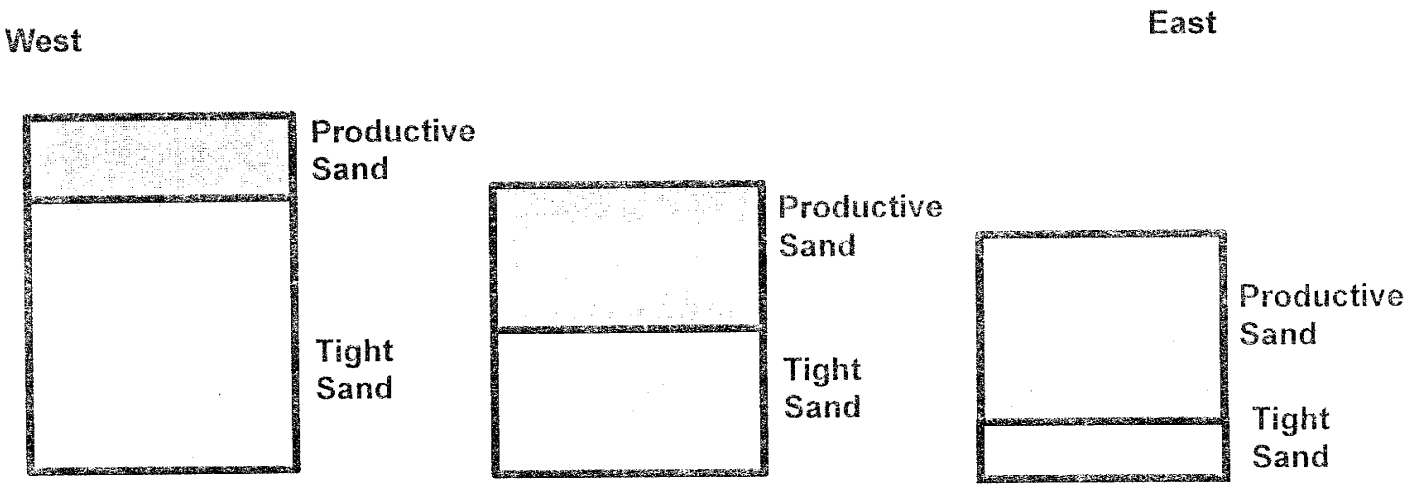

Figure 5.31: Variation of Shattuck Member reservoir thickness along the West-East direction.

data:

$$k = exp^{(A \cdot \phi - B)} \quad (5)$$

Each layer had its own k-ϕ correlation, which required the estimation of four correlation parameters *A* and *B* in Equation 5; *A1* and *B1* for Zone 1 (reservoir zone) and *A2* and *B2* for Zone 2 (non-reservoir zone). The initial guesses for the parameters included in the k-ϕ correlations were derived by using the average porosity and the permeability values estimated during the study. These initial values were adjusted by an automatic history-matching process along with other unknown reservoir properties. The initial and final *A's* and *B's* for Zone 1 and 2 are given in Table 5.4. Permeability maps generated using the initial and final *A's* and *B's* are shown in Figures 5.32 and 5.33. In Zone 1 the initial *A* and *B* gave higher permeability than the final *A* and *B* (Figure 5.32). Automatic history-matching process adjusted the initial *A* and *B* which provided the acceptable permeability values as well as the best production match. There are similarities in the permeability distribution pattern and the ranges between the initial and final maps (Figures 5.32 & 5.33). This suggest, that the initial permeability determined using the gamma ray log derived porosity are also reliable and that the automatic-history matching process did not have to change the permeability considerably. Permeability maps generated using the initial and final *A's* and *B's* for Zone 2 are shown in Figure 5.33.

The advantages of this approach are:

- The geology is honored by considering the k-ϕ relationships in each of the lithofacies.
- The number of reservoir unknowns is reduced by using the correlations. Instead of estimating 6000 values of permeability, we only estimate four correlation parameters
- The permeability provided by the correlation is at the gridblock scale and hence

	Initial A	Initial B	Final A	Final B
Zone 1 (reservoir zone)	0.35	2.00	0.33	2.20
Zone 2 (non-reservoir zone)	0.10	3.50	0.23	3.40

Table 5.4: Comparison of initial and final A's and B's used in Equation 5. These values were used in Equation 5 to generate the permeability distribution.

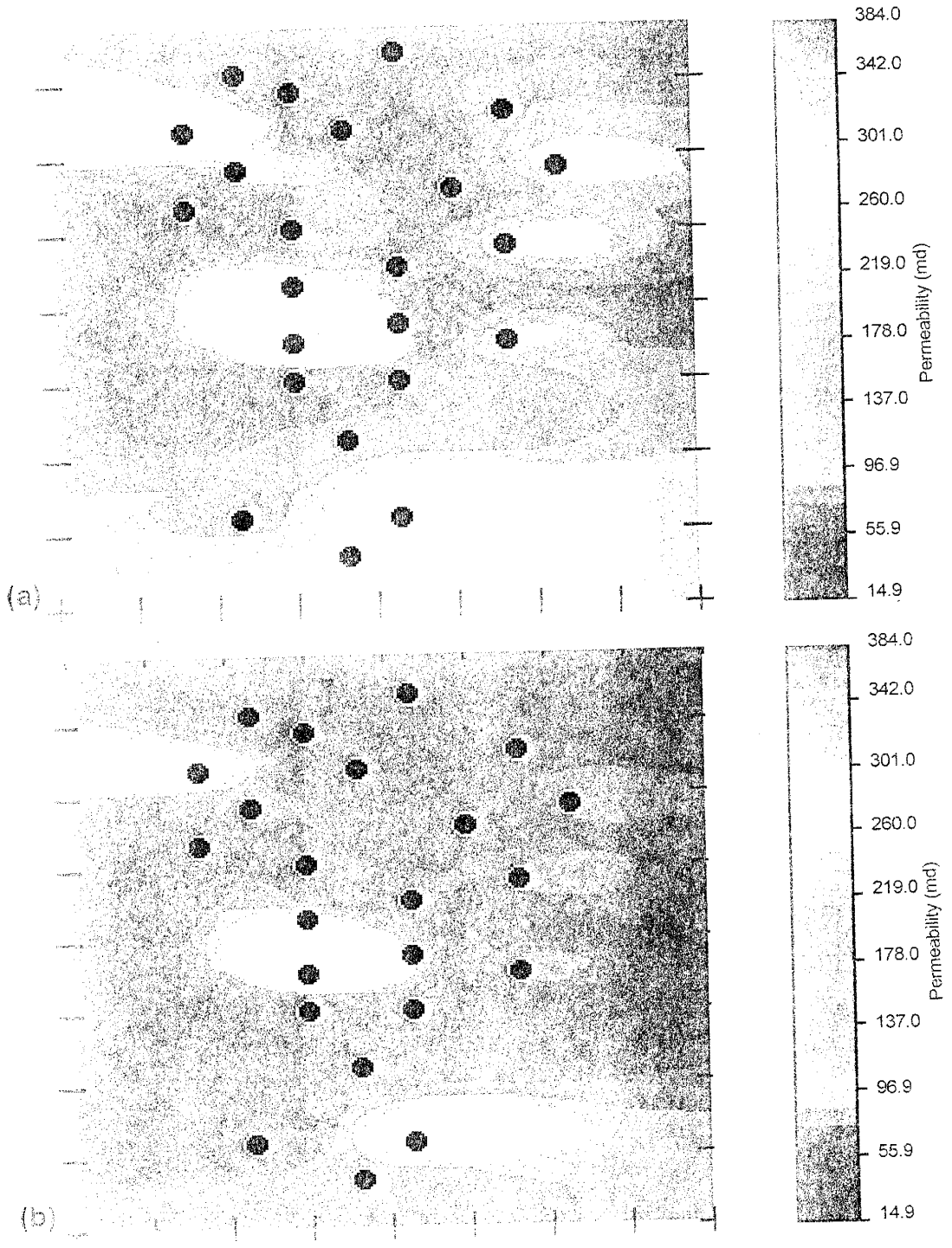

Figure 5.22: Comparison of permeability maps of Zone 1 (reservoir zone) generated using the initial values A1 and B1 (a) and the final values A1 and B1 (b) in [illegible] maps generated using A1 and B1 (a) show higher permeability than [illegible]

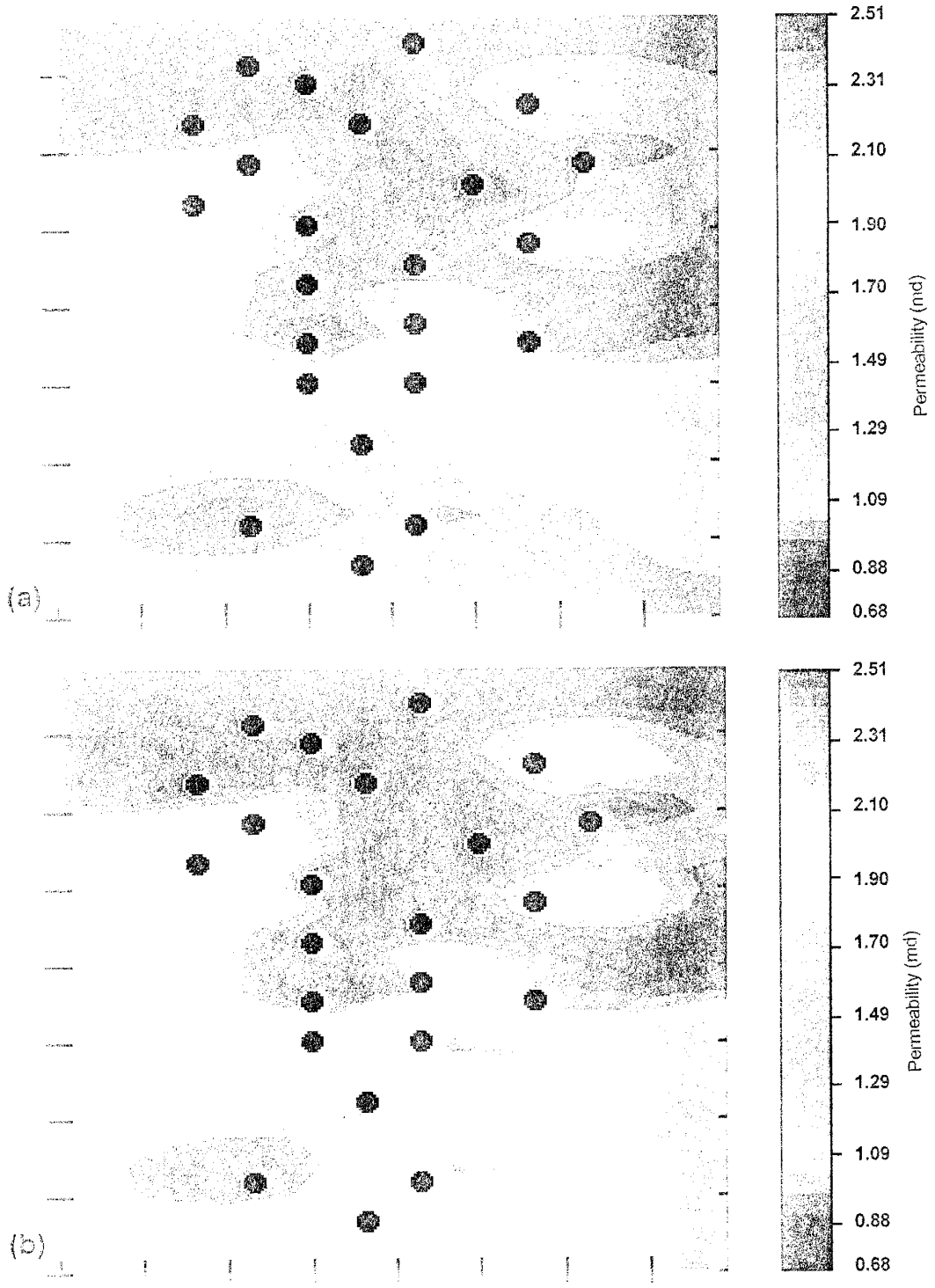

Figure 5.33: Comparison of permeability maps of Zone 2 (non-reservoir zone) generated using initial values A1 and B1 (a) and final values A2 and B2 (b) in Equation [illegible]. Note the significant difference in the permeability between [illegible]

upscaling is avoided.

Permeability is not the only important parameter for the simulation of the Sulimar Queen reservoir. When considering the spatial distribution of the initial GOR, it appeared that the reservoir contained free gas. The result of the initial simulations indicated that there was not enough solution gas to match the large quantities of gas produced. The Sulimar Queen PVT data were not available at the time of preliminary simulations, and the lack of gas was attributed to questionable PVT data from a neighboring field. However, recombined PVT data with Sulimar Queen oil confirmed the low bubble-point pressure and the low amount of dissolved gas.

Since the amount of dissolved gas was not sufficient to produce large quantities of gas from the wells located on the western part of the reservoir, another explanation was required. When examining the initial GOR of the wells, it appeared that the wells located on the structural high had a GOR from 3,000 to 13,000, while the wells downdip had a GOR of around 300. These observations led to the conclusion that free gas existed high on the structure. Therefore, an unique gas saturation distribution was necessary to simulate the large volume of gas produced. Since there is a direct relation between gas saturation and depth, a correlation between these two variables was assumed:

$$S_g = C * depth - D \tag{6}$$

The coefficients C and D were estimated by automatic history-matching. Finally, the water saturation distribution was assumed to be straightforward. In the eastern part of the reservoir where water-oil contact was observed, the water saturation was set to 80%; elsewhere it was set to 30%, the connate water saturation. The reservoir simulator also required flow functions. Corey-type relative permeability curves were used for each layer. The initial curves used to start the history-matching process were similar to those obtained in laboratory experiments. The end-points and exponents of the relative permeability curves were adjusted during the automatic history-matching process. The

final reservoir model was obtained by adjusting the parameters used in the various correlations.

Automatic History-Matching

The various field and laboratory data need to be ultimately integrated with a reservoir simulator. The scale of the reservoir data is dictated by the size of the grid blocks. Selecting proper grid block size requires balancing the need for detailed reservoir description with the need for practical computation times. A very fine geological description that takes into account the thin section core description will lead to prohibitive run-time. In the case of the Sulimar Queen the horizontal grids were sized at 200 feet x 200 feet. These block dimensions resulted in 6,000 grid blocks for the system, which established the final reservoir scale for modeling. An accurate reservoir model must honor all available field data, and most importantly, the production history. Most reservoir properties are not measured at the grid block size; hence, it is necessary to develop innovative ways to estimate the unknowns at the 200 foot scale. This objective was achieved by using automatic history-matching. There are a number of challenging aspects to this task which required extensive research. Two different research directions were explored.

Multiple workstations facilitated the distribution of the optimizing process by increasing the solution speed. The practical aspects of implementing distributed processing have been described by Ouenes *et al.*, (1995). It was determined that this approach requires a high level of expertise in distributed computer systems, mathematical optimization, and reservoir simulation. The feasibility of the concept was demonstrated, but current technology does not permit wide and routine use of such systems. In this approach a message-passing PVM algorithm is required. However, another implementation of the multiple workstation concept was accomplished in this study without the message-passing software. This method relies on remote copying of history-matching files from one workstation to another using the simple UNIX **rcp** protocol.

Another way to achieve faster history-matching is to choose an efficient optimization algorithm. The history-matching process of multiphase flow in porous media is plagued with the local minima problem. Most conventional optimization methods fail to produce a set of reservoir parameters that provide a good match to the real field spatial production history and reservoir pressure. As a result, a stochastic optimization method was tested as a means of escaping the local minima. The large number of unnecessary trials and iterations to reach a satisfactory history-match posed a problem in the application of the stochastic methods. Since each iteration includes one run on the simulator, which can consume from a few minutes to a few hours of computer time, reaching the optimal solution can be expensive. Fortunately, these methods employ algorithms which are entirely automatic and the iterations are performed without user intervention.

History-Matching Primary Production

The Sulimar Queen primary performance was automatically history-matched using the simulated annealing method (Ouenes *et al.*, 1994). Using a black oil model run on a HP 9000-735 workstation, one iteration of the 41-month primary producing period required 20 minutes. Each iteration required the estimation of 42 parameters, four for the k-ϕ correlations, two for the free gas calculation, 16 to estimate the relative permeability curves, and 20 skin value estimates at the producing wells. A reasonable match of the 20 wells was achieved after 350 iterations with a cumulative five days of computer time. This computing time does not require any engineering time to adjust the input parameters. For example, in the Sulimar Queen reservoir, core and field tests have shown that the permeability is in the range of 5-50 md. Hence, the history-matching procedure was constrained with data estimates of the properties.

Gas production was the key to matching the primary producing performance of the reservoir. The quality of the match varied from well to well. The field match of the monthly gas rate during primary is shown in Figure 5.34. During the primary producing period very little water was produced and the history-matching results are not illustrated.

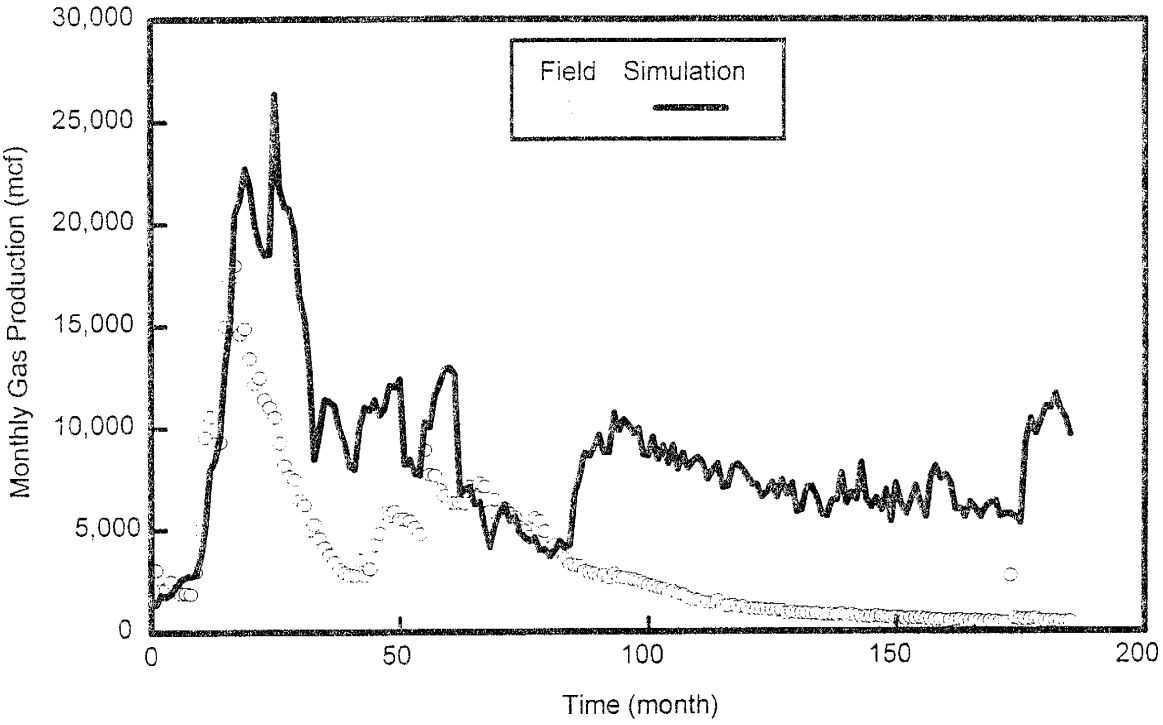

Figure 5.34: Monthly gas production versus time.

Forecasting Secondary Performance

Matching the primary performance led to the estimation of the unknown reservoir parameters and the development of a reservoir model. The reliability of this model was tested by forecasting the secondary performance, essentially the water production. Using the model derived by history-matching the primary gas production with the oil production as the constraint, the black oil simulator provided a forecast of the water monthly rates from 1972 to 1983 (Figure 5.35).

The accuracy of the forecast of water production corroborates the validity of the conditioned model and reservoir parameters. Among these parameters are the mixed-wet relative permeability curves (Figure 5.36), derived by history matching primary performance. Although the primary and secondary mechanisms are completely different, the relative permeability curves derived during primary-matching did provide a good estimate of water production during secondary recovery. The water relative permeability end-point at residual oil saturation was k_{rw}=0.25, which was supported by both the laboratory corefloods and the field tracer tests. This result demonstrates the mixed-wet nature of the Sulimar Queen reservoir.

Since water production during secondary recovery was very sensitive to the water relative permeability curve, two other end-points were tested to simulate the waterflood. The oil-wet and water-wet relative permeabilities curves (Figure 5.36) were used as input to the black oil simulator. The resulting forecast for water production (Figure 5.37) confirms that the mixed wettability curves are the most probable. Average reservoir properties from the history-matched reservoir are presented in Table 5.5.

CONCLUSIONS

In this study, new techniques were applied for improving the quantity and quality of data for better reservoir characterization of old fields. A successful characterization of the Sulimar Queen field was accomplished starting with a meager data set.

A combination of minipermeameter and petrographic analysis allowed the collection of large amount of petrographic data using fewer thin sections and therefore

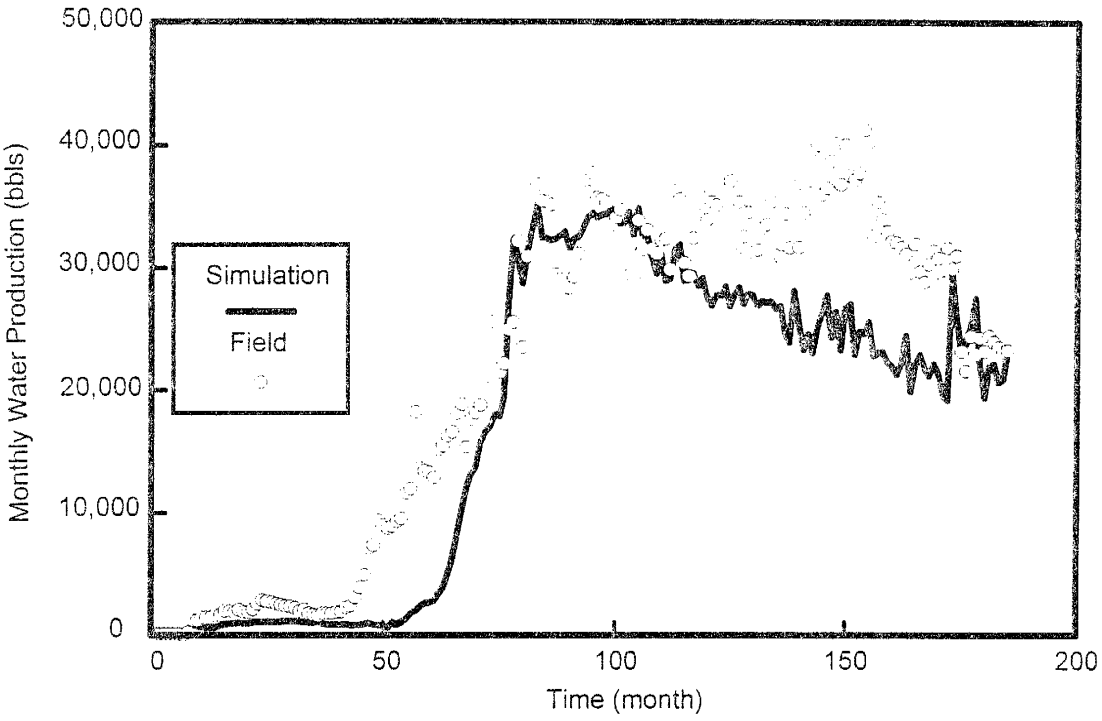

Figure 5.35: Monthly water production versus time.

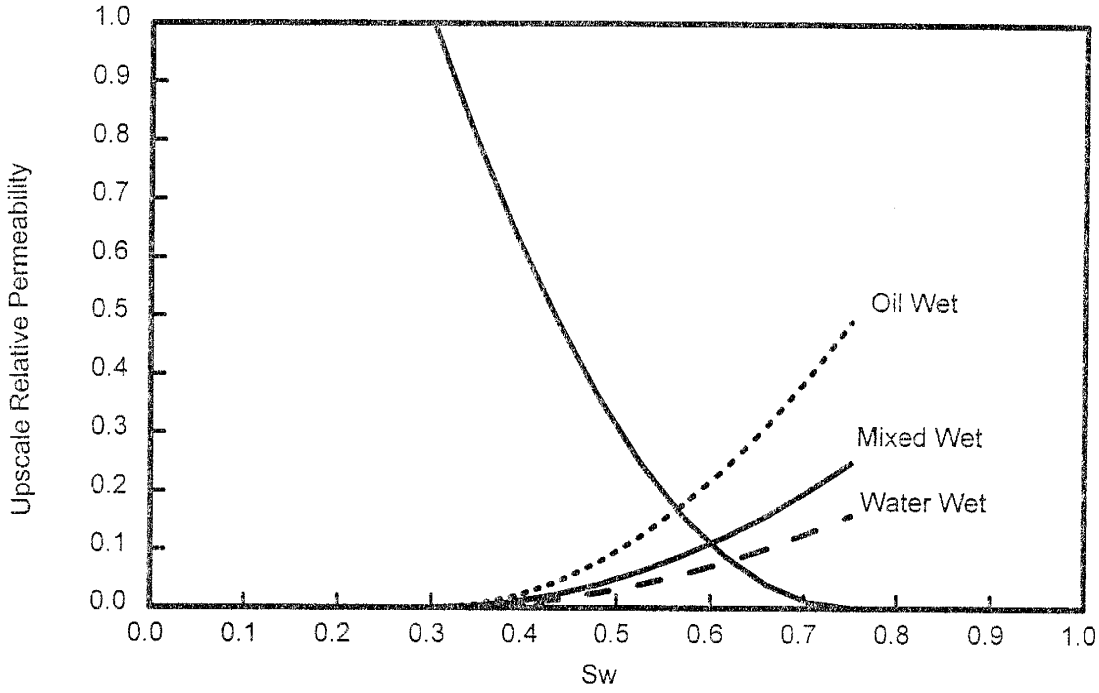

Figure 5.36: Field-scale relative permeabilities.

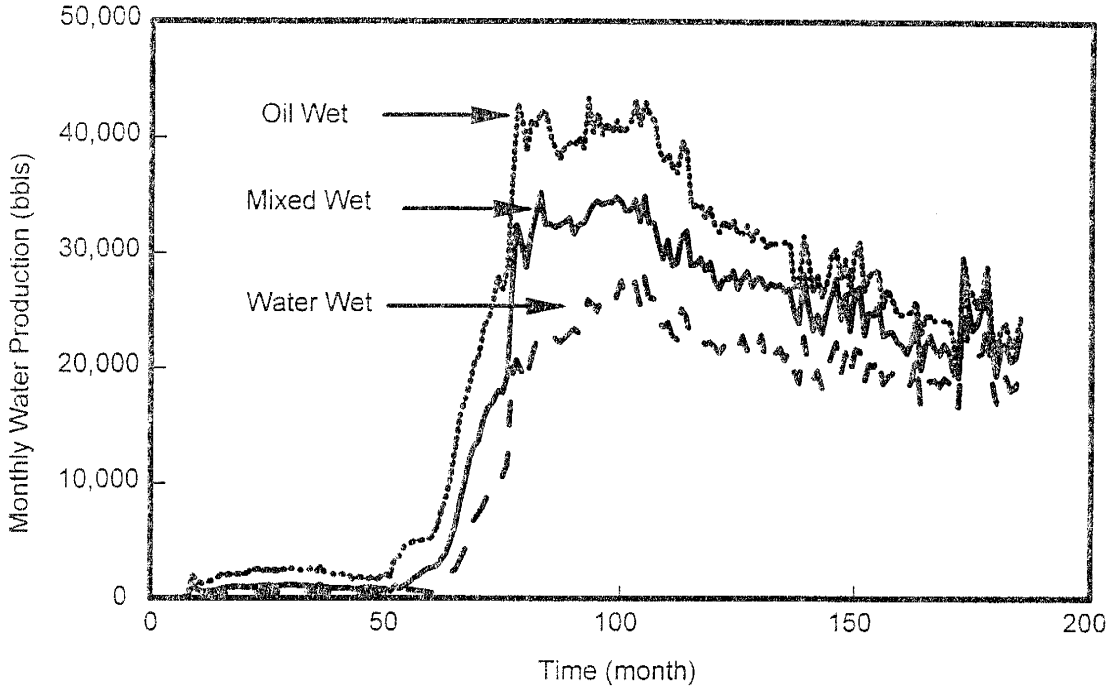

Figure 5.37: Effects of field-scale water relative permeabilities on waterflood forecast.

Sulimar Queen Field: Chaves County, New Mexico		
840 Productive Acres		
Permian Age		
	Before Study	**After Study**
Depositional Environment	Back-Reef Shelf "Lagoonal" Sand	Lagoonal-Sabkha-Eolian
Sandstone	Fine-Grained sandstone	Very fine to fine-grained
Trap	Stratigraphic Trap	Stratigraphic +Minor Structural
Depth	2,000 ft	Same
Well Spacing	~40 Acres	Same
Average Thickness	8 ft	8.5 ft
Permeability	150 md	5 - 50 md
Porosity	20%	20 %
Paraffinic Oil	36° API	Same
Oil Viscosity	4.0 cp @ 113 °F	Same
Connate Water Saturation	34%	30% in Oil Zone 80 % Down Dip
Original Oil in Place	6..3 million Barrels	7.8 Million Barrels
Primary and Secondary Recovery	2.2 Million Barrels	Same
Current Average Oil Saturation	39%	Same

Table 5.5: Parameters of the Sulimar Queen characterization.

helped to conserve valuable core material. This technique is easy to apply and better than the conventional core plug analysis in identifying small-scale heterogeneities, which are important during secondary and tertiary recovery.

A newly developed fuzzy logic algorithm and a neural network were used to establish the ranking of petrographic elements in controlling the permeability and prediction of permeability, respectively.

The control of different petrographic elements on permeability was easily and accurately determined using the newly developed fuzzy logic algorithm. The fuzzy logic algorithm is fast, unbiased and reliable method for establishing the importance of each petrographic element on permeability. Neural networks are fast and reliable tools for predicting permeability using several petrographic elements. A neural network was successfully used to predict permeability in the adjacent South Lucky field.

The rescaling of the old gamma ray logs using the Barrett (1994) technique improved their reliability. In the Shattuck Member, porosity, permeability, and water saturations could be estimated using the gamma ray logs. Rescaling also improved the mapping of the structure and net sand distribution in the field.

Maximum geological and petrophysical information was gathered from the limited database by combining small-, medium-, and large-scale data obtained from minipermeameter, cores, petrographic analysis, logs, outcrops, and field tests. The distribution of the different zones was mapped successfully in the field and a depositional model was developed. Using this meager data set, a successful characterization of the Sulimar Queen was obtained and confirmed through a good history-match of the primary production and a reasonably accurate forecast of the waterflood performance.

PART IV

CHAPTER 6: SUMMARY AND CONCLUSIONS

There is a need to characterize old reservoirs to evaluate the economics for further development. In order to achieve this, an understanding of reservoir structure and the development of diagnostics to characterize heterogeneities are essential. To date, limited and unreliable data have restricted the detailed characterization of such fields. This dissertation presented the results of a Department of Energy (DOE)—State of New Mexico—funded project to study the "Integration of Advanced Geoscience and Engineering Techniques to Quantify Interwell Heterogeneity in Reservoir Models". This project was proposed along the lines of the "New Mexico Improved Oil Recovery Project" (NMIORP) to maximize U.S. oil production.

An old field—the Sulimar Queen—was acquired for this project. The main objective was to develop a methodology to characterize old fields with sparse and unreliable data by developing new and modifying existing techniques. This required an integration of geologic, petrophysical, and engineering data for reservoir simulation to quantify reservoir architecture and fluid dynamics.

For the characterization of old fields all data is important and data ranging from micro- to mega-scale should be incorporated in order to build a reliable reservoir model. Data from outcrops and analog fields in the vicinity is also important for the characterization of old fields in case the available data is not reliable. Unconventional approaches need to be applied to solve the problem at hand.

There is no proven methodology available in the industry for the characterization of old fields. *An objective of this study was to propose such a methodology for the characterization of old fields with limited and unreliable data.*

GENERAL CONCLUSIONS

A successful characterization of the Sulimar Queen field was achieved by increasing the quality and quantity of the data through developing new techniques and modifying the existing ones.

Maximum geological and petrophysical information was extracted by integrating small-, medium-, and large-scale data gathered from minipermeameter, petrographic analysis, cores, logs, analogous fields, outcrops, and field tests. Two main zones with their particular petrophysical parameters were identified in the reservoir and their distribution in the field was mapped. A detailed geologic model was developed for the Shattuck Member in the Sulimar Queen field and adjacent area.

Using this data, a successful characterization of the Sulimar Queen field was obtained and confirmed through a good history-match of the primary production and a reasonably accurate forecast of the waterflood performance.

The methodology developed here can be applied to other fields producing from the Shattuck Member in the southeast New Mexico because of the similarities observed during this study.

SIGNIFICANT CONTRIBUTIONS

(1) New Technique of Collecting Petrographic Data

The combination of minipermeameter and petrographic analysis is easy and more accurate than using the conventional core plugs to determine the control of petrographic elements on permeability. It allows the sampling of the whole permeability range without destroying the core, which again is not possible using the conventional core plugs. This method also allows the collection of large quantities of petrographic data directly related to permeability with fewer thin sections, thus enabling the geologist to improve the quality and quantity of petrographic data. The control of depositional environment and diagenesis on porosity and permeability evolution can also be determined easily. Valuable core material can be conserved using this technique and, therefore, it is more

useful in old fields where cores are scarce.

(2) Fuzzy Logic Analysis to Establish the Ranking of Petrographic Elements in Controlling Permeability

Fuzzy logic analysis was used for the first time to determine the ranking of the petrographic elements in controlling permeability. It is faster and more quantitative than conventional regression analysis; therefore, it is better than the conventional regression analysis, especially when a large set of variables is involved. In this study sixteen petrographic elements were collected for each permeability measurement.

When permeabilities are to be predicted using the petrographic elements, it is important to use only the most influential elements. Otherwise the noise may lead to wrong predictions. The ranking obtained using fuzzy logic analysis was used during permeability prediction using the neural networks.

(3) Permeability Prediction Using Neural Networks

Neural networks are capable of solving complex nonlinear problems comprising several variables. Based on the ranking obtained from the fuzzy logic analysis, a neural network was used to predict permeabilities in the neighboring South Lucky lake field. The results show that a neural network is a reliable and fast tool for prediction of permeability using petrographic elements. In this study, the focus was to use new unconventional techniques in order to improve the results. For this reason we used fuzzy logic and neural networks instead of conventional multiple regression analysis.

The data used for the training of the network was from Sulimar Queen field. The successful prediction of permeabilities in the neighboring South Lucky field confirmed the assumption of similar regional behavior of the Shattuck Member in the Southeast New Mexico. Therefore, other fields in the southeast New Mexico which are producing from the Shattuck Member can easily be characterized using similar techniques to those developed during this study.

(4) Unconventional Use of Old Logs

Old gamma ray logs were made useful by rescaling them to the same datum using the modern logs (Barrett, 1994). Rescaled gamma ray logs helped to delineate the spatial distribution of the sands in the Sulimar Queen field. For the first time gamma ray logs were used to predict porosity and total water content. Total water content was used instead of conventional water saturation to understand the influence of water dissolved species on gamma ray response.

Similar relationships between gamma ray response and porosity, total water content, and permeability were found in adjacent fields producing from the Shattuck Member. Therefore, similar techniques can be used in other Shattuck Member fields in southeast New Mexico.

(5) Depositional Model

A detailed depositional model was developed based on the information obtained from minipermeameter, petrographic analysis, core analysis, rescaled logs, porosity predicted from logs, and information gathered from the adjacent fields. An outcrop study was conducted to gain information about the dimensions and geometries of the sand bodies, to determine the fluid flow barriers, and to evaluate the spatial distribution of porosity and permeability.

The Shattuck Member was deposited in a mixed lagoonal-sabkha-eolian environments. The Sulimar Queen and adjacent fields were formed by the combined effects of minor sea-level changes shifting the environments, lagoon bottom morphology, the distribution of anhydrite, minor structural features, and finally by the development of secondary porosity.

Based on the depositional model, reservoir simulation was carried out on two layers instead of the previously-assumed three layers. After deriving the reservoir model that honors primary production, the secondary performance was forecast and compared to the actual history. A reasonable agreement between the forecast and actual secondary performance attested to the reliability of the developed model.

(6) Development of Methodology for the Characterization of Old Fields

A methodology for the characterization of old fields was developed by increasing the quality and quantity of data and incorporation of micro- to large-scale data (Chapter 5). This methodology describes: (1) techniques to improve the data quality, (2) unconventional use of logs, (3) new techniques for data analysis and prediction, and finally (4) global integration of all information in a simulator.

FUTURE WORK:

A similar study is being carried out on another old field in the Permian Basin owned by Lynx Petroleum. This field was developed in 1950s and is producing from the Lower Queen Formation (Penrose). In this study, in addition to rescaling of the logs, a neural network is also being used to predict porosity and water saturation.

REFERENCES

Adams, J. E., 1965, Stratigraphic-tectonic development of the Delaware Basin: American Association of Petroleum Geologists Bulletin, v. 49, p. 2140 - 2148.

Aleksander, I., and Morton, H., 1990, An introduction to neural computing: Chapman and Hill, London.

Balls, S. M., Roberts, J. W., Norton, J. A., and Pollard, W. D., 1971, Queen Formation (Guadalupian, Permian) outcrops of Eddy County, New Mexico, and their bearing on recently proposed depositional models: American Association of Petroleum geologists Bulletin, v. 55, p. 1348 - 1355.

Barrett, G. D., 1994, Use of computers to perform old log analysis: SPE Computer Applications, August, p. 9 - 12.

Berner, A. R., 1971, Principles of chemical sedimentology: McGraw-Hill Book Company, New York, 240 pp.

Blackband, S., Mansfield, P., Barnes, J. R., Clauge, A. D. H., and Rice, S. A., 1986, Discrimination of crude oil and water in sand and in bore cores with NMR Imaging, SPE Formation Evaluation, v.1, p. 31 - 34.

Blatt, H., 1982, Sedimentary Petrology: W. H. Freeman and Company, New York, 564 pp.

Bourke, L. T., 1993, Core permeability imaging, its relevance to conventional core characterization and potential application to wireline measurements, Marine and Petroleum Geology, v.10, p. 318 - 324.

Boyd, D. W., 1958, Permian sedimentary facies, central Guadalupe Mountains, New Mexico, New Mexico Bureau of Mines and Mineral Resources bulletin. 40, pp. 100.

Chandler, M. A., Goggin, D. J., and Lake, L. W., 1989a, A field permeameter and analytic procedure for making rapid, nondestructive permeability measurements, Journal of Sedimentary Petrology, v. 59, p. 613 - 615.

Chandler, M. A., Kocurek, G., Goggin, D. J., and Lake, L. W., 1989b, Effects of stratigraphic heterogeneity on permeability in eolian sandstone sequence, Page sandstone, Northern Arizona, AAPG Bulletin, v. 73, p. 658 - 668.

Chawathé, A., Ouenes, A., Weiss, W., and Fant, R., 1997, Predicting unconventional logs from conventional logs using neural networks: In Situ, v. 21, No. 2, p. 145 - 159

Choquette, P. W., and Pray, L. C., 1970, Geologic nomenclature and classification of porosity in sedimentary carbonate: The American Association of Petroleum Geologists Bulletin, v. 54, No. 2, p. 201 - 250.

Collins, D. J., and Thompson, B. D., 1982, Sedimentary structures: George Allen and Unwin, London, 194 pp.

Corbett, P. W. M., and Jenson, J. L., 1992, Variations of reservoir statistics according to

sample spacing and measurement type for some intervals in the lower Brent group, The Log Analyst, v. 33, p. 22 - 41.

Corbett, P. W. M., Jensen, J. L., 1993, An application of small-scale permeability measurements - prediction of flow performance in a Rannoch facies, Lower Brent Group, North Sea, Marine and Petroleum geology, v.10, p. 335 - 346.

Cowan, P. E., and Harris, P. M., 1986, Porosity distribution in San Andres Formation (Permian) Cochran and Hockley Counties, Texas: The American Association of Petroleum Geologists Bulletin, v. 70, No. 7, p. 888 - 897.

Crandall, K. H., 1929, Permian stratigraphy of southeastern New Mexico and adjacent parts of western Texas: Bulletin of the American Association of Petroleum Geologists, v. 13, p. 927 - 944.

Darton, N. H., 1922., Geologic structure of parts of New Mexico: U.S. Geological Survey Bulletin, 726E, 725 pp.

Davis, J. M., Lohmann, R. C., Phillips, F. M., Wilson, J. L., and Love, D. W., 1993, Architecture of the Sierra Ladrones Formation, central New Mexico: Depositional control on the permeability correlation structure, GSA Bulletin, v. 105, p. 998 - 1007.

Deutsch, C. V., and Journel, A. G., 1992, GSLIB: Geostatistical Software Library Users Guide: Oxford University Press, New York, 336 pp.

Dewan, J. T., 1983, Essentials of modern open-hole log interpretation: PennWell Publishing Company, Tulsa, Oklahoma, 361 pp.

Doughty, D., and Tomutsa, L., 1992, NMR Microscopy for fluid imaging at pore scale in reservoir rocks. Joint Society of Core Analysts/Society of Professional Well Log Analysts Symposium, Oklahoma City. SCA paper 9222.

Dryer, T., Scheie, A., and Walderttaugh, O., 1990, Minipermeameter based study of permeability trends in channel sand bodies, AAPG Bulletin, v. 74, No. 4, p. 359 - 374.

Dunham, P. J., 1962, Classification of carbonate rocks according to depositional texture: in Ham, E. W., ed., Classification of carbonate rocks, Memoir 1, American Association of Petroleum geologists, p. 108 - 121.

Dykstra, H., and Parson, L. R., 1950, the prediction of oil by water flood: Secondary recovery of oil in united states, American Petroleum Institute, NY. p. 160 - 174.

Earlougher, R. C., and Kersch, K. M., 1994, Analysis of short-time transient test data by type-curve matching: AIME Transaction, p. 793 - 800.

Eijpe, R., and Weber, K. J., 1971, Minipermeameter for consolidated rocks and unconsolidated sands, AAPG Bulletin, v. 55, p. 307 - 309.

Elliot, T., 1986, Siliciclastic shorelines: in *ed.*, Reading, H. G., Sedimentary Environments and Facies, Blackwell Scientific Publications, p. 155 - 189.

Ferris, J. G., and Knowles, D. B., 1954, The slug testing for transmissibility: U.S. Geological Survey Ground Water Notes, v. 26, p. 1 - 7.

Fischer, A. G., 1988, Airborne silts and dune derived sands in the Permian of the Delaware Basin: Journal of Sedimentary Petrology, v. 58, p. 637 - 643.

Georgi, D. T., Harville, D. G., Phillips, C., and Ostroff, G. M., 1993, Extrapolation of core permeability data with wireline logs to uncored intervals, SPWLA 34th Annual Logging Symposium, June 13 - 16, 1993, p. 1 - 19.

Gibbons, K., Halvorsen, C., and Siring, E., 1993, Vertical and horizontal permeability variation within a sandstone reservoir, Marine and Petroleum Geology, v. 10, p. 325 - 334.

Giles, M. R., and de Bore, R. B., 1990, Origin and significance of redistributional secondary porosity: Marine and Petroleum geology, v. 7, p. 378 - 397.

Glennie, K. W., 1970, Desert sedimentary environments: Developments in Sedimentology, v. 12, Elsevier, Amsterdam, 222 pp.

Goggin, D. J., Thrasher, R. L., and Lake, L. W., 1988a, A theoretical and experimental analysis of minipermeameter response including gas slippage and high velocity flow effects, In Situ, v. 12, p. 79 - 116.

Goggin, D. J., Chandler, M. A., Kocurek, G., and Lake, L. W., 1988b, Patterns of permeability in eolian deposits, Page Sandstone (Jurassic), north Arizona, SPE Formation Evaluation, v.3, p. 297 - 306.

Goggin, D. J., Chandler, M. A., Kocurek, G., and Lake, L. W., 1989, Permeability transects in eolian sands and their use in generating random permeability fields, Society of Petroleum Engineers, 19586.

Gautier, D. L., 1985, Interpretation of early diagenesis in ancient marine sediments, *in* Gautier, D. L., Y. K. Kharaka, and R. C. Surdam, *eds.*, Relationship of organic matter and mineral diagenesis, Short Course No. 17; Society of Economic Paleontologists and Mineralogists, p. 6 - 72.

Halvorsen, C., and Hurst, A., 1990, Principles, practice, and applications of laboratory minipermeameter, in Worthington, P. F., ed., Advances in core evaluation, Accuracy and precision in reserves estimates, Gordon and Breach Science Publishers, NY, p. 521 - 549.

Halvorsen, C., 1993, Probe permeametry applied to a highly laminated sandstone reservoir, Marine and Petroleum Geology, v.10, p. 347 - 351.

Hanford, R. C., 1988, Depositional interaction of siliciclastic and marginal marine evaporites: Schreiber, C. B., *ed.*, Evaporite and hydrocarbons: Columbia University Press, New York, p. 139 - 181.

Haykin, S., 1994, Neural networks: A comprehensive foundation: Macmillan College Publishing company, New York, 696 pp.

Heller, J. P., 1992, The PRRC Automatic Scanning Minipermeameter: PRRC report No. 92 - 20, New Mexico Institute of Mining and Technology, 14 pp.

Hilchie, D. W., 1982, Applied openhole log interpretation for geologists and engineers, Douglas W. Hilchie Inc., Golden Colorado.

Hurst. A., and Goggin, D. J., 1995, Probe permeametry: An Over view and bibliography, AAPG Bulletin, v. 79, no. 3, p. 463 - 473.

Hurst. A., and Rosval, K. J., 1991, Permeability variations in sandstones and their relationship to sedimentary structures, in Larry, W. Lake., Herbert, B. Carrol, Jr., and Thomas, C. Wesson., eds., Reservoir Characterization II, Academic Press,

Inc. p. 166 - 196.
Jacka, A. D., and Franco, L. A., 1974, Deposition and diagenesis of Permian evaporites and associated carbonates and clastics on shelf area of the Permian Basin: Fourth Symposium on Salt, v. 1, Northern Ohio Geologic Society, Cleveland, Ohio, p. 67 - 89.
Jackson, Susan., Chang, Ming. Ming., and Tham Min., 1993, Data requirements and acquisition for reservoir characterization: DOE Report No. DE-FC22-83FE60149, IIT Research Institute, National Institute for Petroleum and Energy Research, 26 pp.
Jacobsen, T., and Randel, H., 1991, Permeability patterns in some fluvial sandstones. An outcrop study from Yorkshire, northeast England, in L. W. Lake., H. B. Carrol, Jr., and T. C. Wesson., eds., Reservoir Characterization II: San Diego, Academic Press, Inc., p. 315 - 338.
Journel, A. G., and Huijbergts, Ch. J., 1978, Mining geostatistics: Academic Press, New York, 600 pp.
Journel, A. G., 1989, Fundamentals of geostatistics in five lessons: American Geophysical Union, v. 8.
Kendall, C. G. A. C., 1969, An environmental re-interpretation of the Permian evaporite/carbonate shelf sediments of the Guadalupe Mountains: Geological Society of America Bulletin, v. 80, p. 2503 - 2526.
Kendall, C. G. A. C., and Warren, K. J., 1988, Peritidal evaporites and their sedimentary assemblages: *in* Schreiber. C. B., ed., Evaporites and hydrocarbons; Columbia University Press, New York, p. 66 - 138.
Kerr, D. R., Scott, A. R., Grisby, J. D., and Levy, R. A., 1991, Minipermeameter study of fluvial deposits of the Frio Formation (Oligocene) south Texas: Implications for gas reservoir compartments, in Third International Reservoir Characterization Conference, Tulsa, Oklahoma, Nov. 3 - 5, 1991, Technical papers, 3RC-55.
Kerr, D.S., and Thomson, A., 1963, Origin of nodular and bedded anhydrite in Permian shelf sediments, Texas and New Mexico: American Association of Petroleum Geologists Bulletin, v. 47, p. 1726 - 1732.
Kitteridge, M. G., Lake, L. W., Lucia, F. J., and Fogg, G. E., 1990, Outcrop/subsurface comparisons of heterogeneity in the San Andres Formation, SPE Formation Evaluation, v. 5, p. 223 - 240.
Kosko, B., and Isaka, S., 1993, Fuzzy Logic: Scientific America, July 1993, p. 76 - 81.
Lin, Yinghua., 1994, Input identification of Modeling with fuzzy and neural systems: Ph.D., Dissertation, New Mexico Institute of mining and Technology, Socorro, New Mexico, pp. 89.
Malisce, A., and Mazzullo, J., 1990, Reservoir properties of the desert Shattuck Member, Caprock field, New Mexico: in eds., Barwis, J. H., McPherson, J. G., and Studlick, R. J., Sandstone Petroleum Reservoirs: Springer-Verlag, New York, p. 133 - 152.
Martin, D. F., and Weiss, W. W., 1991, Planning phase for the New Mexico Improved oil recovery project: PRRC Report No. 91-19, 40 pp.

Martin, D. F., Buckley, J., Weiss, W. W. and Ouenes, A., 1996, Integration of advanced geoscience and engineering techniques to quantify interwell heterogeneity, Quarterly Technical Report submitted to DOE under contract no. DE-AC22-93BC14893.

Martin, H., and Naes, T., 1989, Multivariate calibration: John Wiley and Sons Ltd., p. 119 - 125.

Mazzullo, J. M., Williams, M., and Mazzullo, S. J., 1984, The Queen formation of Millard Field, Pecos county, Texas: Its lithologic characteristics, environment of deposition, and reservoir petrophysics: Transactions southwest section American Association of Petroleum Geologists, publication 84-78, p. 103 - 110.

Mazzullo, S. J., Mazzullo, J. M., and Harris, P. M., 1985, significance of quartzose sands on emergent carbonate shelves: Permian of west Texas - New Mexico (abs.): American Association of Petroleum Geologists Bulletin, v. 69, p. 284.

Mazzullo, S. J., and Hendrick, C. L., 1985, Road log and locality guide, lithofacies, stratigraphy, and depositional models of the back-reef Guadalupian section (Queen, Seven Rivers, Yates, and Tansill Formations), SEPM Field Guidebook, p. 1 - 30.

Mazzullo, S., and Carrol, H., 1985, Road Log, Day One - Back-Reef Facies, in Cunningham, B., Hendrick, C, L., and Beard, C., eds., Permian carbonate/clastic sedimentology, Guadalupe Mountains: Analogs for shelf and basin reservoirs, Annual Field Trip Guide Book, April 18, 19, & 20, Road Logs and Locality Guides: Permian Basin Section SEPM Publ. 85-24.

McKee, E. D., 1966, Structures of dunes at White Sands National Monument, New Mexico (and a comparison of structures of dunes from other selected areas). Sedimentology, v. 7 p. 1 - 69.

Meissner, F. F., 1972, Cyclic sedimentation in Middle Permian strata of the Permian Basin, west Texas and New Mexico: West Texas Geological Society Publication, 72 - 60, p. 203 - 232.

Møller, M. F., 1994, A scaled conjugate gradient method algorithm for fast supervised learning: Neural Networks, v. 6, p. 525 - 533.

Moran, W. R., 1954, Proposed type sections for the Queen and Grayburg Formations of Guadalupe age in the Guadalupe Mountains Eddy County, New Mexico (abs.): Geological Society of America Bulletin, v. 65, p. 1288.

Neashan, T. W., 1977., The morphology of dispersed clay in sandstone reservoirs and its effects on sandstone shaliness, pore space, and fluid flow properties: Society of the Petroleum Engineers of the AIME, Denver, SPE Paper 6858.

Newell, N. D., Rigby, J. K., Fischer, A. G., Whiteman, A. J., Hickox, J. E., and Bradley, J. S., 1953, The Permian reef complex of the Guadalupe Mountain region, Texas and New Mexico - A study in paleoecology: San Francisco, W. H. Freeman and Co., 236 pp.

Nocklods, R. S., Knox, O'B. W. R., and Chinner, A. G., 1978, Petrology for students: Cambridge University Press, London, p. 219 - 242.

Ouenes, A., Weiss, W. W., Sultan, A., And Anwar, J., 1995, Parallel reservoir automatic history-matching using a network of workstations and PVM: SPE Paper No. 29107.

Ouenes, A., Bhagavan, A., Bunge, S., and Travis, B. J., 1994, Application of simulated annealing and other global optimization methods to reservoir description: Myths and realities: SPE Paper No. 28415.

Pirson, S. J., 1963, Handbook of well log analysis: Prentice-Hall, Inc, Englewood Cliffs, N.J., 326 pp.

Pray, L. C., 1977, The all wet, constant sea level hypothesis of Upper Guadalupian, shelf and shelf edge strata, Guadalupe Mountains, New Mexico and Texas: West Texas Geological Society, Special Publication 77 - 16.

Pryor, W. A., 1973, permeability and porosity pattern and variations in some Holocene sand bodies, AAPG Bulletin, v. 57, p. 162 - 189.

Ramey, H. J., Agarwal, R. G., and Martin, I., 1977, Analysis of slug test or DST flow period data: JPET (July - Sept. 1975), p. 37 - 42.

Rider, M. H., 1986, The geological interpretation of well logs: John Wiley and Sons, New York, 175 pp.

Robertson, G. M., and McPhee, C. A., 1990, High resolution probe permeability: an aid to reservoir description, in Worthington, P. F., ed., Advances in core evaluation, accuracy and precision in reserves estimates, Amsterdam, Gordon and Breach Publishers, p. 495 - 520.

Rumelhart, D. E., and McClelland, J. L., 1986, Parallel distributing processing, Volume 1: Foundations, MIT Press, Cambridge, MA.

Sarg, J. F., 1977, Locality Guides, Stops VI, VII, VIII, Rocky Arroyo, in Pray, L. C., and Esteban, M. C., eds., Upper Guadalupian Facies, Permian Reef Complex, Guadalupe Mountains, New Mexico and Texas, v.2, Road Logs and Locality Guides: Permian Basin Section SEPM, Publ. 77-16.

Sarg, J. F., 1977, Sedimentology of the carbonate-evaporite facies transition of the Seven Rivers formation (Guadalupian, Permian) in southeast New Mexico: SEPM Permian basin section, special publication, 77 - 16, p. 451 - 478.

Scholle, P. A., 1979, A color illustrated guide to constituents, textures, cements, and porosities of sandstones and associated rocks: AAPG Memoir 28, 201 pp.

Schlumberger Log Interpretation Principles/Application, 1987, 198 pp.

Schmidt, V., and McDonald, D. A., 1979, Secondary reservoir porosity in the course of sandstone diagenesis: AAPG, Education Course Note Series No. 12, 125 pp.

Silver, B. A., and Todd, R. G., 1969, Permian cyclic strata, northern Midland and Delaware Basins, west Texas, and southeastern New Mexico: American Association of Petroleum Geologists bulletin, v. 53, p. 2223 - 2251.

Smith, M., 1993, Neural networks for statistical modeling: Van Nostrand Reinhold, New York, 235 pp.

Stalkup, F. I., 1986, Permeability observed at the faces of cross-bedded sandstone outcrops, in Larry, W. Lake., and Herbert, B. Carrol, Jr., eds., Reservoir Characterization, Academic Press, Inc., New York, p. 141 - 179.

Suboor, M. A., and Heller, J. P., 1995, Minipermeameter characteristics critical to its use: In Situ, v. 19 (3), p. 225 - 248.

Swan, A. R. H., and Sandilands, M., 1992, Introduction to geological data analysis: Blackwell Science, 446 pp.

Tiat, D. B., Ahlen, J. L., Gordon, A., Scott., G. L., Motts, W. S., and Spitler, M. E., 1962, Artesia Group of New Mexico and west Texas: Bulletin of the American Association of Petroleum Geologists, v. 46, No. 4, p. 504 - 517.

Tood, R. G., 1976, Oolite bar progradation, San Andres Formation, Midland Basin, Texas: American Association of Petroleum Geologists Bulletin, v. 60, p. 907 - 925.

Tomutsa, L., Mahmood, S., Brinkmeyer, A., and Honarpour, M., 1990, Application of integrated pore to core image analysis to study field distribution in reservoir rocks. Pres. at SPE Annual Tech. Conf. and Exhibit., New Orleans, Louisiana, SPE Paper 20478, p. 137 - 148.

Tucker, E. M., 1981, Sedimentary petrology, An introduction: John Wiley & Sons, New York, 252 pp.

Turner, P., 1980, Continental red beds: Developments in Sedimentology: v. 29, Elsevier Scientific Publishing Company, New York, 562 pp.

Ward, R. F., Kendall, C. G. C., and Harris, P. M., 1986, Upper Permian (Guadalupian) facies and their association with hydrocarbons - Permian Basin, west Texas and New Mexico: American Association of Petroleum geologists Bulletin, v. 70, No. 3, p. 239 - 262.

Warren, K. J., 1991, Sulfate dominated sea-marginal and platform evaporite settings: Sabkhas and salinas, mudflats and salterns: Melvin, L., J., *ed.*, Evaporites, Petroleum and Mineral Resources, Developments in Sedimentology, v. 50, Elsiver, New York, p. 69 - 188.

Weber, K. J., 1986, How heterogeneity affect oil recovery: in Larry, W. Lake., and Herbert. B. Carrol, Jr., eds., Reservoir Characterization, Academic Press, Inc., p. 487 - 544.

Weiss, W. W., 1997, Reservoir simulation maps old field: Hart's Oil and Gas World, January 1997, p. 29 - 31.

Wellington, S.L. and Vinegar, H. J., 1987, X-Ray Computerized Tomography, Journal of Petroleum Technology., v. 39, no. 8. p. 885 - 898.

Williams, K. W., 1967, Depositional dynamics of the Queen Formation in New Mexico and Texas: Unpublished Master's Thesis, Texas Tech. College, 107 pp.

Willaims, K. W, 1969, Principles of cementation, environmental framework and diagenesis of Grayburg and Queen Formations, New Mexico and Texas: Unpublished Ph.D. Dissertation, Texas Tech. College, 198 pp.

Wilson, J. L., 1975, Carbonate facies in geologic history, Springer-Verlag, New York.

Worthington, P. F., 1991, Reservoir characterization at mesoscopic scale: in Larry, W. Lake., Herbert, B. Carrol, Jr., and Thomas, C. Wesson., eds., Reservoir Characterization II, Academic Press, Inc., p. 123 - 165.

APPENDIX A

- Permeability data for the Santa Rosa Sandstone
- Petrographic data for the Santa Rosa Sandstone
- Permeability data for the San Andres Formation
- Petrographic data for the San Andres Formation

PERMEABILITY DISTRIBUTION IN THE SANTA ROSA SANDSTONE.

Depth(ft.)	K (md)	K (md)	K (md)	K (md)	K (md)	Avg.K (md)
828.167	5.70	5.40	5.80	6.40	5.50	5.76
828.183	5.20	6.30	10.10	9.20	7.30	7.62
828.200	8.20	9.50	7.20	7.20	12.20	8.86
828.217	5.60	6.80	6.60	4.90	8.40	6.46
828.233	9.30	9.10	8.20	8.20	10.30	9.02
828.250	6.90	10.30	10.30	10.50	9.50	9.50
828.267	15.80	15.80	13.10	13.50	11.90	14.02
828.283	6.20	6.20	14.50	8.50	9.00	8.88
828.300	9.60	6.10	8.50	7.50	8.50	8.04
828.317	11.70	14.80	15.80	11.90	8.70	12.58
828.333	22.20	27.80	21.50	26.50	28.90	25.38
828.350	21.90	21.90	21.80	54.00	54.00	34.72
828.367	33.30	25.30	17.20	57.30	105.30	47.68
828.383	16.90	19.30	38.60	38.60	66.00	35.88
828.400	80.60	25.40	26.50	77.30	77.30	57.42
828.417	25.30	27.30	31.90	38.00	95.50	43.60
828.433	35.30	40.40	97.80	144.10	139.50	91.42
828.450	16.50	24.40	46.30	42.90	136.80	53.38
828.467	41.40	37.60	39.80	88.10	101.20	61.62
828.483	20.00	22.00	43.60	71.20	77.20	46.80
828.500	41.40	77.90	126.80	76.90	76.00	79.80
828.517	41.40	77.90	126.00	77.00	77.00	79.86
828.533	17.20	18.70	20.10	16.00	29.20	20.24
828.550	20.60	29.80	21.80	17.70	27.50	23.48
828.567	22.30	21.30	18.30	30.90	30.90	24.74
828.583	28.10	29.10	13.40	14.10	33.40	23.62
828.600	21.80	18.00	14.30	18.90	36.00	21.80
828.617	18.30	17.30	10.00	27.30	33.90	21.36
828.633	10.30	7.50	14.40	12.10	21.10	13.08
828.650	15.00	20.40	13.20	12.60	21.30	16.50
828.667	10.70	12.40	10.30	15.10	15.80	12.86
828.683	4.20	2.20	6.30	6.10	12.70	6.30
828.700	2.80	4.70	2.50	3.90	2.50	3.28
828.717	0.00	2.50	1.90	0.70	2.10	1.44
828.733	0.90	0.00	0.00	1.10	1.30	0.66
828.750	0.00	1.20	1.30	1.40	1.30	1.04
828.767	0.30	0.90	0.90	0.50	0.80	0.68
828.783	0.00	0.00	0.00	0.00	1.10	0.22
828.800	1.30	0.50	0.20	0.20	0.00	0.44
828.817	0.60	0.80	0.50	0.50	0.50	0.58
828.833	1.10	0.60	0.60	0.60	0.00	0.58
828.850	25.10	33.70	4.70	26.20	17.80	21.50
828.867	40.60	28.20	15.10	13.90	20.80	23.72
828.883	28.90	22.40	16.60	18.30	20.10	21.26
828.900	31.50	26.50	21.80	15.80	14.00	21.92

PERMEABILITY DISTRIBUTION IN THE SANTA ROSA SANDSTONE.

Depth(ft.)	K (md)	K (md)	K (md)	K (md)	K (md)	Avg.K (md)
828.917	42.90	14.40	19.60	6.60	19.10	20.52
828.933	52.20	24.20	31.50	9.80	9.80	25.50
828.950	52.80	40.40	20.90	14.30	5.40	26.76
828.967	87.70	43.60	22.20	9.50	9.50	34.50
828.983	31.30	31.30	17.50	17.50	17.50	23.02
829.000	59.80	41.90	41.90	27.80	16.70	37.62
829.017	38.80	41.50	31.60	22.10	0.00	26.80
829.033	0.00	28.40	29.50	18.60	24.50	20.20
829.050	20.00	29.70	34.60	34.60	20.60	27.90
829.067	38.30	19.30	13.20	24.80	22.10	23.54
829.083	4.60	4.60	27.90	29.90	18.90	17.18
829.100	23.20	23.70	36.20	35.00	25.00	28.62
829.117	23.80	23.80	23.80	19.90	0.00	18.26
829.133	52.80	23.50	30.50	21.10	23.50	30.28
829.150	35.10	35.10	24.80	24.80	27.80	29.52
829.167	44.90	35.60	30.10	16.20	23.00	29.96
829.183	23.70	24.40	24.10	23.40	19.40	23.00
829.200	28.80	24.60	27.90	17.60	21.60	24.10
829.217	24.20	42.60	19.80	33.10	33.10	30.56
829.233	0.90	0.90	0.70	0.80	0.80	0.82
829.250	0.90	0.70	0.60	0.80	0.80	0.76
829.267	0.90	0.90	0.90	0.70	0.80	0.84
829.283	1.80	1.60	1.10	1.20	0.00	1.14
829.300	2.00	2.40	1.90	2.10	2.70	2.22
829.317	3.20	2.80	2.80	4.30	4.30	3.48
829.333	4.40	4.40	5.00	4.50	4.00	4.46
829.350	7.70	8.50	9.30	6.80	6.80	7.82
829.367	9.30	15.30	16.00	10.40	7.10	11.62
829.383	19.20	19.20	19.20	9.80	8.60	15.20
829.400	15.30	15.50	16.20	10.40	10.60	13.60
829.417	14.60	11.60	15.50	13.50	11.70	13.38
829.433	18.60	14.30	9.60	13.90	14.90	14.26
829.450	18.90	10.70	13.30	11.90	15.50	14.06
829.467	16.90	12.20	13.00	13.60	18.20	14.78
829.483	25.00	20.60	17.60	11.20	17.10	18.30
829.500	33.20	20.40	16.10	16.10	19.90	21.14
829.517	16.90	16.90	16.90	16.90	16.90	16.90
829.533	24.20	24.20	12.30	16.00	19.30	19.20
829.550	27.60	16.90	23.30	17.00	15.80	20.12
829.567	45.90	19.00	13.80	16.50	16.90	22.42
829.583	45.90	19.00	13.80	16.50	16.90	22.42
829.600	45.90	19.00	13.80	16.50	16.90	22.42
829.617	45.90	19.00	13.80	16.50	16.90	22.42
829.633	45.90	19.00	13.80	16.50	16.90	22.42
829.650	45.90	19.00	13.80	16.50	16.90	22.42

PERMEABILITY DISTRIBUTION IN THE SANTA ROSA SANDSTONE.

Depth(ft.)	K (md)	K (md)	K (md)	K (md)	K (md)	Avg.K (md)
829.667	105.00	94.00	182.00	76.00	93.00	110.00
829.683	153.00	176.00	193.00	166.00	90.00	155.60
829.700	190.00	177.00	157.00	173.00	125.00	164.40
829.717	167.00	162.00	162.00	137.00	80.00	141.60
829.733	136.00	157.00	156.00	156.00	92.00	139.40
829.750	97.00	144.00	155.00	140.00	140.00	135.20
829.767	232.00	185.00	134.00	131.00	155.00	167.40
829.783	134.00	159.00	211.00	105.00	126.00	147.00
829.800	226.00	211.00	158.00	178.00	132.00	181.00
829.817	198.00	117.00	117.00	158.00	154.00	148.80
829.833	171.00	193.00	58.00	136.00	136.00	138.80
829.850	216.00	236.00	162.00	148.00	156.00	183.60
829.867	212.00	131.00	141.00	169.00	130.00	156.60
829.883	215.00	168.00	116.00	195.00	198.00	178.40
829.900	131.00	136.00	220.00	158.00	160.00	161.00
829.917	213.00	229.00	153.00	135.00	159.00	177.80
829.933	246.00	180.00	146.00	106.00	109.00	157.40
829.950	227.00	240.00	196.00	134.00	134.00	186.20
829.967	154.00	190.00	221.00	179.00	0.00	148.80
829.983	0.00	184.00	184.00	164.00	164.00	139.20
830.000	206.00	157.00	127.00	135.00	135.00	152.00
830.017	239.00	179.00	103.00	177.00	140.00	167.60
830.033	256.00	118.00	145.00	155.00	123.00	159.40
830.050	198.00	152.00	235.00	138.00	157.00	176.00
830.067	165.00	195.00	207.00	220.00	133.00	184.00
830.083	75.00	177.00	149.00	148.00	148.00	139.40
830.100	166.00	149.00	193.00	105.00	164.00	155.40
830.117	125.00	125.00	143.00	32.00	166.00	118.20
830.133	157.00	208.00	171.00	223.00	150.00	181.80
830.150	156.00	96.00	108.00	118.00	148.00	125.20
830.167	59.40	24.30	24.70	42.00	17.90	33.66
830.183	66.40	30.20	11.70	12.30	32.90	30.70
830.200	59.70	36.70	23.60	16.90	22.20	31.82
830.217	46.40	48.60	20.40	19.10	13.10	29.52
830.233	52.60	37.20	24.60	4.10	1.10	23.92
830.250	60.20	35.10	33.30	16.40	28.80	34.76
830.267	71.40	41.80	41.80	26.50	36.70	43.64
830.283	138.00	36.10	53.20	9.60	31.90	53.76
830.300	147.00	26.20	48.00	29.00	29.60	55.96
830.317	59.50	49.80	30.90	32.30	27.70	40.04
830.333	54.40	31.50	43.00	43.00	23.70	39.12
830.350	34.30	49.80	43.50	3.53	16.70	29.57
830.367	22.20	17.60	37.50	31.00	14.30	24.52
830.383	49.80	28.10	26.90	18.80	18.70	28.46
830.400	17.60	28.30	45.50	12.40	25.40	25.84

PERMEABILITY DISTRIBUTION IN THE SANTA ROSA SANDSTONE.

Depth(ft.)	K (md)	K (md)	K (md)	K (md)	K (md)	Avg.K (md)
830.417	51.10	44.00	34.60	35.40	18.80	36.78
830.433	44.40	29.20	46.70	21.10	0.00	28.28
830.450	37.90	52.00	18.20	29.60	26.20	32.78
830.467	156.00	176.00	179.00	131.00	116.00	151.60
830.483	179.00	171.00	168.00	135.00	151.00	160.80
830.500	227.00	258.00	231.00	219.00	140.00	215.00
830.517	156.00	196.00	168.00	159.00	75.00	150.80
830.533	181.00	215.00	204.00	168.00	124.00	178.40
830.550	238.00	178.00	159.00	190.00	173.00	187.60
830.567	178.00	154.00	199.00	166.00	150.00	169.40
830.583	200.00	207.00	181.00	166.00	166.00	184.00
830.600					201.00	201.00
830.617	82.00	174.00	183.00	209.00	179.00	165.40
830.633	152.00	171.00	160.00	147.00	150.00	156.00
830.650	188.00	165.00	183.00	213.00	173.00	184.40
830.667	145.00	193.00	154.00	171.00	229.00	178.40
830.683	99.00	125.00	160.00	180.00	84.00	129.60
830.700	109.00	109.00	82.00	168.00	64.00	106.40
830.717	162.00	55.00	54.00	146.00	108.00	105.00
830.733	50.00	149.00	100.00	115.00	146.00	112.00
830.750	107.00	84.00	109.00	121.00	122.00	108.60
830.767	105.00	126.00	112.00	153.00	113.00	121.80
830.783	159.00	95.00	173.00	155.00	180.00	152.40
830.800	88.00	73.00	176.00	144.00	146.00	125.40
830.817	91.00	145.00	145.00	146.00	119.00	129.20
830.833	92.00	135.00	186.00	169.00	210.00	158.40
830.850	24.00	55.00	150.00	106.00	68.00	80.60
830.867	88.00	98.00	170.00	153.00	87.00	119.20
830.883	149.00	107.00	144.00	198.00	135.00	146.60
830.900	159.00	55.00	168.00	171.00	149.00	140.40
830.917	131.00	86.00	109.00	139.00	157.00	124.40
830.933	76.00	63.00	107.00	193.00	133.00	114.40
830.950	94.00	103.00	152.00	129.00	100.00	115.60
830.967	136.00	49.00	158.00	98.00	176.00	123.40
830.983						125.00
831.000	220.00	137.00	109.00	127.00	96.00	137.80
831.017	119.00	139.00	97.00	173.00	122.00	130.00
831.033	124.00	169.00	150.00	124.00	121.00	137.60
831.050	127.00	149.00	106.00	126.00	107.00	123.00
831.067	160.00	118.00	157.00	95.00	112.00	128.40
831.083	194.00	126.00	109.00	62.00	89.00	116.00
831.100	159.00	97.00	114.00	152.00	61.00	116.60
831.117	174.00	141.00	166.00	91.00	68.00	128.00
831.133	187.00	108.00	173.00	96.00	62.00	125.20
831.150	155.00	126.00	120.00	120.00	104.00	125.00

PERMEABILITY DISTRIBUTION IN THE SANTA ROSA SANDSTONE.

Depth(ft.)	K (md)	K (md)	K (md)	K (md)	K (md)	Avg.K (md)
831.167	125.00	149.00	150.00	165.00	87.00	135.20
831.183	105.00	137.00	1106.00	193.00	150.00	338.20
831.200	172.00	134.00	199.00	48.00	99.00	130.40
831.217	182.00	109.00	123.00	87.00	66.00	113.40
831.233	114.00	144.00	163.00	50.00	98.00	113.80
831.250	192.00	166.00	185.00	147.00	131.00	164.20
831.267	154.00	154.00	139.00	132.00	132.00	142.20
831.283	92.00	102.00	70.00	165.00	105.00	106.80
831.300	132.00	61.00	111.00	70.00	74.00	89.60
831.317	142.00	141.00	189.00	122.00	141.00	147.00
831.333	153.00	149.00	163.00	198.00	65.00	145.60
831.350	152.00	134.00	99.00	165.00	182.00	146.40
831.367	177.00	146.00	129.00	115.00	111.00	135.60
831.383	198.00	168.00	180.00	240.00	68.00	170.80
831.400	181.00	172.00	159.00	158.00	226.00	179.20
831.417		561.00	328.00	364.00	339.00	318.40
831.433		332.00	300.00	372.00	322.00	265.20
831.450	361.00	353.00	343.00	298.00	280.00	327.00
831.467	275.00	239.00	247.00	351.00	300.00	282.40
831.483	361.00	341.00	374.00	150.00	261.00	297.40
831.500	258.00	214.00	257.00	187.00	69.00	197.00
831.517	102.00	160.00	122.00	73.00	210.00	133.40
831.533	41.00	140.00	136.00	115.00	188.00	124.00
831.550	142.00	112.00	131.00	79.00	133.00	119.40
831.567	150.00	34.00	117.00	75.00	16.00	78.40
831.583	256.00	361.00	328.00	312.00	274.00	306.20
831.600	392.00	401.00	375.00	313.00	371.00	370.40
831.617	447.00	398.00	0.00	443.00	436.00	344.80
831.633	300.00	447.00	383.00	351.00	380.00	372.20
831.650	361.00	386.00	371.00	315.00	371.00	360.80
831.667	309.00	321.00	319.00	291.00	353.00	318.60
831.683	404.00	278.00	293.00	281.00	210.00	293.20
831.700	300.00	291.00	305.00	189.00	311.00	279.20
831.717	141.00	162.00	253.00	293.00	201.00	210.00
831.733	215.00	243.00	283.00	108.00	271.00	224.00
831.750	210.00	223.00	224.00	267.00	264.00	237.60
831.767	205.00	226.00	213.00	234.00	231.00	221.80
831.783	358.00	285.00	283.00	146.00	310.00	276.40
831.800	273.00	231.00	304.00	260.00	341.00	281.80
831.817	608.00	543.00	594.00	422.00	444.00	522.20
831.833	242.00	374.00	417.00	351.00	361.00	349.00
831.850	328.00	256.00	414.00	401.00	392.00	358.20
831.867	231.00	324.00	292.00	320.00	316.00	296.60
831.883	189.00	254.00	80.00	230.00	290.00	208.60
831.900	270.00	356.00	351.00	304.00	326.00	321.40

PERMEABILITY DISTRIBUTION IN THE SANTA ROSA SANDSTONE.

Depth(ft.)	K (md)	K (md)	K (md)	K (md)	K (md)	Avg.K (md)
831.917	308.00	375.00	326.00	312.00	312.00	326.60
831.933	395.00	300.00	260.00	443.00	277.00	335.00
831.950	386.00	358.00	374.00	408.00	436.00	392.40
831.967	380.00	339.00	343.00	269.00	358.00	337.80
831.983	247.00	318.00	314.00	306.00	274.00	291.80
832.000	279.00	207.00	238.00	277.00	389.00	278.00
832.017	330.00	220.00	271.00	366.00	283.00	294.00
832.033	275.00	306.00	85.00	282.00	197.00	229.00
832.050	66.00	60.00	78.00	68.00	45.00	63.40
832.067	16.80	15.40	18.10	18.00	24.90	18.64
832.083	339.00	323.00	371.00	374.00	421.00	365.60
832.100	144.00	210.00	286.00	302.00	274.00	243.20
832.117	326.00	279.00	358.00	418.00	380.00	352.20
832.133	383.00	283.00	341.00	392.00	363.00	352.40
832.150	607.00	531.00	490.00	593.00	486.00	541.40
832.167	224.00	213.00	215.00	174.00	227.00	210.60
832.183	285.00	276.00	295.00	257.00	214.00	265.40
832.200	288.00	262.00	311.00	308.00	268.00	287.40
832.217	324.00	324.00	308.00	380.00	313.00	329.80
832.233	366.00	356.00	398.00	369.00	395.00	376.80
832.250	348.00	276.00	274.00	436.00	203.00	307.40
832.267	339.00	272.00	401.00	334.00	310.00	331.20
832.283	421.00	293.00	377.00	304.00	319.00	342.80
832.300	421.00	271.00	262.00	127.00	252.00	266.60
832.317	377.00	325.00	303.00	227.00	183.00	283.00
832.333	308.00	317.00	300.00	223.00	353.00	300.20
832.350	306.00	324.00	250.00	222.00	306.00	281.60
832.367	319.00	166.00	212.00	200.00	161.00	211.60
832.383	236.00	173.00	112.00	179.00	118.00	163.60
832.400	56.00	339.00	212.00	153.00	252.00	202.40

SUMMARY OF PETROGRAPHIC DATA FOR THE SANTA ROSA SANDSTONE.

K (md)	Total Porosity (%)	Primary Porosity (%)	Secondary Intergranular Porosity (%)	Secondary Oversized Pores (%)	Secondary Intraconst. Porosity (%)	Micro-Porosity (%)	Cement Dolomite (%)	Clay Authig./ Detrital (%)	Quartz (%)	Rock Frag. (%)	Avg. Grain Size (mm)	Avg. Pore Size (mm)	PS/PI	Grain Shape/ Sorting
0.90	3.00	0.90	0.60	0.00	0.00	1.50	30.00	15.00	50.00	2.00	0.08	0.04	P/P	S.R/M
1.20	3.00	0.90	0.60	0.00	0.00	1.50	30.00	15.00	50.00	2.00	0.08	0.04	P/P	S.R/M
1.60	2.00	1.20	0.00	0.00	0.00	0.80	5.00	25.00	55.00	10.00	0.09	0.05	P/V.P	S.R/M
1.80	3.00	1.80	0.00	0.00	0.00	1.20	5.00	25.00	55.00	10.00	0.09	0.05	P/V.P	S.R/M
2.00	3.00	1.80	0.00	0.00	0.00	1.20	5.00	25.00	55.00	10.00	0.09	0.05	P/V.P	S.R.M
2.20	2.00	0.60	0.60	0.00	0.00	0.80	30.00	12.00	51.00	2.00	0.07	0.04	P/P	S.R/W
2.40	3.00	0.90	0.90	0.00	0.00	1.20	30.00	12.00	51.00	2.00	0.08	0.04	P/P	S.R/W
2.50	3.00	0.90	0.90	0.00	0.00	1.20	30.00	12.00	52.00	2.00	0.10	0.04	P/P	S.R/W
2.80	2.00	0.60	0.60	0.00	0.00	0.80	30.00	12.00	51.00	2.00	0.09	0.04	P/P	S.R/W
2.80	3.00	1.80	0.00	0.00	0.00	1.20	5.00	25.00	55.00	10.00	0.10	0.03	P/V.P	S.R/M
3.20	3.00	1.80	0.00	0.00	0.00	1.20	5.00	25.00	55.00	10.00	0.10	0.03	P/V.P	S.R/M
4.20	3.00	0.90	0.90	0.00	0.00	1.20	30.00	12.00	52.00	2.00	0.09	0.04	P/P	S.R/W
4.40	3.00	1.80	0.00	0.00	0.00	1.20	5.00	25.00	55.00	10.00	0.09	0.03	P/P	S.R/M
4.40	3.00	1.80	0.00	0.00	0.00	1.20	5.00	25.00	55.00	10.00	0.09	0.03	P/P	S.R/M
4.70	4.00	1.20	1.20	0.00	0.00	1.60	30.00	12.00	51.00	2.00	0.09	0.04	P/P	S.R/W
4.10	4.00	2.00	1.40	0.00	0.20	0.40	40.00	8.00	43.00	5.00	0.07	0.01	P/P	SA - SR/M
5.40	4.00	1.60	0.40	0.40	0.00	1.40	10.00	15.00	59.00	10.00	0.10	0.04	P/P	SA - SR/M
5.80	5.00	2.00	0.50	0.50	0.00	1.75	10.00	15.00	59.00	10.00	0.10	0.04	P/P	SA - SR/M
6.10	4.00	1.60	0.80	0.00	0.00	1.60	5.00	20.00	45.00	25.00	0.15	0.05	P/P	SA - SR/P
6.20	5.00	2.00	1.00	0.00	0.00	2.00	5.00	20.00	45.00	25.00	0.15	0.05	P/P	SA - SR/P
6.20	5.00	2.00	1.00	0.00	0.00	2.00	5.00	20.00	45.00	25.00	0.15	0.05	P/P	SA - SR/P
6.30	6.00	2.40	0.60	0.60	0.00	2.10	10.00	15.00	59.00	10.00	0.10	0.04	P/P	SA - SR/M

SUMMARY OF PETROGRAPHIC DATA FOR THE SANTA ROSA SANDSTONE.

K (md)	Total Porosity (%)	Primary Porosity (%)	Secondary Intergranular Porosity (%)	Secondary Oversized Pores (%)	Secondary Intraconst. Porosity (%)	Micro-Porosity (%)	Cement Dolomite (%)	Clay Authig./ Detrital (%)	Quartz (%)	Rock Frag. (%)	Avg. Grain Size (mm)	Avg. Pore Size (mm)	PS/PI	Grain Shape/ Sorting
6.60	6.00	2.40	0.60	0.60	0.00	2.10	10.00	15.00	59.00	10.00	0.10	0.04	P/P	SA - SR/M
6.80	6.00	2.40	0.60	0.60	0.00	2.10	10.00	15.00	59.00	10.00	0.10	0.04	P/P	SA - SR/M
7.20	6.00	2.40	0.60	0.60	0.00	2.10	10.00	15.00	59.00	10.00	0.10	0.04	P/P	SA - SR/M
7.70	6.00	1.80	0.60	0.00	0.00	3.60	5.00	25.00	47.00	13.00	0.10	0.03	P/P	SA - SR/P
8.50	6.00	1.80	0.60	0.00	0.00	3.60	5.00	25.00	47.00	13.00	0.10	0.03	P/P	SA - SR/P
8.50	4.00	1.20	2.00	0.00	0.00	0.80	5.00	20.00	45.00	25.00	0.10	0.05	P/P	SA - SR/P
9.30	6.00	3.00	1.20	0.00	0.00	1.80	20.00	15.00	50.00	9.00	0.10	0.03	P/P	SA - SR/P
9.50	8.00	3.20	0.80	0.80	0.00	2.80	10.00	15.00	60.00	7.00	0.10	0.04	P/P	SA - SR/P
9.60	5.00	2.00	1.00	0.00	0.00	2.00	5.00	20.00	45.00	25.00	0.10	0.03	P/P	SA - SR/P
10.10	7.00	1.40	2.10	0.70	0.35	2.45	10.00	15.00	60.00	7.00	0.10	0.04	P/P	SA - SR/M
10.70	7.00	3.50	2.10	0.00	0.00	1.05	15.00	15.00	61.00	2.00	0.10	0.04	P/P	SA - SR/M
11.70	10.00	7.50	0.50	0.00	0.00	2.00	15.00	20.00	47.00	8.00	0.15	0.06	P/P	SA - SR/P
11.70	6.00	2.40	2.28	0.00	0.12	1.20	10.00	8.00	70.00	6.00	0.10	0.05	M/M	SA - SR/M
12.30	6.00	2.40	2.28	0.00	0.12	1.20	10.00	8.00	70.00	6.00	0.10	0.05	M/M	SA - SR/M
12.40	8.00	4.00	1.60	0.00	0.00	2.00	15.00	15.00	60.00	2.00	0.09	0.04	P/P	SR/M
14.50	10.00	7.50	0.50	0.00	0.00	2.00	15.00	20.00	47.00	8.00	0.10	0.06	M/M	SR/M
14.50	10.00	7.50	0.50	0.00	0.00	2.00	15.00	20.00	47.00	8.00	0.10	0.06	M/M	SR/M
15.00	8.00	4.00	1.60	0.00	0.00	2.00	15.00	15.00	60.00	2.00	0.08	0.04	M/M	SR/M
15.30	12.00	2.40	7.20	0.00	0.00	2.40	5.00	25.00	51.00	7.00	0.10	0.06	M/M	SR/M
15.80	10.00	7.50	0.50	0.00	0.00	2.00	15.00	20.00	47.00	8.00	0.10	0.06	M/M	SR/M
16.90	13.00	5.20	4.94	0.00	0.26	2.60	5.00	20.00	56.00	6.00	0.08	0.04	P/M	SA - SR/M
19.10	13.00	7.15	3.64	0.00	0.26	1.95	5.00	20.00	56.00	6.00	0.08	0.04	P/M	SA - SR/M

SUMMARY OF PETROGRAPHIC DATA FOR THE SANTA ROSA SANDSTONE.

K (md)	Total Porosity (%)	Primary Porosity (%)	Secondary Intergranular Porosity (%)	Secondary Oversized Pores (%)	Secondary Intraconst. Porosity (%)	Micro-Porosity (%)	Cement Dolomite (%)	Clay Authig./ Detrital (%)	Quartz (%)	Rock Frag. (%)	Avg. Grain Size (mm)	Avg. Pore Size (mm)	PS/PI	Grain Shape/ Sorting
19.20	13.00	5.20	3.51	0.00	0.39	3.90	5.00	20.00	51.00	11.00	0.10	0.04	P/M	SA - SR/P
19.20	13.00	5.20	3.51	0.00	0.39	3.90	5.00	20.00	51.00	11.00	0.10	0.04	P/M	SA - SR/P
20.00	10.00	6.50	2.00	0.50	0.50	0.50	10.00	5.00	72.00	3.00	0.08	0.03	P/M	SA - SR/M
20.40	10.00	5.00	3.50	0.00	0.00	1.50	15.00	15.00	58.00	2.00	0.08	0.04	P/M	SA - SR/M
20.40	13.00	6.50	3.64	0.00	0.26	2.60	5.00	20.00	58.00	4.00	0.09	0.04	P/M	SA - SR/M
21.50	10.00	7.50	1.80	0.00	0.20	0.50	5.00	3.00	82.00	0.00	0.10	0.05	M/M	SA - SR/M
22.20	10.00	7.50	1.80	0.00	0.20	0.50	5.00	3.00	82.00	0.00	0.10	0.05	M/M	SA - SR/M
23.60	13.00	6.50	4.16	0.00	0.26	1.95	5.00	20.00	58.00	4.00	0.08	0.04	M/M	SA - SR/M
24.40	12.00	6.00	4.44	0.00	0.36	1.20	2.00	8.00	70.00	8.00	0.13	0.05	P/M	SA - SR/M
24.60	13.00	5.20	3.64	0.00	0.52	3.64	5.00	20.00	58.00	4.00	0.08	0.04	M/M	SA - SR/M
27.80	10.00	6.80	2.80	0.00	0.20	0.20	5.00	1.00	82.00	0.00	0.10	0.05	M/M	SA - SR/M
27.30	8.00	6.00	1.44	0.00	0.16	0.40	3.00	2.00	79.00	6.00	0.13	0.05	W/M	SA - SR/M
28.40	10.00	3.50	5.00	0.50	0.50	0.50	15.00	15.00	58.00	2.00	0.09	0.05	P/M	SA - SR/M
29.70	10.00	4.00	4.50	0.50	0.50	0.50	15.00	15.00	58.00	2.00	0.08	0.05	P/M	SA - SR/M
30.20	12.00	7.20	1.80	0.00	0.60	2.40	10.00	30.00	44.00	4.00	0.10	0.05	P/M	SA - SR/M
31.30	10.00	4.00	4.20	0.80	0.50	0.50	15.00	15.00	58.00	2.00	0.08	0.05	M/M	SA - SR/M
31.30	10.00	4.00	4.20	0.80	0.50	0.50	15.00	15.00	58.00	2.00	0.08	0.05	M/M	SA - SR/M
31.90	10.00	7.50	1.80	0.00	0.20	0.50	3.00	2.00	79.00	6.00	0.13	0.05	M/M	SA - SR/M
36.70	12.00	7.20	3.00	0.00	0.60	1.20	13.00	20.00	50.00	5.00	0.10	0.05	P/M	SA - SR/M
37.20	12.00	6.00	2.40	0.00	0.60	3.00	10.00	20.00	52.00	6.00	0.10	0.05	P/M	SA - SR/M
37.60	12.00	6.00	3.60	0.00	0.00	2.40	2.00	15.00	65.00	6.00	0.13	0.04	P/M	SA - SR/M
38.00	12.00	8.40	1.20	0.00	0.00	2.40	2.00	15.00	65.00	6.00	0.12	0.04	P/M	SA - SR/M

SUMMARY OF PETROGRAPHIC DATA FOR THE SANTA ROSA SANDSTONE.

K (md)	Total Porosity (%)	Primary Porosity (%)	Secondary Intergranular Porosity (%)	Secondary Oversized Pores (%)	Secondary Intraconst. Porosity (%)	Micro-Porosity (%)	Cement Dolomite (%)	Clay Authig./ Detrital (%)	Quartz (%)	Rock Frag. (%)	Avg. Grain Size (mm)	Avg. Pore Size (mm)	PS/PI	Grain Shape/ Sorting
38.80	13.00	4.55	4.55	1.95	0.65	1.30	10.00	8.00	66.00	3.00	0.10	0.07	P/M	SA - SR/M
39.80	12.00	8.40	1.20	0.00	0.00	2.40	2.00	15.00	45.00	8.00	0.14	0.06	P/M	SA - SR/M
40.40	10.00	8.00	0.70	0.00	0.30	1.00	2.00	10.00	70.00	8.00	0.14	0.06	W/M	SA - SR/W
40.40	13.00	4.55	4.55	1.95	0.65	1.30	10.00	8.00	66.00	3.00	0.10	0.06	P/M	SA - SR/M
41.50	13.00	3.90	5.20	1.95	0.65	1.30	10.00	8.00	66.00	3.00	0.12	0.06	P/M	SA - SR/M
41.90	13.00	3.90	5.20	1.95	0.65	1.30	10.00	8.00	66.00	3.00	0.13	0.06	P/M	SA - SR/M
42.90	12.00	8.40	1.20	0.00	0.00	2.40	2.00	15.00	64.00	7.00	0.13	0.06	P/M	SA - SR/M
43.60	13.00	4.55	4.55	1.95	0.65	1.30	10.00	8.00	66.00	3.00	0.10	0.05	P/M	SA - SR/M
46.30	10.00	7.00	1.70	0.00	0.30	1.00	2.00	10.00	70.00	8.00	0.12	0.06	W/M	SA - SR/W
46.40	12.00	6.00	4.80	0.00	0.00	1.20	10.00	5.00	67.00	6.00	0.10	0.07	M/M	SA - SR/M
48.60	12.00	6.00	4.80	0.00	0.00	1.20	10.00	5.00	67.00	6.00	0.10	0.07	M/M	SA - SR/M
52.60	12.00	2.40	8.40	0.00	0.60	0.60	10.00	5.00	67.00	6.00	0.10	0.07	M/M	SA - SR/M
52.80	16.00	4.80	7.20	2.40	0.80	0.80	10.00	8.00	63.00	3.00	0.10	0.05	P/M	SA - SR/M
59.80	16.00	4.80	7.20	2.40	0.80	0.80	10.00	8.00	63.00	3.00	0.11	0.05	P/M	SA - SR/M
59.70	12.00	6.60	4.20	0.00	0.60	0.60	10.00	8.00	63.00	7.00	0.10	0.07	M/M	SA - SR/M
66.40	12.00	6.00	4.80	0.00	0.60	0.60	10.00	8.00	63.00	7.00	0.10	0.07	M/M	SA - SR/M
80.00	15.00	9.00	3.75	0.00	0.75	1.50	5.00	8.00	65.00	7.00	0.13	0.06	M/M	SR/M
87.70	15.00	3.00	9.00	1.50	0.75	0.75	10.00	2.00	68.00	5.00	0.10	0.06	P/M	SA/M
88.10	13.00	5.20	3.25	2.60	0.00	1.95	5.00	10.00	66.00	6.00	0.13	0.08	P/M	SR/M
90.00	15.00	9.00	4.80	0.00	0.75	0.45	5.00	4.00	70.00	6.00	0.13	0.06	M/M	SR/M
92.00	15.00	9.00	4.80	0.00	0.75	0.45	5.00	4.00	70.00	6.00	0.13	0.06	M/M	SR/M
97.80	12.00	9.60	1.56	0.00	0.24	0.60	2.00	5.00	78.00	3.00	0.13	0.08	M/M	SR/M

SUMMARY OF PETROGRAPHIC DATA FOR THE SANTA ROSA SANDSTONE.

K (md)	Total Porosity (%)	Primary Porosity (%)	Secondary Intergranular Porosity (%)	Secondary Oversized Pores (%)	Secondary Intraconst. Porosity (%)	Micro-Porosity (%)	Cement Dolomite (%)	Clay Authig./ Detrital (%)	Quartz (%)	Rock Frag. (%)	Avg. Grain Size (mm)	Avg. Pore Size (mm)	PS/PI	Grain Shape/ Sorting
103.00	10.00	2.00	5.50	1.00	0.00	1.00	15.00	5.00	67.00	3.00	0.11	0.10	M/W	SR/W
107.00	10.00	2.00	5.50	1.00	0.00	1.00	10.00	5.00	72.00	3.00	0.12	0.09	M/W	SA/W
109.00	10.00	2.00	5.50	1.00	0.00	1.00	15.00	5.00	67.00	3.00	0.11	0.10	M/W	SA/W
125.00	20.00	12.00	5.00	0.00	0.00	3.00	5.00	10.00	59.00	6.00	0.08	0.08	M/M	SR/W
126.00	20.00	12.00	5.00	0.00	0.00	3.00	5.00	10.00	59.00	6.00	0.08	0.08	M/M	SR/W
129.00	13.00	3.90	6.50	1.30	0.65	0.65	15.00	5.00	64.00	2.00	0.12	0.11	M/W	SR/W
132.00	15.00	6.00	7.80	0.00	0.90	0.30	5.00	2.00	74.00	4.00	0.13	0.08	W/W	SR/M
134.00	15.00	6.00	7.80	0.00	0.90	0.30	5.00	2.00	74.00	4.00	0.13	0.08	W/W	SR/M
139.00	13.00	3.90	6.50	1.30	0.65	0.65	15.00	5.00	65.00	2.00	0.12	0.10	M/W	SR/W
140.00	15.00	6.75	6.75	0.00	0.00	1.50	8.00	10.00	62.00	5.00	0.08	0.08	M/W	SR/M
141.00	16.00	4.00	11.20	0.00	0.48	0.32	5.00	2.00	74.00	3.00	0.12	0.08	W/W	SR/M
142.00	15.00	6.00	7.80	0.00	0.90	0.30	5.00	2.00	74.00	4.00	0.12	0.08	W/W	SR/M
144.00	15.00	3.00	11.70	0.00	0.00	0.30	3.00	5.00	73.00	4.00	0.14	0.08	P/W	SR/M
146.00	15.00	6.75	6.75	0.00	0.75	0.75	5.00	2.00	73.00	2.00	0.12	0.10	W/W	SR/M
146.00	16.00	2.40	9.12	1.60	0.96	0.96	3.00	3.00	72.00	2.00	0.16	0.10	P/M	SR/M
149.00	15.00	6.75	6.75	0.00	0.75	0.75	5.00	2.00	73.00	2.00	0.13	0.08	W/W	SR/M
152.00	16.00	4.00	11.20	0.00	0.48	0.32	5.00	2.00	75.00	2.00	0.13	0.08	W/W	SR/M
152.00	20.00	5.00	7.80	6.00	0.20	0.40	7.00	3.00	67.00	3.00	0.11	0.11	P/M	SA - SR/W
153.00	16.00	4.00	11.20	0.00	0.48	0.32	5.00	2.00	75.00	2.00	0.13	0.08	W/W	SR/M
154.00	16.00	4.00	11.20	0.00	0.48	0.32	5.00	2.00	75.00	2.00	0.13	0.08	W/W/	SR/M
154.00	16.00	2.40	12.80	0.00	0.48	0.32	5.00	2.00	75.00	2.00	0.13	0.08	W/W/	SR/M
154.00	15.00	3.00	10.50	0.00	0.75	0.75	5.00	5.00	70.00	5.00	0.15	0.13	P/W	SA/M

SUMMARY OF PETROGRAPHIC DATA FOR THE SANTA ROSA SANDSTONE.

K (md)	Total Porosity (%)	Primary Porosity (%)	Secondary Intergranular Porosity (%)	Secondary Oversized Pores (%)	Secondary Intraconst. Porosity (%)	Micro-Porosity (%)	Cement Dolomite (%)	Clay Authig./ Detrital (%)	Quartz (%)	Rock Frag. (%)	Avg. Grain Size (mm)	Avg. Pore Size (mm)	PS/PI	Grain Shape/ Sorting
155.00	25.00	8.75	13.00	0.00	0.75	2.50	8.00	10.00	52.00	5.00	0.08	0.08	M/P	SA/W
156.00	15.00	4.50	9.00	0.00	0.75	0.75	5.00	5.00	70.00	5.00	0.15	0.13	P/W	SA/M
168.00	20.00	5.00	7.80	6.00	0.20	0.40	7.00	3.00	67.00	3.00	0.12	0.11	P/M	SR/W
171.00	20.00	5.00	7.80	6.00	0.20	0.40	7.00	3.00	67.00	3.00	0.12	0.11	P/M	SR/W
171.00	16.00	4.80	10.40	0.00	0.48	0.32	5.00	2.00	70.00	3.00	0.15	0.13	P/M	SA/M
177.00	18.00	3.24	12.78	0.00	1.08	0.90	5.00	3.00	75.00	2.00	0.13	0.08	W/W	SA/M
178.00	16.00	4.80	10.40	0.00	0.48	0.32	5.00	2.00	70.00	3.00	0.15	0.13	P/M	SA/M
178.00	16.00	4.80	10.40	0.00	0.48	0.32	5.00	2.00	70.00	3.00	0.15	0.13	P/M	SA/M
179.00	15.00	4.50	9.75	0.00	0.45	0.30	5.00	2.00	70.00	3.00	0.14	0.13	P/M	SA/M
181.00	15.00	4.50	9.75	0.00	0.45	0.30	5.00	2.00	70.00	3.00	0.14	0.13	P/M	SA/M
193.00	20.00	5.00	8.40	3.00	0.20	0.40	7.00	3.00	67.00	3.00	0.12	0.10	P/M	SR/W
196.00	16.00	4.00	10.40	0.00	0.80	0.80	5.00	2.00	70.00	3.00	0.13	0.10	P/W	SA/M
200.00	15.00	3.75	9.75	0.00	0.75	0.75	5.00	2.00	70.00	3.00	0.14	0.10	P/W	SA/M
205.00	20.00	6.00	8.60	2.00	1.20	1.20	3.00	3.00	72.00	2.00	0.16	0.12	P/W	SA/M
207.00	18.00	4.50	11.70	0.00	0.90	0.90	5.00	2.00	70.00	3.00	0.14	0.10	P/W	SA/M
210.00	20.00	6.00	8.60	2.00	1.20	1.20	3.00	3.00	72.00	2.00	0.15	0.14	P/W	SA/M
215.00	20.00	6.00	8.60	2.00	1.20	1.20	3.00	3.00	72.00	2.00	0.16	0.15	P/W	SA/M
215.00	20.00	5.00	13.00	0.00	1.00	1.00	5.00	2.00	70.00	3.00	0.13	0.11	P/W	SA/M
223.00	20.00	4.00	10.60	2.00	1.20	1.20	3.00	3.00	72.00	2.00	0.16	0.16	P/W	SA/M
226.00	20.00	4.00	10.60	2.00	1.20	1.20	3.00	3.00	72.00	2.00	0.15	0.16	P/W	SA/M
227.00	22.00	8.80	11.00	0.66	1.10	0.44	5.00	3.00	68.00	2.00	0.14	0.11	P/W	SA/W
231.00	22.00	8.80	11.88	0.00	0.66	0.66	2.00	0.00	74.00	2.00	0.16	0.11	M/W	SR/M

SUMMARY OF PETROGRAPHIC DATA FOR THE SANTA ROSA SANDSTONE.

K (md)	Total Porosity (%)	Primary Porosity (%)	Secondary Intergranular Porosity (%)	Secondary Oversized Pores (%)	Secondary Intraconst. Porosity (%)	Micro-Porosity (%)	Cement Dolomite (%)	Clay Authig./ Detrital (%)	Quartz (%)	Rock Frag. (%)	Avg. Grain Size (mm)	Avg. Pore Size (mm)	PS/PI	Grain Shape/ Sorting
231.00	20.00	4.00	10.60	2.00	1.20	1.20	3.00	3.00	72.00	2.00	0.16	0.16	P/W	SA/M
234.00	22.00	8.80	11.88	0.00	0.66	0.66	2.00	0.00	74.00	2.00	0.16	0.12	M/W	SR/M
238.00	22.00	8.80	11.00	0.66	1.10	0.44	5.00	2.00	69.00	2.00	0.14	0.10	M/W	SA/W
242.00	22.00	2.86	9.90	8.80	0.66	0.00	3.00	3.00	70.00	2.00	0.16	0.16	P/W	SA/M
243.00	22.00	2.86	9.90	8.80	0.66	0.00	3.00	3.00	70.00	2.00	0.15	0.16	P/W	SA/M
258.00	22.00	4.40	15.40	0.66	1.10	0.44	5.00	2.00	69.00	2.00	0.14	0.11	M/W	SA/W
260.00	20.00	6.00	12.80	0.00	0.60	0.60	2.00	0.00	76.00	2.00	0.16	0.11	W/W	SR/M
264.00	20.00	6.00	12.80	0.00	0.60	0.60	2.00	0.00	76.00	2.00	0.15	0.12	W/W	SR/M
267.00	20.00	6.00	12.80	0.00	0.60	0.60	2.00	0.00	76.00	2.00	0.16	0.12	W/W	SR/M
271.00	20.00	6.00	12.80	0.00	0.60	0.60	2.00	0.00	76.00	2.00	0.16	0.12	W/W	SR/M
273.00	25.00	6.75	12.50	3.75	1.25	0.50	3.00	3.00	68.00	1.00	0.16	0.18	P/W	SA/M
285.00	25.00	6.75	12.50	3.75	1.25	0.50	3.00	3.00	68.00	1.00	0.15	0.18	P/W	SA/M
310.00	20.00	4.00	15.00	0.00	1.00	0.00	3.00	3.00	74.00	1.00	0.16	0.10	W/V.W	SR/M
341.00	20.00	4.00	15.00	0.00	1.00	0.00	3.00	3.00	74.00	1.00	0.17	0.10	W/V.W	SR/M
351.00	20.00	2.00	17.40	0.00	0.00	0.60	3.00	5.00	71.00	1.00	0.17	0.10	M/V.W	SA/M
358.00	28.00	4.20	17.36	4.20	1.40	0.56	3.00	3.00	65.00	1.00	0.16	0.18	P/W	SA/M
361.00	20.00	2.00	17.40	0.00	0.00	0.60	3.00	5.00	71.00	1.00	0.17	0.10	M/V.W	SA/M
374.00	28.00	4.20	17.36	4.20	1.40	0.56	3.00	3.00	65.00	1.00	0.17	0.17	P/W	SA/M
404.00	25.00	2.50	20.75	0.00	1.25	0.50	5.00	3.00	69.00	1.00	0.20	0.13	W/V.W	SA - SR/W
422.00	25.00	15.00	9.50	0.00	0.00	0.25	3.00	3.00	68.00	1.00	0.20	0.14	W/W	SR/W
440.00	20.00	7.00	9.40	2.00	0.40	0.00	2.00	0.00	76.00	2.00	0.18	0.16	P/W	SA - SR/M
444.00	25.00	11.75	12.00	1.25	0.00	0.25	3.00	3.00	68.00	1.00	0.20	0.14	W/W	SR/W

SUMMARY OF PETROGRAPHIC DATA FOR THE SANTA ROSA SANDSTONE.

K (md)	Total Porosity (%)	Primary Porosity (%)	Secondary Intergranular Porosity (%)	Secondary Oversized Pores (%)	Secondary Intraconst. Porosity (%)	Micro-Porosity (%)	Cement Dolomite (%)	Clay Authig./ Detrital (%)	Quartz (%)	Rock Frag. (%)	Avg. Grain Size (mm)	Avg. Pore Size (mm)	PS/PI	Grain Shape/ Sorting
451.00	25.00	2.50	21.25	0.00	0.75	0.50	5.00	3.00	66.00	1.00	0.18	0.15	W/W	SA - SR/W
452.00	25.00	2.50	20.75	0.00	1.25	0.50	5.00	3.00	66.00	1.00	0.18	0.15	W/W	SA - SR/W
501.00	27.00	5.40	17.55	2.70	1.35	0.00	10.00	0.00	65.00	0.00	0.20	0.17	P/V.W	SR/M
543.00	25.00	2.50	17.25	0.00	0.00	0.25	2.00	3.00	70.00	0.00	0.18	0.18	M/V.W	SA/W
555.00	25.00	5.00	16.25	2.50	1.25	0.00	10.00	0.00	70.00	0.00	0.18	0.18	P/V.W	SR/W
601.00	30.00	6.00	16.50	6.00	1.50	0.00	10.00	0.00	60.00	0.00	0.17	0.20	P/V.W	SR/W
608.00	30.00	9.00	19.50	0.00	1.50	0.00	2.00	3.00	65.00	0.00	0.18	0.20	M/V.W	SA/W

PERMEABILITY DISTRIBUTION IN THE SAN ANDRES FORMATION. WELL: STATE ACCT 2 No.6(

Depth (ft)	K (md)	K (md)	K (md)	K (md)	K (md)	K (md)	Avg K
6745.00	9.30	4.40	4.80	6.40	13.30	15.30	8.92
6745.04	15.40	11.90	17.10	11.00	100.00	14.70	28.35
6745.08	15.00	30.20	10.40	8.00	20.10	5.70	14.90
6745.13	27.30	16.90	32.80	37.70	20.80	8.40	23.98
6745.17	9.50	12.80	3.90	2.20	15.20	7.00	8.43
6745.21	7.80	11.90	2.20	1.90	5.90	17.40	7.85
6745.25	22.40	13.60	0.90	1.00	19.60	13.50	11.83
6745.29	6.60	48.60	16.00	29.70	13.50	12.40	21.13
6745.33	6.40	6.40	6.70	10.30	7.40	4.20	6.90
6745.38	2.50	4.60	4.20	6.10	7.40	7.20	5.33
6745.42	2.50	7.20	13.60	8.90	5.70	4.40	7.05
6745.46	2.10	2.70	3.60	2.60	3.80	3.50	3.05
6745.50	4.40	4.70	2.20	2.90	4.90	3.20	3.72
6745.54	2.30	9.70	12.90	27.40	10.60	9.90	12.13
6745.58	3.10	10.80	23.40	2.50	19.50	19.20	13.08
6745.63	2.80	28.80	19.60	9.70	7.60	5.90	12.40
6745.67	2.40	8.90	40.20	56.80	65.00	13.30	31.10
6745.71	8.30	22.90	15.90	30.50	44.60	23.30	24.25
6745.75	5.60	11.00	11.60	10.70	25.30	16.50	13.45
6745.79	10.00	13.50	11.20	17.90	45.10	12.90	18.43
6745.83	4.70	13.90	32.00	54.20	18.70	17.10	23.43
6745.88	3.80	6.20	6.60	6.60	18.60	19.70	10.98
6745.92	11.50	9.50	9.50	11.50	10.50	10.50	10.50
6745.96	6.70	16.30	10.50	6.60	7.60	10.80	9.75
6746.00	14.30	12.60	24.50	18.90	15.90	100.00	31.03
6746.04	20.70	29.30	24.90	52.90	38.20	26.10	32.02
6746.08	18.20	20.90	10.40	39.90	87.00	49.00	37.57
6746.13	29.40	41.30	42.50	45.10	49.40	62.20	44.98
6746.17	12.00	29.80	23.30	44.30	33.50	59.80	33.78
6746.21	18.30	22.20	20.40	26.50	15.90	9.00	18.72
6746.25	31.40	24.00	13.00	7.90	4.40	6.50	14.53
6746.29	17.30	32.30	18.30	19.30	5.80	32.40	20.90
6746.33	15.30	28.30	32.00	8.20	5.70	6.00	17.90
6746.38	10.40	8.90	5.50	9.00	13.00	12.00	11.60
6746.42	6.60	7.80	23.50	23.50	8.20	6.50	12.68
6746.46	3.80	4.50	5.00	15.20	16.40	18.30	10.53
6746.50	10.20	7.40	15.30	6.00	15.30	12.70	11.15
6746.54	4.10	9.20	9.20	14.50	33.40	7.20	12.93
6746.58	5.90	5.70	6.10	6.10	4.20	0.00	4.67
6746.63	3.80	24.30	10.10	10.10	9.40	9.40	11.18
6746.67	7.80	10.20	9.00	5.20	7.50	2.90	7.10
6746.71	12.90	12.90	12.90	3.30	8.70	2.30	8.83
6746.75	20.60	3.10	3.10	3.10	3.10	0.00	5.50
6746.79	0.00	5.90	3.70	5.00	2.20	1.90	3.12
6746.83	15.70	4.70	4.80	4.10	4.30	4.80	6.40

PERMEABILITY DISTRIBUTION IN THE SAN ANDRES FORMATION. WELL: STATE ACCT 2 No.60.

Depth (ft)	K (md)	K (md)	K (md)	K (md)	K (md)	K (md)	Avg K
6746.88	15.20	11.00	10.50	10.90	31.20	23.50	17.05
6746.92	22.90	24.90	8.40	4.70	6.70	1.30	11.48
6746.96	18.10	21.80	22.20	8.90	8.90	0.90	13.47
6747.00	22.70	35.20	29.20	19.40	7.90	0.50	19.15
6747.04	28.40	21.60	43.80	29.50	1.90	2.00	21.20
6747.08	9.00	11.70	20.50	9.90	0.30	0.40	8.63
6747.13	8.70	17.00	30.20	11.00	5.00	8.20	13.35
6747.17	55.70	15.80	9.90	5.60	22.10	17.50	21.10
6747.21	6.00	11.90	6.90	3.70	18.80	15.80	10.52
6747.25	15.70	6.60	6.10	3.00	14.00	11.40	9.47
6747.29	6.80	10.10	6.80	10.10	6.80	8.20	8.13
6747.33	9.20	11.00	7.50	11.00	7.50	8.50	9.12
6747.38	7.80	6.50	8.20	6.50	6.80	6.30	7.02
6747.42	8.80	9.50	8.90	9.50	8.50	9.40	9.10
6747.46	10.00	11.30	11.20	11.30	11.20	9.50	10.75
6747.50	10.30	10.00	11.80	10.00	11.80	12.10	11.00
6747.54	11.50	6.80	9.90	6.80	10.30	10.30	9.27
6747.58	15.20	9.20	9.80	9.20	9.80	17.20	11.73
6747.63	12.60	7.80	13.60	7.80	12.30	14.10	11.37
6747.67	12.80	8.80	10.50	8.80	10.50	13.40	10.80
6747.71	11.00	10.00	10.20	10.00	9.70	12.00	10.48
6747.75	16.80	10.30	11.50	10.30	11.50	14.00	12.40
6747.79	13.20	11.50	11.30	11.50	11.30	10.60	11.57
6747.83	0.30	100.00	0.50	0.80	0.40	0.30	17.05
6747.88	0.20	0.00	0.30	0.40	0.40	0.20	0.25
6747.92	0.40	0.50	0.60	0.70	0.60	0.70	0.58
6747.96	0.30	0.20	0.50	0.70	0.50	0.50	0.45
6748.00	1.20	0.40	0.40	0.10	0.50	0.40	0.50
6748.04	1.80	0.80	0.60	0.60	0.70	0.60	0.85
6748.08	0.90	0.80	0.70	0.60	0.60	0.90	0.75
6748.13	0.50	1.60	0.40	0.80	0.90	0.60	0.80
6748.17	0.40	0.40	0.40	0.40	0.30	0.50	0.40
6748.21	0.40	0.40	0.30	0.40	0.50	0.30	0.38
6748.25	0.20	1.00	0.40	0.20	0.10	1.90	0.63
6748.29	0.30	0.40	0.40	0.30	0.40	0.30	0.35
6748.33	22.20	0.60	0.30	0.40	0.40	0.30	4.03
6748.38	0.40	0.40	35.70	14.00	0.70	2.10	8.88
6748.42	0.30	0.40	0.80	0.30	0.30	0.20	0.38
6748.46	0.50	0.30	0.30	0.00	0.60	0.30	0.33
6748.50	94.00	0.40	0.30	1.80	0.40	0.20	16.18
6748.54	0.80	0.90	0.70	0.90	0.70	0.60	0.77
6748.58	0.80	0.90	0.80	0.70	0.60	0.80	0.77
6748.63	0.50	0.10	0.30	0.20	0.40	0.10	0.27
6748.67	0.00	0.00	0.00	0.00	0.00	0.00	0.10
6748.71	0.20	0.10	0.00	0.10	0.10	0.10	0.10

PERMEABILITY DISTRIBUTION IN THE SAN ANDRES FORMATION. WELL: STATE ACCT 2 No.60.

Depth (ft)	K (md)	K (md)	K (md)	K (md)	K (md)	K (md)	Avg K
6748.75	0.20	0.30	0.20	0.20	0.20	0.30	0.23
6748.79	0.30	0.00	0.10	0.10	0.10	0.00	0.10
6748.83	0.30	0.20	0.30	0.00	0.20	0.20	0.20
6748.88	0.50	0.30	0.20	0.10	0.20	0.20	0.25
6748.92	0.40	0.40	0.10	0.00	0.00	0.00	0.15
6748.96	0.20	0.30	0.20	0.30	0.20	0.20	0.23
6749.00	0.30	0.00	0.10	0.10	0.10	0.00	0.10
6749.04	0.30	0.20	0.30	0.00	0.20	0.20	0.20
6749.08	0.50	0.30	0.20	0.10	0.20	0.20	0.25
6749.13	0.40	0.40	0.10	0.00	0.00	0.00	0.15
6749.17	0.20	0.30	0.20	0.30	0.20	0.20	0.23
6749.21	6.70	9.60	16.90	7.10	6.40	25.80	12.08
6749.25	7.10	5.50	8.30	16.80	33.80	8.90	13.40
6749.29	16.70	16.30	16.10	11.20	20.60	10.50	15.23
6749.33	8.90	8.70	23.20	8.30	11.30	11.50	11.98
6749.38	14.90	14.90	15.60	16.90	36.20	49.70	24.70
6749.42	9.00	57.30	49.30	18.10	18.40	5.50	26.27
6749.46	6.10	12.30	15.30	22.80	8.90	3.90	11.55
6749.50	7.30	25.70	24.80	19.40	26.30	5.60	18.18
6749.54	11.30	15.90	11.80	11.40	15.10	3.90	11.57
6749.58	8.40	26.60	14.50	14.00	13.60	4.60	13.62
6749.63	12.60	16.70	9.90	11.10	9.10	4.50	10.65
6749.67	4.00	8.50	3.80	3.70	4.20	4.50	4.78
6749.71	7.10	5.70	2.20	1.50	1.80	1.20	3.25
6749.75	11.50	24.10	2.60	1.90	1.70	1.30	7.18
6749.79	3.40	3.20	3.80	3.80	5.60	3.20	3.83
6749.83	4.70	4.80	9.40	4.90	2.80	2.80	4.90
6749.88	2.70	4.50	4.90	6.40	31.80	3.10	8.90
6749.92	2.70	2.70	3.70	6.20	3.00	1.10	3.23
6749.96	2.10	4.10	1.70	2.70	2.60	1.70	2.48
6750.00	3.90	1.90	2.30	2.90	2.10	1.00	2.35
6750.04	2.20	2.60	2.00	3.10	3.20	2.10	2.53
6750.08	1.80	1.80	3.80	4.00	8.40	2.40	3.70
6750.13	1.70	1.70	6.20	5.20	5.50	5.30	4.27
6750.17	1.20	1.20	3.00	3.60	1.80	2.40	2.20
6750.21	14.70	8.00	8.40	6.50	1.00	0.90	6.58
6750.25	4.30	5.30	4.30	4.40	32.40	26.70	12.90
6750.29	4.80	7.10	8.70	8.20	5.80	7.60	7.03
6750.33	6.50	6.30	8.80	10.00	8.00	12.50	8.68
6750.38	9.50	12.60	13.20	14.30	7.10	10.10	11.13
6750.42	3.40	3.20	3.80	3.80	5.60	3.20	3.83
6750.46	4.70	4.80	9.40	4.90	2.80	2.80	4.90
6750.50	2.70	4.50	4.90	6.40	31.80	3.10	8.90
6750.54	2.70	2.70	3.70	6.20	3.00	1.10	3.23
6750.58	2.10	4.10	1.70	2.70	2.60	1.70	2.48

PERMEABILITY DISTRIBUTION IN THE SAN ANDRES FORMATION. WELL: STATE ACCT 2 No.60.

Depth (ft)	K (md)	K (md)	K (md)	K (md)	K (md)	K (md)	Avg K
6750.63	3.90	1.90	2.30	2.90	2.10	1.00	2.35
6750.67	2.20	2.60	2.00	3.10	3.20	2.10	2.53
6750.71	1.80	1.80	3.80	4.00	8.40	2.40	3.70
6750.75	1.70	1.70	6.20	5.20	5.50	5.30	4.27
6750.79	1.20	1.20	3.00	3.60	1.80	2.40	2.20
6750.83	14.70	8.00	8.40	6.50	1.00	0.90	6.58
6750.88	4.30	5.30	4.30	4.40	32.40	26.70	12.90
6750.92	4.80	7.10	8.70	8.20	5.80	7.60	7.03
6750.96	6.50	6.30	8.80	10.00	8.00	12.50	8.68
6751.00	9.50	12.60	13.20	14.30	7.10	10.10	11.13
6751.04	7.50	18.10	13.00	26.60	9.70	15.50	15.07
6751.08	6.80	14.10	9.10	8.10	13.40	47.90	16.57
6751.13	8.40	9.60	10.00	9.80	9.80	8.20	9.30
6751.17	6.60	15.40	9.60	6.40	15.20	39.30	15.42
6751.21	18.60	17.10	11.90	17.20	18.20	12.60	15.93
6751.25	10.80	14.20	7.60	4.50	6.80	6.10	8.33
6751.29	5.40	6.10	7.90	5.30	4.60	3.20	5.42
6751.33	4.60	4.80	7.00	9.20	6.10	5.20	6.15
6751.38	3.10	2.60	2.70	6.10	3.60	4.50	3.77
6751.42	2.20	4.00	3.30	4.70	5.70	2.90	3.80
6751.46	1.50	2.60	1.50	2.70	2.90	2.10	2.22
6751.50	0.30	1.60	1.80	1.70	1.50	1.30	1.37
6751.54	0.30	0.30	0.00	0.00	0.00	0.00	0.10
6751.58	0.00	0.00	0.00	0.00	0.00	0.00	0.01
6751.63	0.40	0.30	0.30	0.30	0.00	0.00	0.22
6751.67	0.00	0.50	0.50	0.50	0.50	0.50	0.42
6751.71	0.00	0.00	0.00	0.00	0.00	0.00	0.01
6751.75	0.50	0.50	0.50	0.20	0.30	0.30	0.38
6751.79	0.90	0.90	0.70	0.70	0.70	0.00	0.65
6751.83	0.00	0.00	0.00	0.00	1.10	1.10	0.37
6751.88	0.80	0.90	0.50	0.80	0.00	0.00	0.50
6751.92	0.60	0.50	0.40	0.40	0.40	0.60	0.48
6751.96	11.20	11.20	0.00	0.00	0.00	0.00	3.73
6752.00	0.00	0.00	0.20	0.30	0.20	0.20	0.15
6752.04	0.10	0.10	0.10	0.10	0.10	0.00	0.08
6752.08	0.00	0.00	0.20	0.20	0.30	0.30	0.17
6752.13	0.80	0.80	0.80	0.00	0.00	0.00	0.40
6752.17	0.00	0.60	0.60	1.40	0.40	0.40	0.57
6752.21	0.40	0.10	0.10	0.50	0.40	0.00	0.25
6752.25	1.20	1.20	1.80	0.70	0.50	0.50	0.98
6752.29	0.60	0.80	0.80	0.80	0.80	0.50	0.72
6752.33	0.00	0.00	0.20	0.20	0.10	0.10	0.10
6752.38	1.90	1.40	1.30	1.30	1.10	0.70	1.28
6752.42	1.10	1.40	1.80	1.70	2.00	1.90	1.65
6752.46	0.90	0.80	1.10	2.10	1.20	1.00	1.18

PERMEABILITY DISTRIBUTION IN THE SAN ANDRES FORMATION. WELL: STATE ACCT 2 No.60.

Depth (ft)	K (md)	K (md)	K (md)	K (md)	K (md)	K (md)	Avg K
6752.50	1.10	1.10	0.90	1.30	1.20	1.40	1.17
6752.54	1.50	1.20	2.10	1.50	1.10	1.20	1.43
6752.58	2.10	1.00	1.40	1.90	1.20	6.40	2.33
6752.63	1.10	1.10	0.90	1.30	1.20	1.40	1.17
6752.67	1.50	1.20	2.10	1.50	1.10	1.20	1.43
6752.71	2.10	1.00	1.40	1.90	1.20	6.40	2.33
6752.75	0.30	0.30	0.00	0.00	0.00	0.00	0.10
6752.79	0.00	0.00	0.00	0.00	0.00	0.00	0.01
6752.83	0.40	0.30	0.30	0.30	0.00	0.00	0.22
6752.88	0.00	0.50	0.50	0.50	0.50	0.50	0.42
6752.92	0.00	0.00	0.00	0.00	0.00	0.00	0.01
6752.96	0.50	0.50	0.50	0.20	0.30	0.30	0.38
6753.00	0.90	0.90	0.70	0.70	0.70	0.00	0.65
6753.04	0.00	0.00	0.00	0.00	1.10	1.10	0.37
6753.08	0.80	0.90	0.50	0.80	0.00	0.00	0.50
6753.13	0.60	0.50	0.40	0.40	0.40	0.60	0.48
6753.17	11.20	11.20	0.00	0.00	0.00	0.00	3.73
6753.21	0.00	0.00	0.20	0.30	0.20	0.20	0.15
6753.25	0.10	0.10	0.10	0.10	0.10	0.00	0.08
6753.29	0.00	0.00	0.20	0.20	0.30	0.30	0.17
6753.33	0.80	0.80	0.80	0.00	0.00	0.00	0.40
6753.38	0.00	0.60	0.60	1.40	0.40	0.40	0.57
6753.42	0.40	0.10	0.10	0.50	0.40	0.00	0.25
6753.46	1.20	1.20	1.80	0.70	0.50	0.50	0.98
6753.50	0.60	0.80	0.80	0.80	0.80	0.50	0.72
6753.54	0.00	0.00	0.20	0.20	0.10	0.10	0.10
6753.58	1.90	1.40	1.30	1.30	1.10	0.70	1.28
6753.63	1.10	1.40	1.80	1.70	2.00	1.90	1.65
6753.67	0.90	0.80	1.10	2.10	1.20	1.00	1.18
6753.71	1.10	1.10	0.90	1.30	1.20	1.40	1.17
6753.75	1.50	1.20	2.10	1.50	1.10	1.20	1.43
6753.79	2.10	1.00	1.40	1.90	1.20	6.40	2.33
6753.83	1.50	17.00	5.00	2.80	3.90	1.10	5.22
6753.88	3.60	1.50	2.10	6.30	2.60	1.50	2.93
6753.92	2.50	3.50	2.70	5.00	2.70	3.20	3.27
6753.96	2.90	2.80	3.90	5.60	4.20	2.90	3.72
6754.00	5.20	5.10	8.60	3.90	7.90	5.20	5.98
6754.04	4.10	5.50	8.20	8.80	4.70	5.50	6.13
6754.08	8.00	12.90	100.00	6.20	5.60	3.90	22.77
6754.13		8.30	12.70	18.40	9.70	8.70	11.50
6754.17	6.00	9.70	16.60	18.90	70.00	31.90	25.52
6754.21	4.40	3.40	4.30	6.60	15.80	8.50	7.17
6754.25	2.90	5.60	15.10	3.80	12.20	4.50	7.35
6754.29	23.40	21.60	17.20	6.50	3.30	3.20	12.53
6754.33	5.80	15.60	8.70	6.50	3.30	4.70	7.43

PERMEABILITY DISTRIBUTION IN THE SAN ANDRES FORMATION. WELL: STATE ACCT 2 No.6(

Depth (ft)	K (md)	K (md)	K (md)	K (md)	K (md)	K (md)	Avg K
6754.38	6.30	18.00	14.30	9.00	8.40	4.20	10.03
6754.42	4.00	10.50	8.10	8.30	5.60	3.60	6.68
6754.46	3.90	9.50	8.50	5.70	10.00	6.20	7.30
6754.50	4.80	4.70	5.00	8.10	11.20	22.70	9.42
6754.54	10.90	5.30	6.10	10.10	16.70	20.10	11.53
6754.58	5.80	6.50	10.50	6.80	18.40	14.10	10.35
6754.63	9.30	14.10	7.40	12.60	13.80	13.10	11.72
6754.67	10.80	10.00	8.30	17.20	11.20	31.30	14.80
6754.71	11.40	17.70	7.20	6.00	9.60	17.80	11.62
6754.75	15.00	8.60	6.40	5.70	6.60	18.10	10.07
6754.79	8.50	8.30	10.70	8.40	8.70	9.30	8.98
6754.83	6.00	9.20	10.10	6.00	8.20	5.90	7.57
6754.88	8.80	12.80	7.40	12.70	8.40	4.70	9.13
6754.92	5.10	13.40	4.70	5.50	3.90	5.20	6.30
6754.96	8.80	13.40	5.00	2.60	2.10	3.00	5.82
6755.00	5.80	6.50	10.50	6.80	18.40	14.10	10.35
6755.04	9.30	14.10	7.40	12.60	13.80	13.10	11.72
6755.08	10.80	10.00	8.30	17.20	11.20	31.30	14.80
6755.13	4.50	5.80	22.20	18.80	18.20	21.30	15.13
6755.17	7.70	14.20	10.90	14.80	15.80	9.40	12.13
6755.21	9.00	21.00	8.80	31.10	12.00	14.00	15.98
6755.25	19.90	12.80	7.80	17.50	11.80	22.10	15.32
6755.29	5.80	17.50	15.90	13.20	24.10	17.30	15.63
6755.33	41.80	55.80	36.90	28.60	27.10	28.70	36.48
6755.38	24.80	25.80	48.70	32.70	35.50	22.10	31.60
6755.42	0.00	2.00	3.60	38.10	114.50	0.00	26.37
6755.46	4.00	10.50	8.10	8.30	5.60	3.60	6.68
6755.50	3.90	9.50	8.50	5.70	10.00	6.20	7.30
6755.54	4.80	4.70	5.00	8.10	11.20	22.70	9.42
6755.58	10.90	5.30	6.10	10.10	16.70	20.10	11.53
6755.63	5.80	6.50	10.50	6.80	18.40	14.10	10.35
6755.67	9.30	14.10	7.40	12.60	13.80	13.10	11.72
6755.71	10.80	10.00	8.30	17.20	11.20	31.30	14.80
6755.75	11.40	17.70	7.20	6.00	9.60	17.80	11.62
6755.79	15.00	8.60	6.40	5.70	6.60	18.10	10.07
6755.83	8.50	8.30	10.70	8.40	8.70	9.30	10.60
6755.88	6.00	9.20	10.10	6.00	8.20	5.90	7.57
6755.92	8.80	12.80	7.40	12.70	8.40	4.70	9.13
6755.96	5.10	13.40	4.70	5.50	3.90	5.20	6.30
6756.00	8.80	13.40	5.00	2.60	2.10	3.00	5.82
6756.04	5.80	6.50	10.50	6.80	18.40	14.10	10.35
6756.08	9.30	14.10	7.40	12.60	13.80	13.10	11.72
6756.13	10.80	10.00	8.30	17.20	11.20	31.30	14.80
6756.17	5.80	15.60	8.70	6.50	3.30	4.70	7.43
6756.21	6.30	18.00	14.30	9.00	8.40	4.20	10.03

PERMEABILITY DISTRIBUTION IN THE SAN ANDRES FORMATION. WELL: STATE ACCT 2 No.6

Depth (ft)	K (md)	K (md)	K (md)	K (md)	K (md)	K (md)	Avg K
6756.25	23.40	21.60	17.20	6.50	3.30	3.20	12.53
6756.29	5.80	15.60	8.70	6.50	3.30	4.70	7.43
6756.33	6.30	18.00	14.30	9.00	8.40	4.20	10.03
6756.38	4.00	10.50	8.10	8.30	5.60	3.60	6.68
6756.42	3.90	9.50	8.50	5.70	10.00	6.20	7.30
6756.46	4.80	4.70	5.00	8.10	11.20	22.70	9.42
6756.50	10.90	5.30	6.10	10.10	16.70	20.10	11.53
6756.54	5.80	6.50	10.50	6.80	18.40	14.10	10.35
6756.58	9.30	14.10	7.40	12.60	13.80	13.10	11.72
6756.63	10.80	10.00	8.30	17.20	11.20	31.30	14.80
6756.67	11.40	17.70	7.20	6.00	9.60	17.80	11.62
6756.71	15.00	8.60	6.40	5.70	6.60	18.10	10.07
6756.75	8.50	8.30	10.70	8.40	8.70	9.30	10.60
6756.79	6.00	9.20	10.10	6.00	8.20	5.90	7.57
6756.83	8.80	12.80	7.40	12.70	8.40	4.70	9.13
6756.88	5.10	13.40	4.70	5.50	3.90	5.20	6.30
6756.92	8.80	13.40	5.00	2.60	2.10	3.00	5.82
6756.96	5.80	6.50	10.50	6.80	18.40	14.10	10.35
6757.00	9.30	14.10	7.40	12.60	13.80	13.10	11.72
6757.04	10.80	10.00	8.30	17.20	11.20	31.30	14.80
6757.08	4.50	5.80	22.20	18.80	18.20	21.30	15.13
6757.13	7.70	14.20	10.90	14.80	15.80	9.40	12.13
6757.17	9.00	21.00	8.80	31.10	12.00	14.00	15.98
6757.21	19.90	12.80	7.80	17.50	11.80	22.10	15.32
6757.25	5.80	17.50	15.90	13.20	24.10	17.30	15.63
6757.29	41.80	55.80	36.90	28.60	27.10	28.70	36.48
6757.33	24.80	25.80	48.70	32.70	35.50	22.10	31.60
6757.38	0.00	2.00	3.60	38.10	114.50	0.00	26.37
6757.42	0.00	0.00	0.00	0.00	0.00	0.00	0.01
6757.46	0.00	0.00	0.00	0.00	16.10	8.10	4.03
6757.50	19.00	11.90	2.40	76.70	76.70	76.70	43.90
6757.54	20.50	6.80	3.10	6.90	5.60	19.50	10.40
6757.58	0.00	8.60	4.10	2.40	2.60	6.30	4.00
6757.63	3.50	4.40	3.30	1.40	1.10	1.10	2.47
6757.67	5.30	14.80	31.90	34.30	31.30	25.30	23.82
6757.71	3.70	4.90	17.00	28.40	27.30	7.30	14.77
6757.75	2.20	3.60	5.60	5.00	1.90	1.30	3.27
6757.79	5.10	7.70	9.90	8.40	3.90	1.70	6.12
6757.83	4.10	8.00	7.70	6.80	3.40	2.10	5.35
6757.88	7.00	6.70	4.30	2.60	2.80	1.90	4.22
6757.92	7.00	6.70	4.30	2.60	2.80	1.90	4.22
6757.96	6.10	9.80	4.20	4.30	6.50	5.70	6.10
6758.00	15.90	20.20	6.90	5.70	7.30	4.50	10.08
6758.04	52.30	18.10	7.90	5.00	11.10	2.90	16.22
6758.08	16.70	21.10	16.10	13.70	5.70	2.70	12.67

PERMEABILITY DISTRIBUTION IN THE SAN ANDRES FORMATION. WELL: STATE ACCT 2 N

Depth (ft)	K (md)	K (md)	K (md)	K (md)	K (md)	K (md)	Avg K
6758.13	8.30	19.10	12.20	9.00	11.00	2.90	10.42
6758.17	6.10	9.00	5.20	4.80	3.80	4.20	5.52
6758.21	7.50	6.70	6.20	8.60	5.20	2.90	6.18
6758.25	6.30	6.00	5.60	3.50	4.80	2.90	4.20
6758.29	8.70	18.70	16.30	23.90	17.40	3.80	14.80
6758.33	20.10	29.30	21.10	10.70	7.50	4.80	15.58
6758.38	17.00	39.50	11.50	6.40	4.00	4.30	13.78
6758.42	4.30	3.50	11.60	11.30	14.90	2.80	8.07
6758.46	8.70	18.70	16.30	23.90	17.40	3.80	14.80
6758.50	20.10	29.30	21.10	10.70	7.50	4.80	15.58
6758.54	17.00	39.50	11.50	6.40	4.00	4.30	13.78
6758.58	6.20	14.40	8.00	12.10	7.70	2.60	8.50
6758.63	4.70	12.20	5.70	7.10	13.50	3.90	7.85
6758.67	2.80	4.90	3.20	2.70	7.20	2.20	3.83
6758.71	7.90	9.50	4.70	3.00	2.10	5.50	5.45
6758.75	3.00	1.80	3.00	0.90	2.60	2.60	2.32
6758.79	1.60	2.20	2.10	1.10	1.30	3.10	1.90
6758.83	3.00	6.70	6.30	3.50	9.60	6.90	6.00
6758.88	4.00	3.80	1.80	6.30	4.90	5.70	4.42
6758.92	19.80	18.60	1.30	24.70	5.20	9.10	13.12
6758.96	13.90	8.60	4.20	3.50	6.20	10.10	7.75
6759.00	20.50	28.30	4.90	5.30	3.70	30.70	15.57
6759.04	8.20	38.00	19.30	2.50	22.70	15.40	17.68
6759.08	26.30	17.70	35.60	16.10	10.00	13.30	19.83
6759.13	14.30	13.30	22.70	4.00	11.70	15.80	13.63
6759.17	49.70	23.80	6.30	3.30	20.30	10.10	18.92
6759.21	14.00	8.30	7.30	2.70	7.00	12.30	8.60
6759.25	7.90	9.50	4.70	3.00	2.10	5.50	5.45
6759.29	3.00	1.80	3.00	0.90	2.60	2.60	2.32
6759.33	1.60	2.20	2.10	1.10	1.30	3.10	1.90
6759.38	2.70	3.40	2.90	0.90	2.80	5.00	2.95
6759.42	3.40	4.10	2.10	1.00	1.00	3.20	2.47
6759.46	2.50	2.50	1.70	0.80	26.00	2.20	5.95
6759.50	11.50	2.10	1.30	0.80	1.30	1.00	3.00
6759.54	0.80	1.60	1.30	0.40	0.70	0.90	0.95
6759.58	1.00	1.50	1.20	1.00	1.60	1.00	1.22
6759.63	1.30	0.80	0.80	0.90	2.80	3.30	1.50
6759.67	2.50	1.60	1.90	2.30	2.20	2.80	2.20
6759.71	1.40	3.40	2.40	2.40	2.20	1.50	2.22
6759.75	3.00	1.50	2.00	1.60	1.60	1.50	1.87
6759.79	1.70	1.70	1.50	1.90	2.00	3.30	2.02
6759.83	2.30	2.00	1.60	2.10	1.40	1.60	1.83
6759.88	1.90	1.80	2.20	3.90	1.60	1.80	2.20
6759.92	1.90	2.50	2.90	2.60	1.20	0.80	1.98
6759.96	2.90	3.30	3.50	9.10	1.30	0.60	3.45

PERMEABILITY DISTRIBUTION IN THE SAN ANDRES FORMATION. WELL: STATE ACCT 2 Nc

Depth (ft)	K (md)	K (md)	K (md)	K (md)	K (md)	K (md)	Avg K
6760.00	4.50	2.50	2.80	5.20	1.50	1.00	2.92
6760.04	2.80	3.70	2.30	2.20	1.40	1.00	2.23
6760.08	3.40	2.80	3.40	16.70	4.00	1.50	5.30
6760.13	7.80	6.80	1.90	4.20	5.00	2.10	4.63
6760.17	5.30	4.20	2.70	8.30	3.60	4.10	4.70
6760.21	7.00	3.70	5.00	5.60	5.40	3.20	4.98
6760.25	2.30	1.40	2.00	6.60	2.70	2.00	2.83
6760.29	2.30	2.80	1.60	1.70	2.10	2.20	2.50
6760.33	1.70	2.50	2.80	1.90	1.40	1.50	1.97
6760.38	1.20	8.70	3.60	5.90	2.21	1.60	3.87
6760.42	3.40	1.80	1.90	2.00	1.30	1.00	1.90
6760.46	3.00	1.30	2.10	1.30	1.50	1.30	1.75
6760.50	4.70	2.00	2.00	1.90	2.20	1.10	2.32
6760.54	1.90	4.70	1.50	1.80	1.10	1.30	2.05
6760.58	3.00	2.00	2.50	1.80	2.20	1.90	2.23
6760.63	2.30	1.80	1.40	1.80	2.30	10.90	3.42
6760.67	2.00	2.00	5.10	2.00	1.40	2.00	2.42
6760.71	1.80	2.20	1.90	1.50	2.00	3.30	2.12
6760.75	18.20	2.60	1.50	2.30	2.90	1.40	4.82
6760.79	1.50	3.80	2.40	7.30	2.80	2.00	3.30
6760.83	4.60	5.00	4.90	6.90	3.20	1.60	4.37
6760.88	2.20	1.30	1.30	7.70	1.70	2.20	2.73
6760.92	3.10	1.70	1.30	4.60	6.20	1.00	2.98
6760.96	13.00	0.90	1.90	2.00	8.00	1.80	4.60
6761.00	4.60	1.10	2.10	2.70	3.90	2.90	2.88
6761.04	17.90	1.30	1.60	1.60	4.00	1.40	4.63
6761.08	7.40	1.30	0.90	1.00			2.60
6761.13	5.70	25.10	2.10	2.90	1.50	0.80	6.35
6761.17	2.00	2.50	8.10	2.10	2.10	2.30	3.18
6761.21	10.00	5.50	4.80	3.00	2.90	2.40	4.77
6761.25	4.60	5.20	5.20	1.70	1.70	1.70	3.35
6761.29	1.50	1.50	1.50	1.50	1.50	0.10	1.27
6761.33	2.60	2.60	2.60	2.60	2.60	2.60	2.60
6761.38			1.50	1.50	1.60	0.00	1.15
6761.42		1.20	1.20	1.80	1.80	1.80	1.30
6761.46	2.20	1.10	2.60	2.60	2.60	2.60	2.28
6761.50	7.50	1.00	2.10	2.10	2.10	4.00	3.13
6761.54	4.20	2.90	3.10	3.10	1.50	0.60	2.57
6761.58	0.00	2.40	1.90			1.90	1.55
6761.63	1.70	2.40	1.30	0.80	3.30	25.20	5.78
6761.67	2.70	2.70	2.70	1.20	1.20	9.10	3.27
6761.71	1.20	1.20	1.20	2.20	2.20	2.00	1.67
6761.75	2.20	7.50	174.70	203.90	8.00	0.00	66.05
6761.79	2.20	2.10	2.70	3.20	2.20	4.20	2.77
6761.83	11.20	11.20	1.60	1.30	3.30	3.50	5.35

PERMEABILITY DISTRIBUTION IN THE SAN ANDRES FORMATION. WELL: STATE ACCT 2 No.6C

Depth (ft)	K (md)	K (md)	K (md)	K (md)	K (md)	K (md)	Avg K
6761.88	2.10	19.50	2.40	1.50	93.80	41.90	26.87
6761.92	3.60	3.80	1.40	0.90	12.10	1.00	3.66
6761.96	2.50	0.70	0.90	2.10	1.90	1.80	1.60
6762.00	2.50	1.10	1.20	1.20	1.10	1.50	1.43
6762.04	3.30	2.60	1.10	1.10	6.30	1.20	2.60
6762.08	5.80	5.20	1.00	2.50	1.70	1.20	2.90
6762.13	6.80	1.40	1.00	1.40	1.50	1.90	2.33
6762.17	2.40	1.80	1.00	1.50	1.40	2.40	1.75
6762.21	1.70	1.30	1.20	1.00	2.60	4.90	2.12
6762.25	6.20	1.50	1.90	1.20	1.20	5.30	2.88
6762.29	9.50	0.70	1.90	2.20	1.60	6.40	3.72
6762.33	2.40	0.60	1.70	2.40	2.10	1.70	1.82
6762.38	1.00	0.50	1.60	1.50	1.50	2.50	1.43
6762.42	4.20	0.80	0.80	1.60	2.80	3.20	2.23
6762.46	1.90	1.00	1.20	1.20	1.20	1.60	1.35
6762.50	2.40	0.90	1.50	1.50	1.80	0.00	1.35
6762.54	0.00	1.10	1.60	1.40	1.10	1.10	1.05
6762.58	7.70	7.70	7.70	7.70	5.30	0.00	6.02
6762.63	0.00	3.40	1.00	1.00	4.80	4.80	2.50
6762.67	0.90	0.90	0.70	2.50	1.60	1.60	1.37
6762.71	6.60	14.00	0.30	0.70	0.70	2.70	4.17

PERMEABILITY DISTRIBUTION IN THE SAN ANDRES FORMATION: WELL; MAYERS A-1 117

Depth (ft)	K (md)	K (md)	K (md)	K (md)	K (md)	K (md)	Avg. k (md)
Oolitic packstone							
3943.00	2.00	1.50	1.30	1.30	1.60	1.40	1.52
3943.03	2.40	3.60	2.30	2.40	2.60	2.20	2.58
3943.05	1.80	1.20	1.40	1.20	1.30	1.20	1.35
3943.08	2.00	1.50	1.50	1.00	1.30	1.20	1.42
3943.10	1.40	1.30	0.80	0.80	1.10	0.80	1.03
3943.13	1.80	1.50	1.00	0.90	1.00	1.10	1.22
3943.15	1.50	1.20	0.90	0.90	0.80	0.90	1.03
3943.18	1.90	2.10	1.80	1.40	1.10	1.40	1.62
3943.20	1.60	1.80	1.40	0.80	0.70	0.60	1.15
3943.23	2.90	1.60	1.40	1.30	1.00	0.70	1.48
3943.25	1.60	1.60	1.90	1.10	0.70	0.60	1.25
3943.28	4.20	3.00	1.40	1.60	1.00	1.00	2.03
3943.30	1.90	1.60	120.00	1.20	1.10	0.90	21.12
3943.33	1.90	2.00	1.40	1.80	1.30	3.90	2.05
3943.35	2.00	0.90	0.60	0.80	0.60	0.40	0.88
3943.38	2.30	1.70	1.10	1.00	1.10	0.80	1.33
3943.40	1.30	1.10	1.10	1.00	0.70	0.60	0.97
3943.43	1.80	1.40	1.60	2.10	1.70	1.60	1.70
3943.45	1.30	1.50	1.50	1.50	2.20	1.80	1.63
3943.48	1.50	1.60	1.20	1.30	1.50	1.60	1.45
3943.50	1.00	1.20	1.50	1.00	1.40	1.20	1.22
3943.53	0.90	1.20	1.20	0.80	1.20	1.20	1.08
3943.55	27.70	0.70	0.90	0.90	1.50	1.20	5.48
3943.58	12.60	16.40	4.20	1.10	1.10	1.70	6.18
3943.60	0.80	2.60	1.10	1.50	1.40	73.20	13.43
3943.63	1.30	1.20	0.90	1.30	1.30	1.20	1.20
3943.65	0.50	0.50	0.60	0.80	1.00	1.20	0.77
3943.68	0.60	0.70	0.50	0.60	0.50	0.10	0.50
3943.70	0.40	0.40	0.70	7.70	300.00	1.30	51.75
3943.73	300.00	300.00	1.80	63.80	1.00	0.90	111.25
3943.75	23.80	200.70	35.10	72.50	42.70	1.10	62.65
3943.78	7.50	13.90	51.70	7.50	1.20	68.10	24.98
3943.80	0.80	2.00	23.60	1.00	0.80	0.80	4.83
3943.83	106.60	1.20	0.70	81.10	111.10	8.40	51.52
3943.85	1.00	1.40	1.80	43.50	347.90	85.70	80.22
3943.88	1.00	70.20	5.70	214.70	60.70	126.30	79.77
3943.90	0.60	2.90	168.70	53.30	228.60	185.40	106.58
3943.93	28.00	207.00	8.30	1.20	0.60	0.80	40.98
3943.95	0.90	1.20	4.00	1.50	0.90	0.80	1.55
3943.98	1.00	4.00	1.20	1.50	0.90	0.80	1.57
3944.00	0.70	12.50	0.60	2.40	0.80	0.80	2.97
3944.03	0.80	12.50	300.00	0.60	1.40	0.90	52.70
3944.05	173.50	0.80	2.70	0.70	1.00	1.70	30.07
3944.08	4.60	2.70	67.30	172.30	178.80	85.10	85.13

PERMEABILITY DISTRIBUTION IN THE SAN ANDRES FORMATION: WELL; MAYERS A-1 217

Depth (ft)	K (md)	K (md)	K (md)	K (md)	K (md)	K (md)	Avg. k (md)
3944.10	5.00	3.00	6.00	2.20	2.30	2.80	3.55
3944.13	2.30	7.30	3.40	2.10	2.40	1.20	3.12
3944.15	3.50	6.00	5.30	1.20	2.80	3.30	3.68
3944.18	4.30	5.80	8.00	1.10	3.00	3.50	4.28
3944.20	7.10	1.10	1.40	1.10	0.60	1.20	2.08
3944.23	10.90	3.50	18.60	12.50	9.20	4.80	9.92
3944.25	4.60	2.80	1.80	1.80	15.30	2.40	4.78
3944.28	12.30	18.20	5.60	10.00	2.30	3.10	8.58
3944.30	11.70	3.20	1.20	1.10	2.40	6.40	4.33
3944.33	6.00	12.40	3.00	4.50	1.30	0.80	4.67
3944.35	6.40	5.30	1.80	1.30	1.10	1.00	2.82
3944.38	4.20	1.50	2.90	1.10	4.40	1.30	2.57
3944.40	2.30	1.30	2.00	1.20	1.60	1.90	1.72
3944.43	97.30	1.60	1.20	1.00	1.10	2.40	17.43
3944.45	300.00	13.50	2.30	1.90	11.70	1.70	55.18
3944.48	11.90	27.50	30.10	0.80	1.20	3.70	12.53
3944.50	20.30	14.30	4.60	1.20	5.00	7.20	8.77
3944.53	2.70	3.40	4.60	2.00	3.60	36.90	8.87
3944.55	1.40	2.20	1.70	1.50	1.10	1.60	1.58
3944.58	1.10	1.30	1.30	0.90	0.80	0.70	1.02
Peloidal wackestone							
4133.00	3.20	0.90	1.00	0.70	0.80	9.40	2.67
4133.02	1.20	5.10	14.80	5.20	6.40	2.70	5.90
4133.03	0.60	39.80	56.00	30.80	2.60	0.30	21.68
4133.05	0.50	1.80	132.00	12.40	1000.00	0.40	29.42
4133.07	2.00	2.00	18.60	25.90	0.20	0.20	8.15
4133.08	0.90	2.30	2.60	8.40	338.00	0.20	58.73
4133.10	5.30	209.00	1.50	2.00	0.40	0.40	36.43
4133.12	0.70	1.20	1.30	0.90	0.20	0.30	0.77
4133.13	0.60	0.80	0.80	0.50	0.40	0.40	0.58
4133.15	0.50	0.20	0.40	0.40	0.40	0.10	0.33
4133.17	0.40	64.00	25.60	31.00	0.90	0.30	20.37
4133.18	65.00	0.30	0.40	0.30	0.30	0.50	11.13
4133.20	0.20	0.20	0.40	0.50	0.80	0.30	0.40
4133.22	0.30	0.40	0.30	0.30	0.30	0.30	0.32
4133.23	0.30	0.30	0.30	0.40	0.60	0.20	0.35
4133.25	0.70	0.70	2.10	1.80	0.80	1.10	1.20
4133.27	0.70	1.70	1.30	0.40	0.50	11.20	2.63
4133.28	0.70	53.00	3.50	3.60	3.30	8.80	12.15
4133.30	0.60	0.10	0.30	0.30	0.30	0.60	0.37
4133.32	0.50	0.20	0.50	0.20	0.30	0.50	0.37
4133.33	0.20	0.00	0.20	0.10	0.30	0.30	0.18

PERMEABILITY DISTRIBUTION IN THE SAN ANDRES FORMATION: WELL; MAYERS A-1 317

Depth (ft)	K (md)	K (md)	K (md)	K (md)	K (md)	K (md)	Avg. k (md)
4133.35	0.20	0.10	0.30	0.60	1.20	0.70	0.52
4133.37	0.20	0.20	0.30	0.50	0.50	0.80	0.42
4133.38	0.20	0.20	0.10	0.20	0.30	22.50	3.92
4133.40	7.90	0.10	0.20	0.40	0.20	0.30	1.52
4133.42	492.00	0.40	0.20	0.30	0.40	0.20	82.25
4133.43	0.40	0.40	0.20	0.10	2.90	2.20	1.03
4133.45	0.20	0.20	0.40	0.20	1.50	0.00	0.42
4133.47	0.30	0.30	0.40	0.60	0.50	0.10	0.37
4133.48	0.90	0.20	0.20	0.50	0.10	66.00	11.32
4133.50	0.50	0.20	0.20	0.50	0.40	0.80	0.43
4133.52	222.00	0.20	0.40	0.60	0.50	0.00	37.28
4133.53	0.30	0.60	0.20	0.10	0.20	0.10	0.25
4133.55	0.10	1000.00	0.00	0.00	0.40	0.10	0.12
4133.57	0.30	0.60	0.10	0.00	0.00	0.00	0.17
4133.58	0.30	0.80	0.00	0.10	0.10	0.10	0.23
4133.60	0.20	0.60	66.00	0.10	0.00	1000.00	13.38
4133.62	6.40	5.90	386.00	0.10	0.00	231.00	104.90
4133.63	6.70	0.70	0.00	0.30	0.50	213.00	36.87
4133.65	0.90	0.50	0.50	0.40	900.00	0.30	150.43
4133.67	0.40	0.60	1.00	0.10	0.20	0.40	0.45
4133.68	1.90	0.30	0.90	0.70	0.30	0.40	0.75
4133.70	0.80	7.20	0.90	1.20	0.40	0.10	1.77
4133.72	0.50	0.10	1.40	0.70	0.30	0.40	0.57
4133.73	0.90	0.50	4.60	0.90	0.30	1.70	1.48
4133.75	0.90	0.50	0.90	0.80	0.30	0.50	0.65
4133.77	1.30	0.50	1.50	0.90	0.30	0.30	0.80
4133.78	1.30	0.40	1.30	3.00	0.70	1.50	2.15
4133.80	0.80	0.80	0.90	2.10	1000.00	1.70	1.37
4133.82	2.00	0.60	3.40	16.70	42.00	2.60	13.06
4133.83	92.00	1.20	2.20	599.00	970.00	28.00	282.07
4133.85	23.40	1.00	5.80	343.00	629.00	0.40	167.10
4133.87	0.40	0.40	787.00	149.00	1.30	3.60	156.95
4133.88	0.20	1.80	1.20	0.90	0.80	5.00	1.65
4133.90	17.30	1.30	1.30	1000.00	0.60	3.40	4.78
4133.92	2.40	8.50	10.00	1000.00	0.20	9.40	6.10
4133.93	662.00	183.00	183.00	99.00	12.30	0.40	189.95
4133.95	158.00	47.20	0.20	448.00	0.20	0.70	109.05
4133.97	0.50	0.50	0.50	9.30	9.30	21.20	6.88
4133.98	0.20	0.20	0.40	5.00	181.00	10.80	32.93
4134.00	0.10	0.20	662.00	513.00	242.00	242.00	276.55
4134.02	0.70	0.70	0.60	2.40	5.90	0.50	1.80
4134.03	0.40	0.40	0.40	0.90	71.00	3.10	12.70
4134.05	0.40	0.10	1.20	110.00	483.00	2.60	99.55
4134.07	0.10	0.10	0.30	0.60	0.20	0.00	0.22
4134.08	0.00	0.50	0.10	0.10	0.30	0.20	0.20

PERMEABILITY DISTRIBUTION IN THE SAN ANDRES FORMATION: WELL; MAYERS A-1 417

Depth (ft)	K (md)	K (md)	K (md)	K (md)	K (md)	K (md)	Avg. k (md)
4134.10	0.20	0.10	0.30	0.10	0.00	15.00	2.62
4134.12	0.40	0.20	2.40	0.30	0.00	0.10	0.57
4134.13	0.40	31.70	0.30	0.20	513.00	62.00	101.27
4134.15	0.30	0.50	0.60	0.30	0.80	0.70	0.53
4134.17	0.50	0.70	0.60	0.80	0.30	0.30	0.53
4134.18	0.60	0.80	0.50	0.80	0.50	0.30	0.58
4134.20	0.50	1.20	1.30	0.80	0.50	0.20	0.75
4134.38	0.50	1.20	1.10	0.80	0.90	0.20	0.78
4134.23	0.80	0.80	0.90	0.60	0.50	0.10	0.62
4134.25	1.00	0.80	0.90	139.00	0.10	0.20	23.67
4134.27	0.60	0.60	62.00	0.20	0.20	0.10	10.62
4134.28	0.30	0.20	0.20	0.30	0.20	0.20	0.23
4134.30	0.30	0.60	0.40	0.30	0.30	0.00	0.32
4134.32	23.20	0.70	0.70	0.00	0.40	0.20	4.20
4134.33	0.50	0.10	0.30	0.40	0.30	0.50	0.35
4134.35	0.30	2.90	0.20	0.30	0.40	0.30	0.73
4134.37	0.20	0.30	0.30	0.10	0.20	0.40	0.25
4134.38	0.40	0.30	0.50	0.30	0.30	0.40	0.37
4134.40	0.20	0.30	0.00	0.00	0.20	0.30	0.17
4134.42	0.40	0.30	0.30	0.40	0.40	0.40	0.37
4134.43	0.10	0.10	0.30	0.30	0.20	0.10	0.18
4134.45	8.90	0.20	0.20	0.30	0.40	0.20	1.70
4134.47	6.00	143.00	0.40	0.10	0.30	0.10	24.98
4134.48	29.30	1000.00	0.10	0.10	0.10	0.00	5.90
4134.50	27.10	3.00	1.00	2.80	0.30	0.20	5.73
4134.52	45.00	17.50	3.40	3.40	0.70	0.50	11.75
4134.53	42.30	13.40	6.30	1.00	0.40	1.10	10.75
4134.55	14.50	250.00	39.50	0.30	0.70	0.50	50.92
4134.57	305.00	275.00	28.80	0.20	0.40	0.30	101.62
4134.58	1000.00	121.00	4.30	2.10	1.50	1.00	25.98
4134.60	1.00	2.00	2.40	0.80	1.00	1.00	1.00
Oolitic-peloidal wackestone/packstone							
4139.17	0.40	0.20	0.10	0.40	0.20	0.10	0.23
4139.18	0.50	0.40	0.40	0.60	0.40	0.40	0.45
4139.20	0.30	0.80	0.20	0.10	0.20	0.20	0.30
4139.22	7.70	7.70	0.60	1.30	1.50	0.70	3.25
4139.23	0.50	0.50	0.50	0.50	0.60	0.50	0.52
4139.25	0.80	0.50	0.10	0.30	1.50	0.20	0.57
4139.27	0.30	0.20	0.20	0.70	0.60	0.30	0.38
4139.28	0.30	0.20	0.20	0.20	0.30	0.30	0.25
4139.30	0.00	0.00	0.00	0.00	0.00	0.00	0.01
4139.32	0.20	0.40	0.40	0.00	0.00	0.60	0.27
4139.33	0.10	0.10	0.10	0.10	1.80	0.30	0.42

PERMEABILITY DISTRIBUTION IN THE SAN ANDRES FORMATION: WELL; MAYERS A-1 517

Depth (ft)	K (md)	K (md)	K (md)	K (md)	K (md)	K (md)	Avg. k (md)
4139.35	0.10	1.00	0.20	0.10	1.30	0.50	0.53
4139.37	0.20	2.40	0.30	348.00	0.90	0.20	58.67
4139.38	0.30	1.20	0.60	0.80	0.40	0.20	0.58
4139.40	0.50	0.90	0.50	2.20	0.50	433.00	72.93
4139.42	0.20	0.20	0.10	0.10	0.20	0.20	0.17
4139.43	0.20	0.20	0.30	9.80	0.20	0.00	1.78
4139.45	0.10	0.20	0.10	0.00	0.10	0.00	0.08
4139.47	0.20	0.10	0.10	0.00	0.20	0.10	0.12
4139.48	0.20	0.20	0.10	0.20	0.30	0.00	0.17
4139.50	0.30	0.20	0.50	11.20	840.00	0.60	142.13
4139.52	0.20	0.10	0.20	585.00	190.00	0.10	129.27
4139.53	0.20	0.30	0.20	1000.00	1000.00	0.30	0.25
4139.55	0.10	0.40	0.40	2.10	90.00	0.20	15.53
4139.57	0.30	0.30	0.00	287.00	0.80	1000.00	57.68
4139.58	1000.00	0.40	0.90	0.00	0.40	0.10	0.40
4139.60	160.00	0.10	313.00	147.00	0.10	0.10	103.38
4139.62	969.00	1000.00	0.70	0.10	0.40	0.20	194.00
4139.63	1000.00	0.40	0.40	0.30	0.10	0.10	0.26
4139.65	0.40	0.30	0.30	0.30	0.30	0.30	0.32
4139.67	0.20	0.00	0.30	0.10	433.00	0.20	72.30
4139.68	0.10	0.10	0.20	0.10	11.30	0.20	2.00
4139.70	0.20	0.20	102.00	0.20	0.10	1000.00	20.54
4139.72	1.40	15.80	29.60	70.00	0.20	0.20	19.53
4139.73	0.30	4.00	1000.00	181.00	0.30	0.20	36.44
4139.75	329.00	0.70	0.30	0.30	0.20	0.90	55.23
4139.77	0.40	0.40	0.50	146.00	0.40	0.30	24.67
4139.78	79.00	1000.00	1.00	115.00	1000.00	1000.00	64.33
4139.80	0.70	0.50	559.00	559.00	0.40	0.20	186.63
4139.82	1.00	1.00	1000.00	0.40	0.30	1000.00	0.67
4139.83	474.00	78.00	0.90	0.30	900.00	0.30	242.25
4139.85	266.00	23.90	1000.00	763.00	699.00	613.00	472.98
4139.87	900.00	840.00	60.00	60.00	0.20	787.00	441.20
4139.88	1000.00	1.70	502.00	122.00	80.00	0.50	141.20
4139.90	363.00	36.70	0.30	629.00	0.50	0.40	171.65
4139.92	0.60	272.00	0.50	0.50	0.50	513.00	131.18
4139.93	1.10	9.10	0.40	1000.00	0.60	235.00	49.24
4139.95	0.30	181.00	813.00	0.40	155.00	629.00	296.45
4139.97	1.10	2.40	1.00	12.00	13.00	101.00	21.75
4139.98	0.60	1.10	0.40	0.30	1.80	0.20	0.73
4140.00	0.60	0.80	0.40	0.40	0.60	0.40	0.53
4140.02	1.00	0.50	0.10	0.30	0.30	0.70	0.48
4140.03	0.50	0.60	0.50	1000.00	0.30	0.50	0.48
4140.05	0.60	0.60	0.20	0.30	0.40	0.20	0.38
4140.07	0.90	0.60	0.50	0.40	51.50	0.60	9.08
4140.08	0.60	0.60	0.50	0.50	0.50	0.50	0.53

PERMEABILITY DISTRIBUTION IN THE SAN ANDRES FORMATION: WELL; MAYERS A-1 617

Depth (ft)	K (md)	K (md)	K (md)	K (md)	K (md)	K (md)	Avg. k (md)
4140.10	4.50	0.90	0.60	0.50	0.40	1.10	1.33
4140.12	33.30	0.50	0.70	398.00	0.60	0.40	72.25
4140.13	1.40	0.60	0.70	0.40	0.60	0.50	0.70
4140.15	0.70	0.50	0.30	0.10	0.30	0.20	0.35
4140.17	0.90	0.80	0.60	0.40	0.50	0.60	0.63
4140.18	0.90	0.50	0.50	0.30	0.70	0.60	0.58
4140.20	0.70	1.90	0.70	1.20	0.70	2.80	1.33
4140.22	21.30	20.40	0.80	1.00	0.50	1.10	7.52
4140.23	1.70	1000.00	0.80	1.90	221.00	1.20	204.43
4140.25	0.80	0.70	12.10	2.40	260.00	0.80	46.13
4140.27	179.00	87.00	102.00	0.80	1000.00	1000.00	394.80
4140.28	102.00	105.00	101.00	105.00	110.00	142.00	110.83
4140.30	108.00	116.00	115.00	102.00	102.00	101.00	107.33
4140.32	108.00	103.00	100.00	106.00	103.00	201.00	120.17
4140.33	1.20	0.70	0.80	48.40	16.60	21.80	14.92
4140.35	1000.00	0.80	1000.00	25.60	1.60	84.00	28.00
4140.37	334.00	334.00	1000.00	3.60	3.00	227.00	180.30
4140.38	1.90	1.40	0.50	613.00	0.70	11.30	104.80
4140.40	1.20	1.30	92.00	0.50	0.90	0.30	16.03
4140.42	0.90	5.10	1.60	1.40	0.30	2.00	1.88
4140.43	0.80	4.70	0.80	0.70	0.70	0.40	1.35
4140.45	0.50	0.50	0.30	0.30	0.50	0.30	0.40
4140.47	229.00	7.40	55.00	0.80	1.00	0.40	48.93
4140.48	0.50	1.50	1000.00	8.60	10.50	19.60	8.14
4140.50	301.00	0.70	425.00	71.00	9.70	1.50	134.82
4140.52	228.00	0.50	1.50	0.80	4.70	3.70	39.87
4140.53	0.70	1.80	2.10	97.00	0.40	0.30	17.05
4140.55	1.10	0.50	2.20	0.80	0.30	79.00	13.98
4140.57	15.30	2.70	2.20	1.00	0.60	10.60	5.40
4140.58	0.70	7.10	0.50	1.00	0.60	1.60	1.92
4140.60	3.00	70.00	1000.00	0.90	0.50	2.80	15.40
4140.62	0.70	1000.00	166.00	2.60	662.00	11.00	168.46
4140.63	1000.00	1000.00	1.80	0.90	1.10	1.40	1.30
4140.65	0.70	0.70	20.50	0.40	0.40	2.50	4.20
4140.67	4.80	2.60	2.60	13.00	0.30	4.80	4.68
4140.68	0.40	0.70	0.40	0.30	0.30	0.30	0.40
4140.70	0.50	0.40	0.40	0.30	0.30	0.40	0.38
4140.72	5.90	48.80	12.70	0.90	0.30	0.40	11.50
4140.73	1.40	5.70	3.50	0.20	15.40	358.00	64.03
4140.75	1000.00	0.40	0.50	0.20	8.20	0.50	1.96
4140.77	0.60	0.60	0.60	0.60	7.50	0.40	1.72
4140.78	0.70	0.60	0.80	1.90	7.80	2.20	2.33
4140.80	0.50	0.60	0.80	0.50	227.00	69.00	49.73
4140.82	0.90	0.80	0.80	0.40	0.70	2.50	1.02

Petrographic data for the San Andres Formation

sample#	k (md)	Total porosity	intercry-stalline Porosity (%)	Intergran-ular Porosity (%)	Vugs (%)	Intracon-stituent Porosity (%)	Mold (%)	Fracture (%)	Vugs size (mm)	Pore size (mm)
Well: Mayers A-1#17										
Oolitic Packstone										
SAD390	0.90	2.00	0.20	0.00	1.80	0.00	0.00	0.00		0.01
SAD390	0.40	0.50	0.50	0.00	0.00	0.00	0.00	0.00		0.01
SAD390	0.30	0.50	0.50	0.00	0.00	0.00	0.00	0.00		0.01
SAD390	0.20	0.50	0.50	0.00	0.00	0.00	0.00	0.00		0.01
SAD390	0.50	0.50	0.50	0.00	0.00	0.00	0.00	0.00		0.01
SAD390	54.70	20.00	0.00	0.00	20.00	0.00	0.00	0.00	1.20	1.20
SAD390	3.40	4.00	2.40	0.00	1.60	0.00	0.00	0.00		0.50
SAD390	212.00	6.00	0.00	0.00	0.00	0.00	0.00	0.00		channel pores
SAD390	163.00	5.00	0.00	0.00	0.00	0.00	0.00	0.00		channel pores
SAD390	2.40	1.00	0.00	0.00	1.00	0.00	0.00	0.00	0.09	0.09
SAD390	201.00	12.00	0.00	1.80	3.00	7.20	0.00	0.00		0.41
SAD390	0.70	1.00	0.00	0.00	1.00	0.00	0.00	0.00	0.10	0.10
SAD390	0.50	1.00	0.00	0.00	1.00	0.00	0.00	0.00	0.10	0.10
SAD390	200.00	40.00	0.00	0.00	40.00	0.00	0.00	0.00	2.30	2.30
SAD390	201.00	40.00	0.00	0.00	40.00	0.00	0.00	0.00	2.80	2.80
SAD390	201.00	15.00	0.00	4.50	6.00	4.50	0.00	0.00		0.30
SAD391	3.50	6.00	0.00	0.00	6.00	0.00	0.00	0.00	0.33	0.33
SAD391	2.30	4.00	0.00	0.00	4.00	0.00	0.00	0.00	0.33	0.33
SAD391	3.70	7.00	0.00	0.00	7.00	0.00	0.00	0.00	0.33	0.33

Petrographic data for the San Andres Formation

sample#	k (md)	Total porosity	intercry-stalline Porosity (%)	Intergran-ular Porosity (%)	Vugs (%)	Intracon-stituent Porosity (%)	Mold (%)	Fracture (%)	Vugs size (mm)	Pore size (mm)
SAD391	6.90	5.00	0.00	0.00	5.00	0.00	0.00	0.00	0.33	0.33
SAD391	3.50	6.00	0.00	0.00	6.00	0.00	0.00	0.00	0.33	0.33
SAD391	0.20	1.00	1.00	0.00	0.00	0.00	0.00	0.00		0.04
SAD391	0.20	1.00	1.00	0.00	0.00	0.00	0.00	0.00		0.04
SAD391	0.10	1.00	1.00	0.00	0.00	0.00	0.00	0.00		0.04
SAD391	0.20	1.00	1.00	0.00	0.00	0.00	0.00	0.00		0.04
SAD391	0.30	1.00	1.00	0.00	0.00	0.00	0.00	0.00		0.04
SAD391	0.20	1.00	1.00	0.00	0.00	0.00	0.00	0.00		0.04
SAD391	0.30	1.00	1.00	0.00	0.00	0.00	0.00	0.00		0.04
SAD391	0.30	1.00	1.00	0.00	0.00	0.00	0.00	0.00		0.04
SAD391	0.10	1.00	1.00	0.00	0.00	0.00	0.00	0.00		0.04
SAD391	0.20	1.00	1.00	0.00	0.00	0.00	0.00	0.00		0.04
SAD391	1.30	1.00	1.00	0.00	0.00	0.00	0.00	0.00		0.04
SAD391	0.20	1.00	1.00	0.00	0.00	0.00	0.00	0.00		0.04
SAD391	0.20	1.00	1.00	0.00	0.00	0.00	0.00	0.00		0.04
SAD391	0.10	1.00	1.00	0.00	0.00	0.00	0.00	0.00		0.04
SAD391	0.20	1.00	1.00	0.00	0.00	0.00	0.00	0.00		0.04
SAD391	0.20	1.00	1.00	0.00	0.00	0.00	0.00	0.00		0.04
SAD432	1.50	10.00	0.00	0.00	0.00	10.00	0.00	0.00		0.40
SAD432	1.00	12.00	0.00	0.00	0.00	12.00	0.00	0.00		0.65
SAD432	1.20	11.00	0.00	0.00	0.00	11.00	0.00	0.00		0.45

Petrographic data for the San Andres Formation

sample#	k (md)	Total porosity	intercry-stalline Porosity (%)	Intergran-ular Porosity (%)	Vugs (%)	Intracon-stituent Porosity (%)	Mold (%)	Fracture (%)	Vugs size (mm)	Pore size (mm)
SAD432	1.50	9.00	0.00	0.00	0.00	9.00	0.00	0.00		0.28
SAD432	0.90	4.00	0.00	0.00	0.00	4.00	0.00	0.00		0.33
SAD432	0.90	6.00	0.00	0.00	0.00	6.00	0.00	0.00		0.33
SAD432	1.20	5.00	0.00	0.00	0.00	5.00	0.00	0.00		0.30
SAD432	1.20	5.00	0.00	0.00	0.00	5.00	0.00	0.00		0.32
SAD432	0.80	4.00	0.00	0.00	0.00	4.00	0.00	0.00		0.15
SAD432	27.70	11.00	0.00	0.00	0.00	11.00	0.00	0.00		0.47
SAD432	0.70	6.00	0.00	0.00	0.00	6.00	0.00	0.00		0.30
SAD432	0.90	8.00	0.00	0.00	0.00	8.00	0.00	0.00		0.28
SAD432	1.70	12.00	0.00	0.00	0.00	12.00	0.00	0.00		0.33
SAD432	12.60	14.00	0.00	0.00	0.00	14.00	0.00	0.00		0.42
SAD432	16.40	12.00	0.00	0.00	0.00	12.00	0.00	0.00		0.48
SAD432	4.20	7.00	0.00	0.00	0.00	7.00	0.00	0.00		0.37
SAD432	0.70	3.00	0.00	0.00	0.00	3.00	0.00	0.00		0.33
SAD432	0.80	3.00	0.00	0.00	0.00	3.00	0.00	0.00		0.33
SAD432	2.60	9.00	0.00	0.00	0.00	9.00	0.00	0.00		0.35
SAD432	1.10	8.00	0.00	0.00	0.00	8.00	0.00	0.00		0.35
SAD432	0.90	4.00	0.00	0.00	0.00	4.00	0.00	0.00		0.30
SAD432	1.30	3.00	0.00	0.00	0.00	3.00	0.00	0.00		0.35
SAD432	1.20	3.00	0.00	0.00	0.00	3.00	0.00	0.00		0.35
SAD432	0.90	4.00	0.00	0.00	0.00	4.00	0.00	0.00		0.28

Petrographic data for the San Andres Formation

sample#	k (md)	Total porosity	intercry-stalline Porosity (%)	Intergran-ular Porosity (%)	Vugs (%)	Intracon-stituent Porosity (%)	Mold (%)	Fracture (%)	Vugs size (mm)	Pore size (mm)
SAD433	111.00	10.00	0.00	6.00	3.00	1.00	0.00	0.00		0.90
SAD433	8.40	15.00	0.00	0.00	10.50	4.50	0.00	0.00		1.02
SAD433	103.00	11.00	0.55	4.40	0.00	6.05	0.00	0.00		0.53
SAD433	348.00	20.00	0.00	6.00	8.00	6.00	0.00	0.00		0.84
SAD433	86.00	25.00	0.00	8.75	0.00	16.25	0.00	0.00		0.33
SAD433	86.00	25.00	0.00	8.75	0.00	16.25	0.00	0.00		0.33
SAD433	61.00	10.00	1.50	5.00	0.00	3.50	0.00	0.00		0.25
SAD433	126.00	22.00	0.00	13.20	0.00	8.80	0.00	0.00		0.50
SAD433	22.00	8.00	0.00	0.80	0.00	7.20	0.00	0.00		0.34
SAD433	229.00	20.00	1.00	9.00	6.00	4.00	0.00	0.00		0.80
SAD433	185.00	25.00	0.00	7.50	0.00	17.50	0.00	0.00		0.50
SAD433	77.00	20.00	0.00	3.00	0.00	17.00	0.00	0.00		0.94
SAD433	0.60	5.00	0.00	0.00	0.00	3.50	1.50	0.00		0.50
SAD433	0.80	5.00	0.00	0.00	0.00	3.50	1.50	0.00		0.50
SAD433	1.10	5.00	0.00	0.00	0.00	3.50	1.50	0.00		0.50
SAD444	24.60	15.00	0.00	2.25	0.00	12.75	0.00	0.00		0.57
SAD444	11.90	5.00	0.75	0.00	3.50	0.75	0.00	0.00		0.50
SAD444	27.50	11.00	0.55	0.00	1.10	9.35	0.00	0.00		0.55
SAD444	3.80	3.00	1.20	0.00	0.00	1.80	0.00	0.00		0.15
SAD444	20.30	7.00	1.40	0.00	5.60	0.00	0.00	0.00		0.50
SAD444	14.30	8.00	0.80	0.00	5.60	1.60	0.00	0.00		0.21

Petrographic data for the San Andres Formation

sample#	k (md)	Total porosity	intercry-stalline Porosity (%)	Intergran-ular Porosity (%)	Vugs (%)	Intracon-stituent Porosity (%)	Mold (%)	Fracture (%)	Vugs size (mm)	Pore size (mm)
SAD444	2.20	1.00	1.00	0.00	0.00	0.00	0.00	0.00		0.05
SAD444	2.70	1.00	1.00	0.00	0.00	0.00	0.00	0.00		0.05
SAD444	3.40	5.00	1.00	0.75	0.00	3.25	0.00	0.00		0.50
SAD444	1.20	1.00	1.00	0.00	0.00	0.00	0.00	0.00		0.05
SAD444	1.40	3.00	1.80	0.00	1.20	0.00	0.00	0.00		0.12
SAD444	2.20	3.00	1.80	0.00	1.20	0.00	0.00	0.00		0.12
Peloidal Wackestone										
SAN331	0.30	1.50	0.45	0.00	1.05	0.00	0.00	0.00		0.50
SAN331	3.20	12.00	1.20	0.00	10.80	0.00	0.00	0.00		0.10
SAN331	0.90	0.50	0.00	0.00	0.50	0.00	0.00	0.00	0.10	0.10
SAN331	1.00	7.00	0.00	0.00	7.00	0.00	0.00	0.00	0.35	0.35
SAN331	0.70	1.00	1.00	0.00	0.00	0.00	0.00	0.00		0.02
SAN331	3.70	15.00	0.00	0.00	15.00	0.00	0.00	0.00	0.38	0.38
SAN331	1.20	8.00	0.00	0.00	8.00	0.00	0.00	0.00	0.50	0.50
SAN331	5.10	5.00	2.00	0.00	3.00	0.00	0.00	0.00		0.30
SAN331	14.80	20.00	0.00	0.00	20.00	0.00	0.00	0.00	1.20	1.20
SAN331	5.20	5.00	4.50	0.00	0.50	0.00	0.00	0.00		0.50
SAN331	15.70	30.00	0.00	0.00	30.00	0.00	0.00	0.00	0.15	0.15
SAN331	0.60	4.00	0.00	0.00	4.00	0.00	0.00	0.00	0.23	0.23

Petrographic data for the San Andres Formation

sample#	k (md)	Total porosity	intercry-stalline Porosity (%)	Intergran-ular Porosity (%)	Vugs (%)	Intracon-stituent Porosity (%)	Mold (%)	Fracture (%)	Vugs size (mm)	Pore size (mm)
SAN331	39.80	30.00	0.00	0.00	30.00	0.00	0.00	0.00	2.50	2.50
SAN331	56.30	15.00	2.25	0.00	6.75	0.00	6.00	0.00		0.35
SAN331	30.80	25.00	1.25	0.00	10.00	0.00	13.75	0.00		0.50
SAN331	0.90	15.00	0.00	0.00	15.00	0.00	0.00	0.00	0.50	0.50
SAN331	0.50	10.00	0.00	0.00	10.00	0.00	0.00	0.00	0.16	0.16
SAN331	1.80	5.00	1.50	0.00	3.50	0.00	0.00	0.00		1.50
SAN331	132.00	45.00	0.00	0.00	45.00	0.00	0.00	0.00	2.80	2.80
SAN331	12.40	5.00	5.00	0.00	0.00	0.00	0.00	0.00		0.04
SAN331	18.60	8.00	4.80	0.00	3.20	0.00	0.00	0.00		0.60
SAN331	25.90	8.00	4.80	0.00	3.20	0.00	0.00	0.00		0.60
SAN332	0.40	2.00	0.00	0.00	2.00	0.00	0.00	0.00	0.08	0.08
SAN332	0.50	2.00	0.00	0.00	2.00	0.00	0.00	0.00	0.09	0.09
SAN332	0.20	1.00	0.00	0.00	1.00	0.00	0.00	0.00	0.06	0.06
SAN332	0.40	2.00	0.00	0.00	2.00	0.00	0.00	0.00	0.08	0.08
SAN332	0.40	2.00	0.00	0.00	2.00	0.00	0.00	0.00	0.08	0.08
SAN332	0.30	2.00	0.00	0.00	2.00	0.00	0.00	0.00	0.07	0.07
SAN332	0.40	2.00	0.00	0.00	2.00	0.00	0.00	0.00	0.09	0.09
SAN332	0.30	2.00	0.00	0.00	2.00	0.00	0.00	0.00	0.08	0.08
SAN332	0.40	2.00	0.00	0.00	2.00	0.00	0.00	0.00	0.09	0.09
SAN332	0.30	3.00	0.00	0.00	3.00	0.00	0.00	0.00	0.07	0.07
SAN332	0.40	2.00	0.00	0.00	2.00	0.00	0.00	0.00	0.08	0.08

Petrographic data for the San Andres Formation

sample#	k (md)	Total porosity	intercry-stalline Porosity (%)	Intergran-ular Porosity (%)	Vugs (%)	Intracon-stituent Porosity (%)	Mold (%)	Fracture (%)	Vugs size (mm)	Pore size (mm)
SAN332	0.20	1.00	0.00	0.00	1.00	0.00	0.00	0.00	0.07	0.07
SAN332	0.20	1.00	0.00	0.00	1.00	0.00	0.00	0.00	0.07	0.07
SAN333	66.00	15.00	0.00	0.00	15.00	0.00	0.00	0.00	0.64	0.64
SAN333	0.10	2.00	0.00	0.00	2.00	0.00	0.00	0.00	0.53	0.53
SAN333	386.00	25.00	0.00	0.00	25.00	0.00	0.00	0.00	1.78	1.78
SAN333	0.10	3.00	0.60	0.00	2.40	0.00	0.00	0.00	0.15	0.15
SAN333	231.00	8.00	1.60	0.00	6.40	0.00	0.00	0.00		0.52
SAN333	0.10	3.00	0.30	0.00	2.70	0.00	0.00	0.00		0.40
SAN333	0.30	4.00	0.80	0.00	3.20	0.00	0.00	0.00		0.25
SAN333	0.50	3.00	0.30	0.00	2.70	0.00	0.00	0.00		0.35
SAN333	213.00	30.00	0.00	0.00	9.00	0.00	0.00	21.00		0.26
SAN333	0.30	1.00	1.00	0.00	0.00	0.00	0.00	0.00		0.06
SAN333	0.50	1.00	0.40	0.00	0.60	0.00	0.00	0.00		0.12
SAN333	0.40	3.00	1.50	0.00	1.50	0.00	0.00	0.00		0.15
SAN333	900.00	20.00	0.00	0.00	0.00	0.00	0.00	20.00		0.80
SAN333	0.30	2.00	0.30	0.00	1.70	0.00	0.00	0.00		0.25
SAN333	0.20	3.00	0.00	0.00	3.00	0.00	0.00	0.00	0.30	0.30
SAN334	599.00	35.00	3.50	0.00	7.00	0.00	0.00	24.50		1.04
SAN334	970.00	20.00	2.00	0.00	8.00	0.00	0.00	10.00		0.80
SAN334	28.00	11.00	1.10	0.00	9.90	0.00	0.00	0.00		0.30
SAN334	0.60	1.00	0.00	0.00	1.00	0.00	0.00	0.00	0.08	0.08

Petrographic data for the San Andres Formation

sample#	k (md)	Total porosity	intercry-stalline Porosity (%)	Intergran-ular Porosity (%)	Vugs (%)	Intracon-stituent Porosity (%)	Mold (%)	Fracture (%)	Vugs size (mm)	Pore size (mm)
SAN334	343.00	20.00	1.00	0.00	19.00	0.00	0.00	0.00		1.25
SAN334	629.00	15.00	0.00	0.00	0.00	0.00	0.00	15.00		3.50
SAN334	0.40	1.00	0.00	0.00	1.00	0.00	0.00	0.00	0.20	0.20
SAN334	0.40	1.00	0.00	0.00	1.00	0.00	0.00	0.00	0.20	0.20
SAN334	1.30	3.00	0.00	0.00	3.00	0.00	0.00	0.00	0.30	0.30
SAN334	3.60	7.00	0.00	0.00	7.00	0.00	0.00	0.00	0.31	0.31
SAN334	3.60	7.00	0.00	0.00	7.00	0.00	0.00	0.00	0.31	0.31
SAN334	0.80	3.00	0.00	0.00	3.00	0.00	0.00	0.00	0.31	0.31
SAN334	5.00	7.00	0.00	0.00	1.40	0.00	0.00	5.60		0.17
SAN334	5.80	7.00	0.00	0.00	1.40	0.00	0.00	5.60		0.17
SAN334	0.60	15.00	0.00	0.00	15.00	0.00	0.00	0.00	0.45	0.45
SAN334	3.40	10.00	0.00	0.00	5.00	0.00	0.00	5.00		0.24
SAN334	0.90	2.00	0.00	0.00	2.00	0.00	0.00	0.00	0.25	0.25
SAN346	32.00	20.00	2.00	0.00	18.00	0.00	0.00	0.00		0.18
SAN346	29.30	20.00	2.00	0.00	18.00	0.00	0.00	0.00		0.18
SAN346	0.10	1.00	1.00	0.00	0.00	0.00	0.00	0.00		0.01
SAN346	0.10	1.00	1.00	0.00	0.00	0.00	0.00	0.00		0.01
SAN346	27.10	15.00	2.25	0.00	12.75	0.00	0.00	0.00		0.30
SAN346	27.10	15.00	2.25	0.00	12.75	0.00	0.00	0.00		0.30
SAN346	0.30	2.00	2.00	0.00	0.00	0.00	0.00	0.00		0.04
SAN346	1.00	3.00	1.80	0.00	1.20	0.00	0.00	0.00		0.10

Petrographic data for the San Andres Formation

sample#	k (md)	Total porosity	intercry-stalline Porosity (%)	Intergran-ular Porosity (%)	Vugs (%)	Intracon-stituent Porosity (%)	Mold (%)	Fracture (%)	Vugs size (mm)	Pore size (mm)
SAN346	2.08	4.00	4.00	0.00	0.00	0.00	0.00	0.00		0.04
SAN346	45.00	10.00	2.00	0.00	7.00	0.00	1.00	0.00		0.43
SAN346	17.50	6.00	0.90	0.00	0.00	0.00	0.00	5.10		0.12
SAN346	3.40	4.00	4.00	0.00	0.00	0.00	0.00	0.00		0.04
SAN346	3.40	4.00	4.00	0.00	0.00	0.00	0.00	0.00		0.04
SAN346	42.30	6.00	6.00	0.00	0.00	0.00	0.00	0.00		0.05
SAN346	42.30	6.00	6.00	0.00	0.00	0.00	0.00	0.00		0.05
SAN346	6.30	3.00	0.00	0.00	3.00	0.00	0.00	0.00	0.05	0.05
SAN346	1.00	2.00	2.00	0.00	0.00	0.00	0.00	0.00		0.04
Oolitic Peloidal Wackestone/Packstone										
SAN391	0.20	1.00	0.00	0.00	0.00	0.00	1.00	0.00		0.05
SAN391	0.40	1.00	0.00	0.00	0.00	0.00	1.00	0.00		0.05
SAN391	0.20	1.00	0.00	0.00	0.00	0.00	1.00	0.00		0.05
SAN391	0.10	0.50	0.00	0.00	0.00	0.00	0.50	0.00		0.05
SAN391	0.40	1.00	0.00	0.00	0.00	0.00	1.00	0.00		0.05
SAN391	0.20	0.50	0.00	0.00	0.00	0.00	0.50	0.00		0.05
SAN391	0.50	1.00	0.00	0.00	0.00	0.00	1.00	0.00		0.05
SAN391	0.50	1.00	0.00	0.00	0.00	0.00	1.00	0.00		0.05
SAN391	0.40	0.50	0.00	0.00	0.00	0.00	0.50	0.00		0.05

Petrographic data for the San Andres Formation

sample#	k (md)	Total porosity	intercry-stalline Porosity (%)	Intergran-ular Porosity (%)	Vugs (%)	Intracon-stituent Porosity (%)	Mold (%)	Fracture (%)	Vugs size (mm)	Pore size (mm)
SAN391	0.40	1.00	0.00	0.00	0.00	0.00	1.00	0.00		0.05
SAN391	0.60	2.00	0.00	0.00	0.00	0.00	2.00	0.00		0.05
SAN391	0.40	2.00	0.00	0.00	0.00	0.00	2.00	0.00		0.05
SAN391	0.30	2.00	0.00	0.00	0.00	0.00	2.00	0.00		0.05
SAN391	0.30	2.00	0.00	0.00	0.00	0.00	2.00	0.00		0.05
SAN391	0.80	1.00	0.00	0.00	0.00	0.00	1.00	0.00		0.05
SAN391	0.20	2.00	0.00	0.00	0.00	0.00	2.00	0.00		0.05
SAN391	0.10	1.00	0.00	0.00	0.00	0.00	1.00	0.00		0.05
SAN391	0.20	1.00	0.00	0.00	0.00	0.00	1.00	0.00		0.05
SAN391	0.20	1.00	0.00	0.00	0.00	0.00	1.00	0.00		0.05
SAN391	7.00	5.00	0.00	0.00	0.00	0.00	5.00	0.00		0.05
SAN391	7.00	5.00	0.00	0.00	0.00	0.00	5.00	0.00		0.05
SAN391	0.60	2.00	0.00	0.00	0.00	0.00	2.00	0.00		0.05
SAN391	1.30	3.00	0.00	0.00	0.00	0.00	3.00	0.00		0.05
SAN391	1.50	3.00	0.00	0.00	0.00	0.00	3.00	0.00		0.05
SAN392	0.50	1.00	0.00	0.00	0.00	0.00	1.00	0.00		0.05
SAN392	11.20	12.00	1.80	0.00	10.20	0.00	0.00	0.00		0.53
SAN392	840.00	20.00	0.00	0.00	20.00	0.00	0.00	0.00	2.50	2.50
SAN392	0.60	1.00	0.00	0.00	0.00	0.00	1.00	0.00		0.05
SAN392	614.00	30.00	0.00	0.00	30.00	0.00	0.00	0.00	2.90	2.90
SAN392	0.20	0.50	0.00	0.00	0.00	0.00	0.50	0.00		0.05

Petrographic data for the San Andres Formation

sample#	k (md)	Total porosity	intercry-stalline Porosity (%)	Intergran-ular Porosity (%)	Vugs (%)	Intracon-stituent Porosity (%)	Mold (%)	Fracture (%)	Vugs size (mm)	Pore size (mm)
SAN392	585.00	30.00	0.00	0.00	30.00	0.00	0.00	0.00	3.50	3.50
SAN392	190.00	20.00	0.00	0.00	20.00	0.00	0.00	0.00	3.50	3.50
SAN392	0.10	1.00	0.00	0.00	0.00	0.00	1.00	0.00		0.05
SAN392	0.40	1.00	0.00	0.00	0.00	0.00	1.00	0.00		0.05
SAN392	0.20	1.00	0.00	0.00	0.00	0.00	1.00	0.00		0.05
SAN392	0.30	3.00	0.00	0.00	3.00	0.00	0.00	0.00	0.80	0.80
SAN392	0.20	0.50	0.50	0.00	0.00	0.00	0.00	0.00		0.01
SAN392	0.40	0.50	0.50	0.00	0.00	0.00	0.00	0.00		0.01
SAN392	2.10	10.00	0.00	0.00	10.00	0.00	0.00	0.00	2.50	2.50
SAN392	0.20	20.00	0.00	0.00	20.00	0.00	0.00	0.00	3.00	3.00
SAN392	0.40	4.00	0.00	0.00	4.00	0.00	0.00	0.00	1.20	1.20
SAN393	474.00	25.00	0.00	0.00	25.00	0.00	0.00	0.00	1.03	1.03
SAN393	78.00	20.00	0.00	0.00	20.00	0.00	0.00	0.00	4.00	4.00
SAN393	0.90	6.00	0.00	0.00	6.00	0.00	0.00	0.00	0.54	0.54
SAN393	0.30	2.00	1.00	0.00	1.00	0.00	0.00	0.00		0.05
SAN393	23.90	15.00	1.50	0.00	13.50	0.00	0.00	0.00		0.43
SAN393	1402.00	35.00	0.00	0.00	35.00	0.00	0.00	0.00	0.80	0.80
SAN393	763.00	35.00	0.00	0.00	35.00	0.00	0.00	0.00	3.50	3.50

Well: State ACCT2 #60
Peloidal Wackestone/Packstone

Petrographic data for the San Andres Formation

sample#	k (md)	Total porosity	intercry-stalline Porosity (%)	Intergran-ular Porosity (%)	Vugs (%)	Intracon-stituent Porosity (%)	Mold (%)	Fracture (%)	Vugs size (mm)	Pore size (mm)
SAN451	15.30	12.00	4.80	0.00	7.20	0.00			0.00	0.20
SAN451	13.30	8.00	7.20	0.00	0.00	0.00			0.00	0.07
SAN451	100.00	15.00	8.25	0.00	0.00	0.00			0.00	0.20
SAN451	14.70	7.00	4.55	0.00	0.00	0.00			0.00	0.06
SAN451	20.10	6.00	5.10	0.00	0.00	0.00			0.00	0.05
SAN451	5.70	6.00	0.90	0.00	0.00	0.00			0.00	0.07
SAN452	2.40	4.00	3.20	0.00	0.00	0.00			0.00	0.07
SAN452	8.90	5.00	4.75	0.00	0.00	0.00			0.00	0.08
SAN452	8.30	3.00	3.00	0.00	0.00	0.00			0.00	0.04
SAN452	22.90	9.00	9.00	0.00	0.00	0.00			0.00	0.05
SAN452	5.60	4.00	4.00	0.00	0.00	0.00			0.00	0.05
SAN452	11.00	10.00	7.50	0.00	0.00	0.00			0.00	0.08
SAN453	65.00	8.00	8.00	0.00	0.00	0.00			0.00	0.30
SAN453	13.30	5.00	3.50	0.00	0.00	0.00			0.00	0.18
SAN453	44.60	8.00	8.00	0.00	0.00	0.00			0.00	0.04
SAN453	23.30	6.00	6.00	0.00	0.00	0.00			0.00	0.04
SAN453	25.30	7.00	7.00	0.00	0.00	0.00			0.00	0.03
SAN453	16.50	11.00	8.25	0.00	2.75	0.00			0.00	0.11
SAN464	14.30	6.00	1.20	0.00	4.80	0.00			0.00	0.13
SAN464	12.60	6.00	1.20	0.00	4.80	0.00			0.00	0.13
SAN464	20.70	10.00	1.00	0.00	9.00	0.00			0.00	0.11

Petrographic data for the San Andres Formation

sample#	k (md)	Total porosity	intercry-stalline Porosity (%)	Intergran-ular Porosity (%)	Vugs (%)	Intracon-stituent Porosity (%)	Mold (%)	Fracture (%)	Vugs size (mm)	Pore size (mm)
SAN464	29.30	15.00	0.75	0.00	14.25	0.00			0.00	0.11
SAN464	18.20	8.00	1.20	0.00	6.80	0.00			0.00	0.11
SAN464	20.90	8.00	1.20	0.00	6.80	0.00			0.00	0.11
SAN465	38.20	8.00	8.00	0.00	0.00	0.00			0.00	0.03
SAN465	26.10	11.00	7.70	0.00	3.30	0.00			0.00	0.23
SAN465	87.00	13.00	13.00	0.00	0.00	0.00			0.00	0.03
SAN465	49.00	9.00	5.85	0.00	3.15	0.00			0.00	0.11
SAN465	49.40	9.00	5.85	0.00	3.15	0.00			0.00	0.11
SAN465	62.20	11.00	7.15	0.00	3.85	0.00			0.00	0.11
SAN476	28.40	6.00	6.00	0.00	0.00	0.00			0.00	0.03
SAN476	21.60	5.00	5.00	0.00	0.00	0.00			0.00	0.03
SAN476	9.00	3.00	3.00	0.00	0.00	0.00			0.00	0.04
SAN476	11.70	5.00	1.50	0.00	3.50	0.00			0.00	0.25
SAN476	8.70	4.00	0.80	0.00	3.20	0.00			0.00	0.12
SAN476	17.00	6.00	5.40	0.00	0.60	0.00			0.00	0.04
SAN477	1.90	2.00	0.10	0.00	1.90	0.00			0.00	0.08
SAN477	2.00	2.00	0.10	0.00	1.90	0.00			0.00	0.08
SAN477	0.30	1.00	0.50	0.00	0.50	0.00			0.00	0.04
SAN477	0.40	1.00	0.50	0.00	0.50	0.00			0.00	0.04
SAN477	50.00	15.00	0.75	0.00	14.25	0.00			0.00	0.50
SAN477	8.20	8.00	3.60	0.00	4.40	0.00			0.00	0.06

Petrographic data for the San Andres Formation

sample#	k (md)	Total porosity	intercry-stalline Porosity (%)	Intergran-ular Porosity (%)	Vugs (%)	Intracon-stituent Porosity (%)	Mold (%)	Fracture (%)	Vugs size (mm)	Pore size (mm)
SAN477	22.10	10.00	10.00	0.00	0.00	0.00			0.00	0.03
SAN477	17.50	10.00	10.00	0.00	0.00	0.00			0.00	0.03
SAN478	0.40	0.50	0.50	0.00	0.00	0.00			0.00	0.03
SAN478	0.30	0.50	0.50	0.00	0.00	0.00			0.00	0.03
SAN478	0.40	0.50	0.50	0.00	0.00	0.00			0.00	0.03
SAN478	0.20	0.50	0.50	0.00	0.00	0.00			0.00	0.03
SAN499	14.90	7.00	4.20	0.00	2.80	0.00			0.00	0.15
SAN499	14.90	7.00	4.20	0.00	2.80	0.00			0.00	0.15
SAN499	9.00	8.00	4.80	0.00	3.20	0.00			0.00	0.15
SAN499	57.30	9.00	3.60	0.00	5.40	0.00			0.00	0.20
SAN499	6.10	4.00	3.20	0.00	0.80	0.00			0.00	0.04
SAN499	12.30	6.00	6.00	0.00	0.00	0.00			0.00	0.02
SAN5111	13.40	7.00	7.00	0.00	0.00	0.00			0.00	0.04
SAN5111	47.90	13.00	9.10	0.00	3.90	0.00			0.00	0.17
SAN5111	9.80	4.00	4.00	0.00	0.00	0.00			0.00	0.04
SAN5111	8.20	6.00	4.50	0.00	1.50	0.00			0.00	0.13
SAN5111	15.20	10.00	3.00	0.00	7.00	0.00			0.00	0.21
SAN5111	39.30	15.00	5.25	0.00	9.75	0.00			0.00	0.25
SAN5314	9.70	10.00	1.50	0.00	8.50	0.00			0.00	0.11
SAN5314	8.70	10.00	1.50	0.00	8.50	0.00			0.00	0.11
SAN5314	70.00	12.00	10.80	0.00	1.20	0.00			0.00	0.08

Petrographic data for the San Andres Formation

sample#	k (md)	Total porosity	intercry-stalline Porosity (%)	Intergran-ular Porosity (%)	Vugs (%)	Intracon-stituent Porosity (%)	Mold (%)	Fracture (%)	Vugs size (mm)	Pore size (mm)
SAN5314	31.90	9.00	7.65	0.00	1.35	0.00			0.00	0.05
SAN5314	15.80	12.00	3.60	0.00	8.40	0.00			0.00	0.25
SAN5314	8.50	6.00	5.40	0.00	0.60	0.00			0.00	0.05
SAN561	23.00	5.00	5.00	0.00	0.00	0.00			0.00	0.01
SAN561	21.60	8.00	3.20	0.00	4.80	0.00			0.00	0.08
SAN561	5.80	3.00	3.00	0.00	0.00	0.00			0.00	0.01
SAN561	15.60	4.00	4.00	0.00	0.00	0.00			0.00	0.03
SAN561	6.30	4.00	4.00	0.00	0.00	0.00			0.00	0.01
SAN561	18.00	15.00	8.25	0.00	6.75	0.00			0.00	0.30
SAN562	11.20	8.00	2.80	0.00	5.20	0.00			0.00	0.22
SAN562	31.30	6.00	5.10	0.00	0.90	0.00			0.00	0.15
SAN562	9.60	4.00	4.00	0.00	0.00	0.00			0.00	0.07
SAN562	17.80	6.00	6.00	0.00	0.00	0.00			0.00	0.04
SAN562	6.60	3.00	3.00	0.00	0.00	0.00			0.00	0.01
SAN562	18.10	7.00	2.80	0.00	4.20	0.00			0.00	0.50
SAN573	24.10	9.00	9.00	0.00	0.00	0.00			0.00	0.03
SAN573	17.30	5.00	5.00	0.00	0.00	0.00			0.00	0.01
SAN573	27.10	11.00	11.00	0.00	0.00	0.00			0.00	0.05
SAN573	28.70	11.00	11.00	0.00	0.00	0.00			0.00	0.05
SAN573	35.50	15.00	15.00	0.00	0.00	0.00			0.00	0.05
SAN573	22.10	10.00	10.00	0.00	0.00	0.00			0.00	0.05

Petrographic data for the San Andres Formation

sample#	k (md)	Total porosity	intercry-stalline Porosity (%)	Intergran-ular Porosity (%)	Vugs (%)	Intracon-stituent Porosity (%)	Mold (%)	Fracture (%)	Vugs size (mm)	Pore size (mm)
SAN574	19.00	7.00	7.00	0.00	0.00	0.00			0.00	0.05
SAN574	11.90	8.00	2.80	0.00	5.20	0.00			0.00	0.22
SAN574	20.50	10.00	10.00	0.00	0.00	0.00			0.00	0.05
SAN574	6.80	4.00	4.00	0.00	0.00	0.00			0.00	0.01
SAN574	8.60	4.00	4.00	0.00	0.00	0.00			0.00	0.07
SAN574	3.50	2.00	0.10	0.00	1.90	0.00			0.00	0.08
SAN574	4.40	2.00	0.10	0.00	1.90	0.00			0.00	0.08
SAN586	15.90	6.00	6.00	0.00	0.00	0.00			0.00	0.04
SAN586	20.20	10.00	10.00	0.00	0.00	0.00			0.00	0.05
SAN586	52.30	13.00	9.10	0.00	3.90	0.00			0.00	0.17
SAN586	18.10	7.00	7.00	0.00	0.00	0.00			0.00	0.05
SAN586	16.70	6.00	6.00	0.00	0.00	0.00			0.00	0.04
SAN586	21.10	10.00	10.00	0.00	0.00	0.00			0.00	0.05
SAN587	7.30	3.00	3.00	0.00	0.00	0.00			0.00	0.01
SAN587	4.50	2.00	0.10	0.00	1.90	0.00			0.00	0.08
SAN587	11.10	8.00	2.80	0.00	5.20	0.00			0.00	0.22
SAN587	2.90	2.00	0.10	0.00	1.90	0.00			0.00	0.08
SAN587	5.70	4.00	4.00	0.00	0.00	0.00			0.00	0.01
SAN587	2.70	2.00	0.10	0.00	1.90	0.00			0.00	0.08
SAN588	4.30	4.00	4.00	0.00	0.00	0.00			0.00	0.01
SAN588	3.50	4.00	4.00	0.00	0.00	0.00			0.00	0.01

Petrographic data for the San Andres Formation

sample#	k (md)	Total porosity	intercry-stalline Porosity (%)	Intergran-ular Porosity (%)	Vugs (%)	Intracon-stituent Porosity (%)	Mold (%)	Fracture (%)	Vugs size (mm)	Pore size (mm)
SAN588	8.70	6.00	6.00	0.00	0.00	0.00			0.00	0.04
SAN588	18.70	7.00	7.00	0.00	0.00	0.00			0.00	0.05
SAN588	20.10	10.00	10.00	0.00	0.00	0.00			0.00	0.05
SAN588	29.30	15.00	15.00	0.00	0.00	0.00			0.00	0.05
SAN589	14.90	6.00	6.00	0.00	0.00	0.00			0.00	0.04
SAN589	2.80	2.00	0.10	0.00	1.90	0.00			0.00	0.08
SAN589	17.40	7.00	7.00	0.00	0.00	0.00			0.00	0.05
SAN589	3.80	2.00	0.10	0.00	1.90	0.00			0.00	0.08
SAN589	7.50	3.00	3.00	0.00	0.00	0.00			0.00	0.01
SAN589	4.80	2.00	0.10	0.00	1.90	0.00			0.00	0.08
SAN5810	3.70	4.00	4.00	0.00	0.00	0.00			0.00	0.01
SAN5810	30.70	15.00	15.00	0.00	0.00	0.00			0.00	0.05
SAN5810	22.70	10.00	10.00	0.00	0.00	0.00			0.00	0.05
SAN5810	15.40	6.00	6.00	0.00	0.00	0.00			0.00	0.04
SAN5810	10.00	6.00	6.00	0.00	0.00	0.00			0.00	0.04
SAN5810	13.30	7.00	7.00	0.00	0.00	0.00			0.00	0.05
SAN6011	4.20	2.00	0.10	0.00	1.90	0.00			0.00	0.08
SAN6011	5.00	3.00	3.00	0.00	0.00	0.00			0.00	0.01
SAN6011	8.30	3.00	3.00	0.00	0.00	0.00			0.00	0.01
SAN6011	3.60	2.00	0.10	0.00	1.90	0.00			0.00	0.08
SAN6011	5.60	4.00	4.00	0.00	0.00	0.00			0.00	0.01

Petrographic data for the San Andres Formation

sample#	k (md)	Total porosity	intercry-stalline Porosity (%)	Intergran-ular Porosity (%)	Vugs (%)	Intracon-stituent Porosity (%)	Mold (%)	Fracture (%)	Vugs size (mm)	Pore size (mm)
SAN6011	5.40	4.00	4.00	0.00	0.00	0.00			0.00	0.01
SAN6012	7.30	3.00	3.00	0.00	0.00	0.00			0.00	0.01
SAN6012	2.80	2.00	0.10	0.00	1.90	0.00			0.00	0.08
SAN6012	6.90	4.00	4.00	0.00	0.00	0.00			0.00	0.01
SAN6012	3.20	2.00	0.10	0.00	1.90	0.00			0.00	0.08
SAN6012	7.70	6.00	6.00	0.00	0.00	0.00			0.00	0.04
SAN6012	1.70	2.00	0.10	0.00	1.90	0.00			0.00	0.08
SAN613	5.70	4.00	4.00	0.00	0.00	0.00			0.00	0.01
SAN613	21.10	10.00	10.00	0.00	0.00	0.00			0.00	0.05
SAN613	2.00	2.00	0.10	0.00	1.90	0.00			0.00	0.08
SAN613	2.50	2.00	0.10	0.00	1.90	0.00			0.00	0.08
SAN613	10.00	6.00	6.00	0.00	0.00	0.00			0.00	0.04
SAN613	5.50	4.00	4.00	0.00	0.00	0.00			0.00	0.01
SAN6114	2.10	2.00	0.10	0.00	1.90	0.00			0.00	0.08
SAN6114	2.30	2.00	0.10	0.00	1.90	0.00			0.00	0.08
SAN6114	2.90	2.00	0.10	0.00	1.90	0.00			0.00	0.08
SAN6114	2.40	2.00	0.10	0.00	1.90	0.00			0.00	0.08
SAN6114	1.70	2.00	0.10	0.00	1.90	0.00			0.00	0.08
SAN6114	1.70	2.00	0.10	0.00	1.90	0.00			0.00	0.08

APPENDIX B

- Old gamma ray log data including the rescaled logs in the Sulimar Queen and Adjacent fields

Well: 1-2 TVDSS (ft)	Old Gamma (API)	Corrected Gamma (API)	Porosity (%) from Gamma	Neutron (API)
1971.00	56.46	29.53	1.59	1190.41
1970.50	38.15	22.54	1.10	1199.30
1970.00	35.39	18.90	0.91	1227.50
1969.50	33.06	15.82	0.77	1296.74
1969.00	30.19	12.03	0.63	1359.05
1968.50	30.11	11.93	0.63	1401.09
1968.00	30.43	12.35	0.64	1405.31
1967.50	30.70	12.70	0.65	1404.66
1967.00	31.31	13.51	0.68	1397.69
1966.50	35.18	18.62	0.89	1370.74
1966.00	38.60	23.14	1.13	1373.22
1965.50	46.85	34.03	2.02	1289.47
1965.00	50.69	39.10	2.64	1252.32
1964.50	55.81	45.85	3.77	1193.58
1964.00	66.43	59.87	7.90	1170.76
1963.50	68.14	62.13	8.91	1177.66
1963.00	68.54	62.65	9.16	1163.51
1962.50	70.75	65.57	10.68	1067.97
1962.00	75.40	71.70	14.77	1036.44
1961.50	76.32	72.92	15.76	973.59
1961.00	77.04	73.88	16.57	959.16
1960.50	79.80	77.52	20.09	953.34
1960.00	81.91	80.30	23.27	944.24
1959.50	80.54	78.50	21.16	934.72
1959.00	78.46	75.74	18.29	917.36
1958.50	77.09	73.94	16.63	862.47
1958.00	77.25	74.15	16.82	880.93
1957.50	77.03	73.85	16.55	897.70
1957.00	75.82	72.26	15.22	901.30
1956.50	68.48	62.58	9.12	903.96
1956.00	68.17	62.16	8.92	902.94
1955.50	69.99	64.57	10.13	906.59
1955.00	77.67	74.70	17.31	922.87
1954.50	80.95	79.03	21.76	930.54
1954.00	74.45	70.45	13.83	947.99
1953.50	66.42	59.85	7.90	957.60
1953.00	65.86	59.12	7.60	972.53
1952.50	59.11	50.21	4.74	997.25
1952.00	53.81	43.21	3.28	1033.62
1951.50	50.92	39.39	2.68	1067.86
1951.00	49.50	37.53	2.43	1094.96
1950.50	50.48	38.82	2.60	1137.49
1950.00	50.71	39.11	2.64	1194.36
1949.50	46.07	33.00	1.91	1255.19
1949.00	43.58	29.70	1.60	1293.68
1948.50	43.18	29.18	1.56	1319.77
1948.00	43.35	29.40	1.58	1326.51
1947.50	41.67	27.19	1.40	1324.65
1947.00	39.22	23.95	1.18	1331.10
1946.50	37.27	21.38	1.03	1348.97
1946.00	40.38	25.48	1.28	1340.23
1945.50	48.07	35.63	2.19	1315.93
1945.00	52.21	41.10	2.93	1273.06
1944.50	51.99	40.81	2.89	1208.89
1944.00	53.03	42.19	3.10	1169.35
1943.50	58.17	48.96	4.44	1152.68
1943.00	59.77	51.08	4.97	1143.40

Well: 1-3 TVDSS (ft)	Old Gamma (API)	Corrected Gamma (API)	Porosity (%) from Gamma	Neutron (API)
1986.00	41.88	26.79	1.38	1138.89
1985.50	40.32	23.89	1.18	1236.30
1985.00	40.62	24.44	1.21	1332.47
1984.50	38.62	20.72	1.00	1370.07
1984.00	34.35	12.79	0.66	1357.32
1983.50	33.96	12.05	0.63	1505.84
1983.00	35.90	15.66	0.76	1525.35
1982.50	36.78	17.30	0.83	1531.30
1982.00	38.13	19.81	0.95	1503.86
1981.50	41.07	25.27	1.27	1483.34
1981.00	45.81	34.10	2.02	1439.57
1980.50	50.26	42.38	3.14	1365.73
1980.00	54.60	50.44	4.80	1285.27
1979.50	57.91	56.60	6.65	1198.51
1979.00	59.38	59.34	7.69	1173.54
1978.50	62.66	65.43	10.61	1144.82
1978.00	65.72	71.13	14.33	1117.03
1977.50	68.95	77.14	19.70	1043.64
1977.00	71.02	80.98	24.13	976.13
1976.50	69.80	78.71	21.40	898.83
1976.00	69.28	77.75	20.34	877.89
1975.50	70.37	79.78	22.64	851.80
1975.00	70.20	79.45	22.26	848.82
1974.50	70.07	79.22	21.98	859.57
1974.00	70.80	80.58	23.63	866.76
1973.50	70.38	79.80	22.67	864.33
1973.00	70.03	79.15	21.90	877.39
1972.50	68.31	75.95	18.49	891.45
1972.00	65.00	69.79	13.35	904.16
1971.50	65.71	71.11	14.32	907.62
1971.00	64.00	67.92	12.10	909.01
1970.50	61.67	63.60	9.63	916.61
1970.00	59.89	60.28	8.08	926.31
1969.50	59.52	59.59	7.79	954.92
1969.00	58.08	56.91	6.76	973.56
1968.50	55.31	51.77	5.15	1037.46
1968.00	52.15	45.88	3.77	1035.44
1967.50	49.04	40.11	2.78	1122.03
1967.00	46.19	34.81	2.10	1147.65
1966.50	45.80	34.08	2.02	1174.54
1966.00	46.99	36.30	2.27	1222.70
1965.50	47.41	37.07	2.37	1277.50
1965.00	46.45	35.29	2.16	1338.16
1964.50	46.85	36.03	2.24	1385.13
1964.00	47.12	36.53	2.30	1451.15
1963.50	43.57	29.94	1.62	1485.23
1963.00	39.44	22.25	1.08	1500.48
1962.50	38.35	20.21	0.97	1527.80
1962.00	39.49	22.33	1.09	1537.91
1961.50	44.26	31.21	1.74	1491.50
1961.00	49.02	40.08	2.78	1424.16
1960.50	50.48	42.78	3.20	1376.04

Well: 1-4 TVDSS (ft)	Old Gamma (API)	Corrected Gamma (API)	Porosity (%) from Gamma	Neutron (API)
1958.00	50.05	35.86	2.22	831.27
1957.50	44.41	29.65	1.60	877.28
1957.00	44.59	29.85	1.62	945.71
1956.50	42.13	27.14	1.40	958.34
1956.00	39.18	23.90	1.18	982.26
1955.50	32.14	16.16	0.78	1064.86
1955.00	30.38	14.21	0.71	1134.08
1954.50	29.68	13.45	0.68	1137.23
1954.00	28.36	11.99	0.63	1148.21
1953.50	29.32	13.05	0.67	1156.83
1953.00	30.26	14.08	0.70	1162.11
1952.50	33.63	17.79	0.85	1165.64
1952.00	39.31	24.04	1.19	1159.59
1951.50	50.71	36.58	2.31	1143.83
1951.00	59.60	46.36	3.87	1121.53
1950.50	69.34	57.07	6.82	1085.06
1950.00	74.83	63.11	9.38	1007.70
1949.50	80.20	69.02	12.82	914.17
1949.00	90.62	80.48	23.50	791.37
1948.50	85.44	74.78	17.39	752.57
1948.00	78.57	67.23	11.66	754.14
1947.50	79.53	68.29	12.33	751.78
1947.00	80.92	69.82	13.37	746.27
1946.50	83.18	72.30	15.25	743.97
1946.00	84.66	73.93	16.62	754.91
1945.50	83.62	72.78	15.64	759.19
1945.00	84.29	73.51	16.26	755.16
1944.50	82.48	71.53	14.64	749.85
1944.00	84.84	74.12	16.79	746.04
1943.50	78.79	67.47	11.81	748.00
1943.00	76.20	64.62	10.16	742.93
1942.50	77.31	65.85	10.84	739.77
1942.00	78.27	66.90	11.46	742.37
1941.50	79.32	68.05	12.18	742.85
1941.00	78.28	66.91	11.47	755.21
1940.50	84.02	73.22	16.01	759.75
1940.00	84.98	74.28	16.93	761.36
1939.50	78.97	67.66	11.93	763.30
1939.00	70.98	58.88	7.50	776.92
1938.50	70.54	58.40	7.31	786.73
1938.00	63.72	50.90	4.92	809.46
1937.50	60.56	47.42	4.09	852.91
1937.00	59.08	45.79	3.75	885.75
1936.50	54.04	40.24	2.80	921.97
1936.00	52.54	38.60	2.57	968.99
1935.50	52.42	38.46	2.55	966.55
1935.00	52.81	38.89	2.61	994.07
1934.50	53.37	39.50	2.69	1012.83
1934.00	52.63	38.69	2.58	1032.47
1933.50	53.70	39.87	2.75	1086.86
1933.00	52.61	38.67	2.58	1108.44
1932.50	52.33	38.36	2.54	1134.06
1932.00	44.68	29.95	1.63	1156.85
1931.50	35.55	19.91	0.96	1174.67
1931.00	27.30	10.83	0.59	1188.25
1930.50	28.37	12.01	0.63	1176.05
1930.00	39.27	24.00	1.19	1170.45
1929.50	42.62	27.68	1.44	1149.71
1929.00	49.40	35.14	2.14	1099.92
1928.50	56.43	42.87	3.22	1046.50
1928.00	57.52	44.07	3.43	1033.88

Well: 1-5 TVDSS (ft)	Old Gamma (API)	Corrected Gamma (API)	Porosity (%) from Gamma	Neutron (API)
1941.00	66.29	44.12	3.44	1170.44
1940.50	58.54	29.64	1.60	1192.89
1940.00	57.30	27.32	1.41	1237.67
1939.50	57.60	27.89	1.46	1253.16
1939.00	52.11	17.62	0.85	1281.09
1938.50	49.15	12.08	0.63	1323.91
1938.00	48.97	11.75	0.62	1393.20
1937.50	49.96	13.60	0.69	1429.81
1937.00	50.44	14.49	0.72	1440.16
1936.50	53.13	19.53	0.94	1453.40
1936.00	57.99	28.62	1.51	1460.80
1935.50	63.64	39.17	2.65	1455.50
1935.00	70.18	51.41	5.05	1445.35
1934.50	77.58	65.25	10.50	1377.63
1934.00	82.76	74.94	17.53	1345.75
1933.50	85.50	80.05	22.97	1253.74
1933.00	83.88	77.03	19.58	1182.56
1932.50	82.44	74.34	16.99	1095.89
1932.00	83.83	76.94	19.49	1056.75
1931.50	81.49	72.56	15.46	1045.01
1931.00	80.08	69.93	13.45	1023.48
1930.50	80.08	69.93	13.45	1018.82
1930.00	80.86	71.38	14.52	1028.56
1929.50	75.56	61.46	8.60	1038.67
1929.00	79.75	69.31	13.02	1053.24
1928.50	83.41	76.14	18.68	1068.39
1928.00	84.47	78.13	20.75	1073.61
1927.50	83.67	76.64	19.18	1061.76
1927.00	83.50	76.31	18.85	1046.30
1926.50	85.90	80.80	23.90	1044.14
1926.00	82.41	74.28	16.93	1065.48
1925.50	79.56	68.94	12.77	1077.80
1925.00	79.19	68.26	12.31	1086.81
1924.50	78.37	66.73	11.36	1097.97
1924.00	78.86	67.65	11.92	1104.16
1923.50	75.40	61.18	8.47	1100.46
1923.00	75.92	62.14	8.91	1135.21
1922.50	75.98	62.25	8.96	1142.71
1922.00	73.68	57.96	7.15	1130.53
1921.50	70.54	52.08	5.24	1119.66
1921.00	67.50	46.39	3.88	1094.89
1920.50	64.26	40.34	2.82	1091.46
1920.00	62.22	36.51	2.30	1094.05
1919.50	61.43	35.05	2.13	1114.91
1919.00	60.65	33.58	1.97	1159.26
1918.50	62.20	36.48	2.30	1178.18
1918.00	62.00	36.11	2.25	1212.15
1917.50	62.08	36.25	2.27	1279.31
1917.00	62.51	37.07	2.37	1273.39
1916.50	64.38	40.57	2.85	1314.77
1916.00	67.11	45.66	3.73	1347.77
1915.50	68.66	48.56	4.35	1395.11
1915.00	69.10	49.38	4.54	1448.94
1914.50	64.00	39.85	2.74	1462.43
1914.00	54.55	22.18	1.08	1462.43
1913.50	54.12	21.38	1.03	1464.90
1913.00	61.32	34.83	2.10	1427.10

Well: 1-6 TVDSS (ft)	Old Gamma (API)	Corrected Gamma (API)	Porosity (%) from Gamma	Neutron (API)
1997.00	59.04	35.32	2.16	1140.13
1996.50	57.59	32.53	1.86	1192.43
1996.00	53.10	23.91	1.18	1226.30
1995.50	49.94	17.85	0.86	1305.19
1995.00	48.20	14.50	0.72	1465.16
1994.50	47.29	12.75	0.65	1498.53
1994.00	46.98	12.16	0.63	1519.63
1993.50	49.26	16.53	0.80	1526.01
1993.00	50.97	19.83	0.95	1531.45
1992.50	54.06	25.75	1.30	1536.20
1992.00	56.85	31.11	1.73	1365.85
1991.50	60.41	37.95	2.48	1349.58
1991.00	73.45	62.98	9.32	1298.33
1990.50	78.83	73.32	16.09	1251.23
1990.00	81.80	79.02	21.75	1089.30
1989.50	82.28	79.93	22.83	1065.75
1989.00	80.83	77.15	19.71	1037.25
1988.50	76.98	69.76	13.33	979.36
1988.00	78.85	73.36	16.12	922.97
1987.50	81.63	78.69	21.37	870.55
1987.00	81.93	79.27	22.04	836.06
1986.50	82.06	79.52	22.33	798.88
1986.00	81.25	77.95	20.56	770.96
1985.50	79.91	75.38	17.95	755.37
1985.00	78.96	73.55	16.29	748.32
1984.50	79.52	74.64	17.26	759.05
1984.00	80.82	77.14	19.70	773.67
1983.50	81.94	79.28	22.06	783.21
1983.00	82.44	80.24	23.20	778.20
1982.50	82.72	80.79	23.88	781.36
1982.00	82.66	80.66	23.72	781.09
1981.50	82.28	79.93	22.82	800.69
1981.00	81.94	79.29	22.06	824.49
1980.50	81.10	77.66	20.25	855.50
1980.00	80.33	76.18	18.72	890.24
1979.50	78.54	72.75	15.62	967.62
1979.00	76.65	69.12	12.89	1010.79
1978.50	72.24	60.67	8.24	1111.87
1978.00	65.09	46.93	3.99	1109.91
1977.50	61.55	40.14	2.79	1151.63
1977.00	59.93	37.02	2.36	1240.53
1976.50	57.27	31.91	1.80	1307.82
1976.00	57.53	32.42	1.85	1343.76
1975.50	57.12	31.63	1.78	1378.07
1975.00	57.95	33.22	1.93	1399.55
1974.50	56.67	30.76	1.70	1428.85
1974.00	54.62	26.83	1.38	1441.12
1973.50	53.28	24.26	1.20	1451.01
1973.00	50.30	18.53	0.89	1413.60
1972.50	48.64	15.35	0.75	1400.44
1972.00	50.60	19.11	0.92	1336.89
1971.50	53.11	23.94	1.18	1267.37
1971.00	58.40	34.08	2.02	1215.19

Well: 1-7 TVDSS (ft)	Old Gamma (API)	Corrected Gamma (API)	Porosity (%) from Gamma	Neutron (API)
1977.00	37.38	25.87	1.31	1128.39
1976.50	32.58	19.88	0.95	1238.75
1976.00	30.43	17.19	0.83	1313.85
1975.50	28.97	15.36	0.75	1326.62
1975.00	26.26	11.98	0.63	1410.19
1974.50	27.35	13.34	0.68	1504.42
1974.00	29.63	16.18	0.79	1632.40
1973.50	31.66	18.73	0.90	1626.13
1973.00	36.11	24.29	1.21	1617.80
1972.50	42.97	32.86	1.90	1618.37
1972.00	47.96	39.10	2.64	1574.17
1971.50	53.88	46.50	3.90	1533.89
1971.00	57.00	50.41	4.79	1225.44
1970.50	62.77	57.62	7.02	1247.05
1970.00	66.17	61.87	8.78	1180.46
1969.50	66.81	62.66	9.16	1140.12
1969.00	69.27	65.74	10.78	1094.36
1968.50	74.05	71.71	14.78	1044.09
1968.00	78.38	77.13	19.68	996.15
1967.50	81.03	80.43	23.44	948.52
1967.00	79.82	78.92	21.64	924.55
1966.50	74.43	72.19	15.16	921.67
1966.00	72.64	69.95	13.47	949.46
1965.50	71.38	69.00	12.81	964.14
1965.00	70.43	67.18	11.63	976.27
1964.50	68.27	64.48	10.09	996.64
1964.00	68.40	64.65	10.18	1026.82
1963.50	69.15	65.59	10.69	1033.91
1963.00	68.37	64.61	10.16	1005.41
1962.50	67.87	63.99	9.83	977.10
1962.00	67.72	63.81	9.73	987.69
1961.50	67.30	63.28	9.47	1009.32
1961.00	67.02	62.93	9.29	1043.86
1960.50	69.50	66.02	10.94	1083.69
1960.00	75.40	73.41	16.17	1089.60
1959.50	76.58	74.88	17.48	1096.26
1959.00	79.09	78.02	20.63	1109.24
1958.50	81.03	80.43	23.44	1116.76
1958.00	80.59	79.89	22.77	1128.80
1957.50	76.42	74.67	17.28	1135.85
1957.00	70.40	67.15	11.61	1121.99
1956.50	66.14	61.82	8.76	1064.84
1956.00	63.37	58.36	7.30	1044.16
1955.50	58.76	52.59	5.38	1038.12
1955.00	56.17	49.36	4.53	1011.02
1954.50	56.32	49.55	4.58	957.51
1954.00	56.39	49.63	4.60	938.06
1953.50	55.46	48.47	4.33	949.37
1953.00	55.66	48.73	4.39	969.18
1952.50	57.97	51.62	5.11	1048.38
1952.00	60.07	54.24	5.87	1116.50
1951.50	60.31	54.54	5.96	1202.77
1951.00	61.95	56.59	6.65	1233.38
1950.50	60.04	54.20	5.86	1212.55
1950.00	57.03	50.44	4.80	1181.43
1949.50	55.87	48.98	4.45	1213.08
1949.00	60.84	55.20	6.18	1280.54
1948.50	69.86	66.47	11.20	1284.92
1948.00	75.21	73.17	15.96	1245.41
1947.50	76.88	75.25	17.82	1196.72
1947.00	75.04	72.95	15.78	1181.93

Well: 1-8 TVDSS (ft)	Old Gamma (API)	Corrected Gamma (API)	Porosity (%) from Gamma	Neutron (API)
1958.00	53.31	12.64	0.65	1048.13
1957.50	52.82	11.99	0.63	1091.20
1957.00	54.59	14.35	0.71	1098.97
1956.50	55.35	15.35	0.75	1096.51
1956.00	55.14	15.07	0.74	1099.82
1955.50	56.42	16.77	0.81	1097.68
1955.00	57.68	18.45	0.88	1101.43
1954.50	63.32	25.92	1.31	1094.70
1954.00	73.88	39.94	2.76	1070.39
1953.50	81.15	49.59	4.59	1038.62
1953.00	87.58	58.12	7.21	997.03
1952.50	91.11	62.80	9.23	949.45
1952.00	97.35	71.09	14.30	926.58
1951.50	101.84	77.05	19.60	872.44
1951.00	104.01	79.92	22.81	813.39
1950.50	103.56	79.32	22.10	791.73
1950.00	103.11	78.73	21.42	763.68
1949.50	103.41	79.13	21.88	728.44
1949.00	103.05	78.65	21.33	702.78
1948.50	103.37	79.07	21.81	686.47
1948.00	104.45	80.50	23.52	677.71
1947.50	101.35	76.39	18.92	678.53
1947.00	99.66	74.15	16.82	674.91
1946.50	92.52	64.68	10.19	672.79
1946.00	90.54	62.04	8.87	676.68
1945.50	89.91	61.21	8.48	674.57
1945.00	87.85	58.48	7.34	678.85
1944.50	83.61	52.85	5.45	687.34
1944.00	81.66	50.27	4.76	699.98
1943.50	77.96	45.35	3.67	714.85
1943.00	78.25	45.74	3.75	734.65
1942.50	72.56	38.19	2.51	744.60
1942.00	67.61	31.61	1.78	747.76
1941.50	64.98	28.12	1.48	760.73
1941.00	63.78	26.53	1.36	795.66
1940.50	63.87	26.65	1.37	813.93
1940.00	63.50	26.17	1.33	851.00
1939.50	63.16	25.71	1.30	877.93
1939.00	59.97	21.48	1.04	893.92
1938.50	58.19	19.12	0.92	923.35
1938.00	58.41	19.40	0.93	975.76

Well: 1-9 TVDSS (ft)	Old Gamma (API)	Corrected Gamma (API)	Porosity (%) from Gamma	Neutron (API)
1988.00	65.47	46.20	3.84	1072.47
1987.50	64.21	44.36	3.48	1205.21
1987.00	59.29	37.20	2.38	1293.98
1986.50	50.06	23.75	1.17	1360.68
1986.00	43.69	14.49	0.72	1344.76
1985.50	39.95	9.04	0.54	1354.70
1985.00	41.40	11.15	0.60	1382.68
1984.50	43.46	14.14	0.70	1393.32
1984.00	43.85	14.71	0.73	1417.61
1983.50	41.99	12.00	0.63	1429.69
1983.00	44.26	15.32	0.75	1421.86
1982.50	46.91	19.17	0.92	1368.25
1982.00	52.81	27.77	1.45	1329.93
1981.50	66.51	47.71	4.16	1270.18
1981.00	75.31	60.52	8.18	1181.86
1980.50	80.48	68.05	12.18	1118.22
1980.00	82.24	70.62	13.95	1036.90
1979.50	89.02	80.48	23.50	970.39
1979.00	89.20	80.75	23.83	952.59
1978.50	83.24	72.06	15.06	948.08
1978.00	80.77	68.47	12.46	948.88
1977.50	77.42	63.59	9.62	936.25
1977.00	77.19	63.26	9.45	931.09
1976.50	79.28	66.30	11.11	910.06
1976.00	77.87	64.25	9.96	886.37
1975.50	76.66	62.49	9.08	876.88
1975.00	76.82	62.72	9.19	884.24
1974.50	77.94	64.35	10.02	896.75
1974.00	78.02	64.47	10.08	902.31
1973.50	77.30	63.41	9.53	918.64
1973.00	77.83	64.19	9.93	930.85
1972.50	80.57	68.19	12.27	930.49
1972.00	81.27	69.20	12.94	914.80
1971.50	82.79	71.42	14.55	913.88
1971.00	80.53	68.12	12.23	925.91
1970.50	80.94	68.72	12.62	958.04
1970.00	74.70	59.64	7.81	1001.67
1969.50	73.28	57.56	7.00	1034.66
1969.00	73.50	57.88	7.12	1073.26
1968.50	71.34	54.74	6.03	1106.73
1968.00	66.51	47.71	4.16	1134.11
1967.50	63.36	43.13	3.26	1158.74
1967.00	61.95	41.07	2.93	1198.76
1966.50	61.37	40.23	2.80	1238.03
1966.00	64.59	44.91	3.59	1244.44
1965.50	69.30	51.77	5.15	1250.58
1965.00	65.65	46.46	3.89	1265.90
1964.50	59.62	37.68	2.45	1268.00
1964.00	62.92	42.49	3.15	1236.17

Well: 1-10 TVDSS (ft)	Old Gamma (API)	Corrected Gamma (API)	Porosity (%) from Gamma	Neutron (API)
1928.00	67.73	45.96	3.79	1145.66
1927.50	47.33	23.52	1.16	1165.87
1927.00	47.48	23.69	1.17	1200.23
1926.50	47.84	24.09	1.19	1300.31
1926.00	47.79	24.03	1.19	1403.36
1925.50	46.23	22.31	1.09	1504.48
1925.00	36.24	11.32	0.61	1597.51
1924.50	36.27	11.35	0.61	1684.49
1924.00	37.19	12.37	0.64	1784.99
1923.50	37.72	12.95	0.66	1896.91
1923.00	38.11	13.38	0.68	2027.96
1922.50	38.45	13.76	0.69	2073.65
1922.00	43.71	19.54	0.94	2162.05
1921.50	50.04	26.50	1.35	2155.19
1921.00	62.54	40.25	2.80	2170.85
1920.50	64.66	42.59	3.17	2079.44
1920.00	65.28	43.27	3.29	1906.09
1919.50	64.61	42.53	3.16	1912.78
1919.00	65.50	43.51	3.33	1793.99
1918.50	75.48	54.49	5.95	1645.96
1918.00	76.92	56.07	6.47	1485.24
1917.50	79.92	59.38	7.70	1373.03
1917.00	81.96	61.62	8.67	1359.25
1916.50	84.08	63.95	9.81	1359.25
1916.00	63.46	41.27	2.96	1392.00
1915.50	64.54	42.45	3.15	1399.40
1915.00	69.91	48.36	4.30	1397.12
1914.50	91.02	71.59	14.68	1408.76
1914.00	90.90	71.45	14.58	1448.50
1913.50	80.86	60.40	8.13	1501.33
1913.00	74.45	53.35	5.60	1566.83
1912.50	84.87	64.82	10.27	1593.57
1912.00	98.41	79.71	22.56	1596.61
1911.50	99.14	80.51	23.53	1475.34
1911.00	74.73	53.66	5.69	1419.25
1910.50	63.88	41.72	3.03	1400.31
1910.00	63.24	41.03	2.92	1403.20
1909.50	63.34	41.13	2.94	1446.34
1909.00	83.22	63.00	9.33	1494.80
1908.50	84.38	64.28	9.98	1510.34
1908.00	53.15	29.93	1.62	1520.81
1907.50	48.34	24.63	1.23	1540.93
1907.00	58.56	35.87	2.22	1557.40
1906.50	58.03	35.30	2.16	1597.97
1906.00	65.77	43.80	3.38	1622.49
1905.50	64.76	42.70	3.19	1625.31
1905.00	64.24	42.12	3.09	1575.95
1904.50	64.15	42.02	3.08	1547.72
1904.00	62.84	40.58	2.85	1544.06
1903.50	41.85	17.49	0.84	1558.06
1903.00	41.01	16.58	0.80	1580.83
1902.50	45.60	21.62	1.05	1747.31
1902.00	47.53	23.74	1.17	1729.04
1901.50	48.26	24.55	1.22	1917.53
1901.00	47.72	23.95	1.18	1935.70
1900.50	51.78	28.42	1.50	2006.08
1900.00	51.07	27.64	1.44	2056.24
1899.50	42.96	18.72	0.90	2154.00

Well: 1-11 TVDSS (ft)	Old Gamma (API)	Corrected Gamma (API)	Porosity (%) from Gamma	Neutron (API)
1999.00	27.55	14.84	0.73	1080.17
1998.50	28.10	15.82	0.77	1227.80
1998.00	27.96	15.57	0.76	1297.04
1997.50	26.84	13.56	0.68	1354.51
1997.00	25.98	11.99	0.63	1440.37
1996.50	26.30	12.57	0.65	1491.14
1996.00	26.82	13.52	0.68	1631.90
1995.50	26.58	13.07	0.67	1626.85
1995.00	27.50	14.74	0.73	1645.86
1994.50	29.63	18.60	0.89	1578.35
1994.00	32.98	24.67	1.23	1547.19
1993.50	37.30	32.49	1.86	1517.08
1993.00	42.82	42.47	3.15	1479.22
1992.50	46.55	49.22	4.50	1415.24
1992.00	53.19	61.25	8.50	1308.31
1991.50	58.44	70.74	14.04	1140.25
1991.00	59.98	73.53	16.27	1071.77
1990.50	61.94	77.07	19.62	999.85
1990.00	63.83	80.51	23.53	966.90
1989.50	62.33	77.79	20.38	944.48
1989.00	56.28	66.83	11.42	931.40
1988.50	56.20	66.70	11.34	914.92
1988.00	55.55	65.52	10.65	900.29
1987.50	56.28	66.84	11.42	871.98
1987.00	59.01	71.79	14.84	850.08
1986.50	60.93	75.26	17.82	827.07
1986.00	59.77	73.16	15.95	825.41
1985.50	59.43	72.54	15.44	821.99
1985.00	57.10	68.31	12.35	815.78
1984.50	56.59	67.40	11.77	811.26
1984.00	55.29	65.05	10.39	823.11
1983.50	53.21	61.28	8.51	833.84
1983.00	52.54	60.07	7.99	856.87
1982.50	54.18	63.03	9.34	872.14
1982.00	53.47	61.76	8.73	899.12
1981.50	51.27	57.76	7.07	925.96
1981.00	48.98	53.62	5.68	964.94
1980.50	48.32	52.42	5.33	981.91
1980.00	43.55	43.80	3.38	1028.34
1979.50	37.74	33.29	1.94	1023.46
1979.00	33.79	26.12	1.33	1183.49
1978.50	34.70	27.77	1.45	1262.42
1978.00	35.36	28.97	1.54	1342.05
1977.50	35.54	29.30	1.57	1391.90
1977.00	36.24	30.57	1.68	1429.10
1976.50	37.49	32.83	1.89	1469.79
1976.00	35.89	29.93	1.62	1523.52
1975.50	31.74	22.41	1.09	1573.48
1975.00	32.77	24.28	1.20	1612.70
1974.50	37.84	33.46	1.96	1606.97
1974.00	43.28	43.30	3.29	1608.43
1973.50	47.66	51.24	5.01	1603.84
1973.00	51.98	59.06	7.57	1610.15
1972.50	55.63	65.66	10.73	1465.36
1972.00	55.54	65.50	10.64	1411.86
1971.50	56.86	67.89	12.08	1324.30

Well: 1-12 TVDSS (ft)	Old Gamma (API)	Corrected Gamma (API)	Porosity (%) from Gamma	Neutron (API)
1979.00	29.63	26.07	1.32	612.10
1978.50	29.61	26.04	1.32	666.64
1978.00	25.96	19.47	0.93	692.86
1977.50	23.06	14.25	0.71	705.36
1977.00	22.43	13.12	0.67	722.32
1976.50	21.78	11.94	0.63	743.93
1976.00	23.07	14.27	0.71	747.71
1975.50	25.98	19.50	0.94	729.38
1975.00	30.38	27.43	1.42	701.57
1974.50	32.70	31.59	1.77	635.68
1974.00	34.83	35.44	2.17	582.61
1973.50	38.52	42.07	3.09	544.83
1973.00	44.40	52.66	5.40	512.41
1972.50	48.08	59.29	7.66	484.95
1972.00	50.35	63.37	9.51	458.63
1971.50	50.88	64.32	10.00	445.03
1971.00	53.97	69.89	13.42	429.70
1970.50	56.39	74.24	16.90	412.53
1970.00	56.55	74.52	17.15	400.86
1969.50	55.42	72.49	15.40	399.30
1969.00	56.64	74.69	17.30	397.62
1968.50	59.88	80.52	23.55	397.76
1968.00	58.74	78.48	21.14	397.92
1967.50	54.62	71.05	14.27	394.08
1967.00	51.09	64.70	10.20	386.00
1966.50	46.91	57.17	6.85	382.66
1966.00	42.72	49.64	4.60	388.69
1965.50	40.45	45.55	3.71	392.77
1965.00	40.01	44.75	3.55	393.55
1964.50	40.94	46.43	3.88	391.22
1964.00	43.07	50.26	4.76	389.76
1963.50	45.85	55.26	6.20	392.73
1963.00	47.27	57.82	7.09	393.37
1962.50	48.15	59.41	7.71	404.25
1962.00	49.54	61.91	8.80	408.05
1961.50	49.99	62.72	9.19	422.31
1961.00	50.01	62.77	9.21	439.28
1960.50	48.91	60.78	8.30	452.10
1960.00	45.30	54.28	5.88	460.81
1959.50	44.14	52.20	5.27	465.54
1959.00	42.73	49.65	4.61	480.87
1958.50	42.92	50.00	4.69	503.16
1958.00	41.39	47.25	4.06	543.53
1957.50	39.53	43.90	3.40	576.86
1957.00	38.35	41.76	3.04	618.35
1956.50	37.33	39.93	2.75	658.52
1956.00	35.75	37.09	2.37	673.49
1955.50	33.92	33.80	1.99	678.42
1955.00	33.50	33.04	1.91	667.41
1954.50	37.69	40.59	2.85	585.90
1954.00	42.48	49.20	4.50	528.25
1953.50	45.22	54.13	5.84	477.25
1953.00	45.96	55.46	6.26	457.34
1952.50	46.63	56.68	6.68	456.03
1952.00	47.42	58.10	7.20	455.75
1951.50	48.52	60.07	7.99	455.88
1951.00	48.69	60.38	8.12	456.13

Well: 1-13

TVDSS (ft)	Old Gamma (API)	Corrected Gamma (API)	Porosity (%) from Gamma	Neutron (API)
1984.00	28.79	14.39	0.71	344.89
1983.50	28.67	14.13	0.70	379.67
1983.00	29.00	14.86	0.73	460.77
1982.50	28.35	13.41	0.68	587.50
1982.00	28.25	13.20	0.67	621.82
1981.50	26.94	10.28	0.57	658.41
1981.00	27.72	12.02	0.63	685.14
1980.50	29.64	16.27	0.79	703.95
1980.00	31.76	20.98	1.01	709.88
1979.50	34.50	27.06	1.40	697.60
1979.00	38.19	35.27	2.15	668.58
1978.50	42.77	45.43	3.68	552.71
1978.00	46.74	54.23	5.87	486.50
1977.50	53.05	68.26	12.32	407.88
1977.00	58.36	80.05	22.96	337.54
1976.50	59.07	81.62	24.95	310.07
1976.00	58.93	81.30	24.54	252.14
1975.50	58.34	79.98	22.89	177.37
1975.00	51.86	65.61	10.71	129.85
1974.50	50.85	63.37	9.51	95.69
1974.00	41.62	42.87	3.22	82.07
1973.50	40.52	40.42	2.83	78.18
1973.00	39.64	38.49	2.55	81.77
1972.50	39.13	37.34	2.40	85.73
1972.00	39.03	37.12	2.37	86.68
1971.50	40.97	41.42	2.98	108.38
1971.00	42.15	44.06	3.43	118.88
1970.50	42.61	45.08	3.62	124.23
1970.00	42.43	44.68	3.54	124.57
1969.50	41.21	41.97	3.07	133.78
1969.00	40.10	39.50	2.69	144.99
1968.50	44.12	48.43	4.32	167.16
1968.00	45.60	51.72	5.14	183.03
1967.50	47.30	55.49	6.27	205.38
1967.00	51.80	65.48	10.63	233.26
1966.50	56.79	76.55	19.08	267.37
1966.00	57.72	78.62	21.30	314.15
1965.50	58.23	79.76	22.62	356.58
1965.00	58.00	79.25	22.02	377.36
1964.50	57.15	77.36	19.92	412.03
1964.00	54.95	72.46	15.38	464.68
1963.50	47.09	55.03	6.12	536.14
1963.00	45.50	51.49	5.08	594.42
1962.50	44.50	49.27	4.51	639.90
1962.00	42.80	45.49	3.70	647.02

Well: 1-14 TVDSS (ft)	Old Gamma (API)	Corrected Gamma (API)	Porosity (%) from Gamma	Neutron (API)
1973.00	46.24	29.43	1.58	887.72
1972.50	44.59	26.99	1.39	976.91
1972.00	42.32	23.64	1.16	1080.45
1971.50	39.46	19.40	0.93	1191.84
1971.00	35.21	13.11	0.67	1240.47
1970.50	34.46	12.01	0.63	1250.62
1970.00	36.94	15.67	0.76	1321.45
1969.50	39.84	19.96	0.96	1316.87
1969.00	43.17	24.90	1.24	1269.21
1968.50	47.65	31.53	1.77	1169.53
1968.00	53.85	40.70	2.87	987.90
1967.50	57.05	45.43	3.68	992.50
1967.00	60.59	50.67	4.86	803.98
1966.50	66.71	59.73	7.85	717.19
1966.00	71.47	66.78	11.39	626.42
1965.50	77.63	75.89	18.44	500.59
1965.00	79.80	79.10	21.85	457.96
1964.50	80.64	80.34	23.33	443.43
1964.00	80.74	80.49	23.51	440.92
1963.50	80.44	80.05	22.97	441.54
1963.00	80.12	79.58	22.40	442.04
1962.50	78.08	76.56	19.10	443.57
1962.00	74.57	71.37	14.52	455.42
1961.50	73.35	69.56	13.19	475.09
1961.00	66.09	58.81	7.47	493.39
1960.50	62.37	53.31	5.59	515.58
1960.00	62.38	53.33	5.59	542.96
1959.50	63.65	55.20	6.18	563.75
1959.00	63.80	55.43	6.25	604.52
1958.50	62.89	54.08	5.82	634.73
1958.00	63.04	54.30	5.89	664.86
1957.50	63.95	55.65	6.32	729.69
1957.00	64.01	55.74	6.35	731.78
1956.50	63.34	54.74	6.03	746.21
1956.00	62.49	53.48	5.64	767.47
1955.50	61.57	52.13	5.25	788.87
1955.00	65.42	57.82	7.09	810.37
1954.50	68.83	62.87	9.26	823.82
1954.00	68.27	62.04	8.87	803.72
1953.50	66.69	59.70	7.83	825.32
1953.00	62.93	54.14	5.84	875.65
1952.50	50.70	36.04	2.24	932.86
1952.00	46.76	30.20	1.65	1040.65
1951.50	45.91	28.94	1.54	1121.55
1951.00	50.26	35.39	2.17	1165.93
1950.50	55.77	43.53	3.33	1172.42
1950.00	58.50	47.58	4.13	1179.88
1949.50	58.82	48.05	4.23	1188.19
1949.00	59.80	49.51	4.57	1197.01
1948.50	62.28	53.18	5.55	1199.43
1948.00	62.19	53.05	5.51	1192.26
1947.50	61.20	51.58	5.10	1175.21
1947.00	52.26	38.35	2.53	1169.77

Well: 1-15

TVDSS (ft)	Old Gamma (API)	Corrected Gamma (API)	Porosity (%) from Gamma	Neutron (API)
1974.00	38.42	30.14	1.64	1574.63
1973.50	30.48	17.84	0.86	1726.40
1973.00	26.72	12.01	0.63	1902.86
1972.50	28.08	14.12	0.70	1947.59
1972.00	30.11	17.27	0.83	1940.12
1971.50	30.76	18.28	0.88	1919.11
1971.00	29.10	15.71	0.77	1938.09
1970.50	28.84	15.30	0.75	1965.42
1970.00	29.98	17.07	0.82	1977.01
1969.50	31.25	19.03	0.91	1944.37
1969.00	33.85	23.06	1.13	1863.99
1968.50	37.74	29.09	1.55	1772.00
1968.00	43.72	38.36	2.54	1700.43
1967.50	51.54	50.48	4.81	1529.22
1967.00	57.03	59.00	7.55	1356.88
1966.50	61.59	66.07	10.97	1263.96
1966.00	66.46	73.61	16.34	1225.13
1965.50	70.38	79.68	22.53	1226.82
1965.00	69.19	77.84	20.44	1216.58
1964.50	70.37	79.68	22.52	1193.95
1964.00	70.91	80.52	23.54	1173.79
1963.50	68.56	76.87	19.42	1173.01
1963.00	69.00	77.56	20.13	1195.24
1962.50	66.96	74.39	17.03	1233.55
1962.00	64.09	69.94	13.46	1282.81
1961.50	62.73	67.84	12.04	1325.68
1961.00	60.67	64.64	10.17	1390.58
1960.50	59.04	62.11	8.90	1461.23
1960.00	56.80	58.64	7.41	1607.53
1959.50	53.95	54.22	5.86	1686.66
1959.00	51.55	50.50	4.82	1829.01
1958.50	50.84	49.41	4.55	1881.29
1958.00	49.26	46.95	3.99	1905.44
1957.50	50.02	48.13	4.25	1903.04
1957.00	52.48	51.95	5.20	1884.83
1956.50	53.88	54.12	5.83	1869.15
1956.00	52.49	51.95	5.20	1857.09
1955.50	52.48	51.94	5.20	1851.96
1955.00	54.72	55.41	6.24	1839.84
1954.50	57.58	59.85	7.90	1832.85
1954.00	60.01	63.62	9.64	1891.31
1953.50	61.11	65.32	10.54	2133.57
1953.00	44.64	39.79	2.73	2269.96
1952.50	34.86	24.63	1.23	2320.34
1952.00	32.66	21.22	1.02	2328.74
1951.50	41.03	34.20	2.03	2272.20
1951.00	48.78	46.21	3.84	2126.29
1950.50	55.50	56.63	6.66	1996.28
1950.00	61.68	66.21	11.05	1792.10

Well: 2-1 TVDSS (ft)	Old Gamma (API)	Corrected Gamma (API)	Porosity (%) from Gamma
1950.00	37.98	26.61	1.36
1950.50	37.78	26.47	1.35
1951.00	35.21	24.66	1.23
1951.50	27.68	19.33	0.93
1952.00	20.15	14.00	0.70
1952.50	18.04	12.51	0.65
1953.00	17.65	12.24	0.64
1953.50	17.31	12.00	0.63
1954.00	17.88	12.40	0.64
1954.50	18.96	13.16	0.67
1955.00	23.96	16.70	0.81
1955.50	31.60	22.10	1.07
1956.00	39.78	27.88	1.46
1956.50	50.87	35.73	2.21
1957.00	64.21	45.15	3.63
1957.50	71.46	50.28	4.76
1958.00	70.64	49.71	4.62
1958.50	79.99	56.32	6.55
1959.00	79.14	55.71	6.35
1959.50	81.17	57.15	6.84
1960.00	88.88	62.60	9.13
1960.50	91.74	64.62	10.16
1961.00	91.90	64.73	10.22
1961.50	95.73	67.44	11.79
1962.00	95.41	67.22	11.66
1962.50	90.73	63.90	9.78
1963.00	87.98	61.96	8.83
1963.50	87.41	61.56	8.64
1964.00	92.03	64.82	10.27
1964.50	98.55	69.43	13.10
1965.00	100.44	70.77	14.06
1965.50	106.78	75.26	17.83
1966.00	114.16	80.47	23.49
1966.50	112.63	79.39	22.18
1967.00	108.89	76.75	19.29
1967.50	102.93	72.53	15.44
1968.00	97.52	68.71	12.61
1968.50	94.40	66.50	11.22
1969.00	87.05	61.30	8.53
1969.50	80.42	56.62	6.66
1970.00	78.49	55.25	6.19
1970.50	76.38	53.76	5.72
1971.00	70.66	49.71	4.62
1971.50	70.57	49.66	4.61
1972.00	69.94	49.21	4.50
1972.50	69.87	49.16	4.49
1973.00	75.00	52.79	5.44
1973.50	81.63	57.47	6.96
1974.00	85.97	60.54	8.19

Well: 2-3 TVDSS (ft)	Old Gamma (API)	Corrected Gamma (API)	Porosity (%) from Gamma	Neutron (API)
1955.00	40.86	26.20	1.33	1307.92
1954.50	32.30	16.30	0.79	1428.72
1954.00	29.91	13.54	0.68	1465.87
1953.50	28.57	11.99	0.63	1477.35
1953.00	29.01	12.49	0.65	1488.04
1952.50	29.26	12.78	0.66	1489.01
1952.00	28.86	12.32	0.64	1489.87
1951.50	28.63	12.06	0.63	1481.80
1951.00	29.83	13.45	0.68	1460.03
1950.50	34.18	18.48	0.89	1429.55
1950.00	39.14	24.21	1.20	1407.13
1949.50	48.10	34.58	2.08	1360.31
1949.00	53.03	40.29	2.81	1339.73
1948.50	63.69	52.62	5.39	1266.96
1948.00	85.19	77.49	20.07	1214.69
1947.50	85.46	77.81	20.41	1187.08
1947.00	86.13	78.58	21.25	1113.12
1946.50	86.60	79.13	21.88	1103.39
1946.00	87.75	80.46	23.47	1099.97
1945.50	82.84	74.78	17.38	1102.11
1945.00	80.08	71.59	14.69	1116.41
1944.50	77.15	68.20	12.28	1126.48
1944.00	77.18	68.22	12.29	1135.09
1943.50	75.98	66.84	11.42	1139.98
1943.00	73.40	63.86	9.76	1145.28
1942.50	66.08	55.39	6.24	1149.79
1942.00	65.07	54.21	5.86	1149.60
1941.50	66.75	56.16	6.50	1153.47
1941.00	65.02	54.16	5.84	1155.51
1940.50	60.40	48.81	4.41	1158.57
1940.00	61.73	50.35	4.78	1159.60
1939.50	55.84	43.54	3.33	1175.05
1939.00	55.00	42.56	3.17	1182.14
1938.50	55.34	42.96	3.23	1198.75
1938.00	61.71	50.33	4.77	1190.84
1937.50	67.51	57.04	6.80	1205.49
1937.00	69.55	59.41	7.71	1234.64
1936.50	62.83	51.62	5.11	1271.15
1936.00	58.55	46.67	3.93	1293.02
1935.50	53.72	41.09	2.93	1334.38
1935.00	53.20	40.48	2.84	1344.24
1934.50	52.54	39.72	2.72	1350.38
1934.00	53.16	40.44	2.83	1366.89
1933.50	46.58	32.83	1.89	1388.35
1933.00	43.63	29.41	1.58	1406.71
1932.50	38.53	23.51	1.16	1413.05
1932.00	37.30	22.08	1.07	1407.63
1931.50	39.61	24.75	1.24	1393.37
1931.00	50.50	37.36	2.41	1365.66

Well: 2-4 TVDSS (ft)	Old Gamma (API)	Corrected Gamma (API)	Porosity (%) from Gamma	Neurton (API)
1956.00	35.36	12.68	0.65	1110.98
1955.50	34.77	11.90	0.63	1173.93
1955.00	36.39	14.03	0.70	1243.56
1954.50	36.45	14.11	0.70	1277.04
1954.00	37.03	14.87	0.73	1281.80
1953.50	38.86	17.27	0.83	1279.86
1953.00	43.01	22.70	1.11	1273.37
1952.50	47.48	28.56	1.51	1259.30
1952.00	51.29	33.55	1.97	1232.06
1951.50	55.15	38.61	2.57	1170.39
1951.00	64.92	51.41	5.05	1090.73
1950.50	71.97	60.64	8.23	1054.10
1950.00	75.01	64.63	10.16	1017.14
1949.50	79.85	70.96	14.21	1024.97
1949.00	82.89	74.95	17.54	986.14
1948.50	86.85	80.13	23.06	976.35
1948.00	86.94	80.25	23.21	978.69
1947.50	83.04	75.15	17.72	923.58
1947.00	81.13	72.64	15.53	910.37
1946.50	81.32	72.89	15.73	915.78
1946.00	80.10	71.29	14.46	919.85
1945.50	75.46	65.21	10.48	921.68
1945.00	73.47	62.60	9.13	931.40
1944.50	70.22	58.35	7.29	927.68
1944.00	69.18	56.98	6.79	929.49
1943.50	68.52	56.12	6.48	937.75
1943.00	67.84	55.23	6.18	936.82
1942.50	65.65	52.36	5.32	927.76
1942.00	62.04	47.64	4.14	924.99
1941.50	59.27	44.01	3.42	920.34
1941.00	54.96	38.35	2.53	920.04
1940.50	53.97	37.06	2.37	908.20
1940.00	55.30	38.81	2.60	901.03
1939.50	56.25	40.04	2.77	922.21
1939.00	55.50	39.06	2.63	934.05
1938.50	55.50	39.06	2.63	939.17
1938.00	57.05	41.09	2.93	944.53
1937.50	59.77	44.66	3.54	949.56
1937.00	61.95	47.51	4.11	950.57
1936.50	61.96	47.53	4.12	956.79
1936.00	58.25	42.67	3.18	964.54
1935.50	55.30	38.81	2.60	981.88
1935.00	57.56	41.76	3.03	1011.31
1934.50	60.14	45.14	3.63	1019.74
1934.00	60.73	45.91	3.78	1024.41
1933.50	59.19	43.91	3.40	1035.87
1933.00	58.22	42.62	3.18	1047.41
1932.50	54.99	38.40	2.54	1066.99
1932.00	52.58	35.24	2.15	1086.54
1931.50	47.54	28.64	1.52	1109.65
1931.00	45.49	25.96	1.32	1148.38
1930.50	47.72	28.87	1.54	1169.02
1930.00	52.93	35.69	2.20	1158.30

Well: 2-5 TVDSS (ft)	Old Gamma (API)	Corrected Gamma (API)	Porosity (%) frm Gamma	Neutron (API)
2014.50	36.80	18.47	0.89	457.06
2015.00	34.41	14.40	0.71	566.46
2015.50	32.93	11.88	0.63	600.50
2016.00	33.67	13.14	0.67	607.43
2016.50	35.02	15.44	0.75	612.38
2017.00	35.38	16.05	0.78	632.18
2017.50	35.21	15.76	0.77	640.90
2018.00	36.31	17.64	0.85	634.80
2018.50	39.01	22.21	1.08	599.71
2019.00	43.10	29.17	1.56	553.63
2019.50	46.23	34.49	2.07	515.52
2020.00	49.52	40.08	2.78	492.59
2020.50	54.45	48.47	4.33	405.65
2021.00	58.15	54.75	6.03	376.62
2021.50	61.89	61.11	8.44	349.04
2022.00	64.27	65.16	10.45	354.94
2022.50	68.35	72.09	15.08	357.54
2023.00	70.17	75.19	17.76	366.90
2023.50	72.44	79.05	21.79	377.95
2024.00	73.17	80.28	23.26	395.00
2024.50	71.50	77.45	20.01	395.79
2025.00	68.46	72.28	15.24	246.86
2025.50	65.32	66.94	11.48	140.19
2026.00	63.97	64.65	10.18	118.89
2026.50	62.80	62.65	9.16	177.40
2027.00	60.30	58.40	7.32	205.36
2027.50	57.31	53.33	5.59	199.39
2028.00	56.08	51.24	5.01	195.83
2028.50	57.20	53.14	5.54	216.80
2029.00	59.72	57.43	6.95	262.73
2029.50	60.73	59.14	7.60	372.77
2030.00	59.61	57.24	6.88	368.14
2030.50	58.89	56.02	6.45	540.84
2031.00	59.75	57.47	6.96	668.81
2031.50	58.31	55.03	6.12	817.33
2032.00	56.01	51.11	4.97	930.20

Well: 2-6 TVDSS (ft)	Old Gamma (API)	Corrected Gamma (API)	Porosity (%) frm Gamma	Neutron (API)
1951.00	45.58	34.60	2.08	1061.17
1950.50	46.29	35.28	2.15	898.23
1950.00	35.60	25.09	1.26	1714.19
1949.50	32.65	22.28	1.08	1971.50
1949.00	26.97	16.86	0.81	2041.92
1948.50	21.86	11.99	0.63	2141.24
1948.00	23.28	13.35	0.68	2231.52
1947.50	26.10	16.04	0.78	2383.20
1947.00	28.77	18.57	0.89	2428.34
1946.50	33.18	22.78	1.11	2579.90
1946.00	34.02	23.58	1.16	2672.66
1945.50	32.28	21.93	1.06	2764.05
1945.00	34.76	24.29	1.21	2930.32
1944.50	41.09	30.32	1.66	2950.19
1944.00	50.76	39.54	2.70	2867.12
1943.50	61.76	50.02	4.70	2832.82
1943.00	74.32	61.99	8.84	2961.02
1942.50	87.83	74.86	17.46	2749.57
1942.00	93.73	80.48	23.50	2281.94
1941.50	91.82	78.66	21.34	1814.31
1941.00	92.24	79.07	21.81	1963.75
1940.50	83.30	70.54	13.90	1938.31
1940.00	79.78	67.19	11.64	1792.05
1939.50	82.43	69.71	13.30	2957.41
1939.00	83.70	70.93	14.18	3061.35
1938.50	84.50	71.69	14.76	3120.31
1938.00	86.71	73.79	16.50	3230.44
1937.50	88.70	75.69	18.24	2391.75
1937.00	85.99	73.11	15.91	892.05
1936.50	72.48	60.23	8.06	891.17
1936.00	67.56	55.54	6.29	891.17
1935.50	63.62	51.79	5.16	799.56
1935.00	62.77	50.98	4.94	3266.72
1934.50	68.16	56.11	6.48	3086.73
1934.00	66.19	54.24	5.87	3132.95
1933.50	62.18	50.42	4.80	3012.95
1933.00	60.08	48.41	4.31	3007.97
1932.50	58.89	47.29	4.06	2944.54
1932.00	58.13	46.55	3.91	2842.97
1931.50	45.75	34.76	2.10	2741.40
1931.00	37.49	26.89	1.38	2636.66
1930.50	30.43	20.16	0.97	2450.34
1930.00	26.92	16.82	0.81	2356.23
1929.50	25.32	15.29	0.75	2214.37
1929.00	25.38	15.34	0.75	2164.71

Well: 3-1 TVDSS (ft)	Old Gamma (API)	Corrected Gamma (API)	Porosity (%) frm Gamma	Density (G/CC)
1933.00	27.22	34.51	2.07	2.29
1932.50	22.74	28.64	1.52	2.60
1932.00	21.27	26.72	1.37	2.64
1931.50	19.55	24.46	1.22	2.62
1931.00	10.21	12.22	0.64	2.65
1930.50	10.28	12.31	0.64	2.85
1930.00	10.65	12.81	0.66	2.90
1929.50	11.57	14.01	0.70	2.89
1929.00	12.41	15.11	0.74	2.85
1928.50	14.75	18.18	0.87	2.82
1928.00	18.77	23.45	1.15	2.81
1927.50	26.05	32.97	1.91	2.78
1927.00	33.58	42.84	3.21	2.73
1926.50	43.58	55.94	6.42	2.63
1926.00	49.07	63.13	9.39	2.56
1925.50	50.78	65.37	10.57	2.51
1925.00	51.36	66.14	11.01	2.41
1924.50	52.16	67.18	11.64	2.36
1924.00	51.41	66.19	11.04	2.26
1923.50	51.23	65.96	10.91	2.17
1923.00	50.80	65.40	10.59	2.10
1922.50	49.84	64.14	9.91	2.06
1922.00	52.43	67.54	11.85	2.04
1921.50	54.26	69.93	13.45	2.04
1921.00	54.12	69.75	13.33	2.04
1920.50	55.69	71.81	14.86	2.07
1920.00	55.29	71.28	14.45	2.07
1919.50	56.12	72.37	15.30	2.06
1919.00	56.51	72.89	15.73	2.01
1918.50	57.10	73.65	16.38	1.98
1918.00	57.70	74.43	17.07	1.96
1917.50	57.84	74.63	17.25	1.95
1917.00	58.10	74.96	17.55	1.94
1916.50	60.00	77.45	20.02	2.15
1916.00	62.28	80.44	23.45	2.14
1915.50	59.10	76.27	18.81	2.20
1915.00	60.25	77.78	20.37	2.22
1914.50	45.75	58.79	7.47	2.24
1914.00	41.08	52.67	5.40	2.27
1913.50	39.49	50.58	4.84	2.31
1913.00	37.48	47.96	4.21	2.34
1912.50	34.42	43.94	3.41	2.40
1912.00	33.69	42.99	3.24	2.42
1911.50	35.79	45.74	3.75	2.45
1911.00	36.15	46.21	3.84	2.48
1910.50	35.98	45.99	3.80	2.53
1910.00	35.35	45.16	3.63	2.56
1909.50	33.86	43.21	3.28	2.61
1909.00	31.60	40.25	2.80	2.64
1908.50	31.21	39.74	2.73	2.67
1908.00	28.83	36.62	2.31	2.70
1907.50	25.18	31.84	1.80	2.73
1907.00	19.29	24.13	1.20	2.83
1906.50	13.84	16.99	0.82	2.82
1906.00	17.51	21.79	1.06	2.79
1905.50	20.36	25.52	1.29	2.79
1905.00	22.49	28.31	1.49	2.62

Well: 3-2 TVDSS (ft)	Old Gamma (API)	Corrected Gamma (API)	Porosity (%) from Gamma	Neutron (API)
1952.00	53.47	30.94	1.71	2340.59
1951.50	47.19	23.76	1.17	2545.54
1951.00	40.18	15.76	0.77	2653.50
1950.50	37.32	12.49	0.65	2660.83
1950.00	38.54	13.88	0.70	2700.56
1949.50	38.58	13.93	0.70	2730.29
1949.00	38.31	13.62	0.69	2723.22
1948.50	40.90	16.57	0.80	2703.39
1948.00	44.78	21.00	1.01	2671.48
1947.50	50.44	27.47	1.43	2579.40
1947.00	66.76	46.11	3.82	2457.08
1946.50	82.61	64.21	9.94	2265.86
1946.00	85.01	66.96	11.50	2128.60
1945.50	81.20	62.60	9.13	1985.15
1945.00	81.15	62.55	9.11	1878.22
1944.50	81.75	63.23	9.44	1869.31
1944.00	80.72	62.05	8.87	1855.45
1943.50	85.93	68.00	12.15	1833.96
1943.00	92.32	75.30	17.87	1820.66
1942.50	92.61	75.63	18.18	1805.56
1942.00	91.65	74.53	17.16	1797.45
1941.50	91.29	74.13	16.80	1803.21
1941.00	90.25	72.94	15.77	1809.15
1940.50	96.90	80.53	23.55	1806.51
1940.00	90.73	73.49	16.24	1807.59
1939.50	85.43	67.43	11.79	1797.76
1939.00	81.78	63.26	9.46	1784.94
1938.50	83.58	65.32	10.54	1799.61
1938.00	81.79	63.27	9.46	1805.52
1937.50	82.61	64.21	9.94	1801.91
1937.00	89.67	72.28	15.23	1799.38
1936.50	90.97	73.76	16.47	1800.08
1936.00	91.56	74.43	17.07	1794.73
1935.50	88.79	71.27	14.44	1788.51
1935.00	87.98	70.34	13.75	1762.43
1934.50	88.15	70.53	13.89	1737.42
1934.00	89.31	71.86	14.90	1731.79
1933.50	83.62	65.36	10.57	1759.64
1933.00	78.40	59.40	7.71	1794.84
1932.50	73.15	53.41	5.62	1824.34
1932.00	71.73	51.79	5.16	1913.06
1931.50	67.43	46.87	3.98	1953.47
1931.00	64.71	43.76	3.37	1992.72
1930.50	63.35	42.21	3.11	2018.24
1930.00	63.05	41.87	3.05	2057.95
1929.50	57.21	35.20	2.15	2102.02
1929.00	59.55	37.87	2.47	2132.67
1928.50	60.13	38.53	2.56	2157.34
1928.00	60.10	38.51	2.56	2244.67
1927.50	61.07	39.61	2.71	2327.14
1927.00	62.21	40.91	2.90	2480.63
1926.50	59.76	38.11	2.50	2548.10
1926.00	54.72	32.36	1.85	2589.95
1925.50	48.36	25.10	1.26	2607.84
1925.00	38.64	14.00	0.70	2610.06
1924.50	36.90	12.01	0.63	2572.03
1924.00	42.23	18.10	0.87	2473.03
1923.50	49.63	26.55	1.36	2343.74
1923.00	57.86	35.94	2.23	2248.14

Well: 3-3 TVDSS (ft)	Old Gamma (API)	Corrected Gamma (API)	Porosity (%) from Gamma	Neutron (API)
1926.00	63.00	35.65	2.20	1054.93
1925.50	63.05	35.77	2.21	1070.87
1925.00	62.01	33.68	1.98	1092.51
1924.50	58.81	27.29	1.41	1119.79
1924.00	55.22	20.10	0.97	1155.31
1923.50	51.50	12.65	0.65	1223.24
1923.00	51.16	11.99	0.63	1312.34
1922.50	51.98	13.62	0.69	1335.20
1922.00	52.76	15.18	0.74	1338.70
1921.50	54.14	17.94	0.86	1339.72
1921.00	56.59	22.84	1.12	1333.64
1920.50	59.76	29.18	1.56	1310.18
1920.00	62.44	34.54	2.07	1284.05
1919.50	64.91	39.48	2.69	1256.60
1919.00	67.84	45.33	3.67	1221.00
1918.50	70.70	51.06	4.96	1194.25
1918.00	72.69	55.03	6.12	1164.70
1917.50	74.62	58.90	7.51	1134.48
1917.00	77.11	63.87	9.77	1093.70
1916.50	79.48	68.62	12.55	1057.01
1916.00	80.51	70.68	14.00	994.72
1915.50	81.88	73.42	16.18	960.42
1915.00	82.51	74.69	17.30	945.79
1914.50	83.20	76.07	18.61	941.49
1914.00	83.09	75.84	18.38	933.81
1913.50	81.68	73.02	15.84	926.71
1913.00	81.74	73.14	15.94	918.27
1912.50	82.78	75.23	17.80	918.94
1912.00	84.45	78.56	21.23	924.83
1911.50	85.43	80.51	23.54	924.86
1911.00	82.48	74.62	17.24	917.86
1910.50	78.63	66.92	11.48	909.44
1910.00	73.79	57.23	6.88	909.09
1909.50	72.56	54.78	6.04	914.10
1909.00	71.56	52.78	5.43	921.87
1908.50	70.00	49.66	4.61	931.86
1908.00	66.17	42.00	3.07	943.57
1907.50	64.81	39.29	2.66	953.53
1907.00	67.20	44.06	3.43	958.55
1906.50	68.09	45.84	3.77	964.56
1906.00	67.18	44.02	3.42	975.07
1905.50	66.14	41.93	3.06	996.68
1905.00	62.94	35.53	2.18	1015.92
1904.50	61.06	31.77	1.79	1031.11
1904.00	58.18	26.02	1.32	1049.67
1903.50	59.93	29.53	1.59	1071.06
1903.00	63.54	36.74	2.33	1099.05
1902.50	65.42	40.50	2.84	1110.81
1902.00	64.85	39.36	2.67	1125.36
1901.50	62.67	35.01	2.12	1144.37
1901.00	60.91	31.49	1.76	1155.35
1900.50	61.14	31.95	1.81	1162.51
1900.00	60.74	31.13	1.73	1176.58
1899.50	60.79	31.24	1.74	1195.14
1899.00	62.73	35.13	2.14	1225.61
1898.50	63.04	35.75	2.21	1251.15
1898.00	61.84	33.34	1.94	1257.92
1897.50	58.78	27.23	1.41	1260.45
1897.00	57.25	24.16	1.20	1267.67

Well: 3-4 TVDSS (ft)	Old Gamma (API)	Corrected Gamma (API)	Porosity (%) from Gamma	Neutron (API)
1936.00	44.08	20.72	1.00	1018.34
1935.50	43.71	20.10	0.97	1047.31
1935.00	42.40	17.93	0.86	1091.73
1934.50	40.43	14.65	0.72	1178.83
1934.00	38.88	12.08	0.63	1258.00
1933.50	40.75	15.18	0.74	1310.55
1933.00	41.30	16.10	0.78	1322.45
1932.50	43.22	19.28	0.93	1332.37
1932.00	46.01	23.92	1.18	1338.29
1931.50	50.89	32.01	1.81	1319.00
1931.00	57.80	43.50	3.33	1284.83
1930.50	63.17	52.40	5.33	1256.00
1930.00	65.72	56.63	6.66	1153.90
1929.50	74.00	70.38	13.78	1055.74
1929.00	80.08	80.48	23.49	953.61
1928.50	79.84	80.07	22.99	872.31
1928.00	77.07	75.47	18.03	826.04
1927.50	75.16	72.31	15.26	800.22
1927.00	72.13	67.27	11.69	784.33
1926.50	73.90	70.22	13.66	778.34
1926.00	76.45	74.44	17.08	789.32
1925.50	76.47	74.48	17.11	786.52
1925.00	75.20	72.38	15.31	783.36
1924.50	76.59	74.68	17.29	772.00
1924.00	76.58	74.67	17.28	763.63
1923.50	73.59	69.70	13.29	760.82
1923.00	75.71	73.22	16.01	753.21
1922.50	72.77	68.35	12.37	756.67
1922.00	70.92	65.27	10.52	768.46
1921.50	70.03	63.78	9.72	773.06
1921.00	73.23	69.11	12.88	789.84
1920.50	73.74	69.96	13.47	837.53
1920.00	74.58	71.35	14.50	832.43
1919.50	74.77	71.65	14.73	910.44
1919.00	73.57	69.67	13.27	955.15
1918.50	70.66	64.84	10.28	974.70
1918.00	70.27	64.18	9.93	1000.47
1917.50	67.75	60.00	7.96	995.47
1917.00	64.28	54.24	5.87	985.89
1916.50	61.61	49.81	4.64	986.93
1916.00	59.26	45.92	3.78	995.67
1915.50	58.69	44.97	3.60	1043.76
1915.00	60.28	47.61	4.13	1050.86
1914.50	61.71	49.98	4.69	1023.69
1914.00	62.95	52.04	5.22	1000.69
1913.50	60.41	47.82	4.18	991.88
1913.00	58.78	45.11	3.62	1017.71
1912.50	57.10	42.33	3.13	1061.14
1912.00	56.68	41.63	3.01	1134.90
1911.50	58.21	44.17	3.45	1178.31
1911.00	58.82	45.18	3.64	1197.75
1910.50	60.23	47.53	4.12	1213.61
1910.00	61.96	50.40	4.79	1203.79
1909.50	65.71	56.61	6.65	1184.76
1909.00	63.61	53.13	5.53	1183.54
1908.50	58.04	43.88	3.40	1227.25
1908.00	59.37	46.09	3.82	1282.75

Well: 3-6 TVDSS (ft)	Old Gamma (API)	Corrected Gamma (API)	Porosity (%) from Gamma	Neutron (API)
1949.00	31.74	37.22	2.39	591.99
1948.50	33.03	39.81	2.74	587.53
1948.00	29.77	33.29	1.94	743.90
1947.50	25.98	25.70	1.30	865.01
1947.00	24.64	23.03	1.13	870.53
1946.50	21.00	15.74	0.77	822.01
1946.00	20.44	14.63	0.72	788.88
1945.50	19.45	12.65	0.65	771.12
1945.00	19.09	11.93	0.63	761.57
1944.50	21.89	17.53	0.84	748.55
1944.00	25.05	23.85	1.18	696.47
1943.50	25.48	24.71	1.23	573.57
1943.00	28.28	30.30	1.66	456.97
1942.50	31.54	36.83	2.34	432.90
1942.00	33.91	41.57	3.01	397.95
1941.50	38.28	50.31	4.77	347.62
1941.00	43.51	60.76	8.29	299.10
1940.50	48.30	70.35	13.75	290.50
1940.00	49.67	73.09	15.90	276.09
1939.50	52.28	78.31	20.95	252.42
1939.00	52.56	78.86	21.57	243.30
1938.50	51.79	77.34	19.90	229.32
1938.00	53.26	80.27	23.24	236.64
1937.50	53.33	80.42	23.42	250.40
1937.00	51.41	76.57	19.11	255.62
1936.50	48.30	70.36	13.76	266.70
1936.00	48.78	71.31	14.47	288.06
1935.50	48.88	71.52	14.63	323.51
1935.00	47.63	69.00	12.81	362.14
1934.50	47.49	68.73	12.62	408.31
1934.00	49.71	73.17	15.96	456.11
1933.50	48.50	70.76	14.05	507.48
1933.00	50.44	74.63	17.24	568.81

Well: 4-1 TVDSS (ft)	Old Gamma (API)	Corrected Gamma (API)	Porosity (%) from Gamma
1980.00	39.71	39.24	2.66
1979.50	35.78	32.95	1.90
1979.00	28.33	21.00	1.01
1978.50	28.14	20.68	1.00
1978.00	28.47	21.22	1.02
1977.50	24.18	14.34	0.71
1977.00	22.72	12.00	0.63
1976.50	23.93	13.93	0.70
1976.00	26.04	17.32	0.83
1975.50	28.54	21.32	1.03
1975.00	34.81	31.39	1.75
1974.50	43.85	45.88	3.77
1974.00	48.63	53.56	5.66
1973.50	50.51	56.57	6.64
1973.00	52.19	59.26	7.65
1972.50	53.70	61.69	8.70
1972.00	51.34	57.90	7.12
1971.50	50.11	55.93	6.42
1971.00	52.39	59.58	7.79
1970.50	56.01	65.39	10.58
1970.00	59.36	70.77	14.06
1969.50	61.93	74.89	17.49
1969.00	62.97	76.55	19.09
1968.50	63.10	76.76	19.30
1968.00	64.10	78.36	21.01
1967.50	64.81	79.50	22.31
1967.00	65.23	80.18	23.13
1966.50	64.00	78.20	20.83
1966.00	61.10	73.55	16.29
1965.50	61.23	73.76	16.47
1965.00	60.70	72.91	15.75
1964.50	61.20	73.71	16.43
1964.00	64.82	79.52	22.34
1963.50	65.41	80.47	23.48
1963.00	59.94	71.70	14.77
1962.50	57.37	67.58	11.88
1962.00	55.54	64.63	10.17
1961.50	58.40	69.22	12.96
1961.00	59.40	70.83	14.11
1960.50	59.50	70.98	14.22
1960.00	57.73	68.14	12.24
1959.50	55.80	65.06	10.40
1959.00	53.25	60.97	8.38
1958.50	52.65	59.99	7.96
1958.00	51.37	57.95	7.14
1957.50	46.77	50.56	4.83
1957.00	43.06	44.61	3.53
1956.50	38.54	37.36	2.41
1956.00	36.74	34.48	2.07
1955.50	36.18	33.58	1.97
1955.00	38.69	37.60	2.44
1954.50	44.06	46.23	3.84
1954.00	49.15	54.39	5.92

Well: 4-2

TVDSS (ft)	Old Gamma (API)	Corrected Gamma (API)	Porosity (%) from Gamma	Density (G/CC)
1999.00	36.33	32.67	1.88	2.68
1998.50	34.27	30.67	1.69	2.69
1998.00	23.25	19.99	0.96	2.66
1997.50	17.76	14.65	0.72	2.70
1997.00	15.09	12.07	0.63	2.83
1996.50	15.03	12.01	0.63	2.89
1996.00	23.28	20.02	0.96	2.92
1995.50	20.78	17.59	0.85	2.92
1995.00	35.95	32.30	1.84	2.91
1994.50	48.93	44.89	3.58	2.89
1994.00	51.79	47.67	4.15	2.85
1993.50	55.86	51.62	5.11	2.74
1993.00	62.46	58.02	7.17	2.65
1992.50	62.76	58.31	7.28	2.60
1992.00	62.52	58.07	7.19	2.52
1991.50	61.87	57.45	6.95	2.48
1991.00	61.20	56.80	6.72	2.47
1990.50	60.15	55.78	6.37	2.45
1990.00	61.11	56.70	6.69	2.44
1989.50	64.52	60.01	7.96	2.43
1989.00	67.64	63.04	9.35	2.41
1988.50	70.75	66.06	10.96	2.40
1988.00	74.66	69.85	13.40	2.37
1987.50	77.26	72.37	15.31	2.35
1987.00	80.31	75.34	17.90	2.32
1986.50	83.14	78.07	20.69	2.29
1986.00	85.73	80.59	23.63	2.28
1985.50	85.64	80.50	23.52	2.26
1985.00	84.95	79.83	22.70	2.26
1984.50	81.94	76.91	19.46	2.26
1984.00	82.37	77.33	19.89	2.24
1983.50	83.92	78.83	21.53	2.22
1983.00	84.71	79.60	22.43	2.23
1982.50	80.64	75.65	18.20	2.25
1982.00	79.22	74.28	16.93	2.29
1981.50	75.82	70.98	14.22	2.39
1981.00	74.16	69.37	13.06	2.55
1980.50	72.45	67.70	11.96	2.63
1980.00	71.31	66.60	11.28	2.62
1979.50	68.73	64.10	9.88	2.63
1979.00	59.52	55.16	6.16	2.63
1978.50	45.58	41.64	3.02	2.64
1978.00	38.97	35.24	2.15	2.68
1977.50	31.00	27.50	1.43	2.69
1977.00	21.21	18.01	0.86	2.78
1976.50	17.41	14.32	0.71	2.88
1976.00	18.72	15.58	0.76	2.91
1975.50	26.65	23.28	1.14	2.94
1975.00	63.66	59.18	7.62	2.93

Well: 5-1 TVDSS (ft)	Old Gamma (API)	Corrected Gamma (API)	Porosity (%) from Gamma
1960.00	58.24	37.47	2.42
1959.50	56.49	35.08	2.13
1959.00	53.78	31.38	1.75
1958.50	50.10	26.34	1.34
1958.00	45.67	20.28	0.98
1957.50	40.90	13.77	0.69
1957.00	40.32	12.98	0.66
1956.50	39.64	12.05	0.63
1956.00	39.59	11.98	0.63
1955.50	40.80	13.63	0.69
1955.00	42.74	16.29	0.79
1954.50	48.69	24.43	1.21
1954.00	52.86	30.12	1.64
1953.50	58.10	37.29	2.40
1953.00	64.29	45.75	3.75
1952.50	69.23	52.50	5.35
1952.00	71.05	54.98	6.10
1951.50	74.52	59.73	7.85
1951.00	74.51	59.72	7.84
1950.50	75.40	60.94	8.36
1950.00	77.84	64.27	9.97
1949.50	84.06	72.77	15.63
1949.00	84.93	73.96	16.64
1948.50	85.06	74.14	16.80
1948.00	84.59	73.50	16.24
1947.50	83.79	72.40	15.33
1947.00	85.00	74.05	16.72
1946.50	87.17	77.02	19.56
1946.00	86.15	75.63	18.18
1945.50	87.89	78.01	20.61
1945.00	87.28	77.17	19.72
1944.50	88.35	78.63	21.31
1944.00	89.44	80.13	23.06
1943.50	88.69	79.09	21.83
1943.00	88.40	78.70	21.38
1942.50	88.75	79.18	21.93
1942.00	86.47	76.07	18.61

Well: 5-2 TVDSS (ft)	Old Gamma (API)	Corrected Gamma (API)	Porosity (%) from Gamma	Neutron (API)
1968.00	16.29	20.07	0.96	1035.93
1967.50	15.69	18.70	0.90	1086.77
1967.00	14.94	16.95	0.82	1157.64
1966.50	12.81	12.04	0.63	1207.32
1966.00	13.24	13.04	0.67	1307.16
1965.50	15.19	17.54	0.84	1364.81
1965.00	18.95	26.23	1.34	1442.32
1964.50	18.43	25.03	1.25	1513.85
1964.00	21.02	31.02	1.72	1516.19
1963.50	25.56	41.50	2.99	1524.91
1963.00	24.85	39.86	2.74	1514.31
1962.50	39.47	73.62	16.35	1451.49
1962.00	42.01	79.49	22.29	1367.59
1961.50	42.49	80.60	23.65	1264.75
1961.00	40.13	75.16	17.74	1107.55
1960.50	37.65	69.43	13.10	995.05
1960.00	37.21	68.40	12.41	941.58
1959.50	37.48	69.04	12.83	915.18
1959.00	36.36	66.44	11.19	919.11
1958.50	35.89	65.35	10.56	907.36
1958.00	36.54	66.85	11.43	894.66
1957.50	37.66	69.44	13.11	872.40
1957.00	39.99	74.82	17.42	871.72
1956.50	41.76	78.91	21.62	881.53
1956.00	41.47	78.25	20.88	858.71
1955.50	39.66	74.06	16.74	846.87
1955.00	38.02	70.27	13.69	838.76
1954.50	36.64	67.08	11.57	835.40
1954.00	34.38	61.87	8.79	815.59
1953.50	32.58	57.72	7.06	776.81
1953.00	30.82	53.65	5.69	765.45
1952.50	28.72	48.80	4.40	804.13
1952.00	28.20	47.60	4.13	847.64
1951.50	29.61	50.86	4.91	918.55
1951.00	32.94	58.53	7.36	927.42

Well: 5-3 TVDSS (ft)	Old Gamma (API)	Corrected Gamma (API)	Porosity (%) from Gamma	Neutron (API)
1973.00	37.43	30.99	1.72	1193.03
1972.50	39.69	33.17	1.93	1227.52
1972.00	37.65	31.21	1.74	1293.11
1971.50	30.91	24.73	1.23	1461.14
1971.00	22.48	16.64	0.80	1667.97
1970.50	18.52	12.84	0.66	1650.89
1970.00	17.58	11.94	0.63	1692.41
1969.50	18.77	13.08	0.67	1712.28
1969.00	22.55	16.71	0.81	1707.66
1968.50	28.87	22.77	1.11	1621.73
1968.00	28.32	22.25	1.08	1632.65
1967.50	51.27	44.28	3.47	1364.16
1967.00	69.07	61.36	8.55	1202.65
1966.50	76.06	68.07	12.20	1136.28
1966.00	80.66	72.49	15.40	1057.12
1965.50	81.13	72.95	15.78	1020.31
1965.00	74.40	66.49	11.21	1005.23
1964.50	71.06	63.28	9.47	1000.55
1964.00	73.59	65.70	10.76	981.32
1963.50	75.43	67.47	11.81	964.35
1963.00	75.64	67.67	11.94	938.27
1962.50	74.64	66.72	11.35	912.08
1962.00	73.17	65.30	10.53	923.18
1961.50	70.44	62.68	9.17	942.67
1961.00	69.08	61.37	8.56	989.56
1960.50	70.87	63.09	9.37	1009.14
1960.00	73.37	65.50	10.64	1016.84
1959.50	77.61	69.57	13.20	984.14
1959.00	82.49	74.25	16.91	964.56
1958.50	84.80	76.47	19.01	964.49
1958.00	86.27	77.88	20.48	961.98
1957.50	86.00	77.62	20.20	978.09
1957.00	84.05	75.74	18.29	1064.71
1956.50	79.37	71.25	14.43	1143.50
1956.00	74.15	66.24	11.07	1148.14
1955.50	75.73	67.76	12.00	1115.57
1955.00	79.35	71.23	14.41	1048.04
1954.50	80.88	72.71	15.58	1042.99
1954.00	85.26	76.91	19.46	1069.80
1953.50	88.03	79.57	22.39	1059.47
1953.00	88.68	80.20	23.15	1048.92
1952.50	88.13	79.66	22.50	1064.28
1952.00	83.33	75.06	17.64	1113.06
1951.50	74.14	66.24	11.07	1203.35
1951.00	63.07	55.61	6.31	1401.50
1950.50	59.00	51.70	5.13	1398.01
1950.00	60.57	53.21	5.56	1369.79
1949.50	62.90	55.45	6.26	1319.01
1949.00	66.13	58.55	7.37	1246.98
1948.50	66.10	58.52	7.36	1174.10
1948.00	61.58	54.17	5.85	1169.03
1947.50	51.61	44.61	3.53	1478.89
1947.00	46.44	39.64	2.71	1489.41
1946.50	54.08	46.98	4.00	1509.52
1946.00	67.69	60.05	7.98	1465.57

Well: 8-1 TVDSS (ft)	Old Gamma (API)	Corrected Gamma (API)	Porosity (%) from Gamma	Density (G/CC)
1964.00	42.42	41.88	3.05	2.68
1963.50	35.26	34.72	2.09	2.76
1963.00	30.18	29.64	1.60	2.78
1962.50	26.57	26.03	1.32	2.86
1962.00	18.20	17.66	0.85	2.92
1961.50	13.37	12.83	0.66	2.94
1961.00	12.67	12.13	0.63	2.91
1960.50	13.81	13.27	0.67	2.88
1960.00	15.59	15.05	0.74	2.84
1959.50	17.40	16.86	0.81	2.79
1959.00	21.76	21.22	1.02	2.74
1958.50	31.74	31.20	1.74	2.67
1958.00	37.14	36.60	2.31	2.60
1957.50	49.31	48.77	4.40	2.53
1957.00	60.29	59.75	7.85	2.47
1956.50	66.13	65.59	10.70	2.40
1956.00	73.62	73.08	15.89	2.32
1955.50	74.91	74.37	17.01	2.28
1955.00	78.53	77.99	20.60	2.24
1954.50	81.04	80.50	23.53	2.22
1954.00	76.91	76.37	18.91	2.21
1953.50	74.59	74.05	16.72	2.21
1953.00	73.30	72.76	15.62	2.22
1952.50	71.45	70.91	14.17	2.24
1952.00	66.02	65.48	10.63	2.22
1951.50	64.18	63.64	9.65	2.21
1951.00	63.74	63.20	9.43	2.21
1950.50	62.75	62.21	8.95	2.18
1950.00	61.50	60.96	8.38	2.18
1949.50	63.04	62.50	9.08	2.19
1949.00	63.84	63.30	9.48	2.21
1948.50	66.01	65.47	10.63	2.22
1948.00	66.75	66.21	11.05	2.24
1947.50	65.45	64.91	10.32	2.26
1947.00	63.94	63.40	9.53	2.28
1946.50	61.67	61.13	8.45	2.29
1946.00	61.90	61.36	8.55	2.33
1945.50	59.07	58.53	7.36	2.38
1945.00	55.83	55.29	6.21	2.43
1944.50	53.20	52.66	5.40	2.47
1944.00	49.82	49.28	4.52	2.48
1943.50	47.05	46.51	3.90	2.48
1943.00	44.97	44.43	3.49	2.46
1942.50	44.35	43.81	3.38	2.49
1942.00	40.71	40.17	2.79	2.54
1941.50	38.88	38.34	2.53	2.62
1941.00	38.21	37.67	2.45	2.64
1940.50	39.52	38.98	2.62	2.68
1940.00	39.80	39.26	2.66	2.70
1939.50	36.48	35.94	2.23	2.73
1939.00	30.45	29.91	1.62	2.78
1938.50	24.65	24.11	1.19	2.83
1938.00	24.06	23.52	1.16	2.82
1937.50	27.33	26.79	1.38	2.76
1937.00	36.27	35.73	2.21	2.68

Well: 9-1 TVDSS (ft)	Old Gamma (API)	Corrected Gamma (API)	Porosity (%) frm Gamma
1998.00	39.99	41.83	3.05
1997.50	33.48	34.67	2.09
1997.00	27.75	28.37	1.49
1996.50	22.60	22.70	1.11
1996.00	17.75	17.36	0.84
1995.50	13.77	12.99	0.66
1995.00	13.38	12.56	0.65
1994.50	13.12	12.27	0.64
1994.00	13.29	12.46	0.64
1993.50	14.94	14.27	0.71
1993.00	15.93	15.37	0.75
1992.50	19.99	19.83	0.95
1992.00	23.07	23.22	1.14
1991.50	26.89	27.42	1.42
1991.00	31.45	32.43	1.85
1990.50	35.48	36.87	2.34
1990.00	36.79	38.31	2.53
1989.50	38.04	39.69	2.72
1989.00	36.34	37.81	2.46
1988.50	35.06	36.41	2.29
1988.00	33.08	34.22	2.04
1987.50	39.72	41.54	3.00
1987.00	43.21	45.37	3.67
1986.50	44.04	46.28	3.85
1986.00	41.12	43.08	3.25
1985.50	43.48	45.67	3.73
1985.00	44.05	46.30	3.86
1984.50	40.86	42.79	3.20
1984.00	39.61	41.41	2.98
1983.50	46.81	49.33	4.53
1983.00	53.21	56.37	6.57
1982.50	61.73	65.74	10.78
1982.00	73.53	78.73	21.42
1981.50	76.48	81.97	25.42
1981.00	73.49	78.68	21.36
1980.50	67.76	72.38	15.31
1980.00	62.59	66.69	11.33
1979.50	60.47	64.35	10.02
1979.00	60.00	63.84	9.75
1978.50	60.68	64.59	10.14
1978.00	60.80	64.72	10.22
1977.50	55.17	58.53	7.36
1977.00	50.68	53.58	5.67
1976.50	46.70	49.21	4.50
1976.00	44.02	46.26	3.85
1975.50	45.99	48.42	4.32
1975.00	57.38	60.95	8.37

Well: 10-1

TVDSS (ft)	Old Gamma (API)	Corrected Gamma (API)	Porosity (%) from Gamma	Neutron (API)
1910.00	33.89	25.82	1.31	1305.88
1910.50	33.42	25.31	1.27	1331.67
1911.00	30.58	22.19	1.08	1363.63
1911.50	26.56	17.77	0.85	1401.19
1912.00	23.88	14.82	0.73	1478.96
1912.50	22.14	12.90	0.66	1470.09
1913.00	21.30	11.98	0.63	1607.22
1913.50	21.24	11.92	0.63	1630.56
1914.00	23.23	14.10	0.70	1635.13
1914.50	27.45	18.74	0.90	1622.98
1915.00	35.20	27.26	1.41	1596.70
1915.50	41.21	33.89	2.00	1547.70
1916.00	48.89	42.33	3.13	1396.94
1916.50	56.72	50.94	4.93	1346.93
1917.00	63.50	58.40	7.31	1306.50
1917.50	65.72	60.85	8.32	1278.23
1918.00	67.17	62.44	9.05	1255.34
1918.50	67.58	62.88	9.27	1248.09
1919.00	67.27	62.55	9.11	1247.76
1919.50	69.00	64.45	10.07	1252.54
1920.00	71.65	67.36	11.75	1257.11
1920.50	75.63	71.74	14.80	1263.31
1921.00	76.77	73.00	15.82	1263.58
1921.50	77.67	73.99	16.67	1263.60
1922.00	78.70	75.12	17.70	1262.56
1922.50	79.88	76.42	18.96	1260.30
1923.00	80.60	77.21	19.76	1261.44
1923.50	81.39	78.08	20.70	1262.65
1924.00	82.51	79.31	22.09	1266.15
1924.50	83.27	80.15	23.09	1271.05
1925.00	82.75	79.57	22.39	1264.81
1925.50	81.34	78.02	20.63	1262.07
1926.00	80.06	76.62	19.16	1254.57
1926.50	79.69	76.20	18.74	1247.28
1927.00	77.94	74.29	16.94	1230.84
1927.50	77.11	73.37	16.14	1209.90
1928.00	77.07	73.32	16.10	1196.13
1928.50	76.68	72.90	15.74	1190.05
1929.00	76.01	72.16	15.14	1186.98
1929.50	75.11	71.17	14.37	1183.98
1930.00	72.97	68.82	12.68	1183.87
1930.50	70.71	66.33	11.12	1188.10
1931.00	69.74	65.27	10.51	1199.50
1931.50	67.07	62.33	9.00	1220.96
1932.00	67.62	62.93	9.29	1247.90
1932.50	56.68	50.90	4.92	1279.19
1933.00	48.09	41.45	2.99	1313.84
1933.50	46.87	40.11	2.78	1329.36
1934.00	45.30	38.38	2.54	1333.36
1934.50	44.46	37.46	2.42	1328.78
1935.00	42.64	35.45	2.17	1319.71
1935.50	40.68	33.30	1.94	1314.65
1936.00	38.81	31.24	1.74	1309.26
1936.50	37.65	29.96	1.63	1311.10
1937.00	38.17	30.54	1.68	1307.66
1937.50	40.45	33.04	1.91	1294.36
1938.00	47.52	40.82	2.89	1266.82

Well: 11-1 TVDSS (ft)	Old Gamma (API)	Corrected Gamma (API)	Porosity (%) from Gamma	Neutron (API)
1997.00	40.72	18.05	0.87	1931.66
1996.50	37.91	14.52	0.72	2049.08
1996.00	37.16	13.58	0.68	2308.49
1995.50	40.86	18.23	0.87	2439.80
1995.00	42.65	20.49	0.99	2456.98
1994.50	42.43	20.21	0.97	2505.87
1994.00	43.75	21.87	1.06	2649.16
1993.50	49.30	28.86	1.53	2682.49
1993.00	56.87	38.40	2.54	2641.46
1992.50	63.24	46.43	3.88	2471.99
1992.00	63.98	47.36	4.08	2453.67
1991.50	68.96	53.65	5.69	2372.05
1991.00	82.27	70.41	13.80	2213.79
1990.50	86.78	76.10	18.64	1988.90
1990.00	84.91	73.74	16.45	1782.48
1989.50	81.64	69.61	13.23	1725.39
1989.00	73.01	58.74	7.45	1723.43
1988.50	73.66	59.56	7.78	1735.24
1988.00	80.41	68.07	12.19	1710.31
1987.50	82.63	70.86	14.13	1680.52
1987.00	74.38	60.46	8.16	1674.40
1986.50	73.91	59.88	7.91	1635.18
1986.00	73.42	59.25	7.65	1609.60
1985.50	73.53	59.39	7.71	1601.63
1985.00	84.33	73.00	15.82	1600.93
1984.50	82.92	71.22	14.41	1610.79
1984.00	79.48	66.89	11.46	1621.05
1983.50	84.98	73.82	16.52	1638.62
1983.00	90.12	80.30	23.28	1662.41
1982.50	88.60	78.39	21.04	1686.67
1982.00	85.23	74.14	16.80	1800.03
1981.50	68.78	53.41	5.62	1868.85
1981.00	65.44	49.20	4.50	1871.29
1980.50	63.42	46.65	3.93	1795.82
1980.00	67.79	52.17	5.26	1783.37
1979.50	75.13	61.41	8.58	1784.13
1979.00	74.14	60.16	8.03	1771.75
1978.50	76.49	63.13	9.39	1791.61
1978.00	73.32	59.14	7.60	1779.93
1977.50	65.64	49.46	4.56	1750.89
1977.00	67.87	52.27	5.29	1896.60
1976.50	39.03	15.93	0.77	1889.28
1976.00	40.74	18.08	0.87	2048.59
1975.50	49.42	29.02	1.55	2075.95
1975.00	54.08	34.89	2.11	2133.20
1974.50	57.56	39.28	2.66	2229.46
1974.00	58.64	40.64	2.86	2277.22
1973.50	55.73	36.97	2.36	2283.97
1973.00	51.83	32.06	1.82	2271.20
1972.50	42.46	20.25	0.97	2310.11
1972.00	35.85	11.93	0.63	2414.97
1971.50	48.21	27.49	1.43	2428.17
1971.00	64.93	48.57	4.35	2362.99
1970.50	66.24	50.21	4.74	2227.32
1970.00	65.09	48.77	4.40	2172.43
1969.50	72.58	58.20	7.24	2141.03
1969.00	69.40	54.19	5.85	2120.92

Well: 13-1 TVDSS (ft)	Old Gamma (API)	Corrected Gamma (API)	Porosity (%) from Gamma	Neutron (API)
2036.00	41.50	29.20	1.56	474.92
2035.50	39.01	23.56	1.16	496.77
2035.00	37.25	19.58	0.94	513.33
2034.50	33.84	11.89	0.63	518.08
2034.00	33.96	12.15	0.63	525.40
2033.50	36.62	18.16	0.87	536.44
2033.00	36.38	17.63	0.85	542.30
2032.50	37.30	19.71	0.95	541.27
2032.00	39.58	24.86	1.24	536.62
2031.50	38.96	23.44	1.15	529.85
2031.00	44.33	35.58	2.19	520.91
2030.50	56.37	62.81	9.23	515.74
2030.00	61.05	73.38	16.14	514.16
2029.50	60.85	72.92	15.75	501.10
2029.00	62.93	77.61	20.19	478.67
2028.50	63.82	79.64	22.48	466.77
2028.00	64.10	80.26	23.23	466.18
2027.50	62.61	76.89	19.44	466.90
2027.00	58.03	66.55	11.25	467.63
2026.50	56.08	62.13	8.91	467.81
2026.00	55.79	61.49	8.61	471.35
2025.50	54.42	58.39	7.31	481.36
2025.00	55.73	61.34	8.54	487.40
2024.50	59.53	69.93	13.46	484.26
2024.00	61.90	75.30	17.87	480.81
2023.50	60.87	72.96	15.79	482.10
2023.00	58.78	68.25	12.31	489.08
2022.50	59.85	70.65	13.98	501.12
2022.00	60.22	71.49	14.61	510.64
2021.50	57.20	64.67	10.19	514.24
2021.00	56.15	62.29	8.98	516.83
2020.50	55.98	61.91	8.80	519.64
2020.00	55.99	61.95	8.82	521.69
2019.50	60.41	71.92	14.95	523.62
2019.00	62.56	76.80	19.34	523.25
2018.50	57.57	65.52	10.65	520.03
2018.00	53.69	56.74	6.70	517.04
2017.50	53.91	57.24	6.88	516.58
2017.00	52.49	54.04	5.81	521.49
2016.50	47.93	43.73	3.37	527.84
2016.00	44.70	36.42	2.29	525.60
2015.50	44.29	35.50	2.18	521.19
2015.00	43.33	33.32	1.94	528.83
2014.50	42.07	30.48	1.67	540.31
2014.00	42.13	30.61	1.68	541.75
2013.50	41.90	30.10	1.64	541.55
2013.00	43.21	33.05	1.92	552.99
2012.50	44.86	36.78	2.33	566.59
2012.00	43.68	34.13	2.03	568.11
2011.50	47.90	43.66	3.35	571.06
2011.00	57.98	66.43	11.18	582.44
2010.50	63.01	77.81	20.40	572.96
2010.00	64.55	81.28	24.51	542.07

Well: 14-1 TVDSS (ft)	Old Gamma (API)	Corrected Gamma (API)	Porosity (%) from Gamma	Neutron (API)
2012.00	39.12	42.02	3.08	2157.94
2011.50	32.37	33.79	1.99	2189.50
2011.00	24.93	24.70	1.23	2192.96
2010.50	17.62	15.79	0.77	2127.77
2010.00	14.77	12.32	0.64	2062.73
2009.50	14.57	12.07	0.63	2036.10
2009.00	15.57	13.29	0.67	2047.68
2008.50	16.71	14.68	0.73	2120.00
2008.00	17.07	15.12	0.74	2172.58
2007.50	18.08	16.34	0.79	2298.40
2007.00	18.85	17.28	0.83	2382.17
2006.50	19.77	18.41	0.88	2475.64
2006.00	21.05	19.97	0.96	2523.99
2005.50	26.09	26.12	1.33	2610.23
2005.00	34.64	36.55	2.30	2680.06
2004.50	38.32	41.04	2.92	2735.06
2004.00	39.33	42.27	3.12	2785.02
2003.50	40.85	44.13	3.44	2833.99
2003.00	42.54	46.19	3.83	2855.10
2002.50	43.37	47.21	4.05	2849.43
2002.00	43.57	47.45	4.10	2836.59
2001.50	43.39	47.23	4.05	2815.54
2001.00	43.00	46.75	3.95	2803.09
2000.50	43.53	47.40	4.09	2792.49
2000.00	43.74	47.65	4.14	2774.22
1999.50	43.65	47.54	4.12	2725.82
1999.00	45.35	49.62	4.60	2666.94
1998.50	48.16	53.05	5.51	2595.83
1998.00	49.64	54.85	6.06	2541.98
1997.50	50.58	55.99	6.44	2499.12
1997.00	48.10	52.98	5.49	2459.07
1996.50	46.18	50.63	4.85	2423.86
1996.00	44.17	48.17	4.26	2388.53
1995.50	41.76	45.23	3.65	2324.02
1995.00	40.63	43.86	3.39	2290.57
1994.50	38.57	41.35	2.97	2279.11
1994.00	34.30	36.13	2.25	2277.29
1993.50	30.00	30.89	1.71	2277.28
1993.00	26.99	27.22	1.41	2286.62
1992.50	28.23	28.74	1.52	2295.40
1992.00	30.81	31.88	1.80	2305.89
1991.50	39.08	41.97	3.07	2323.42
1991.00	52.34	58.14	7.21	2367.84
1990.50	58.62	65.80	10.82	2382.41
1990.00	63.03	71.19	14.38	2385.43
1989.50	68.11	77.38	19.95	2378.43
1989.00	69.34	78.88	21.59	2347.91
1988.50	69.65	79.27	22.04	2312.87
1988.00	70.36	80.13	23.06	2298.55
1987.50	70.58	80.40	23.40	2299.27
1987.00	69.15	78.65	21.33	2307.95
1986.50	65.51	74.22	16.87	2312.72
1986.00	62.21	70.18	13.64	2312.70

Well: 15-3 TVDSS (ft)	Old Gamma (API)	Corrected Gamma (API)	Porosity (%) from Gamma	Neutron (API)
1948.00	2.95	14.96	0.74	535.63
1948.50	2.86	14.76	0.73	538.40
1949.00	3.44	16.05	0.78	543.15
1949.50	3.45	16.08	0.78	544.00
1950.00	2.49	13.95	0.70	547.68
1950.50	1.76	12.35	0.64	541.49
1951.00	1.71	12.22	0.64	539.98
1951.50	2.11	13.10	0.67	522.86
1952.00	3.19	15.50	0.76	497.08
1952.50	5.81	21.28	1.03	486.26
1953.00	7.83	25.76	1.30	483.57
1953.50	10.01	30.57	1.68	468.50
1954.00	12.14	35.28	2.16	428.06
1954.50	15.06	41.73	3.03	420.76
1955.00	19.18	50.83	4.90	418.45
1955.50	25.49	64.78	10.25	416.93
1956.00	28.25	70.89	14.16	420.36
1956.50	28.30	70.99	14.23	420.98
1957.00	27.03	68.19	12.27	429.42
1957.50	23.61	60.62	8.22	431.39
1958.00	18.46	49.25	4.51	432.36
1958.50	18.88	50.18	4.74	432.01
1959.00	20.76	54.34	5.90	435.04
1959.50	21.06	55.00	6.11	435.96
1960.00	18.41	49.13	4.48	432.08
1960.50	19.01	50.46	4.81	422.96
1961.00	20.78	54.38	5.91	419.75
1961.50	23.90	61.26	8.51	418.03
1962.00	25.61	65.04	10.39	418.59
1962.50	27.15	68.44	12.44	418.20
1963.00	28.92	72.37	15.31	418.40
1963.50	30.15	75.08	17.66	419.29
1964.00	31.11	77.21	19.76	420.72
1964.50	31.35	77.73	20.31	416.39
1965.00	31.37	77.78	20.37	414.12
1965.50	29.95	74.64	17.26	416.62
1966.00	28.90	72.33	15.27	424.84
1966.50	28.00	70.34	13.75	434.64
1967.00	25.52	64.85	10.29	449.85
1967.50	20.82	54.47	5.94	455.95
1968.00	16.87	45.74	3.74	455.99
1968.50	17.10	46.24	3.85	435.80
1969.00	20.64	54.06	5.81	419.90
1969.50	30.81	76.54	19.07	415.64
1970.00	32.08	79.35	22.14	417.05
1970.50	32.52	80.31	23.29	417.87
1971.00	30.50	75.85	18.40	433.73
1971.50	30.16	75.10	17.68	448.69
1972.00	31.78	78.67	21.36	455.58
1972.50	32.32	79.87	22.75	458.63
1973.00	29.00	72.53	15.44	466.93
1973.50	27.27	68.72	12.62	482.23
1974.00	24.68	62.98	9.32	523.21
1974.50	16.43	44.77	3.56	575.16
1975.00	10.36	31.34	1.75	604.00
1975.50	3.13	15.36	0.75	581.78
1976.00	1.60	11.98	0.63	545.51
1976.50	1.68	12.17	0.64	511.19
1977.00	3.55	16.30	0.79	505.27
1977.50	4.86	19.19	0.92	512.76
1978.00	5.63	20.88	1.01	538.21
1978.50	5.06	19.62	0.94	609.18
1979.00	2.23	13.38	0.68	653.84
1979.50	1.91	12.68	0.65	650.14
1980.00	2.88	14.81	0.73	637.80

Well: 1-16 (New Log)

TVDSS (ft)	Gamma (API)	Porosity (%) from Gamma
1970.00	42.68	3.19
1969.50	33.55	1.97
1969.00	25.10	1.26
1968.50	17.57	0.85
1968.00	13.55	0.68
1967.50	11.35	0.61
1967.00	11.45	0.61
1966.50	11.66	0.62
1966.00	10.73	0.59
1965.50	11.13	0.60
1965.00	17.69	0.85
1964.50	23.85	1.18
1964.00	35.29	2.16
1963.50	46.77	3.95
1963.00	54.13	5.84
1962.50	59.25	7.65
1962.00	64.46	10.07
1961.50	68.10	12.21
1961.00	74.04	16.72
1960.50	75.12	17.70
1960.00	77.27	19.83
1959.50	77.11	19.66
1959.00	78.11	20.73
1958.50	76.93	19.48
1958.00	76.50	19.04
1957.50	75.11	17.69
1957.00	76.51	19.05
1956.50	75.99	18.53
1956.00	78.20	20.83
1955.50	76.89	19.44
1955.00	77.87	20.47
1954.50	73.95	16.64
1954.00	74.03	16.71
1953.50	75.01	17.60
1953.00	75.96	18.50
1952.50	74.16	16.82
1952.00	73.09	15.90
1951.50	65.95	10.90
1951.00	61.50	8.62
1950.50	53.19	5.55
1950.00	53.13	5.54
1949.50	48.63	4.36
1949.00	47.00	4.00
1948.50	45.00	3.60
1948.00	44.00	3.42
1947.50	40.00	2.77
1947.00	38.00	2.49
1946.50	36.59	2.31

Well: 2-2 (New Log)

TVDSS (ft)	Gamma (API)	Porosity (%) from Neutron	Porosity (%) from Gamma
1962.00	26.07	4.86	1.32
1961.50	19.37	1.65	0.93
1961.00	17.29	1.02	0.83
1960.50	16.31	0.65	0.79
1960.00	16.54	0.42	0.80
1959.50	14.60	0.30	0.72
1959.00	15.08	0.30	0.74
1958.50	19.14	0.58	0.92
1958.00	26.89	1.44	1.38
1957.50	40.01	3.92	2.77
1957.00	56.84	7.96	6.73
1956.50	68.44	12.17	12.43
1956.00	72.73	14.24	15.60
1955.50	73.72	18.36	16.43
1955.00	72.48	21.11	15.39
1954.50	70.96	23.19	14.20
1954.00	69.71	22.65	13.30
1953.50	68.17	21.74	12.26
1953.00	67.00	21.50	11.52
1952.50	66.65	24.76	11.31
1952.00	66.88	28.95	11.45
1951.50	67.92	30.48	12.09
1951.00	69.12	28.63	12.89
1950.50	70.99	26.10	14.23
1950.00	71.82	26.13	14.87
1949.50	71.61	26.53	14.70
1949.00	71.46	27.11	14.59
1948.50	72.14	27.55	15.12
1948.00	72.47	24.56	15.38
1947.50	73.42	22.72	16.17
1947.00	75.14	20.56	17.72
1946.50	77.68	18.68	20.26
1946.00	78.97	18.38	21.69
1945.50	77.42	18.02	19.98
1945.00	74.92	17.38	17.51
1944.50	72.16	16.05	15.13
1944.00	69.94	15.08	13.46
1943.50	65.20	11.18	10.48
1943.00	59.73	9.06	7.84
1942.50	55.37	8.08	6.23
1942.00	54.05	6.22	5.81
1941.50	55.91	4.70	6.41
1941.00	57.19	4.60	6.86

Well: 16-1 (New Log)

TVDSS (ft)	Gamma (API)	Porosity (%) from Gamma	Porosity (%) from Neutron
1900.00	29.73	1.61	4.91
1900.50	19.64	0.94	2.21
1901.00	20.34	0.98	1.23
1901.50	13.08	0.67	0.33
1902.00	12.41	0.64	0.10
1902.50	13.73	0.69	0.18
1903.00	18.03	0.87	1.08
1903.50	25.30	1.27	2.62
1904.00	36.46	2.29	6.35
1904.50	81.32	24.57	7.77
1905.00	84.06	28.40	8.91
1905.50	68.20	12.28	13.09
1906.00	57.60	7.01	13.76
1906.50	54.47	5.94	14.47
1907.00	53.31	5.59	15.10
1907.50	53.74	5.72	15.73
1908.00	56.09	6.47	17.56
1908.50	58.01	7.16	18.25
1909.00	59.41	7.72	17.52
1909.50	61.01	8.39	15.69
1910.00	61.55	8.64	15.98
1910.50	61.94	8.82	16.48
1911.00	59.60	7.79	17.23
1911.50	61.22	8.49	17.26
1912.00	63.09	9.37	17.97
1912.50	66.35	11.13	18.71
1913.00	67.28	11.70	19.19
1913.50	63.49	9.57	18.57
1914.00	59.48	7.74	17.22
1914.50	58.84	7.49	16.52
1915.00	62.47	9.07	15.69
1915.50	64.86	10.29	14.52
1916.00	65.73	10.77	13.49
1916.50	65.45	10.61	12.34
1917.00	64.21	9.94	11.60
1917.50	60.41	8.14	11.12
1918.00	54.90	6.08	9.90
1918.50	49.89	4.66	8.63
1919.00	45.70	3.74	7.21
1919.50	42.76	3.20	5.96
1920.00	41.11	2.93	5.38
1920.50	40.82	2.89	4.86
1921.00	40.76	2.88	4.65
1921.50	40.39	2.82	4.42
1922.00	38.32	2.53	4.19
1922.50	38.00	2.49	3.86
1923.00	43.23	3.28	3.53
1923.50	49.00	4.45	3.06
1924.00	51.55	5.09	2.38
1924.50	33.78	1.99	1.08
1925.00	19.82	0.95	0.82
1925.50	19.89	0.96	0.76
1926.00	28.24	1.49	1.07

Well: Boomer Federal TVDSS (ft)	(New Log) Gamma (API)	Porosity (%) from Gamma	Porosity (%) from Neutron
1806.00	28.43	1.52	7.94
1806.50	18.20	0.88	6.28
1807.00	14.37	0.72	5.61
1807.50	11.94	0.63	2.05
1808.00	10.21	0.58	1.37
1808.50	8.76	0.54	1.06
1809.00	9.45	0.56	0.58
1809.50	13.20	0.68	0.19
1810.00	20.00	0.97	0.15
1810.50	27.99	1.48	0.15
1811.00	34.40	2.08	0.86
1811.50	43.23	3.32	2.09
1812.00	51.64	5.18	3.51
1812.50	60.15	8.11	6.10
1813.00	67.07	11.70	7.63
1813.50	70.41	13.96	9.81
1814.00	69.75	13.49	12.18
1814.50	68.49	12.61	14.16
1815.00	66.82	11.55	15.46
1815.50	65.40	10.71	15.88
1816.00	62.74	9.31	14.91
1816.50	59.66	7.91	13.03
1817.00	60.82	8.41	12.38
1817.50	64.24	10.08	12.27
1818.00	65.04	10.51	13.54
1818.50	66.65	11.45	14.51
1819.00	68.76	12.79	14.51
1819.50	72.46	15.56	13.84
1820.00	73.88	16.77	13.76
1820.50	79.24	22.26	14.31
1821.00	80.63	23.97	15.02
1821.50	79.01	22.00	15.14
1822.00	76.51	19.27	15.42
1822.50	75.42	18.19	16.17
1823.00	75.79	18.55	16.85
1823.50	77.90	20.74	16.85
1824.00	77.83	20.66	16.68
1824.50	72.06	15.23	16.22
1825.00	62.68	9.28	13.82
1825.50	55.58	6.38	11.87
1826.00	51.41	5.11	8.14
1826.50	48.51	4.39	5.41
1827.00	44.86	3.62	3.79
1827.50	41.25	2.99	3.35
1828.00	40.86	2.93	3.16
1828.50	45.10	3.66	3.23
1829.00	49.64	4.66	4.03
1829.50	48.88	4.47	5.18
1830.00	45.12	3.67	8.30

Well: LL1 (Old Log)

TVDSS (ft)	Old Gamma (API)	Corrected Gamma (API)	Porosity (%) from Gamma	Neutron (API)
1954.00	46.69	46.02	3.80	1111.71
1954.50	40.89	38.37	2.54	1152.78
1955.00	37.62	34.04	2.02	1219.20
1955.50	31.51	25.98	1.32	1313.54
1956.00	25.17	17.61	0.85	1384.76
1956.50	21.00	12.11	0.63	1556.61
1957.00	20.92	12.00	0.63	1753.33
1957.50	22.35	13.89	0.70	1794.87
1958.00	23.59	15.53	0.76	1789.67
1958.50	27.01	20.04	0.96	1779.80
1959.00	30.68	24.88	1.24	1866.23
1959.50	35.22	30.89	1.71	1892.43
1960.00	39.18	36.10	2.25	1766.58
1960.50	46.68	46.01	3.80	1656.05
1961.00	52.84	54.15	5.84	1499.64
1961.50	55.39	57.50	6.97	1346.34
1962.00	56.59	59.09	7.58	1224.28
1962.50	59.44	62.85	9.25	1108.67
1963.00	61.62	65.73	10.77	1034.68
1963.50	63.43	68.12	12.22	979.19
1964.00	63.67	68.44	12.43	976.20
1964.50	62.88	67.39	11.76	976.77
1965.00	62.75	67.22	11.66	986.81
1965.50	63.12	67.70	11.96	1019.84
1966.00	63.48	68.19	12.27	1043.95
1966.50	62.22	66.52	11.23	1068.91
1967.00	61.26	65.26	10.51	1094.82
1967.50	62.69	67.14	11.61	1102.94
1968.00	63.45	68.14	12.24	1093.05
1968.50	61.10	65.05	10.39	1086.04
1969.00	61.63	65.75	10.78	1060.47
1969.50	59.90	63.45	9.55	1023.46
1970.00	58.97	62.23	8.96	964.67
1970.50	60.30	63.99	9.83	954.59
1971.00	64.40	69.40	13.08	949.32
1971.50	68.11	74.29	16.94	963.09
1972.00	71.97	79.39	22.18	964.55
1972.50	72.78	80.46	23.47	978.06
1973.00	71.21	78.39	21.04	992.86
1973.50	70.27	77.15	19.70	1021.14
1974.00	68.35	74.62	17.24	1039.86
1974.50	67.11	72.98	15.80	1049.41
1975.00	64.27	69.23	12.96	1070.08
1975.50	56.54	59.03	7.56	1096.10
1976.00	53.54	55.06	6.13	1175.61
1976.50	49.42	49.63	4.60	1252.78
1977.00	45.35	44.25	3.46	1318.05
1977.50	42.16	40.04	2.77	1375.31
1978.00	42.08	39.93	2.76	1496.24
1978.50	35.51	31.27	1.74	1589.79
1979.00	33.04	28.01	1.47	1728.69
1979.50	28.31	21.76	1.05	1818.02
1980.00	27.99	21.34	1.03	1865.40

Well: LL2 TVDSS (ft)	Old Gamma (API)	Corrected Gamma (API)	Porosity (%) from Gamma	Neutron (API)
1962.00	32.81	26.00	1.32	802.44
1962.50	29.94	19.97	0.96	826.63
1963.00	28.34	16.61	0.80	895.85
1963.50	26.57	12.89	0.66	952.25
1964.00	26.26	12.24	0.64	967.63
1964.50	28.57	17.11	0.82	969.76
1965.00	29.57	19.21	0.92	970.45
1965.50	29.99	20.08	0.96	975.69
1966.00	30.06	20.22	0.97	957.76
1966.50	35.31	31.25	1.74	933.32
1967.00	40.31	41.75	3.03	873.54
1967.50	43.61	48.69	4.38	829.63
1968.00	44.32	50.17	4.73	786.33
1968.50	45.06	51.74	5.14	769.67
1969.00	46.35	54.44	5.93	748.07
1969.50	48.56	59.08	7.58	725.03
1970.00	51.72	65.71	10.77	664.44
1970.50	55.66	73.98	16.67	666.67
1971.00	57.67	78.21	20.84	647.96
1971.50	59.00	81.00	24.15	642.33
1972.00	56.30	75.34	17.91	644.77
1972.50	52.83	68.04	12.17	654.29
1973.00	49.58	61.23	8.49	688.36
1973.50	49.53	61.11	8.44	705.44
1974.00	49.05	60.11	8.01	730.21
1974.50	49.48	61.00	8.39	740.70
1975.00	52.64	67.64	11.92	747.99
1975.50	55.13	72.87	15.71	734.84
1976.00	56.99	76.78	19.32	713.32
1976.50	57.18	77.18	19.73	699.13
1977.00	55.62	73.90	16.59	690.71
1977.50	55.33	73.28	16.06	704.43
1978.00	55.81	74.30	16.95	721.18
1978.50	55.87	74.42	17.06	733.87
1979.00	54.49	71.53	14.64	745.61
1979.50	54.22	70.96	14.21	757.35
1980.00	54.82	72.23	15.19	779.13
1980.50	55.78	74.23	16.89	803.95
1981.00	52.10	66.50	11.22	849.65
1981.50	45.69	53.04	5.51	881.29
1982.00	41.91	45.10	3.62	911.36
1982.50	39.48	40.00	2.76	952.98
1983.00	39.41	39.86	2.74	978.61
1983.50	38.16	37.24	2.39	994.95
1984.00	33.83	28.14	1.48	1024.83
1984.50	28.28	16.49	0.80	1045.53
1985.00	27.02	13.84	0.69	1054.40
1985.50	28.65	17.25	0.83	1054.02
1986.00	32.12	24.55	1.22	1015.61
1986.50	38.38	37.69	2.45	942.34
1987.00	40.23	41.59	3.01	901.34
1987.50	40.91	43.02	3.24	839.90

Well: LL3 (Old Log) TVDSS (ft)	Old Gamma (API)	Corrected Gamma (API)	Porosity (%) from Gamma	Neutron (API)
1934.00	32.52	26.83	1.38	811.04
1934.50	30.40	23.18	1.14	818.48
1935.00	29.53	21.69	1.05	841.96
1935.50	28.38	19.71	0.95	875.00
1936.00	25.85	15.36	0.75	902.01
1936.50	24.21	12.54	0.65	1021.80
1937.00	23.83	11.88	0.63	1070.87
1937.50	26.83	17.05	0.82	1112.87
1938.00	29.56	21.75	1.05	1087.74
1938.50	34.26	29.83	1.62	1070.66
1939.00	35.50	31.95	1.81	1046.16
1939.50	39.91	39.55	2.70	1015.02
1940.00	48.87	54.96	6.10	952.79
1940.50	57.21	69.29	13.01	850.83
1941.00	58.55	71.61	14.70	779.30
1941.50	56.11	67.41	11.77	669.33
1942.00	55.55	66.45	11.19	636.14
1942.50	55.76	66.81	11.41	554.01
1943.00	55.89	67.04	11.55	539.56
1943.50	56.95	68.86	12.71	538.88
1944.00	60.95	75.73	18.28	569.49
1944.50	63.22	79.63	22.47	579.96
1945.00	63.13	79.48	22.29	578.46
1945.50	60.04	74.18	16.84	584.40
1946.00	57.22	69.31	13.02	593.28
1946.50	56.09	67.37	11.75	598.42
1947.00	57.33	69.51	13.15	604.36
1947.50	56.58	68.21	12.28	620.30
1948.00	56.91	68.78	12.66	638.56
1948.50	57.96	70.58	13.93	637.65
1949.00	59.88	73.90	16.59	616.34
1949.50	59.74	73.65	16.37	605.75
1950.00	59.85	73.84	16.54	589.00
1950.50	60.30	74.62	17.24	549.34
1951.00	60.35	74.71	17.32	547.31
1951.50	60.66	75.24	17.81	553.13
1952.00	62.13	77.77	20.36	573.31
1952.50	63.03	79.31	22.09	586.29
1953.00	63.65	80.39	23.38	590.92
1953.50	62.53	78.44	21.10	594.24
1954.00	60.77	75.43	17.99	605.16
1954.50	60.25	74.53	17.16	611.33
1955.00	58.69	71.84	14.88	616.08
1955.50	53.57	63.04	9.35	623.66
1956.00	49.12	55.38	6.23	645.85
1956.50	44.35	47.18	4.04	659.56
1957.00	44.00	46.58	3.91	679.72
1957.50	45.09	48.46	4.32	710.41
1958.00	44.43	47.32	4.07	767.21
1958.50	39.96	39.63	2.71	826.38
1959.00	39.76	39.29	2.66	885.95
1959.50	38.88	37.77	2.46	926.44
1960.00	37.83	35.96	2.23	977.94
1960.50	42.49	43.98	3.41	995.10
1963.50	46.47	50.83	4.90	888.17
1964.00	53.23	62.46	9.06	850.72

Sulimar Queen Field Log Data

Well	Old Gamma Ray Log Scale Range (API units)	Old Log Average (API units)	Old Log Standard Deviation (API units)	Rescaled Gamma Ray Logs Scale Range (API units)	Rescaled Logs Average (API units)	Rescaled Logs Standard Deviation (API units)
1-2	30 - 82	56	19	12 - 80	45	23
1-3	34 - 71	46	23	12 - 81	45	24
1-4	28 - 91	60	19	12 - 80	46	21
1-5	49 - 86	70	17	12 - 81	48	23
1-6	47 - 83	65	18	12 - 81	49	27
1-7	26 - 81	63	14	12 - 80	60	18
1-8	53 - 105	67	29	12 - 81	40	25
1-9	40 - 89	65	19	9 - 81	48	22
1-10	36 - 99	61	18	11 - 81	38	18
1-11	26 - 64	44	14	12 - 81	45	23
1-12	22 - 60	42	12	12 - 81	48	19
1-13	27 - 59	42	13	10 - 82	46	24
1-14	34 - 81	58	19	12 - 80	47	21
1-15	27 - 71	47	19	12 - 81	45	24
2-1	17 - 114	65	34	12 - 81	46	24
2-3	29 - 88	54	21	12 - 80	42	22
2-4	35 - 87	58	20	12 - 80	42	20
2-5	33 - 73	48	19	12 - 80	44	23
2-6	22 - 94	51	27	12 - 81	41	24
3-1	10 - 62	38	17	12 - 80	47	23
3-2	37 - 97	70	19	13 - 81	49	21
3-3	51 - 85	67	10	12 - 81	44	19
3-4	39 - 80	63	16	12 - 80	51	21
3-6	19 - 53	32	14	12 - 80	43	23
4-1	23 - 65	48	16	12 - 80	53	23
4-2	15 - 86	52	27	12 - 81	48	25
5-1	40 - 90	61	24	12 - 80	47	25

Sulimar Queen Field Log Data

Well	Old Gamma Ray Log Scale Range (API units)	Old Log Average (API units)	Old Log Standard Deviation (API units)	Rescaled Gamma Ray Logs Scale Range (API units)	Rescaled Logs Average (API units)	Rescaled Logs Standard Deviation (API units)
5-2	13 - 42	29	11	12 - 81	50	24
5-3	18 - 87	62	24	12 - 80	54	22
8-1	13 - 81	47	21	12 - 81	46	21
9-1	13 - 76	39	19	12 - 82	41	20
10-1	21 - 83	58	23	12 - 80	50	24
11-1	36 - 90	65	19	12 - 80	47	21
13-1	34 - 64	50	14	12 - 80	49	23
14-1	15 - 71	39	18	12 - 80	42	21
15-3	1.6 - 33	20	10	12 - 80	51	23
	New Logs					
1-16				11 - 79	51	24
2-2				15 - 79	55	24
Boomer				9 - 81	47	20
16-1				12 - 84	50	24

APPENDIX C

- Permeability and petrographic data for the Shattuck Member in the Sulimar Queen, South Lucky Lake, and Queen fields

Permeability Distribution in the Shattuck Member in the Sulimar Queen field (Well: 1-16)

Depth (ft)	K (md)	K (md)	K (md)	K (md)	Avg. K (md)
1994.000	0.90	0.10	0.40	0.60	0.50
1994.042	0.02	0.01	0.02	0.70	0.19
1994.125	0.02	0.03	0.02	0.09	0.04
1994.167	0.05	0.09	0.59	0.03	0.19
1994.208	0.01	0.02	0.04	0.28	0.09
1994.250	0.03	0.06	0.04	0.03	0.04
1994.292	0.08	0.07	0.11	0.05	0.08
1994.333	0.17	0.20	0.19	0.08	0.16
1994.375	0.53	0.33	0.26	0.19	0.33
1994.417	0.71	0.54	0.25	0.34	0.46
1994.458	0.17	0.20	0.19	0.41	0.24
1994.500	0.53	0.33	0.26	0.35	0.37
1994.542	0.71	0.54	0.25	0.43	0.48
1994.583	0.11	0.46	0.94	0.48	0.50
1994.625	0.67	0.12	0.12	0.50	0.35
1994.667	0.34	1.87	0.11	0.23	0.64
1994.708	0.28	0.35	1.30	0.99	0.73
1994.750	0.49	0.74	0.40	0.53	0.54
1994.792	1.09	0.90	0.64	0.54	0.79
1994.833	0.80	0.90	0.50	0.79	0.75
1994.875	0.83	1.29	1.85	1.10	1.27
1994.917	0.62	0.98	0.67	1.58	0.96
1994.958	0.46	0.29	0.33	1.10	0.55
1995.000	0.45	1.33	0.66	0.82	0.82
1995.042	0.18	0.75	2.00	2.30	1.31
1995.083	1.48	0.22	0.38	0.86	0.74
1995.125	0.50	0.50	0.71	0.57	0.57
1995.167	0.50	0.50	1.42	0.72	0.79
1995.208	0.50	0.50	1.42	1.65	1.02
1995.250	0.80	0.95	1.50	0.90	1.04
1995.292	0.59	0.50	0.60	0.56	0.56
1995.333	1.26	0.65	0.78	0.89	0.90
1995.375	1.22	1.04	1.18	1.42	1.22
1995.417	1.83	4.83	3.80	3.33	3.45
1995.458	0.83	0.89	0.84	0.99	0.89
1995.500	0.62	0.98	0.67	1.80	1.02
1995.542	1.83	4.83	3.80	3.40	3.47
1995.583	6.30	4.90	3.30	4.40	4.73
1995.625	8.70	5.10	5.10	6.30	6.30
1995.667	13.60	5.10	6.90	13.60	9.80
1995.708	12.30	8.66	9.50	10.50	10.24
1995.750	7.79	3.92	2.50	7.05	5.32
1995.792	2.46	2.80	2.08	3.29	2.66
1995.833	41.20	18.00	27.07	27.25	28.38
1995.875	35.69	25.46	35.82	32.75	32.43
1995.917	55.96	51.24	88.36	63.00	64.64
1995.958	66.28	87.57	89.09	94.00	84.24

Permeability Distribution in the Shattuck Member in the Sulimar Queen field (Well: 1-16)

Depth (ft)	K (md)	K (md)	K (md)	K (md)	Avg. K (md)
1996.000	152.00	118.00	68.00	110.00	112.00
1996.042	157.00	104.00	98.00	105.00	116.00
1996.083	157.00	104.00	98.00	106.00	116.25
1996.125	138.00	124.00	76.00	108.00	111.50
1996.167	221.00	165.00	82.00	134.00	150.50
1996.208	292.00	33.00	2.36	109.00	109.09
1996.250	7.64	9.94	9.89	9.20	9.17
1996.292	112.00	106.00	45.00	88.00	87.75
1996.333	93.00	78.00	52.00	74.00	74.25
1996.375	72.00	165.00	80.00	106.00	105.75
1996.417	78.00	85.30	79.80	73.00	79.03
1996.458	6.30	4.80	4.60	5.56	5.32
1996.500	110.00	135.00	122.00	112.00	119.75
1996.542	74.00	76.80	44.90	53.50	62.30
1996.583	22.40	18.60	17.50	17.00	18.88
1996.625	21.10	18.90	19.60	19.00	19.65
1996.667	21.10	18.90	19.60	19.00	19.65
1996.708	35.69	25.46	35.82	32.75	32.43
1996.750	41.00	23.40	42.00	38.00	36.10
1996.792	5.90	8.70	8.30	7.00	7.48
1996.833	25.00	21.40	21.40	22.00	22.45
1996.875	8.80	8.50	14.60	11.00	10.73
1996.917	8.80	8.50	13.30	11.00	10.40
1996.958	6.70	9.60	5.80	9.00	7.78
1997.000	11.60	11.10	15.80	12.00	12.63
1997.042	25.00	21.40	25.80	25.40	24.40
1997.083	15.00	34.00	37.00	33.00	29.75
1997.125	45.00	74.00	57.00	59.00	58.75
1997.167	70.00	81.00	72.00	74.00	74.25
1997.208	86.00	73.00	86.00	82.00	81.75
1997.250	58.00	65.00	57.00	58.00	59.50
1997.292	72.00	72.00	68.00	72.00	71.00
1997.333	31.00	41.00	47.00	31.00	37.50
1997.375	23.00	8.00	6.00	15.00	13.00
1997.417	5.00	3.00	22.00	10.00	10.00
1997.458	5.00	2.00	4.00	4.00	3.75
1997.500	4.00	17.00	19.00	13.50	13.38
1997.542	22.00	16.00	14.00	20.20	18.05
1997.583	23.50	19.00	28.00	26.40	24.23
1997.625	26.00	45.00	33.50	38.00	35.63
1997.667	11.60	9.80	8.70	10.00	10.03
1997.708	11.60	9.80	8.70	10.00	10.03
1997.750	31.00	41.00	47.00	37.00	39.00
1997.792	26.00	45.00	33.50	39.00	35.88
1997.833	23.00	15.30	14.70	17.00	17.50
1997.875	31.50	45.00	33.50	37.50	36.88
1997.917	15.00	34.00	37.00	33.40	29.85

Permeability Distribution in the Shattuck Member in the Sulimar Queen field (Well: 1-16)

Depth (ft)	K (md)	K (md)	K (md)	K (md)	Avg. K (md)
1997.958	33.40	45.00	35.30	39.20	38.23
1998.000	33.80	45.00	39.50	41.00	39.83
1998.042	110.00	135.00	122.00	110.00	119.25
1998.083	143.00	116.00	137.00	132.00	132.00
1998.125	83.00	90.00	70.00	81.00	81.00
1998.167	45.00	98.00	83.00	75.00	75.25
1998.208	30.00	29.00	54.00	38.00	37.75
1998.250	98.00	121.00	107.00	108.00	108.50
1998.292	99.00	89.00	61.00	81.00	82.50
1998.333	77.40	82.60	80.50	85.00	81.38
1998.375	98.00	87.00	76.00	87.00	87.00
1998.417	76.00	76.00	69.00	76.00	74.25
1998.458	13.00	8.00	17.00	13.00	12.75
1998.500	14.30	14.10	15.10	15.00	14.63
1998.542	14.80	14.80	16.90	16.00	15.63
1998.583	14.30	15.80	13.70	15.00	14.70
1998.625	17.00	19.00	19.00	20.00	18.75
1998.667	9.00	14.00	18.00	11.50	13.13
1998.708	10.00	13.00	10.00	10.00	10.75
1998.750	14.00	4.00	13.00	9.25	10.06
1998.792	10.00	11.00	11.00	11.00	10.75
1998.833	15.00	8.00	9.00	10.00	10.50
1998.875	6.80	8.80	6.40	8.00	7.50
1998.917	7.00	10.00	4.00	7.00	7.00
1998.958	20.00	29.00	14.00	21.00	21.00
1999.000	7.50	7.70	9.13	8.00	8.08
1999.042	18.50	25.60	21.30	21.50	21.73
1999.083	13.00	15.00	43.00	20.25	22.81
1999.125	2.19	2.63	2.62	3.26	2.68
1999.167	1.50	1.76	3.39	2.66	2.33
1999.208	1.94	2.69	4.23	3.73	3.15
1999.250	1.01	0.95	1.47	1.12	1.14
1999.292	0.17	0.67	0.99	0.55	0.60
1999.333	1.86	0.57	1.49	1.32	1.31
1999.375	0.51	0.91	0.92	0.95	0.82
1999.417	9.00	12.00	13.00	11.75	11.44
1999.458	27.00	30.00	32.00	33.00	30.50
1999.500	1.91	9.46	7.89	10.57	7.46
1999.542	8.47	6.59	8.90	8.00	7.99
1999.583	7.10	7.10	5.40	6.00	6.40
1999.625	8.14	2.36	2.01	4.39	4.23
1999.667	0.69	1.05	1.36	2.47	1.39
1999.708	11.85	11.03	11.10	11.44	11.36
1999.750	3.94	3.49	4.92	4.12	4.12
1999.792	44.00	130.00	25.00	66.00	66.25
1999.833	84.00	82.00	68.00	76.00	77.50
1999.875	88.00	87.00	81.00	86.00	85.50

Permeability Distribution in the Shattuck Member in the Sulimar Queen field (Well: 1-16)

Depth (ft)	K (md)	K (md)	K (md)	K (md)	Avg. K (md)
1999.917	120.00	110.00	105.00	110.00	111.25
1999.958	133.00	156.00	145.00	148.00	145.50
2000.000	136.00	125.00	112.00	122.00	123.75
2000.042	140.00	141.00	109.00	127.00	129.25
2000.083	144.00	178.00	88.00	133.00	135.75
2000.125	69.50	68.30	67.00	66.00	67.70
2000.167	132.50	153.00	147.00	148.00	145.13
2000.208	99.00	114.00	110.00	107.00	107.50
2000.250	72.00	87.00	82.00	88.00	82.25
2000.292	73.00	75.00	71.00	75.00	73.50
2000.333	71.00	75.00	67.00	70.00	70.75
2000.375	69.00	71.00	63.00	66.00	67.25
2000.417	133.00	154.00	148.00	150.00	146.25
2000.458	187.00	178.00	169.00	178.00	178.00
2000.500	185.00	85.00	83.00	118.00	117.75
2000.542	137.00	123.00	123.00	125.00	127.00
2000.583	144.00	178.00	88.00	137.00	136.75
2000.625	121.00	70.00	72.00	94.00	89.25
2000.667	148.00	123.00	123.00	131.00	131.25
2000.708	185.00	85.00	83.00	118.00	117.75
2000.750	98.00	125.00	109.00	113.00	111.25
2000.792	101.00	114.00	110.00	109.00	108.50
2000.833	71.50	88.00	80.90	80.00	80.10
2000.875	85.30	84.70	85.00	85.00	85.00
2000.917	71.00	75.00	67.00	70.00	70.75
2000.958	48.00	57.00	52.00	54.00	52.75
2001.000	103.00	89.00	85.00	93.00	92.50
2001.042	88.00	90.00	104.00	95.00	94.25
2001.083	85.30	84.70	85.00	85.00	85.00
2001.125	101.00	70.00	76.00	86.00	83.25
2001.167	71.50	88.00	80.90	80.00	80.10
2001.208	67.00	52.00	48.00	51.00	54.50
2001.250	25.00	15.00	24.00	26.00	22.50
2001.292	48.00	42.00	41.00	45.00	44.00
2001.333	144.00	178.00	92.00	138.00	138.00
2001.375	160.00	85.00	83.00	112.00	110.00
2001.417	121.00	88.00	80.00	96.00	96.25
2001.458	73.00	77.00	78.00	77.00	76.25
2001.500	145.00	159.00	158.00	158.00	155.00
2001.542	84.00	89.00	179.00	115.00	116.75
2001.583	151.00	85.00	83.00	106.00	106.25
2001.625	133.00	121.00	137.00	130.00	130.25
2001.667	73.00	77.00	78.00	76.00	76.00
2001.708	37.00	37.00	31.00	37.00	35.50
2001.750	9.00	10.00	13.00	11.50	10.88
2001.792	25.00	15.00	24.00	26.20	22.55
2001.833	14.00	11.00	7.00	10.20	10.55

Permeability Distribution in the Shattuck Member in the Sulimar Queen field (Well: 1-16)

Depth (ft)	K (md)	K (md)	K (md)	K (md)	Avg. K (md)
2001.875	16.00	12.00	15.00	15.00	14.50
2001.917	37.00	33.00	23.00	31.00	31.00
2001.958	36.00	30.00	27.00	32.00	31.25
2002.000	25.00	15.00	24.00	26.00	22.50
2002.042	27.00	24.00	32.00	28.00	27.75
2002.083	7.52	11.11	8.17	10.14	9.24
2002.125	7.76	8.38	6.35	12.12	8.65
2002.167	3.61	11.00	5.67	6.35	6.66
2002.208	2.55	2.50	5.47	3.94	3.62
2002.250	2.81	2.74	3.17	5.18	3.48
2002.292	6.82	6.70	13.00	9.38	8.98
2002.333	31.00	18.00	28.00	24.25	25.31
2002.375	31.00	19.00	53.00	34.33	34.33
2002.417	21.00	59.00	15.00	29.00	31.00
2002.458	32.50	27.00	53.00	37.70	37.55
2002.500	3.80	10.89	6.00	7.00	6.92
2002.542	27.00	24.00	32.00	29.00	28.00
2002.583	32.00	20.00	52.00	35.00	34.75
2002.625	50.00	34.30	39.70	40.00	41.00
2002.667	43.80	71.30	66.00	60.00	60.28
2002.708	25.00	15.00	24.00	22.00	21.50
2002.750	48.00	41.60	42.00	44.00	43.90
2002.792	59.80	56.10	50.20	55.00	55.28
2002.833	130.00	121.00	137.00	127.00	128.75
2002.875	141.00	136.00	131.00	134.00	135.50
2002.917	101.00	90.00	84.00	92.00	91.75
2002.958	31.00	19.00	53.00	34.00	34.25
2003.000	20.80	14.40	14.00	16.00	16.30
2003.042	48.00	41.60	42.00	42.00	43.40
2003.083	59.80	56.10	50.20	54.00	55.03
2003.125	21.00	27.00	33.00	28.00	27.25
2003.167	13.50	11.00	11.90	13.00	12.35
2003.208	43.80	71.30	66.00	63.00	61.03
2003.250	101.00	90.00	84.00	91.00	91.50
2003.292	59.80	56.10	50.20	55.00	55.28
2003.333	25.00	15.00	24.00	22.00	21.50
2003.375	44.00	70.00	67.00	61.00	60.50
2003.417	47.00	68.00	62.00	58.00	58.75
2003.458	12.00	5.54	11.34	9.60	9.62
2003.500	10.50	14.68	4.92	9.80	9.98
2003.542	9.87	7.44	6.80	8.70	8.20
2003.583	32.00	34.00	31.00	33.00	32.50
2003.625	1.95	4.57	3.86	3.50	3.47
2003.667	0.52	0.84	1.66	1.00	1.01
2003.708	3.90	4.00	4.40	4.20	4.13
2003.750	4.80	6.20	5.60	5.60	5.55
2003.792	3.40	3.60	4.50	4.10	3.90

Permeability Distribution in the Shattuck Member in the Sulimar Queen field (Well: 1-16)

Depth (ft)	K (md)	K (md)	K (md)	K (md)	Avg. K (md)
2003.833	7.50	10.30	10.10	9.60	9.38
2003.875	15.00	8.90	8.50	10.00	10.60
2003.917	9.87	7.44	6.80	8.70	8.20
2003.958	4.80	6.20	5.60	5.60	5.55
2004.000	15.00	8.90	8.50	9.80	10.55
2004.042	11.50	14.30	13.20	13.00	13.00
2004.083	9.40	9.80	13.60	12.50	11.33
2004.125	14.10	14.60	12.50	13.00	13.55
2004.167	6.30	9.70	8.00	8.00	8.00
2004.208	6.60	6.50	7.90	7.00	7.00
2004.250	6.20	6.10	5.70	6.00	6.00
2004.292	1.20	3.30	3.90	3.00	2.85
2004.333	4.10	4.90	5.70	5.00	4.93
2004.375	2.80	2.90	3.30	3.00	3.00
2004.417	1.90	2.40	1.70	2.00	2.00
2004.458	4.50	3.10	3.90	4.00	3.88
2004.500	4.50	4.50	4.50	4.50	4.50
2004.542	3.10	3.60	2.80	3.30	3.20
2004.583	4.40	4.30	4.70	4.50	4.48
2004.625	2.60	5.50	7.10	5.20	5.10
2004.667	5.50	3.10	7.80	6.10	5.63
2004.708	4.60	4.60	4.40	4.50	4.53
2004.750	5.90	5.10	8.30	7.50	6.70
2004.792	6.10	6.90	6.10	6.40	6.38
2004.833	5.20	8.30	5.90	6.80	6.55
2004.875	0.40	0.53	0.53	0.50	0.49
2004.917	0.58	0.41	0.52	0.50	0.50
2004.958	0.32	0.39	0.45	0.40	0.39
2005.000	0.32	0.47	0.60	0.50	0.47
2005.042	0.55	0.56	0.70	0.60	0.60
2005.083	2.80	1.10	1.40	2.10	1.85
2005.125	3.76	5.04	5.10	4.40	4.58
2005.167	7.90	9.11	9.80	9.11	8.98
2005.208	2.68	1.66	1.19	1.84	1.84
2005.250	5.15	8.11	7.20	7.13	6.90
2005.292	4.48	3.33	1.08	2.96	2.96
2005.333	3.10	3.80	4.70	3.90	3.88
2005.375	10.60	8.10	9.10	8.06	8.97
2005.417	0.45	0.41	0.48	0.45	0.45
2005.458	0.32	0.21	0.81	0.45	0.45
2005.500	1.04	1.03	1.05	1.04	1.04
2005.542	1.80	2.30	2.30	2.10	2.13
2005.583	2.90	3.90	2.50	3.50	3.20
2005.625	4.00	5.00	3.10	3.90	4.00
2005.667	3.60	4.20	4.50	4.20	4.13
2005.708	3.50	3.80	3.10	3.60	3.50
2005.750	2.40	2.90	3.40	3.10	2.95

Permeability Distribution in the Shattuck Member in the Sulimar Queen field (Well: 1-16)

Depth (ft)	K (md)	K (md)	K (md)	K (md)	Avg. K (md)
2005.792	3.80	3.10	2.90	3.40	3.30
2005.833	2.20	1.90	3.30	2.60	2.50
2005.875	3.00	4.20	2.60	3.50	3.33
2005.917	5.50	5.10	5.30	5.40	5.33
2005.958	4.40	8.00	4.90	6.30	5.90
2006.000	4.90	6.80	6.90	6.20	6.20
2006.042	4.30	4.10	6.40	5.40	5.05
2006.083	3.30	3.00	2.90	3.10	3.08
2006.125	3.80	4.70	3.90	4.20	4.15
2006.167	2.70	3.80	3.70	3.70	3.48
2006.208	3.60	3.80	3.50	3.60	3.63
2006.250	2.20	2.90	2.90	3.30	2.83
2006.292	2.20	2.90	3.20	2.80	2.78
2006.333	1.90	3.80	2.10	2.90	2.68
2006.375	2.10	2.80	2.10	2.50	2.38
2006.417	1.50	1.60	3.10	2.10	2.08
2006.458	2.60	2.30	2.10	2.40	2.35
2006.500	2.80	3.40	3.20	3.10	3.12
2006.542	3.45	4.60	2.10	3.30	3.36
2006.583	2.20	2.90	2.90	3.40	2.85
2006.625	2.50	1.90	2.20	2.90	2.38
2006.667	1.50	2.60	3.00	2.70	2.45
2006.708	3.00	3.40	2.70	3.10	3.05
2006.750	3.00	3.00	2.80	2.90	2.93
2006.792	1.60	2.10	3.00	2.82	2.38
2006.833	1.00	0.80	2.10	1.16	1.27
2006.875	3.20	4.10	6.50	4.71	4.63
2006.917	0.90	1.80	1.70	1.46	1.47
2006.958	0.50	0.30	0.70	0.47	0.49
2007.000	1.00	1.00	1.30	1.01	1.08
2007.042	2.80	1.50	2.30	2.10	2.18
2007.083	3.15	4.10	2.80	3.15	3.30
2007.125	4.29	3.81	3.90	4.05	4.01
2007.167	0.38	0.20	1.16	0.58	0.58
2007.208	1.50	1.47	1.67	1.67	1.58
2007.250	0.57	0.68	2.92	1.39	1.39
2007.292	0.41	0.89	2.29	1.20	1.20
2007.333	2.10	2.20	1.80	1.90	2.00
2007.375	1.10	1.40	1.40	1.30	1.30
2007.417	2.10	2.30	2.22	2.22	2.21
2007.458	2.36	2.82	2.18	2.45	2.45
2007.500	1.04	1.14	4.44	2.20	2.21
2007.542	0.43	0.43	0.83	0.56	0.56
2007.583	0.60	0.48	0.71	0.60	0.60
2007.625	4.51	0.88	1.06	2.15	2.15
2007.667	1.61	2.61	1.76	2.00	2.00
2007.708	1.76	3.40	2.78	2.50	2.61

Permeability Distribution in the Shattuck Member in the Sulimar Queen field (Well: 1-16)

Depth (ft)	K (md)	K (md)	K (md)	K (md)	Avg. K (md)
2007.750	2.50	2.83	2.11	2.47	2.48
2007.792	0.45	0.50	0.71	0.58	0.56
2007.833	0.34	0.37	0.35	0.35	0.35
2007.875	0.22	0.45	0.80	0.49	0.49
2007.917	0.17	0.21	0.40	0.26	0.26
2007.958	0.20	0.20	0.20	0.20	0.20
2008.000	0.36	0.31	0.37	0.35	0.35
2008.042	0.37	0.42	0.39	0.43	0.40
2008.083	0.35	0.29	0.29	0.31	0.31
2008.125	0.53	0.62	0.59	0.51	0.56
2008.167	0.31	0.28	0.19	0.25	0.26
2008.208	0.37	0.27	0.30	0.30	0.31
2008.250	0.32	0.29	0.34	0.33	0.32
2008.292	0.37	0.34	0.37	0.37	0.36
2008.333	0.35	0.32	0.33	0.33	0.33
2008.375	0.99	0.31	0.28	0.49	0.52
2008.417	0.55	0.39	0.41	0.45	0.45
2008.458	0.26	0.51	0.38	0.38	0.38
2008.500	0.20	0.22	0.29	0.26	0.24
2008.542	0.32	0.27	0.24	0.32	0.29
2008.583	0.35	0.31	0.31	0.33	0.33
2008.625	0.41	0.45	0.39	0.41	0.42
2008.667	0.72	0.20	0.66	0.53	0.53
2008.708	0.29	0.43	0.21	0.31	0.31
2008.750	0.19	0.26	0.39	0.21	0.26
2008.792	0.14	0.18	0.15	0.16	0.16
2008.833	0.11	0.11	0.21	0.14	0.14
2008.875	0.11	0.13	0.12	0.12	0.12
2008.917	0.11	0.13	0.13	0.11	0.12
2008.958	0.11	0.11	0.14	0.12	0.12
2009.000	0.17	0.14	0.14	0.15	0.15
2009.042	0.32	0.28	0.35	0.30	0.31
2009.083	0.32	0.54	0.39	0.43	0.42
2009.125	0.16	0.45	0.48	0.36	0.36
2009.167	0.11	0.18	0.41	0.23	0.23
2009.208	0.14	0.10	0.18	0.14	0.14
2009.250	0.11	0.11	0.13	0.12	0.12
2009.292	0.24	0.21	0.11	0.17	0.18
2009.333	0.64	0.31	1.91	0.95	0.95
2009.375	0.80	0.56	0.42	0.59	0.59
2009.417	0.68	0.85	1.06	0.86	0.86
2009.458	0.26	1.29	1.13	0.89	0.89
2009.500	0.16	0.29	1.08	0.51	0.51
2009.542	0.18	0.15	0.27	0.21	0.20
2009.583	0.07	0.15	0.22	0.15	0.15
2009.625	0.14	0.10	0.26	0.15	0.16
2009.667	0.06	0.12	0.08	0.15	0.10

Permeability Distribution in the Shattuck Member in the Sulimar Queen field (Well: 1-16)

Depth (ft)	K (md)	K (md)	K (md)	K (md)	Avg. K (md)
2009.708	0.06	0.07	0.06	0.09	0.07
2009.750	0.06	0.07	0.06	0.06	0.06
2009.792	0.05	0.06	0.06	0.06	0.06
2009.833	0.04	0.05	0.05	0.05	0.05
2009.875	0.04	0.04	0.04	0.04	0.04
2009.917	0.05	0.06	0.05	0.05	0.05
2009.958	0.04	0.05	0.04	0.04	0.04
2010.000	0.90	1.10	1.80	0.13	0.98
2010.042	0.02	0.08	0.04	0.05	0.05
2010.083	1.10	1.60	1.30	0.13	1.03
2010.125	0.57	0.48	0.61	0.57	0.56
2010.167	0.50	0.45	0.62	0.50	0.52
2010.208	6.94	2.01	4.50	4.47	4.48
2010.250	0.46	0.23	0.77	0.46	0.48
2010.292	6.99	2.85	3.80	4.92	4.64
2010.333	1.10	2.60	2.30	2.30	2.08
2010.375	0.42	7.22	4.10	3.82	3.89
2010.417	1.00	1.20	1.60	1.40	1.30
2010.458	0.22	0.58	0.45	0.40	0.41
2010.500	0.20	0.60	0.40	0.40	0.40
2010.542	0.09	1.60	0.20	0.21	0.53
2010.583	0.25	0.33	0.30	0.30	0.30
2010.625	0.03	0.14	0.09	0.08	0.09
2010.667	0.08	0.01	0.01	0.08	0.05
2010.708	0.11	0.06	0.07	0.08	0.08
2010.750	0.04	0.20	0.08	0.08	0.10
2010.792	0.04	0.15	0.09	0.09	0.09
2010.833	0.03	0.08	0.04	0.06	0.05
2010.875	0.02	0.05	0.05	0.03	0.04
2010.917	0.15	0.13	0.10	0.11	0.12
2010.958	0.09	0.11	0.15	0.15	0.13
2011.000	0.07	0.09	0.20	0.09	0.11
2011.042	0.12	0.09	0.20	0.09	0.13
2011.083	0.28	0.10	0.16	0.19	0.18
2011.125	1.10	0.80	0.60	0.90	0.85
2011.167	0.56	1.50	1.10	1.03	1.05
2011.208	1.20	0.80	1.00	1.10	1.03
2011.250	0.15	1.31	0.90	0.73	0.77
2011.292	0.30	0.50	0.40	0.40	0.40
2011.333	0.09	0.13	0.10	0.11	0.11
2011.375	0.10	0.50	0.30	0.35	0.31
2011.417	0.04	0.81	0.41	0.42	0.42
2011.458	0.15	0.90	0.11	0.13	0.32
2011.500	0.04	0.01	0.03	0.03	0.03
2011.542	0.01	0.01	0.01	0.01	0.01
2011.583	0.02	0.01	0.02	0.02	0.02
2011.625	0.03	0.07	0.05	0.06	0.05

Permeability Distribution in the Shattuck Member in the Sulimar Queen field (Well: 1-16)

Depth (ft)	K (md)	K (md)	K (md)	K (md)	Avg. K (md)
2011.667	0.16	0.02	0.09	0.09	0.09
2011.708	0.10	1.50	0.20	0.12	0.48
2011.750	0.22	0.17	0.18	0.19	0.19
2011.792	0.10	0.09	0.14	0.13	0.12
2011.833	0.11	0.10	0.10	0.10	0.10
2011.875	0.08	0.09	0.13	0.10	0.10
2011.917	0.18	0.05	0.11	0.11	0.11
2011.958	0.15	0.20	0.34	0.25	0.24
2012.000	0.41	0.21	0.30	0.31	0.31
2012.042	0.04	0.09	0.09	0.08	0.08
2012.083	0.07	0.01	0.04	0.04	0.04
2012.125	0.02	0.04	0.01	0.03	0.03
2012.167	0.01	0.04	0.01	0.02	0.02
2012.208	0.05	0.01	0.01	0.03	0.03
2012.250	0.03	0.04	0.03	0.04	0.03
2012.292	0.09	0.10	0.09	0.09	0.09
2012.333	0.29	0.09	0.20	0.19	0.19
2012.375	0.08	0.12	0.08	0.09	0.09
2012.417	0.04	0.03	0.03	0.04	0.03
2012.458	0.12	0.10	0.10	0.11	0.11
2012.500	0.29	0.04	0.16	0.16	0.16
2012.542	0.18	0.26	0.25	0.23	0.23
2012.583	0.18	0.50	0.35	0.34	0.34
2012.625	0.40	0.25	0.32	0.30	0.32
2012.667	0.09	0.46	0.28	0.28	0.28
2012.708	0.25	0.41	0.30	0.31	0.32
2012.750	0.52	0.38	0.36	0.43	0.42
2012.792	0.35	0.40	0.27	0.33	0.34
2012.833	0.51	0.54	0.52	0.52	0.52
2012.875	0.19	0.28	0.40	0.35	0.31
2012.917	0.28	0.25	0.27	0.27	0.27
2012.958	0.51	0.28	0.35	0.41	0.39
2013.000	0.50	0.40	0.40	0.45	0.44
2013.042	0.97	0.87	1.50	1.03	1.09
2013.083	0.47	3.55	0.81	1.61	1.61
2013.125	0.46	1.47	1.33	1.10	1.09
2013.167	0.47	0.36	0.62	0.48	0.48
2013.208	0.74	0.33	0.58	0.55	0.55
2013.250	0.58	0.45	0.45	0.50	0.50
2013.292	1.52	1.00	0.94	1.15	1.15
2013.333	0.70	0.42	0.60	0.57	0.57
2013.375	0.29	0.25	0.17	0.24	0.24
2013.417	1.10	1.50	1.10	1.30	1.25
2013.458	3.60	2.10	2.40	2.80	2.73
2013.500	4.00	6.35	5.00	5.20	5.14
2013.542	1.27	2.05	1.60	1.66	1.65
2013.583	1.10	1.60	1.40	1.50	1.40

Permeability Distribution in the Shattuck Member in the Sulimar Queen field (Well: 1-16)

Depth (ft)	K (md)	K (md)	K (md)	K (md)	Avg. K (md)
2013.625	1.30	2.10	1.90	1.80	1.78
2013.667	1.10	5.24	3.20	3.17	3.18
2013.708	1.80	1.90	2.00	1.90	1.90
2013.750	1.53	0.41	0.90	0.97	0.95
2013.792	0.98	0.78	1.60	1.13	1.12
2013.833	0.36	1.85	1.10	1.10	1.10
2013.875	1.30	1.00	1.00	1.20	1.13
2013.917	0.97	1.03	1.00	1.00	1.00
2013.958	0.87	1.00	0.85	0.92	0.91
2014.000	0.71	0.95	0.80	0.83	0.82
2014.042	0.68	0.94	0.78	0.84	0.81
2014.083	0.87	0.74	0.80	0.82	0.81
2014.125	1.10	0.75	0.71	0.93	0.87
2014.167	0.12	2.35	1.20	1.23	1.23
2014.208	0.55	0.69	0.71	0.65	0.65
2014.250	0.10	0.16	0.60	0.58	0.36
2014.292	0.33	0.21	0.24	0.28	0.27
2014.333	0.23	0.15	0.20	0.19	0.19
2014.375	0.21	0.21	0.21	0.21	0.21
2014.417	0.28	0.28	0.28	0.28	0.28
2014.458	0.52	0.51	0.38	0.41	0.46
2014.500	0.33	0.68	0.50	0.51	0.51
2014.542	0.41	0.42	0.58	0.49	0.48
2014.583	0.92	0.26	0.60	0.59	0.59
2014.625	0.23	0.54	0.50	0.43	0.43
2014.667	0.27	0.46	0.40	0.36	0.37
2014.708	0.33	0.39	0.39	0.37	0.37
2014.750	0.36	0.38	0.38	0.37	0.37
2014.792	0.38	0.39	0.41	0.40	0.40
2014.833	0.65	0.29	0.50	0.47	0.48
2014.875	0.42	0.60	0.52	0.50	0.51
2014.917	0.50	0.55	0.50	0.52	0.52
2014.958	0.08	0.06	0.09	0.08	0.08
2015.000	0.06	0.09	0.09	0.08	0.08
2015.042	0.09	0.07	0.09	0.09	0.09

Permeability Distribution in the Sahttuck Member in the South Lucky Lake field

Depth (ft)	K (md)	Depth (ft)	K (md)	Depth (ft)	K (md)
1786.00	1.75	1788.08	185.00	1790.17	41.00
1786.04	0.90	1788.13	200.00	1790.21	27.00
1786.08	1.60	1788.17	204.00	1790.25	13.70
1786.13	2.29	1788.21	101.00	1790.29	13.70
1786.17	1.80	1788.25	141.00	1790.33	14.30
1786.21	2.11	1788.29	150.00	1790.38	18.60
1786.25	3.60	1788.33	177.00	1790.42	17.50
1786.29	3.80	1788.38	77.00	1790.46	16.50
1786.33	3.90	1788.42	108.00	1790.50	3.90
1786.38	6.30	1788.46	104.00	1790.54	3.80
1786.42	3.90	1788.50	92.00	1790.58	4.90
1786.46	4.50	1788.54	90.00	1790.63	12.30
1786.50	4.20	1788.58	93.00	1790.67	16.00
1786.54	3.50	1788.63	201.00	1790.71	19.00
1786.58	3.40	1788.67	250.00	1790.75	24.00
1786.63	2.90	1788.71	195.00	1790.79	9.50
1786.67	2.40	1788.75	180.00	1790.83	11.30
1786.71	1.80	1788.79	299.00	1790.88	10.50
1786.75	2.80	1788.83	294.00	1790.92	12.10
1786.79	3.54	1788.88	153.00	1790.96	14.00
1786.83	8.30	1788.92	153.00	1791.00	11.00
1786.88	3.80	1788.96	204.00	1791.04	4.90
1786.92	2.20	1789.00	294.00	1791.08	5.90
1786.96	2.96	1789.04	323.00	1791.13	3.40
1787.00	3.50	1789.08	370.00	1791.17	4.30
1787.04	4.40	1789.13	334.00	1791.21	63.00
1787.08	3.60	1789.17	232.00	1791.25	149.00
1787.13	2.50	1789.21	301.00	1791.29	158.00
1787.17	2.80	1789.25	385.00	1791.33	178.00
1787.21	4.30	1789.29	132.00	1791.38	160.00
1787.25	3.50	1789.33	175.00	1791.42	108.00
1787.29	3.90	1789.38	115.00	1791.46	135.00
1787.33	4.40	1789.42	212.00	1791.50	226.00
1787.38	4.40	1789.46	178.00	1791.54	75.50
1787.42	4.30	1789.50	175.00	1791.58	59.80
1787.46	4.10	1789.54	108.00	1791.63	66.00
1787.50	4.40	1789.58	203.00	1791.67	45.70
1787.54	3.60	1789.63	208.00	1791.71	25.50
1787.58	6.76	1789.67	170.00	1791.75	12.30
1787.63	4.60	1789.71	162.00	1791.79	18.00
1787.67	3.60	1789.75	79.00	1791.83	17.70
1787.71	5.50	1789.79	97.00	1791.88	45.00
1787.75	76.00	1789.83	89.00	1791.92	53.00
1787.79	95.00	1789.88	90.00	1791.96	30.20
1787.83	114.00	1789.92	38.00	1792.00	32.50
1787.88	232.00	1789.96	68.00	1792.04	25.50
1787.92	227.00	1790.00	56.00	1792.08	18.80
1787.96	108.00	1790.04	60.00	1792.13	16.20
1788.00	185.00	1790.08	54.00	1792.17	23.80
1788.04	156.00	1790.13	35.00	1792.21	27.70

Permeability Distribution in the Sahttuck Member in the South Lucky Lake field

Depth (ft)	K (md)	Depth (ft)	K (md)	Depth (ft)	K (md)
1792.25	38.00	1794.33	150.00	1796.42	1.30
1792.29	35.20	1794.38	199.00	1796.46	1.40
1792.33	27.80	1794.42	100.00	1796.50	1.28
1792.38	30.50	1794.46	124.00	1796.54	1.50
1792.42	31.10	1794.50	86.00	1796.58	1.69
1792.46	33.00	1794.54	115.00	1796.63	2.80
1792.50	47.00	1794.58	61.00	1796.67	3.10
1792.54	52.70	1794.63	99.00	1796.71	2.60
1792.58	147.00	1794.67	102.00	1796.75	2.98
1792.63	25.00	1794.71	129.00	1796.79	3.20
1792.67	23.00	1794.75	178.00	1796.83	3.85
1792.71	22.00	1794.79	192.00	1796.88	0.91
1792.75	26.00	1794.83	134.00	1796.92	0.25
1792.79	21.00	1794.88	125.00	1796.96	1.20
1792.83	24.00	1794.92	140.00	1797.00	1.80
1792.88	28.00	1794.96	150.00	1797.04	1.70
1792.92	15.00	1795.00	170.00	1797.08	1.60
1792.96	14.00	1795.04	169.00	1797.13	1.10
1793.00	8.40	1795.08	185.00	1797.17	0.45
1793.04	24.00	1795.13	204.00	1797.21	0.90
1793.08	19.00	1795.17	144.00	1797.25	0.33
1793.13	9.50	1795.21	244.00	1797.29	0.85
1793.17	8.30	1795.25	256.00	1797.33	0.21
1793.21	7.40	1795.29	286.00	1797.38	0.23
1793.25	29.00	1795.33	289.00	1797.42	0.10
1793.29	12.80	1795.38	285.00	1797.46	0.16
1793.33	5.90	1795.42	150.00	1797.50	0.14
1793.38	95.00	1795.46	166.00	1797.54	0.47
1793.42	113.00	1795.50	171.00	1797.58	0.26
1793.46	142.00	1795.54	195.00	1797.63	0.14
1793.50	201.00	1795.58	205.00	1797.67	0.45
1793.54	247.00	1795.63	161.00	1797.71	0.72
1793.58	84.00	1795.67	134.00	1797.75	0.62
1793.63	88.00	1795.71	175.00	1797.79	0.89
1793.67	48.00	1795.75	145.00	1797.83	0.53
1793.71	84.00	1795.79	102.00	1797.88	0.71
1793.75	85.00	1795.83	115.00	1797.92	0.51
1793.79	78.00	1795.88	95.00	1797.96	0.68
1793.83	46.00	1795.92	68.00	1798.00	0.63
1793.88	56.00	1795.96	29.00	1798.04	0.71
1793.92	78.00	1796.00	23.00	1798.08	2.80
1793.96	91.00	1796.04	5.80	1798.13	1.20
1794.00	117.00	1796.08	2.80	1798.17	0.22
1794.04	97.00	1796.13	2.40	1798.21	0.16
1794.08	45.00	1796.17	2.50	1798.25	0.17
1794.13	103.00	1796.21	2.40	1798.29	0.15
1794.17	106.00	1796.25	2.63	1798.33	0.23
1794.21	65.00	1796.29	2.30	1798.38	0.31
1794.25	64.00	1796.33	2.40	1798.42	0.65
1794.29	73.00	1796.38	1.80	1798.46	0.15

Permeability Distribution in the Sahttuck Member in the South Lucky Lake field

Depth (ft)	K (md)	Depth (ft)	K (md)
1798.50	0.18	1800.58	0.27
1798.54	0.14	1800.63	0.35
1798.58	0.13	1800.67	0.29
1798.63	0.08	1800.71	0.33
1798.67	0.30	1800.75	0.42
1798.71	0.17	1800.79	0.58
1798.75	0.90	1800.83	0.47
1798.79	0.50	1800.88	0.32
1798.83	0.60	1800.92	0.20
1798.88	0.38	1800.96	0.25
1798.92	2.10	1801.00	0.24
1798.96	3.60	1801.04	0.21
1799.00	5.50	1801.08	0.19
1799.04	4.10	1801.13	0.18
1799.08	3.50	1801.17	0.25
1799.13	2.70	1801.21	0.25
1799.17	0.70	1801.25	0.22
1799.21	0.80	1801.29	0.23
1799.25	0.50	1801.33	0.22
1799.29	0.81	1801.38	0.25
1799.33	0.72	1801.42	0.28
1799.38	0.54	1801.46	0.35
1799.42	0.51	1801.50	0.70
1799.46	0.62	1801.54	0.50
1799.50	0.29	1801.58	0.28
1799.54	0.25	1801.63	0.26
1799.58	0.38	1801.67	0.24
1799.63	0.27	1801.71	0.23
1799.67	0.23	1801.75	0.26
1799.71	0.21	1801.79	0.25
1799.75	0.36	1801.83	0.23
1799.79	0.52	1801.88	0.23
1799.83	0.36	1801.92	0.95
1799.88	0.40	1801.96	0.81
1799.92	0.43	1802.00	0.60
1799.96	0.39	1802.04	0.33
1800.00	0.37	1802.08	0.34
1800.04	0.35	1802.13	0.35
1800.08	0.31	1802.17	0.29
1800.13	0.29	1802.21	0.24
1800.17	0.25	1802.25	0.23
1800.21	0.25	1802.29	0.21
1800.25	0.24	1802.33	0.19
1800.29	0.26	1802.38	0.13
1800.33	0.26	1802.42	0.22
1800.38	0.24	1802.46	0.26
1800.42	0.25		
1800.46	0.28		
1800.50	0.29		
1800.54	0.25		

Permeability Distribution in the Shattuck Member in the Queen field

Depth (ft)	K (md)
2975.000	3.270
2975.042	1.400
2975.083	0.530
2975.125	2.420
2975.167	1.020
2975.208	5.100
2975.250	6.280
2975.292	4.500
2975.333	1.910
2975.375	1.960
2975.417	1.880
2975.458	3.300
2975.500	4.700
2975.542	4.010
2975.583	2.470
2975.625	6.930
2975.667	2.400
2975.708	5.800
2975.750	3.100
2975.792	6.400
2975.833	5.800
2975.875	1.210
2975.917	4.900
2975.958	1.200
2976.000	2.500
2976.042	2.720
2976.083	3.200
2976.125	6.800
2976.167	2.600
2976.208	3.150
2976.250	0.330
2976.292	0.180
2976.333	0.400
2976.375	0.320
2976.417	0.160
2976.458	0.300
2976.500	1.110
2976.542	0.600
2976.583	2.900
2976.625	0.360
2976.667	0.270
2976.708	2.300
2976.750	5.130
2976.792	6.200
2976.833	11.600
2976.875	4.800
2976.917	2.000
2976.958	6.590
2977.000	7.200
2979.083	149.000

Depth (ft)	K (md)
2977.042	24.300
2977.083	21.900
2977.125	23.800
2977.167	31.220
2977.208	19.500
2977.250	26.400
2977.292	22.100
2977.333	33.700
2977.375	32.600
2977.417	31.800
2977.458	21.100
2977.500	31.000
2977.542	40.500
2977.583	47.300
2977.625	62.800
2977.667	2.330
2977.708	2.050
2977.750	7.760
2977.792	8.300
2977.833	13.000
2977.875	76.500
2977.917	50.700
2977.958	63.800
2978.000	72.900
2978.042	70.500
2978.083	64.000
2978.125	31.700
2978.167	40.400
2978.208	7.200
2978.250	31.100
2978.292	43.800
2978.333	71.700
2978.375	57.500
2978.417	77.600
2978.458	49.000
2978.500	43.200
2978.542	46.400
2978.583	60.900
2978.625	71.630
2978.667	108.000
2978.708	201.000
2978.750	270.000
2978.792	432.000
2978.833	300.000
2978.875	308.000
2978.917	126.000
2978.958	135.000
2979.000	147.000
2979.042	136.000
2979.125	8.300

Depth (ft)	K (md)
2979.167	18.500
2979.208	13.500
2979.250	7.600
2979.292	4.340
2979.333	2.960
2979.375	4.800
2979.417	16.400
2979.458	25.700
2979.500	25.000
2979.542	23.030
2979.583	22.300
2979.625	23.000
2979.667	27.000
2979.708	29.000
2979.750	7.500
2979.792	6.500
2979.833	0.730
2979.875	4.200
2979.917	3.170
2979.958	10.700
2980.000	31.000
2980.042	39.000
2980.083	31.000
2980.125	22.680
2980.167	31.200
2980.208	44.500
2980.250	28.600
2980.292	6.250
2980.333	10.300
2980.375	9.600
2980.417	8.500
2980.458	13.900
2980.500	9.800
2980.542	41.600
2980.583	35.500
2980.625	23.800
2980.667	24.400
2980.708	18.900
2980.750	17.600
2980.792	35.500
2980.833	16.300
2980.875	12.900
2980.917	21.700
2980.958	9.800
2981.000	8.500
2981.042	15.900
2981.083	16.600
2981.125	9.800
2981.167	15.300
2981.208	11.200

Permeability Distribution in the Shattuck Member in the Queen field

Depth (ft)	K (md)	Depth (ft)	K (md)	Depth (ft)	K (md)
2981.250	11.100	2983.333	19.500	2985.417	3.200
2981.292	16.600	2983.375	30.400	2985.458	1.300
2981.333	15.300	2983.417	37.800	2985.500	3.230
2981.375	14.600	2983.458	45.000	2985.542	3.300
2981.417	14.900	2983.500	47.000	2985.583	3.900
2981.458	10.000	2983.542	58.000	2985.625	5.100
2981.500	10.500	2983.583	44.000	2985.667	1.300
2981.542	25.700	2983.625	52.300	2985.708	2.900
2981.583	24.600	2983.667	59.000	2985.750	3.600
2981.625	32.200	2983.708	11.500	2985.792	4.500
2981.667	52.400	2983.750	3.700	2985.833	6.800
2981.708	70.200	2983.792	12.770	2985.875	10.600
2981.750	8.940	2983.833	19.900	2985.917	9.300
2981.792	72.000	2983.875	7.700	2985.958	16.900
2981.833	67.300	2983.917	7.700	2986.000	14.800
2981.875	33.900	2983.958	1.400	2986.042	28.400
2981.917	32.700	2984.000	1.300	2986.083	21.600
2981.958	22.800	2984.042	1.300	2986.125	29.700
2982.000	17.500	2984.083	0.840	2986.167	36.900
2982.042	18.200	2984.125	1.800	2986.208	22.000
2982.083	11.100	2984.167	1.300	2986.250	19.000
2982.125	9.300	2984.208	1.030	2986.292	15.400
2982.167	9.900	2984.250	0.500	2986.333	10.300
2982.208	10.300	2984.292	0.740	2986.375	11.200
2982.250	8.500	2984.333	2.700	2986.417	4.700
2982.292	8.500	2984.375	2.000	2986.458	4.900
2982.333	8.100	2984.417	0.400	2986.500	5.800
2982.375	15.600	2984.458	0.400	2986.542	6.900
2982.417	11.100	2984.500	0.370	2986.583	2.320
2982.458	11.040	2984.542	0.500	2986.625	4.320
2982.500	8.500	2984.583	0.550	2986.667	5.440
2982.542	9.800	2984.625	1.600	2986.708	2.800
2982.583	3.900	2984.667	1.380	2986.750	3.400
2982.625	7.400	2984.708	3.490	2986.792	2.100
2982.667	9.300	2984.750	2.610	2986.833	6.000
2982.708	11.600	2984.792	3.980	2986.875	7.200
2982.750	7.500	2984.833	1.030	2986.917	11.030
2982.792	11.600	2984.875	0.930	2986.958	7.350
2982.833	15.900	2984.917	0.690	2987.000	9.000
2982.875	31.700	2984.958	3.920	2987.042	8.300
2982.917	25.500	2985.000	5.710	2987.083	11.500
2982.958	29.600	2985.042	4.440	2987.125	14.500
2983.000	41.700	2985.083	1.900	2987.167	19.900
2983.042	41.300	2985.125	2.800	2987.208	13.300
2983.083	106.000	2985.167	3.690	2987.250	11.700
2983.125	108.000	2985.208	3.520	2987.292	13.200
2983.167	62.000	2985.250	4.990	2987.333	14.300
2983.208	85.000	2985.292	2.800	2987.375	17.700
2983.250	51.000	2985.333	2.600	2987.417	19.700
2983.292	33.000	2985.375	6.100	2987.458	21.300

Permeability Distribution in the Shattuck Member in the Queen field

Depth (ft)	K (md)
2987.500	14.200
2987.542	4.890
2987.583	23.810
2987.625	8.900
2987.667	19.900
2987.708	31.700
2987.750	31.300
2987.792	8.700
2987.833	7.200
2987.875	6.900
2987.917	7.300
2987.958	8.730
2988.000	6.550
2988.042	4.300
2988.083	6.800
2988.125	4.300
2988.167	5.600
2988.208	4.400
2988.250	5.600
2988.292	1.300
2988.333	1.600
2988.375	0.920
2988.417	2.600
2988.458	0.950
2988.500	0.700
2988.542	0.500
2988.583	0.700
2988.625	0.500
2988.667	0.530
2988.708	0.600
2988.750	0.150
2988.792	0.160
2988.833	0.920
2988.875	3.040
2988.917	0.760
2988.958	1.100
2989.000	1.320
2989.042	1.440
2989.083	1.100
2989.125	0.440
2989.167	0.550
2989.208	0.450
2989.250	0.300
2989.292	0.500
2989.333	2.100
2989.375	2.200
2989.417	2.900
2989.458	2.050
2989.500	2.000
2989.542	1.800
2989.583	5.300
2989.625	0.750
2989.667	2.200
2989.708	1.530
2989.750	1.980
2989.792	2.400
2989.833	2.300
2989.875	2.500
2989.917	2.000
2989.958	4.000
2990.000	1.300
2990.042	2.200
2990.083	2.400
2990.125	1.800
2990.167	1.200
2990.208	3.100
2990.250	2.700
2990.292	0.530
2990.333	1.600
2990.375	1.700
2990.417	2.300
2990.458	1.700
2990.500	1.900
2990.542	1.040
2990.583	1.400
2990.625	0.540
2990.667	0.500
2990.708	0.330
2990.750	0.930
2990.792	0.850
2990.833	0.820
2990.875	0.500
2990.917	1.000
2990.958	1.300
2991.000	0.800
2991.042	3.250
2991.083	1.800
2991.125	2.700
2991.167	1.700
2991.208	6.000
2991.250	7.960
2991.292	6.600
2991.333	7.500
2991.375	1.600
2991.417	2.500
2991.458	1.100
2991.500	0.530
2991.542	0.460
2991.583	0.500
2991.625	0.520
2991.667	0.600
2991.708	0.650
2991.750	1.000
2991.792	0.860
2991.833	0.750
2991.875	0.850
2991.917	1.000
2991.958	0.900
2992.000	0.830
2992.042	1.700
2992.083	2.300
2992.125	2.800
2992.167	2.300
2992.208	0.910
2992.250	1.350
2992.292	1.400
2992.333	1.740
2992.375	1.400
2992.417	1.560
2992.458	1.940
2992.500	1.800
2992.542	1.550
2992.583	1.310
2992.625	1.200
2992.667	1.160
2992.708	1.300
2992.750	1.410
2992.792	1.430
2992.833	1.560
2992.875	1.960
2992.917	1.990
2992.958	0.580
2993.000	0.960
2993.042	0.620
2993.083	0.320
2993.125	0.320
2993.167	0.700
2993.208	1.250
2993.250	1.100
2993.292	0.870
2993.333	0.850
2993.375	0.740
2993.417	0.510
2993.458	0.540
2993.500	0.780
2993.542	0.830
2993.583	0.810
2993.625	0.610
2993.667	0.740
2993.708	1.100

Permeability Distribution in the Shattuck Member in the Queen field

Depth (ft)	K (md)
2993.750	1.000
2993.792	0.880
2993.833	0.640
2993.875	0.470
2993.917	0.980
2993.958	2.900
2994.000	0.190
2994.042	0.390
2994.083	0.410
2994.125	0.410
2994.167	0.340
2994.208	0.340
2994.250	0.400
2994.292	0.500
2994.333	0.620
2994.375	0.104
2994.417	2.610
2994.458	6.090
2994.500	3.800
2994.542	2.500
2994.583	2.800
2994.625	2.550
2994.667	1.900
2994.708	2.140
2994.750	1.650
2994.792	2.200
2994.833	3.100
2994.875	3.500
2994.917	3.200
2994.958	5.000
2995.000	4.600
2995.042	2.800
2995.083	2.230
2995.125	1.370
2995.167	0.940
2995.208	1.860
2995.250	2.400
2995.292	1.970
2995.333	1.220
2995.375	3.300
2995.417	2.600
2995.458	2.000
2995.500	2.500
2995.542	3.230
2995.583	3.600
2995.625	3.310
2995.667	2.750
2995.708	2.750
2995.750	2.900
2995.792	3.010

Petrographic Data for the Shattuck Member

K (md)	Total Porosity	Primary Porosity	Total Secondary Porosity	Secondary Intergran. Porosity	Intracons-tituent Porosity	Micro-Porosity	Quartz	Feldspar	Rock Frag.	Anhydrite Gypsum	Dolomite	Hema-tite	Clay Detrital	Pore Size	Grain Size	Grain Sorting	Pore Sorting/ Connection
	(%)	(%)	(%)	(%)	(%)	(%)	(%)	(%)	(%)	(%)	(%)	(%)	(%)	(microns)	(microns)		
0.04	2.00	2.00	0.00	0.00	0.00	0.00	36.00	4.00	1.00	2.00	55.00	0.00	0.00	10.00	30.00	poor	P/P
0.04	3.00	3.00	0.00	0.00	0.00	0.00	35.00	3.00	1.00	5.00	53.00	0.00	0.00	10.00	30.00	poor	P/P
0.07	2.00	2.00	0.00	0.00	0.00	0.00	35.00	4.00	1.00	3.00	55.00	0.00	0.00	10.00	30.00	poor	P/P
0.09	1.50	1.50	0.00	0.00	0.00	0.00	35.00	4.50	1.00	3.00	55.00	0.00	0.00	10.00	30.00	poor	P/P
0.09	1.50	1.50	0.00	0.00	0.00	0.00	38.00	2.50	1.00	2.00	55.00	0.00	0.00	10.00	30.00	poor	P/P
0.09	2.00	2.00	0.00	0.00	0.00	0.00	34.00	5.00	1.00	4.00	54.00	0.00	0.00	10.00	30.00	poor	P/P
0.08	2.50	2.50	0.00	0.00	0.00	0.00	38.00	3.50	1.00	1.00	54.00	0.00	0.00	10.00	30.00	poor	P/P
0.08	1.50	1.50	0.00	0.00	0.00	0.00	38.00	3.50	1.00	1.00	55.00	0.00	0.00	10.00	30.00	poor	P/P
0.07	2.00	2.00	0.00	0.00	0.00	0.00	37.00	4.00	1.00	2.00	54.00	0.00	0.00	10.00	30.00	poor	P/P
0.07	2.00	2.00	0.00	0.00	0.00	0.00	38.00	4.00	1.00	1.00	54.00	0.00	0.00	10.00	30.00	poor	P/P
0.23	4.00	0.00	4.00	0.00	0.00	4.00	49.00	2.00	0.00	1.00	40.00	2.00	2.00	10.00	40.00	poor	P/P
0.24	3.00	0.00	3.00	0.00	0.00	3.00	47.00	3.00	0.00	2.00	41.00	2.00	2.00	10.00	40.00	poor	P/P
0.22	4.00	0.00	4.00	0.00	0.00	4.00	48.00	2.00	0.00	1.00	41.00	2.00	2.00	10.00	40.00	poor	P/P
0.22	5.00	0.00	5.00	0.00	0.00	5.00	47.00	2.00	0.00	1.00	41.00	2.00	2.00	10.00	40.00	poor	P/P
0.32	3.00	0.00	3.00	0.00	0.00	3.00	45.00	5.00	0.00	1.00	42.00	2.00	2.00	10.00	40.00	poor	P/P
0.31	3.00	0.00	3.00	0.00	0.00	3.00	46.00	4.00	0.00	2.00	42.00	2.00	1.00	10.00	40.00	poor	P/P
0.41	4.00	0.00	4.00	0.00	0.00	4.00	49.00	2.00	0.00	2.00	40.00	2.00	1.00	10.00	40.00	poor	P/P
0.41	4.00	0.00	4.00	0.00	0.00	4.00	47.00	2.00	0.00	2.00	40.00	2.00	3.00	10.00	40.00	poor	P/P
0.42	4.00	0.00	4.00	0.00	0.00	4.00	48.00	2.00	0.00	1.00	41.00	2.00	2.00	10.00	40.00	poor	P/P
0.43	5.00	0.00	5.00	0.00	0.00	5.00	46.00	2.00	0.00	1.00	42.00	2.00	2.00	10.00	40.00	poor	P/P
0.38	3.00	0.00	3.00	0.00	0.00	3.00	46.00	3.00	0.00	1.00	43.00	2.00	2.00	10.00	40.00	poor	P/P
0.38	4.00	0.00	4.00	0.00	0.00	4.00	46.00	2.00	0.00	1.00	43.00	2.00	2.00	10.00	40.00	poor	P/P
0.95	3.00	0.00	1.00	1.00	0.00	2.00	58.00	12.00	2.00	3.00	14.00	1.00	7.00	10.00	100.00	poor	P/P
0.91	3.00	0.00	1.00	1.00	0.00	2.00	57.00	10.00	3.00	3.00	16.00	1.00	7.00	10.00	100.00	poor	P/P
0.31	4.00	0.00	1.00	1.00	0.00	2.00	59.00	10.00	2.00	3.00	15.00	0.50	6.50	10.00	100.00	poor	P/P
0.34	2.00	0.00	1.00	1.00	0.00	2.00	58.00	11.00	2.00	3.00	15.00	1.00	8.00	10.00	100.00	poor	P/P
26.00	10.00	1.00	9.00	6.00	1.50	1.50	57.00	13.00	1.00	5.00	8.00	1.00	5.00	35.00	110.00	Mod.	M/M
9.30	8.00	1.50	7.00	4.00	0.00	3.00	56.00	12.00	3.00	6.00	9.00	1.00	5.00	35.00	110.00	Mod.	M/M
25.00	9.00	1.50	8.00	5.00	1.20	1.80	57.00	13.00	3.00	5.00	7.00	1.00	5.00	35.00	110.00	Mod.	M/M
18.00	10.00	1.00	9.00	5.00	1.50	1.50	58.00	12.00	2.00	5.00	7.00	1.00	5.00	35.00	110.00	Mod.	M/M
89.80	16.00	0.00	16.00	12.00	1.00	0.00	60.00	15.00	1.00	3.50	3.50	1.00	0.00	40.00	100.00	well	W/G
82.30	19.50	0.00	19.50	16.00	2.00	0.00	58.00	13.70	1.00	3.80	2.00	1.00	1.00	40.00	100.00	well	W/G
56.00	16.00	0.00	16.00	14.00	1.00	0.00	60.00	14.00	1.00	7.00	0.00	2.00	0.00	40.00	100.00	well	W/G
81.00	19.00	0.00	19.00	16.00	2.00	0.00	58.00	15.10	1.00	2.90	2.00	1.00	1.00	40.00	100.00	well	W/G
68.00	17.00	0.00	17.00	14.00	2.50	0.00	59.00	14.00	1.00	5.00	2.00	1.00	1.00	40.00	100.00	well	W/G

Petrographic Data for the Shattuck Member

K (md)	Total Porosity	Primary Porosity	Total Secondary Porosity	Secondary Intergran. Porosity	Intracons-tituent Porosity	Micro-Porosity	Quartz	Feldspar	Rock Frag.	Anhydrite Gypsum	Dolomite	Hema-tite	Clay Detrital	Pore Size	Grain Size	Grain Sorting	Pore Sorting/ Connection
	(%)	(%)	(%)	(%)	(%)	(%)	(%)	(%)	(%)	(%)	(%)	(%)	(%)	(microns)	(microns)		
79.00	17.50	0.00	17.50	14.00	2.00	0.00	60.00	15.50	1.00	2.00	2.00	1.00	1.00	40.00	100.00	well	W/G
95.00	18.00	0.00	18.00	16.00	1.00	0.00	59.00	15.00	1.00	4.00	1.00	1.00	1.00	40.00	100.00	well	W/G
133.00	20.00	0.00	20.00	17.00	1.00	0.00	61.00	14.00	0.00	3.00	1.00	1.00	0.00	50.00	100.00	well	W/G
108.00	18.50	0.00	18.50	18.50	1.00	0.00	61.00	15.50	0.00	3.00	1.00	1.00	0.00	50.00	100.00	well	W/G
147.00	21.00	0.00	20.00	18.00	1.00	0.00	61.00	13.00	0.00	3.00	1.00	1.00	0.00	55.00	100.00	well	W/G
143.00	20.00	0.00	20.00	19.00	1.00	0.00	61.00	14.00	0.00	3.00	1.00	1.00	0.00	55.00	100.00	well	W/G
175.00	22.00	0.00	22.00	20.00	1.00	0.00	59.00	14.00	0.00	3.00	1.00	1.00	0.00	55.00	100.00	well	W/G
12.30	7.00	2.00	5.00	3.00	0.00	2.00	57.00	11.00	5.00	5.00	10.00	1.00	4.00	20.00	80.00	poor	P/P
4.57	4.00	0.00	4.00	1.00	0.00	3.00	56.00	10.00	5.00	5.00	15.00	1.00	4.00	10.00	80.00	poor	P/P
1.67	3.50	0.00	3.50	0.50	0.00	3.00	56.00	10.00	5.50	5.00	15.00	1.00	4.00	10.00	80.00	poor	P/P
1.52	3.00	0.00	3.00	0.50	0.00	2.50	56.00	10.00	6.00	5.00	15.00	1.00	4.00	10.00	80.00	poor	P/P
2.70	4.00	0.00	2.70	1.00	0.00	1.70	56.00	10.00	5.00	5.00	15.00	1.00	4.00	10.00	80.00	poor	P/P
1.50	3.00	0.00	3.00	1.00	0.00	2.00	56.00	10.00	6.00	5.00	15.00	1.00	4.00	10.00	80.00	poor	P/P
8.80	11.00	3.00	8.00	5.00	0.00	3.00	56.00	17.00	2.00	4.00	5.00	0.00	5.00	35.00	80.00	Mod	M/P
4.40	6.00	2.00	4.00	2.00	0.00	2.00	53.00	19.00	1.00	10.00	3.00	0.00	8.00	35.00	80.00	Mod	M/P
23.00	11.80	2.00	9.80	7.00	0.00	2.80	52.00	17.00	2.00	10.20	2.00	1.00	4.00	50.00	105.00	Mod	M/P
7.00	6.00	2.00	4.00	2.00	0.00	2.00	54.00	17.00	1.00	10.00	3.00	1.00	8.00	30.00	80.00	Mod	M/P
33.00	14.00	1.00	13.00	9.00	1.40	1.60	51.00	18.00	1.00	8.00	3.00	1.00	4.00	50.00	100.00	Mod	M/P
23.00	11.00	2.00	9.00	7.00	0.00	2.00	51.00	19.00	2.00	10.00	2.00	1.00	4.00	55.00	100.00	Mod	M/P
33.00	13.00	1.00	12.00	10.50	0.00	1.50	51.00	18.00	1.00	8.00	4.00	1.00	4.00	50.00	100.00	Mod	M/P
3.00	5.00	1.00	4.00	3.00	0.00	1.00	54.00	17.00	2.00	13.00	3.00	1.00	5.00	30.00	75.00	Mod	M/P
18.00	18.00	2.00	16.00	10.00	1.00	5.00	43.00	16.00	2.00	5.00	6.00	0.00	10.00	20.00	65.00	poor	P/M
5.60	9.00	1.00	8.00	4.00	0.00	4.00	55.00	14.00	1.00	6.00	5.00	0.00	10.00	15.00	65.00	poor	P/P
8.00	7.00	2.00	5.00	3.00	0.50	1.50	63.00	18.00	1.00	1.00	4.00	0.00	6.00	15.00	65.00	poor	P/P
19.00	10.00	1.00	9.00	7.00	1.00	1.00	60.00	19.00	2.00	2.00	4.00	0.00	3.00	36.00	65.00	Mod	M/M
28.00	15.00	3.00	12.00	10.00	1.50	0.50	57.00	20.00	1.00	3.00	3.00	0.00	1.00	36.00	70.00	Mod	M/M
29.00	15.00	3.00	12.00	10.00	1.10	0.90	57.00	20.00	1.00	3.00	3.00	0.00	1.00	35.00	70.00	Mod	M/M
65.00	17.00	3.00	14.00	11.00	1.50	0.50	59.00	16.00	2.00	2.00	1.00	0.00	3.00	45.00	110.00	Mod	M/M
55.00	18.00	4.00	14.00	11.50	1.00	1.50	59.00	16.00	2.00	1.00	1.00	0.00	3.00	50.00	110.00	Mod	M/M
108.00	23.00	3.00	19.00	16.00	1.60	0.80	47.00	18.90	1.00	4.10	1.00	0.00	5.00	55.00	110.00	Mod	M/G
93.00	23.00	4.00	19.00	15.00	1.00	1.00	47.00	20.10	2.00	3.90	1.00	0.00	3.00	50.00	110.00	Mod	M/G
93.00	23.00	3.50	19.50	15.50	0.50	0.50	46.00	18.70	2.00	5.30	2.00	0.00	3.00	45.00	110.00	Mod	M/G
86.00	20.00	3.00	17.00	14.00	1.00	0.00	48.50	19.00	1.00	6.50	1.00	0.00	4.00	50.00	110.00	Mod	M/G
70.00	20.00	3.00	17.00	14.00	1.00	0.00	49.00	18.00	1.00	6.00	1.00	0.00	5.00	50.00	110.00	Mod	M/G
56.00	14.00	1.00	13.00	9.00	1.20	2.80	53.00	18.00	3.00	4.00	0.00	0.00	8.00	45.00	100.00	Mod	M/G

Petrographic Data for the Shattuck Member

K (md)	Total Porosity	Primary Porosity	Total Secondary Porosity	Secondary Intergran. Porosity	Intracons-tituent Porosity	Micro-Porosity	Quartz	Feldspar	Rock Frag.	Anhydrite Gypsum	Dolomite	Hema-tite	Clay Detrital	Pore Size	Grain Size	Grain Sorting	Pore Sorting/ Connection
	(%)	(%)	(%)	(%)	(%)	(%)	(%)	(%)	(%)	(%)	(%)	(%)	(%)	(microns)	(microns)		
13.50	5.00	0.00	5.00	2.50	0.00	1.50	55.00	20.00	5.00	3.00	2.00	0.00	10.00	15.00	70.00	poor	P/P
5.60	4.00	0.00	4.00	2.00	0.00	2.00	56.00	20.00	5.00	3.00	2.00	0.00	10.00	15.00	65.00	poor	P/P
9.30	4.00	0.00	4.00	1.50	0.00	2.50	56.00	20.00	5.00	3.00	2.00	0.00	10.00	20.00	75.00	poor	P/P
8.60	4.00	0.00	4.00	2.00	0.00	2.00	54.00	20.00	7.00	3.00	2.00	0.00	10.00	15.00	70.00	poor	P/P
27.00	12.00	1.00	11.00	7.00	1.00	3.00	54.00	19.00	5.00	2.00	3.00	0.00	5.00	25.00	75.00	poor	P/P
28.00	12.00	1.00	11.00	7.00	1.40	2.60	56.00	19.00	3.00	2.00	3.00	0.00	5.00	20.00	75.00	poor	P/P
0.93	3.50	0.00	3.50	1.00	0.00	2.50	55.00	16.00	2.00	5.50	6.00	0.00	12.00	10.00	60.00	poor	P/P
1.20	3.00	0.00	3.00	1.00	0.00	2.00	55.00	16.00	2.00	6.00	6.00	0.00	12.00	10.00	60.00	poor	P/P
27.00	7.00	0.00	7.00	5.00	0.00	2.00	53.00	16.00	2.00	5.00	6.00	0.00	12.00	20.00	70.00	poor	P/P
27.00	6.00	0.00	6.00	5.00	0.00	2.00	51.00	16.00	3.00	6.00	6.00	0.00	12.00	20.00	70.00	poor	P/P
10.00	5.50	1.00	4.50	4.00	0.00	0.50	53.00	18.00	5.00	5.00	4.50	1.00	8.00	20.00	75.00	poor	P/P
7.00	7.00	1.00	6.00	3.00	0.00	2.00	54.00	18.00	5.00	4.00	3.00	1.00	8.00	20.00	75.00	poor	P/P
7.10	8.00	1.00	7.00	4.00	0.00	3.00	52.00	18.00	5.00	4.00	4.00	1.00	8.00	20.00	75.00	poor	P/P
2.00	3.00	0.00	3.00	1.00	0.00	2.00	42.00	17.00	6.00	7.00	8.00	1.00	16.00	10.00	70.00	poor	P/P
0.71	2.00	0.00	2.00	0.50	0.00	1.50	42.00	17.00	6.00	7.00	8.00	1.00	17.00	10.00	70.00	poor	P/P
0.52	2.00	0.00	2.00	0.50	0.00	1.50	42.00	17.00	6.00	7.00	8.00	1.00	17.00	10.00	70.00	poor	P/P
0.29	2.00	0.00	2.00	1.00	0.00	1.00	42.00	17.00	6.00	7.00	8.00	1.00	17.00	10.00	70.00	poor	P/P
0.56	2.00	0.00	2.00	1.00	0.00	1.00	42.00	17.00	6.00	7.00	8.00	1.00	17.00	10.00	70.00	poor	P/P
0.38	2.00	0.00	2.00	1.00	0.00	1.00	42.00	17.00	6.00	7.00	8.00	1.00	17.00	10.00	70.00	poor	P/P
0.53	3.00	0.00	3.00	1.50	0.00	1.50	42.00	17.00	6.00	6.00	8.00	1.00	17.00	10.00	70.00	poor	P/P
0.44	2.00	0.00	2.00	1.00	0.00	1.00	42.00	17.00	6.00	7.00	8.00	1.00	17.00	10.00	70.00	poor	P/P
1.04	2.00	0.00	2.00	1.00	0.00	1.00	42.00	17.00	6.00	7.00	8.00	1.00	17.00	10.00	70.00	poor	P/P
0.49	3.00	0.00	3.00	1.50	0.00	1.50	42.00	17.00	6.00	6.00	8.00	1.00	17.00	10.00	70.00	poor	P/P
3.32	3.00	0.00	3.00	1.00	0.00	2.00	42.00	17.00	6.00	7.00	8.00	1.00	16.00	10.00	70.00	poor	P/P
1.29	3.00	0.00	3.00	1.00	0.00	2.00	42.00	17.00	6.00	7.00	8.00	1.00	16.00	10.00	70.00	poor	P/P
0.95	2.00	0.00	2.00	1.00	0.00	1.00	42.00	17.00	6.00	7.00	8.00	1.00	17.00	10.00	70.00	poor	P/P
0.48	2.50	0.00	2.50	1.50	0.00	1.00	42.00	17.00	6.00	6.50	8.00	1.00	17.00	10.00	70.00	poor	P/P
0.41	2.00	0.00	2.00	1.00	0.00	1.00	42.00	17.00	6.00	7.00	8.00	1.00	17.00	10.00	70.00	poor	P/P
0.51	2.70	0.00	2.70	1.30	0.00	1.40	42.00	17.00	6.00	6.30	8.00	1.00	17.00	10.00	70.00	poor	P/P
1.90	2.00	0.00	2.00	1.00	0.00	1.00	42.00	17.00	6.00	7.00	8.00	1.00	17.00	10.00	70.00	poor	P/P
2.70	2.00	0.00	2.00	1.00	0.00	1.00	42.00	17.00	6.00	7.00	8.00	1.00	17.00	10.00	70.00	poor	P/P
2.30	2.00	0.00	2.00	0.00	0.00	2.00	42.00	17.00	6.00	7.00	8.00	1.00	17.00	10.00	70.00	poor	P/P
1.13	2.00	0.00	2.00	1.00	0.00	1.00	42.00	17.00	6.00	7.00	8.00	1.00	17.00	10.00	70.00	poor	P/P
100.00	18.00	3.00	15.00	10.00	1.60	2.40	49.00	16.00	4.00	4.00	3.00	0.00	4.00	35.00	80.00	Mod.	M/G
61.00	14.00	4.00	10.00	7.00	1.05	1.95	49.00	20.70	3.00	7.30	2.00	0.00	3.00	35.00	80.00	Mod.	M/G

Petrographic Data for the Shattuck Member

K (md)	Total Porosity	Primary Porosity	Total Secondary Porosity	Secondary Intergran. Porosity	Intracons-tituent Porosity	Micro-Porosity	Quartz	Feldspar	Rock Frag.	Anhydrite Gypsum	Dolomite	Hema-tite	Clay Detrital	Pore Size	Grain Size	Grain Sorting	Pore Sorting/ Connection
	(%)	(%)	(%)	(%)	(%)	(%)	(%)	(%)	(%)	(%)	(%)	(%)	(%)	(microns)	(microns)		
62.00	13.00	4.00	9.00	6.00	1.40	1.60	48.00	22.50	3.00	6.50	2.00	0.00	3.00	35.00	80.00	Mod.	M/G
57.00	14.00	4.00	10.00	7.00	1.20	1.80	48.00	18.00	3.00	10.00	2.00	0.00	3.00	35.00	80.00	Mod.	M/G
36.00	12.00	1.00	11.00	9.00	0.00	2.00	50.00	17.00	3.00	10.00	2.00	0.00	4.00	35.00	80.00	Mod.	M/M
47.00	11.00	1.00	10.00	8.00	0.00	2.00	50.00	18.00	3.00	11.00	2.00	0.00	4.00	30.00	80.00	Mod.	M/M
34.00	12.00	0.00	12.00	10.50	0.00	1.50	49.00	19.00	3.00	10.00	2.00	0.00	4.00	30.00	80.00	Mod.	M/M
38.00	12.00	1.00	11.00	9.00	0.00	2.00	49.00	19.00	3.00	10.00	2.00	0.00	4.00	30.00	80.00	Mod.	M/M
78.00	8.00	1.00	7.00	2.00	0.00	2.00	47.00	20.00	3.00	4.00	7.00	0.00	6.00	35.00	85.00	Mod.	M/M
48.00	13.00	2.00	11.00	6.00	0.00	5.00	48.00	18.00	3.00	3.00	6.00	0.00	5.00	35.00	85.00	Mod.	M/M
39.00	9.00	3.00	6.00	5.00	0.00	1.00	50.00	16.00	2.00	12.00	3.00	0.00	3.00	35.00	85.00	Mod.	M/M
2.30	3.00	0.00	3.00	1.00	0.00	2.00	53.00	17.00	2.00	4.00	8.00	0.00	7.00	10.00	65.00	poor	P/P
6.70	5.00	0.00	5.00	3.00	0.00	3.00	51.00	17.00	2.00	4.00	8.00	0.00	7.00	10.00	65.00	poor	P/P
1.70	1.50	0.00	1.50	0.00	0.00	1.50	65.00	17.00	2.00	4.50	2.00	0.00	8.00	10.00	65.00	poor	P/P
2.80	3.00	0.00	3.00	1.00	0.00	2.00	65.00	17.00	2.00	3.00	2.00	0.00	8.00	10.00	65.00	poor	P/P
2.40	2.00	0.00	2.00	0.00	0.00	2.00	65.00	17.00	2.00	4.00	2.00	0.00	8.00	10.00	65.00	poor	P/P
3.20	2.00	0.00	1.50	0.00	0.00	0.50	65.00	17.00	2.00	4.00	2.00	0.00	8.00	10.00	65.00	poor	P/P
3.20	3.00	0.00	3.00	0.00	0.00	3.00	64.00	17.00	4.00	4.00	2.00	0.00	6.00	10.00	65.00	poor	P/P
4.00	3.00	0.00	3.00	1.00	0.00	2.00	64.00	17.00	4.00	4.00	2.00	0.00	6.00	10.00	65.00	poor	P/P
5.00	5.00	1.00	4.00	3.00	0.00	1.00	58.00	18.00	4.00	4.00	5.00	0.00	4.00	15.00	65.00	poor	P/P
5.30	5.00	1.00	4.00	2.00	0.00	2.00	60.00	18.00	2.00	4.00	5.00	0.00	4.00	15.00	65.00	poor	P/P
20.00	13.00	2.00	11.00	7.00	0.00	4.00	51.00	20.00	2.00	4.00	2.00	0.00	3.00	35.00	100.00	Mod.	M/M
58.00	11.00	1.00	10.00	4.00	0.00	3.00	53.00	20.00	2.00	4.00	2.00	0.00	3.00	60.00	100.00	Mod.	P/G
9.00	9.00	1.00	8.00	6.00	0.00	2.00	52.00	18.00	3.00	3.00	4.00	0.00	3.00	25.00	100.00	Mod.	P/P
15.00	8.00	1.00	7.00	4.00	0.00	1.00	53.00	18.00	3.00	3.00	4.00	0.00	3.00	25.00	100.00	Mod.	P/P
22.00	9.00	1.00	8.00	3.00	0.00	2.00	52.00	18.00	3.00	3.00	4.00	0.00	3.00	35.00	100.00	Mod.	P/P
12.00	7.00	1.00	6.00	4.00	0.00	2.00	52.00	18.00	3.00	5.00	4.00	0.00	3.00	25.00	100.00	Mod.	P/P
7.00	5.00	0.00	5.00	0.00	0.00	3.00	53.00	18.00	5.00	4.00	3.00	0.00	5.00	25.00	100.00	Mod.	P/P
29.00	7.00	0.00	7.00	3.00	0.00	1.00	51.00	18.00	5.00	4.00	3.00	0.00	5.00	35.00	100.00	Mod.	P/P
34.00	16.00	1.00	15.00	8.00	1.40	2.60	51.00	20.00	1.00	2.00	3.00	0.00	4.00	50.00	100.00	Mod.	M/P
48.00	18.00	3.00	15.00	11.20	1.00	1.00	49.00	20.00	1.00	2.00	3.00	0.00	4.00	50.00	100.00	Mod.	M/M
19.00	16.00	3.00	13.00	10.00	0.00	3.00	55.00	18.00	1.00	1.00	2.00	0.00	3.00	45.00	100.00	Mod.	M/P
26.00	14.00	3.00	11.00	9.00	0.00	2.00	55.00	18.00	1.00	3.00	2.00	0.00	3.00	45.00	100.00	Mod.	M/M
27.00	15.00	2.00	13.00	10.00	0.00	1.00	56.00	18.00	1.00	1.00	2.00	0.00	3.00	45.00	100.00	Mod.	M/M
39.00	18.00	2.00	16.00	11.00	1.70	1.30	55.00	16.00	1.00	1.00	2.00	0.00	3.00	45.00	100.00	Mod.	M/M
17.00	16.00	3.00	13.00	10.00	0.00	1.00	53.00	18.00	1.00	1.00	2.00	0.00	3.00	45.00	100.00	Mod.	M/M
22.00	16.00	2.00	14.00	11.00	0.00	1.00	53.00	18.00	1.00	1.00	2.00	0.00	3.00	45.00	100.00	Mod.	M/M

Petrographic Data for the Shattuck Member

K (md)	Total Porosity	Primary Porosity	Total Secondary Porosity	Secondary Intergran. Porosity	Intracons-tituent Porosity	Micro-Porosity	Quartz	Feldspar	Rock Frag.	Anhydrite Gypsum	Dolomite	Hema-tite	Clay Detrital	Pore Size	Grain Size	Grain Sorting	Pore Sorting/ Connection
	(%)	(%)	(%)	(%)	(%)	(%)	(%)	(%)	(%)	(%)	(%)	(%)	(%)	(microns)	(microns)		
1.80	4.00	1.00	3.00	2.00	0.00	1.00	64.00	16.00	2.00	4.00	4.00	0.00	5.00	15.00	70.00	Mod.	P/P
4.30	4.00	1.00	3.00	2.50	0.00	0.50	64.00	16.00	2.00	4.00	4.00	0.00	5.00	15.00	70.00	Mod.	P/P
0.90	2.00	0.00	2.00	1.00	0.00	1.00	64.00	16.00	2.00	4.00	4.00	0.00	7.00	10.00	60.00	poor	P/P
4.00	4.00	1.00	3.00	1.50	0.00	1.50	64.00	16.00	2.00	4.00	4.00	0.00	5.00	10.00	60.00	poor	P/P
0.80	2.00	0.00	2.00	1.00	0.00	1.00	63.00	13.00	3.00	6.00	6.00	0.00	7.00	7.00	65.00	poor	P/P
1.30	2.00	0.00	2.00	1.00	0.00	1.00	63.00	13.00	3.00	6.00	6.00	0.00	7.00	8.00	60.00	poor	P/P
48.00	15.00	0.00	15.00	9.00	0.00	3.00	52.00	17.00	2.00	2.00	3.00	0.00	4.00	55.00	100.00	Mod.	M/M
32.00	10.00	0.00	10.00	6.00	0.00	0.00	52.00	17.00	2.00	2.00	3.00	0.00	3.00	60.00	100.00	Mod.	M/M
0.50	7.00	0.00	7.00	0.00	2.00	3.00	52.00	17.00	1.00	17.00	2.00	0.00	2.00	25.00	60.00	Well	M/P
0.80	6.00	0.00	6.00	0.00	1.00	3.00	53.00	16.00	3.00	16.00	2.00	0.00	2.00	20.00	65.00	Well	M/P
0.31	7.00	0.00	7.00	0.00	2.00	3.50	51.00	18.00	2.00	18.00	1.00	0.00	2.00	20.00	60.00	Well	M/P
0.34	5.00	0.00	5.00	0.00	0.00	3.00	52.00	17.00	1.00	18.00	2.00	0.00	3.00	25.00	60.00	Well	M/P
0.50	4.50	0.00	4.50	0.00	0.00	1.50	52.00	19.00	1.50	18.00	1.00	0.00	2.00	25.00	60.00	Well	M/P
0.50	3.00	0.00	3.00	0.00	0.00	1.50	55.00	17.00	3.00	16.00	2.00	0.00	1.00	18.00	65.00	Well	M/P
0.40	5.00	0.00	5.00	0.00	0.00	3.00	52.00	19.00	2.00	17.00	2.00	0.00	1.00	20.00	60.00	Well	M/P
0.50	7.00	0.00	7.00	0.00	2.00	3.00	51.00	18.00	1.00	18.00	1.00	0.00	3.00	25.00	60.00	Well	M/P
0.43	6.00	0.00	6.00	0.00	1.00	3.00	53.00	18.00	1.00	16.00	1.00	0.00	3.00	25.00	60.00	Well	M/P
0.50	5.00	0.00	5.00	0.00	0.00	3.00	54.00	17.00	2.00	15.00	2.00	0.00	3.00	20.00	65.00	Well	M/P
2.20	5.00	0.00	5.00	0.00	0.00	2.20	52.00	17.00	1.00	19.00	2.00	0.00	2.00	20.00	65.00	Well	M/P
0.63	3.00	0.00	3.00	0.80	0.00	0.00	52.00	18.00	3.00	18.00	2.00	0.00	2.00	20.00	65.00	Well	M/P
3.50	6.00	0.00	6.00	2.50	1.00	0.00	52.00	17.00	1.00	18.00	2.00	0.00	2.00	25.00	60.00	Well	M/P
4.60	6.00	0.00	6.00	3.00	1.00	0.00	53.00	17.00	1.00	18.00	1.00	0.00	2.00	25.00	60.00	Well	M/P
1.50	4.00	0.00	4.00	1.00	1.00	0.00	40.00	18.00	6.00	9.00	2.00	0.00	19.00	20.00	40.00	Well	M/P
0.42	2.00	0.00	2.00	1.00	0.50	0.50	63.00	14.00	1.00	19.00	0.00	0.00	1.00	10.00	70.00	Well	P/P
0.74	2.00	0.00	2.00	1.00	0.50	0.50	63.00	14.00	1.00	19.00	0.00	0.00	1.00	10.00	70.00	Well	P/P
1.40	4.00	0.00	4.00	2.00	1.00	1.00	59.00	14.00	1.00	17.00	0.00	0.00	2.00	10.00	70.00	Well	P/P
2.40	4.50	0.00	4.50	2.00	1.50	1.00	60.00	12.50	1.00	17.00	0.00	0.00	2.00	10.00	70.00	Well	P/P
2.60	3.50	0.00	3.50	1.50	1.00	1.00	61.00	13.50	1.00	16.00	0.00	0.00	2.00	10.00	70.00	Well	P/P
2.90	4.00	0.00	4.00	2.00	1.00	1.00	59.00	15.00	1.00	16.00	0.00	0.00	2.00	10.00	70.00	Well	P/P
1.03	5.50	0.00	5.50	2.00	2.00	1.50	59.00	12.50	1.00	17.00	0.00	0.00	2.00	10.00	70.00	Well	P/P
1.50	3.00	0.00	3.00	1.00	1.00	1.00	60.00	15.00	1.00	16.00	0.00	0.00	2.00	10.00	70.00	Well	P/P
3.50	3.00	0.00	4.00	2.00	0.50	0.50	51.00	18.00	2.00	17.00	0.00	0.00	4.00	15.00	70.00	Well	P/P
6.00	4.00	0.00	4.00	2.00	0.50	0.50	50.00	18.00	2.00	17.00	0.00	0.00	4.00	15.00	70.00	Well	P/P
2.70	13.00	0.00	13.00	10.00	1.00	2.00	52.00	15.00	0.00	7.00	0.00	0.00	2.00	20.00	100.00	Mod.	P/P
1.23	13.00	0.00	13.00	10.00	1.00	2.00	52.00	15.00	0.00	7.00	0.00	0.00	2.00	20.00	100.00	Mod.	P/P

Petrographic Data for the Shattuck Member

K (md)	Total Porosity	Primary Porosity	Total Secondary Porosity	Secondary Intergran. Porosity	Intracons-tituent Porosity	Micro-Porosity	Quartz	Feldspar	Rock Frag.	Anhydrite Gypsum	Dolomite	Hema-tite	Clay Detrital	Pore Size	Grain Size	Grain Sorting	Pore Sorting/ Connection
	(%)	(%)	(%)	(%)	(%)	(%)	(%)	(%)	(%)	(%)	(%)	(%)	(%)	(microns)	(microns)		
2.20	9.00	0.00	9.00	5.00	2.00	2.00	57.00	16.00	2.00	5.00	0.00	0.00	5.00	15.00	100.00	poor	P/P
1.50	8.00	0.00	8.00	4.00	1.50	1.50	63.00	14.00	0.00	12.00	0.00	0.00	1.00	20.00	100.00	Mod.	M/P
3.01	7.00	0.00	7.00	5.00	1.00	1.00	58.00	17.00	0.00	9.00	3.00	0.00	0.00	15.00	100.00	Mod.	M/P
1.03	8.00	0.00	8.00	5.00	1.00	2.00	62.00	16.00	0.00	10.00	0.00	0.00	0.00	20.00	100.00	Mod.	M/P
1.35	4.00	0.00	4.00	2.00	1.00	1.00	61.00	17.00	0.00	16.00	0.00	0.00	0.00	10.00	100.00	Mod.	P/P
1.03	2.00	0.00	2.00	1.00	0.00	1.00	58.00	19.00	0.00	21.00	0.00	0.00	0.00	10.00	100.00	Mod.	P/P
1.11	3.00	0.00	3.00	1.50	0.00	1.50	52.00	18.00	0.00	27.00	0.00	0.00	0.00	5.00	100.00	well	P/P
1.20	2.00	0.00	2.00	1.00	0.00	1.00	52.00	19.00	0.00	27.00	0.00	0.00	0.00	5.00	100.00	well	P/P
1.10	7.00	0.00	7.00	2.00	0.70	2.30	51.00	17.00	0.00	17.00	7.00	0.00	0.00	15.00	95.00	Mod.	P/P
1.40	6.00	0.00	6.00	0.00	1.00	3.00	50.00	17.00	0.00	20.00	6.00	0.00	0.00	15.00	95.00	Mod.	P/P
1.20	4.00	0.00	4.00	0.00	1.50	2.00	53.00	17.00	0.00	17.00	8.00	0.00	0.00	10.00	100.00	Mod.	P/P
1.30	5.00	0.00	5.00	1.00	1.00	1.50	52.00	17.00	0.00	20.00	5.00	0.00	0.00	15.00	100.00	Mod.	P/P
0.21	6.00	0.00	6.00	1.00	2.00	3.00	51.00	17.00	0.00	19.00	6.00	0.00	0.00	10.00	95.00	Mod.	P/P
0.70	7.00	0.00	7.00	0.00	1.00	4.00	50.00	19.00	0.00	16.00	6.00	0.00	0.00	10.00	100.00	Mod.	P/P
3.60	9.00	0.00	9.00	3.00	1.50	3.00	49.00	15.00	0.00	18.00	8.00	0.00	0.00	10.00	100.00	Mod.	P/P
0.60	7.00	0.00	7.00	3.00	1.00	1.00	49.00	18.00	0.00	19.00	6.00	0.00	0.00	15.00	100.00	Mod.	P/P
3.40	6.00	0.00	6.00	3.00	1.00	0.00	49.00	19.00	0.00	17.00	7.00	0.00	0.00	15.00	100.00	Mod.	P/P
0.74	8.00	0.00	8.00	1.50	1.70	2.50	53.00	15.00	0.00	21.00	2.00	0.00	0.00	15.00	100.00	Mod.	P/P
0.31	7.00	0.00	7.00	1.00	1.60	3.00	43.00	15.00	0.00	34.00	0.00	0.00	0.00	15.00	95.00	Mod.	P/P
0.32	6.00	0.00	6.00	0.50	0.80	2.50	43.00	15.00	0.00	35.00	0.00	0.00	0.00	15.00	95.00	Mod.	P/P
0.32	4.00	0.00	4.00	1.00	1.00	1.00	44.00	16.00	0.00	35.00	0.00	0.00	0.00	10.00	100.00	Mod.	P/P
0.31	5.00	0.00	5.00	3.00	1.10	0.00	41.00	16.00	0.00	36.00	0.00	0.00	0.00	15.00	100.00	Mod.	P/P
0.37	4.50	0.00	4.50	1.50	1.00	1.00	43.00	16.50	0.00	34.00	0.00	0.00	0.00	10.00	95.00	Mod.	P/P
0.30	7.00	0.00	7.00	2.00	1.30	2.00	44.00	15.00	0.00	33.00	0.00	0.00	0.00	10.00	100.00	Mod.	P/P
0.37	4.00	0.00	4.00	1.00	1.00	2.00	44.00	17.00	0.00	34.00	0.00	0.00	0.00	10.00	100.00	Mod.	P/P
0.34	7.00	0.00	7.00	3.00	1.40	1.00	41.00	16.00	0.00	34.00	0.00	0.00	0.00	15.00	100.00	Mod.	P/P
0.37	5.00	0.00	5.00	1.00	1.50	0.00	45.00	16.00	0.00	32.00	0.00	0.00	0.00	15.00	100.00	Mod.	P/P
0.32	6.00	0.00	6.00	2.00	1.00	0.00	41.00	16.00	0.00	35.00	0.00	0.00	0.00	15.00	100.00	Mod.	P/P
0.15	1.00	0.00	1.00	1.00	0.00	0.00	50.00	15.00	0.00	30.00	0.00	1.00	2.00	10.00	110.00	well	P/P
0.12	1.00	0.00	1.00	1.00	0.00	0.00	49.00	15.00	0.00	29.00	0.00	1.00	3.00	10.00	110.00	well	P/P
0.12	1.50	0.00	1.50	1.50	0.00	0.00	48.00	17.00	0.00	30.00	0.00	1.50	1.00	15.00	110.00	well	P/P
0.12	2.50	0.00	2.50	2.50	0.00	0.00	47.00	18.00	0.00	28.00	0.00	0.50	2.00	10.00	110.00	well	P/P
0.12	2.00	0.00	2.00	2.00	0.00	0.00	48.00	16.00	0.00	30.00	0.00	1.00	2.00	10.00	110.00	well	P/P
0.11	1.00	0.00	1.00	1.00	0.00	0.00	49.00	17.00	0.00	29.00	0.00	1.00	2.00	10.00	110.00	well	P/P
1.20	2.80	0.00	2.80	0.80	0.00	0.00	58.00	18.00	0.00	13.00	0.00	0.00	8.20	10.00	100.00	well	P/P

Petrographic Data for the Shattuck Member

K (md)	Total Porosity	Primary Porosity	Total Secondary Porosity	Secondary Intergran. Porosity	Intracons-tituent Porosity	Micro-Porosity	Quartz	Feldspar	Rock Frag.	Anhydrite Gypsum	Dolomite	Hema-tite	Clay Detrital	Pore Size	Grain Size	Grain Sorting	Pore Sorting/ Connection
	(%)	(%)	(%)	(%)	(%)	(%)	(%)	(%)	(%)	(%)	(%)	(%)	(%)	(microns)	(microns)		
1.12	2.00	0.00	2.00	0.00	0.00	0.00	57.00	17.00	0.00	16.00	0.00	0.00	8.00	10.00	100.00	well	P/P
2.40	3.20	0.00	3.20	0.00	0.00	1.20	56.00	17.00	0.00	18.00	0.00	0.00	5.80	10.00	100.00	well	P/P
2.20	1.80	0.00	1.80	0.00	0.00	0.80	56.00	17.00	0.00	17.00	0.00	0.00	8.20	10.00	100.00	well	P/P
1.20	2.00	0.00	2.00	0.00	0.00	0.00	56.00	17.00	0.00	17.00	0.00	0.00	8.00	10.00	100.00	well	P/P
1.50	2.00	0.00	2.00	0.00	0.00	0.00	58.00	17.00	0.00	15.00	0.00	0.00	8.00	10.00	100.00	well	P/P
1.30	2.50	0.00	2.50	0.00	0.00	0.50	58.00	17.00	0.00	15.00	0.00	0.00	7.50	10.00	100.00	well	P/P
1.14	2.00	0.00	2.00	0.00	0.00	0.00	58.00	17.00	0.00	15.00	0.00	0.00	8.00	10.00	100.00	well	P/P
1.40	2.50	0.00	2.50	0.00	0.00	0.50	58.00	17.00	0.00	15.00	0.00	0.00	7.50	10.00	100.00	well	P/P
1.03	2.00	0.00	2.00	0.00	0.00	0.00	58.00	17.00	0.00	16.00	0.00	0.00	7.00	10.00	100.00	well	P/P
4.40	6.00	0.00	6.00	1.50	0.50	4.00	59.00	12.00	3.00	7.00	5.00	0.00	8.00	5.00	80.00	Mod.	P/P
5.20	6.00	0.00	6.00	2.50	0.50	3.00	59.00	12.00	3.00	7.00	5.00	0.00	8.00	5.00	80.00	Mod.	P/P
3.70	5.00	0.00	5.00	2.00	0.00	3.00	57.00	15.00	3.00	8.00	6.00	0.00	6.00	5.00	80.00	Mod.	P/P
2.40	4.00	0.00	4.00	1.50	0.00	2.50	57.00	15.00	3.00	8.00	6.00	0.00	7.00	5.00	80.00	Mod.	P/P
4.20	4.00	0.00	4.00	2.00	0.00	2.00	68.00	16.00	2.00	3.00	4.00	0.00	3.00	10.00	80.00	Mod.	P/P
2.50	4.00	0.00	4.00	2.00	0.00	2.00	68.00	16.00	2.00	3.00	4.00	0.00	3.00	10.00	80.00	Mod.	P/P
244.00	25.00	0.00	25.00	23.00	2.00	0.00	44.00	19.50	1.00	4.50	0.00	0.00	3.00	60.00	120.00	Mod.	G/G
222.00	27.00	0.00	27.00	24.00	2.00	0.00	42.00	20.80	1.00	5.20	0.00	0.00	2.00	60.00	120.00	Mod.	G/G
117.00	19.00	0.00	19.00	15.00	2.00	0.00	50.00	20.40	1.00	4.60	0.00	0.00	2.00	60.00	120.00	Mod.	G/G
149.00	18.00	0.00	18.00	14.00	2.00	0.00	48.00	21.70	1.00	6.30	0.00	0.00	2.00	60.00	120.00	Mod.	G/G
149.00	19.00	0.00	19.00	15.00	2.00	0.00	50.70	20.00	1.00	5.30	0.00	0.00	2.00	60.00	120.00	Mod.	G/G
140.00	19.00	0.00	19.00	15.00	2.00	0.00	51.00	20.00	1.00	5.00	0.00	0.00	2.00	60.00	120.00	Mod.	G/G
5.00	5.00	0.00	5.00	4.00	1.00	0.00	47.00	19.00	1.00	23.00	1.00	1.00	1.00	15.00	110.00	well	G/P
2.22	2.50	0.00	2.50	1.70	0.80	0.00	44.00	18.00	2.50	28.00	1.00	1.00	1.00	15.00	110.00	well	G/P
3.10	3.00	0.00	3.00	2.00	1.00	0.00	44.00	18.00	2.00	28.00	1.00	1.00	1.00	15.00	110.00	well	G/P
5.00	5.00	0.00	5.00	3.20	1.80	0.00	50.00	19.00	2.00	19.00	1.00	1.00	1.00	15.00	110.00	well	G/P
5.00	3.00	0.00	3.00	3.00	0.00	0.00	50.00	19.00	3.00	20.00	1.00	1.00	1.00	15.00	110.00	well	G/P
5.00	6.00	0.00	6.00	4.50	1.50	0.00	50.00	18.00	1.00	20.00	1.00	1.00	1.00	15.00	110.00	well	G/P
139.00	17.00	0.00	17.00	13.00	2.00	0.70	52.50	21.00	0.00	7.50	0.00	0.00	0.00	65.00	90.00	well	G/G
200.00	22.00	0.00	22.00	18.00	2.00	1.00	48.00	19.00	1.00	5.00	4.00	0.00	0.00	65.00	90.00	well	G/G
182.00	18.00	0.00	18.00	16.00	1.50	0.50	50.00	18.00	0.00	6.00	0.00	0.00	0.00	65.00	90.00	well	G/G
117.00	19.00	0.00	19.00	15.00	2.00	1.00	49.00	21.00	0.00	6.00	3.00	0.00	0.00	50.00	110.00	well	G/G
147.00	18.00	0.00	18.00	14.00	2.00	0.00	51.00	19.00	4.00	4.00	1.00	0.00	0.00	50.00	110.00	well	G/G

Petrographic Data for the Shattuck Member

K (md)	Total Porosity	Primary Porosity	Total Secondary Porosity	Secondary Intergran. Porosity	Intraconstituent Porosity	Micro-Porosity	Quartz	Feldspar	Rock Frag.	Anhydrite Gypsum	Dolomite	Hematite	Clay Detrital	Pore Size	Grain Size	Grain Sorting	Pore Sorting/ Connection
	(%)	(%)	(%)	(%)	(%)	(%)	(%)	(%)	(%)	(%)	(%)	(%)	(%)	(microns)	(microns)		
143.00	21.00	0.00	21.00	17.00	3.00	0.00	51.00	19.00	2.00	3.00	1.00	0.00	0.00	50.00	110.00	well	G/G
257.00	21.00	0.00	21.00	17.50	3.50	0.00	57.00	18.00	0.00	3.00	0.00	0.00	0.00	65.00	90.00	well	G/G
101.00	16.00	0.00	16.00	14.00	2.00	0.00	59.00	18.00	0.00	6.00	0.00	0.00	0.00	50.00	110.00	well	G/G
21.20	9.00	0.00	9.00	8.00	0.00	0.00	55.00	14.00	2.00	17.00	0.00	0.00	0.00	25.00	105.00	well	G/P
22.40	9.00	0.00	9.00	8.00	0.00	1.00	54.00	15.00	2.00	17.00	0.00	0.00	0.00	25.00	105.00	well	G/P
21.20	10.00	0.00	10.00	8.50	0.00	1.50	54.00	16.00	1.00	15.00	0.00	0.00	0.00	25.00	105.00	well	G/P
18.10	10.00	0.00	10.00	7.00	0.00	1.00	53.00	15.00	2.00	17.00	0.00	0.00	0.00	25.00	105.00	well	G/P
17.20	9.00	0.00	9.00	7.00	0.00	2.00	52.00	17.00	1.00	17.00	0.00	0.00	0.00	25.00	105.00	well	G/P
18.00	9.00	0.00	9.00	8.00	0.00	1.00	53.00	17.00	2.00	15.00	0.00	0.00	0.00	25.00	105.00	well	G/P
12.20	5.00	0.00	5.00	5.00	0.00	0.00	63.00	16.00	1.00	14.00	0.00	0.00	0.00	45.00	110.00	well	P/P
6.00	5.00	0.00	5.00	5.00	0.00	0.00	63.00	16.00	1.00	14.00	0.00	0.00	0.00	30.00	110.00	well	P/P
5.10	7.00	0.00	7.00	5.20	1.80	0.00	55.00	18.00	0.00	16.00	1.00	0.00	0.00	30.00	110.00	well	P/P
4.40	7.00	0.00	7.00	6.00	1.00	0.00	55.00	18.00	0.00	16.00	1.00	0.00	0.00	30.00	110.00	well	P/P
24.00	17.00	0.00	17.00	15.00	2.00	0.00	51.00	18.00	0.00	8.00	0.00	0.00	0.00	45.00	110.00	well	P/P
8.40	15.00	0.00	15.00	13.70	1.30	0.00	49.00	18.00	0.00	11.00	1.00	0.00	0.00	45.00	110.00	well	P/P
200.00	19.00	0.00	19.00	15.00	0.00	0.00	53.00	21.00	2.00	2.00	3.00	0.00	0.00	65.00	100.00	Mod.	G/G
294.00	21.00	0.00	21.00	16.00	0.00	0.00	50.00	19.00	4.00	5.00	1.00	0.00	0.00	60.00	100.00	Mod.	G/G
87.00	15.00	0.00	15.00	13.00	1.00	0.00	54.00	20.00	4.00	3.00	4.00	0.00	0.00	50.00	100.00	Mod.	G/G
82.00	16.00	0.00	16.00	14.00	1.00	0.00	54.00	20.00	3.00	3.00	4.00	0.00	0.00	50.00	100.00	Mod.	G/G
104.00	17.00	0.00	17.00	15.50	1.50	0.00	54.00	20.00	2.00	3.00	4.00	0.00	0.00	50.00	100.00	Mod.	G/G
73.00	16.00	0.00	16.00	14.00	1.00	1.00	54.00	20.00	3.00	3.00	4.00	0.00	0.00	50.00	100.00	Mod.	G/G
3.20	4.00	0.00	4.00	0.50	0.00	3.50	58.00	18.00	7.00	3.00	1.00	0.00	9.00	10.00	75.00	poor	P/P
8.40	7.00	0.00	7.00	5.00	0.00	2.00	57.00	17.00	7.00	3.00	1.00	0.00	8.00	10.00	75.00	poor	P/P
2.30	4.00	0.00	4.00	1.00	0.00	3.00	52.00	19.00	9.00	5.00	1.00	0.00	10.00	10.00	75.00	poor	P/P
3.30	4.00	0.00	4.00	1.50	0.00	2.50	53.00	18.00	9.00	5.00	1.00	0.00	10.00	10.00	75.00	poor	P/P

This dissertation is accepted on behalf of the faculty
of the Institute by the following committee

10/27/97 Peter Mozley

Adviser

09/04/1997 ADWAIT CHAWATHÉ

9/04/97 ALLAN GUTJAHR

9/08/97 John Heller

15 October 1997 Fred M. Phillips

10/31/97 David B. Johns

Date

I release this document to New Mexico Institute of Mining and Technology.

Student's Signature Date